



**HAL**  
open science

# Development of stimuli-responsive cellulose nanocrystals hydrogels for smart applications

Erwan Gicquel

► **To cite this version:**

Erwan Gicquel. Development of stimuli-responsive cellulose nanocrystals hydrogels for smart applications. Chemical Physics [physics.chem-ph]. Université Grenoble Alpes, 2017. English. NNT : 2017GREAI105 . tel-01756932

**HAL Id: tel-01756932**

**<https://theses.hal.science/tel-01756932>**

Submitted on 3 Apr 2018

**HAL** is a multi-disciplinary open access archive for the deposit and dissemination of scientific research documents, whether they are published or not. The documents may come from teaching and research institutions in France or abroad, or from public or private research centers.

L'archive ouverte pluridisciplinaire **HAL**, est destinée au dépôt et à la diffusion de documents scientifiques de niveau recherche, publiés ou non, émanant des établissements d'enseignement et de recherche français ou étrangers, des laboratoires publics ou privés.

## **THÈSE**

Pour obtenir le grade de

### **DOCTEUR DE LA COMMUNAUTE UNIVERSITE GRENOBLE ALPES**

Spécialité : **Matériaux, mécanique, génie civil, Electrochimie**

Arrêté ministériel : 25 mai 2016

Présentée par

**Erwan GICQUEL**

Thèse dirigée par **Julien BRAS** et  
codirigée par **Céline MARTIN**

préparée au sein du **Laboratoire de Génie des Procédés  
Papetiers**  
dans l'**École Doctorale I-MEP2 – Ingénierie – Matériaux,  
Mécanique, Environnement, Energétique, Procédés, Production**

## **Development of stimuli-responsive cellulose nanocrystals hydrogels for smart applications**

Thèse soutenue publiquement le «**01 décembre 2017**»,  
devant le jury composé de :

**Dr. Bernard CATHALA**

Directeur de recherche à l'INRA de Nantes, Rapporteur

**Pr. Wim THIELEMANS**

Professeur à l'Université de Louvain, Rapporteur

**Pr. Emily CRANSTON**

Professeur à l'université McMaster à Hamilton, Examinatrice

**Pr. Frédéric BOSSARD**

Professeur des universités au LRP de Grenoble, Président

**Dr. Julien, BRAS**

Maître de Conférences à Grenoble INP, Directeur de thèse

**Dr. Céline MARTIN**

Maître de Conférences à Grenoble INP, Co-encadrante de thèse

**Dr. Bruno JEAN**

Chargé de recherche au CERMAV, Membre invité

**Dr. Frédéric PIGNON**

Directeur de recherche au LRP de Grenoble, Membre invité





# Remerciements

*A vous, lecteurs-res, je tiens à vous remercier pour votre intérêt et votre lecture de ce manuscrit de recherche traçant mes trois années de thèse.*

*Avant d'oublier quiconque, j'adresse ma plus profonde gratitude à toutes les personnes de mon entourage proche ou lointain pour leur soutien au cours de mes trois années de thèse : **Merci à tous et toutes !***

*J'adresse ensuite ma gratitude au Professeur Frédéric BOSSARD pour sa présidence à mon jury de thèse, au Directeur de recherche Bernard CATHALA et au Professeur Wim THIELEMANS pour leur engagement sur mon manuscrit de thèse en tant que rapporteurs. De plus, je remercie la Professeure Emily CRANSTON pour son importante participation en tant qu'examinatrice mais aussi pour son aide et ses conseils tout au long de nos travaux collaboratifs. Un grand merci pour votre présence.*

*A Frédéric PIGNON et Bruno JEAN, milles mercis pour nos discussions, nos manip et nos travaux (aussi bien en rhéologie, qu'en chimie) ainsi que pour votre présence au sein de mon comité de suivi de thèse. Celle-ci n'aurait pas été aussi riche et variée sans votre aide.*

*A Céline et Julien, mes deux directeurs de thèse, je vous exprime toute ma gratitude pour votre confiance. Je vous remercie pour le temps conséquent que vous m'avez accordé durant ses trois années (il était très rare qu'une réunion ne déborde pas généreusement), votre rigueur scientifique, votre excellent et complémentaire encadrement, vos très nombreux conseils pendant la rédaction ainsi que votre amitié. Je vous dois la bonne réussite de ce travail.*

*Merci Julien pour ta confiance, ton enthousiasme, ta disponibilité, ton écoute, tes méthodes d'organisation du travail (le mur de post-it qui m'a bien aidé) et tes énormes qualités scientifiques et humaines. Chacune de nos réunions furent d'énormes coups de boost pour la réussite de ma thèse (avec 50 nouvelles idées à chaque fois). Bien que tu ais dû faire le deuil d'une thèse 100% Chimie, notre collaboration a fourni un travail d'excellente qualité : je t'en remercie. Et ne t'inquiète pas, je viendrai t'apporter un peu de terroir Nantais quand je passerai au laboratoire :D.*

*Merci Céline d'avoir été en quelque sorte ma maman de thèse. Tu as toujours été présente, disponible, à l'écoute, patiente et pédagogue. Avec tes qualités scientifiques, tu m'as fait prendre goût à la rhéologie. A chaque point que nous faisons, alors que j'avais l'impression de n'avoir jamais assez de résultats, tu me démontrais, à chaque fois, la qualité de ceux-ci à travers la pluralité des domaines abordés. Tu as toujours été une source de conseils et de motivation : je t'en remercie.*

*Par ailleurs, je tiens à remercier toutes les personnes extérieures au laboratoire qui ont répondu à mes sollicitations. En particulier, un grand merci à Jean-Luc Putaux et Christine Lancelon-Pin pour leur disponibilité sur la microscopie TEM et pour nos nombreuses et variées discussions.*

*Merci aux personnels techniques du LGP2 qui ont toujours été disponibles et à l'écoute pour m'aider et discuter (surtout) : Anne-Marie, Charlotte, Chu, Olivier, Momo, Philippe (et quel arbre des thèses), Stéphane D., Cécile S., Sylvie, Isabelle, Stéphane V., Emmanuelle, Bertine, Raphaël, Nevin, Nathalie, Frank et Lydia. Merci aussi à Mazen, Martine, Marc, Anne, Lionel, Didier, Naceur, Evelyne, Denis, Isabelle, Alain, José, Guillaume, Gérard, Frédéric, Nadège,... J'en oublie sûrement.*

*Merci également à Vivek, Antoine, Clara et Quentin que j'ai eu la chance d'encadrer. Merci pour votre travail. Je vous souhaite bon courage dans vos carrières respectives.*

*Merci à toute l'équipe MATBIO, les doctorants et post-doctorants pour nos franches rigolades, nos nombreuses discussions (je suis quelque peu bavard :D) et votre bonne humeur à tous et toutes : Johanna, Fanny H., Claire M., Manon, Fleur (un joli road trip aux USA), Lucas, Valentin, Seema, Hélène, Flavien, Karim (et son joyeux franc-parler), Hugo et Gabriel. Mention spéciale pour le petit groupe avec qui j'ai partagé aussi bien soirées festives que babyfoot tout au long de ses trois années : Charlène, Vivien, Vincent, Benoit, Fanny B., Hippo et Marie-Alix.*

*Je ne peux manquer l'occasion de faire une dédicace spéciale à mes amis du bureau B120. Charlène : nos coups de gueule et nos fous rires, Madame Ronchon, vont me manquer. Megan : Avec ton humour américain et ta bonne humeur, avec toute mon amitié merci pour ce bout de chemin parcouru. Hippolyte : Avec toujours son sourire et sa bonne humeur, c'était un plaisir de venir au labo :D. En plus, on s'est découvert pleins de points communs : « Broooooforce », geekade, whisky, ski... Merci pour votre amitié.*

*A mes amis Nantais, qui m'ont soutenu de l'autre côté de la France sans jamais vraiment comprendre ce que c'était que faire une thèse ; mais qui trouvaient sacrément classe de m'appeler « Doc' Want ».*

*Enfin un grand merci à mes parents et à toute ma famille pour m'avoir toujours soutenu et encouragé, en traversant la France pour assister à ma soutenance. Merci à ma petite sœur et à mon petit frère pour m'avoir encouragé, sans jamais vraiment comprendre le travail pharaonique qu'est de faire une thèse :D.*

*Je vais conclure en remerciant celle qui partage ma vie et mon quotidien depuis presque 6 ans : Anne. Merci pour tes encouragements, ta confiance en moi et tout ton soutien durant mes trois années de doctorat. Et surtout pour m'avoir supporté les six derniers mois, c'était rude...*

*Merci ma puce : Je t'aime.*

# Table of content

<b>General Introduction</b> .....	11
<b>I. Literature review</b> .....	19
Introduction .....	23
1. <i>Cellulose Nanocrystals: From the cellulose fiber to the nanomaterial functionalization</i> .....	25
2. <i>Rheology of Cellulose Nanocrystals</i> .....	53
3. <i>Cellulose nanocrystals and stimuli-responsive applications</i> .....	65
Conclusion .....	79
References .....	81
<b>II. CNCs chemical modification</b> .....	99
Introduction .....	103
1. <i>Optimization of cellulose nanocrystals surface grafting with Poly(N-isopropyl acrylamide) using aqueous conditions and microwaves assisted</i> .....	105
2. <i>Low molecular weight amino-poly(N-isopropyl acrylamide) adsorption configuration onto carboxylated cellulose nanocrystals for designing thermo-responsive hydrogels</i> .....	129
Conclusion .....	149
References .....	151
<b>III. Rheological study of CNCs hydrogels</b> .....	159
Introduction .....	163
1. <i>Impact of sonication on the rheological and colloidal properties of high concentrated cellulose nanocrystals suspensions</i> .....	165
2. <i>Cellulose nanocrystals grafted with Poly(N-isopropyl acrylamide) suspensions as thermo-sensitive hydrogel</i> .....	187
3. <i>PDMAEMA-g-PDEGMA Polymer adsorption on carboxylated cellulose nanocrystals and corresponding thermo-sensitive hydrogel</i> .....	205
Conclusion .....	231
References .....	233
<b>IV. Smart materials and CNCs</b> .....	241
Introduction .....	245
1. <i>Cellulose nanocrystals as new bio-based coating layer for improving fiber-based mechanical &amp; barrier properties</i> .....	247
2. <i>Thermo-reversible cellulose nanocrystals system coated on cellulosic substrate: a water reversible surface</i> .....	269
3. <i>Thermo-responsive hydrogel based on Cellulose nanocrystals for injectable applications</i> ...	279
Conclusion .....	293
References .....	295
<b>General conclusion and perspectives</b> .....	301
<b>Résumé Français</b> .....	311
<b>Appendix - Posters</b> .....	321



# Scientific contributions (2014-2017)

## Publications in scientific journal

1. E. Gicquel, C. Martin, J. Garrido Yanez, J. Bras. "Cellulose nanocrystals as new bio-based coating layer for improving fiber-based mechanical & barrier properties". *Journal of Materials Science*, **2017**, 52, 6
2. E. Gicquel, C. Martin, L. Heux, S. Fort, B. Jean, J. Bras. "Optimization of cellulose nanocrystals surface grafting with Poly(N-isopropyl acrylamide) using aqueous conditions and microwaves assisting". Submitted in *Carbohydrate Polymers*
3. E. Gicquel, B. Jean, J. Bras, C. Martin. "Cellulose nanocrystals grafted with Poly(N-isopropyl acrylamide) suspensions as thermo-sensitive hydrogel". Submitted in *Journal of Colloid and Interface Science*
4. E. Gicquel, C. Martin, B. Jean, E. D. Cranston, J. Bras. "Low molecular weight amino-poly(N-isopropyl acrylamide) adsorption configuration onto carboxylated cellulose nanocrystals for designing thermo-responsive hydrogels". Submitted in *ACS Applied Materials & Interfaces*
5. E. Gicquel, C. Martin, Q. Gauthier, J. Engström, C. Abbattista, A. Carlmark, E. D. Cranston, B. Jean, J. Bras. "PDMAEMA-g-PDEGMA Polymer adsorption on carboxylated cellulose nanocrystals and corresponding thermo-sensitive hydrogel". Submitted in *Biomacromolecules*
6. E. Gicquel, C. Rey, B. Jean, J-L. Putaux, F. Pignon, J. Bras, C. Martin. "Impact of sonication on the rheological and colloidal properties of high concentrated cellulose nanocrystals suspensions". Submitted in *Cellulose*

## Oral presentation

1. E. Gicquel, C. Martin, J. Bras. "Cellulose Nanocrystals as new bio-based coating layer for improving fiber-based surface properties" in *TAPPI - International Conference on Nanotechnology for Renewable Materials*. **2016**
2. E. Gicquel, B. Jean, C. Martin, J. Engström, A. Carlmark, J. Bras. "Rheological behavior of thermosensitive hydrogel suspensions based on Cellulose Nanocrystals with adsorbed thermo-responsive polymer" in *ACS - National Meeting & Exposition*. **2017**

## Posters presentation

1. V. Hitaishi, E. Gicquel, C. Martin, J. Bras, B. Jean. "Grafting process optimization of stimuli responsive polymer onto cellulose nanocrystals via peptidic coupling" in *EPNOE - International Polysaccharide Conference*. **2015**
2. E. Gicquel, C. Martin, C. Sillard, J. Bras. "Cellulose nanocrystals as new bio based coating for improving fiber based mechanical & barrier properties" in *EPNOE - International Polysaccharide Conference*. **2015**
3. E. Gicquel, C. Abbattista, B. Jean, F. Pignon, C. Martin, J. Bras. "Cellulose Nanocrystals as new bio-based support in thermo-sensitive hydrogels for bio-compatible smart applications" in *TAPPI - International Conference on Nanotechnology for Renewable Materials*. **2016**

## Other communications

1. *Oral*: C. Martin, E. Gicquel, J. Bras. "Rheological behavior of cellulose nanocrystalline suspensions" in *EPNOE - International Polysaccharide Conference*. **2015**
2. *Oral*: E. Gicquel, C. Martin, F. Pignon, B. Jean, J. Bras. "Stimuli responsive cellulose nanocrystals hydrogel for smart applications" in *ACS - National Meeting & Exposition*. **2016**
3. *Oral*: A. De Geyer, C. Rey, N. Hengl, B. Jean, E. Gicquel, J. Bras, F. Pignon, S. Prevost. "Structure and rheological behavior of nanocrystal cellulose dispersions probed by in-situ Rheo-SAXS and local birefringence" in *TAPPI - International Conference on Nanotechnology for Renewable Materials*. **2016**
4. *Oral*: A. De Geyer, C. Rey, N. Hengl, E. Gicquel, J. Bras, B. Jean, F. Pignon. "In situ Rheo-SAXS study of cellulose nanocrystals suspensions" in *ACS - National Meeting & Exposition*. **2017**
5. *Publication*: F. Hoeng, J. Bras, E. Gicquel, G. Krosnicki, A. Denneulin. "Inkjet printing of nanocellulose–silver ink onto nanocellulose coated cardboard". *RSC Advances*, **2017**, 7, 25

# Abbreviations

## *Chemical and materials*

<b>CNCs</b>	Cellulose nanocrystals
<b>CNC-g-Pnipam<sub>2500</sub></b>	Peptidic coupling between CNCs and Pnipam <sub>2500</sub>
<b>CNFs</b>	Cellulose nanofibrils
<b>Diblock</b>	Block copolymer composed with PDMAEMA-PDEGMA
<b>DB</b>	Diblock
<b>EDC</b>	N-(3-Dimethylaminopropyl)-N'-ethylcarbodiimide
<b>HA</b>	Hyaluronic acid
<b>HCl</b>	Hydrochloric acid
<b>KBr</b>	Potassium bromide
<b>LCST</b>	Lower critical solution temperature
<b>NaCl</b>	Sodium chloride
<b>NHS</b>	N-Hydroxysuccinimide
<b>NIPAM</b>	N(isopropyl acrylamide)
<b>PDEGMA</b>	Poly(di(ethylene glycol)methyl ether methacrylate)
<b>PDMAEMA</b>	Poly(2-(Dimethylamino)ethyl methacrylate)
<b>PEG</b>	Polyethylene glycol
<b>PEI</b>	Polyethyleneimine
<b>PNIPAM</b>	Polymer of Poly(N-isopropyl acrylamide)
<b>Pnipam<sub>2500</sub></b>	Oligomer of PNIPAM with 2500 g·mol <sup>-1</sup>
<b>Pnipam<sub>5500</sub></b>	Oligomer of PNIPAM with 5500 g·mol <sup>-1</sup>
<b>POEGMA</b>	Poly(oligo(ethyleneglycol)methyl ether methacrylate)
<b>TEMPO</b>	2,2,6,6-Tetramethylpiperidine 1-oxyl
<b>TEMPO CNCs</b>	TEMPO-oxidized cellulose nanocrystals

## *Methods*

<b>AFM</b>	Atomic force microscopy
<b>CA</b>	Contact angle
<b>DLS</b>	Dynamic light scattering
<b>EA</b>	Elemental analysis
<b>FEG-STEM</b>	Field emission gun-scanning transmission electron microscopy
<b>FTIR</b>	Fourier-transform infrared spectroscopy
<b>ITC</b>	Isothermal calorimetry titration
<b>MP-SPR</b>	Multi parametric surface Plasmon resonance
<b>QCM-d</b>	Quartz crystal microbalance with dissipation
<b>SANS</b>	Small angle neutron scattering
<b>SAXS</b>	Small angle X-Ray scattering
<b>SEM</b>	Scanning electron microscopy
<b>TEM</b>	Transmission electron microscopy



# General introduction

---



# General introduction

With the end of fossil based economy and the continuous progress in Sciences, new generation of materials more “Bio” (bio-based, bio-compatible, bio-degradable) and more “SMART” (functionalities, performance, stimuli-responsive) see the light of day.

Regarding stimuli-responsive polymer (Reineke, 2016; Schattling et al., 2014; Wei et al., 2017), a particular focus was done since the last decades on thermo-responsive polymer like **Poly(N-isopropyl acrylamide) (PNIPAM)** for their application in bio-medical science. This polymer presents a *lower critical solution temperature* (LCST) closed to physiological temperature (Okahata et al., 1986) which make PNIPAM-based materials particularly relevant for biomedical applications like tissue engineering or drug delivery (Alosmanov et al., 2017; Chen et al., 2014; Pentlavalli et al., 2017).

Meanwhile, nanoparticles extract from cellulose sources have been considered as a promising solution for creating **thermo-responsive materials**. Regarding the green and smart aspects, these nanoparticles, also called **nanocellulose**, come directly from nature (or industrial wastes products) and exhibit remarkable properties such as high chemical reactivity or high mechanical properties. Since the last two decade, interest on nanocellulose and especially on cellulose nanocrystal has been growing as shown in **figure 1** by the exponential number of publications per year.

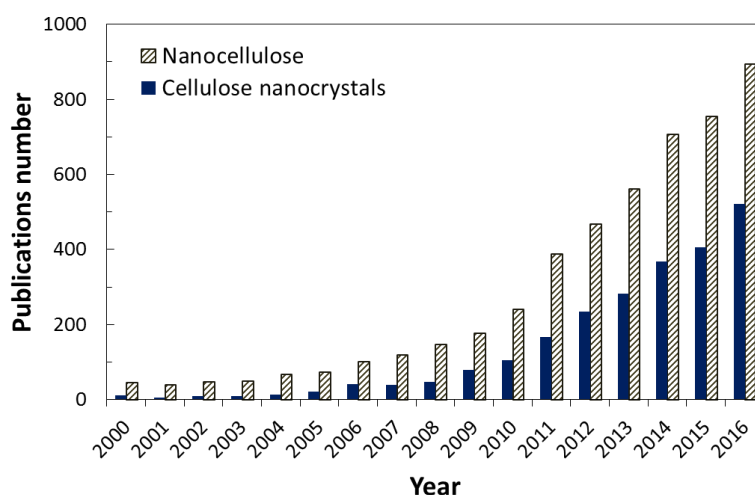


**Figure 1:** Evolution of annual publications on nanocellulose and cellulose nanocrystals (extracted from ACS scifinder® in June 2017) with descriptors: “microfibrillated cellulose”, “nanofibrillated cellulose”, “cellulose microfibrils”, “cellulose nanofibrils”, “cellulose nanocrystals”, “cellulose nanowhiskers”, “nanocrystalline cellulose” and “cellulose whiskers”. Cellulose nanocrystals is refined with the 4 last terms.

In the nanocellulose field, two major families exist: cellulose nanofibers (CNFs) and cellulose nanocrystals (CNCs). The difference comes from the isolation treatment, dimensions and core properties. CNFs are flexible filaments of several micrometer lengths and CNFs suspensions present a gel-like behavior with a high cohesive entangled network. Oppositely, CNCs are rigid rod-like particles with nano-metric dimensions. CNCs present a high area and consequently a high chemical reactivity which is ideal to achieve the grafting of molecules or polymer on their surface. Taken advantage on the increasing interest of CNCs and their unique properties, several manufacturing facilities propose a large available amount of CNCs suspension, almost 2 tons per day (Celluforce, American Process, Holmen, Blue Goose Biorefineries ...) (Tang et al., 2017).

During the last decade, such CNCs have been used for several applications, i.e. composites (Mariano et al., 2014), liquid crystals (Giese et al., 2015; Kelly et al., 2014), aerogels (De France et al., 2017). But the last researches focus on using such bio-templates to produce smart materials (dried or in suspension). Some researchers deposit metals (e.g. Ag, Pd ...) on their surface for various applications at dry state whereas other graded fluorescent particles for tumor tracking in medical applications. In our project, we have decided to focus on stimuli-responsive applications.

LGP2 (UMR CNRS 5518) - a research laboratory expert in nanocellulose - has proposed a project to overcome these issues with the support of “Ministère de l’enseignement supérieur, de la recherche et de l’innovation” and partially support by the PolyNat Carnot Institute (Investissements d’Avenir - grant agreement n°ANR-11-CARN-007-01). My PhD project RHEONANO was launched and named *“Development of stimuli-responsive cellulose nanocrystal hydrogels for smart applications”*.

Through PolyNat Carnot institute, my PhD has benefited from interesting collaborations with different laboratories like:

- (i) CERMAV (UPR CNRS 5301, France) - a fundamental research laboratory expert in glyco-sciences
- (ii) LRP (UMR CNRS 5520, France) - a research laboratory expert in material flow and rheology

For active discussions with some complementary expertise in the field, led us to build very good collaboration with:

- (i) KTH, chemistry division (Royal institute of technology, Sweden) - a research laboratory expert in organic chemistry
- (ii) McMaster University, chemical engineering division (Canada) - a research laboratory expert in biomaterials and polymer science

This PhD proposes to evaluate the development of stable bio-based hydrogel with thermo-responsive properties. Several objectives can be announced for this project:

- (i) Establish a green process for grafting stimuli-responsive polymers onto CNCs
- (ii) Understand rheological behaviors of thermo-responsive hydrogels based on CNCs
- (iii) Develop “smart” and high added values biomaterials for applications in packaging and biomedical gel

In response to these objectives, the present manuscript is divided into four chapters based on scientific papers as described in **figure 2**.

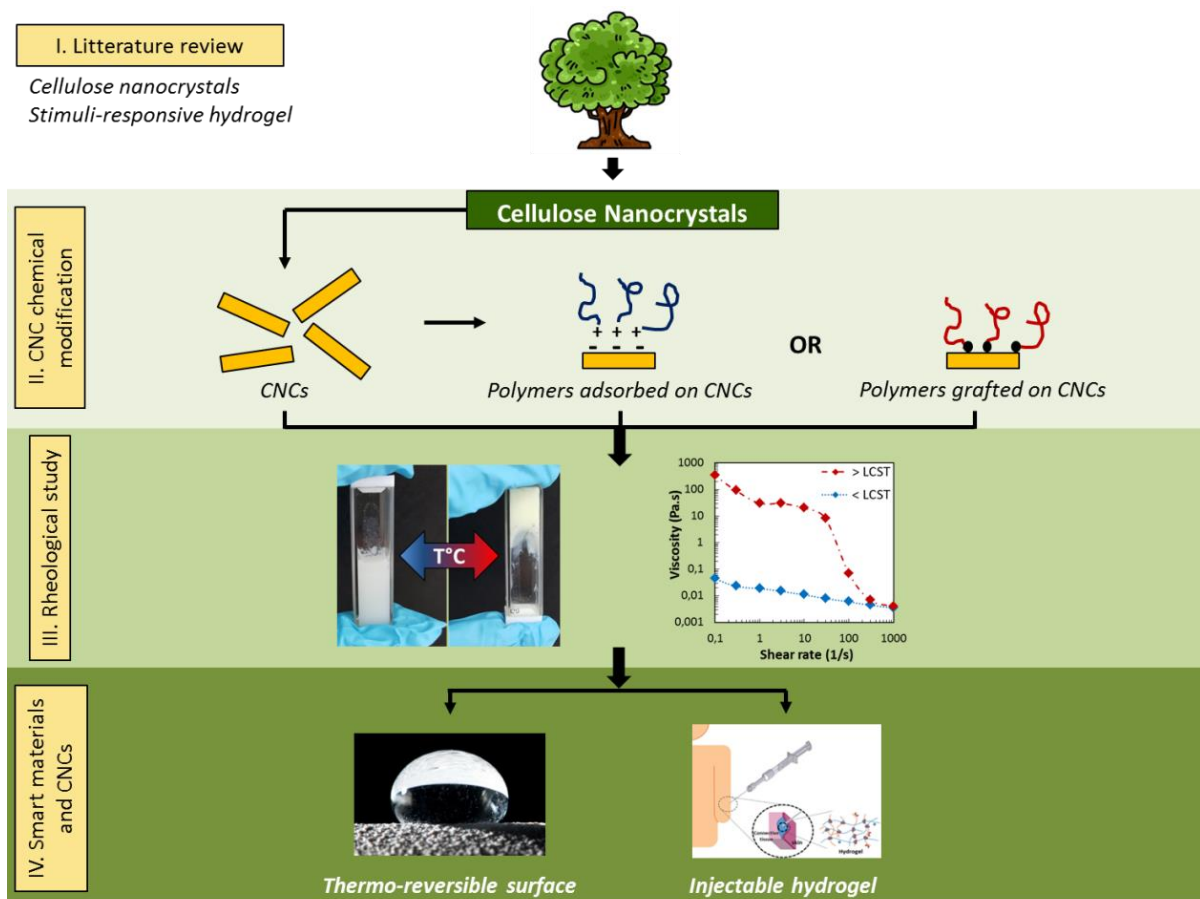


**Figure 2:** Schematic representation of this PhD manuscript organization

In **chapter I**, a literature review describes the context and objectives of this PhD project through both the nanocellulose (in particular cellulose nanocrystals) and stimuli-responsive hydrogel field. Extended details on the use of CNCs in hydrogel are also provided which draw the main challenges of this project in the nanoscale. Following chapter propose the evolution from green chemical modification of CNCs (**chapter II**) to stimuli-responsive hydrogel behavior (**chapter III**). Finally, **chapter IV** presents smart application for these hydrogel.

In **chapter II**, the chemical reactivity of CNCs will be used to graft thermo-responsive polymer via green chemistry. Different ways are proposed to incorporate thermal sensibility on CNCs. *Chapter II.1* first investigates the peptidic grafting of Poly(N-isopropyl acrylamide) onto CNCs (*Scientific paper n°1*). Then, *Chapter II.2* develops the PNIPAM polymer adsorption on CNCs in order to take out chemical modification from the system and propose a simple way to produce thermo-responsive and bio-compatible hydrogels. Small angle neutron scattering (SANS) gives access to the polymer configuration depending on the temperature (*Scientific paper n°2*).

In **chapter III**, the rheological behavior of thermo-responsive hydrogel is developed to highlight the impact of such polymer on CNCs rheology. *Chapter III.1* focuses on the influence of sonication on the rheological behavior of CNCs suspension (*Scientific paper n°3*). Then, the study of hydrogel based on PNIPAM polymer grafted via amidation on CNCs is developed in *chapter III.2* (*Scientific paper n°4*). In *chapter III.3*, thermo-responsive hydrogel based on home-made diblock polymer and CNCs is detailed (*Scientific paper n°5*).

Finally **chapter IV** proposes applications for these thermo-responsive systems. New bio-based coating of CNCs on cellulosic substrate is described in *chapter IV.1*. It improves the mechanical and barrier properties of fiber-based material (*Scientific paper n°6*). Then, building on its expertise, *chapter IV.2* reports the realization of thermo-sensitive surface with waterproof properties tuned by the temperature. The final part *chapter IV.3* examines various hydrogels system in biomedical field. Very promising results are provided with hydrogels based on CNCs and diblock copolymers.

All chapters of this PhD project are mainly based on scientific publications or structured as scientific publications.

This complete work will provide new strategies on the realization of thermo-responsive hydrogel based on cellulose nanocrystals and green chemistry. These systems pave the way of large field of applications such as biomedical, cosmetic, packaging or functional materials.

## References

- Alosmanov, R., Wolski, K., and Zapotoczny, S. (2017). Grafting of thermosensitive poly(N-isopropylacrylamide) from wet bacterial cellulose sheets to improve its swelling-drying ability. *Cellulose* 24, 285–293.
- Chen, X., Huang, L., Sun, H.-J., Cheng, S.Z.D., Zhu, M., and Yang, G. (2014). Stimuli-Responsive Nanocomposite: Potential Injectable Embolization Agent. *Macromol. Rapid Commun.* 35, 579–584.
- De France, K.J., Hoare, T., and Cranston, E.D. (2017). Review of Hydrogels and Aerogels Containing Nanocellulose. *Chem. Mater.* 29, 4609–4631.
- Giese, M., Blusch, L.K., Khan, M.K., and MacLachlan, M.J. (2015). Functional Materials from Cellulose-Derived Liquid-Crystal Templates. *Angew. Chem. Int. Ed.* 54, 2888–2910.
- Kelly, J.A., Giese, M., Shopsowitz, K.E., Hamad, W.Y., and MacLachlan, M.J. (2014). The Development of Chiral Nematic Mesoporous Materials. *Acc. Chem. Res.* 47, 1088–1096.
- Mariano, M., El Kissi, N., and Dufresne, A. (2014). Cellulose nanocrystals and related nanocomposites: Review of some properties and challenges. *J. Polym. Sci. Part B Polym. Phys.* 52, 791–806.
- Okahata, Y., Noguchi, H., and Seki, T. (1986). Thermoselective permeation from a polymer-grafted capsule membrane. *Macromolecules* 19, 493–494.
- Pentlavalli, S., Chambers, P., Sathy, B.N., O’Doherty, M., Chalanqui, M., Kelly, D.J., Haut-Donahue, T., McCarthy, H.O., and Dunne, N.J. (2017). Simple Radical Polymerization of Poly (Alginate-Graft-N-Isopropylacrylamide) Injectable Thermoresponsive Hydrogel with the Potential for Localized and Sustained Delivery of Stem Cells and Bioactive Molecules. *Macromol. Biosci.* 10.1002/mabi.201700118.
- Reineke, T.M. (2016). Stimuli-Responsive Polymers for Biological Detection and Delivery. *ACS Macro Lett.* 5, 14–18.
- Schattling, P., D. Jochum, F., and Theato, P. (2014). Multi-stimuli responsive polymers – the all-in-one talents. *Polym. Chem.* 5, 25–36.
- Tang, J., Sisler, J., Grishkewich, N., and Tam, K.C. (2017). Functionalization of cellulose nanocrystals for advanced applications. *J. Colloid Interface Sci.* 494, 397–409.
- Wei, M., Gao, Y., Li, X., and Serpe, M.J. (2017). Stimuli-responsive polymers and their applications. *Polym Chem* 8, 127–143.

# *Chapter I*

## **Literature review**

---



# Table of content

<b>Introduction</b> .....	23
<b>I. Cellulose Nanocrystals: From the cellulose fiber to the nanomaterial functionalization</b> .....	25
1.1. From Cellulose to Nanocellulose .....	25
1.1.1. Origin of the cellulose fiber .....	26
1.1.2. Nanocellulose: Cellulose Nanofibrils and Cellulose Nanocrystals .....	28
1.1.3. Cellulose Nanocrystals: origin, fabrication and applications.....	30
1.2. Applications of CNCs.....	35
1.3. Chemical functionalization of Cellulose Nanocrystals .....	38
1.3.1. TEMPO oxidation of Cellulose Nanocrystals .....	39
1.3.2. Non-covalent functionalization: adsorption .....	40
1.3.3. Covalent functionalization of CNCs with molecules in aqueous conditions.....	43
1.3.4. Polymer chains grafting on cellulose nanocrystals .....	44
<b>II. Rheology of Cellulose Nanocrystals</b> .....	53
2.1. Rheology Concepts .....	53
2.2. Cellulose Nanocrystals and rheology.....	54
2.2.1. CNCs liquid crystals organization and phase separation.....	54
2.2.2. CNCs suspension behavior in aqueous solution.....	57
2.2.3. CNCs suspension behavior in polymer solution .....	61
<b>III. Cellulose nanocrystals and stimuli-responsive applications</b> .....	65
3.1. Stimuli-responsive polymers .....	65
3.2. CNCs and Stimuli-responsive polymers .....	70
3.3. Cellulose based stimuli-responsive hydrogels and applications .....	75
<b>Conclusion</b> .....	79
<b>References</b> .....	81



## Introduction

The following literature review has two major objectives: (i) develop the global context of the Ph.D. thesis and (ii) provide numerous resources in order to understand its scientific challenges, through more than 300 references. This chapter attempts to address both 'non expert' and 'expert' readers. Through the introduction of general concepts and data in each topic, 'non experts' will have access to tools to understand scientific principles that are outside of his or her expertise. Several exhaustive tables and figures are included in this chapter for the interest of the 'expert' readers. The link between the Ph.D. project and literature review will be emphasized in *italic dark gray letters*.

As already stated in the general introduction, this Ph.D. deals with surface functionalization of cellulose nanocrystals in the design of a thermo-sensitive hydrogel. Four challenges to reach this goal are: (i) CNCs functionalization via green chemistry and green grafting, (ii) understanding of rheological behavior of CNCs and CNCs-polymer suspensions, (iii) realization of stimuli-responsive system based on cellulose nanocrystals and thermo-responsive polymers and (iv) development of "smart" and high added values applications with these thermo-responsive hydrogels.

The first part of this literature review will focus on the raw materials: **cellulose nanocrystals (CNCs)**. From cellulosic fiber to nanomaterials, the production and chemical modification of this biodegradable and renewable material is presented. This part will finish outlining the various applications using this remarkable material.

The second part will present the **rheological behavior** of this tiny cellulosic material. General concepts of rheology are presented, and then continue to describe a particular behavior of CNCs: liquid crystalline behavior. Finally, the presence of polymer in CNCs suspension is presented, related to induced rheological modifications.

This Ph.D. has an important objective: to create **thermo-sensitive hydrogels** based on CNCs for 'smart' applications. The third part of this literature review will present an overview of these 'smart' applications for **stimuli-responsive hydrogels** composed of cellulose and derivatives. This literature review will help in presenting the main challenges of this project and highlighting scientific questions to investigate and understand in future chapters.



# I. Cellulose Nanocrystals: From the cellulose fiber to the nanomaterial and its functionalization

## 1.1. From Cellulose to Nanocellulose

The paper and textile industries are the biggest consumers of cellulosic fibers for centuries. For industrial applications, cellulose is usually extracted from wood pulp and cotton. Nonetheless, these are not the only applications of cellulose which can be found in bio degradable composites, cosmetics, medicine, building materials, food, energy, etc. The increasing interest to use this biodegradable, renewable, and non-toxic material to replace petroleum-based chemical components has even motivated researchers to use cellulose in advanced materials at the nanoscale (at least one dimension lower than 100 nm). This cellulosic material is called nanocellulose and **Figure 1** illustrates this increasing interest by presenting the number of publications and patents covering nanocellulose. As several types of nanocellulose exists (detailed in a following section), a focus on cellulose nanocrystals will be presented. In 2016 about three new publications and one patent every two days are produced which are only about CNCs. This enthusiasm is also confirmed by numerous books and reviews concerning the scientific study of nanocellulose since the last decade (Abitbol et al., 2016; Charreau et al., 2013; De France et al., 2017; Dufresne, 2013; Eichhorn et al., 2010; Habibi et al., 2010; Isogai et al., 2011; Klemm et al., 2011; Lavoine et al., 2012; Moon et al., 2011).

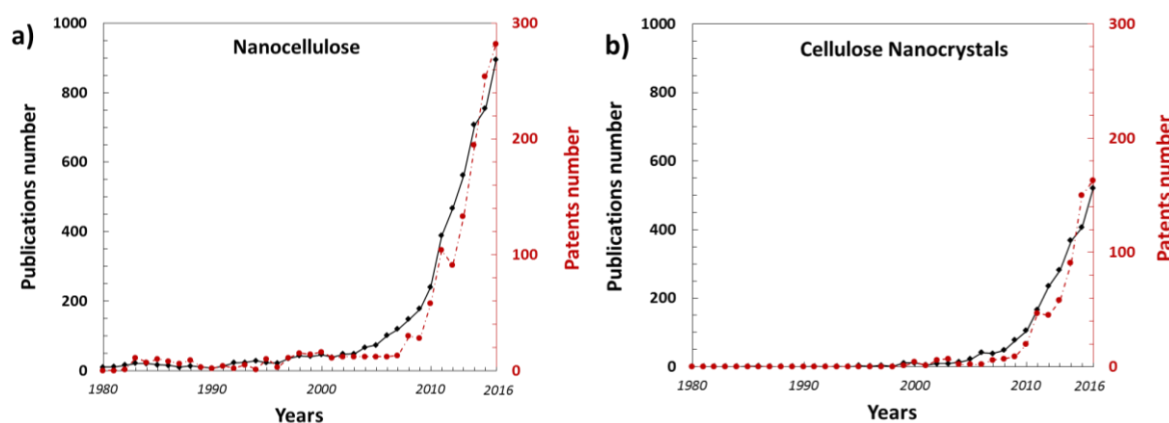


**Figure 1:** Publications and patents extracted from ACS scifinder® in June 2017 with keywords: a) *nanocellulose* = “microfibrillated cellulose”, “nanofibrillated cellulose”, “cellulose microfibrils”, “cellulose nanofibrils”, “cellulose nanocrystals”, “cellulose nanowhiskers”, “nanocrystalline cellulose” and “cellulose whiskers”. b) cellulose nanocrystals is refined with the 4 last terms of key words.

### **1.1.1. Origin of the cellulose fiber**

With a huge availability and abundance on earth, cellulose is an important material in our life. With approximately 250 megatons produced annually by biomass, cellulose is considered as the most abundant organic polymer in nature (Urruzola et al., 2014). In 1838, the first chemist who isolated cellulose from several plants was Anselm Payen (Payen, 1838).

According to the work of Haworth et al. (Haworth et al., 1930), cellulose is a linear homopolymer composed of anhydroglucopyranose linked by glycosidic linkage  $\beta(1-4)$  (D-glucopyranosyl- $\alpha$ -1,4-D-glucopyranose). The repeated segment of the cellulose polymer chain is named cellobiose ( $C_{11}H_{22}O_{11}$ ). The anhydro-glucose units (AGU), constituting half of the cellobiose chain, is twisted every unit at  $180^\circ$  and used to define the degree of polymerization ( $DP = n/2$ ). These particular units have three hydroxyls groups, which are responsive to strong intra and inter hydrogens bonds between each chain at the origin of cellulose organization and properties. A schematic of the tree hierarchical structure and the molecular structure of cellulose is presented in **Figure 2a** and **2b**. Cellulose polymer presents two ends groups which are chemically different with a non-reducing end and a reducing end (aldehyde group).

The source of cellulose can vary from plants, such as wood and cotton, to tunicates, and bacteria species (Klemm et al., 2011). The amount of cellulose extracted depends on the source:  $\sim 90\%$  for cotton and  $\sim 40\%$  for wood. Contrary to synthetic polymers, cellulose is produced through an enzymatic process. In all organisms which can produce cellulose, the synthesizing enzymes (also called “synthase cellulose”) are grouped in terminal complexes. These complexes rigorously coordinate the extrusion and simultaneous crystallization of a well-defined number of cellulose molecules. Micro-fibrillated crystallites are created in this manner (Brown, 1996; Haigler, 1990; Williamson et al., 2002). This biogenesis gives to cellulose a perfect structure and morphology that does not exist in synthetic polymers.

What also differs between sources is the amorphous and crystalline domains organization of the cellulose fibers, which are dependent on the cellulose source. Cellulose molecules are arranged by biomass in order to create larger units, which are considered to be elementary fibrils. These elementary fibrils are then included in an amorphous matrix of hemicellulose,

pectin, lignin, and proteins to create a natural composite structure which is the base of the vegetal cell walls.

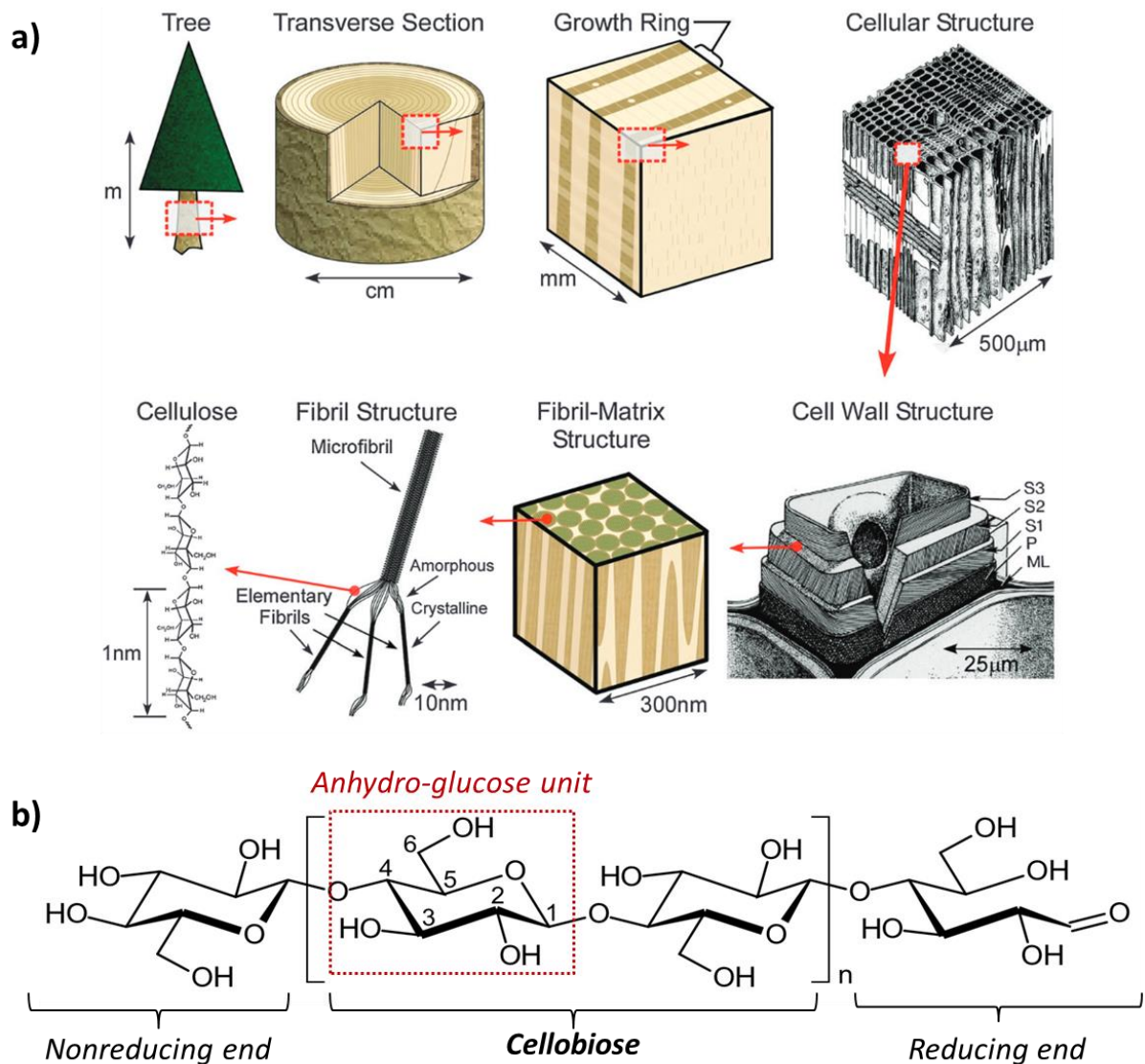


**Figure 2:** a) Schematic of the tree hierarchical structure (Postek et al., 2011) and b) molecular structure of cellulose fibrils

Since the 1970s, numerous publications present the structure of native cellulose in cell walls and its allomorphs. The review of Brown in 1996 (Brown, 1996) presents all of these cellulose structures and the link between them. **Figure 3** shows the relation between the cellulose allomorphs. Native cellulose is named Cellulose I. It presents two allomorphs:  $I_{\alpha}$  and  $I_{\beta}$ . The proportion between each of them depends on the origin of the species. Most of cellulose  $I_{\alpha}$  come from primitive organisms, such as bacteria or algae, while cellulose  $I_{\beta}$  is produced by superior plants (wood, cotton) and tunicates. Then by chemical or thermal

treatment of native cellulose I, five other allomorphs exist: II, III<sub>I</sub>, III<sub>II</sub>, IV<sub>I</sub>, IV<sub>II</sub>. These transitions are possible due to cellulose I which is metastable. The most commonly known allomorph is cellulose II, which is usually obtained when regenerated cellulose is prepared (E.G. viscose process, mercerization and sulfurization).

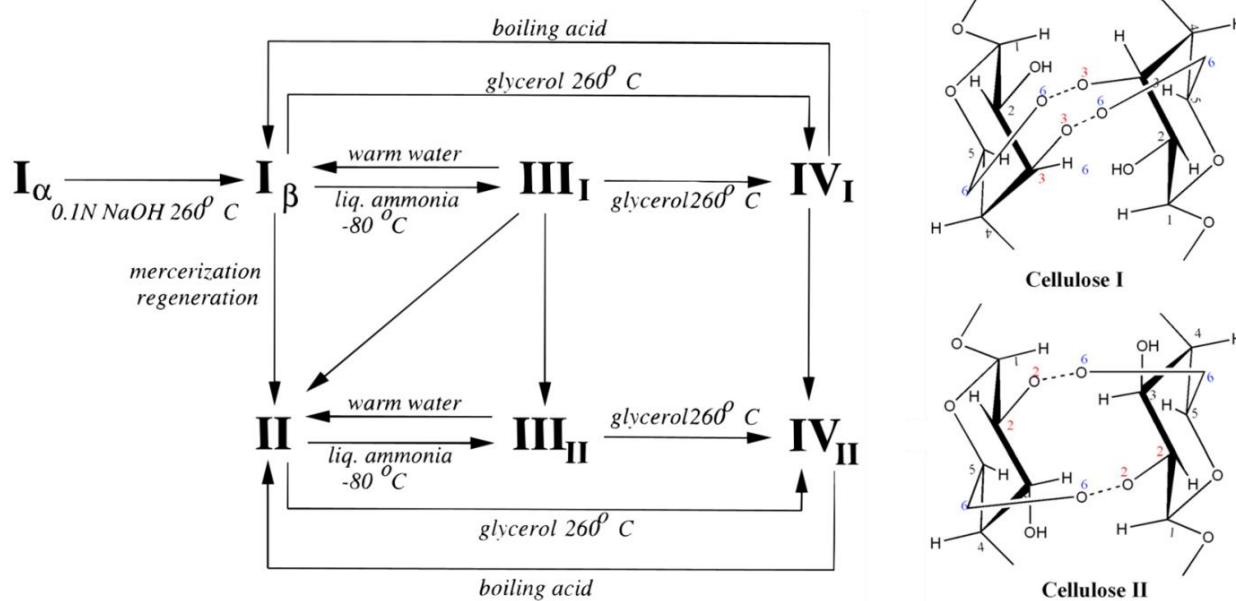


**Figure 3 :** Relationship between different cellulose allomorphs (extracted from (Kroon-Batenburg et al., 1996) and (Zuber et al., 2012))

During this Ph.D. project, cellulose nanocrystals were used and the final product was composed with cellulose I and a small part of cellulose II (may be due to the mercerization and regeneration of cellulose during the washing steps of the process).

### 1.1.2. Nanocellulose: Cellulose Nanofibrils and Cellulose Nanocrystals

From the elementary cellulose fibers, it is possible to extract via acid hydrolysis or mechanical treatment different types of nanocellulose: cellulose nanocrystals (CNCs) or cellulose nanofibrils (CNFs), as shown in **figure 4**. It is important to keep in mind that even if the starting materials to produce nanocellulose is the same, CNCs and CNFs should be considered as two completely different families of nanomaterials (different crystallinity, flexibility, and aspect ratio).

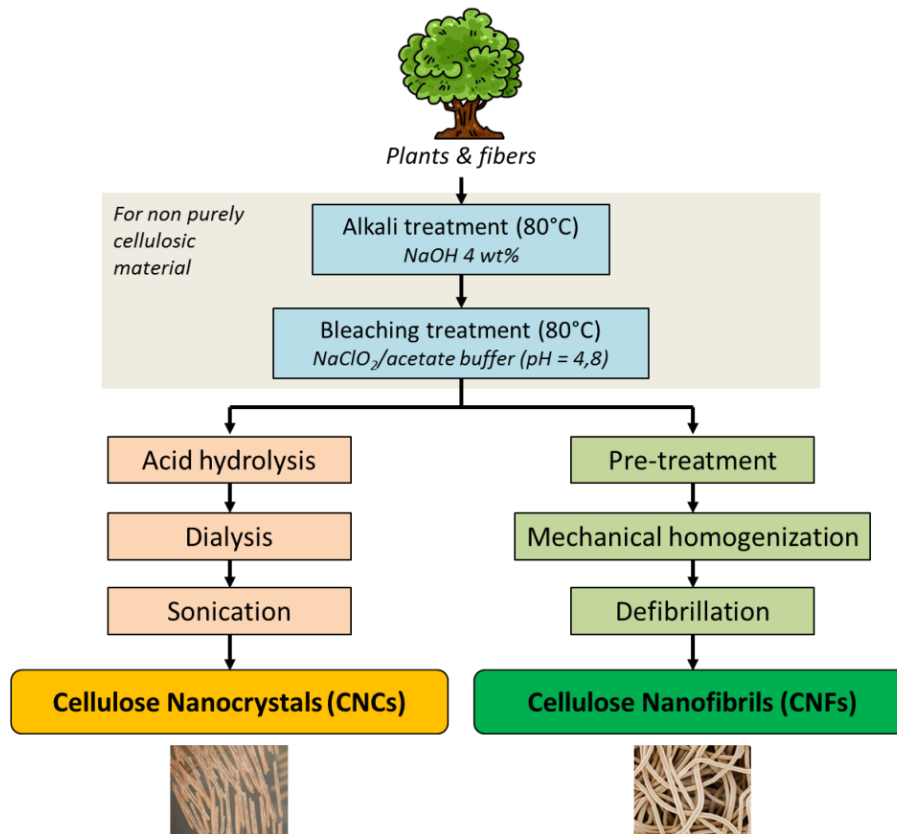


**Figure 4:** General procedure to obtain nanocellulose

In the 1980s, CNFs, originally called Microfibrillated Cellulose (MFCs), were discovered by two research groups managed by Herrick and Turbak (Herrick et al., 1983; Turbak et al., 1983). A dilute cellulosic fiber suspension was passed through several times in a high-pressure homogenizer (80°C at 8000 psi) to create CNFs by longitudinal cleavage of the cellulosic fibers. During this mechanical fibrillation, the bond between elementary fibrils and bundles of fibrils were opened, which promotes the formation of CNFs. A shear thinning aqueous gel was produced with low solid content (2-7 wt%) (Herrick et al., 1983) with fibrils having a diameter ranging from 20-60 nm and several microns in length (Siró and Plackett, 2010; Turbak et al., 1983). This suspension can turn into a translucent “gel” structure mainly through enzymatic (Henriksson et al., 2007) and chemical (Saito et al., 2007) pretreatments, which were first proposed at the end of the 2000’s. CNFs contain the crystalline and amorphous parts of cellulose. Nowadays, processes commonly involved for mechanical fibrillation are grinding, micro-fluidization, or homogenization, where the cellulose suspension passes several times in the process to obtain a CNFs suspension. Nonetheless, these processes and limited energy consumption require chemical pre-treatments to

facilitate the fibrillation. A recent review discusses the recent advances in CNF production (Nechporchuk et al., 2016a). Since the 1980s, CNFs suspensions were used as a rheological modifier (Hoeng et al., 2017a; Nechporchuk et al., 2016b; Turbak et al., 1983), nanocomposites (Missoum et al., 2013; Siqueira et al., 2010a), a paper additive and coating (Bardet and Bras, 2014; Brodin et al., 2014; Lavoine et al., 2012), or biomedical applications (Jorfi and Foster, 2015).

The second type of nanocellulose derived from biomass are CNCs. CNCs have a rod-like shape and typically dimensions of approximately 150-500 nm in length and a diameter of 5-30 nm (Dufresne, 2013; Habibi et al., 2010). CNCs are derived from the destruction of the amorphous regions of cellulose fibers by acid hydrolysis. The first reported production of stable CNCs suspension was conducted by Rånby et al. in the 1950s (Rånby, 1951; Rånby and Ribí, 1950). In this work, CNCs were produced from wood and cotton by sulfuric acid hydrolysis, which is still the most common method used today. The final suspension presents a birefringent behavior under cross polarized light. **Figure 5** shows images of the two nanocellulose types.

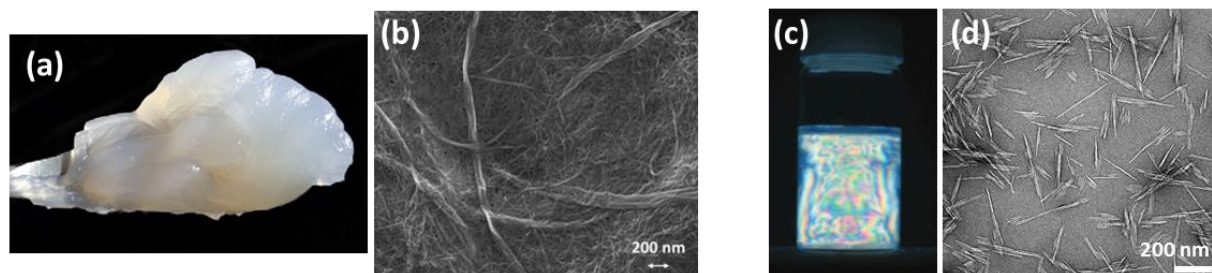


**Figure 5:** CNF: (a) Photograph of CNF gel(Lavoine et al., 2012), (b) FE-SEM image of the dried CNF suspension (Lavoine et al., 2014). CNCs: (c) aqueous CNCs suspension observed between crossed polarizers (Araki and Kuga, 2001) and (d) TEM images of CNCs.

*Cellulose nanocrystals isolation and applications are described in details in the following part as this material is the main raw materials used in this Ph.D.*

### **1.1.3. Cellulose Nanocrystals: origin, fabrication and applications**

#### **1.1.3.1. CNCs isolation**

Cellulose nanocrystals preparation involves a chemical acid hydrolysis process intended to dissolve amorphous chains from the cellulose fibers, and to release crystal domains after

sonication. CNCs are considered to be the smallest building blocks that can be extracted from cellulose.

Historically, cellulose crystallites were isolated the first time by Nickerson and Harble in the 1940s (Nickerson and Harble, 1947). They observed that the degradation induced by boiling cellulose fibers in acidic solution (hydrochloric and sulfuric acids) reached a limit after a certain time of treatment. This work inspired Rånby et al. in 1950 (Rånby, 1951; Rånby and Ribí, 1950) to prepare cellulose nanocrystals. It was found that CNCs isolated from hydrolysis of wood and cotton pulp present negative charge and a well-dispersed suspension at a pH range of 3 to 10.5.

Chemical techniques to isolate CNCs consist to expose the cellulosic material to an acid hydrolysis under controlled temperature, agitation, and time followed by sonication to separate the crystal domains. The cellulose amorphous regions are randomly oriented in a spaghetti-like arrangement leading to lower density cellulose compared to nanocrystalline regions. The amorphous regions act as structural defects which are susceptible to be attacked by acid and, under controlled conditions, they may be removed leaving crystalline regions intact (de Souza Lima and Borsali, 2004; Thielemans et al., 2009). During the acid hydrolysis process, the hydronium ions ( $\text{H}_3\text{O}^+$ ) can penetrate the cellulose chains in the amorphous domains promoting the hydrolytic cleavage of the glycosidic bonds and releasing individual crystallites. Hydrochloric (HCl) and sulfuric acids ( $\text{H}_2\text{SO}_4$ ) are commonly used as hydrolyzing agents. In literature, several other mineral and organic acids have been tested such as phosphoric acid (Camarero Espinosa et al., 2013), hydro bromic acid (Sadeghifar et al., 2011), nitric acid (Rehman et al., 2014) or subcritical water (Novo et al., 2015).

Referring to **Figure 4**, the isolation of CNCs from a cellulosic source follows several steps. For non-purely cellulosic materials, chemical pre-treatment and bleaching steps are necessary to remove lignin and hemicellulose from the material matrices. The removal of the lignin and hemicellulose is necessary to ensure maximum crystallinity of the produced CNCs (Chaker et al., 2013). As previously described, the third step is the acid hydrolysis. Sulfuric acid is the most common method employed in literature and was described in details by Revol et al. in 1992 (Revol et al., 1992). The final yield and the morphology of CNCs are affected by multiple parameters: cellulose source, acid choice and related concentration, hydrolysis

time, and temperature. Reaction time of the acid hydrolysis using traditional methods (64 wt% sulfuric acid, 40-45°C, 30 min) has been shown to have the greatest impact on the final yield. It has been noted that with increased reaction time the yield decreases due to the increased destruction of the CNCs (Beck-Candanedo et al., 2005; Elazzouzi-Hafraoui et al., 2008). To stop the isolation of CNCs, the hydrolyzed mixture is extensively diluted to inhibit the reaction. Then, the suspension is submitted to several separations (centrifugation and filtration) and washing steps such as a prolonged dialysis against deionized water to remove the remaining reagents and salt residues. A final centrifuge separation or micro-filtration steps are often used to remove larger agglomerates (Bai et al., 2009). The last step in the process is ultrasonic treatment to facilitate the dispersion of the crystalline cellulose in the suspension (Beck-Candanedo et al., 2005). **Figure 6** presents a schematic illustration of the cellulose nanocrystal isolation procedure via sulfuric acid hydrolysis. This process will introduce negatively charged half-ester sulfate groups on the CNC surface. These anionic groups induce repulsive forces between CNCs, which induces stable colloidal suspension in aqueous solvent.

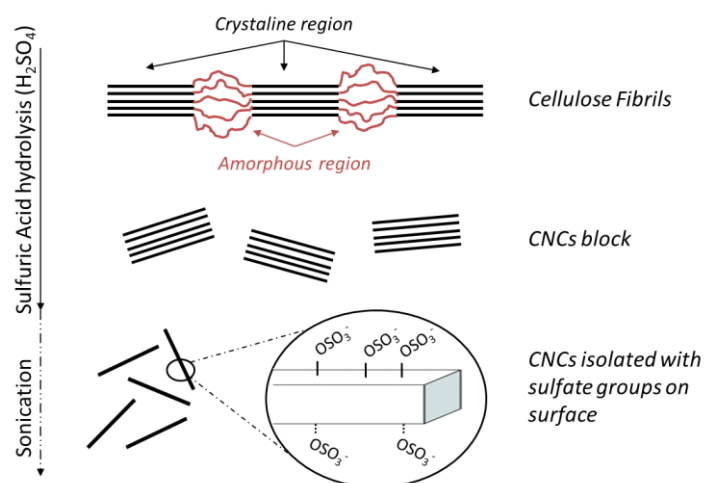


**Figure 6:** Schematic illustration of the cellulose nanocrystal isolation via sulfuric acid hydrolysis, which break down amorphous region and isolates nanocrystals.

In this Ph.D. project, CNCs from wood obtained via sulfuric acid hydrolysis were used in most instances. These CNCs present sulfate group at their surface as shown on **figure 6**. More precisely, semi-industrially available CNCs from University of Maine process Development Center (University of Maine, USA) were used, which are known to have a small part of cellulose II (Reid et al., 2017).

### 1.1.3.2. CNCs safety and toxicology assessment

The increasing interest on CNCs induces the question of nano-toxicology and safety issues. Cellulose is considered as non-toxic material (no impact on health). Regarding the size and the high specific area, the question of interactions with physiological medium is still under investigation. Several studies have reported that CNCs seem to be non-toxic (Dong et al., 2012; Jia et al., 2013; Kovacs et al., 2010; Pitkänen et al., 2014). In November 2012, the Canadian government added CNCs nanomaterial to the list of “domestic substances list” with no suspicion of toxicity. This list is an inventory of substances that may be imported and/or manufactured in Canada in luxury, food, and drug applications. Besides, nanocellulose is currently exempted from registration in the REACH list. Very recent studies also investigate the impact of CNCs in genotoxicity and immune-toxicity *in vitro* (Catalán et al., 2015), the impact of surface modified CNCs on their toxicity (Harper et al., 2016), and review the pulmonary, oral, dermal, and cytotoxicity of CNCs (Roman, 2015). These studies report an overall low-toxicity for these materials.

### 1.1.3.3. CNCs properties

CNCs are favorable in terms of biodegradability, renewability, and abundance all over the world. They also present numerous advantages and interesting properties. **Figure 7** shows an overview of the physical and chemical properties of CNCs.

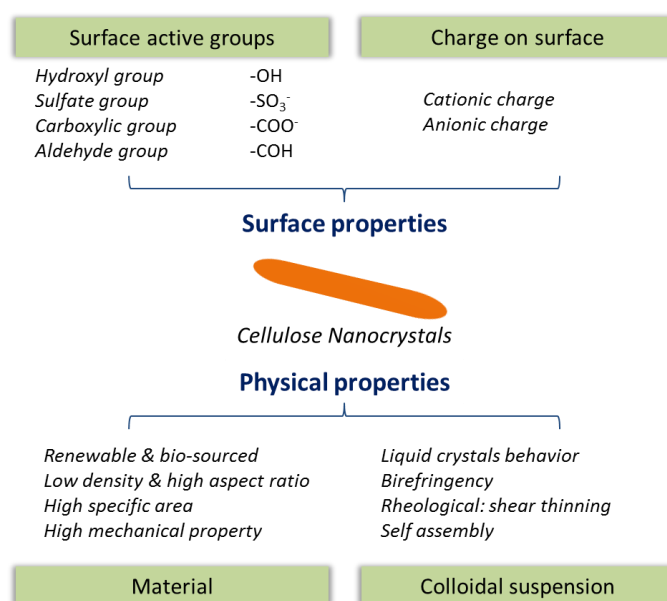


**Figure 7:** Summary of properties of cellulose nanocrystals (adapted from (Tang et al., 2017))

CNCs have a low density ( $1.606 \text{ g}\cdot\text{cm}^{-3}$ ) and exhibit a high aspect ratio with dimension: a diameter of  $\sim 5 \text{ nm}$  to several tens of nanometers and length of  $\sim 100 \text{ nm}$  to a few micrometers (Habibi et al., 2010). As previously described, their size, shape, and surface properties depend on the origin of the cellulosic source and on the hydrolysis conditions (Beck-Candanedo et al., 2005; Bras et al., 2011; Klemm et al., 2011; Moon et al., 2011).

Regarding the mechanical properties, their well-defined dimensions, their high crystallinity (70~90%) and their bond packing organization induce excellent mechanical properties. CNCs are characterized by their high elastic modulus ( $\sim 150 \pm 50 \text{ GPa}$ ) and high tensile strength ( $\sim 7.5 \pm 0.5 \text{ GPa}$ ). These specific properties historically induce reinforcement of mechanical properties with addition of nanocellulose into a polymer matrix as detailed in several reviews (Herrera et al., 2014; Lee et al., 2014; Mariano et al., 2014; Oksman et al., 2016; Siqueira et al., 2010a).

As other colloidal rods like DNA fragments, viruses, metallic oxides, or chitin nanocrystals, CNCs suspensions exhibit very interesting properties to self-organize into liquid crystalline phases. Above a critical concentration, the suspension phase separates into an upper isotropic phase and a lower anisotropic chiral nematic phase (Revol et al., 1992, 1994). The chiral nematic structure and iridescent behavior of CNCs suspension have been studied by researchers to obtain iridescent dried films (**Figure 8**) (Beck et al., 2010).

Thanks to the presence of negative charges ( $\text{SO}_3^-$ ) on the surface, CNCs materials present a colloidal stability in aqueous media. The unique rheological behavior of CNCs suspension is detailed in major works (Bercea and Navard, 2000; Shafiei-Sabet et al., 2012; Ureña-Benavides et al., 2011). These works explain that CNCs suspension rheological behavior is concentration dependent (link to the presence of isotropic/anisotropic region). At low concentrations ( $< 3 \text{ wt\%}$ ), CNCs suspensions appear as a near-Newtonian fluid with small shear thinning behavior at high shear rate ( $> 1000 \text{ s}^{-1}$ ). At higher concentrations ( $> 3 \text{ wt\%}$ ), a shear thinning behavior is observed due to the organization of rods-like particles in the sense of the flow (induced by the shear rate applied during rheological tests).

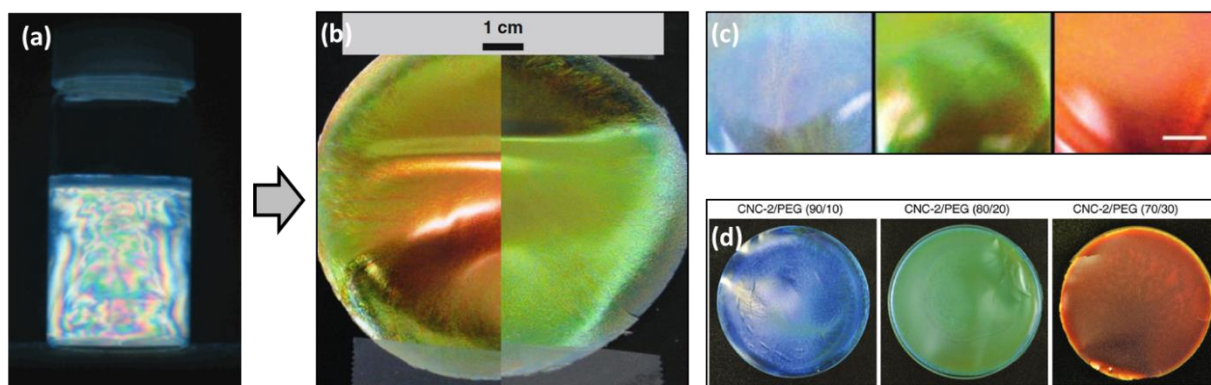


**Figure 8:** (a) aqueous CNC suspension (Araki and Kuga, 2001), (b) Solid CNC film in diffuse light, showing its iridescence when viewed normal to the surface (left) and at an oblique angle (right) (Beck et al., 2013), (c) From left to right, CNC films prepared from different sonicated suspensions showing the normal light reflection (scale marker = 1 cm) (Beck et al., 2010) and (d) Photographs of CNC & PEG composite films showing various structural colors under white light illumination (diameter of the film, 9 cm) (Yao et al., 2017).

The rheological behavior of CNCs suspension is an important part of this Ph.D. project. A future part in this chapter will explain in details the latest development in this research area.

Industries and researchers are attracted by the isolation of nanoparticles with a high surface area ( $> 200 \text{ m}^2 \cdot \text{g}^{-1}$ ) to create 'smart' materials, such as nanocomposites, hydrogels, aerogels, etc. CNCs exhibit a high surface area ( $150\text{-}800 \text{ m}^2 \cdot \text{g}^{-1}$ ) (Habibi, 2014) and can be used as a template to create new hybrid materials with metals or minerals (Hoeng et al., 2015; Kaushik and Moores, 2016a; Majoinen et al., 2011, 2016; Olivier et al., 2012; Padalkar et al., 2010; Rezayat et al., 2014). Due to the presence of three hydroxyl groups in each anhydroglucose unit, CNCs exhibit also good surface reactivity and allow the introduction of new groups by OH functionalization (Habibi, 2014).

These CNCs properties allow their utility in a broad range of applications detailed in the following section.

## 1.2. Applications of CNCs

CNCs are excellent candidates for the design and development of high performance nanomaterials in many applications due to several attractive features such as morphology, high surface area, hydroxyl groups for functionalization, colloidal stability, low toxicity, chirality, and mechanical strength. Since the last decade, around the world, several large scale manufacturing facilities have been commissioned to produce CNCs. Some of these

facilities include the following: (a) Celluforce 1000 kg/day (Canada), (b) American Process 500 kg/day (USA), (c) Holmen 100 kg/day (Sweden), (d) Alberta Innovates 20 kg/day (Canada), (e) US Forest Products Lab 10 kg/day (USA), (f) Blue Goose Biorefineries 10 kg/day (Canada), and (g) India Council for Agriculture Research 10 kg/day (India) (Chauve and Bras, 2014; Tang et al., 2017). Thanks to these facilities, the average price for 1 kilogram of dried CNCs is around 400 €.

This promising interest of scientific community has allowed several recent reviews on potential applications of CNCs and functionalized CNCs (Abitbol et al., 2016; De France et al., 2017; Giese et al., 2015; Kaushik and Moores, 2016b; Salas et al., 2014; Sunasee et al., 2016; Tang et al., 2017). **Figure 9** shows different field of applications with CNCs.

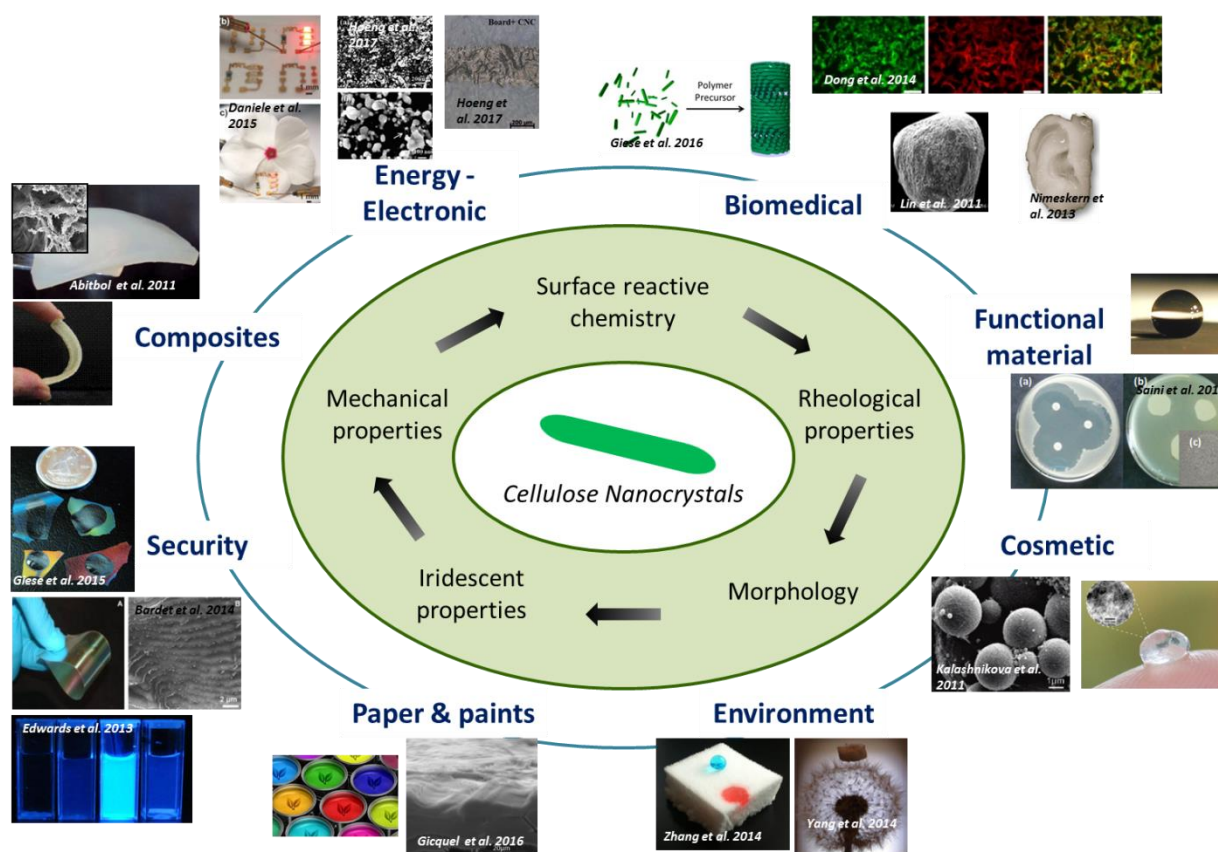


**Figure 9:** Illustration of different cellulose nanocrystals field of application

**Composites:** material applications take advantage of the outstanding mechanical properties of CNCs. Used as a reinforcement or a crosslinker, several works investigate the effect of CNCs in polymeric matrices (Fujisawa et al., 2014; Habibi et al., 2013; Mariano et al., 2015, 2016; Peresin et al., 2014a; Petersson et al., 2007; Siqueira et al., 2011). A recent review on this field of material science are present in literature (Oksman et al., 2016; Peresin et al.,

2014b). **Security:** Iridescent properties combined with unique morphology of CNCs open the possibility of use in security paper and inks (Bardet et al., 2015; Chen et al., 2016; Chindawong and Johannsmann, 2014). **Paper & paints:** this field encompasses several applications such as food packaging, hygienic tissues, specific paper, printing papers or paints facilities (Gicquel et al., 2017; Li et al., 2013; Mascheroni et al., 2016). **Energy & electronics:** This field takes advantages from the reactive surface of CNCs and their unique morphology in order to realize conductive bio-sourced inks (Hoeng et al., 2015, 2017b), flexible piezo electric devices (Csoka et al., 2012), semiconductors (Hamad, 2015), to stabilize metal particles (Kaushik and Moores, 2016b; Lam et al., 2012), and other material applications (George et al., 2012; Olivier et al., 2012; Tang et al., 2014b; Valentini et al., 2014). **Environment:** Wastewater (Batmaz et al., 2014; Chen et al., 2014a; He et al., 2013) and pollution adsorbent (Abraham et al., 2017; Ahmadi et al., 2016; Zhang et al., 2014) are important fields of research to help with protecting the environment, which is possible due to the high specific area of CNCs. In the same area, CNCs are used to increase the thermal isolation of materials thanks to their possible configuration in aerogels (Kobayashi et al., 2014; Yang and Cranston, 2014). **Cosmetics:** The rheological behavior of CNCs is used in this field of application and in particular, the possibility of CNCs to create pickering emulsions for foam formation (Capron and Cathala, 2013; Cherhal et al., 2016; Kalashnikova et al., 2011; Saidane et al., 2016; Tasset et al., 2014). **Functional materials:** antimicrobial properties (Drogat et al., 2011; Tang et al., 2015; Zoppe et al., 2014), barrier to water, air, or oil (Gicquel et al., 2017; Mascheroni et al., 2016), or super-hydrophobic surfaces. **Biomedical:** Because of the possibility of chemical modification, colloidal stability, chirality for template and bio compatibility, the field of biomedical research is one of the most recent application area for CNCs based materials (Jorfi and Foster, 2015; Lin and Dufresne, 2014). Several examples are present in literature using CNCs as drug delivery (Akhlaghi et al., 2013, 2014; Dong et al., 2014; Jackson et al., 2011; Lin et al., 2016), fluorescent labeling for bio-imaging (Chen et al., 2015a; Dong and Roman, 2007), tissue engineering and 3D printing for tissue (Camarero Espinosa et al., 2016; Domingues et al., 2014; Naseri et al., 2016; Siqueira et al., 2017; Zhang et al., 2015), as a template for medical devices (Giese et al., 2015; Kelly et al., 2014) and injectable hydrogel (Domingues et al., 2015).

The large range of potential applications presented in this section is possible due to the large investigation on the functionalization of CNCs particles. Possible chemical modifications of CNCs are detailed in the following section. One challenge of this Ph.D. is to modify their surface to obtain thermo-sensitive properties.

### 1.3. Chemical functionalization of Cellulose Nanocrystals

In order to add new functionalities onto the CNC surface (reactive groups, fluorescent labelling, electric charge, hydrophobicity in polymer matrices...), a wide variety of chemical modification techniques were developed as summarized in recent reviews (Eyley and Thielemans, 2014; Habibi, 2014; Tang et al., 2017). A challenge of these modifications is to prevent the degradation of the CNC crystallinity during the chemical alteration. The following section describes different types of surface modification used in this Ph.D. work: TEMPO-mediated oxidation of CNCs, non-covalent bonding via adsorption and covalent linkage on the surface of CNCs in aqueous medium.

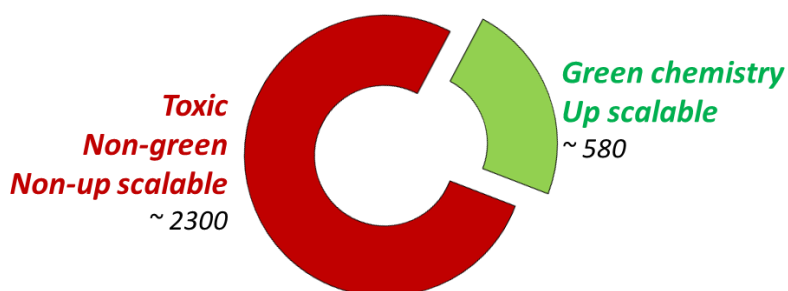


**Figure 10:** schematic representation of up scalable versus non-up scalable work on CNCs systems in 2016 extracted from ACS scifinder® from 1980 to 2016.

In this Ph.D. project, the **first challenge** is the modification of CNCs via green chemistry and green grafting. The twelve principles of green chemistry were proposed by Mulvihill et al. in 2011 (Anastas and Warner, 2000; Mulvihill et al., 2011). Important goals are to use renewable and safer products, prevent waste and chemical pollution, create environmentally-friendly and efficient protocols. **Figure 10** presents schematically the ratio between green and up scalable CNC system and non-green system.

### 1.3.1. TEMPO oxidation of Cellulose Nanocrystals

The oxidation of the surface of CNCs by a TEMPO radical is used as a common post-treatment of CNCs to introduce carboxylate groups on their surface. In 2001, Araki et al. introduced for the first time the TEMPO oxidation on CNCs from cellulosic fiber (Araki et al., 2001). Then, this technique was optimized by several teams of researchers (Habibi et al., 2006; Isogai et al., 2011; Montanari et al., 2005; Rattaz et al., 2011). **Figure 11** represents the TEMPO oxidation mechanism. Cellulose and an oxidized agent (TEMPO radical) are introduced into a medium composed with NaClO and NaBr. In presence of NaBr, the hypochlorite ion (principal oxidizing agent -  $\text{ClO}^-$ ) will react to form the hypobromite ion ( $\text{BrO}^-$ ). This ion will then reacts with TEMPO radical and oxidize the primary alcohol groups  $\text{CH}_2\text{OH}$  (on the carbon  $\text{C}_6$ ) into aldehyde groups. By maintaining the medium at basic pH ( $\sim 10$ ), the TEMPO radical is regenerated and a second oxidation takes place on aldehyde groups to create acid carboxylic groups.

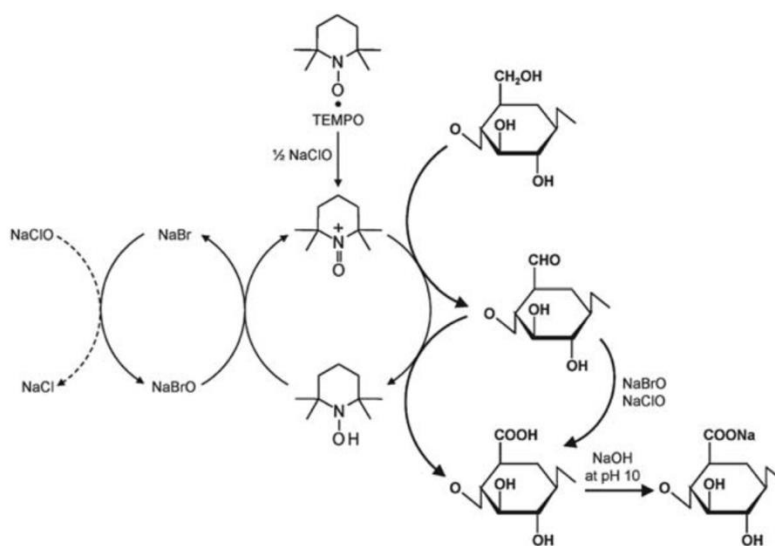


**Figure 11:** Regioselective oxidation of  $\text{C}_6$  primary hydroxyls of cellulose to  $\text{C}_6$  carboxylate groups by TEMPO/NaBr/NaClO oxidation in water at pH 10–11 (Isogai et al., 2011).

It has been shown that the reactivity of nanocellulose is more pronounced at the primary hydroxyl group present on carbon  $\text{C}_6$  compared to the secondary alcohols at  $\text{C}_2$  and  $\text{C}_3$  (carbon number on **Figure 2b**), and that the reaction takes place only on the surface of CNCs (Montanari et al., 2005). This oxidation does not significantly degrade the structure and crystallinity (Habibi et al., 2006). Due to an addition of repulsive charges on the surface (up to  $1600 \mu\text{mol}\cdot\text{g}^{-1}$ ), the final suspension has a high colloidal stability and is a translucent gel.

The introduction of carboxyl function on the cellulose surface offers potential locations for adsorption or grafting reaction. Some examples are presented in additional section.

*In this study, TEMPO CNCs have been used for their surface reactivity in order to adsorb or graft polymer chains on CNCs surface in aqueous conditions.*

### **1.3.2. Non-covalent functionalization: adsorption**

CNC surface can be modified and tuned by physical interaction or adsorption of molecules (like a surfactant), macromolecules, or polyelectrolytes. Electrostatic phenomena are usually involved in the “linkage” process: negatively charged CNCs (sulfate groups or carboxylic acid groups from TEMPO oxidation) attract positively charged molecules. Other “adsorptions” can occur using hydrogen bonding, Van der Waals interactions, or supramolecular interactions are also possible but less efficient than ionic interaction. These adsorption methods occur using similar methods than chemical grafting because of the absence of chemical reactions and preservation the crystallinity of CNC rods. Nevertheless, their reversibility and the complexity of different adsorption profiles and behavior are not adaptable for all applications.

Most of the previous work following this strategy focus on the adsorption of surfactant on cellulose nanocrystals in order to stabilize particles in non-aqueous/organic solvent (Mariano et al., 2017) or polymer matrices (Nagalakshmaiah et al., 2016), or to create new architecture used in pickering emulsions (Cherhal et al., 2015, 2016; Gong et al., 2017; Hu et al., 2015a; Saidane et al., 2016). The drawback of this strategy is the possible molecules released during storage, dilution, or processing. A recent review by Tardy et al. discusses the different surfactant interactions on CNCs particles (Tardy et al., 2017).

In some cases the strategy is not to combine particles or polymer and CNCs to add new properties in a system, but to use the ionic adsorption facility to remove waste product from water, such as methylene blue (Batmaz et al., 2014; Mohammed et al., 2016) or silver ions (Liu et al., 2014).

The colloidal stability of the CNC system can be also enhanced by macromolecules or polyelectrolytes adsorbed onto the CNC surface (Napper, 1977, 1983). **Figure 12** shows a schematic illustration of the adsorption of polymeric molecules onto a particle surface. An adsorbed polymer presents three type of configuration. *Train* is the part in touch with the surface. *Loops* are polymer configuration as loop-like free chains in the medium. *Tails* are the “end” of the polymer and free in the medium. Loops and tails contribute to the colloidal stabilization.

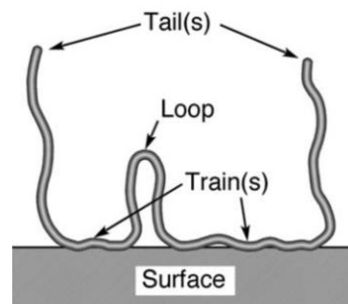


**Figure 12:** Schematic illustration of a surface-adsorbed polymer molecule presenting tails, loop and trains configuration (Araki, 2013).

Several publications have used ionic connection between polymers and CNCs to create new properties using green chemical methods. An example, the ionic adsorption of poly(2-(dimethylamino)ethyl methacrylate) (PDMAEMA) on CNCs combined with a copolymer of poly(oligo(ethylene glycol)methyl ether methacrylate) (POEGMA) to introduce a thermo-reversibility system was investigated by different research teams (Larsson et al., 2013; Vuoriluoto et al., 2015). Another method is to build up multilayer films by electrostatic-driven layer-by layer (Decher et al., 1992) (LbL) assembly of nanocellulose substrates (either positively or negatively charged) with oppositely charged entities constitutes a way to create tailored nano-materials. Generally, LbL deposition is carried out by dipping the substrate into polyelectrolyte solution, or by spin coating (Cranston and Gray, 2006; Moreau et al., 2016). Cathala and coworkers propose a different system based on LbL composed of CNCs and , carbon nanotubes (Olivier et al., 2012), xyloglucan (Cerclier et al., 2010, 2013; Villares et al., 2015), cationic xylans (Dammak et al., 2013), or poly(allylamine hydrochloride) (PAH) (Azzam et al., 2017). A recent review by Martin and Jean focuses on the use of CNCs facilitate self-assembly in multi-layer thin films (Martin and Jean, 2014).

Cranston et al. proposed a broad range of works on the adsorption of non-ionic polymers on CNCs such as xyloglucan (Bensselfelt et al., 2016), or other polymers (HEC, HPC...) (Hu et al., 2014, 2015b).

Different techniques were developed since the 90's to measure and understand the adsorption phenomenon. Among these, most popular are Quartz Crystal Microbalance with dissipation (QCM-d) (principle explained by (Rodahl et al., 1995)), Multi-Parametric Surface Plasmon Resonance (MP-SPR) (Details in (Homola et al., 1999; Liedberg et al., 1983)), and Isothermal Titration Calorimetry (ITC) (Details in (Freire et al., 1990)). The first two investigate the mass adsorbed on a film during a polymer solution flow. QCM-d follows the shift in frequency of the quartz during adsorption, which is directly related to the mass adsorbed. Despite of it being an "easy" process, it is sensitive to the bounded water on the film and data processing can be challenging. In MP-SPR experiments, a laser is reflected on the surface of the sensor at a specific angle of incidence. The change in refractive index near the sensor surface is then measured and the mass adsorbed is calculated. This technique is more complicated than QCM-d, but the solvent bound on the film has low impact on the measurement. Depending on the studied system, literature proposes a rich amount of publications on the comparison between QCM-d and MP-SPR and their complementary properties (Köβlinger et al., 1995; Liu et al., 2011b). ITC experiments also measure the mass adsorbed for dilute suspensions. The experiment consists of collecting the energy released or consumed during the reaction on the surface of particles. A full thermodynamic behavior of the linkage during the adsorption is obtained with details on maximum coverage amount or the adhesion mechanism (hydrogen bounding or ionic adhesion).

*Adhesion of polymer on CNCs via hydrogen bounding or ionic force is a relevant option to create CNCs and polymer system via green chemistry. We developed a hydrogel based on CNCs and PNIPAM or PDMAEMA-PDEGMA polymer and used QCM-d, MP-SPR and ITC to understand the adsorption behavior. Details on these three techniques and calculation are described in results sections and publications of this Ph.D. project.*

### 1.3.3. Covalent functionalization of CNCs with molecules in aqueous conditions

*As previously described, one of the main objectives of this Ph.D. is to use green grafting on the surface of CNCs. Chemical surface functionalization in aqueous condition or with a low environmental impact will be described in this section.*

Chemical reactions on CNCs, whatever the solvent is, have been well described in literature review since the early 2010s (Dufresne, 2013; Eyley and Thielemans, 2014; Habibi, 2014; Moon et al., 2011; Tang et al., 2017). The presence of hydroxyl groups on the surface of CNCs and a large specific surface area provide numerous active sites for chemical modification. Functional groups can be introduced onto nanocellulose via several chemical reactions, e.g. oxidation (Sun et al., 2015), esterification (Espino-Pérez et al., 2014; Filpponen and Argyropoulos, 2010), silylation (Huang et al., 2014), or carbamation (Siqueira et al., 2010b). Major drawbacks of covalent functionalization are the low grafting efficiency and sometimes the impossibility to graft in aqueous media. In some cases, the reagent is reactive with water (as the reaction is on OH group of cellulose) or in other cases water is one of the reaction products.

As an example, esterification is possible between OH groups of cellulose and carboxylic acid or with the carboxylic groups on the TEMPO CNCs surface with an alcohol. **Figure 13** presents the mechanism involved in esterification. This reaction produces H<sub>2</sub>O molecules which are a problem when the reaction occurs in aqueous media due to the excess of water and Le Chatelier's principle (modification of the chemical equilibrium).

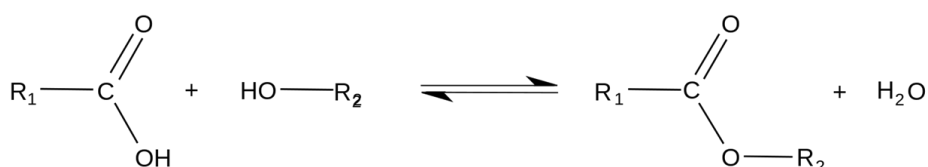


**Figure 13:** Esterification mechanism (*R<sub>1</sub>* and *R<sub>2</sub>* are molecules, radical...)

Previous work has designed esterification experiments on CNCs. Braun et al. present the first work through Fisher esterification of acid (organic, butyric, and acetic) (Braun and Dorgan, 2009). A one-step method was developed which consists of adding these acids during the hydrochloric acid hydrolysis of cellulose fibers. Modified CNCs were directly extracted with a

substitution close to 50%. A similar "in situ" functionalization approach has also been proposed (Boujemaoui et al., 2015). In 2014, Espino-Perez et al. proposed a green method (solvent-free) for CNCs esterification called SolReact (Espino-Pérez et al., 2014). Carboxylic acids are the solvent and the grafting agent at the same time. The water evaporation during the reaction encourages the esterification via solvent exchange at a temperature above the melting point of the carboxylic acids. Then the carboxylic acid solvent is evaporated and can be used again for another SolReact reaction, which correlates with green chemistry principles. Other solutions by adsorption and then esterification during the drying step have been proposed for nanocellulose (Castro et al., 2016) but this has limits with applications. Another recent process allows amidation (also called peptidic linkage) in aqueous condition by using 1-ethyl-3,3-dimethylaminopropylcarbodi-imide (EDAC) and N-hydroxysuccinimide (NHS) coupling. In this case carboxylic acid is necessary at the surface of CNCs.

*During this Ph.D., to functionalize with a polymer chain the surface of CNCs was proposed. Different strategies are possible as detailed in following chapter.*

#### **1.3.4. Polymer chains grafting on cellulose nanocrystals**

The main objectives for grafting a polymer on the surface of nanocellulose, particularly cellulose nanocrystals, are to turn the surface hydrophobicity (dispersion in non-polar medium), to enhance the mechanical properties for composite materials, and to add new properties for smart application. More details are available in the recent reviews previously quoted (Eyley and Thielemans, 2014; Habibi, 2014; Tang et al., 2017). Two main strategies can be used to realize polymer grafting on surfaces of CNCs, "grafting-onto" and "grafting-from", they are schematically illustrated in **Figure 14**.

In the first strategy (**Figure 14a**), polymers are previously synthesized with a terminal groups that can react with the material surface. Then a polymer, nanoparticles, and coupling agent are mixed together. The grafting reaction occurs by the reaction between the terminal functional groups of the polymer and the surface functional groups of the surface in presence of coupling agent. Nonetheless, steric repulsion of grafted polymer chains can prevent optimal grafting and have low surface density grafts. This strategy allows a control of the resulting material since the molecular weight of the attached polymer can be

characterized before grafting. The second strategy (**Figure 14b**), requires the surface to be first functionalized with an “initiator”. Then monomers are added in the reaction process and the polymerization *in situ* starts on these initiators. This strategy allows a high grafting density by limiting the steric hindrance on the surface. However, the “grafting-from” method induces the presence of homopolymer and generally uses toxic solvent or reagent, and it is difficult to control and determine precisely the molecular weight of the grafted polymer.

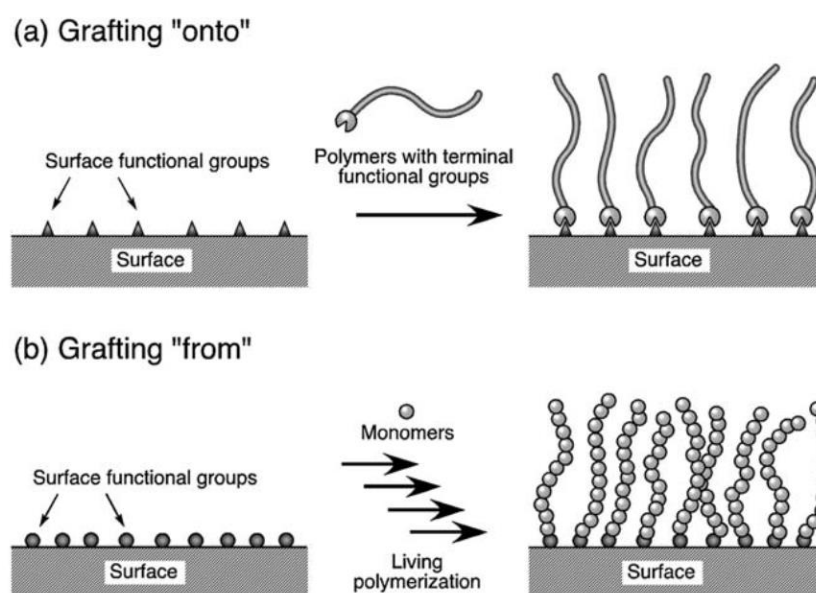


**Figure 14:** Schematic illustrations of (a) “grafting onto” and (b) “grafting from” strategies (Araki, 2013)

### “Grafting-from” strategy

The most commonly used ways to graft polymer with grafting-from are free or living radical polymerization or ring opening polymerization.

*Ring opening polymerization* (ROP) is a traditional way to graft and polymerize cyclic monomers on the CNCs surface, mainly lactones, such as, as polycaprolactone (PCL) or lactides like polylactic acid (PLA). Tin(II) 2-ethylhexanoate ( $\text{Sn}(\text{Oct})_2$ ) is a commonly used catalyst in ROP reactions. **Figure 15** shows the scheme of ROPs. The hydroxyl groups on CNCs surface act as initiator and the ratio of monomer on initiating groups determines the polymerization degree of the reaction. A review by Carlmark et al. (Carlmark et al., 2012) presents different ROPs which have been done on CNCs.

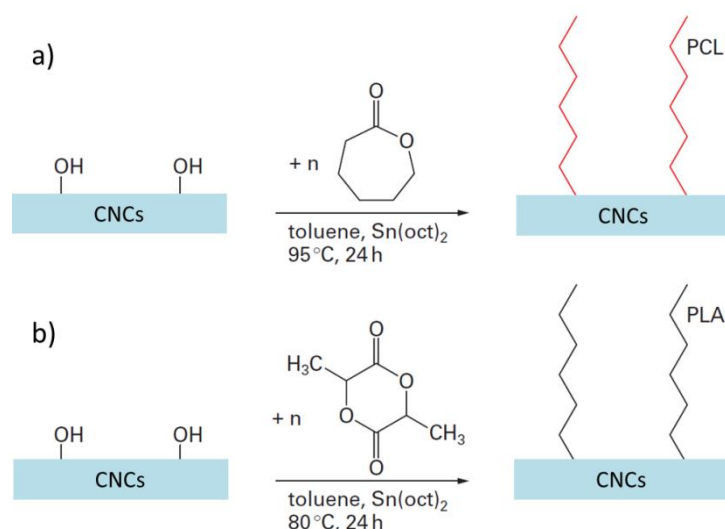


**Figure 15:** scheme of ring opening polymerization of (a) caprolactone (Habibi et al., 2008) and (b) L-lactide (Goffin et al., 2011) as initiated from the surface of cellulose nanocrystals (CNCs) (Dufresne, 2013)

Concerning the grafting from using *radical polymerization*, two steps are involved. The first is the creation of an initial site with an initiator immobilized on the surface of nanoparticle. Then, the second step is the reaction of the initiator-modified surface with a monomer to induce radical polymerization propagation. **Figure 16** shows schematically the reaction involved. Copper-mediated polymerization is commonly used for the large monomer choice and the ease of synthesis. In this chemical area, two main mechanisms are distinguished: Atom Transfer Radical Polymerization (ATRP) and Single Electron Transfer-Living Radical Polymerization (SET-LRP).

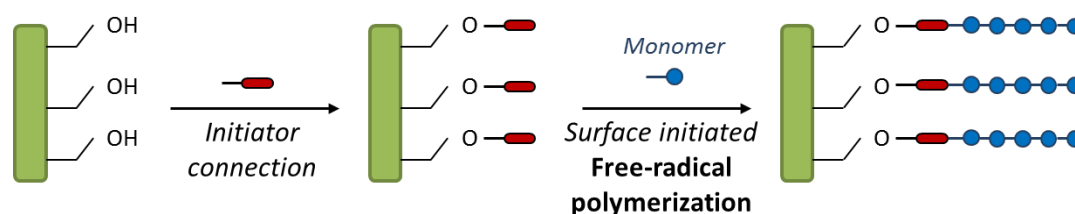


**Figure 16:** Reaction scheme of a free-radical polymerization

Among the first works, Yi et al. in 2008 grafted PS on CNC surface via atom transfer radical polymerization (ATRP), presented in **Figure 17** (Yi et al., 2008), by using 2-bromoisobutyryl bromide (BriB) as an initiator. Hydroxyl groups were activated by 2-bromoisobutyrylbromide in presence of trimethylamine and 4-dimethylaminopyridine in toluene at room temperature during 24h. After freeze drying, initiator-modified CNCs were mixed with  $\text{CuBr}$ , 1.1.4.7.10.10-

Hexamethyltrielenetetramine (HMTETA), and monomer of styrene at 110°C during 12h for polymerization. The final system conserved the chiral nematic particular structure of CNCs. Morandi et al. developed the same protocol by optimization of parameters and found a higher polystyrene grafting density (Morandi et al., 2009).

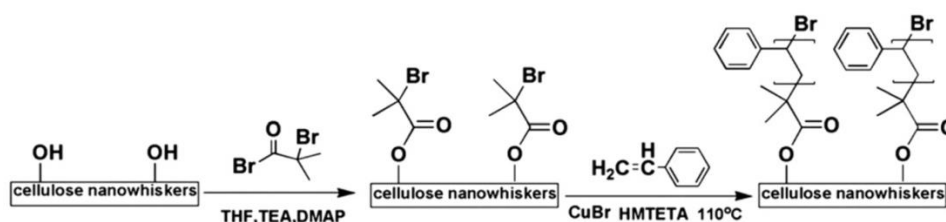


**Figure 17:** Formation of Polystyrene grafted on cellulose nanocrystals (Yi et al., 2008).

Kan et al. used a similar approach to polymerize 4-vinylpyridine (4VP) on CNCs and create a pH-responsive system based on cellulose nanocrystals by ceric-ion initiation in aqueous media under inert atmosphere (Kan et al., 2013). Most of these “grafting-from” procedures were firstly developed with cellulose fibers by several researchers like Malmström’s group at KTH. Among them, some has focused with stimuli-responsive solutions (Hansson et al., 2009; Lindqvist et al., 2008; Porsch et al., 2011).

*Regarding our objective to graft thermo-responsive polymer on CNCs, no more than 15 papers can be cited at this date.*

Zoppe et al. (Zoppe et al., 2010) developed, via SET-LRP, a thermo-responsive system based on CNCs and poly(N-isopropylacrylamide). Different proportion of BriB initiator and N-isopropyl acrylamide monomer were studied in order to create different grafting densities and degrees of polymerization. This system was then used to introduce thermo-responsive functionalities on silica surface (Zoppe et al., 2010), or to stabilize pickering emulsions (Zoppe et al., 2012). Inspired by this system, Hemraz et al. (Hemraz et al., 2014) investigated another ratio of BriB/NIPAM in order to create a system with the highest thermo-responsivity possible. They found that the lowest density increased the thermal functionalities and reversibility, because of a lower steric hindrance between each polymer chains induced highest polymer mobility in aqueous media. Wu et al. (Wu et al., 2015) combined thermo-sensitive (N-Isopropylacrylamide) and pH-sensitive (4-Ethoxy-9-allyl-1,8-naphthalimide - EANI) properties on cellulose nanocrystals via a similar process (**Figure 18**).

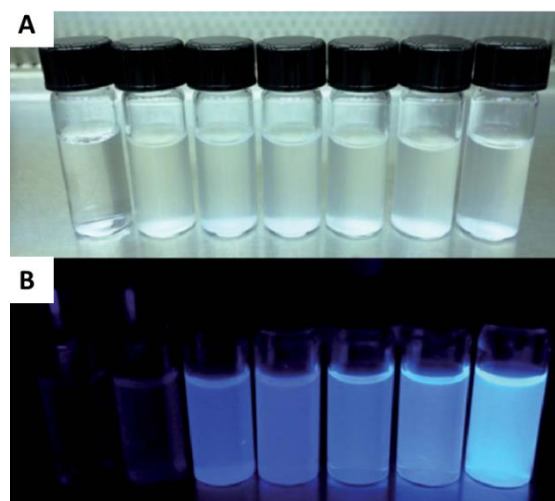


**Figure 18:** Photographs of CNCs suspensions (0.05%) under (A) sunlight and (B) 365 nm UV illumination. Samples are, from left to right, CNCs, CNCs–initiator and CNCs grafted with PNIPAM-EANI complex with an increase ratio PNIPAM/EANI.

Grishkewich et al. used another polymer and produced a system composed on cellulose nanocrystal and poly(oligo(ethyleneglycol)methacrylate) (POEGMA) brushes with thermo-reversible functionalities (Grishkewich et al., 2016). After initiated the CNCs surface with BriB, multiple POEGMA-g-CNC system with different ratio of MEO<sub>2</sub>MA/OEGMA<sub>300</sub> were synthesized. These systems present a large range of lower critical system temperature (LCST) in aqueous media depending on the ratio (from 23 °C to 34°C).

*In any case such polymer grafting strategies used either toxic solvent, toxic catalyst/initiator, or both. In our project, as biomedical systems were targeted, the main idea is to focus on non-toxic condition consistent with “grafting-onto” strategy.*

### **“Grafting-onto” strategy**

This strategy, in cellulose chemistry, was inspired from previous grafting of polymer onto cellulose fibers (Belgacem et al., 2011; Felix and Gatenholm, 1991). Since the 1990s, several works investigated the “grafting-onto” process for polymer-CNCs systems. Most of them used toxic solvent but, in literature, different types of polymers can be grafted in aqueous conditions on CNCs such as waterbone polyurethane (Cao et al., 2009), chitosan (Akhlaghi et al., 2013), and polyethylene oxide (Kloser and Gray, 2010). In respect with green chemistry, an interesting way is to use a “click” reaction between CNCs, with a specific end, and a polymer with an end that can react without any catalyzer on the CNCs surface (Filpponen and Argyropoulos, 2010; Zhang et al., 2009).

In accordance with the green chemistry objectives, Araki et al. (Araki et al., 2001) were the first to modify the surface of CNC with polyethylene glycol (PEG) via a carboxylation-amidation (also called peptidic grafting) in presence of 1-ethyl-3,3-dimethylaminopropyl)carbodi-imide (EDAC) and N-hydroxysuccinimide (NHS). The grafting yield was 12%. Filpponen et al. later applied the same technique of peptidic coupling with propargyl amine and 11-azido-3,6,9-trioxaundecan-1-amine. The grafting success was evaluated at 17% and 10% respectively (Filpponen and Argyropoulos, 2010). The aim is to create, by peptidic coupling, a covalent amide bond between a primary amine-terminated polymer and carboxylated CNCs as shown in **Figure 19**. First, CNCs are TEMPO oxidized to introduce carboxylic groups on the surface. Then, the polymer with amine derivatives on surface reacts with carboxylic group by a peptidic coupling reaction using a carbo-diimide as amidation agent. Such reactions can be successfully performed in solvent (DMF) or in aqueous media. In the case of nanocellulose substrate, it was reported that the favorable pH range is 7 to 10. Principal benefits of this grating process are the green feasibility at room temperature in aqueous media, the absence of harsh component, and the lack of sensitivity to the ionic strength of the system (steric repulsion between the grafted brushes). Nonetheless, major drawbacks are a long reaction time (16-96h) and low grafting yield (between 10-30%).

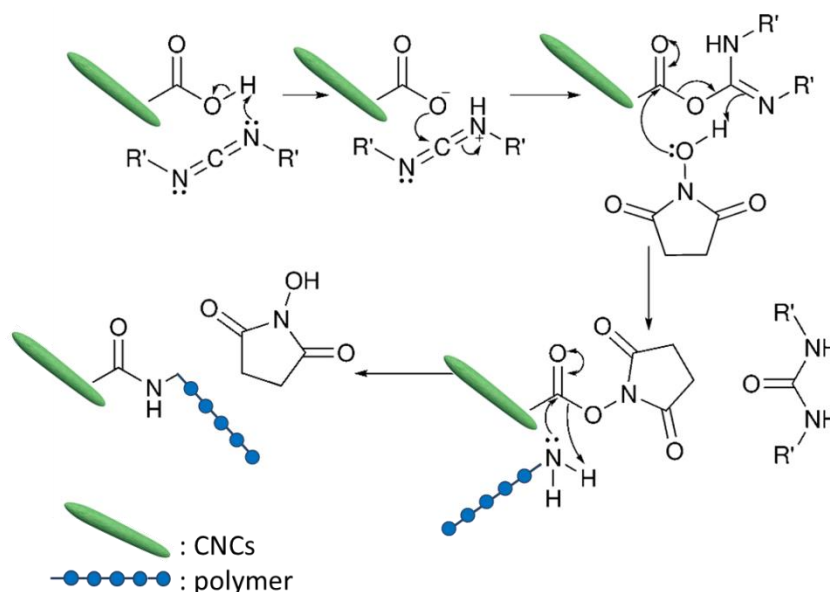


**Figure 19:** Schematic reaction amine terminated polymer onto TEMPO oxidized cellulose in presence of coupling agent: EDAC and NHS. First, EDAC gives to acid carboxylic function an O-acylurea unstable compound. In second time, NHS reacts with this compound and blocks the reorganization of this function in N-acylurea stable. Then, amine terminated polymer reacts with the CNCs surface activated (Eyley and Thielemans, 2014).

This approach has been successfully applied by Azzam et al. to graft copolymers of ethylene oxide and propylene oxide with thermo-sensitive properties (named Jeffamine by Huntsman Corporation) onto TEMPO oxidized CNCs in order to increase the stability at high ionic strength (Azzam et al., 2010, 2016). Three different kinds of amine-terminated Jeffamines with different molecular weights (1000, 2070 and 2005 g·mol<sup>-1</sup>) were grafted onto the CNCs during 24h at neutral pH and low temperature. A high grafting yield was reported around 26% in aqueous media (Azzam et al., 2016) and around 50% in DMF solvent (Azzam et al., 2010). Using the same process, polymers that cannot be produced by polymerization, such as polysaccharides and DNA, can be introduced as polymer brushes on the surface of CNC (Mangalam et al., 2009).

One recent study by Hoeng et al. presents the grafting of low molecular weight amines instead of polymer with a grafting yield about 60-70% (Hoeng et al., 2015). As a result, the thermal stability of the system increased to 250°C due to the decrease in charge density. A recent investigation of the grafting of PEG-NH<sub>2</sub> on the surface of TEMPO oxidized CNF (TOCNF) was also proposed by Lavoine et al. (Lavoine et al., 2016). Ionic bonds between the protonated carboxyl groups of TOCNF and the amine groups of PEG-NH<sub>2</sub> were converted to amide bonds by heating to 150°C and present a promising application in the fabrication of nanocomposites.

*In the present Ph.D., “grafting-onto” was investigated to connect Poly(N-isopropylacrylamide) polymer and TEMPO CNCs. In particular, the peptidic grafting described in this section was used in order to respect green chemistry objectives.*

This section of the chapter gives a synthetic overview of the cellulose nanocrystals main properties, functionalization, and applications. For more information, the following **Table 1** provides additional publications and reviews dealing with different CNCs topics (adapted and completed from the Ph.D. thesis of Hoeng (Hoeng, 2016)).

**Table 1:** Key reviews and publications on cellulose nanocrystals

<b>CNCs topic</b>	<b>Review/publication</b>	<b>Reference</b>
Properties	Cellulose Nanocrystals: Chemistry, Self-Assembly, and Applications <i>Habibi et al. 2010</i>	(Habibi et al., 2010)
Surface modification	Key advances in the chemical modification of nanocelluloses <i>Habibi et al. 2014</i> Surface modification of cellulose nanocrystals <i>Thielemans et Eyley 2014</i> Functionalization of cellulose nanocrystals for advanced applications <i>Tang et al. 2017</i>	(Eyley and Thielemans, 2014; Habibi, 2014; Tang et al., 2017)
TEMPO oxidation	TEMPO-mediated surface oxidation of cellulose whiskers <i>Habibi et al. 2006</i>	(Habibi et al., 2006)
Patents on CNCs	Nanocellulose Patents Trends: A Comprehensive Review on Patents on Cellulose Nanocrystals, Microfibrillated and Bacterial Cellulose <i>Charreau et al. 2013</i>	(Charreau et al., 2013)
General Applications	Nanocellulose, a tiny fiber with huge applications <i>Abitbol et al. 2016</i> Functionalization of cellulose nanocrystals for advanced applications <i>Tang et al. 2017</i> Nanocellulose properties and applications in colloids and interfaces <i>Salas et al. 2014</i>	(Abitbol et al., 2016; Salas et al., 2014; Tang et al., 2017)
Composites	Cellulose nanocrystals and related nanocomposites: Review of some properties and challenges - <i>Mariano et al. 2014</i>	(Mariano et al., 2014)
Hydrogel	Cellulose nanocrystals and related nanocomposites: Review of some properties and challenges - <i>De France et al. 2017</i>	(De France et al., 2017)
Biomedical	Recent advances in nanocellulose for biomedical applications <i>Jorfi et Foster 2015</i> Cellulose nanocrystals: a versatile nanoplatform for emerging biomedical applications - <i>Sunasee et al. 2016</i>	(Jorfi and Foster, 2015; Sunasee et al., 2016)

The key reviews and papers cited in this section were published before or at the start of this Ph.D. project. Many of the reviews published in 2017 have focused on the application of CNCs, which illustrates that more research is being dedicated to the use of CNCs in industrial applications.

*In material science associated with CNCs and functionalized CNCs, a large field of applications focuses on coatings, suspensions modifiers or hydrogels. In this Ph.D. project, one of the target applications is a hydrogel system based on CNCs and thermo-sensitive polymers. In order to understand and use these systems rheological behavior must be understood.* The following section focuses on the rheological behavior of CNCs.



## II. Rheology of Cellulose Nanocrystals

### 1.1. Rheology Concept

Rheology is the study of deformation and flow of a material under shear. In this Ph.D. study, related to CNCs suspension and hydrogels experimentation, only ‘fluid’ rheological studies are applied. Nevertheless, the term ‘fluid’ is complex and includes different systems: some fluids are very liquid like water, dispersed suspensions, and organic solvents, but other fluids are highly viscous and thick like a network of entangled polymers. These mechanisms are time dependent. For example, a liquid with a low viscosity will immediately flow under gravitation, but glass (a solid fluid) will take centuries to flow under gravitation.

Rheology is present everywhere in human activities and natural phenomena, for example, the plastic material industry, red blood cells, emulsions and food sauces, magma and snow, cement and paint, or cosmetic creams and lipsticks. This area of scientific study involves mechanics, physics, chemistry, and mathematic concepts. Books on rheology (Coussot, 2005, 2012), written by Coussot et al., were a source of knowledge reported in this section.

The **rheological study of a suspension** is rich and complex. Each system can present a different behaviors related to its composition and structure. These behaviors can be described either by the evolution of the shear stress  $\tau$  or viscosity  $\eta$  versus the shear rate  $\dot{\gamma}$ , also called flow curve. Viscosity is related to shear stress and can be defined by  $\eta = \tau/\dot{\gamma}$ . Principal rheological behaviors are presented in **figure 20**. In following chapter, we use the flow curves representation as  $\eta = f(\dot{\gamma})$ .

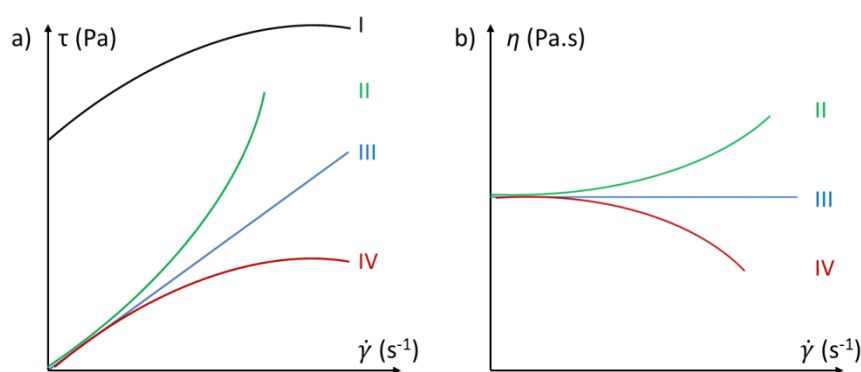


**Figure 20:** General flow curves used to define typical rheological behavior of fluids a)  $\tau = f(\dot{\gamma})$  and b)  $\eta = f(\dot{\gamma})$  at  $\dot{\gamma} > 0 s^{-1}$ .

- *Plastic fluid* (Bingham fluids), number **I**: the rheological behavior presents a flow threshold. The system needs a critical shear stress to flow (toothpaste, dry sand, shaving foam, mayonnaise).
- *Shear thickening fluid* (dilatant fluid), number **II**: when the shear rate increases, the viscosity increases and the system is thicker (quicksand, cornstarch).
- *Newtonian fluids*, number **III**: the viscosity value is constant over the whole shear rate range. The flow curve presents proportionality between shear rate and shear stress. Water is a good example of this kind of fluid.
- *Shear thinning fluids* (pseudo plastic fluids), number **IV**: The viscosity of this sort of fluid decreases when the shear rate increases. It is the most common type of fluid behavior. Blood and paint are good example of this type of fluid.

*The description of basic concepts in rheology was necessary to understand and appreciate following section. In particular, nanocellulose fluids present a shear thinning behavior, due to the nanoparticles within the system. The following section will describe in detail the rheological behavior of cellulose nanocrystals, and its particular properties regarding the liquid crystal phase.*

## **1.2. Cellulose Nanocrystals and rheology**

*The **second challenge** of this Ph.D. is to investigate and understand the effect of shear rate on the CNCs suspension's rheological behavior. This chapter will describe in detail the latest developments in literature about the CNCs configuration in the liquid crystal phase and their rheological behavior.*

### **1.2.1. CNCs liquid crystals organization and phase separation**

A liquid crystal is an intermediate state of matter with the characteristics of a liquid (fluidity) and solid crystal (some long-range order and anisotropy)(Chandrasekhar, 1992). They may flow like liquid, and at the same time molecules are oriented in a crystal-like way (typically for rod-like and rigid particles). **Figure 22** shows schematically different types of organized structures which exist in nature.

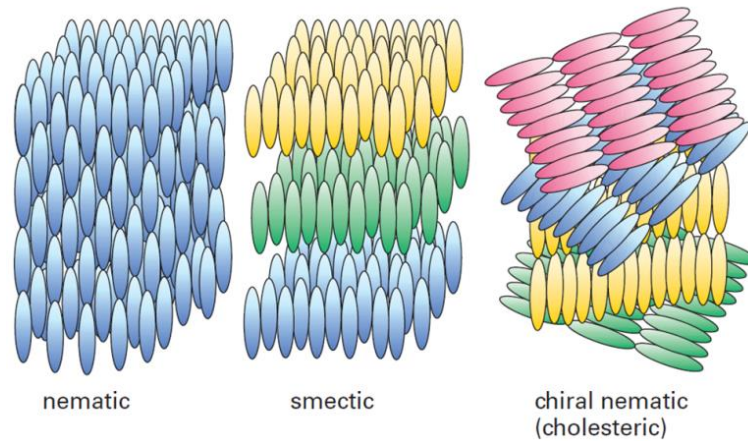


**Figure 22:** scheme of different type of liquid crystal structure (Dufresne, 2013)

A nematic structure is characterized by the absence of positional order between each particle, but all particles tend to align in the same direction. The smectic structure presents one more degree of orientation. Particles are aligned along the same direction, and tend to align themselves in layers or planes. The chiral nematic (also named cholesteric) structure is described as layers of particles organized in the same direction, and rotated along an axis with respect to the layers above and below it, which causes a helical structure. The pitch of the helix is defined as the distance required for a full rotation. When the pitch is in the order of the wavelength of visible light, it will reflect polarized light (De Vries, 1951). The wavelength of this selectively reflected light changes with the viewing angle, causing an iridescent appearance.

Liquid crystals are divided into two categories: thermotropic and lyotropic. Thermotropic liquid crystals present a phase transition of liquid to liquid-crystal phase due to temperature. Lyotropic ones exhibit a phase transition caused by changes in concentration.

Historically, the first macroscopic evidence of a self-organization in CNCs suspensions appears in the work of Marchessault et al. published in 1959 (Marchessault et al., 1959), where a flow birefringence of a cellulosic suspension was observed through cross polarizers (**Figure 23a**). This observation was refined by Revol et al. (Revol et al., 1992, 1994). They describe this property of CNCs to display a lyotropic liquid-crystalline behavior in water. At the diluted regime, CNCs exhibit a stable colloidal particle suspension (**Figure 23b**). The birefringence appears only during agitation of the suspension. When a critical concentration is reached, the suspension starts to self-organize in a cholesteric structure; CNCs are

organized in the same direction along a vector direction. Two phases appear: an upper phase totally isotropic and a lower phase which is anisotropic (**Figure 23c**). After a maximum critical concentration, the entire suspension is anisotropic and exhibits a birefringence gel-like form.

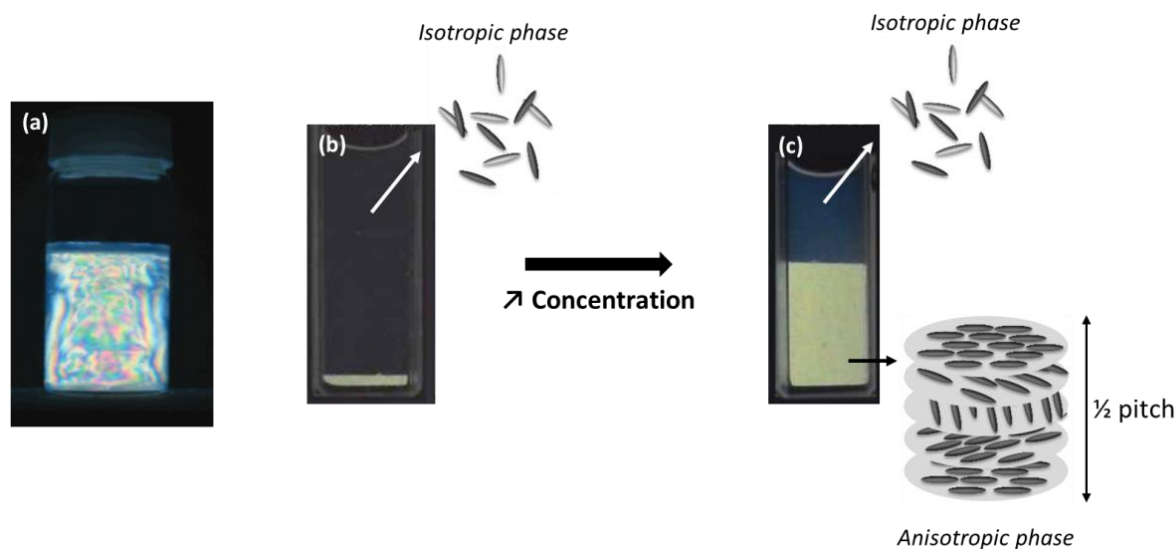


**Figure 23:** (a) 0.63 wt% aqueous CNCs suspension observed between crossed polarizers (Araki and Kuga, 2001), (b) Isotropic structure at dilute suspension (2.99 vol%) and (c) biphasic region (6.23 vol%) with upper isotropic and lower anisotropic structure (image from reference (Ureña-Benavides et al., 2011))

Several other systems exhibit a liquid-crystalline form (DNA, peptides, and polysaccharides (Hamley, 2010)); the formation of this phase can be explained by Onsager's theory (Onsager, 1949), which predicts the critical transition density for rods with a small aspect ratio. This theory was extended via a numeric simulation in order to incorporate a defined form factor (Lee, 1987), polydispersity effect (Vroege et al., 2006), and generalized for all liquid crystals (Xiao and Sheng, 2013)

As previously described in **figure 23**, all liquid-crystalline have a director and all chiral nematic liquid-crystalline have a pitch. CNCs have the same behavior. Several studies explain the origin of this pitch, and the effect CNCs suspension concentration on the pitch distance (Revol et al., 1992, 1994; Schütz et al., 2015; Ureña-Benavides et al., 2011). In 1998, Orts et al. (Orts et al., 1998) described, by using small angle neutron scattering, that CNCs are screw-like rods, and they are packed tighter along the cholesteric axis as shown in **figure 24a**.

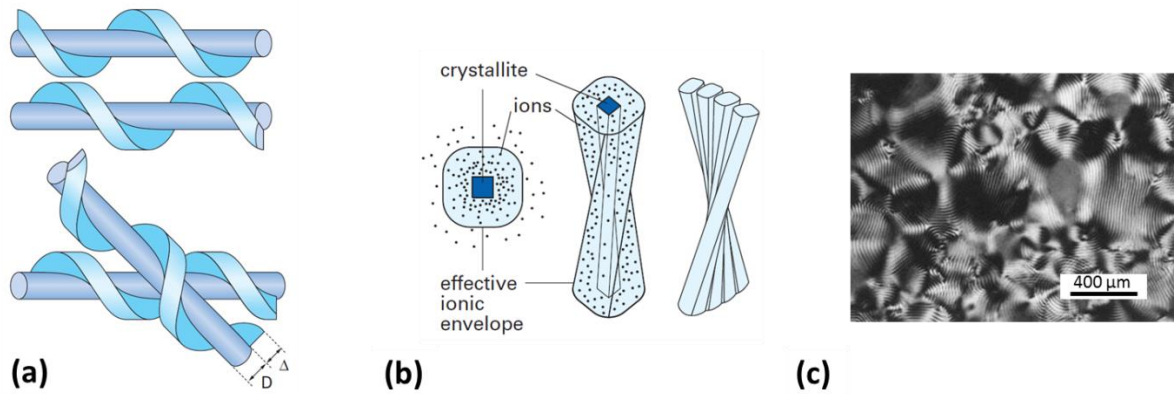


**Figure 24:** (a) Representations of the tighter packing achievable by the chiral interactions of twisted rods. When the distance between rods is inferior to the section of particles (diameter  $D$  and ionic envelope  $\Delta$ ), rods packed with axes parallel will be packed with a twist. (b) For nanocrystals with an electrostatic double layer, a threaded rod would alter the surrounding electric double layer and affect packing over relatively large distances (Orts et al., 1998). (c) shows a fingerprint structure for CNC suspension through cross polarized light (Dong et al., 1996).

**Figure 24b** shows the presence of electric double layers which are transmitted to the chiral twist of CNCs to create liquid crystals. This electric double layer and pitch can be modified by the presence of an electrolyte (Araki and Kuga, 2001; Dong and Gray, 1997; Dong et al., 1996). Figure 24c shows a fingerprint configuration for a CNC suspension with a pitch that can be measured by polarized optical microscopy (POM) as proposed by Gray and Revol (Revol et al., 1994).

Due to the crystal-liquid behavior of CNCs, the presence of two phases in suspension (isotropic and anisotropic) induces particular rheological behavior described in following section.

### 1.2.2. CNCs suspension behavior in aqueous solution

As presented in previous section, CNCs in an aqueous suspension are able to form a spontaneous liquid crystalline phase. A lot of studies investigated these properties to create model for liquid crystals, and to understand how to use the shear dependent behavior in industrial material production. With an applied shear rate, CNCs rod-like particles are strongly aligned in the direction of the flow. It makes them a good model for understanding the ordering phenomenon and the rheological behavior of long rigid rods. Marchessault et al. (Marchessault et al., 1961) demonstrated in their pioneering work in 1961 that the hydrodynamic properties of CNCs are directly related to the size and the length distribution

of the nanoparticles (aspect ratio). In 1998, Orts et al. (Orts et al., 1998) studied the rheological behavior and the liquid crystalline ordering of CNCs from black spruce kraft pulp via small angle neutron scattering (SANS). Above a certain mass concentration the CNC suspension behaves as shear-thinning fluid: when the shear rate increases, the viscosity decreases. At a higher concentration, as for common crystal liquids polymer suspensions (theory in (Onogi and Asada, 1980)), Orts et al. have shown that there are three different regions in the shear-dependent viscosity profile. These results were confirmed by Lima and Borsali in 2004 for CNCs from cotton linter (de Souza Lima and Borsali, 2004), as shown in **figure 25**.

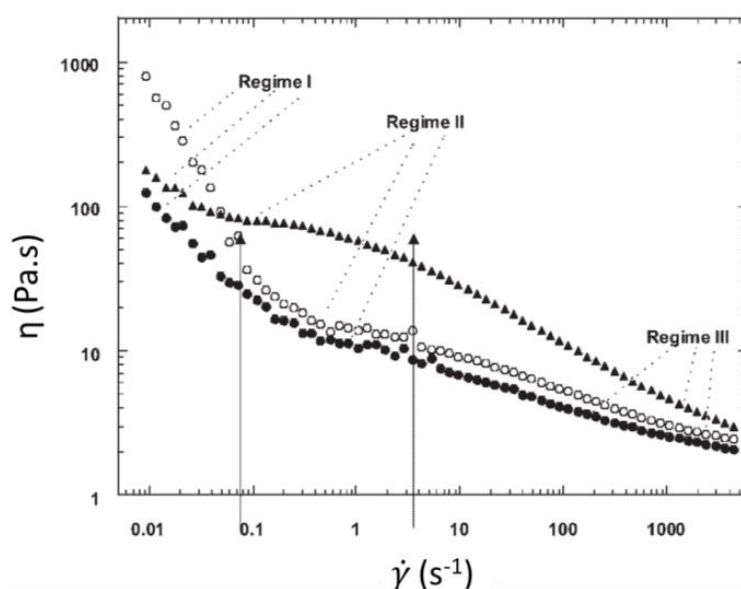


**Figure 25:** Viscosity versus shear rate for cellulose nanocrystals of cotton linter at concentrations of 1.2 wt% (●), 1.7 wt% (○) and 2.7 wt% (▲). Three regimes appear: Regime 1: shear thinning behavior at low  $\dot{\gamma}$ , Regime 2: Newtonian behavior at intermediate  $\dot{\gamma}$ , and Regime 3: shear thinning behavior at high  $\dot{\gamma}$  (adapted from (de Souza Lima and Borsali, 2004))

At lower shear rates the viscosity continuously decreases. They proposed a shear thinning regime (Regime I) where the domains formed by the CNCs starts to flow. At an intermediate shear rate (Regime II), a plateau region appears. This corresponds to CNCs domains which start to break up and align in the flow direction. At a higher shear rate, a further shear thinning behavior appears (Regime III). This corresponds to the breakdown of these domains and to the alignment of individual CNCs in the flow direction. The cholesteric structure of the suspension is destroyed in favor of a simple nematic structure. In 1999, Ebeling et al. confirmed this observation with Small Angle X-ray Scattering (SAXS) (Ebeling et al., 1999). Critical concentration, when three regime appears, depends on the aspect ratio which

determines the degree of shear induced order (Orts et al., 1998). Observations with polarized filters reveal that the “fingerprint” patterns related to the chiral nematic phase were deformed when the shear rate was increased and totally disappeared with an applied high shear rate (Shafiei-Sabet et al., 2014).

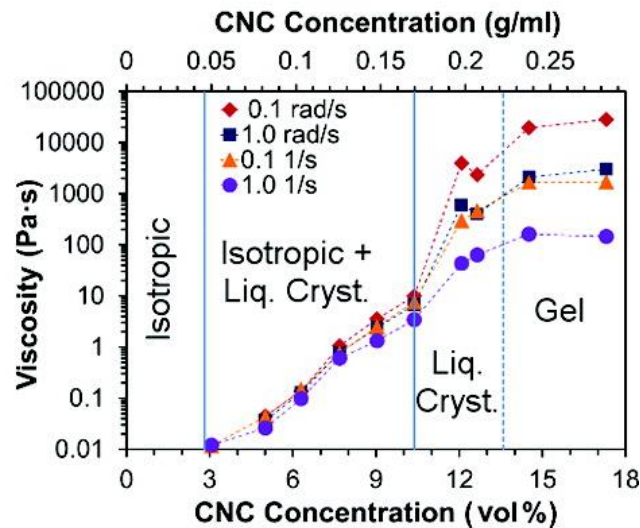


**Figure 26:** Viscosity versus CNCs concentration at different frequency (Ureña-Benavides et al., 2011).

Ureña-benavides et al. (Ureña-Benavides et al., 2011) studied cotton CNCs suspension at different concentrations, and proposed a phase diagram relevant for each CNCs suspension (Figure 26). They identified several critical concentrations in this diagram which separate each liquid crystal behavior. At less than 3 vol% the suspension is full isotropic. Between 3 and 10 vol% a biphasic domain composed with isotropic and liquid crystals appears. Up to 10 vol% the fraction of liquid crystalline phase increases until a full chiral nematic structure appears (at 12.1 vol% with fingerprint texture), and finally forms a gel at 14.5 vol% (a random texture with bright colours). This critical concentration depends on the aspect ratio of the CNCs.

A broad range of publications investigated the suspension concentration, ionic strength, temperature, or ultrasonic effect on rheological behavior of CNCs suspensions. **Table 2** is an overview of different publications which investigated CNCs suspension concentration in relation to the cellulose source. A recent review by Oguzlu et al. in 2017 summarizes different works on CNCs from wood and their rheological behavior (Oguzlu et al., 2017).

**Table 2:** Overview of publications that investigated the CNCs rheological behavior since 2000

Cellulose source	Aspect ratio	CNCs concent. (NaCl amount)	Comments	References
<b>Tunicin</b>	~140	0 to 0.85 wt% <sup>i</sup> 1 to 3.5 wt% <sup>a</sup>	<sup>i</sup> : Newtonian viscosity regime with CNC orientation at high shear rate. <sup>a</sup> : 3 regions viscosity behavior	(Bercea and Navard, 2000)
<b>Cotton</b>	~17	1 to 3 wt% <sup>a</sup>	3 regions behavior description	(de Souza Lima and Borsali, 2004)
	~12	3.07 vol% <sup>i</sup> 6.99 vol% <sup>a</sup> 12.1 to 17.3 vol% <sup>g</sup>	<sup>i</sup> : Newtonian <sup>a</sup> : 3 regions viscosity behavior <sup>g</sup> : shear thinning & gel form <i>Low impact of the temperature</i>	(Ureña-Benavides et al., 2011)
<b>Cotton &amp; Switchgrass</b>	~13 ~39	0.75 to 5.2 wt% 0.5 to 3.7 wt%	Both CNCs displayed 3 different regimes in a viscosity–concentration graph with 2 critical concentrations: overlap and gelation point <b>L/D switchgrass CNC &gt; L/D cotton CNCs → switchgrass CNC formed a liquid crystal structure and hydrogel at lower concentrations than cotton CNCs</b>	(Wu et al., 2014)
<b>Wood</b>	~40	0.25 to 1 g/dL <sup>i</sup> (0 to 10 mM)	Shear thinning behavior starts at 1 g/dL ↗ of NaCl in suspension → η ↘	(Boluk et al., 2011)
	~15	3 wt% <sup>i</sup> 5 & 7 wt% <sup>a</sup> 10 wt% <sup>g</sup>	<sup>i</sup> : Newtonian <sup>a</sup> : 3 regions viscosity behavior <sup>g</sup> : shear thinning & gel form ↗ T°C for <sup>i</sup> and <sup>a</sup> → ↗ η ↗ T°C for <sup>a</sup> → no effect <i>After sonication, ↘ η (↘ aggregates)</i>	(Shafiei-Sabet et al., 2012)
	~15	1 to 15 wt% <sup>i, a, g</sup> (0 to 10 mM)	<sup>i</sup> : ↗ NaCl → ↘ η <sup>a</sup> : up to 5 mM NaCl → ↘ chiral nematic domains so ↘ η <sup>g</sup> : ↗ NaCl → ↘ η due to interference between CNC connection	(Shafiei-Sabet et al., 2014)
	~14	1 to 12 wt% <sup>i, a, g</sup> (0.001 to 1 M NaCl)	Same results than (Shafiei-Sabet et al., 2012) pH <2 and >10 → ↗ η Phase diagramme: CNCs concentration VS NaCl concentration	(Xu et al., 2017b)
<b>CNF</b>	~10	0.91 wt% <sup>i</sup> 2.03 & 3.17 wt% <sup>a</sup>	3.17 wt% present a gel structure and films from this suspension are iridescent.	(Liu et al., 2011a)
	~27 ~45	1 to 6 wt% <sup>i, a</sup>	Shear rate > Critical value → breakup of CNCs aggregates <i>Reversible process</i>	(Xu et al., 2017a)
	<sup>a</sup> : anisotropic	<sup>g</sup> : Gel	<sup>γ</sup> : Shear rate	<sup>η</sup> : viscosity

### 1.2.3. CNCs suspension behavior in polymer solution

Numerous works discussed the interaction between cellulose nanocrystals and soluble polymers (CMC, PEO, HEC, PVA, POEGMA, PNIPAM, Agarose, glycerol...). The following present recent works on this topic where rheological behavior is discussed.

The addition of macromolecules or polymers into CNC suspensions can be characterized by adsorption or non-adsorption. In this kind of suspension, the presence of polymer chains and CNCs particles can induce two types of steric interactions (Fleer et al., 1993). First, bridging can appear in suspension with CNCs acting as a crosslinker when adsorption between CNCs and the polymer occurs (De France et al., 2016; Le Goff et al., 2015; Yang et al., 2013; Zhou et al., 2011). In some cases, the suspension can turn into a gel form with shear thinning properties due to the presence of CNCs (Oguzlu and Boluk, 2016; Oguzlu et al., 2016). Secondly, in the case of sufficient amount of polymer molecules, phase transition and phase separation occur as a result of depletion of colloidal particles (Edgar and Gray, 2002; El Kissi et al., 2008; Sieglauff, 1959).

Recent works from Oguzlu et al. (Oguzlu and Boluk, 2016; Oguzlu et al., 2016, 2017) investigated the synergic effect of carboxymethyl Cellulose (CMC) on a CNC suspension (isolated from wood) in dilute and semi-dilute polymer solutions. **Figure 26** shows the major results of their publications. By adding 0.5 to 3 wt% of CMC (700 kDa) in a dilute CNCs suspension (0.67 vol%) a gel is formed by bridging between semi-rigid CMC and rigid CNCs. When these samples were turned upside down the suspension did not flow, and were suspended from the top (the stirred magnet is trapped inside these gels) (**Figure 26a and b**). Up to 2 wt% of CMC two phases appear and induce polymer depletion because of the higher amount of polymer compared to the surface area of the CNCs. The top phase is rich in CNCs and bottom poor. In **Figure 26c** it is shown that the CMC solution presents a near Newtonian rheological behavior, but with the addition of a small amount of CNCs (0.5 to 4 vol%) the viscosity at low shear rate drastically increases (about five decades). An important shear thinning behavior appears when shear rate increases with the addition of any concentration of CNCs. This is due to CNCs aligning in the direction of the flow. The shear-thickening behavior at low shear rates comes from the entanglement of polyelectrolyte chains which dominate the CNCs rheological behavior.

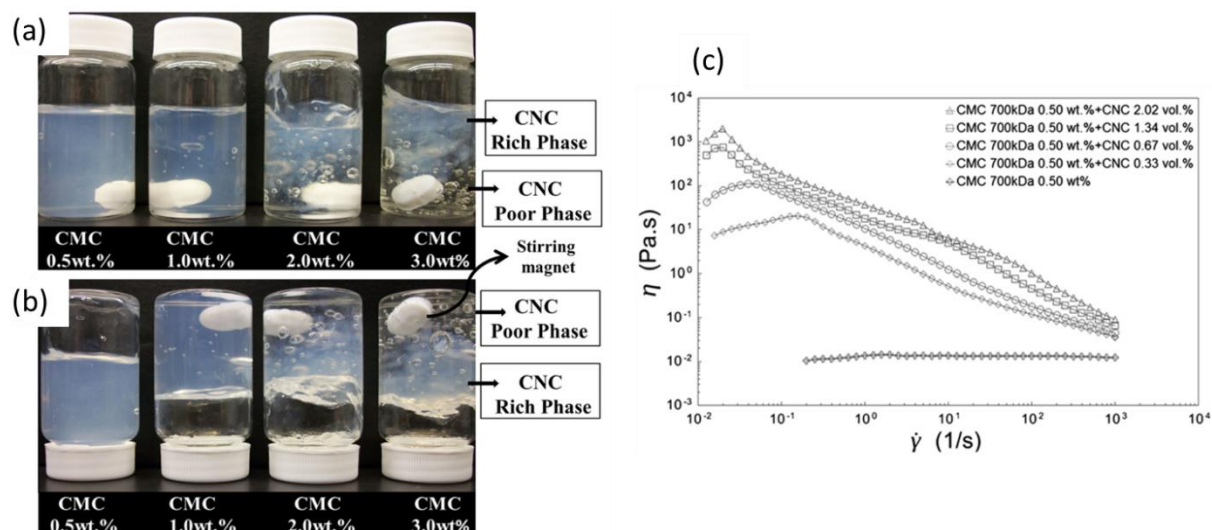


**Figure 26:** Photographs of 0.67 vol% CNC suspensions in CMC (700 kDa) solutions. Vials are in (a) upward position and (b) 180°rotated position. (c) Steady state shear viscosities of various CNC suspensions with 0.5% CMC addition measured at 25 °C(Oguzlu et al., 2017)

Hydroxyethyl cellulose (HEC) with CNC suspension was explored by Boluk et al.(Boluk et al., 2012) and presented similar results to what was previously reported. An addition of rod-shaped nanoparticles in a semi-dilute HEC solution caused weak gels and significantly altered the viscoelastic properties and shear flow behavior of these suspensions in a similar manner to CMC.

In the case of polyethylene oxide (PEO), the same researcher group (Oguzlu and Boluk, 2016) showed that no synergetic effect on rheology appears between CNCs and PEO. Isotropic-nematic phase transition for a maximum of 2 wt% of CNCs with 5 wt% of PEO was observed. After saturation of the PEO chains, weak depletion interactions occurred in the CNC suspension.

A recent work of Chen et al. in 2017 (Chen et al., 2017) investigated the rheological effect of CNCs in a poly(vinylalcohol) (PVA) polymer solution. PVA has a flexible chain structure and is comparable to aqueous CMC with a semi-rigid chain structure. The concentration of PVA solution was 10 wt% (same viscosity of a CMC solution at 1 wt%) and CNCs addition occurred between 0.1 and 3 wt%. In both cases, CNCs were well dispersed in the polymer solution. The flexibility of the PVA chains had a stronger interaction with CNCs compared to the CMC polymer, which induced a lower percolation threshold of CNCs in a PVA aqueous solution. Gel formation is caused by the flocculation of CNCs and polymer.

In 2014, McKee et al. (McKee et al., 2014) proposed a thermo-responsive bio-based gel system based on CNCs physically bound with methylcellulose (MC). MC has a LCST between 40 and 50°C. **Figure 27** shows an overview of the published results.

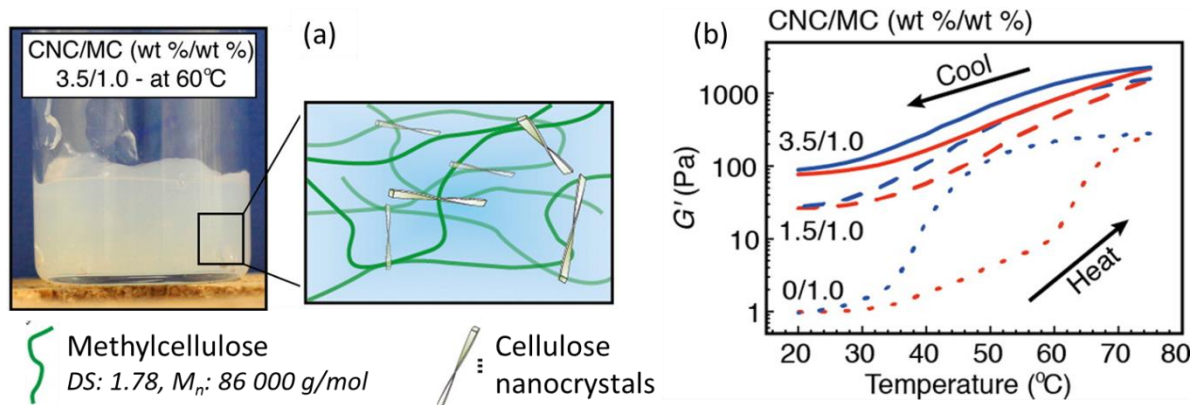


**Figure 27:** (a) Photograph showing gelation of the sample CNCs/MC 3.5 wt%/1.0 wt% at 60°C and schematic presentation of the MC cross-linked with CNCs. (b) Cyclic heating of the samples with 0, 1.5, and 3.5 wt% CNCs loading while keeping a fixed amount 1 wt% of methyl cellulose (MC), where  $G'$  was determined at an angular frequency of 6.283 rad/s and 2.0% strain with a temperature ramp of 2.5°C per minutes (adapted from (McKee et al., 2014)).

In this work, 1 wt% of MC was dissolved in a CNCs aqueous suspension with a concentration up to 3.5 wt% at 20°C and always presented a homogenous suspension. The storage modulus ( $G'$ ) was then tunable from 1 to 75 Pa. Above the LCST, a distinct gel form is obtained (**Figure 28a**). At 60°C, by increasing the CNCs content  $G'$  increases from 100 to 900 Pa and presents thermo-reversibility (**Figure 28b**). By changing the CNCs concentration and temperature, the storage modulus of the nanocomposite hydrogels could be modified over a broad range with three orders of magnitude: from 1 Pa (20°C) to 2200 Pa (75°C) with a fixed amount of MC (1 wt%).

*This section has reported a part of the recent studies on cellulose nanocrystals rheological behavior. This section ends with the rheological impact of CNCs and polymer together in a suspension. Interesting results were shown, but to link with an industrial objective, CNCs and polymer have been able to be used in high added values materials. Different systems can be imagined as reported in first chapter of this state of the art section (tissues engineering, bones scaffolds, drug delivery, wound dressing, packaging, cosmetics...). In this Ph.D., efforts*

*were focused on hydrogels composed with CNCs and thermo-sensitive polymers to create injectable hydrogels for surgery applications.*

The following section will propose an investigation on stimuli-responsive polymers and particularly thermo-sensitive polymers. Then, their combination with CNCs to produce hydrogels will be detailed.

### III. Cellulose nanocrystals and stimuli-responsive applications

#### 3.1. Stimuli-responsive polymers

The concept of a “smart” material is commonly based on the presence of a stimuli-responsive polymer. Stimuli-responsive polymers are polymers with properties designed to sharply and quickly respond to small environmental changes (physical or chemical). These behaviors are dictated by the functional groups present within or on polymer chain. At the macromolecular level, polymer chains can be modified in different ways such as, hydrophilic-to-hydrophobic balance, conformation, solubility, degradation, and bond cleaving. Over the past 20 years several fields of material applications were innovated by using these polymers. A large library of functional polymers has been studied in biomedical applications for bio-sensing diagnostics, drug delivery, tissue engineering (regenerative medicine), cell culture, or smart coatings. This is highlighted by a large variety of reviews (Alarcón et al., 2005; Bawa et al., 2009; Cabane et al., 2012; Hoffman, 2013; Reineke, 2016; Schattling et al., 2014; Wei et al., 2017).

In the present chapter, we will focus only on stimuli-responsive polymers soluble in aqueous solutions. **Figure 28** presents the most commonly used stimuli in literature and a selection of polymers and functional groups which exhibit stimuli-responsive behavior.

##### ***Stimulus: Photo - UV - light***

These polymers are sensitive to light exposure at a specific wavelength. The whole light spectra from the UV to infrared can allow a diversity of stimuli which is not accessible by any other stimulus. Exposure time and intensity are additional level of control. The light can be directly used at the surface of the polymer or through tissues without damage on human cells (biological-friendly applications). Common examples of photo-responsive polymer contain light-sensitive chromophores such as azobenzene groups (Jochum and Theato, 2009; Mahimwalla et al., 2012), spiropyran groups (Pietsch et al., 2011), or nitrobenzyl groups (Li et al., 2010).

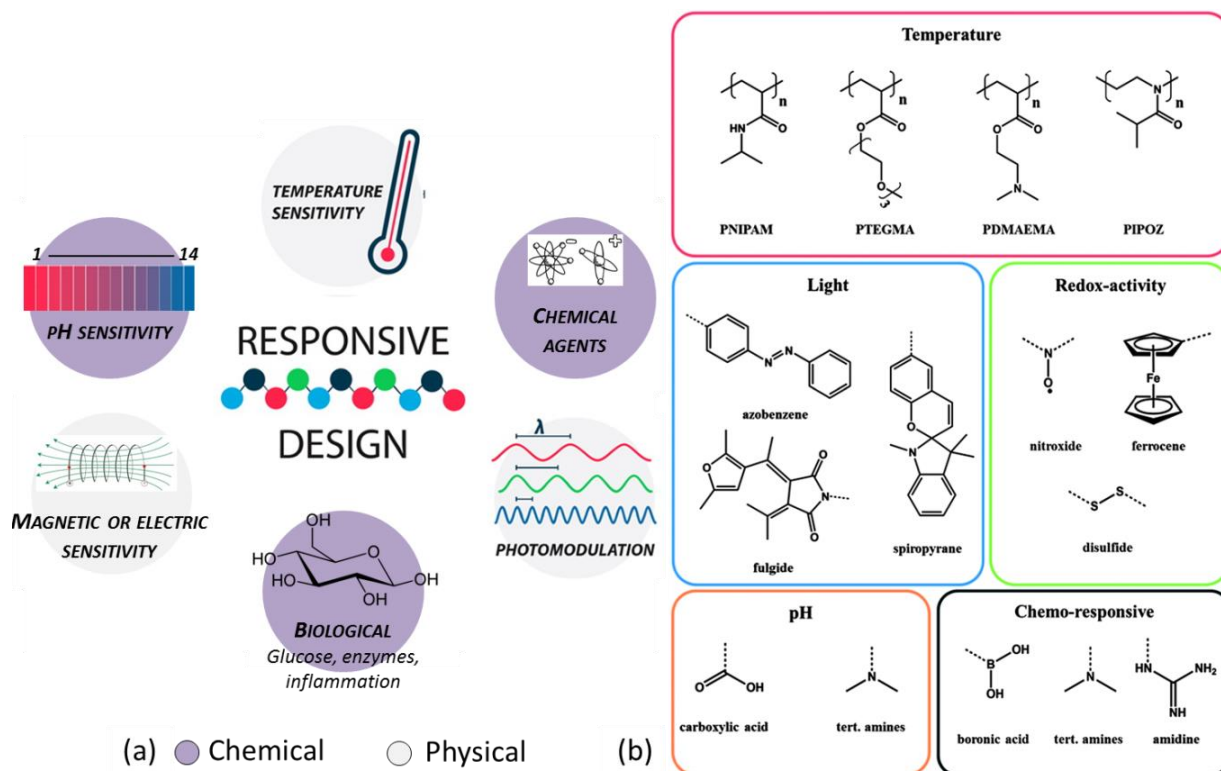


**Figure 28:** (a) Classification of stimuli for stimuli-responsive polymers (adapted from (Reineke, 2016)). (b) Selection of important polymers and functional groups, exhibiting stimuli-responsive behavior (Schattling et al., 2014)

### Stimulus: pH

A polymer is pH responsive if it has the capability to donate or accept protons during a pH environmental modification. The pH adjustment triggers ionic interactions on the polymer which leads to extending or collapsing of the polymer chain in aqueous media (Dai et al., 2008). Typical pH responsive polymers which exhibit very abrupt protonation-deprotonation functionalities are carboxylic and amino groups (Lee and Shim, 1997; Way et al., 2012), poly(acrylic acid) (Li et al., 2008), or chitosan (Abdelaal et al., 2007).

### Stimulus: redox responsive

A redox stimulus is defined as an electrochemical address of the redox-sensitive group, which causes a change in its oxidation state. Some polymers can react to electric impulses and oxidize or reduce inducing a hydrophilic/phobic inversion like with ferrocene (Mazurowski et al., 2012) or disulfides (Phillips and Gibson, 2012). For example, polymers with disulfide groups are degraded when exposed to cysteine or glutathione, which are reductive amino-acid based molecules (Matsumoto et al., 2008). An interesting redox polymer, or chemical pacemaker, is Poly(NiPAAm-co-Ru(bpy)<sub>3</sub>) (Yoshida et al., 1999). The

self-oscillation redox reaction of the  $\text{Ru}(\text{bpy})_3$  modified the hydrophobicity and the hydrophilicity properties of the polymer like a heartbeat.

### ***Stimulus: chemical responsive***

These stimuli-responsive polymers are sensitive to chemical changes in the environment. Boronic acid is an example. It is sensitive to diols, and has a particular application in a reaction with glucose (Elmas et al., 2007; Pasparakis et al., 2009; Xu et al., 2012). The diol sensitivity is based on the existence of a neutral form and an anionic form of boronic acid. In the neutral form boronic acid is hydrophobic. The anionic species can link diols in a reversible reaction inducing an increase of the polymer hydrophilicity. Alginate can be another example which uses the presence of cations to completely modify its behavior by crosslinking.

### ***Stimulus: temperature***

Thermo-responsive polymers are sensitive to a change in external temperature. They have attracted high interest from researchers and industries because these stimuli can easily be applied externally to the system. A large variety of applications using this stimuli in aqueous solvent exists such as tissue engineering (Zhang et al., 2012), drug delivery (Bawa et al., 2009; Schmaljohann, 2006), catalysis (Liu et al., 2010), surface engineering (Hakalahti et al., 2016; Xue et al., 2013; Zoppe et al., 2011), or information processing (Roth et al., 2010; Schattling et al., 2011). Recent reviews propose an overview of potential applications (Reineke, 2016; Schattling et al., 2014; Wei et al., 2017).

These polymers are characterized by a lower or upper critical solution temperature (LCST or UCST) around which the hydrophilic and hydrophobic interactions between the polymer and the aqueous media sharply change in a small range of temperature. **Figure 29** shows schematically this transition. This phenomenon is driven by entropy to minimize the system's free energy. Water molecules of the aqueous media associated with the side-chain isopropyl functionalities are released into the aqueous suspension when the temperature crosses a critical value. The polymer chain collapses or expands after this critical temperature.

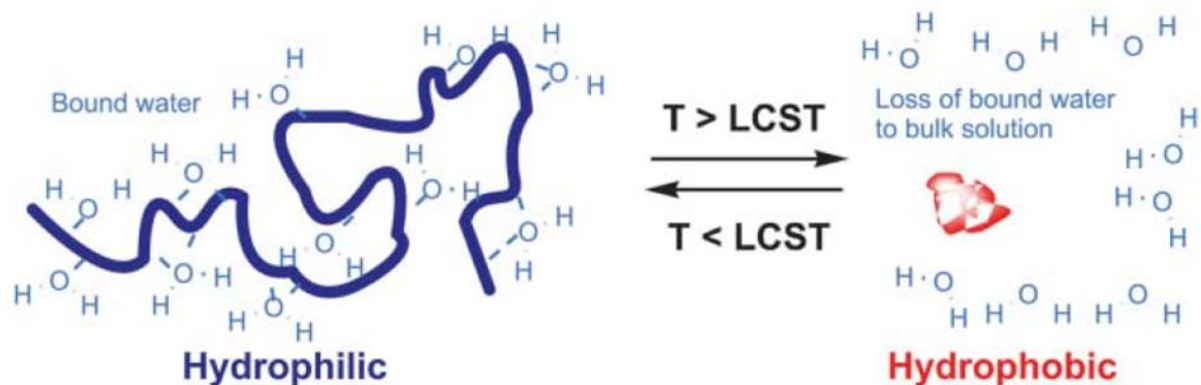


**Figure 29:** Schematic behavior of a thermo-sensitive polymer with a Lower Critical Solution Temperature (LCST) (Alarcón et al., 2005)

**Table 3** shows a list of polymers having a LCST in water.

One of the most studied synthetic thermo-sensitive polymer is Poly(N-isopropylacrylamide) (PNIPAM), which presents a sharp coil-globule transition in water at 32°C. Below this temperature, the polymer chains are in a swollen coil conformation with highly hydrated chains. Above the LCST, PNIPAM becomes more hydrophobic and turn into a collapsed globule (Lai et al., 2013; Plunkett et al., 2006; Schild, 1992). The fact that the LCST of PNIPAM is close to physiological temperature whatever the length is (Okahata et al., 1986) make PNIPAM-based materials particularly relevant for biomedical applications (Alosmanov et al., 2017; Chen et al., 2014b; Pentlavalli et al., 2017).

**Table 3:** Polymers presenting a LCST in water (adapted and completed from (Jeong et al., 2002))

<i>Polymer</i>		<i>LCST (°C)</i>
Poly(N-isopropylacrylamide)	<i>PNIPAM</i>	~32
Poly(acrylamide) derivated		22-72
Poly(vinyl methylether)	<i>PVME</i>	~40
Poly(ethylene glycol)	<i>PEG</i>	~120
Poly(propylene glycol)	<i>PPG</i>	~50
Poly(methacrylic acid)	<i>PMAA</i>	~75
Poly(vinyl alcohol),	<i>PVA</i>	~125
Poly(vinyl methyl oxazolidone)	<i>PVMO</i>	~65
Poly(vinyl pyrrolidone)	<i>PVP</i>	~140
Poly(silamine)		~37
Methylcellulose	<i>MC</i>	~80
Hydroxypropylcellulose	<i>HPC</i>	~45
Polyphosphazene derivatives		33-100
Poly(N-vinylcaprolactam)	<i>PNVCL</i>	25-35
Poly(siloxyethylene glycol)		10-60
Jeffamine®		16 or 65
Poly(ethylene oxide)	<i>PEO</i>	~120
Poly(propylene oxide)	<i>PPO</i>	~50
Pluronic, Poloxamers, Tetronics	<i>PEO-PPO co-polymers</i>	20-85
Poly (ethylene glycol) methacrylate	<i>PEGMA</i>	~25

### 3.2. CNCs and Stimuli-responsive polymers

The **third challenge** of this Ph.D. is to combine cellulose nanocrystals and thermo-responsive polymers to create a “smart” system. The goal is to create these systems via simple green chemistry and investigate the rheological behavior. The interest of the scientific community is schematically presented in **Figure 30** with publications published before and after the beginning of the present Ph.D. on CNCs and stimuli-responsive polymers.

This section will discuss CNCs and stimuli-responsive polymer systems present in literature, followed by a focus on the thermo-responsive system which inspired this Ph.D.

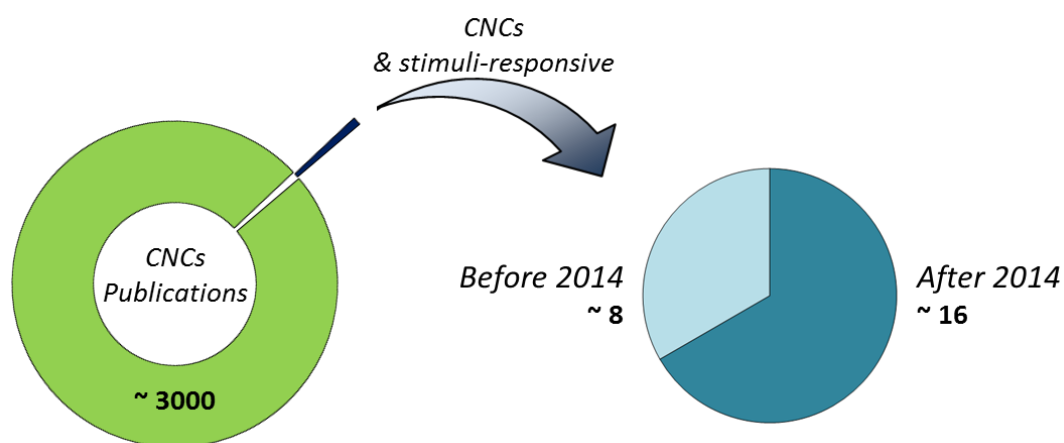


**Figure 30:** schematic representation of number of publication on CNCs and stimuli-responsive dated before and after the beginning of the present Ph.D. (data extracted from ACS scifinder from 1980 to June 2017).

The previous section described the interest in material science to use stimuli-sensitive polymers to create smart materials. In order to create bio-compatible and bio-based systems, nanocelluloses are good candidates to use in these materials. In fact, due to their abundance, high specific area, biodegradability, and large amount of reactive hydroxyl groups on the surface (described in Section I), CNCs are an exceptional candidate for smart materials. **Table 4** presents recent progress in this field of material science since 2010. UV light, pH, and temperature are presented in this table.

**Table 4:** publications dealing with stimuli-responsive system based on CNCs in aqueous media (publications, which are present in different categories, propose dual responsive system).

Stimuli	Polymers	Synthesis method	Intended Applications	References
Photo (UV)	PNIPAM-EANI	ATRP	Sensor	(Wu et al., 2015)
	PAMAM	Amidation	Sensors & nano-reactors	(Chen et al., 2015b)
	Coumarin Anthracene	Click	Sensor Photosensible nanoarrays	(Filpponen et al., 2011)
	FITC & RBITC	Reaction in NaOH	Sensors	(Nielsen et al., 2010)
pH	PNIPAM-AA	RAFT	Drug delivery	(Haqani et al., 2017)
	PNIPAM-EANI	ATRP	Sensor	(Wu et al., 2015)
	PAMAM	Amidation	Sensors & nano-reactors	(Chen et al., 2015b)
	NIPAM-AA	RAFT	-	(Zeinali et al., 2014)
	Polyrhodamine	FRP	pH sensor	(Tang et al., 2014a)
	P4VP	CAN	Separation processes (remove pharmaceuticals from wastewater)	(Kan et al., 2013)
	Carboxylic and amine ends	-	Sensors	(Way et al., 2012)
	PNIPAM – TEMPO	FP	-	(Cha et al., 2012)
	PNVCL	ATRP	-	(Zhang et al., 2017)
	PNIPAM	FRP	Wound dressing	(Zubik et al., 2017)
Temperature	PNIPAM-AA	RAFT	Drug delivery	(Haqani et al., 2017)
	Jeffamine	Peptidic grafting	-	(Azzam et al., 2010, 2016)
	POEGMA	FRP	-	(Grishkewich et al., 2016)
	PNIPAM - Clay	FRP	Drug delivery	(Chen et al., 2015c)
	PNIPAM-EANI	ATRP	Sensor	(Wu et al., 2015)
	NIPAM-AA	RAFT	-	(Zeinali et al., 2014)
	PNIPAM	LRP	Injectable hydrogel	(Hemraz et al., 2014)
	PNIPAM	IPN	Injectable hydrogel	(Hebeish et al., 2014)
	MC	Adsorption	-	(McKee et al., 2014)
	PNVCL	FP	-	(Sanna et al., 2013)
	PNIPAM – TEMPO	FP	-	(Cha et al., 2012)
	PNIPAM	SET-LRP	Sensor	(Zoppe et al., 2010, 2011)
	PDMAEMA	ATRP	-	(Yi et al., 2009)

PNIPAM: poly(*N*-isopropylacrylamide)

AA: Acrylic acid

POEGMA: poly(oligo(ethylene glycol) methacrylate)

P4VP: Poly(4-vinylpyridine)

PDMAEMA: poly(*N,N*-dimethylaminoethyl methacrylate)

RAFT: reversible addition fragmentation chain transfer

FRP: Free-radical polymerization

LRP: living radical polymerization

ATRP: atom transfer radical polymerization

CAN: Ceric-ion-initiated radical polymerization

IPN: interpenetrated network

PNVCL: Poly (*N*-vinylcaprolactam)

FP: frontal polymerization

SET-LRP: Single Electron Transfer-Living Radical Polymerization

EANI: 4-Ethoxy-9-allyl-1,8-naphthalimide

TEMPO: carboxylated CNCs

PAMAM : Poly (amidoamine)

MC: methylcellulose

The most popular thermo-sensitive polymer is Poly(*N*-isopropyl)acrylamide (PNIPAM). This polymer presents a commercial availability with different chemical terminations. It was chosen for biomedical applications possibilities in an injectable system.

An interesting work developed by Hemraz et al. in 2014 (Hemraz et al., 2014) investigated the rheological behavior of systems based on PNIPAM grafted on CNCs via living radical polymerization (reaction developed in Section §1.2.4.). This grafting process was published by Zoppe et al. in 2010 (Zoppe et al., 2010). Depending on the ratio between grafting initiator and monomer the grafting density and the polymer length can be tuned. In the work of Hemraz et al. two cases are presented: one with a high grafting density, but high steric hindrance (**Figure 31C, NIPAAm-CNC1**), and one with a low grafting density, but with low steric hindrance (**Figure 31D and E, NIPAAm-CNC2**).

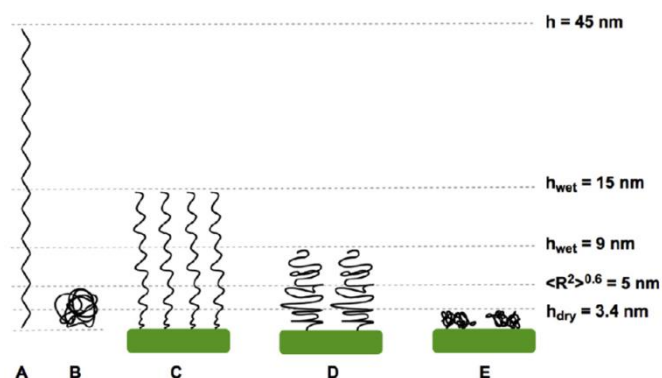


**Figure 31:** Schematic illustration of conformations of PNIPAM chains with length noted on the right side. (A) Fully elongated polymer; (B) swollen polymer; (C) wet thickness of polymer on NIPAAm-CNC1 and (D) on NIPAAm-CNC2; (E) dry film thickness of polymer on NIPAAm-CNC2 (Hemraz et al., 2014).

Grafting efficiency was validated by elemental analysis, infrared transmission, and X-ray photoelectron spectrometry analysis. **Figure 32** shows very promising results in the rheological properties of such suspensions. The dynamic storage modulus ( $G'$ ) is presented in both cases and the physical behavior is changing at and above the LCST. **Figure 32A** shows NIPAAm-CNC1, corresponding to a high grafting density. A small temperature effect is noted, but because of steric hindrance the system does not have the area to collapse and form a gel. After crossing the LCST the entanglement is not totally reversible. **Figure 32B** presents NIPAAm-CNC2 with a lower grafting density. In this promising case,  $G'$  changes from 0.003 Pa to 15 Pa under and above the LCST respectively. This system is totally reversible via

temperature stimuli. Nonetheless, the drawback of this hydrophilic/hydrophobic system is a phase separation above the LCST.

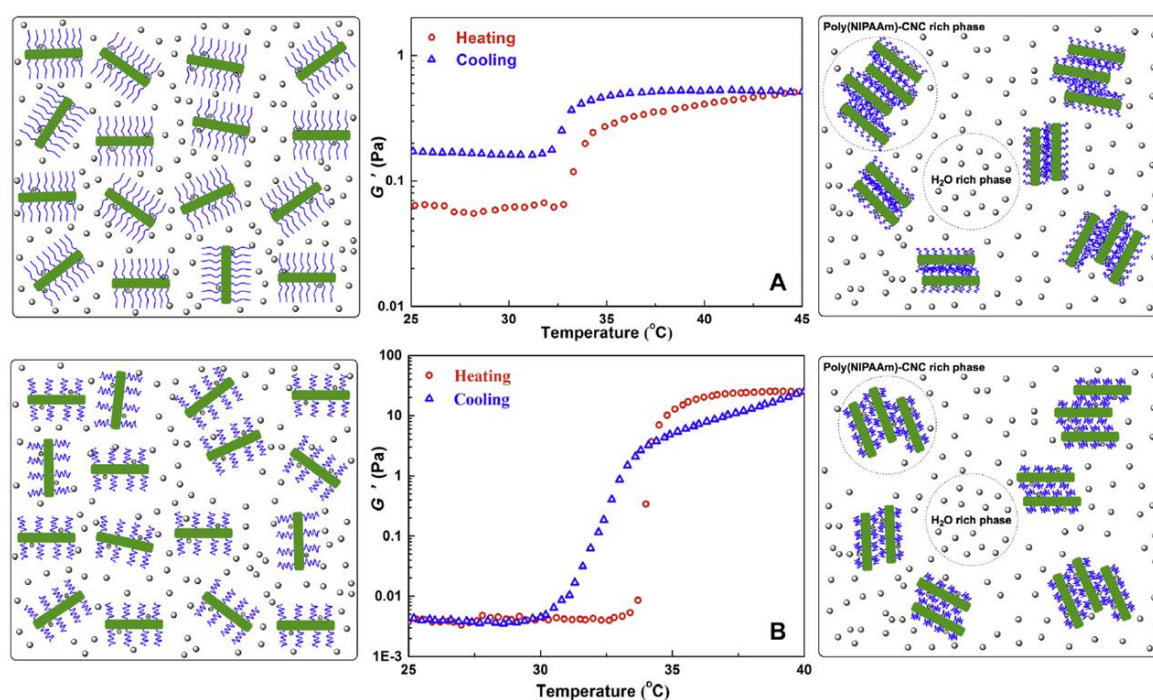


**Figure 32:** Dynamic storage modulus ( $G'$ ) as a function of temperature in a heating and cooling process for 1.0 wt% NIPAAm-CNC1 (A) and 3.0 wt% NIPAAm-CNC2 (B) suspensions at a rate of  $1^\circ\text{C}/\text{min}$  and oscillation frequency of 6.4 Hz (Hemraz et al., 2014)

In order to respect the first challenge (namely *green chemical modification of CNCs*) the publications of Azzam et al. (Azzam et al., 2010, 2016) used the same grafting process that in this Ph.D. project with PNIPAM. Indeed, Azzam et al. grafted Jeffamine<sup>®</sup> on CNCs via amidation of polymer  $-\text{NH}_2$  termination on TEMPO CNCs (source cotton). The grafting process is described in section §1.2.4. They proved the grafting efficiency via infra-red transmission and  $^{13}\text{C}$  solid state NMR. This system presents very good colloidal stability in organic solvent (due to polymer stability and steric repulsion) and in presence of electrolyte in aqueous media. At a concentration up to 1 wt% a thermo-reversible gelation occurs (proved by viscoelastic measurements and dynamic light scattering on **Figure 33c**), and is attributed to the formation and disruption of aggregates formed above the polymer LCST. This system presents multi-responsive properties: temperature, pH, and ionic strength. **Figure 33** shows an overview of results obtained during this work.

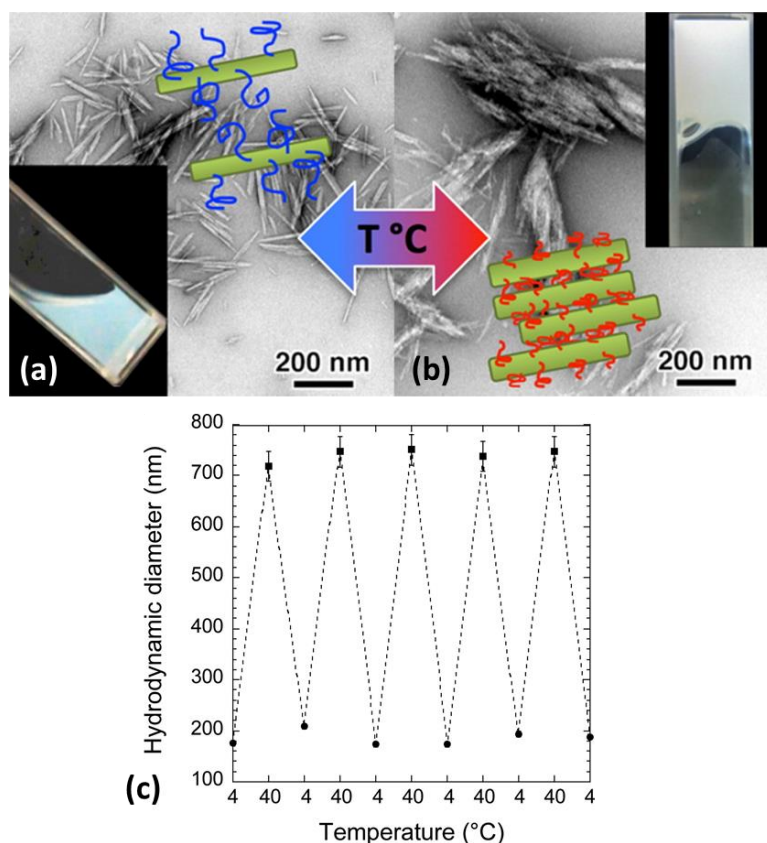


**Figure 33:** CNCs grafted with Jeffamine (a) under the LCST and (b) above the LCST with TEM image in the background and photos of the visual system. (c) Hydrodynamic diameter variation exhibited by a 0.5 wt % system in aqueous suspension submitted to 4°C- 40°C-4°C temperature cycles. Dotted lines were added as guides (Azzam et al., 2016).

A second option developed in this Ph.D. is the adsorption of thermo-sensitive polymer on CNCs and TEMPO CNCs. PNIPAM was investigated in the following chapter and another block polymer poly(di(ethylene glycol)methyl ether methacrylate) (PDEGMA). This second part of the project was conducted in collaboration with Anna Carlmark and co-workers based on one of their publications in 2013 (Larsson et al., 2013).

In the study of Larsson et al. (Larsson et al., 2013), three block copolymers, containing a thermo-responsive block based on poly(di(ethylene glycol) methyl ether methacrylate) (PDEGMA with a LCST tuned between 26 and 28°C) and a quaternized poly(2-(dimethylamino)ethylmethacrylate) (PDMAEMA) polyelectrolyte block, were synthesized via ATRP (Figure 34a). A complete study of the block copolymer was done (polyelectrolyte titration, size exclusion chromatography, and dynamic light scattering). These polymers were then adsorbed on carboxylate CNF proved by QCM-d measurement. Thermo-responsive behavior was shown by visual inspection of suspensions under and above the LCST

(Figure 34b). In conclusion, a thermo-reversible system based on nanocellulose without any chemical modification of the cellulose surface was developed. One drawback is the phase separation above the LCST. Via optimization of the density and colloidal stability of this system a thermo-sensitive hydrogel could be produced just by mixing polymers and negatively charged nanocellulose.

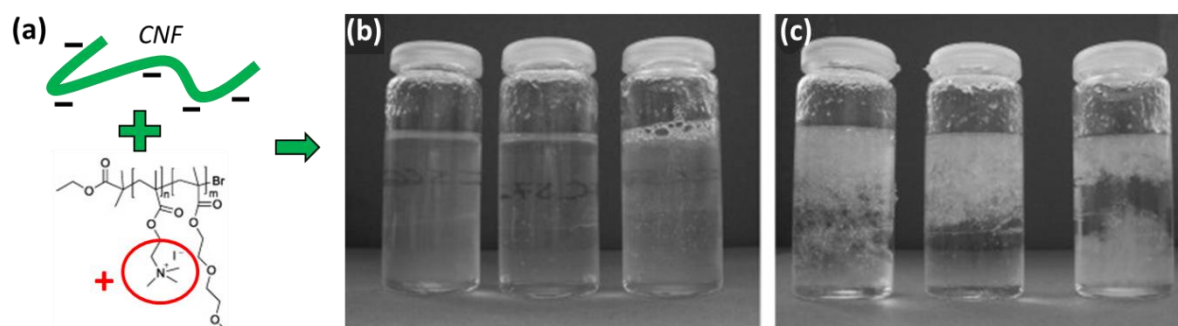


**Figure 34:** (a) Schematic CNF and copolymer block adsorption, (b) Image of modified NFC in aqueous solutions, with increasing molecular weight of the PDEGMA block from left to right, below LCST and (c) Same system above the LCST (Larsson et al., 2013).

To our knowledge, the copolymer block has never been tested onto CNCs or TEMPO CNCs. In this Ph.D., it was proposed to study the development of thermo-responsive hydrogels with a copolymer block onto CNCs, and an investigation of the potential applications for the stimuli-responsive systems.

### 3.3. Cellulose based stimuli-responsive hydrogels and applications

The **fourth challenge** of this Ph.D. is to use a thermo-responsive hydrogel based on CNCs in “smart” and high added value applications. This section describes major fields which use hydrogels for “smart” applications. Applications of interest for this system will further be identified, such as biomedical applications.

A gel is tri-dimensional network of solid dispersed and connected in fluid. It presents an elastic structure. A hydrogel is a class of gel with the capacity to absorb large amounts of water in aqueous conditions. This capacity is due to an abundant presence of hydrophilic groups on the hydrogels’ components (example: CNCs). In particular, cellulose-based hydrogels exhibit interesting properties such as biocompatibility and biodegradability. A lot of reviews present different fields of “smart” applications for hydrogels comprised of

cellulosic material (Chang and Zhang, 2011; De France et al., 2017; Lin and Dufresne, 2014; Qiu and Hu, 2013; Sannino et al., 2009). These reviews present two main types of gels: covalently linked hydrogels and physical hydrogels. Both have the capacity to swell and release water. The first one exhibits a crosslinked network and will be never dissolved in a solvent. The second one is based on physical interactions between polymers (as entanglement), and could be dissolved in a sufficient amount of time in a solvent.

The smart behavior of some cellulose derivatives in response to physiological stimuli (such as pH, ionic strength, temperature) paves the way for *in vivo* applications of the resulting hydrogels. Hydrogels can be ideal platforms for the design of scaffold biomaterials in the field of tissue engineering and regenerative medicine. **Figure 35** presents a list of several applications based on a cellulose derivative structure. Biomedical applications are in highlighted in green and other industrial applications are in blue.

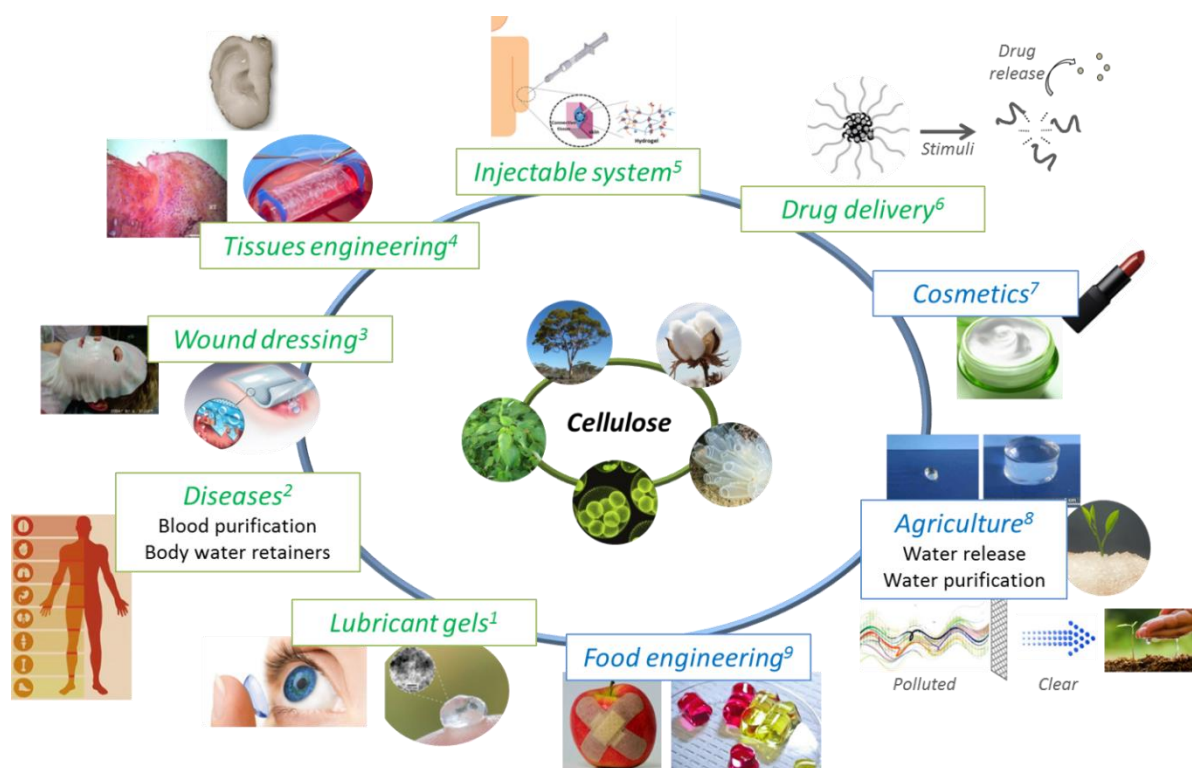


**Figure 35:** Illustration of several cellulose nanocrystals hydrogel fields of applications

<sup>1</sup>**Lubricant gels** can be used like water or release drugs depending on the pH stimuli contact length, ophthalmic materials, and joint surgery (Valle-Delgado et al., 2016). <sup>2</sup>**Diseases:** cellulose based hydrogels can be used for blood purification (Ye et al., 2003), as a stomach bulking agent (Sannino et al., 2006), personal hygiene superabsorbent (Sannino et al., 2004),

and body water retainers in cases of disease with renal edemas for example. Hydrogels can release water in a particular pH stimuli to heal a special area in body (pH of intestine is 6-7 while stomach is 1) (Esposito et al., 2005). <sup>3</sup>**Wound dressing**: this corresponds to the development of biological substitutes that restore or improve tissue functions when applied to the wound. An active molecule or water can be released in presence of external stimuli such as pH changes due to injury or temperature increased caused by the inflammatory response (Czaja et al., 2007; Sannino et al., 2003). <sup>4</sup>**Tissue engineering**: these cellulose based hydrogels are produced to mimic and replace degraded tissues such as skin, bones, soft tissues, cartilages, menisci, and sometimes organs (ear) (Domingues et al., 2014; Naseri et al., 2016; Nimeskern et al., 2013). Cellulose and polymers are mixed together to create a matrix which can be a template for regenerative medicine. For example, BIOMEDICAL TISSUES<sup>®</sup> is a start-up which produces dental and skin tissue using cellulose. <sup>5</sup>**Injectable system**: these hydrogels are often based on stimuli-responsive polymers to facilitate injection. PNIPAM is the commonly used in this application (referred to in the previous section §3.1). Hyaluronic acid is considered to be one of the best polymers for hydration and regeneration of body cells. This application is highly represented in recent publications (De France et al., 2016; Domingues et al., 2015; Yang et al., 2013) and in industrial products (Vivacy<sup>®</sup>, LIOAD<sup>®</sup>, BIOMATLANTE<sup>®</sup>). <sup>6</sup>**Drug delivery**: this concept based upon the trapping of drug molecules in a hydrogel matrix composed with nanocellulose and stimuli-responsive polymers. When the external stimuli is applied the system “opens” and releases medications in the desired location (Lin et al., 2016; Pal et al., 2006; Tomatsu et al., 2011). <sup>7</sup>**Cosmetics** are a field of application for hydrogels due to the shear thinning properties of CNCs (Fei et al., 2000). <sup>8</sup>**Agriculture**: water release can be based on the super adsorbent properties of the hydrogel (capacity to swell/release water depending on the stimuli) (Chang et al., 2010). This can be incredibly applicable in arid climates. Hydrogel granules, composed with water and nutrients for plants, have a high water composition (1L/g of material)(Ibrahim et al., 2007). Water purification (Zhou et al., 2005) is another application which follows the same idea: conserve water and use it with caution. <sup>9</sup>**Food engineering** is referred to a broad range of applications like creams, foams, and to protect damaged fruits and vegetables.

In the present Ph.D. the high added value application chosen is the use injectable hydrogels for biomedical applications. CNCs and thermo-responsive polymer hydrogels are used in an injectable system into the body because of change from room temperature to body temperature (around LCST). This application, injectable hydrogels, can present numerous complications and research challenges as presented in **figure 36**.

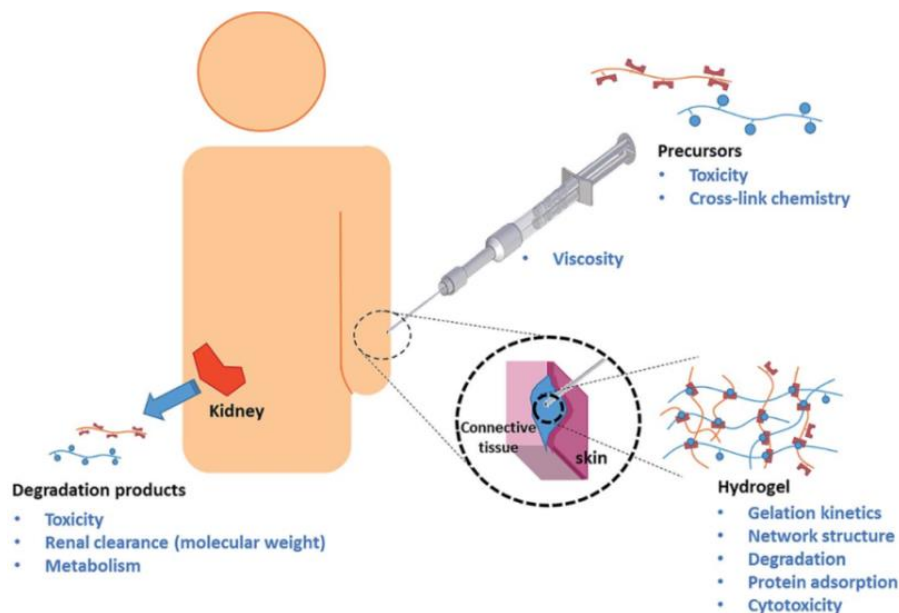


**Figure 36:** Schematic representations of the various design criteria for in situ gelling hydrogels (Bakaic et al., 2015).

## Conclusion

To conclude, cellulose nanocrystals are a promising biomaterial for a large range of applications, such as biomedical, packaging, paper, and cosmetics. In medical science, an important research field focuses on injectable hydrogels for regenerative cell therapy, wound healing, and for use in surgery. Thermo-responsive polymers present exciting properties for use in injections: liquid at room temperature and a gel at body temperature (especially PNIPAM). Because of the high aspect ratio and chemical modification capabilities of CNCs thermo-responsive hydrogels with the combination of CNCs and PNIPAM present a future for bio-sourced injectable system. A couple of challenges appear for the viability of these hydrogels: stability in the body, toxicity, gelation kinetics, and network structure are major points of interest (**Figure 36**).

This Ph.D. project targets to use CNCs and thermo-sensitive polymers linked via green chemistry methods in the creation of thermo-responsive hydrogels. **Figure 37** presents the Ph.D. project strategies that will be detailed in the next chapters. Two majors strategies of functionalization will be developed: grafting and adsorption.

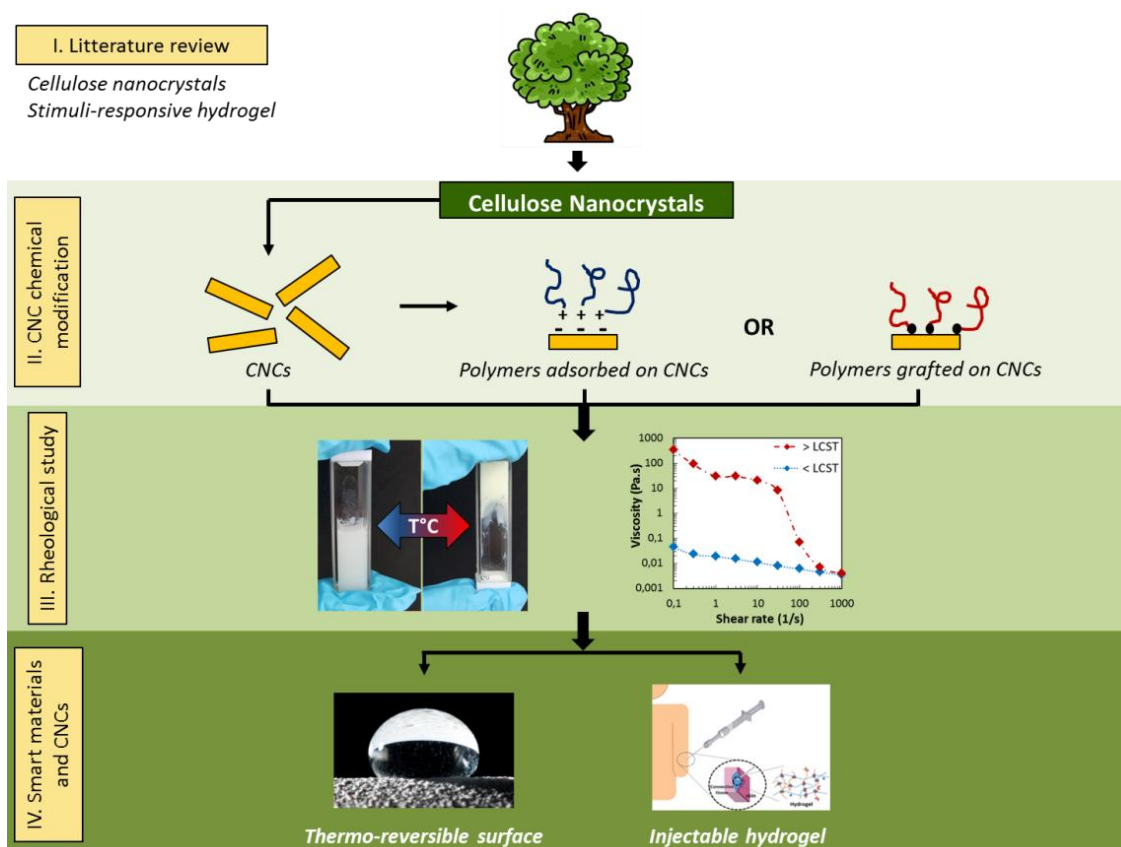


**Figure 37:** Schematic representation of the Ph.D. project strategies.

The present literature review chapter highlighted the potential to use CNCs as a hydrogel support with the benefit of thermal reversibility due to the biocompatible polymers. The first results section will present the green chemistry involved in this Ph.D. project to realize this system. The second part will investigate the rheological behavior of these thermo-responsive hydrogels. Finally, the third results section will discuss the possible use of these 'smart' systems in biomedical and paper industry applications.

## References

- Abdelaal, M.Y., Abdel-Razik, E.A., Abdel-Bary, E.M., and El-Sherbiny, I.M. (2007). Chitosan-based interpolymeric pH-responsive hydrogels for in vitro drug release. *J. Appl. Polym. Sci.* *103*, 2864–2874.
- Abitbol, T., Rivkin, A., Cao, Y., Nevo, Y., Abraham, E., Ben-Shalom, T., Lapidot, S., and Shoseyov, O. (2016). Nanocellulose, a tiny fiber with huge applications. *Curr. Opin. Biotechnol.* *39*, 76–88.
- Abraham, E., Weber, D.E., Sharon, S., Lapidot, S., and Shoseyov, O. (2017). Multifunctional Cellulosic Scaffolds from Modified Cellulose Nanocrystals. *ACS Appl. Mater. Interfaces* *9*, 2010–2015.
- Ahmadi, M., Madadlou, A., and Saboury, A.A. (2016). Whey protein aerogel as blended with cellulose crystalline particles or loaded with fish oil. *Food Chem.* *196*, 1016–1022.
- Akhlaghi, S.P., Berry, R.C., and Tam, K.C. (2013). Surface modification of cellulose nanocrystal with chitosan oligosaccharide for drug delivery applications. *Cellulose* *20*, 1747–1764.
- Akhlaghi, S.P., Tiong, D., Berry, R.M., and Tam, K.C. (2014). Comparative release studies of two cationic model drugs from different cellulose nanocrystal derivatives. *Eur. J. Pharm. Biopharm.* *88*, 207–215.
- Alarcón, C. de las H., Pennadam, S., and Alexander, C. (2005). Stimuli responsive polymers for biomedical applications. *Chem Soc Rev* *34*, 276–285.
- Alosmanov, R., Wolski, K., and Zapotoczny, S. (2017). Grafting of thermosensitive poly(N-isopropylacrylamide) from wet bacterial cellulose sheets to improve its swelling-drying ability. *Cellulose* *24*, 285–293.
- Anastas, P.T., and Warner, J.C. (2000). *Green chemistry: theory and practice* (Oxford university press).
- Araki, J. (2013). Electrostatic or steric? – preparations and characterizations of well-dispersed systems containing rod-like nanowhiskers of crystalline polysaccharides. *Soft Matter* *9*, 4125–4141.
- Araki, J., and Kuga, S. (2001). Effect of Trace Electrolyte on Liquid Crystal Type of Cellulose Microcrystals. *Langmuir* *17*, 4493–4496.
- Araki, J., Wada, M., and Kuga, S. (2001). Steric Stabilization of a Cellulose Microcrystal Suspension by Poly(ethylene glycol) Grafting. *Langmuir* *17*, 21–27.
- Azzam, F., Heux, L., Putaux, J.-L., and Jean, B. (2010). Preparation By Grafting Onto, Characterization, and Properties of Thermally Responsive Polymer-Decorated Cellulose Nanocrystals. *Biomacromolecules* *11*, 3652–3659.
- Azzam, F., Siqueira, E., Fort, S., Hassaini, R., Pignon, F., Travelet, C., Putaux, J.-L., and Jean, B. (2016). Tunable Aggregation and Gelation of Thermoresponsive Suspensions of Polymer-Grafted Cellulose Nanocrystals. *Biomacromolecules* *17*, 2112–2119.
- Azzam, F., Chaunier, L., Moreau, C., Lourdin, D., Bertocini, P., and Cathala, B. (2017). Relationship between Young's Modulus and Film Architecture in Cellulose Nanofibril-Based Multilayered Thin Films. *Langmuir* *33*, 4138–4145.
- Bai, W., Holbery, J., and Li, K. (2009). A technique for production of nanocrystalline cellulose with a narrow size distribution. *Cellulose* *16*, 455–465.
- Bakaic, E., Smeets, N.M.B., and Hoare, T. (2015). Injectable hydrogels based on poly(ethylene glycol) and derivatives as functional biomaterials. *RSC Adv* *5*, 35469–35486.
- Bardet, R., and Bras, J. (2014). Cellulose Nanofibers and Their Use in Paper Industry. In *Handbook of Green Materials : Processing Technologies, Properties and Applications*, pp. 207–232.

- Bardet, R., Belgacem, N., and Bras, J. (2015). Flexibility and Color Monitoring of Cellulose Nanocrystal Iridescent Solid Films Using Anionic or Neutral Polymers. *ACS Appl. Mater. Interfaces* 7, 4010–4018.
- Batmaz, R., Mohammed, N., Zaman, M., Minhas, G., Berry, R.M., and Tam, K.C. (2014). Cellulose nanocrystals as promising adsorbents for the removal of cationic dyes. *Cellulose* 21, 1655–1665.
- Bawa, P., Pillay, V., Choonara, Y.E., and du Toit, L.C. (2009). Stimuli-responsive polymers and their applications in drug delivery. *Biomed. Mater.* 4, 022001.
- Beck, S., Bouchard, J., and Berry, R. (2010). Controlling the Reflection Wavelength of Iridescent Solid Films of Nanocrystalline Cellulose. *Biomacromolecules* 12, 167–172.
- Beck, S., Bouchard, J., Chauve, G., and Berry, R. (2013). Controlled production of patterns in iridescent solid films of cellulose nanocrystals. *Cellulose* 20, 1401–1411.
- Beck-Candanedo, S., Roman, M., and Gray, D.G. (2005). Effect of Reaction Conditions on the Properties and Behavior of Wood Cellulose Nanocrystal Suspensions. *Biomacromolecules* 6, 1048–1054.
- Belgacem, M.N., Salon-Brochier, M.C., Krouit, M., and Bras, J. (2011). Recent Advances in Surface Chemical Modification of Cellulose Fibres. *J. Adhes. Sci. Technol.* 25, 661–684.
- Benselfelt, T., Cranston, E.D., Ondaral, S., Johansson, E., Brumer, H., Rutland, M.W., and Wågberg, L. (2016). Adsorption of Xyloglucan onto Cellulose Surfaces of Different Morphologies: An Entropy-Driven Process. *Biomacromolecules* 17, 2801–2811.
- Bercea, M., and Navard, P. (2000). Shear Dynamics of Aqueous Suspensions of Cellulose Whiskers. *Macromolecules* 33, 6011–6016.
- Boluk, Y., Lahiji, R., Zhao, L., and McDermott, M.T. (2011). Suspension viscosities and shape parameter of cellulose nanocrystals (CNC). *Colloids Surf. Physicochem. Eng. Asp.* 377, 297–303.
- Boluk, Y., Zhao, L., and Incani, V. (2012). Dispersions of Nanocrystalline Cellulose in Aqueous Polymer Solutions: Structure Formation of Colloidal Rods. *Langmuir* 28, 6114–6123.
- Boujemaoui, A., Mongkhontreerat, S., Malmström, E., and Carlmark, A. (2015). Preparation and characterization of functionalized cellulose nanocrystals. *Carbohydr. Polym.* 115, 457–464.
- Bras, J., Viet, D., Bruzzese, C., and Dufresne, A. (2011). Correlation between stiffness of sheets prepared from cellulose whiskers and nanoparticles dimensions. *Carbohydr. Polym.* 84, 211–215.
- Braun, B., and Dorgan, J.R. (2009). Single-Step Method for the Isolation and Surface Functionalization of Cellulosic Nanowhiskers. *Biomacromolecules* 10, 334–341.
- Brodin, F.W., Gregersen, O.W., and Syverud, K. (2014). Cellulose nanofibrils: Challenges and possibilities as a paper additive or coating material—A review. *Nord. Pulp Pap. Res. J.* 29, 156–166.
- Brown, R.M. (1996). The Biosynthesis of Cellulose. *J. Macromol. Sci. Part A* 33, 1345–1373.
- Cabane, E., Zhang, X., Langowska, K., Palivan, C.G., and Meier, W. (2012). Stimuli-Responsive Polymers and Their Applications in Nanomedicine. *Biointerphases* 7, 9.
- Camarero Espinosa, S., Kuhnt, T., Foster, E.J., and Weder, C. (2013). Isolation of thermally stable cellulose nanocrystals by phosphoric acid hydrolysis. *Biomacromolecules* 14, 1223–1230.
- Camarero Espinosa, S., Rothen-Rutishauser, B., Johan Foster, E., and Weder, C. (2016). Articular cartilage: from formation to tissue engineering. *Biomater. Sci.* 4, 734–767.
- Cao, X., Habibi, Y., and Lucia, L.A. (2009). One-pot polymerization, surface grafting, and processing of waterborne polyurethane-cellulose nanocrystal nanocomposites. *J. Mater. Chem.* 19, 7137–7145.
- Capron, I., and Cathala, B. (2013). Surfactant-free high internal phase emulsions stabilized by cellulose nanocrystals. *Biomacromolecules* 14, 291–296.

- Carlmark, A., Larsson, E., and Malmström, E. (2012). Grafting of cellulose by ring-opening polymerisation—A review. *Eur. Polym. J.* *48*, 1646–1659.
- Castro, D.O., Tabary, N., Martel, B., Gandini, A., Belgacem, N., and Bras, J. (2016). Effect of different carboxylic acids in cyclodextrin functionalization of cellulose nanocrystals for prolonged release of carvacrol. *Mater. Sci. Eng. C* *69*, 1018–1025.
- Catalán, J., Ilves, M., Järventausta, H., Hannukainen, K.-S., Kontturi, E., Vanhala, E., Alenius, H., Savolainen, K.M., and Norppa, H. (2015). Genotoxic and immunotoxic effects of cellulose nanocrystals in vitro. *Environ. Mol. Mutagen.* *56*, 171–182.
- Cerclier, C., Cousin, F., Bizot, H., Moreau, C., and Cathala, B. (2010). Elaboration of Spin-Coated Cellulose-Xyloglucan Multilayered Thin Films. *Langmuir* *26*, 17248–17255.
- Cerclier, C.V., Guyomard-Lack, A., Cousin, F., Jean, B., Bonnin, E., Cathala, B., and Moreau, C. (2013). Xyloglucan–Cellulose Nanocrystal Multilayered Films: Effect of Film Architecture on Enzymatic Hydrolysis. *Biomacromolecules* *14*, 3599–3609.
- Cha, R., He, Z., and Ni, Y. (2012). Preparation and characterization of thermal/pH-sensitive hydrogel from carboxylated nanocrystalline cellulose. *Carbohydr. Polym.* *88*, 713–718.
- Chaker, A., Alila, S., Mutjé, P., Vilar, M.R., and Boufi, S. (2013). Key role of the hemicellulose content and the cell morphology on the nanofibrillation effectiveness of cellulose pulps. *Cellulose* *20*, 2863–2875.
- Chandrasekhar, S. (1992). *Liquid crystals*, (1992). Camb. Univ. *Cambridge*.
- Chang, C., and Zhang, L. (2011). Cellulose-based hydrogels: Present status and application prospects. *Carbohydr. Polym.* *84*, 40–53.
- Chang, C., Duan, B., Cai, J., and Zhang, L. (2010). Superabsorbent hydrogels based on cellulose for smart swelling and controllable delivery. *Eur. Polym. J.* *46*, 92–100.
- Charreau, H., L. Foresti, M., and Vazquez, A. (2013). Nanocellulose Patents Trends: A Comprehensive Review on Patents on Cellulose Nanocrystals, Microfibrillated and Bacterial Cellulose. *Recent Pat. Nanotechnol.* *7*, 56–80.
- Chauve, G., and Bras, J. (2014). Industrial point of view of nanocellulose materials and their possible applications. *Handb. Green Mater.* World Sci. 233–252.
- Chen, L., Berry, R.M., and Tam, K.C. (2014a). Synthesis of  $\beta$ -Cyclodextrin-modified cellulose nanocrystals (CNCs)@ Fe<sub>3</sub>O<sub>4</sub>@ SiO<sub>2</sub> superparamagnetic nanorods. *ACS Sustain. Chem. Eng.* *2*, 951–958.
- Chen, L., Liu, Y., Lai, C., Berry, R.M., and Tam, K.C. (2015a). Aqueous synthesis and biostabilization of CdS@ ZnS quantum dots for bioimaging applications. *Mater. Res. Express* *2*, 105401.
- Chen, L., Cao, W., Grishkewich, N., Berry, R.M., and Tam, K.C. (2015b). Synthesis and characterization of pH-responsive and fluorescent poly (amidoamine) dendrimer-grafted cellulose nanocrystals. *J. Colloid Interface Sci.* *450*, 101–108.
- Chen, L., Lai, C., Marchewka, R., Berry, R.M., and Tam, K.C. (2016). Use of CdS quantum dot-functionalized cellulose nanocrystal films for anti-counterfeiting applications. *Nanoscale* *8*, 13288–13296.
- Chen, X., Huang, L., Sun, H.-J., Cheng, S.Z.D., Zhu, M., and Yang, G. (2014b). Stimuli-Responsive Nanocomposite: Potential Injectable Embolization Agent. *Macromol. Rapid Commun.* *35*, 579–584.
- Chen, Y., Xu, W., Liu, W., and Zeng, G. (2015c). Responsiveness, swelling, and mechanical properties of PNIPAA nanocomposite hydrogels reinforced by nanocellulose. *J. Mater. Res.* *30*, 1797–1807.

- Chen, Y., Xu, C., Huang, J., Wu, D., and Lv, Q. (2017). Rheological properties of nanocrystalline cellulose suspensions. *Carbohydr. Polym.* *157*, 303–310.
- Cherhal, F., Cousin, F., and Capron, I. (2015). Influence of Charge Density and Ionic Strength on the Aggregation Process of Cellulose Nanocrystals in Aqueous Suspension, as Revealed by Small-Angle Neutron Scattering. *Langmuir* *31*, 5596–5602.
- Cherhal, F., Cousin, F., and Capron, I. (2016). Structural Description of the Interface of Pickering Emulsions Stabilized by Cellulose Nanocrystals. *Biomacromolecules* *17*, 496–502.
- Chindawong, C., and Johannsmann, D. (2014). An anisotropic ink based on crystalline nanocellulose: Potential applications in security printing. *J. Appl. Polym. Sci.* *131*.
- Coussot, P. (2005). *Rheometry of pastes, suspensions, and granular materials: applications in industry and environment* (John Wiley & Sons).
- Coussot, P. (2012). *Comprendre la rhéologie: de la circulation du sang à la prise du béton* (EDP Sciences).
- Cranston, E.D., and Gray, D.G. (2006). Formation of cellulose-based electrostatic layer-by-layer films in a magnetic field. *Sci. Technol. Adv. Mater.* *7*, 319–321.
- Csoka, L., Hoeger, I.C., Rojas, O.J., Peszlen, I., Pawlak, J.J., and Peralta, P.N. (2012). Piezoelectric effect of cellulose nanocrystals thin films. *ACS Macro Lett.* *1*, 867–870.
- Czaja, W.K., Young, D.J., Kawecki, M., and Brown, R.M. (2007). The Future Prospects of Microbial Cellulose in Biomedical Applications. *Biomacromolecules* *8*, 1–12.
- Dai, S., Ravi, P., and Chiu Tam, K. (2008). pH-Responsive polymers: synthesis, properties and applications. *Soft Matter* *4*, 435–449.
- Dammak, A., Moreau, C., Beury, N., Schwikal, K., Winter, H.T., Bonnin, E., Saake, B., and Cathala, B. (2013). Elaboration of multilayered thin films based on cellulose nanocrystals and cationic xylans: application to xylanase activity detection. *Holzforschung* *67*, 579–586.
- De France, K.J., Chan, K.J.W., Cranston, E.D., and Hoare, T. (2016). Enhanced Mechanical Properties in Cellulose Nanocrystal–Poly(oligoethylene glycol methacrylate) Injectable Nanocomposite Hydrogels through Control of Physical and Chemical Cross-Linking. *Biomacromolecules* *17*, 649–660.
- De France, K.J., Hoare, T., and Cranston, E.D. (2017). Review of Hydrogels and Aerogels Containing Nanocellulose. *Chem. Mater.* *29*, 4609–4631.
- De Vries, H. (1951). Rotatory power and other optical properties of certain liquid crystals. *Acta Crystallogr.* *4*, 219–226.
- Decher, G., Hong, J.D., and Schmitt, J. (1992). Buildup of ultrathin multilayer films by a self-assembly process: III. Consecutively alternating adsorption of anionic and cationic polyelectrolytes on charged surfaces. *Thin Solid Films* *210*, 831–835.
- Domingues, R.M.A., Gomes, M.E., and Reis, R.L. (2014). The Potential of Cellulose Nanocrystals in Tissue Engineering Strategies. *Biomacromolecules* *15*, 2327–2346.
- Domingues, R.M.A., Silva, M., Gershovich, P., Betta, S., Babo, P., Caridade, S.G., Mano, J.F., Motta, A., Reis, R.L., and Gomes, M.E. (2015). Development of Injectable Hyaluronic Acid/Cellulose Nanocrystals Bionanocomposite Hydrogels for Tissue Engineering Applications. *Bioconjug. Chem.* *26*, 1571–1581.
- Dong, S., and Roman, M. (2007). Fluorescently Labeled Cellulose Nanocrystals for Bioimaging Applications. *J. Am. Chem. Soc.* *129*, 13810–13811.
- Dong, X.M., and Gray, D.G. (1997). Effect of Counterions on Ordered Phase Formation in Suspensions of Charged Rodlike Cellulose Crystallites. *Langmuir* *13*, 2404–2409.

- Dong, S., Hirani, A.A., Colacino, K.R., Lee, Y.W., and Roman, M. (2012). Cytotoxicity and cellular uptake of cellulose nanocrystals. *Nano LIFE* 02, 1241006.
- Dong, S., Cho, H.J., Lee, Y.W., and Roman, M. (2014). Synthesis and cellular uptake of folic acid-conjugated cellulose nanocrystals for cancer targeting. *Biomacromolecules* 15, 1560–1567.
- Dong, X.M., Kimura, T., Revol, J.-F., and Gray, D.G. (1996). Effects of Ionic Strength on the Isotropic–Chiral Nematic Phase Transition of Suspensions of Cellulose Crystallites. *Langmuir* 12, 2076–2082.
- Drogat, N., Granet, R., Sol, V., Memmi, A., Saad, N., Koerkamp, C.K., Bressollier, P., and Krausz, P. (2011). Antimicrobial silver nanoparticles generated on cellulose nanocrystals. *J. Nanoparticle Res.* 13, 1557–1562.
- Dufresne, A. (2013). Nanocellulose: from nature to high performance tailored materials (Walter de Gruyter).
- Ebeling, T., Paillet, M., Borsali, R., Diat, O., Dufresne, A., Cavaille, J.Y., Chanzy, H., and others (1999). Shear-induced orientation phenomena in suspensions of cellulose microcrystals, revealed by small angle X-ray scattering. *Langmuir* 15, 6123–6126.
- Edgar, C.D., and Gray, D.G. (2002). Influence of Dextran on the Phase Behavior of Suspensions of Cellulose Nanocrystals. *Macromolecules* 35, 7400–7406.
- Eichhorn, S.J., Dufresne, A., Aranguren, M., Marcovich, N.E., Capadona, J.R., Rowan, S.J., Weder, C., Thielemans, W., Roman, M., Renneckar, S., et al. (2010). Review: current international research into cellulose nanofibres and nanocomposites. *J. Mater. Sci.* 45, 1–33.
- El Kissi, N., Alloin, F., Dufresne, A., Sanchez, J., Bossard, F., D'Aprèa, A., and Leroy, S. (2008). Influence of Cellulose Nanofillers on the Rheological Properties of Polymer Electrolytes. *AIP Conf. Proc.* 1027, 87–89.
- Elazzouzi-Hafraoui, S., Nishiyama, Y., Putaux, J.-L., Heux, L., Dubreuil, F., and Rochas, C. (2008). The Shape and Size Distribution of Crystalline Nanoparticles Prepared by Acid Hydrolysis of Native Cellulose. *Biomacromolecules* 9, 57–65.
- Elmas, B., Senel, S., and Tuncel, A. (2007). A new thermosensitive fluorescent probe for diol sensing: Poly (N-isopropylacrylamide-co-vinylphenylboronic acid)-alizarin red S complex. *React. Funct. Polym.* 67, 87–96.
- Espino-Pérez, E., Domenek, S., Belgacem, N., Sillard, C., and Bras, J. (2014). Green Process for Chemical Functionalization of Nanocellulose with Carboxylic Acids. *Biomacromolecules* 15, 4551–4560.
- Esposito, A., Sannino, A., Cozzolino, A., Quintiliano, S.N., Lamberti, M., Ambrosio, L., and Nicolais, L. (2005). Response of intestinal cells and macrophages to an orally administered cellulose-PEG based polymer as a potential treatment for intractable edemas. *Biomaterials* 26, 4101–4110.
- Eyley, S., and Thielemans, W. (2014). Surface modification of cellulose nanocrystals. *Nanoscale* 6, 7764–7779.
- Fei, B., Wach, R.A., Mitomo, H., Yoshii, F., and Kume, T. (2000). Hydrogel of biodegradable cellulose derivatives. I. Radiation-induced crosslinking of CMC. *J. Appl. Polym. Sci.* 78, 278–283.
- Felix, J.M., and Gatenholm, P. (1991). The nature of adhesion in composites of modified cellulose fibers and polypropylene. *J. Appl. Polym. Sci.* 42, 609–620.
- Filpponen, I., and Argyropoulos, D.S. (2010). Regular Linking of Cellulose Nanocrystals via Click Chemistry: Synthesis and Formation of Cellulose Nanoplatelet Gels. *Biomacromolecules* 11, 1060–1066.

- Filpponen, I., Sadeghifar, H., and Argyropoulos, D.S. (2011). Photoresponsive cellulose nanocrystals. *Nanomater. Nanotechnol.* *1*, 7.
- Fleer, G., Stuart, M.A.C., Scheutjens, J.M.H.M., Cosgrove, T., and Vincent, B. (1993). *Polymers at Interfaces* (Springer Science & Business Media).
- Freire, E., Mayorga, O.L., and Straume, M. (1990). Isothermal titration calorimetry. *Anal. Chem.* *62*, 950A–959A.
- Fujisawa, S., Saito, T., Kimura, S., Iwata, T., and Isogai, A. (2014). Comparison of mechanical reinforcement effects of surface-modified cellulose nanofibrils and carbon nanotubes in PLLA composites. *Compos. Sci. Technol.* *90*, 96–101.
- George, J., Sajeevkumar, V.A., Ramana, K.V., Sabapathy, S.N., and others (2012). Augmented properties of PVA hybrid nanocomposites containing cellulose nanocrystals and silver nanoparticles. *J. Mater. Chem.* *22*, 22433–22439.
- Gicquel, E., Martin, C., Yanez, J.G., and Bras, J. (2017). Cellulose nanocrystals as new bio-based coating layer for improving fiber-based mechanical and barrier properties. *J. Mater. Sci.* *52*, 3048–3061.
- Giese, M., Blusch, L.K., Khan, M.K., and MacLachlan, M.J. (2015). Functional Materials from Cellulose-Derived Liquid-Crystal Templates. *Angew. Chem. Int. Ed.* *54*, 2888–2910.
- Goffin, A.-L., Raquez, J.-M., Duquesne, E., Siqueira, G., Habibi, Y., Dufresne, A., and Dubois, P. (2011). From interfacial ring-opening polymerization to melt processing of cellulose nanowhisker-filled polylactide-based nanocomposites. *Biomacromolecules* *12*, 2456–2465.
- Gong, X., Wang, Y., and Chen, L. (2017). Enhanced emulsifying properties of wood-based cellulose nanocrystals as Pickering emulsion stabilizer. *Carbohydr. Polym.* *169*, 295–303.
- Grishkewich, N., Akhlaghi, S.P., Zhaoling, Y., Berry, R., and Tam, K.C. (2016). Cellulose nanocrystal-poly(oligo(ethylene glycol) methacrylate) brushes with tunable LCSTs. *Carbohydr. Polym.* *144*, 215–222.
- Habibi, Y. (2014). Key advances in the chemical modification of nanocelluloses. *Chem. Soc. Rev.* *43*, 1519–1542.
- Habibi, Y., Chanzy, H., and Vignon, M.R. (2006). TEMPO-mediated surface oxidation of cellulose whiskers. *Cellulose* *13*, 679–687.
- Habibi, Y., Goffin, A.-L., Schiltz, N., Duquesne, E., Dubois, P., and Dufresne, A. (2008). Bionanocomposites based on poly( $\epsilon$ -caprolactone)-grafted cellulose nanocrystals by ring-opening polymerization. *J. Mater. Chem.* *18*, 5002–5010.
- Habibi, Y., Lucia, L.A., and Rojas, O.J. (2010). Cellulose Nanocrystals: Chemistry, Self-Assembly, and Applications. *Chem. Rev.* *110*, 3479–3500.
- Habibi, Y., Aouadi, S., Raquez, J.-M., and Dubois, P. (2013). Effects of interfacial stereocomplexation in cellulose nanocrystal-filled polylactide nanocomposites. *Cellulose* *20*, 2877–2885.
- Haigler, C.H. (1990). *Biosynthesis and biodegradation of cellulose* (CRC Press).
- Hakalahti, M., Mautner, A., Johansson, L.-S., Hänninen, T., Setälä, H., Kontturi, E., Bismarck, A., and Tammelin, T. (2016). Direct Interfacial Modification of Nanocellulose Films for Thermoresponsive Membrane Templates. *ACS Appl. Mater. Interfaces* *8*, 2923–2927.
- Hamad, W.Y. (2015). Photonic and semiconductor materials based on cellulose nanocrystals. In *Cellulose Chemistry and Properties: Fibers, Nanocelluloses and Advanced Materials*, (Springer), pp. 287–328.
- Hamley, I.W. (2010). Liquid crystal phase formation by biopolymers. *Soft Matter* *6*, 1863–1871.

- Hansson, S., Östmark, E., Carlmark, A., and Malmström, E. (2009). ARGET ATRP for Versatile Grafting of Cellulose Using Various Monomers. *ACS Appl. Mater. Interfaces* *1*, 2651–2659.
- Haqani, M., Roghani-Mamaqani, H., and Salami-Kalajahi, M. (2017). Synthesis of dual-sensitive nanocrystalline cellulose-grafted block copolymers of N-isopropylacrylamide and acrylic acid by reversible addition-fragmentation chain transfer polymerization. *Cellulose* *24*, 2241–2254.
- Harper, B.J., Clendaniel, A., Sinche, F., Way, D., Hughes, M., Schardt, J., Simonsen, J., Stefaniak, A.B., and Harper, S.L. (2016). Impacts of chemical modification on the toxicity of diverse nanocellulose materials to developing zebrafish. *Cellulose* *23*, 1763–1775.
- Haworth, W.N., Hirst, E.L., and Thomas, H.A. (1930). The existence of the cellobiose residue in cellulose. *Nature* *126*, 438.
- He, X., Male, K.B., Nesterenko, P.N., Brabazon, D., Paull, B., and Luong, J.H. (2013). Adsorption and desorption of methylene blue on porous carbon monoliths and nanocrystalline cellulose. *ACS Appl. Mater. Interfaces* *5*, 8796–8804.
- Hebeish, A., Farag, S., Sharaf, S., and Shaheen, T.I. (2014). Thermal responsive hydrogels based on semi interpenetrating network of poly(NIPAM) and cellulose nanowhiskers. *Carbohydr. Polym.* *102*, 159–166.
- Hemraz, U.D., Lu, A., Sunasee, R., and Boluk, Y. (2014). Structure of poly(N-isopropylacrylamide) brushes and steric stability of their grafted cellulose nanocrystal dispersions. *J. Colloid Interface Sci.* *430*, 157–165.
- Henriksson, M., Henriksson, G., Berglund, L.A., and Lindström, T. (2007). An environmentally friendly method for enzyme-assisted preparation of microfibrillated cellulose (MFC) nanofibers. *Eur. Polym. J.* *43*, 3434–3441.
- Herrera, M.A., Mathew, A.P., and Oksman, K. (2014). Gas permeability and selectivity of cellulose nanocrystals films (layers) deposited by spin coating. *Carbohydr. Polym.* *112*, 494–501.
- Herrick, F.W., Casebier, R.L., Hamilton, J.K., and Sandberg, K.R. (1983). Microfibrillated Cellulose: Morphology and Accessibility. *J Appl Polym Sci Appl Polym Symp U. S.* *37*.
- Hoeng, F. (2016). Thèse: Utilisation des nanocelluloses pour la préparation d'encre conductrices. Thesis. Grenoble Alpes, LGP2 - Laboratoire de Génie des Procédés Papetiers.
- Hoeng, F., Denneulin, A., Neuman, C., and Bras, J. (2015). Charge density modification of carboxylated cellulose nanocrystals for stable silver nanoparticles suspension preparation. *J. Nanoparticle Res.* *17*, 244.
- Hoeng, F., Denneulin, A., Reverdy-Bruas, N., Krosnicki, G., and Bras, J. (2017a). Rheology of cellulose nanofibrils/silver nanowires suspension for the production of transparent and conductive electrodes by screen printing. *Appl. Surf. Sci.* *394*, 160–168.
- Hoeng, F., Bras, J., Gicquel, E., Krosnicki, G., and Denneulin, A. (2017b). Inkjet printing of nanocellulose–silver ink onto nanocellulose coated cardboard. *RSC Adv.* *7*, 15372–15381.
- Hoffman, A.S. (2013). Stimuli-responsive polymers: Biomedical applications and challenges for clinical translation. *Adv. Drug Deliv. Rev.* *65*, 10–16.
- Homola, J., Yee, S.S., and Gauglitz, G. (1999). Surface plasmon resonance sensors. *Sens. Actuators B Chem.* *54*, 3–15.
- Hu, Z., Cranston, E.D., Ng, R., and Pelton, R. (2014). Tuning Cellulose Nanocrystal Gelation with Polysaccharides and Surfactants. *Langmuir* *30*, 2684–2692.
- Hu, Z., Ballinger, S., Pelton, R., and Cranston, E.D. (2015a). Surfactant-enhanced cellulose nanocrystal Pickering emulsions. *J. Colloid Interface Sci.* *439*, 139–148.

- Hu, Z., Patten, T., Pelton, R., and Cranston, E.D. (2015b). Synergistic Stabilization of Emulsions and Emulsion Gels with Water-Soluble Polymers and Cellulose Nanocrystals. *ACS Sustain. Chem. Eng.* **3**, 1023–1031.
- Huang, J.-L., Li, C.-J., and Gray, D.G. (2014). Functionalization of cellulose nanocrystal films via “thiol–ene” click reaction. *RSC Adv.* **4**, 6965–6969.
- Ibrahim, S.M., El Salmawi, K.M., and Zahran, A.H. (2007). Synthesis of crosslinked superabsorbent carboxymethyl cellulose/acrylamide hydrogels through electron-beam irradiation. *J. Appl. Polym. Sci.* **104**, 2003–2008.
- Isogai, A., Saito, T., and Fukuzumi, H. (2011). TEMPO-oxidized cellulose nanofibers. *Nanoscale* **3**, 71–85.
- Jackson, J.K., Letchford, K., Wasserman, B.Z., Ye, L., Hamad, W.Y., and Burt, H.M. (2011). The use of nanocrystalline cellulose for the binding and controlled release of drugs. *Int. J. Nanomedicine* **6**, 321.
- Jeong, B., Kim, S.W., and Bae, Y.H. (2002). Thermosensitive sol-gel reversible hydrogels. *Adv. Drug Deliv. Rev.* **54**, 37–51.
- Jia, B., Li, Y., Yang, B., Xiao, D., Zhang, S., Rajulu, A.V., Kondo, T., Zhang, L., and Zhou, J. (2013). Effect of microcrystal cellulose and cellulose whisker on biocompatibility of cellulose-based electrospun scaffolds. *Cellulose* **20**, 1911–1923.
- Jochum, F.D., and Theato, P. (2009). Temperature and light sensitive copolymers containing azobenzene moieties prepared via a polymer analogous reaction. *Polymer* **50**, 3079–3085.
- Jorfi, M., and Foster, E.J. (2015). Recent advances in nanocellulose for biomedical applications. *J. Appl. Polym. Sci.* **132**.
- Kalashnikova, I., Bizot, H., Cathala, B., and Capron, I. (2011). New Pickering Emulsions Stabilized by Bacterial Cellulose Nanocrystals. *Langmuir* **27**, 7471–7479.
- Kan, K.H.M., Li, J., Wijesekera, K., and Cranston, E.D. (2013). Polymer-Grafted Cellulose Nanocrystals as pH-Responsive Reversible Flocculants. *Biomacromolecules* **14**, 3130–3139.
- Kaushik, M., and Moores, A. (2016a). Review: nanocelluloses as versatile supports for metal nanoparticles and their applications in catalysis. *Green Chem* **18**, 622–637.
- Kaushik, M., and Moores, A. (2016b). Nanocelluloses as versatile supports for metal nanoparticles and their applications in catalysis. *Green Chem.* **18**, 622–637.
- Kelly, J.A., Giese, M., Shopsowitz, K.E., Hamad, W.Y., and MacLachlan, M.J. (2014). The Development of Chiral Nematic Mesoporous Materials. *Acc. Chem. Res.* **47**, 1088–1096.
- Klemm, D., Kramer, F., Moritz, S., Lindström, T., Ankerfors, M., Gray, D., and Dorris, A. (2011). Nanocelluloses: A New Family of Nature-Based Materials. *Angew. Chem. Int. Ed.* **50**, 5438–5466.
- Kloser, E., and Gray, D.G. (2010). Surface Grafting of Cellulose Nanocrystals with Poly(ethylene oxide) in Aqueous Media. *Langmuir* **26**, 13450–13456.
- Kobayashi, Y., Saito, T., and Isogai, A. (2014). Aerogels with 3D Ordered Nanofiber Skeletons of Liquid-Crystalline Nanocellulose Derivatives as Tough and Transparent Insulators. *Angew. Chem.* **126**, 10562–10565.
- Kovacs, T., Naish, V., O’Connor, B., Blaise, C., Gagné, F., Hall, L., Trudeau, V., and Martel, P. (2010). An ecotoxicological characterization of nanocrystalline cellulose (NCC). *Nanotoxicology* **4**, 255–270.
- Köblinger, C., Uttenthaler, E., Drost, S., Aberl, F., Wolf, H., Brink, G., Stanglmaier, A., and Sackmann, E. (1995). Comparison of the QCM and the SPR method for surface studies and immunological applications. *Sens. Actuators B Chem.* **24**, 107–112.

- Kroon-Batenburg, L.M.J., Bouma, B., and Kroon, J. (1996). Stability of Cellulose Structures Studied by MD Simulations. Could Mercerized Cellulose II Be Parallel? *Macromolecules* *29*, 5695–5699.
- Lai, H., Chen, Q., and Wu, P. (2013). The core–shell structure of PNIPAM collapsed chain conformation induces a bimodal transition on cooling. *Soft Matter* *9*, 3985.
- Lam, E., Male, K.B., Chong, J.H., Leung, A.C., and Luong, J.H. (2012). Applications of functionalized and nanoparticle-modified nanocrystalline cellulose. *Trends Biotechnol.* *30*, 283–290.
- Larsson, E., Sanchez, C.C., Porsch, C., Karabulut, E., Wågberg, L., and Carlmark, A. (2013). Thermo-responsive nanofibrillated cellulose by polyelectrolyte adsorption. *Eur. Polym. J.* *49*, 2689–2696.
- Lavoine, N., Desloges, I., Dufresne, A., and Bras, J. (2012). Microfibrillated cellulose – Its barrier properties and applications in cellulosic materials: A review. *Carbohydr. Polym.* *90*, 735–764.
- Lavoine, N., Desloges, I., Khelifi, B., and Bras, J. (2014). Impact of different coating processes of microfibrillated cellulose on the mechanical and barrier properties of paper. *J. Mater. Sci.* *49*, 2879–2893.
- Lavoine, N., Bras, J., Saito, T., and Isogai, A. (2016). Improvement of the Thermal Stability of TEMPO-Oxidized Cellulose Nanofibrils by Heat-Induced Conversion of Ionic Bonds to Amide Bonds. *Macromol. Rapid Commun.* *37*, 1033–1039.
- Le Goff, K.J., Gaillard, C., Helbert, W., Garnier, C., and Aubry, T. (2015). Rheological study of reinforcement of agarose hydrogels by cellulose nanowhiskers. *Carbohydr. Polym.* *116*, 117–123.
- Lee, S.-D. (1987). A numerical investigation of nematic ordering based on a simple hard-rod model. *J. Chem. Phys.* *87*, 4972–4974.
- Lee, Y.M., and Shim, J.K. (1997). Preparation of pH/temperature responsive polymer membrane by plasma polymerization and its riboflavin permeation. *Polymer* *38*, 1227–1232.
- Lee, K.-Y., Aitomäki, Y., Berglund, L.A., Oksman, K., and Bismarck, A. (2014). On the use of nanocellulose as reinforcement in polymer matrix composites. *Compos. Sci. Technol.* *105*, 15–27.
- Li, F., Biagioni, P., Bollani, M., Maccagnan, A., and Piergiovanni, L. (2013). Multi-functional coating of cellulose nanocrystals for flexible packaging applications. *Cellulose* *20*, 2491–2504.
- Li, G., Song, S., Guo, L., and Ma, S. (2008). Self-assembly of thermo- and pH-responsive poly(acrylic acid)-*b*-poly(N-isopropylacrylamide) micelles for drug delivery. *J. Polym. Sci. Part Polym. Chem.* *46*, 5028–5035.
- Li, Y., Jia, X., Gao, M., He, H., Kuang, G., and Wei, Y. (2010). Photoresponsive nanocarriers based on PAMAM dendrimers with a *o*-nitrobenzyl shell. *J. Polym. Sci. Part Polym. Chem.* *48*, 551–557.
- Liedberg, B., Nylander, C., and Lunström, I. (1983). Surface plasmon resonance for gas detection and biosensing. *Sens. Actuators* *4*, 299–304.
- Lin, N., and Dufresne, A. (2014). Nanocellulose in biomedicine: current status and future prospect. *Eur. Polym. J.* *59*, 302–325.
- Lin, N., Gèze, A., Wouessidjewe, D., Huang, J., and Dufresne, A. (2016). Biocompatible Double-Membrane Hydrogels from Cationic Cellulose Nanocrystals and Anionic Alginate as Complexing Drugs Codelivery. *ACS Appl. Mater. Interfaces* *8*, 6880–6889.
- Lindqvist, J., Nyström, D., Östmark, E., Antoni, P., Carlmark, A., Johansson, M., Hult, A., and Malmström, E. (2008). Intelligent Dual-Responsive Cellulose Surfaces via Surface-Initiated ATRP. *Biomacromolecules* *9*, 2139–2145.
- Liu, D., Chen, X., Yue, Y., Chen, M., and Wu, Q. (2011a). Structure and rheology of nanocrystalline cellulose. *Carbohydr. Polym.* *84*, 316–322.

- Liu, P., Sehaqui, H., Tingaut, P., Wichser, A., Oksman, K., and Mathew, A.P. (2014). Cellulose and chitin nanomaterials for capturing silver ions (Ag<sup>+</sup>) from water via surface adsorption. *Cellulose* 21, 449–461.
- Liu, X.-Y., Cheng, F., Liu, Y., Liu, H.-J., and Chen, Y. (2010). Preparation and characterization of novel thermoresponsive gold nanoparticles and their responsive catalysis properties. *J. Mater. Chem.* 20, 360–368.
- Liu, Z., Choi, H., Gatenholm, P., and Esker, A.R. (2011b). Quartz Crystal Microbalance with Dissipation Monitoring and Surface Plasmon Resonance Studies of Carboxymethyl Cellulose Adsorption onto Regenerated Cellulose Surfaces. *Langmuir* 27, 8718–8728.
- Mahimwalla, Z., Yager, K.G., Mamiya, J., Shishido, A., Priimagi, A., and Barrett, C.J. (2012). Azobenzene photomechanics: prospects and potential applications. *Polym. Bull.* 69, 967–1006.
- Majoinen, J., Walther, A., McKee, J.R., Kontturi, E., Aseyev, V., Malho, J.M., Ruokolainen, J., and Ikkala, O. (2011). Polyelectrolyte Brushes Grafted from Cellulose Nanocrystals Using Cu-Mediated Surface-Initiated Controlled Radical Polymerization. *Biomacromolecules* 12, 2997–3006.
- Majoinen, J., Hassinen, J., Haataja, J.S., Rekola, H.T., Kontturi, E., Kostianen, M.A., Ras, R.H.A., Törmä, P., and Ikkala, O. (2016). Chiral Plasmonics Using Twisting along Cellulose Nanocrystals as a Template for Gold Nanoparticles. *Adv. Mater.* 28, 5262–5267.
- Mangalam, A.P., Simonsen, J., and Benight, A.S. (2009). Cellulose/DNA Hybrid Nanomaterials. *Biomacromolecules* 10, 497–504.
- Marchessault, R.H., Morehead, F.F., and Walter, N.M. (1959). Liquid Crystal Systems from Fibrillar Polysaccharides. *Nature* 184, 632–633.
- Marchessault, R.H., Morehead, F.F., and Koch, M.J. (1961). Some hydrodynamic properties of neutral suspensions of cellulose crystallites as related to size and shape. *J. Colloid Sci.* 16, 327–344.
- Mariano, M., El Kissi, N., and Dufresne, A. (2014). Cellulose nanocrystals and related nanocomposites: Review of some properties and challenges. *J. Polym. Sci. Part B Polym. Phys.* 52, 791–806.
- Mariano, M., El Kissi, N., and Dufresne, A. (2015). Melt processing of cellulose nanocrystal reinforced polycarbonate from a masterbatch process. *Eur. Polym. J.* 69, 208–223.
- Mariano, M., El Kissi, N., and Dufresne, A. (2016). Cellulose nanocrystal reinforced oxidized natural rubber nanocomposites. *Carbohydr. Polym.* 137, 174–183.
- Mariano, M., Pilate, F., de Oliveira, F.B., Khelifa, F., Dubois, P., Raquez, J.-M., and Dufresne, A. (2017). Preparation of Cellulose Nanocrystal-Reinforced Poly(lactic acid) Nanocomposites through Noncovalent Modification with PLLA-Based Surfactants. *ACS Omega* 2, 2678–2688.
- Martin, C., and Jean, B. (2014). Nanocellulose/polymer multilayered thin films: tunable architectures towards tailored physical properties. *Nord Pulp Pap. Res J* 19–30.
- Mascheroni, E., Rampazzo, R., Ortenzi, M.A., Piva, G., Bonetti, S., and Piergiovanni, L. (2016). Comparison of cellulose nanocrystals obtained by sulfuric acid hydrolysis and ammonium persulfate, to be used as coating on flexible food-packaging materials. *Cellulose* 23, 779–793.
- Matsumoto, S., Christie, R.J., Nishiyama, N., Miyata, K., Ishii, A., Oba, M., Koyama, H., Yamasaki, Y., and Kataoka, K. (2008). Environment-responsive block copolymer micelles with a disulfide cross-linked core for enhanced siRNA delivery. *Biomacromolecules* 10, 119–127.
- Mazurowski, M., Gallei, M., Li, J., Didzoleit, H., Stühn, B., and Rehahn, M. (2012). Redox-responsive polymer brushes grafted from polystyrene nanoparticles by means of surface initiated atom transfer radical polymerization. *Macromolecules* 45, 8970–8981.

- McKee, J.R., Hietala, S., Seitsonen, J., Laine, J., Kontturi, E., and Ikkala, O. (2014). Thermoresponsive Nanocellulose Hydrogels with Tunable Mechanical Properties. *ACS Macro Lett.* *3*, 266–270.
- Missoum, K., Martoia, F., Belgacem, M.N., and Bras, J. (2013). Effect of chemically modified nanofibrillated cellulose addition on the properties of fiber-based materials. *Ind. Crops Prod.* *48*, 98–105.
- Mohammed, N., Grishkewich, N., Waeijen, H.A., Berry, R.M., and Tam, K.C. (2016). Continuous flow adsorption of methylene blue by cellulose nanocrystal-alginate hydrogel beads in fixed bed columns. *Carbohydr. Polym.* *136*, 1194–1202.
- Montanari, S., Roumani, M., Heux, L., and Vignon, M.R. (2005). Topochemistry of Carboxylated Cellulose Nanocrystals Resulting from TEMPO-Mediated Oxidation. *Macromolecules* *38*, 1665–1671.
- Moon, R.J., Martini, A., Nairn, J., Simonsen, J., and Youngblood, J. (2011). Cellulose nanomaterials review: structure, properties and nanocomposites. *Chem. Soc. Rev.* *40*, 3941.
- Morandi, G., Heath, L., and Thielemans, W. (2009). Cellulose Nanocrystals Grafted with Polystyrene Chains through Surface-Initiated Atom Transfer Radical Polymerization (SI-ATRP). *Langmuir* *25*, 8280–8286.
- Moreau, C., Villares, A., Capron, I., and Cathala, B. (2016). Tuning supramolecular interactions of cellulose nanocrystals to design innovative functional materials. *Ind. Crops Prod.* *93*, 96–107.
- Mulvihill, M.J., Beach, E.S., Zimmerman, J.B., and Anastas, P.T. (2011). Green Chemistry and Green Engineering: A Framework for Sustainable Technology Development. *Annu. Rev. Environ. Resour.* *36*, 271–293.
- Nagalakshmaiah, M., Pignon, F., Kissi, N.E., and Dufresne, A. (2016). Surface adsorption of triblock copolymer (PEO–PPO–PEO) on cellulose nanocrystals and their melt extrusion with polyethylene. *RSC Adv.* *6*, 66224–66232.
- Napper, D.H. (1977). Steric stabilization. *J. Colloid Interface Sci.* *58*, 390–407.
- Napper, D.H. (1983). *Polymeric stabilization of colloidal dispersions* (Academic Pr).
- Naseri, N., Deepa, B., Mathew, A.P., Oksman, K., and Girandon, L. (2016). Nanocellulose-Based Interpenetrating Polymer Network (IPN) Hydrogels for Cartilage Applications. *Biomacromolecules* *17*, 3714–3723.
- Nechyporchuk, O., Belgacem, M.N., and Bras, J. (2016a). Production of cellulose nanofibrils: A review of recent advances. *Ind. Crops Prod.* *93*, 2–25.
- Nechyporchuk, O., Belgacem, M.N., and Pignon, F. (2016b). Current Progress in Rheology of Cellulose Nanofibril Suspensions. *Biomacromolecules* *17*, 2311–2320.
- Nickerson, R.F., and Habrle, J.A. (1947). Cellulose intercrystalline structure. *Ind. Eng. Chem.* *39*, 1507–1512.
- Nielsen, L.J., Eyley, S., Thielemans, W., and Aylott, J.W. (2010). Dual fluorescent labelling of cellulose nanocrystals for pH sensing. *Chem. Commun.* *46*, 8929–8931.
- Nimeskern, L., Martínez Ávila, H., Sundberg, J., Gatenholm, P., Müller, R., and Stok, K.S. (2013). Mechanical evaluation of bacterial nanocellulose as an implant material for ear cartilage replacement. *J. Mech. Behav. Biomed. Mater.* *22*, 12–21.
- Novo, L.P., Bras, J., García, A., Belgacem, N., and Curvelo, A.A.S. (2015). Subcritical Water: A Method for Green Production of Cellulose Nanocrystals. *ACS Sustain. Chem. Eng.* *3*, 2839–2846.
- Oguzlu, H., and Boluk, Y. (2016). Interactions between cellulose nanocrystals and anionic and neutral polymers in aqueous solutions. *Cellulose* *24*, 131–146.

- Oguzlu, H., Danumah, C., and Boluk, Y. (2016). The role of dilute and semi-dilute cellulose nanocrystal (CNC) suspensions on the rheology of carboxymethyl cellulose (CMC) solutions. *Can. J. Chem. Eng.* *94*, 1841–1847.
- Oguzlu, H., Danumah, C., and Boluk, Y. (2017). Colloidal behavior of aqueous cellulose nanocrystal suspensions. *Curr. Opin. Colloid Interface Sci.* *29*, 46–56.
- Okahata, Y., Noguchi, H., and Seki, T. (1986). Thermoselective permeation from a polymer-grafted capsule membrane. *Macromolecules* *19*, 493–494.
- Oksman, K., Aitomäki, Y., Mathew, A.P., Siqueira, G., Zhou, Q., Butylina, S., Tanpichai, S., Zhou, X., and Hooshmand, S. (2016). Review of the recent developments in cellulose nanocomposite processing. *Compos. Part Appl. Sci. Manuf.* *83*, 2–18.
- Olivier, C., Moreau, C., Bertocini, P., Bizot, H., Chauvet, O., and Cathala, B. (2012). Cellulose Nanocrystal-Assisted Dispersion of Luminescent Single-Walled Carbon Nanotubes for Layer-by-Layer Assembled Hybrid Thin Films. *Langmuir* *28*, 12463–12471.
- Onogi, S., and Asada, T. (1980). Rheology and Rheo-Optics of Polymer Liquid Crystals. In *Rheology*, G. Astarita, G. Marrucci, and L. Nicolais, eds. (Springer US), pp. 127–147.
- Onsager, L. (1949). The Effects of Shape on the Interaction of Colloidal Particles. *Ann. N. Y. Acad. Sci.* *51*, 627–659.
- Orts, W.J., Godbout, L., Marchessault, R.H., and Revol, J.-F. (1998). Enhanced Ordering of Liquid Crystalline Suspensions of Cellulose Microfibrils: A Small Angle Neutron Scattering Study. *Macromolecules* *31*, 5717–5725.
- Padalkar, S., Capadona, J.R., Rowan, S.J., Weder, C., Won, Y.-H., Stanciu, L.A., and Moon, R.J. (2010). Natural Biopolymers: Novel Templates for the Synthesis of Nanostructures. *Langmuir* *26*, 8497–8502.
- Pal, K., Banthia, A.K., and Majumdar, D.K. (2006). Development of carboxymethyl cellulose acrylate for various biomedical applications. *Biomed. Mater.* *1*, 85.
- Pasparakis, G., Vamvakaki, M., Krasnogor, N., and Alexander, C. (2009). Diol–boronic acid complexes integrated by responsive polymers—a route to chemical sensing and logic operations. *Soft Matter* *5*, 3839–3841.
- Payen, A. (1838). *Comptes Rendus De L Academie Des Sciences Serie Iii-Sciences De La Vie*. *Life Sci.* *7*, 1052.
- Pentlavalli, S., Chambers, P., Sathy, B.N., O’Doherty, M., Chalanqui, M., Kelly, D.J., Haut-Donahue, T., McCarthy, H.O., and Dunne, N.J. (2017). Simple Radical Polymerization of Poly (Alginate-Graft-N-Isopropylacrylamide) Injectable Thermoresponsive Hydrogel with the Potential for Localized and Sustained Delivery of Stem Cells and Bioactive Molecules. *Macromol. Biosci.* *10.1002/mabi.201700118*.
- Peresin, M.S., Vesterinen, A.-H., Habibi, Y., Johansson, L.-S., Pawlak, J.J., Nevzorov, A.A., and Rojas, O.J. (2014a). Crosslinked PVA nanofibers reinforced with cellulose nanocrystals: Water interactions and thermomechanical properties. *J. Appl. Polym. Sci.* *131*.
- Peresin, M.S., Zoppe, J.O., Vallejos, M.E., Habibi, Y., Hubbe, M.A., and Rojas, O.J. (2014b). Nano- and micro-fiber composites reinforced with cellulose nanocrystals. *Cellul. Based Compos. New Green Nanomater.* Wiley-VCH Verl. GmbH.
- Petersson, L., Kvien, I., and Oksman, K. (2007). Structure and thermal properties of poly (lactic acid)/cellulose whiskers nanocomposite materials. *Compos. Sci. Technol.* *67*, 2535–2544.
- Phillips, D.J., and Gibson, M.I. (2012). Degradable thermoresponsive polymers which display redox-responsive LCST Behaviour. *Chem. Commun.* *48*, 1054–1056.

- Pietsch, C., S. Schubert, U., and Hoogenboom, R. (2011). Aqueous polymeric sensors based on temperature-induced polymer phase transitions and solvatochromic dyes. *Chem. Commun.* *47*, 8750–8765.
- Pitkänen, M., Kangas, H., and Vartiainen, J. (2014). Toxicity and health issues. *Handb. Green Mater.* World Sci. 181–205.
- Plunkett, K.N., Zhu, X., Moore, J.S., and Leckband, D.E. (2006). PNIPAM Chain Collapse Depends on the Molecular Weight and Grafting Density. *Langmuir* *22*, 4259–4266.
- Porsch, C., Hansson, S., Nordgren, N., and Malmström, E. (2011). Thermo-responsive cellulose-based architectures: tailoring LCST using poly(ethylene glycol) methacrylates. *Polym. Chem.* *2*, 1114.
- Postek, M.T., Vladár, A., Dagata, J., Farkas, N., Ming, B., Wagner, R., Raman, A., Moon, R.J., Sabo, R., Wegner, T.H., et al. (2011). Development of the metrology and imaging of cellulose nanocrystals. *Meas. Sci. Technol.* *22*, 024005.
- Qiu, X., and Hu, S. (2013). “Smart” Materials Based on Cellulose: A Review of the Preparations, Properties, and Applications. *Materials* *6*, 738–781.
- Rånby, B.G. (1951). Fibrous macromolecular systems. Cellulose and muscle. The colloidal properties of cellulose micelles. *Discuss. Faraday Soc.* *11*, 158–164.
- Rånby, B.G., and Ribí, E. (1950). Über den feinbau der zellulose. *Experientia* *6*, 12–14.
- Rattaz, A., Mishra, S.P., Chabot, B., and Daneault, C. (2011). Cellulose nanofibres by sonocatalysed-TEMPO-oxidation. *Cellulose* *18*, 585.
- Rehman, H.U., Nawaz, M.A., Aman, A., Baloch, A.H., and Qader, S.A.U. (2014). Immobilization of pectinase from *Bacillus licheniformis* KIBGE-IB21 on chitosan beads for continuous degradation of pectin polymers. *Biocatal. Agric. Biotechnol.* *3*, 282–287.
- Reid, M.S., Villalobos, M., and Cranston, E.D. (2017). Benchmarking Cellulose Nanocrystals: From the Laboratory to Industrial Production. *Langmuir* *33*, 1583–1598.
- Reineke, T.M. (2016). Stimuli-Responsive Polymers for Biological Detection and Delivery. *ACS Macro Lett.* *5*, 14–18.
- Revol, J.-F., Bradford, H., Giasson, J., Marchessault, R.H., and Gray, D.G. (1992). Helicoidal self-ordering of cellulose microfibrils in aqueous suspension. *Int. J. Biol. Macromol.* *14*, 170–172.
- Revol, J.-F., Godbout, L., Dong, X.-M., Gray, D.G., Chanzy, H., and Maret, G. (1994). Chiral nematic suspensions of cellulose crystallites; phase separation and magnetic field orientation. *Liq. Cryst.* *16*, 127–134.
- Rezayat, M., Blundell, R.K., Camp, J.E., Walsh, D.A., and Thielemans, W. (2014). Green One-Step Synthesis of Catalytically Active Palladium Nanoparticles Supported on Cellulose Nanocrystals. *ACS Sustain. Chem. Eng.* *2*, 1241–1250.
- Rodahl, M., Höök, F., Krozer, A., Brzezinski, P., and Kasemo, B. (1995). Quartz crystal microbalance setup for frequency and *Q*-factor measurements in gaseous and liquid environments. *Rev. Sci. Instrum.* *66*, 3924–3930.
- Roman, M. (2015). Toxicity of Cellulose Nanocrystals: A Review. *Ind. Biotechnol.* *11*, 25–33.
- Roth, P.J., Jochum, F.D., Forst, F.R., Zentel, R., and Theato, P. (2010). Influence of End Groups on the Stimulus-Responsive Behavior of Poly [oligo (ethylene glycol) methacrylate] in Water. *Macromolecules* *43*, 4638–4645.
- Sadeghifar, H., Filpponen, I., Clarke, S.P., Brougham, D.F., and Argyropoulos, D.S. (2011). Production of cellulose nanocrystals using hydrobromic acid and click reactions on their surface. *J. Mater. Sci.* *46*, 7344–7355.

- Saidane, D., Perrin, E., Cherhal, F., Guellec, F., and Capron, I. (2016). Some modification of cellulose nanocrystals for functional Pickering emulsions. *Phil Trans R Soc A* 374, 20150139.
- Saito, T., Kimura, S., Nishiyama, Y., and Isogai, A. (2007). Cellulose Nanofibers Prepared by TEMPO-Mediated Oxidation of Native Cellulose. *Biomacromolecules* 8, 2485–2491.
- Salas, C., Nypelö, T., Rodriguez-Abreu, C., Carrillo, C., and Rojas, O.J. (2014). Nanocellulose properties and applications in colloids and interfaces. *Curr. Opin. Colloid Interface Sci.* 19, 383–396.
- Sanna, R., Fortunati, E., Alzari, V., Nuvoli, D., Terenzi, A., Casula, M.F., Kenny, J.M., and Mariani, A. (2013). Poly(N-vinylcaprolactam) nanocomposites containing nanocrystalline cellulose: a green approach to thermoresponsive hydrogels. *Cellulose* 20, 2393–2402.
- Sannino, A., Esposito, A., Rosa, A.D., Cozzolino, A., Ambrosio, L., and Nicolais, L. (2003). Biomedical application of a superabsorbent hydrogel for body water elimination in the treatment of edemas. *J. Biomed. Mater. Res. A* 67, 1016–1024.
- Sannino, A., Mensitieri, G., and Nicolais, L. (2004). Water and synthetic urine sorption capacity of cellulose-based hydrogels under a compressive stress field. *J. Appl. Polym. Sci.* 91, 3791–3796.
- Sannino, A., Madaghiele, M., Lionetto, M.G., Schettino, T., and Maffezzoli, A. (2006). A cellulose-based hydrogel as a potential bulking agent for hypocaloric diets: An in vitro biocompatibility study on rat intestine. *J. Appl. Polym. Sci.* 102, 1524–1530.
- Sannino, A., Demitri, C., and Madaghiele, M. (2009). Biodegradable Cellulose-based Hydrogels: Design and Applications. *Materials* 2, 353–373.
- Schattling, P., Jochum, F.D., and Theato, P. (2011). Multi-responsive copolymers: using thermo-, light- and redox stimuli as three independent inputs towards polymeric information processing. *Chem. Commun.* 47, 8859–8861.
- Schattling, P., D. Jochum, F., and Theato, P. (2014). Multi-stimuli responsive polymers – the all-in-one talents. *Polym. Chem.* 5, 25–36.
- Schild, H.G. (1992). Poly(N-isopropylacrylamide): experiment, theory and application. *Prog. Polym. Sci.* 17, 163–249.
- Schmaljohann, D. (2006). Thermo- and pH-responsive polymers in drug delivery. *Adv. Drug Deliv. Rev.* 58, 1655–1670.
- Schütz, C., Agthe, M., Fall, A.B., Gordeyeva, K., Guccini, V., Salajková, M., Plivelic, T.S., Lagerwall, J.P.F., Salazar-Alvarez, G., and Bergström, L. (2015). Rod Packing in Chiral Nematic Cellulose Nanocrystal Dispersions Studied by Small-Angle X-ray Scattering and Laser Diffraction. *Langmuir* 31, 6507–6513.
- Shafiei-Sabet, S., Hamad, W.Y., and Hatzikiriakos, S.G. (2012). Rheology of nanocrystalline cellulose aqueous suspensions. *Langmuir ACS J. Surf. Colloids* 28, 17124–17133.
- Shafiei-Sabet, S., Hamad, W.Y., and Hatzikiriakos, S.G. (2014). Ionic strength effects on the microstructure and shear rheology of cellulose nanocrystal suspensions. *Cellulose* 21, 3347–3359.
- Sieglauff, C.L. (1959). Phase separation in mixed polymer solutions. *J. Polym. Sci. Part Polym. Chem.* 41, 319–326.
- Siqueira, G., Bras, J., and Dufresne, A. (2010a). Cellulosic Bionanocomposites: A Review of Preparation, Properties and Applications. *Polymers* 2, 728–765.
- Siqueira, G., Bras, J., and Dufresne, A. (2010b). New Process of Chemical Grafting of Cellulose Nanoparticles with a Long Chain Isocyanate. *Langmuir* 26, 402–411.

- Siqueira, G., Mathew, A.P., and Oksman, K. (2011). Processing of cellulose nanowhiskers/cellulose acetate butyrate nanocomposites using sol–gel process to facilitate dispersion. *Compos. Sci. Technol.* *71*, 1886–1892.
- Siqueira, G., Kokkinis, D., Libanori, R., Hausmann, M.K., Gladman, A.S., Neels, A., Tingaut, P., Zimmermann, T., Lewis, J.A., and Studart, A.R. (2017). Cellulose Nanocrystal Inks for 3D Printing of Textured Cellular Architectures. *Adv. Funct. Mater.* *27*.
- Siró, I., and Plackett, D. (2010). Microfibrillated cellulose and new nanocomposite materials: a review. *Cellulose* *17*, 459–494.
- de Souza Lima, M.M., and Borsali, R. (2004). Rodlike cellulose microcrystals: structure, properties, and applications. *Macromol. Rapid Commun.* *25*, 771–787.
- Sun, B., Hou, Q., Liu, Z., and Ni, Y. (2015). Sodium periodate oxidation of cellulose nanocrystal and its application as a paper wet strength additive. *Cellulose* *22*, 1135–1146.
- Sunasee, R., Hemraz, U.D., and Ckless, K. (2016). Cellulose nanocrystals: a versatile nanoplatform for emerging biomedical applications. *Expert Opin. Drug Deliv.* *13*, 1243–1256.
- Tang, J., Song, Y., Berry, R.M., and Tam, K.C. (2014a). Polyrhodanine coated cellulose nanocrystals as optical pH indicators. *RSC Adv* *4*, 60249–60252.
- Tang, J., Song, Y., Tanvir, S., Anderson, W.A., Berry, R.M., and Tam, K.C. (2015). Polyrhodanine coated cellulose nanocrystals: a sustainable antimicrobial agent. *ACS Sustain. Chem. Eng.* *3*, 1801–1809.
- Tang, J., Sisler, J., Grishkewich, N., and Tam, K.C. (2017). Functionalization of cellulose nanocrystals for advanced applications. *J. Colloid Interface Sci.* *494*, 397–409.
- Tang, Y., He, Z., Mosseler, J.A., and Ni, Y. (2014b). Production of highly electro-conductive cellulosic paper via surface coating of carbon nanotube/graphene oxide nanocomposites using nanocrystalline cellulose as a binder. *Cellulose* *21*, 4569–4581.
- Tardy, B.L., Yokota, S., Ago, M., Xiang, W., Kondo, T., Bordes, R., and Rojas, O.J. (2017). Nanocellulose–surfactant interactions. *Curr. Opin. Colloid Interface Sci.* *29*, 57–67.
- Tasset, S., Cathala, B., Bizot, H., and Capron, I. (2014). Versatile cellular foams derived from CNC-stabilized Pickering emulsions. *Rsc Adv.* *4*, 893–898.
- Thielemans, W., Warbey, C.R., and Walsh, D.A. (2009). Permselective nanostructured membranes based on cellulose nanowhiskers. *Green Chem.* *11*, 531–537.
- Tomatsu, I., Peng, K., and Kros, A. (2011). Photoresponsive hydrogels for biomedical applications. *Adv. Drug Deliv. Rev.* *63*, 1257–1266.
- Turbak, A.F., Snyder, F.W., and Sandberg, K.R. (1983). Microfibrillated Cellulose, a New Cellulose Product: Properties, Uses, and Commercial Potential. *J Appl Polym Sci Appl Polym Symp U. S.* *37*.
- Ureña-Benavides, E.E., Ao, G., Davis, V.A., and Kitchens, C.L. (2011). Rheology and Phase Behavior of Lyotropic Cellulose Nanocrystal Suspensions. *Macromolecules* *44*, 8990–8998.
- Urruzola, I., Robles, E., Serrano, L., and Labidi, J. (2014). Nanopaper from almond (*Prunus dulcis*) shell. *Cellulose* *21*, 1619–1629.
- Valentini, L., Bon, S.B., Cardinali, M., Fortunati, E., and Kenny, J.M. (2014). Cellulose nanocrystals thin films as gate dielectric for flexible organic field-effect transistors. *Mater. Lett.* *126*, 55–58.
- Valle-Delgado, J.J., Johansson, L.-S., and Österberg, M. (2016). Bioinspired lubricating films of cellulose nanofibrils and hyaluronic acid. *Colloids Surf. B Biointerfaces* *138*, 86–93.
- Villares, A., Moreau, C., Dammak, A., Capron, I., and Cathala, B. (2015). Kinetic aspects of the adsorption of xyloglucan onto cellulose nanocrystals. *Soft Matter* *11*, 6472–6481.

- Vroege, G.J., Thies-Weesie, D.M., Petukhov, A.V., Lemaire, B.J., and Davidson, P. (2006). Smectic Liquid-Crystalline Order in Suspensions of Highly Polydisperse Goethite Nanorods. *Adv. Mater.* *18*, 2565–2568.
- Vuoriluoto, M., Orelma, H., Johansson, L.-S., Zhu, B., Poutanen, M., Walther, A., Laine, J., and Rojas, O.J. (2015). Effect of Molecular Architecture of PDMAEMA–POEGMA Random and Block Copolymers on Their Adsorption on Regenerated and Anionic Nanocelluloses and Evidence of Interfacial Water Expulsion. *J. Phys. Chem. B* *119*, 15275–15286.
- Way, A.E., Hsu, L., Shanmuganathan, K., Weder, C., and Rowan, S.J. (2012). pH-Responsive Cellulose Nanocrystal Gels and Nanocomposites. *ACS Macro Lett.* *1*, 1001–1006.
- Wei, M., Gao, Y., Li, X., and Serpe, M.J. (2017). Stimuli-responsive polymers and their applications. *Polym Chem* *8*, 127–143.
- Williamson, R.E., Burn, J.E., and Hocart, C.H. (2002). Towards the mechanism of cellulose synthesis. *Trends Plant Sci.* *7*, 461–467.
- Wu, Q., Meng, Y., Wang, S., Li, Y., Fu, S., Ma, L., and Harper, D. (2014). Rheological Behavior of Cellulose Nanocrystal Suspension: Influence of Concentration and Aspect Ratio. *J. Appl. Polym. Sci.* *131*, 40525.
- Wu, W., Huang, F., Pan, S., Mu, W., Meng, X., Yang, H., Xu, Z., Ragauskas, A.J., and Deng, Y. (2015). Thermo-responsive and fluorescent cellulose nanocrystals grafted with polymer brushes. *J. Mater. Chem. A* *3*, 1995–2005.
- Xiao, X., and Sheng, P. (2013). Generalized Onsager theory of liquid crystals. *Phys. Rev. E* *88*, 062501.
- Xu, H.-N., Tang, Y.-Y., and Ouyang, X.-K. (2017a). Shear-Induced Breakup of Cellulose Nanocrystal Aggregates. *Langmuir* *33*, 235–242.
- Xu, Y., Atrens, A.D., and Stokes, J.R. (2017b). Rheology and microstructure of aqueous suspensions of nanocrystalline cellulose rods. *J. Colloid Interface Sci.* *496*, 130–140.
- Xu, Z., Uddin, K.M.A., and Ye, L. (2012). Boronic acid terminated thermo-responsive and fluorogenic polymer: controlling polymer architecture for chemical sensing and affinity separation. *Macromolecules* *45*, 6464–6470.
- Xue, B., Gao, L., Hou, Y., Liu, Z., and Jiang, L. (2013). Temperature controlled water/oil wettability of a surface fabricated by a block copolymer: application as a dual water/oil on–off switch. *Adv. Mater.* *25*, 273–277.
- Yang, X., and Cranston, E.D. (2014). Chemically cross-linked cellulose nanocrystal aerogels with shape recovery and superabsorbent properties. *Chem. Mater.* *26*, 6016–6025.
- Yang, X., Bakaic, E., Hoare, T., and Cranston, E.D. (2013). Injectable Polysaccharide Hydrogels Reinforced with Cellulose Nanocrystals: Morphology, Rheology, Degradation, and Cytotoxicity. *Biomacromolecules* *14*, 4447–4455.
- Yao, K., Meng, Q., Bulone, V., and Zhou, Q. (2017). Flexible and Responsive Chiral Nematic Cellulose Nanocrystal/Poly(ethylene glycol) Composite Films with Uniform and Tunable Structural Color. *Adv. Mater.* *29*.
- Ye, S.H., Watanabe, J., Iwasaki, Y., and Ishihara, K. (2003). Antifouling blood purification membrane composed of cellulose acetate and phospholipid polymer. *Biomaterials* *24*, 4143–4152.
- Yi, J., Xu, Q., Zhang, X., and Zhang, H. (2008). Chiral-nematic self-ordering of rodlike cellulose nanocrystals grafted with poly(styrene) in both thermotropic and lyotropic states. *Polymer* *49*, 4406–4412.

- Yi, J., Xu, Q., Zhang, X., and Zhang, H. (2009). Temperature-induced chiral nematic phase changes of suspensions of poly(N,N-dimethylaminoethyl methacrylate)-grafted cellulose nanocrystals. *Cellulose* 16, 989–997.
- Yoshida, R., Yamaguchi, T., and Kokufuta, E. (1999). New intelligent polymer gels: a self-oscillating gel with pacemaking and actuating functions. *J. Artif. Organs* 2, 135–140.
- Zeinali, E., Haddadi-Asl, V., and Roghani-Mamaqani, H. (2014). Nanocrystalline cellulose grafted random copolymers of N-isopropylacrylamide and acrylic acid synthesized by RAFT polymerization: effect of different acrylic acid contents on LCST behavior. *RSC Adv.* 4, 31428–31442.
- Zhang, C., Salick, M.R., Cordie, T.M., Ellingham, T., Dan, Y., and Turng, L.-S. (2015). Incorporation of poly (ethylene glycol) grafted cellulose nanocrystals in poly (lactic acid) electrospun nanocomposite fibers as potential scaffolds for bone tissue engineering. *Mater. Sci. Eng. C* 49, 463–471.
- Zhang, J., Xu, X.-D., Wu, D.-Q., Zhang, X.-Z., and Zhuo, R.-X. (2009). Synthesis of thermosensitive P(NIPAAm-co-HEMA)/cellulose hydrogels via “click” chemistry. *Carbohydr. Polym.* 77, 583–589.
- Zhang, J., Wu, Q., Li, M.-C., Song, K., Sun, X., Lee, S.-Y., and Lei, T. (2017). Thermoresponsive Copolymer Poly(N-Vinylcaprolactam) Grafted Cellulose Nanocrystals: Synthesis, Structure, and Properties. *ACS Sustain. Chem. Eng.* 5, 7439–7447.
- Zhang, N., Salzinger, S., and Rieger, B. (2012). Poly (vinylphosphonate) s with widely tunable LCST: a promising alternative to conventional thermoresponsive polymers. *Macromolecules* 45, 9751–9758.
- Zhang, Z., Sèbe, G., Rentsch, D., Zimmermann, T., and Tingaut, P. (2014). Ultralightweight and flexible silylated nanocellulose sponges for the selective removal of oil from water. *Chem. Mater.* 26, 2659–2668.
- Zhou, C., Wu, Q., and Zhang, Q. (2011). Dynamic rheology studies of in situ polymerization process of polyacrylamide–cellulose nanocrystal composite hydrogels. *Colloid Polym. Sci.* 289, 247–255.
- Zhou, D., Zhang, L., and Guo, S. (2005). Mechanisms of lead biosorption on cellulose/chitin beads. *Water Res.* 39, 3755–3762.
- Zoppe, J.O., Habibi, Y., Rojas, O.J., Venditti, R.A., Johansson, L.-S., Efimenko, K., Österberg, M., and Laine, J. (2010). Poly(N-isopropylacrylamide) Brushes Grafted from Cellulose Nanocrystals via Surface-Initiated Single-Electron Transfer Living Radical Polymerization. *Biomacromolecules* 11, 2683–2691.
- Zoppe, J.O., Österberg, M., Venditti, R.A., Laine, J., and Rojas, O.J. (2011). Surface Interaction Forces of Cellulose Nanocrystals Grafted with Thermoresponsive Polymer Brushes. *Biomacromolecules* 12, 2788–2796.
- Zoppe, J.O., Venditti, R.A., and Rojas, O.J. (2012). Pickering emulsions stabilized by cellulose nanocrystals grafted with thermo-responsive polymer brushes. *J. Colloid Interface Sci.* 369, 202–209.
- Zoppe, J.O., Ruottinen, V., Ruotsalainen, J., Rönkkö, S., Johansson, L.-S., Hinkkanen, A., Järvinen, K., and Seppälä, J. (2014). Synthesis of cellulose nanocrystals carrying tyrosine sulfate mimetic ligands and inhibition of alphavirus infection. *Biomacromolecules* 15, 1534–1542.
- Zuber, M., Zia, K.M., Bhatti, I.A., Ali, Z., Arshad, M.U., and Saif, M.J. (2012). Modification of cellulosic fibers by UV-irradiation. Part II: After treatments effects. *Int. J. Biol. Macromol.* 51, 743–748.
- Zubik, K., Singhsa, P., Wang, Y., Manuspiya, H., and Narain, R. (2017). Thermo-Responsive Poly(N-Isopropylacrylamide)-Cellulose Nanocrystals Hybrid Hydrogels for Wound Dressing. *Polymers* 9, 119.



# *Chapter II*

## **CNCs chemical modification**

---



## Table of content

<b>Introduction</b> .....	103
<b>1. Optimization of cellulose nanocrystals surface grafting with Poly(N-isopropylacrylamide) using aqueous conditions and microwaves assisted</b> .....	105
1.1. Introduction.....	106
1.2. Materials and Methods .....	109
1.2.1. Materials.....	109
1.2.2. Carboxylation of cellulose nanocrystals by TEMPO oxidation .....	109
1.2.3. Polymer grafting by peptidic coupling in water .....	110
1.2.4. Peptidic grafting assisted by microwave in water.....	111
1.2.5. Conductometric and pH-metric titrations: Carboxyl content .....	111
1.2.6. Fourier Transform Infrared Spectroscopy (FTIR).....	112
1.2.7. Elemental analysis (EA).....	113
1.2.8. Transmission Electron Microscopy (TEM).....	114
1.2.9. Dynamic Light Scattering (DLS) .....	114
1.3. Results and Discussion.....	115
1.3.1. Tempo oxidation of CNCs .....	115
1.3.2. Grafting of amine terminated Pnipam <sub>2500</sub> onto TEMPO CNCs .....	115
1.3.3. Quantitative analysis of Pnipam <sub>2500</sub> onto CNCs.....	119
1.3.4. Thermosensitive behavior of CNCs decorated with Pnipam <sub>2500</sub> .....	121
1.3.5. CNCs and Pnipam <sub>2500</sub> grafted onto CNCs (CNC-g-Pnipam <sub>2500</sub> ) characterization .....	123
1.3.6. Microwave optimization of CNC decorated with Pnipam <sub>2500</sub> .....	126
1.4. Conclusions.....	128
<b>2. Low molecular weight amino-poly(N-isopropyl acrylamide) adsorption configuration onto carboxylated cellulose nanocrystals for designing thermo-responsive hydrogels</b> .....	129
2.1. Introduction.....	130
2.2. Materials and Methods .....	132
2.2.1. Materials.....	132
2.2.2. TEMPO oxidation of CNC surfaces .....	132
2.2.3. Transmission Electron Microscopy (TEM).....	133
2.2.4. Pnipam <sub>2500</sub> adsorption on CNCs and TEMPO CNCs .....	133
2.2.5. Quartz Crystal Microbalance with dissipation (QCM-d).....	133
2.2.6. Isothermal titration calorimetry (ITC) of the Pnipam <sub>2500</sub> adsorption on CNCs and TEMPO CNCs .....	135
2.2.7. Small angle neutron scattering: Polymer conformation .....	135

2.2.8.	Dynamic light scattering (DLS) .....	136
2.2.9.	Atomic force microscopy (AFM) .....	136
2.2.10.	Viscoelasticity experiments on thermo-reversible hydrogel .....	136
2.3.	Results and discussion .....	137
2.3.1.	Oxidation of cellulose nanocrystals .....	137
2.3.2.	Adsorption characterization .....	138
2.3.3.	Small angle neutron scattering (SANS) of Pnipam <sub>2500</sub> and TEMPO CNCs .....	141
2.3.4.	DLS of Pnipam <sub>2500</sub> adsorbed on TEMPO CNCs system.....	144
2.3.5.	Viscoelasticity properties of thermo-responsive hydrogel based on TEMPO CNCs and Pnipam <sub>2500</sub> .....	145
2.4.	Conclusions.....	147
<b>Conclusions</b> .....		<b>149</b>
<b>References</b> .....		<b>151</b>

## II. CNCs chemical modification

### Introduction

As described in *Chapter I*, the CNCs high surface area and surface reactivity make them good candidate for chemical modification. The main objective of this Ph.D. is the realization of stimuli-responsive system based on cellulose nanocrystals and thermo-responsive polymers.

In this chapter, we have investigated the first Ph.D. challenge which is (i) CNCs functionalization with thermo-responsive polymers via green chemistry and up scalable grafting. Two strategies have been developed during this Ph.D.: chemical grafting versus irreversible surface adsorption.

Based on the literature, the first part (*Chapter II.1*) is dedicated to the modification of the TEMPO oxidized CNCs surface via peptidic coupling (or amidation). The grafting efficiency will be investigated for low molecular weight PNIPAM terminated with  $\text{NH}_2$ .

In *Chapter II.2*, the polymer physico-chemical adsorption strategy will be characterized in details. The surface of CNCs will be TEMPO oxidized to increase the amount of negative charges on the surface and ease the positively charged polymer adsorption. Some rheological properties will be introduced at the end of each part.



# 1. Optimization of cellulose nanocrystals surface grafting with Poly(N-isopropylacrylamide) using aqueous conditions and microwaves assisted.

*This section is adapted from "Erwan GICQUEL, Céline MARTIN, Laurent HEUX, Sébastien FORT, Bruno JEAN, Julien BRAS - Optimization of cellulose nanocrystals surface grafting with Poly(N-isopropylacrylamide) using aqueous conditions and microwaves assisting. Submitted in Carbohydrate Polymers, 2017"*

## ABSTRACT

This study presents the grafting of thermo-sensitive amine-terminated oligomers onto the surface of Cellulose NanoCrystals (CNCs). Pnipam<sub>2500</sub> grafting in aqueous condition via peptide coupling agent was explored to obtain CNC hydrogel with thermo-reversible aggregation and new colloidal properties. A large range of experimental techniques was used to investigate the properties of the CNC decorated with polymer and to confirm the grafting. Elemental analysis, infrared spectroscopy, solid state NMR and conductometric titration of washed CNC-g-Pnipam<sub>2500</sub> demonstrate that at least a part of Pnipam<sub>2500</sub> was covalently bonded with CNC, whereas TEM images present the individual dispersion of modified objects. A thermo-reversible aggregation was observed by Dynamic Light Scattering experiments. Microwave-assisted grafting was then used to optimize such reaction and it has been confirmed to improve the Pnipam<sub>2500</sub> density on surface using a much lower reaction time.

This thermo-reversible, bio-based and biocompatible system paves the way for the design of injectable hydrogel and biomedical nanocomposite materials.

## 1.1. Introduction

Cellulose is the most abundant organic polymer in nature. The increasing interest to use biodegradable, renewable, non-toxic and sustainable material has conducted to the increasing use of nanoscale cellulose in advanced materials. Among such nanoscale cellulose, Cellulose Nanocrystals (CNC) are obtained by acid hydrolysis and are rigid rod-shape particles with dimensions ranging from 3 to 30 nm in cross-section and from 100 to 500 nm in length. Known since 50's (Rånby, 1951), they exhibit several interesting properties including excellent mechanical strength, high aspect ratio, low density and an ability to self-organize into liquid crystalline phases (Habibi, 2014; Klemm et al., 2011; Moon et al., 2011; Revol et al., 1992). Besides, this treatment introduces also sulfate ester groups on the surface of CNC which induces a colloidal stability in aqueous media. Owing to their specific physical properties and high aspect ratio (depending on the source), CNC are used in several domains (Oksman et al., 2014) like environmentally friendly nanocomposites (Dufresne, 2013a; Eichhorn et al., 2010; Siqueira et al., 2010a), biomedical applications (Camarero Espinosa et al., 2016; Domingues et al., 2014; Endes et al., 2016; Jorfi and Foster, 2015; Klemm et al., 2011; Lin and Dufresne, 2014; Naseri et al., 2016), coatings & printing electronics (Gicquel et al., 2017; Hoeng et al., 2016; Li et al., 2013), hydrogels & aerogels (De France et al., 2016, 2017; Eichhorn et al., 2010). For the past 10 years, CNC are not only produced at laboratory scale but are now industrially available in high quantities (Chauve and Bras, 2014).

New properties can even be implemented to CNC by modify the numerous hydroxyl group at their surface. Several reviews focus on the chemical surface modification of CNC with molecule or polymers like in these studies (Eyley and Thielemans, 2014; Habibi, 2014; Tang et al., 2017). Two main approaches can be used to fabricate polymer brushes on surfaces of CNC, “grafting-from” or “grafting-onto”. The “grafting-from” creates high grafting densities polymer structures on CNC surfaces. As first steps, the surface is functionalized with an initiator monolayer. Then, polymerization is realized on the surface-initiated, resulting on the growth of the polymer brush directly from the surface (Alosmanov et al., 2017; Dong and Roman, 2007; Follain et al., 2010; Kan et al., 2013; Wu et al., 2015; Zoppe et al., 2010). However, the “grafting-from” method induces the presence of homopolymer and generally uses toxic solvent or reagent.

In the “grafting-onto” approach, a greener process can be tested. Presynthesized and well characterized polymer chains are attached directly to cellulose hydroxyl groups. Nonetheless, steric repulsion of grafted polymer chains can prevent optimal grafting and limit to low surface density grafts. As examples of the “grafting-to” process, Araki et al. and Kloser et al. grafted respectively epoxy-terminated polyethylene glycol (PEG) and polyethylene oxide (PEO) on CNC to create a sterically stabilized system (Araki et al., 2001; Kloser and Gray, 2010).

In this study, the “grafting-to” strategy is used. The aim is to create, by peptidic grafting, a covalent amide bond between a primary amine-terminated thermo-sensitive polymer and carboxylated CNC as shown in general scheme (**Figure 1**). In the literature, this approach has been successfully applied by coauthors to the grafting of copolymers of ethylene oxide and propylene oxide (named Jeffamines by Huntsman Corporation) on TEMPO oxidized CNC (Azzam et al., 2010, 2016). First, CNC are oxidized and then a polymer with amine derivatives on surface reacts with carboxylic group by a peptidic coupling reaction using a carbodiimide as amidation agent. Such reactions can be performed in organic solvent (Azzam et al., 2010) or in aqueous media (Azzam et al., 2016) but requires long duration and washing steps and presents a low yield. As reported in the literature, the realization of stimuli-sensitive CNC complex represents an interesting way to design smart biosourced materials, in particular in the field biomedical applications (Jorfi and Foster, 2015; Naseri et al., 2016).

In this work, we have focused on the peptidic grafting of one of the most common thermo-sensitive polymer Poly(N-isopropylacrylamide) also called PNIPAM. This polymer presents a lower critical solution temperature (LCST) at 32°C. Below the LCST, the polymer chains are in swollen coil conformation with highly hydrated chains. When the LCST is reached, the polymer becomes more hydrophobic and turns in a collapsed globule (Lai et al., 2013; Pelton, 2010; Plunkett et al., 2006; Schild, 1992). PNIPAM shows a LCST close to physiological temperature whatever the length is (Okahata et al., 1986), and has a huge potential in biomedical applications (Alosmanov et al., 2017; Chen et al., 2014; Hebeish et al., 2014).

In the literature, the “grafting-from” method has mainly been used to graft this thermo-sensitive chains (Alosmanov et al., 2017; Hemraz et al., 2014; Zoppe et al., 2010, 2011; Zubik et al., 2017). Zoppe and co-workers (Zoppe et al., 2010, 2011) grafted PNIPAM brushes from

CNC via SET-LRP, in which they control exactly the density and the length of brushes depending on the ratio of initiator and molecular ratio of NiPAAm monomer. In our knowledge, no previous works propose green “grafting-to” of PNIPAM on CNC.

Nevertheless, the peptidic grafting on CNC is a time-consuming process with low yield. To optimize this process, some assisted technologies such as ultrasonic wave and microwave are applied to accelerate organic reactions. In particular, microwave-assisted synthesis was first demonstrated in 1980's (Gedye et al., 1986; Giguere et al., 1986). Microwave chemistry is based on the efficient heating of materials by “microwave dielectric heating” effects (Kappe, 2004, 2008; Mingos and Baghurst, 1991). This phenomenon is dependent on the ability of a specific material (polar solvent or ion-conducting reagent) to absorb microwave energy and convert it into heat. This process also enhanced the probability of molecule to be in contact by increasing molecular entropy. Compared to conventional method, the benefits of microwave process are reduction of reaction times, improved yields, reproducibility and selectivity. A new field in green chemistry was opened (Caddick, 1995; Danks, 1999; Deshayes et al., 1999; Gabriel et al., 1998; Kaur and Gupta, 2017; Lew et al., 2002; Polshettiwar and Varma, 2008). Several works used this the microwave irradiation of cellulose to enhance its hydrolysis and create CNC (Lu et al., 2013) or bioethanol (Orozco et al., 2007; Zhang and Zhao, 2009). Also, researchers use it to graft molecules on cellulose: esterification of N,N-dimethyl-4-aminopyridine (DMAP) (Satgé et al., 2002), acrylic acid (Lin et al., 2010), metallic particles (Chen et al., 2008; Li et al., 2011), polycaprolactone (Lin et al., 2009) or glutaraldehyde (Cao et al., 2001). But only few use it in aqueous conditions and almost no study use it with CNC.

In this paper, we describe the grafting of thermo-sensitive polymer PNIPAM (with amine termination) onto the surface of cellulose nanocrystals using peptidic grafting method. To prove the functionalization of CNC, we characterize this new system by conductometric titration, infrared spectroscopy, solid state NMR and elemental analysis. Then, dynamic light scattering (DLS) and transmission electron microscopy (TEM) describe the structural modification on the nanoparticles. To complete this conventional grafting, we conclude this paper with a promising grafting optimization using microwave assisted reaction.

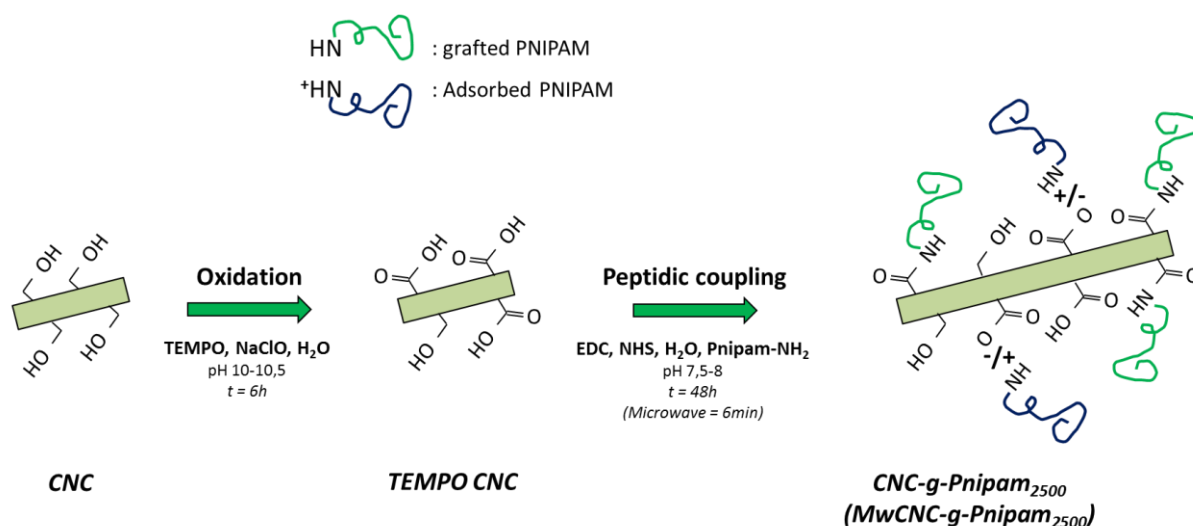


**Figure 1:** Schematic representation of chemical modification on CNCs presents in this work

## 1.2. Materials and Methods

### 1.2.1. Materials

Colloidal suspension of ~12%wt Commercial Cellulose NanoCrystals (CNCs) was purchased from UMaine process Development Center (University of Maine, USA). They have been produced from wood pulp using sulfuric acid hydrolysis process and have been never freeze-dried. The concentration was measured using a moisture analyzer (Ohaus® MB-35, Sigma-Aldrich, USA). Poly(N-isopropylacrylamide) with amine terminated was purchased from Sigma-Aldrich (USA). The molecular weight is about 2500 g·mol<sup>-1</sup>, and the LCST is close to 32°C. For the TEMPO oxidation, following chemicals are purchased from Sigma-Aldrich: 2,2,6,6-Tetramethyl-1-piperidinyloxy (TEMPO, 2564-83-2), Sodium hypochlorite (NaClO, 12%wt, 7681-52-9) and Sodium bromide (NaBr, 7647-15-6). For the peptidic grafting, chemicals are purchased from Sigma-Aldrich: N-(3-Dimethylaminopropyl)-N'-ethylcarbodiimide hydrochloride (EDC, 25952-53-8) and N-Hydroxysuccinimide (NHS, 6066-82-6). Other chemicals were purchased from Sigma-Aldrich. Distilled water was used for all experiments.

### 1.2.2. Carboxylation of cellulose nanocrystals by TEMPO oxidation

CNCs were subjected to TEMPO-mediation oxidation using a previously reported procedure (Habibi et al., 2006). 11 g of CNC were dispersed in 730mL of distilled water. Then, this suspension was exposed to an ultrasonic dispersive energy of 5 kJ per gram of dry CNC using

a 250 Watt sonication probe (Sonifier S-250A, Branson, USA) at 50% of maximum energy during 15 minutes in this case. To prevent burning of CNC during the dispersion, the suspension was placed in a crystallizer full of ice. TEMPO (323 mg, 2.07 mmol) and NaBr (3.564 mg, 34.61 mmol) were dissolved in 250mL of deionized water by magnetic stirring and slowly added to the CNC suspension. Then, 66 g (0.12M) of NaClO suspension was added dropwise to the suspension to start the oxidation. The mixture was stirred for 3 h at room temperature. The pH condition of the suspension was maintained between 10 and 10.5 by addition of sodium hydroxide solution (NaOH) at 0.5M during the reaction. Reaction was then quenched by the addition of ethanol (40 ml), the suspension color turned from yellow to white. The resulting CNC were washed with hydrochloric acid (HCl) at 0.5M, to decrease the pH to 1-2, at least three times by centrifugation (10 000 rpm, 30 min). After the last centrifugation, the oxidized CNC were re-dispersed in distilled water using the minimum volume to recover all CNC. This suspension was dialyzed against distilled water at least one week until a neutral pH was obtained (membrane 6-8 kDa). TEMPO CNCs were stored in the fridge at constant neutral pH to allow the CNC to be in their carboxylate form.

### 1.2.3. Polymer grafting by peptidic coupling in water

Grafting of amine-terminated PNIPAM<sub>2500</sub> on TEMPO CNCs was performed by peptidic coupling in water according to protocol of Bulpitt and Aeschlimann (Bulpitt and Aeschlimann, 1999). The reaction was performed at ambient temperature, and started with a ~1%wt TEMPO CNCs suspension,  $N_{COOH}$  is the mole of carboxyl unit measured by conductometry. This suspension was exposed to an ultrasonic dispersive energy using a 250 Watt sonication probe (Sonifier S-250A, Branson, USA) at 50% of maximum energy during 80 seconds per dry grams of CNC to remove any aggregates. The pH was adjusted to 4.5 (CNC-COOH configuration) with 0.5M HCl. Then, 2mL of EDC solution was added to the suspension ( $N_{EDC}$ : mol per carboxyl group) and stirred during 30 min. Then, 2mL of NHS solution was added ( $N_{NHS}$ : mol per carboxyl group) and stirred during 30 min. The pH was then adjusted to 7.5-8.0 before the addition of 10mL of an aqueous suspension containing PNIPAM-NH<sub>2</sub> ( $N_P$ : mol per carboxyl group). In accordance with the protocol of Azzam et al. (Azzam et al., 2010), all results were obtained with  $N_{EDC} = N_{NHS} = N_P = 4 \times N_{COOH}$ . The reaction lasted 48 h at room temperature under stirring while maintaining the pH at 7.5-8.0 by addition of 0.5M NaOH or 0.5M HCl. The reaction was quenched by the decreasing of the pH

at 1-2 by addition of 0.5M HCl and the resulting suspension was dialyzed against distilled water to remove excess of reagents at least seven days with exchange of water regularly until neutral pH is obtained. PNIPAM<sub>2500</sub> grafted CNC will be referred to as CNC-g-Pnipam<sub>2500</sub>.

#### 1.2.4. Peptidic grafting assisted by microwave in water

The microwave reactor used for the grafting was a Biotage® initiator classic at 2.45 GHz (BIOTAGE®, Sweden). All the procedure remained the same for microwave reaction than the regular peptidic grafting. CNC suspension, polymer, and coupling agents were mixed properly as stated above and the reaction was carried out in microwave conditions. The pH of the suspension was maintained at 7.5-8 before keeping it inside microwave reactor. The reaction was carried out for 6 min at 100°C with a pre-stirring of 30 seconds. After the completion of reaction ultra-filtration was performed over a night for purification with an EMD Millipore Amicon® bio separations stirred cell (Merck KGaA, Darmstadt, Germany). PNIPAM<sub>2500</sub> grafted CNC by microwave will be referred to as MWCNC-g-Pnipam<sub>2500</sub>.

#### 1.2.5. Conductometric and pH-metric titrations: Carboxyl content

The carboxyl content of oxidized CNC and grafted CNC were determined by conductometric titration coupled with pH-metric titration. About 15 mg of CNC was suspended in 200 mL of distilled water and treated by ultrasonic bath for 5min to remove gas and increase the dispersion. The pH of the suspension is adjusted to acidic condition (pH = 3) with 0.1 M HCl to replace the sodium counter-ions by protons. The suspension was then titrated with 0.2 mL increment of 0.01 M NaOH. The titration curves exhibit two turns: the first one corresponds to the NaOH neutralization of the strong acid due to the excess of HCl, and then follows by the neutralization of the weak acid related to the carboxyl content.

Degree of Oxidation (DO) of oxidized CNC is the number of primary hydroxyl groups that have been oxidized into carboxyl groups per AnhydroGlucose Unit (AGU). It was calculated according to the following **Equation 1** from Da Silva Perez et al. (Da Silva Perez et al., 2003):

$$(1) \quad DO = \frac{162 \times C \times (V_{eq2} - V_{eq1})}{m - 36 \times C \times (V_{eq2} - V_{eq1})}$$

Where 162 (g·mol<sup>-1</sup>) corresponds to the molar mass of an AGU,  $C$  (mol·L<sup>-1</sup>) is the exact concentration of the NaOH solution,  $m$  (g) is the weight of the oven-dried sample, 36 in

$\text{g}\cdot\text{mol}^{-1}$  corresponds to the difference between the molecular weight of an AGU ( $162 \text{ g}\cdot\text{mol}^{-1}$ ) and that of the sodium salt of a glucuronic acid moiety ( $198 \text{ g}\cdot\text{mol}^{-1}$ ), and  $V_{eq1}$  and  $V_{eq2}$  are the equivalent volumes of NaOH on the bends during the titration. To minimize errors, titrations were reproduced at least three times and an average value was used for the discussion.

**Equation 2** gives the calculation of the oxidation charge concentration ( $X_{ox}$ ), in  $\mu\text{mol}\cdot\text{g}^{-1}$ :

$$(2) \quad X_{ox} = \frac{C \times (V_{eq2} - V_{eq1})}{m}$$

Where  $C$  ( $\text{mol}\cdot\text{L}^{-1}$ ),  $m$  (g),  $V_{eq1}$  and  $V_{eq2}$  are the same as previously.

After grafting by peptidic coupling, a part of the carboxyl groups are consumed in the reaction with the amine-terminated polymer. A new oxidation rate  $X_{res}$  (in  $\mu\text{mol}\cdot\text{g}^{-1}$ ), corresponded to the residual carboxyl content, was calculated after conductometric titration as given by the following **Equation 3**:

$$(3) \quad X_{res} = \frac{C \times (V_{eq4} - V_{eq3})}{w}$$

Where  $C$  ( $\text{mol}\cdot\text{L}^{-1}$ ) is the exact concentration of the NaOH solution,  $w$  (g) is the pure dry CNC weight in total sample weight of the oven-dried sample (CNC and polymer) and  $V_{eq3}$  and  $V_{eq4}$  are the equivalent volumes of NaOH on the post-grafting titration.

Finally, the percentage of carboxyl groups which has been substituted ( $\%\text{COOH}_{\text{grafted}}$ ) was calculated according to the equation **Equation 4**, and represents the peptidic coupling yield:

$$(4) \quad \%\text{COOH}_{\text{grafted}} = \frac{X_{ox} - X_{res}}{X_{ox}} \times 100$$

### 1.2.6. Fourier transform infra-red spectroscopy (FTIR)

Infrared spectra of oxidized CNC and grafted CNC were performed using a Perkin-Elmer spectrum 65 (PerkinElmer, USA). Prior to avoid the superposition of the carbonyl band with the one of the water, CNC suspensions were acidified to pH 3. Samples were dried during 2 h in an oven at  $80^\circ\text{C}$  and reduced in powder form prior to analysis. KBr pellets containing 1%wt solid cellulose sample were prepared. At least spectra of two samples (to check the

reproducibility) per type of CNC were recorded in transmission mode with 16 scans in the 400-4000  $\text{cm}^{-1}$  wavenumber range.

### 1.2.7. Elemental analysis (EA)

Elemental analysis was carried out by the Analysis science institute of the “centre national de la recherche scientifique”, Lyon, France. The Carbon, Hydrogen, Oxygen, Sulfur and Nitrogen contents for CNC, TEMPO CNC, CNC-g-Pnipam<sub>2500</sub> and MwCNC-g-Pnipam<sub>2500</sub> were measured independently. The obtained results from elemental analysis were used to determine the Degree of Oxidation after TEMPO oxidation ( $DO_{EA}$ ) and the Percentage of COOH grafted ( $\%COOH_{grafted_{EA}}$ ), which is an average number of substituted cellulose hydroxyl groups per AGU by polymer groups. **Equation 5** and **Equation 6** give respectively these two parameters:

$$(5) \quad DO_{EA} = \frac{72.07 - \%C1 \times 162.14}{\%C1 \times 35.93}$$

$$(6) \quad \%COOH_{grafted_{EA}} = \frac{72.07 - 162.14 \times \%C2}{2500 \times \%C2 - 1609.47}$$

Where %C1 corresponds to the relative carbon content in oxidized sample, %C2 to the relative carbon content in grafted sample and 72.07, 162.14, 35.93, 2500 and 1609.47 are respectively the molecular weight of carbon in AGU, molecular weight of an AGU, the difference between the molecular weight of an AGU and an oxidized AGU with sodium salt, the molecular weight of the grafted polymer termination and the molecular weight of carbon in polymer termination.

### **Solid-State NMR**

NMR experiments were performed with a Bruker Avance DSX 400 MHz spectrometer operating at 100.6 MHz for  $^{13}\text{C}$ , using the combination of cross-polarization, high-power proton decoupling and magic angle spinning (CP/MAS) methods. The spinning speed was set at 12 kHz. The  $^1\text{H}$  radio frequency field strength was set to give a  $90^\circ$  pulse duration at  $2.5\mu\text{s}$ . The  $^{13}\text{C}$  radio frequency field strength was obtained by matching the Hartman-Hahn conditions at 60 kHz. Recording at least 2000 transients with contact time and recycle delay, respectively, of 2 ms and 2 s represented standard conditions. The acquisition time was set at 30 ms and the sweep width at 29400 Hz. The position and width of the lines were

maintained constant throughout a series of samples. The area corresponding to the integration of the  $C_1$  signal was used as an internal standard and set to one.

### **1.2.8. Transmission Electron Microscopy (TEM)**

Drops of about 0.001 %wt of CNC suspension were deposited onto glow-discharged carbon-coated TEM grids. After 2 minutes, the liquid in excess was absorbed with filter paper, and prior to drying, a drop of Urany-Less (Delta Microscopies, France) was deposited on the specimen. Then, after 2 minutes, the solution in excess was adsorbed and the grid was dried under room temperature. The sampling was observed using a Philips CM200 (FEI, USA) operating at 200 kV.

This protocol was adapted to account for the LCST of the grafted thermo-sensitive polymer ( $\sim 32^\circ\text{C}$ ). In a first case, TEM specimens were prepared at room temperature. In a second case, TEM specimens were prepared with CNC-g-Pnipam<sub>2500</sub> suspension and Urany-Less solution both preheated at  $50^\circ\text{C}$ .

### **1.2.9. Dynamic light scattering (DLS)**

DLS measurements were performed on Malvern Nano ZS instrument (Malvern instruments, United Kingdom). Samples were diluted in deionized water at  $10^{-2}$  %wt and the conductivity was adjusted to  $500 \mu\text{S}\cdot\text{cm}^{-1}$  by addition of NaCl solution. All measurements were made at a well-controlled ( $\pm 0.05^\circ\text{C}$ ) temperature at a backscattering detection angle of  $173^\circ$ . Non-negative least squares analysis (NNLS) was performed to achieve the intensity size distribution (corresponding to hydrodynamic diameter  $z^*$ ) from the analysis of the correlation function on the Malvern DTS software. For each samples, the final data in this paper represent an average of at least 3 acquisitions with 10 measurements.

## 1.3. Results and Discussion

### 1.3.1. TEMPO oxidation of CNCs

Aqueous commercial CNC suspensions were carboxylated using TEMPO oxidation process. By conductometric titration with equivalent volume  $V_{eq1}$  and  $V_{eq2}$  from **Figure 2a** and calculation with **Equation 1**, a degree of surface oxidation DO of 0.25 (mol/mol of anhydroglucose unit) and a oxidation rate  $X_{ox}$  of  $1450 \text{ } (\mu\text{mol}\cdot\text{g}^{-1})$  were obtained.

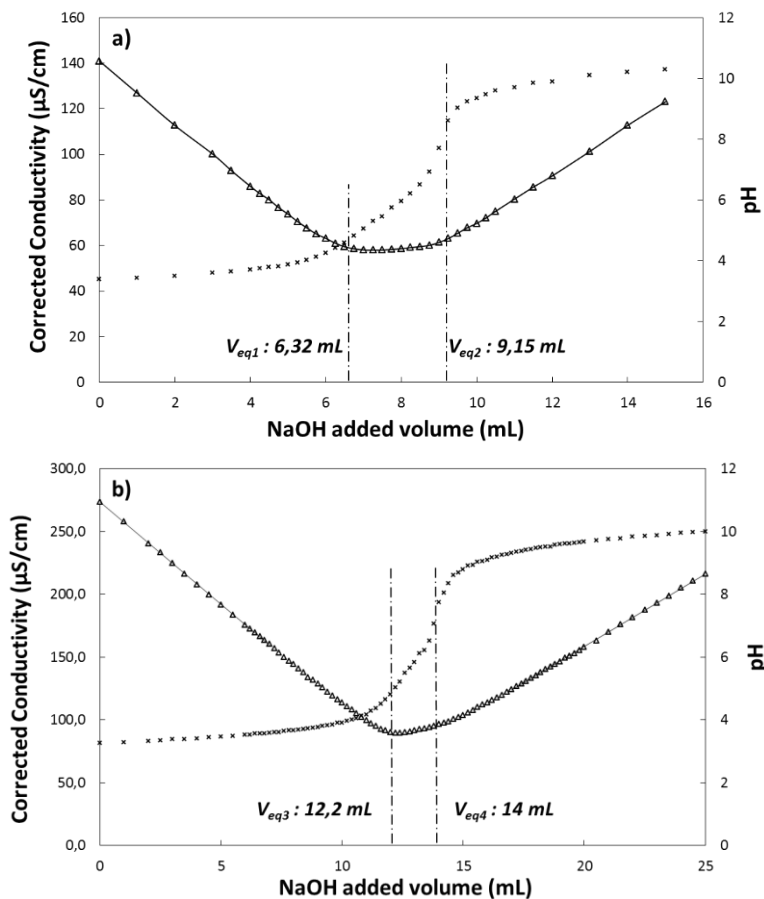


**Figure 2:** Conductometric ( $\Delta$ ) and pH (x) titration for a) TEMPO CNCs and b) CNC-g-Pnipam<sub>2500</sub>. Equivalent volumes  $V_{eq1}$ ,  $V_{eq2}$ ,  $V_{eq3}$  and  $V_{eq4}$  are respectively 6.32 mL, 9.15 mL, 12 mL and 14 mL.

### 1.3.2. Grafting of amine terminated Pnipam<sub>2500</sub> onto TEMPO CNCs

Aqueous TEMPO CNCs were grafted with amine terminated Pnipam<sub>2500</sub> via peptidic coupling. **Figure 2b** reports conductometric titration with equivalent volume  $V_{eq3}$  and  $V_{eq4}$ , respectively 12 mL and 14 mL. After calculation with **Equation 2** and **Equation 3**, the residual carboxyl content ( $X_{res}$ ) is  $1010 \text{ } (\mu\text{mol}\cdot\text{g}^{-1})$  and the percentage of carboxyl groups which has been substituted by amine groups ( $\% \text{COOH}_{\text{grafted}}$ ) is 30 %.

Nevertheless, these results are indirect proof of the grafting and would be similar in case of adsorption. FTIR spectroscopy and Elemental Analysis were performed to confirm the presence of the polymer chains onto the CNC. **Figure 3** shows FTIR spectra of **(Figure 3a)** regular CNC, **(Figure 3b)** TEMPO CNCs, **(Figure 3c)** TEMPO CNCs mixed with Pnipam<sub>2500</sub> and **(Figure 3d)** CNC-g-Pnipam<sub>2500</sub>. All samples have been extensively washed before any characterization using dialysis.

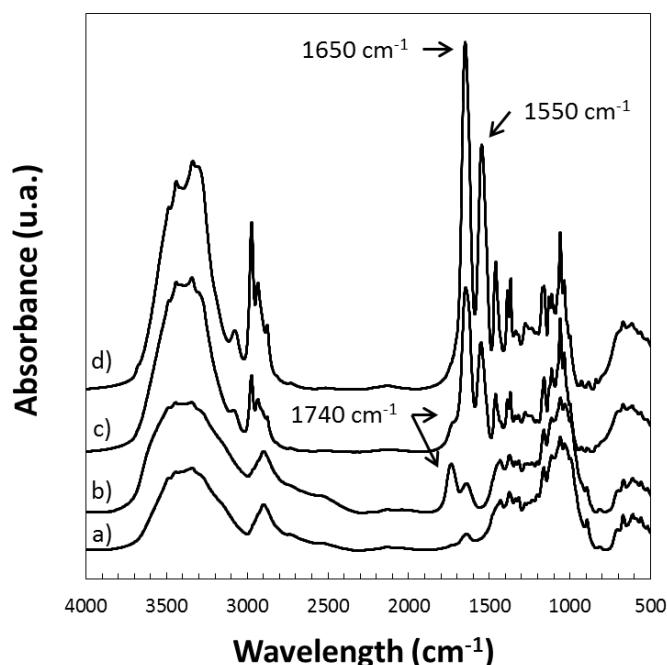


**Figure 3:** Infrared spectra of a) sulfated commercial CNCs, b) TEMPO CNCs c) TEMPO CNCs mixed with Pnipam<sub>2500</sub> and d) Pnipam<sub>2500</sub> grafted onto CNCs: CNC-g-Pnipam<sub>2500</sub>. Each spectra is normalized at 1110 cm<sup>-1</sup>.

Clear changes occur in each steps of the chemical modification. By comparing to the commercial CNCs, the spectra of the TEMPO CNCs exhibits a high absorption band at 1740 cm<sup>-1</sup>. This peak is characteristic to the acidic form of the carboxylic acid function (COOH), which validated the oxidation of CNCs. In the case of a peptidic grafting, peaks characteristic of the amide bonding appear in two absorption bands. Unfortunately in our case such amide bonds are also present in the polymer and cannot prove the grafting but mainly the presence or not of the polymer. The first band at 1650 cm<sup>-1</sup> can be attributed to the amide bond (amide I absorption band) but also to the residual water adsorbs on the cellulose (or polymer). Furthermore, at 1550 cm<sup>-1</sup>, another absorption peak characteristic of the N-H bond exists (called amide II band). On the **Figure 3c**, referring to Pnipam<sub>2500</sub> only mixed with TEMPO CNCs without coupling agent and following similar washing steps, the

two characteristic peaks of amide are present ( $1650$  and  $1550\text{ cm}^{-1}$ ). They prove the presence of Pnipam<sub>2500</sub> on the surface of CNCs even without grafting and after the washing steps. This result was surprising and we have first checked the efficiency of our washing procedure. By dialysis of pure Pnipam<sub>2500</sub> during 7 days, we have checked that most of the polymer (ab. 80-85%) pass through the membrane and is eliminated during the dialysis. The 15-20% still present seems to be non-solubilized polymer or impurities nanoparticles (like catalyst) present in this commercial grades, as proved by some DLS measurement showing some “dust” impurities of about 200nm dimensions. So as most of the Pnipam<sub>2500</sub> is eliminated, the **Figure 3c** confirms that such oligomer tends to be strongly physically adsorbed onto the CNC surface. This adsorption might be due to the hydrogen bonds and will be investigated more in details in another scientific paper.

However, the presence of a small peak at  $1740\text{ cm}^{-1}$  (e.g. COOH characteristic pic) indicates that still some carboxylic ends are available after adsorption and washing. In the case of the grafted sample (**Figure 3d**), the two characteristic peaks of the amide bond are present ( $1650$  and  $1550\text{ cm}^{-1}$ ). Even if it is not quantitative proof, the intensities of these peaks are largely superior to those one of Pnipam<sub>2500</sub> adsorbed on CNCs. Besides, as previously said PNIPAM-NH<sub>2</sub> contains N-H bonds in the repeating NIPAM monomer. The molecular weight  $\sim 2500\text{ g}\cdot\text{mol}^{-1}$  corresponds to  $\sim 22$  time of monomer ( $\sim 22$  amine groups) and one amine on the termination. So, with a superior intensity compared to **Figure 3c**, more Pnipam<sub>2500</sub> are present on the CNCs' surface which might be due to a different polymer configuration on the surface. In this case, the grafting efficiency is also revealed thanks to the disappearance of the  $1740\text{ cm}^{-1}$  peak which probably reveals the consumption of CNC's carboxyl groups in the reaction with the amine-terminated polymers. Probably one part of Pnipam<sub>2500</sub> is adsorbed and one part is grafted in this case but it is difficult to separate the amount of grafted and adsorbed polymer on CNCs.

So this FTIR analyses proves that Pnipam<sub>2500</sub> adsorbed onto oxidized CNCs surface and stay on the surface in spite of washing steps but also that when grafting is performed a higher quantity seems present and a major part of carboxylic group disappears.

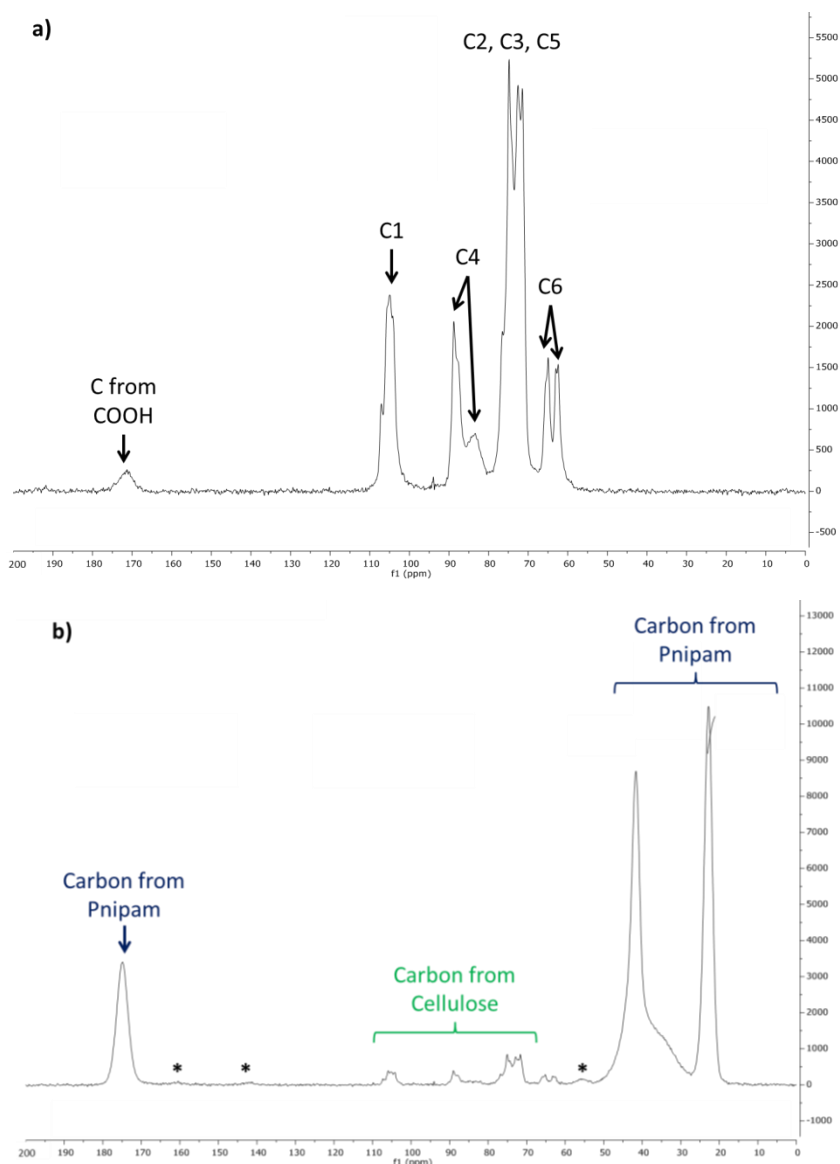


**Figure 4:**  $^{13}\text{C}$  Solid-state NMR spectra of A. TEMPO CNCs and B. CNC-g-Pnipam<sub>2500</sub>. Stars (\*) correspond to the spinning side band of Pnipam<sub>2500</sub> at 10 kHz (results not shown).

**Figure 4** shows the  $^{13}\text{C}$  solid-state NMR of TEMPO CNCs and CNC-g-Pnipam<sub>2500</sub>. In the case of TEMPO CNCs (**Figure 4a**), carbon contribution of the cellulose were clearly identified (Atalla and VanderHart, 1999; Montanari et al., 2005). The region between 60 and 70 ppm correspond to the C<sub>6</sub> carbon of the AGU, and between 70 and 80 ppm to the carbon contribution of the C<sub>2</sub>, C<sub>3</sub> and C<sub>5</sub>. C<sub>4</sub> contribution is the region between 83 and 88 ppm. The C<sub>1</sub> carbon appears at 105 ppm. The area corresponding to the integration of the C<sub>1</sub> signal was used as an internal standard and set to one. The contribution of the carboxyl group is located at 174 ppm (Montanari et al., 2005). The **Figure 4b** represents the NMR spectra after the grafting of Pnipam<sub>2500</sub> on CNCs (after dialysis washing steps). On this spectrum, the contribution of the carbon from the polymer is very high related to the internal standard on

C<sub>1</sub> (from 20 to 36 times the integration of the C<sub>1</sub> signal). The peptidic grafting creates a new link between carbon and nitrogen (i.e. a new amide). As already said, this link is also present inside the NIPAM monomer of the polymer chain, so it is difficult to separate the contribution of the carbon amide occurring after the grafting from the carbon amide in polymer contribution. The disappearance of the peak at 174 ppm could be due to the grafting but also to solid “dilution” due to the presence of Pnipam<sub>2500</sub>. The **Figure 4b** reveals indeed the presence in huge amount of PNIPAM on the CNCs surface after several washing steps. These values are in accordance with a presence of Pnipam<sub>2500</sub> on TEMPO CNCs surface, but cannot confirm if it is grafted or adsorbed. A comparison with only mixed Pnipam<sub>2500</sub> would not help due to this dilution but could give us more quantitative information. For such quantitative data, we have preferred using elemental analysis.

### 1.3.3. Quantitative analysis of Pnipam<sub>2500</sub> onto CNCs

Further evidence of the grafting of Pnipam<sub>2500</sub> from CNCs was supported by the elemental analysis of extensively washed CNC and used to quantify the amount of polymer present on the surface. **Table 1** shows the experimental atomic composition (C, H, N, O and S) of CNCs, TEMPO CNCs, CNC-g-Pnipam<sub>2500</sub> and CNCs mixed with Pnipam<sub>2500</sub>.

**Table 1:** Atomic composition determined by Elemental Analysis (standard deviation is considered to be related to equipment at 0.1 % for each value).

	Experimental values					Corrected values	
	% C	% H	% N	% O	% S	% C	%O
CNCs	40.2	6.0	< 0.1	49.7	0.9	44.44	49.37
TEMPO CNCs	37.0	5.9	< 0.1	52.2	0.8	40.91	51.80
CNC-g-Pnipam <sub>2500</sub>	53.8	8.9	8.9	24.3	0.3	59.50	24.13
TEMPO CNCs + Pnipam <sub>2500</sub>	53.9	8.8	9.1	24.2	0.2	59.69	24.04

In the case of pure cellulose, theoretical values of the weight fraction of carbon are 44.44% and 49.37% for oxygen, and theoretical ratio of oxygen-to-carbon is close to 1.11. Therefore, experimental value presents a ratio about 1.24 for CNC. It is well known that the difference between the theoretical and the experimental values in the case of the carbon content is probably due to sulfate content, the impurities present in the sample and experimental error. To incorporate this difference, the experimental values reported in **Table 1** are

corrected with the product between the experimental value obtained for a given material and the ratio of the theoretical to experimental value for non-grafted nanoparticles. This strategy has already been used to determine the degree of substitution (Missoum et al., 2012; Siqueira et al., 2010b).

In the case of TEMPO CNCs, the  $DO_{EA}$  calculated from the **Equation 5** gives an oxidation rate of about 0,38 which is close and in accordance with conductometry titration value (i.e.  $DO = 0,25$ ) if we consider the standard deviation of E.A. From these results, it is possible to estimate the surface density of the carboxyl content and to calculate the maximum amount possible of polymers which can be grafted. After a TEMPO oxidation, carboxylic groups are mainly on the surface of CNCs (Isogai et al., 2011). With a DO of about 0.25 and assuming that the surface of an AGU is  $1 \text{ nm}^2$ , it corresponds to a density  $\sim 25 \text{ COOH}$  every  $100 \text{ nm}^2$ . As the surface of CNC is  $150 \times 10 \times 10 \text{ nm}^2$  (i.e.  $6000 \text{ nm}^2$ ), the maximum grafting molecule will be with 1500 polymer chains per CNC. This value is equivalent to 75 wt% of Pnipam<sub>2500</sub> and 25wt% of CNC in the final system by using density and dimension for CNCs mass, and molecular weight and Avogadro Number for Pnipam<sub>2500</sub>.

The presence of a high amount of nitrogen content in the CNC-g-Pnipam<sub>2500</sub>, extensively washed confirms that Pnipam<sub>2500</sub> is present after grafting on TEMPO CNCs. This value is equivalent to the quantity of Pnipam<sub>2500</sub> of 5 wt% (using ratio of %C/%N), meaning 300 polymer chains on the surface of TEMPO CNCs. This value shows that all the COOH have not been grafted. But it is difficult to say if it is grafted or adsorbed. Indeed, unfortunately similar amount of Pnipam<sub>2500</sub> is present when only adsorption and washing occurs.

If we consider only adsorption, the surface of adsorbed polymer chains should be characterized by a mushroom regime, in which they do not interact together, in the case of moderate polymer densities. The size of the polymer is in the order of the gyration radius, which is 1.5 nm, given by  $R_g = 0.022 \times M_w^{0.54}$  (Kubota et al., 1990). To be in mushroom regime, each polymer needs to be at a distance higher than twice time the  $R_g$ . The CNC size is  $150 \times 10 \times 10 \text{ nm}^3$ . The surface occupied by a polymer is  $9 \text{ nm}^2$ , so on a CNC the maximum adsorbed polymer is  $\sim 600$  polymer chains. This value is in the range of grafting calculation. So in both case, adsorption and grafting similar amount of polymer chain can be present on CNC surface.

As a conclusion, it is difficult to have a direct proof of the grafting vs adsorption with techniques we have used. Our assumption is that similar amount of Pnipam<sub>2500</sub> is at the surface of CNC but in the case of adsorbed polymer, all polymer stick to the surface whereas when it is grafted, one part is grafted on the surface and another part is adsorbed. Indirect methods have then been performed to check if we have a difference between grafted and adsorbed system. Furthermore the elemental analysis gave us an idea of the ratio of Pnipam<sub>2500</sub> and CNC. This has been confirmed by weight measurement of suspensions. Indeed after grafting, all samples are washed directly with dialysis, so we are sure that CNCs stays (does not pass through dialysis membrane). So, knowing the initial CNCs mass and just by measuring the final mass, we can calculate the quantity of Pnipam<sub>2500</sub> which is still present (adsorbed or grafted or both). In our case this weight measurement gives a ratio of 25% of CNC and 75% of PNIPAM after adsorption and after grafting, which is in accordance with the similar value obtained by elemental analysis.

#### 1.3.4. Thermosensitive behavior of CNCs decorated with Pnipam<sub>2500</sub>

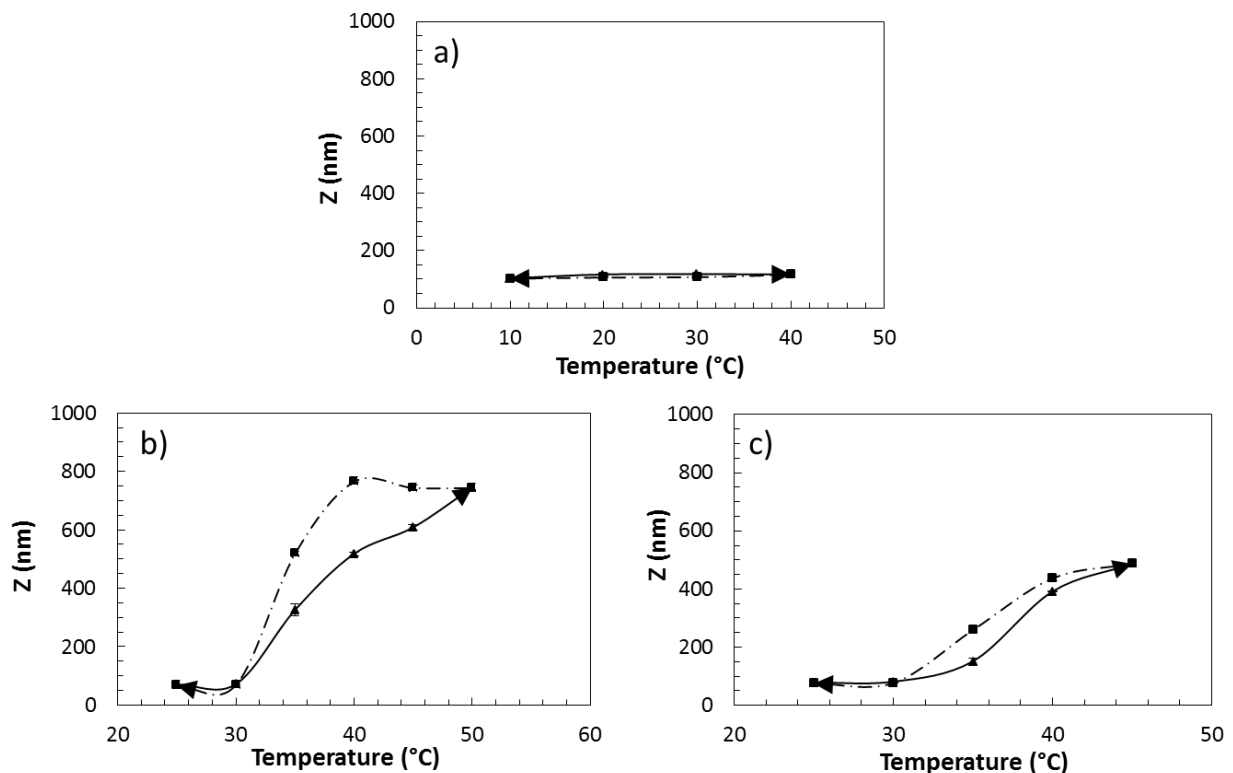


**Figure 5:** DLS curve for (a) TEMPO CNCs at 0.1 %wt, (b) CNC-g-Pnipam<sub>2500</sub> at 0.1 %wt (ratio estimated at 25% CNC and 75% Pnipam<sub>2500</sub>) and (c) TEMPO CNCs + Pnipam<sub>2500</sub> (ratio at 25% TEMPO CNCs and 75% Pnipam<sub>2500</sub>). Full line: temperature increases and dot line: Temperature decreases.

In **Figure 5**, the hydrodynamic diameter of CNC-g-Pnipam<sub>2500</sub> and TEMPO CNCs + Pnipam<sub>2500</sub> suspension and CNCs raw materials were measured as function of temperature. For TEMPO CNCs (**Figure 5a**), temperature has no clear influence on the size of the particles. Referring to the literature (Fujishige et al., 1989; Wu, 1998), PNIPAM shows sensitivity to the temperature. In works of Kubota (Fujishige et al., 1989; Kubota et al., 1990; Senff and Richtering, 1999; Wu, 1998) and Wu (Wang and Wu, 1999; Wu, 1998), under the LCST (~34°C), PNIPAM polymer presents coil conformation with hydrodynamic diameter about 100 nm. In our case the measurement of DLS was difficult due to the presence of impurities (catalyst nanoparticles or other) detected with an initial DLS value of 500nm which is not possible for a so short oligomer. Then above the LCST, the polymer turns in globule conformation and presents a hydrodynamic diameter about 20 nm. For the grafting sample CNC-g-Pnipam<sub>2500</sub> (**Figure 5b**), under the LCST the hydrodynamic diameter is low and constant (close to the CNC size as it is a short oligomer). After 30°C, an increase in size was observed (750 nm), probably due to aggregates formation. When the sample is cooling back to 20°C, the hydrodynamic diameter decreases and, at  $T < 30^{\circ}\text{C}$  the system recovers a low and constant value similar to the one measured during the heating process. This phenomenon is considered reversible, even if a 5°C hysteresis is observed. This result is very positive and confirms indirectly that (at least a part of) CNC is grafted mainly when it is compared with only adsorbed Pnipam<sub>2500</sub> (**Figure 5c**). In this case, the aggregation is limited compared to grafted molecule, and the maximum collapse system size is close to 480 nm. Nonetheless, the thermo-reversible behavior is similar in the case of grafted or adsorbed Pnipam<sub>2500</sub>. So the thermo-stimuli properties of CNC-g-Pnipam<sub>2500</sub> and TEMPO CNCs + Pnipam<sub>2500</sub> are different. This confirms indirectly that we don't have only adsorption in the first case.

The grafting of Pnipam<sub>2500</sub> polymer chain on the surface of CNCs gives a thermo-reversible behavior to the suspension, as proved by the thermo-reversible aggregation in DLS data. The behavior of a thermosensitive polymer was previously explained (Lai et al., 2013). In this study, when the temperature is below the LCST of Pnipam<sub>2500</sub>, grafted chains are under good solvent conditions. Steric repulsion forces between particles are maximal, and dispersion with individual objects appears. For temperature higher than the LCST, the polymer is in

poor solvent condition in water, resulting in individual collapsed and CNC-g-Pnipam<sub>2500</sub> are aggregated together. This process is reversible and generates a hysteresis effect.

### 1.3.5. CNCs and Pnipam<sub>2500</sub> grafted onto CNCs (CNC-g-Pnipam<sub>2500</sub>) characterization

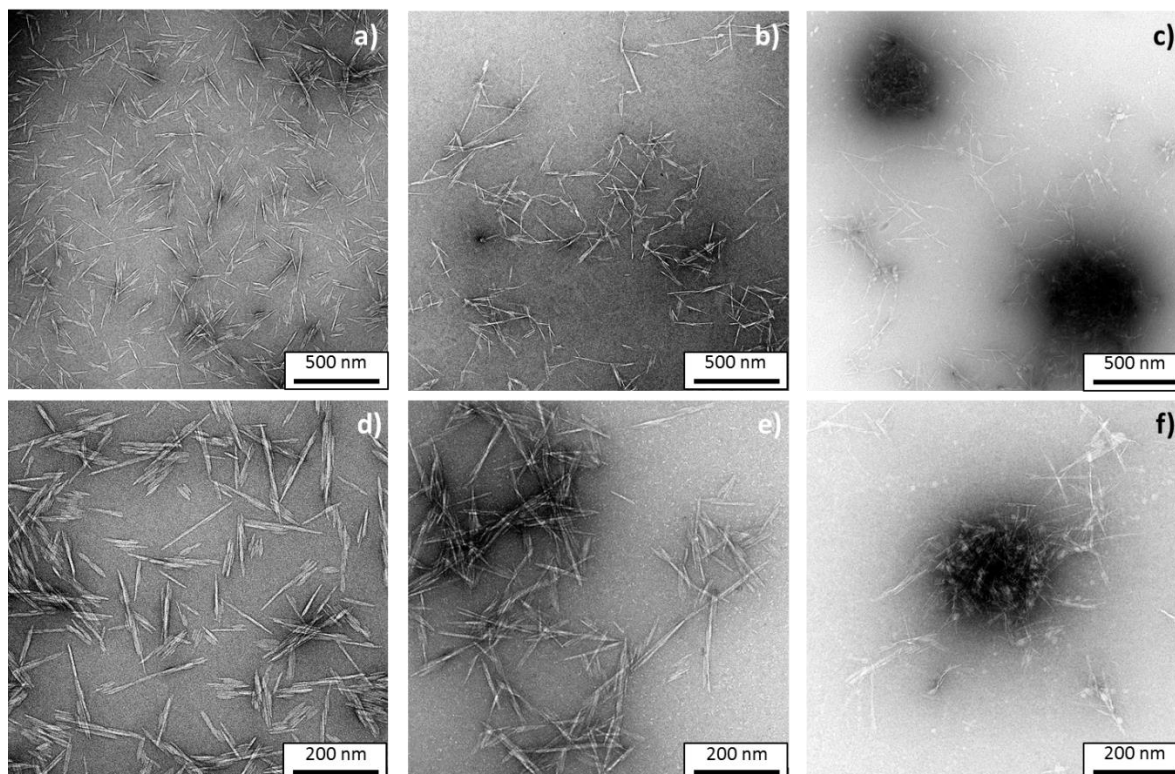


**Figure 6:** TEM images of a)-d) Cellulose NanoCrystals (CNCs) before any treatment and b)-e) CNC-g-Pnipam<sub>2500</sub> deposited on TEM grid at 20°C and c)-f) CNC-g-Pnipam<sub>2500</sub> deposited at 50°C. Pictures are representatives of each sample.

As confirmed in **Figure 6a** and **6d**, CNC have a rod-like shape. Size measurements on TEM images show an average length of  $150 \pm 30$  nm and a section of  $10 \pm 5$  nm. These values are comparable with the literature data (Habibi et al., 2010).

**Table 2:** Physical and chemical properties of CNCs from university of Maine.

Properties	Tools	Value	S.D.
Morphology	AFM & TEM	Length (nm)	150 (30)
		Thickness (nm)	10 (5)
		Aspect ratio	15 -
Chemical	EA	Sulfur content ( $\mu\text{mol}/g_{\text{CNC}}$ )	305 (15)
Physicochemical	Calculation based on EA & TEM	Surface charge density ( $\text{e}/\text{nm}^2$ )	0.46 (0.02)

In details in **Table 2**, the sulfur content estimated by elemental analysis is  $305 \mu\text{mol/g}_{\text{CNC}}$ . The surface charge density is approximately  $0.46 \text{ e/nm}^2$ , as calculated using TEM and EA data.

**Figure 6** presents TEM images of negatively stained CNC (**Figure 6a** and **6d**), CNCs decorated with Pnipam<sub>2500</sub> under LCST condition (**Figure 6b** and **6e**) and CNC-g-Pnipam<sub>2500</sub> after LCST (**Figure 6c** and **6f**). By comparison between **Figure 6d** and **Figure 6e**, the morphology of the rod-like particles is unchanged after peptidic grafting. Under LCST, Pnipam<sub>2500</sub> grafted CNCs seems to be well-dispersed. The individualization of nanocrystals can be attributed to the presence of polymer chains on the surface, which generate entropic repulsion forces between nanoparticles. Nonetheless, polymer chains are not visible on TEM images, due to their tiny size and a low surface density (hinder a detectable contrast in TEM stained grid). After LCST (**Figure 6c** and **6f**), CNC-g-Pnipam<sub>2500</sub> seems to be packed together and shows a ‘bird-nest’ configuration, due to the collapse Pnipam<sub>2500</sub> on the surface of TEMPO CNCs. These pictures are in agreement with Pnipam<sub>2500</sub> grafting and thermal aggregation of the system when the temperature is above the polymer LCST. Nonetheless, the system does not present CNC-g-Pnipam<sub>2500</sub> packed by 3-4 CNCs (as previously published by Azzam et al. (Azzam et al., 2016)) but a huge aggregate without well-defined size.

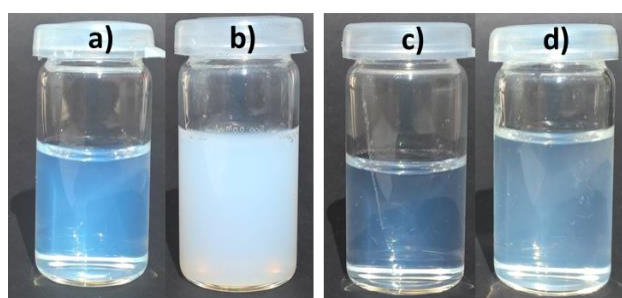


**Figure 7:** Pictures of cellulose nanocrystals suspension: a) oxidized CNC without salt, b) TEMPO CNCs with 1M NaCl, c) CNC-g-Pnipam<sub>2500</sub> without salt and d) CNC-g-Pnipam<sub>2500</sub> with 1M NaCl. Each suspension has a concentration of 2 wt%.

An interesting property acquired by the presence of polymer chains (adsorbed or grafted) on the CNC surface is the colloidal stability with presence of electrolyte. **Figure 7** shows the behavior of TEMPO CNCs and polymer grafted CNCs when NaCl is added. Colloidal suspension of TEMPO CNCs (**Figure 7a**) immediately precipitates after addition of 1 M NaCl

and forms a turbid suspension (**Figure 7b**). At the opposite, Pnipam<sub>2500</sub> grafted on CNCs suspension (**Figure 7c**) prevent any precipitation and remain stable the suspension in presence of electrolyte (**Figure 7d**). Steric stabilization caused by the presence of polymer (grafted or adsorbed) was already reported in literature (Araki et al., 2001; Azzam et al., 2010; Kloser and Gray, 2010).

**Figure 8** presents the rheological behavior of CNC-g-Pnipam<sub>2500</sub> and TEMPO CNCs + Pnipam<sub>2500</sub> under and above the PNIPAM LCST. System concentrations are 6.1 wt% (estimated ratio is 25% of CNCs and 75% of Pnipam<sub>2500</sub>). For grafted polymer (**Figure 8a**) the viscosity increases from 0.008 to 40 Pa·s at low shear rate when the LCST is reached. Nonetheless, in the case of polymer adsorption exclusively (**Figure 8b**), the viscosity increases only from 0.002 to 0.3 Pa·s when the LCST is reached. This visual observation shows a difference in kinetics of aggregation whereas similar amount of polymer is present. This confirms once again indirectly that there is a difference between these two CNCs materials. *A detailed study on the rheological behavior of these systems is presented in Chapter III.2.*

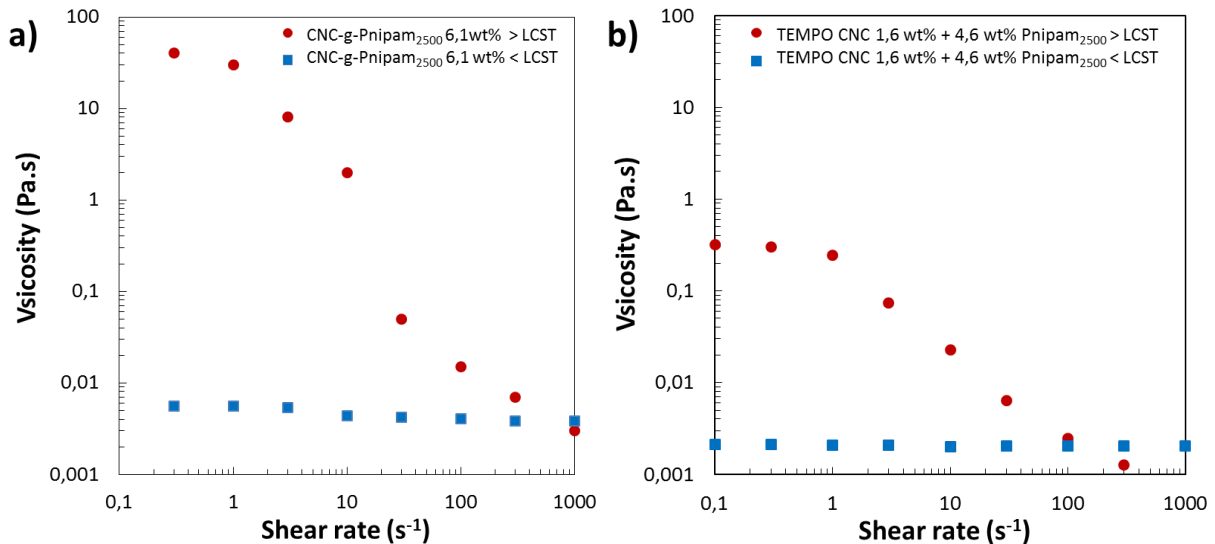


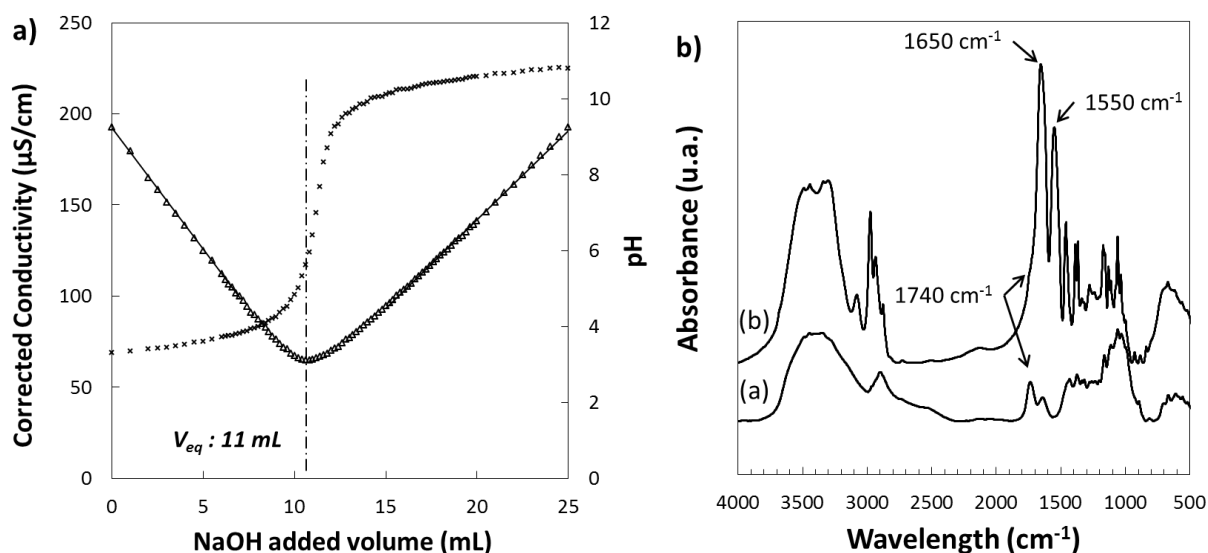
**Figure 8:** flow curves of a) CNC-g-Pnipam<sub>2500</sub> at 6.1 wt% and b) TEMPO CNCs at 1.6 wt% + Pnipam<sub>2500</sub> at 4.6 wt% (final concentration 6.2 wt%). Each graph presents the system flow curve under (blue square) and above (red dot) the PNIPAM LCST.

This peptidic grafting is promising and can modify CNCs suspension properties by using water based grafting or adsorption. One drawback could be attributed to the low quantity of grafting (similar to adsorption) and to the time duration of such treatment. One idea was then to use microwave to accelerate this surface modification and increase the grafting.

### 1.3.6. Microwave optimization of CNCs decorated with Pnipam<sub>2500</sub>

The last point investigated in this study is the optimization of the peptidic grafting process by microwave assisted reaction during only 6 minutes (48h under classical conditions). **Figure 9** reports main results of MwCNC-g-Pnipam<sub>2500</sub>. **Figure 9a** presents conductometric titration with equivalent volume  $V_{eq}$  at 11 mL. The weak acid has totally disappeared, the conductometric titration normally reveals a second equivalent volume. No carboxylic groups are available on the surface of TEMPO CNCs after grafting in the microwave condition. This means that COOH are not any more accessible either by adsorption or by grafting or a combination of both phenomena. In the second case, we could say that the degree of oxidation residual ( $DO_{res}$ ) is null and the yield of the peptidic coupling ( $DS_{COOH}$ ) is 100 %. In the case of only adsorption, it is possible that temperature increase adsorption but washing by long and successive dialysis at low pH and room temperature should eliminate similar amount than previous study. This has not been confirmed by experimental data due to a lack of samples.

TEMPO CNCs and TEMPO CNCs mixed with EDC and NHS were exposed to microwave assisted reaction to verify if an alteration of carboxylic acids occurred during the process. No changes are found with the degree of oxidation before and after microwaves. CNCs keeps also their rod-like structure as proved by AFM (*Chapter II.1*). Thereby, the microwave optimizes the peptidic grafting (or adsorption), and it seems that 100% of the available carboxylic groups are linked or occupied with Pnipam<sub>2500</sub> (grafted or adsorbed).



c)	Experimental values					Corrected values	
	% C	% H	% N	% O	% S	% C	%O
TEMPO CNC	40.1	5.8	< 0.10	50.2	0.9	44.41	49.93
CNC-g-Pnipam <sub>2500</sub>	53.8	8.9	8.9	24.3	0.3	59.50	24.13
MwCNC-g-Pnipam <sub>2500</sub>	56.3	9.2	9.9	22.9	0.2	62.31	22.81

**Figure 9:** a) Conductometric ( $\Delta$ ) and pH ( $x$ ) titration of CNCs grafted Pnipam<sub>2500</sub> after peptidic coupling optimized by microwave reaction: MwCNC-g-Pnipam<sub>2500</sub>. Equivalent volume  $V_{eq}$  is 11 mL. b) Infrared spectra of (a) TEMPO CNCs and (b) MwCNC-g-Pnipam<sub>2500</sub> and c) Atomic composition determined by Elemental Analysis of TEMPO CNCs, CNC-g-Pnipam<sub>2500</sub> and MwCNC-g-Pnipam<sub>2500</sub> (standard deviation is considered to be related to equipment and between 0.05 and 0.1 % for each value).

To complete these results, **Figure 9b** presents FTIR spectra of the MwCNC-g-Pnipam<sub>2500</sub>. As previously presented results, two characteristic peaks of the amine bond are present (1650 and 1550  $\text{cm}^{-1}$ ), but the presence of N-H bonds in the Pnipam<sub>2500</sub> polymer distorts the N-H grafting proof. By comparison with the spectra of CNC-g-Pnipam<sub>2500</sub> (**Figure 3c**) obtained for conventional grafting, the peak at 1740  $\text{cm}^{-1}$  disappears which proves a higher covering of carboxylic groups by Pnipam<sub>2500</sub>, mainly due to more numerous grafted PNIPAM on the surface of CNCs. The C=O involved in the amide link are identified at 1650 $\text{cm}^{-1}$ . **Figure 9c** completes these proofs with elemental analysis of extensively washed sample. The nitrogen content increases from 8.9% to 9.9% for normal reaction and microwave assisted reaction respectively. The %C also increases and the ratio of %C/%O decreases which confirm higher amount of Pnipam<sub>2500</sub>. With using the carbon content of MwCNC-g-Pnipam<sub>2500</sub> and the **Equation 6**, the microwave assisted percentage of COOH grafted ( $\% \text{COOH}_{\text{graftedEA}}$ ) is 0.56 on only 0.25 COOH available. The “grafting” yield is then 226%. This result suggests a grafting efficiency close to 100% and the presence of ‘extra’ grafting yield can be due to a strong adsorption of Pnipam<sub>2500</sub> on the surface of TEMPO CNCs during the adsorption of microwave radiative energy. Maybe the higher temperature induces a stronger aggregation which has difficulty to disaggregate and so to be eliminated during the washing steps. The yield obtained by elemental analysis is higher than the one obtained by conductometric titration and still higher than the one grafted in classic conditions. After microwave assisted reaction, the yield is maximized on the surface of TEMPO CNCs.

This result is very promising. When comparing with literature, this is the first time that such strategy is proposed with PNIPAM. Coauthors have already worked with success on similar approach but with other thermo-responsive polymer (e.g. Jeffamine).

## 1.4. Conclusions

In this study, thermo-sensitive Pnipam<sub>2500</sub> were successfully adsorbed and grafted (or both) onto oxidized cellulose nanocrystals by a green peptidic coupling. Results demonstrate the presence and the formation of the polymer onto the nanocrystals after extensive washings. The polymer density was sufficient to create a steric stabilization of the CNC-g-Pnipam<sub>2500</sub> in high ionic strength which prevents the flocculation. Microwave assisted grafting strongly improve the density of Pnipam<sub>2500</sub> on the surface of nanocrystals by decreasing the reaction time. This microwave process opens the potential of upscaling the final product. In spite of several methods, it has been difficult to distinguish the adsorbed from the grafted CNCs. However indirect methods show clearly a difference between the two samples indicating that of CNC-g-Pnipam<sub>2500</sub> has at least one part which is grafted. Whatever the case, thanks to this sufficient density, the thermo-reversible behavior of the polymer allows us to realize a thermo-reversible system composed with bio particles, CNCs, and biocompatible polymers, Pnipam<sub>2500</sub>. CNCs give good mechanical properties to the system and the polymer, a thermosensitive behavior. These results open the road to biomedical applications such as injectable hydrogel for reparative surgery and esthetic surgery.

## 2. Low molecular weight amino-poly(N-isopropyl acrylamide) adsorption configuration onto carboxylated cellulose nanocrystals for designing thermo-responsive hydrogels.

*This section is adapted from "Erwan GICQUEL, Céline MARTIN, Bruno JEAN, Emily D. CRANSTON, Julien BRAS - Low molecular weight Amino-Poly(N-isopropyl acrylamide) adsorption configuration onto carboxylated cellulose nanocrystals for designing thermo-responsive hydrogels Submitted in ACS Applied Materials & Interfaces, 2017"*

### ABSTRACT

The poly(N-isopropyl acrylamide) (PNIPAM) adsorption on cellulose nanocrystals (CNCs) was investigated. Commercial sulfated CNCs and TEMPO CNCs were compared to study the influence of surface chemistry and surface charge density on adsorption behavior. PNIPAM used in this study has an amine end group and a low molecular weight ( $2500 \text{ g}\cdot\text{mol}^{-1}$ ). At pH 6, amine groups are below their pKa and present positive charge favoring brush adsorption. Quartz crystal microbalance with dissipation (QCM-d) confirmed the adsorption of PNIPAM on cellulosic films indicating higher adsorption with more highly charged CNCs. Isothermal titration calorimetry (ITC) experiments determined that the polymer adsorption in suspension is an exothermic phenomenon driven by anionic-cationic interactions. The adsorbed polymer conformation on CNCs in suspension was analyzed using small angle neutron scattering (SANS) experiments which indicated that PNIPAM is in elongated conformation on the surface. The resulting polymer decorated CNCs exhibit new colloidal properties such as thermo-responsive behavior. Dynamic light scattering (DLS) and rheology were used to investigate the effect of temperature. This new and straightforward functionalization route for CNCs paves the way for the design of smart nanocellulose-based materials for application in injectable biomedical system.

**Keywords:** Cellulose nanocrystals, CNCs, PNIPAM, poly(N-isopropyl acrylamide), small angle neutron scattering

## 2.1. Introduction

With a huge availability and abundance on earth, cellulose is an important material in our day to day life. With approximately 250 megatons produced annually by biomass, cellulose is also considered as the most abundant organic polymer in nature (Urruzola et al., 2014). Over the past 15 years, growing interest from the scientific community has been reported for the nanoscaled particles derived from cellulose. In particular, cellulose nanocrystals (CNCs) is the sphere of interest with their recent industrial availability and the numerous reviews focusing on their unique properties (Abitbol et al., 2016; Dufresne, 2013b; Habibi, 2014; Habibi et al., 2010; J. Eichhorn, 2011; Klemm et al., 2011).

CNCs are the crystalline part of cellulose and are obtained through an acid hydrolysis process that removes the amorphous regions of natural cellulose fibrils. CNCs are rigid rod-like particles with dimension of 5 to 15 nm in cross section and 150 to 500 nm in length depending on the source (Bras et al., 2011; Dufresne, 2013b). Known since 1950's (Rånby, 1951), they exhibit several interesting properties including excellent mechanical strength, high aspect ratio, high surface area, chemically modifiable surfaces, low density and the ability to self-organize into liquid crystalline phases (Dong and Gray, 1997; Dong et al., 1996; Moon et al., 2011; Revol et al., 1992). All of these properties pave the way for a broad range of smart applications such as biomedical (Jorfi and Foster, 2015; Lin and Dufresne, 2014), composite material (Mariano et al., 2014; Siqueira et al., 2010c), electronics (Hoeng et al., 2016) or for example, as wastewater environmental adsorbents (Ahmadi et al., 2016; Batmaz et al., 2014; Yang and Cranston, 2014).

To take advantage of the CNC surface reactivity, surface oxidation by 2,2,6,6-tetramethyl-1-piperidinyloxy (TEMPO) has been widely used to introduce carboxylate groups on the surface (Araki et al., 2001; Habibi et al., 2006; Montanari et al., 2005). Several studies used TEMPO CNCs to functionalized the surface with carboxylate groups in order to try different modification chemistry strategies than OH grafting (Azzam et al., 2010; Carlmark et al., 2012; Filpponen and Argyropoulos, 2010; Zoppe et al., 2010). Carboxylate groups on CNCs introduce negative charges on the reactive surface which favor dispersion but also allow adsorption via cationic-anionic interaction. This strategy was already proposed in literature to connect CNCs and cationic polyelectrolytes or metal cations for example. In one of our

recent work (*Chapter III.3*), a block copolymer of poly(2-(dimethylamino) ethylmethacrylate) and poly(di(ethyleneglycol) methyl ether methacrylate) (PDMAEMA-PDEGMA) was adsorbed on TEMPO CNCs in order to produce a thermo-responsive hydrogel for biomedical applications. Similarly, De France et al. adsorbed poly(oligoethylene glycol methacrylate) on sulfated CNCs to use it as a cross-linker for injectable hydrogels (De France et al., 2016). Hoeng et al. used the interaction between carboxylated CNCs interaction with silver ions to produce a stable silver nanoparticle suspensions for printing electronics facilities (Hoeng et al., 2015).

Meanwhile the concept of “smart” materials is becoming increasingly studied. Among them, stimuli-responsive polymers especially designed to sharply and quickly respond to small environmental changes (physical or chemical) are of interest in several fields. Over the past 20 years, several fields of material applications were innovated by using these polymers. A large library of functional polymers has been studied as highlighted by a variety of reviews (Alarcón et al., 2005; Bawa et al., 2009; Cabane et al., 2012; Hoffman, 2013; Reineke, 2016; Schattling et al., 2014; Wei et al., 2017). One of the most studied synthetic thermo-sensitive polymers is poly(N-isopropylacrylamide) also commonly called PNIPAM, which presents a sharp coil-globule transition in water at its lower critical solution temperature (LCST) about 34°C (Lai et al., 2013; Plunkett et al., 2006; Schild, 1992). This LCST, close to physiological temperature whatever the length is (Okahata et al., 1986), and its biocompatibility renders PNIPAM-based materials particularly relevant for biomedical applications (Alosmanov et al., 2017; Chen et al., 2014; Pentlavalli et al., 2017).

Combining CNCs and thermo-responsive polymers has already been tested in previous studies (Azzam et al., 2016; Grishkewich et al., 2016; Haqani et al., 2017; Zhang et al., 2017; Zubik et al., 2017). More specifically, some researchers have grafted PNIPAM on CNC surfaces (Hemraz et al., 2014; Zoppe et al., 2010) as described in *Chapter II.2*, whereas others just mixed this stimuli responsive polymer with CNCs. Best results in the second case were achieved with TEMPO oxidized cellulose nanofibrils (Larsson et al., 2013; Lavoine et al., 2016; Vuoriluoto et al., 2015). It has been shown or admitted that this polymer can develop strong hydrogen bonds with cellulose. To the best of our knowledge, there is no previous study that monitors the conformation of adsorbed PNIPAM with the aim to understand the role of such organization on rheological measurements. Indeed such questions are critical.

The current study presents a thermo-responsive nanocellulose system assembled via anionic-cationic adsorption. In particular, the interactions between sulfated CNCs or TEMPO CNCs and amine-terminated PNIPAM were studied. The “connection” between cellulose and polymer was inferred from quartz crystal microbalance (QCM-d) and isothermal titration calorimetric (ITC). Small angle neutron scattering (SANS) experiments were performed to understand the polymer conformation on the CNC surface. Finally, a small rheological examination was developed to demonstrate a thermo-responsive hydrogel system.

## 2.2. Materials and Methods

### 2.2.1. Materials

A commercial suspension of cellulose nanocrystals (CNCs) from wood was purchased from UMaine Development Center (University of Maine, USA - CNCs produced at the Forest Products Lab in Maddison, WI) and was delivered at a concentration of ~12%wt. CNCs were been produced via sulfuric acid hydrolysis. The dry matter was measured using a moisture analyzer (Ohaus® MB-35, Sigma-Aldrich, USA). For the TEMPO oxidation, following chemicals are purchased from Sigma-Aldrich: 2,2,6,6-Tetramethyl-1-piperidinyloxy (TEMPO, 2564-83-2), Sodium hypochlorite (NaClO, 12%wt, 7681-52-9) and Sodium bromide (NaBr, 7647-15-6). Poly(N-isopropylacrylamide) with amine terminated were purchased from Sigma-Aldrich (USA) with molecular weight of 2500 g·mol<sup>-1</sup>. The LCST is close to 32°C. Other chemicals (HCl, NaOH) were purchased from Sigma-Aldrich. Distilled water was used for all experiments.

### 2.2.2. TEMPO oxidation of CNC surfaces

Carboxylic acid were added on CNC surface via TEMPO oxidation of primary alcohol of the cellulose unit as reported in literature (Habibi et al., 2006). Briefly, 11 g of CNCs were dispersed with ultrasonic energy (5 kJ·g<sub>CNC</sub> with 250 Watt sonic probe at 50% of maximum energy during 15 minutes) in 730 mL of distilled water. TEMPO (323 mg, 2.07 mmol) and NaBr (3.564 mg, 34.61 mmol) were dissolved in 250mL of deionized water by magnetic stirring and slowly added to the CNCs suspension. Then, the oxidation process starts with the addition dropwise of 66 g (0.12 M) of NaClO. The reaction runs during 3 h at room temperature, and the pH was maintained between 10 and 10.5 by addition of sodium hydroxide solution (NaOH) at 0.5 M. In order to stop the reaction, 40 mL of ethanol was

added in the suspension. Then, oxidant reagents were removed from the suspension thanks to three washing steps by centrifugation (10 000 rpm, 30 min) with hydrochloric acid (HCl) at 0.5 M. A final dialyzed step against distilled water for at least one week neutral pH was obtained (membrane 6-8 kDa). TEMPO CNCs were stored in the fridge at constant neutral pH to allow the CNC to be in their carboxylate form.

### **2.2.3. Transmission Electron Microscopy (TEM)**

Drops of about 0.001 %wt of CNC suspension were deposited onto glow-discharged carbon-coated TEM grids. After 2 minutes, the liquid in excess was absorbed with filter paper, and prior to drying, a drop of Urany-Less (Delta Microscopies, France) was deposited on the specimen. Then, after 2 minutes, the solution in excess was adsorbed with filter paper and the grid was dried under room temperature. The sampling was observed using a Philips CM200 (FEI, USA) operating at 200 kV and the most representative images among at least 10 views were selected.

### **2.2.4. Pnipam<sub>2500</sub> adsorption on CNCs and TEMPO CNCs**

The polymer adsorption on CNCs and TEMPO CNCs were performed at room temperature (between 20 and 25°C), i.e. a temperature inferior to the Lower Critical Solution Temperature (LCST) of the PNIPAM: 34°C. Polymer powder was directly added to the suspension of CNCs at different weight percent, and dispersed by magnetic stirring during 30 minutes.

### **2.2.5. Quartz crystal microbalance with dissipation (QCM-d)**

Cellulose model surfaces were prepared on QCM-d crystals coated with SiO<sub>2</sub> (QSX 303), supplied by Biolin Scientific AB (Sweden). QCM-d sensors were cleaned using UV-Ozone treatment for 15 minutes. Next, the sensor were spin-coated with a suspension of CNCs or TEMPO CNCs (2 %wt), at 4000 rpm for 30 seconds using a spin coater (SPIN150i Tabletop, spin coating POLOS, The Netherlands). The coating is considered successful when a uniform violet color across the sensor is visible. The spin-coated films were heat-treated at 80°C over night to ensure the stability of the CNC film on the sensor when submerge in water. Sensors were then rinsed with deionized water to remove loosely bound CNCs from the surface and

heat-treated at 80°C for another 2 hours. Full coverage of the spin coated layer was verified by atomic force microscopy (AFM).

The interactions between CNCs (TEMPO or unmodified) and Pnipam<sub>2500</sub>, in particular the adsorbed amount, were measured using a quartz crystal microbalance with dissipation (QCM-d, E4 model, Biolin Scientific Holding AB, Gothenburg, Sweden). Crystals coated with cellulose were mounted in the QCM-d chamber and exposed to a flow of MilliQ water at 0.07  $\mu\text{L}\cdot\text{min}^{-1}$  for a night to create a stable baseline before polymer injection. Then, experiments were run with a flow rate of 100  $\mu\text{L}\cdot\text{min}^{-1}$ . All experiments were conducted at constant temperature of 20°C. Pnipam<sub>2500</sub> polymer was injected with the same flow rate at 0.1 wt%. After reaching a plateau region, a rinsing step with a flow of MilliQ water was applied at 100  $\mu\text{L}\cdot\text{min}^{-1}$ .

The principles of the technique have been described by Rodahl et al (Rodahl et al., 1995). The change in resonance frequency is related to the mass added to the crystal, and thus adsorption or desorption of material induces a frequency shift. QTools software (version 3.0.15, Biolin) was used for data analysis of frequency and dissipation data (overtones 1, 3, 5, 7, 9, 11 and 13). The estimated adsorbed polymer amount ( $\Delta m$ ) was calculating using the Sauerbrey equation (**Equation 1**) (Sauerbrey, 1959) with assumption that created film is (i) rigid (it is valid if the dissipation change is inferior to 10 times the frequency change,  $\Delta f$ ) (Irwin et al., 2005; Voinova et al., 1999), (ii) uniform on the crystal and (iii) that mass is small compared to the mass of the crystal (Vuoriluoto et al., 2015). In complement, studies have shown that there is only a small difference between Sauerbrey and more advanced viscoelastic models like Voigt (Aulin et al., 2008; Karabulut et al., 2012; Krivosheeva et al., 2013).

$$(1) \quad \Delta m = -C \frac{\Delta f}{n}$$

With  $C$  is a constant related to the density and thickness of the quartz crystals with a value of 17.7  $\text{ng}\cdot\text{cm}^{-2}\cdot\text{Hz}^{-1}$  for 5 MHz crystal (provided by the manufacturer),  $\Delta f$  is the change in frequency and  $n$  is the overtone number. In this study the third overtone was used for the calculation of  $\Delta m$ . Q-tools frequency values are normalized, so  $n=1$  is utilized.

The layer thickness  $\Delta e$  in nanometer can be estimated via internal calculation of the QTools software (version 3.0.15, Biolin). The CNCs density about 1.65 was used for the calculation.

### **2.2.6. Isothermal titration calorimetry (ITC) of the Pnipam<sub>2500</sub> adsorption on CNCs and TEMPO CNCs**

The adsorptions of polymer onto TEMPO CNCs or CNCs were performed via calorimetric titrations on a Nano ITC low-volume system (TA Instruments-Waters LLC, Newcastle, DE). The experiment consists in collecting the energy released or consumed during the reaction on the surface of particles. Each injection lightly increases the amount of polymer on surface until a maximum. At this point, no energy modification is noted and the molar heat of injection ( $\Delta H$  in  $\text{kJ}\cdot\text{mol}^{-1}$ ) is determined. The measurements consisted of 18 successive injections of 2.5  $\mu\text{L}$  of Pnipam<sub>2500</sub> polymer (2.5 wt% in milliQ water) into a reaction cell containing 170  $\mu\text{L}$  of a 1 wt% CNCs (or TEMPO CNCs) suspension in distilled water. Prior to manipulation, all solutions and suspensions were degassed. All experiments were performed at room temperature under constant stirring at 350 rpm and at least duplicate. The software NanoAnalyze software (TA Instruments–Waters LLC, Newcastle, DE) was used to process titration heat signals on the reaction. In order to remove errors originating from the diffusion of titrant into the calorimetric cell, the first injections data were removed from the analysis (Velazquez-Campoy and Freire, 2006). A blank experiment (heat of dilution during polymer addition) was performed with the injection of Pnipam<sub>2500</sub> solution in MilliQ water into distilled water. These data were subtracted from the enthalpies measured for each run. The molar heat of injection per repeated unit ( $\Delta H$  in  $\text{kJ}\cdot\text{mol}^{-1}$ ) was determined by integrating each individual injection peak, as demonstrated previously for other polymer adsorbed onto the surface of CNCs (Boluk et al., 2012; De France et al., 2016).

### **2.2.7. Small angle neutron scattering: Polymer conformation**

In order to investigate the polymer conformation on the surface of CNC after Pnipam<sub>2500</sub> adsorption, small angle neutron scattering (SANS) experiments were performed. The concentrations of the different suspensions measured are 1 wt. % for TEMPO CNCs, 0.75 wt. % for Pnipam<sub>2500</sub> and 0.75 wt% of Pnipam<sub>2500</sub> adsorbed on 0.25 wt% TEMPO CNCs. As SANS is sensitive to the isotopic composition, all samples were dialyzed against deuterium oxide ( $\text{D}_2\text{O}$ ) in order to obtain the best contrast possible and to minimize the incoherent scattering

due to hydrogen. SANS experiments were carried out using the PA20 spectrometer at Laboratoire Léon Brillouin (CEA, Saclay, France). A large range of scattering vector,  $Q$ , between  $0.0024$  and  $0.44 \text{ \AA}^{-1}$  was probed using three different neutron wavelength/sample-detector distances ( $5 \text{ \AA}/18 \text{ m}$ ,  $5 \text{ \AA}/8 \text{ m}$ , and  $5 \text{ \AA}/1.5 \text{ m}$ ). Samples were studied at  $20^\circ\text{C}$  and  $40^\circ\text{C}$ , i.e. respectively below and above the polymer LCST. Samples were loaded in quartz cells (Hellma) with a path length equal to  $2 \text{ mm}$ . The averaged spectra were corrected for solvent ( $\text{D}_2\text{O}$ ), cell, and incoherent scattering (cell with  $1 \text{ mm}$  of  $\text{H}_2\text{O}$ ) as well as for background noise (Brûlet et al., 2007) and spectra  $I(Q) = f(Q)$  on an absolute scale were obtained. The data were fitted using the SasView® 4.0.1 modeling software.

### **2.2.8. Dynamic light scattering (DLS)**

DLS measurements were performed on Malvern Nano ZS instrument (Malvern instruments, United Kingdom). Samples were diluted in deionized water at  $10^{-2}$  %wt and the conductivity was adjusted to  $500 \mu\text{S}\cdot\text{cm}^{-1}$  by addition of NaCl solution. All measurements were made at a well-controlled ( $\pm 0.05^\circ\text{C}$ ) temperature at a backscattering detection angle of  $173^\circ$ . Non-negative least squares analysis (NNLS) was performed to achieve the intensity size distribution (corresponding to hydrodynamic diameter  $z^*$ ) from the analysis of the correlation function on the Malvern DTS software. For each samples, the final data in this paper represent an average of at least 3 acquisitions with 10 measurements.

### **2.2.9. Atomic force microscopy (AFM)**

Homogeneity of QCM-d films were imaged using AFM (Dimension icon®, Bruker, USA). QCM-d sensor, after spin-coating and drying over a night, were characterized in tapping mode using silica coated cantilever (OTESPA® 300 kHz - 42 N/m, Bruker, USA). Scans of  $5 \times 5 \mu\text{m}^2$  were performed to analyze dimensions of CNC. At least 4 images per samples were obtained and the most representative were taken into consideration.

### **2.2.10. Viscoelasticity experiments on thermo-reversible hydrogel**

Viscoelastic properties of the hydrogel based on Pnipam<sub>2500</sub> polymer adsorbed on TEMPO CNCs were carried out in the oscillatory mode with a rotatic rheometer Physica MCR 301 (Anton-Paar, Austria) with a cone-plate configuration (diameter of  $50 \text{ mm}$  and angle of  $1^\circ$ ). Oscillatory measurements were performed to collect transition from liquid to gel of each

sample. The strain imposed to the sample was inside the linear viscoelastic region (LVE) as determined by performing strain sweep experiments at a frequency of 1 Hz. Then the optimal frequency was determined by performing oscillation sweep experiments at the previously obtained strain in the LVE. These two values were fixed to achieve the storage modulus ( $G'$ , Pa) and the loss modulus ( $G''$ , Pa) on temperature plateau experiments at 20°C and 50°C. Experiments were at least triplicate to confirm its rheological behavior.

## 2.3. Results and discussion

### 2.3.1. Oxidation of cellulose nanocrystals

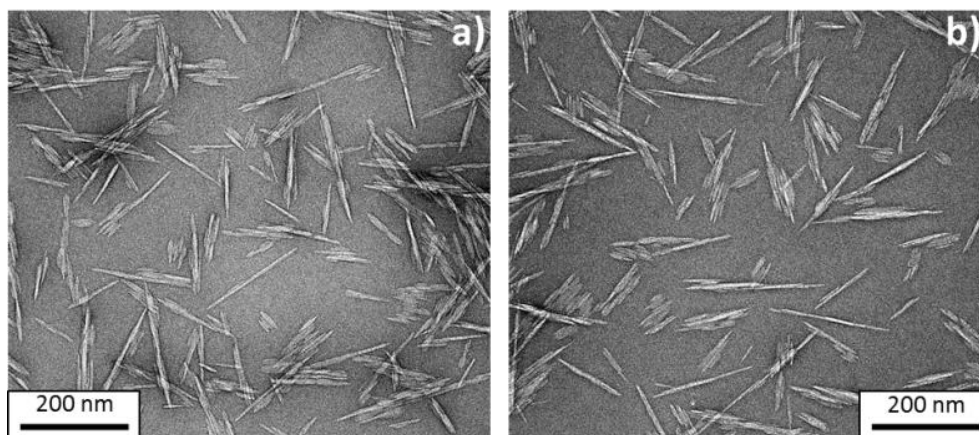


**Figure 1:** TEM images of a) CNCs and b) TEMPO CNCs.

After extraction from wood, CNC exhibits a rod-like shape, presented in **Figure 1a**. Size measurements on TEM images show an average length of  $150 \pm 30$  nm and a cross section of  $10 \pm 5$  nm. These values are comparable with the literature data (Reid et al., 2016). As CNCs used in this work were produced by sulfuric acid hydrolysis, some sulfate half ester groups are present on the CNC surfaces. After oxidation, TEMPO CNCs sizes are similar to CNC (**Figure 1b**) with length of  $150 \pm 10$  nm and diameter of  $10 \pm 5$  nm.

CNCs were oxidized using the well-known TEMPO procedure which provides regio-selective  $C_6$  oxidation (Da Silva Perez et al., 2003; Follain et al., 2010; Isogai et al., 2011). As detailed in *Chapter II.1*, by conductometric titration, a degree of oxidation DO of 0.25 (mol/mol of anhydroglucose unit) and an oxidation rate  $X_{ox}$  of  $1450$  ( $\mu\text{mol}\cdot\text{g}^{-1}$ ) were obtained.

### 2.3.2. Adsorption characterization

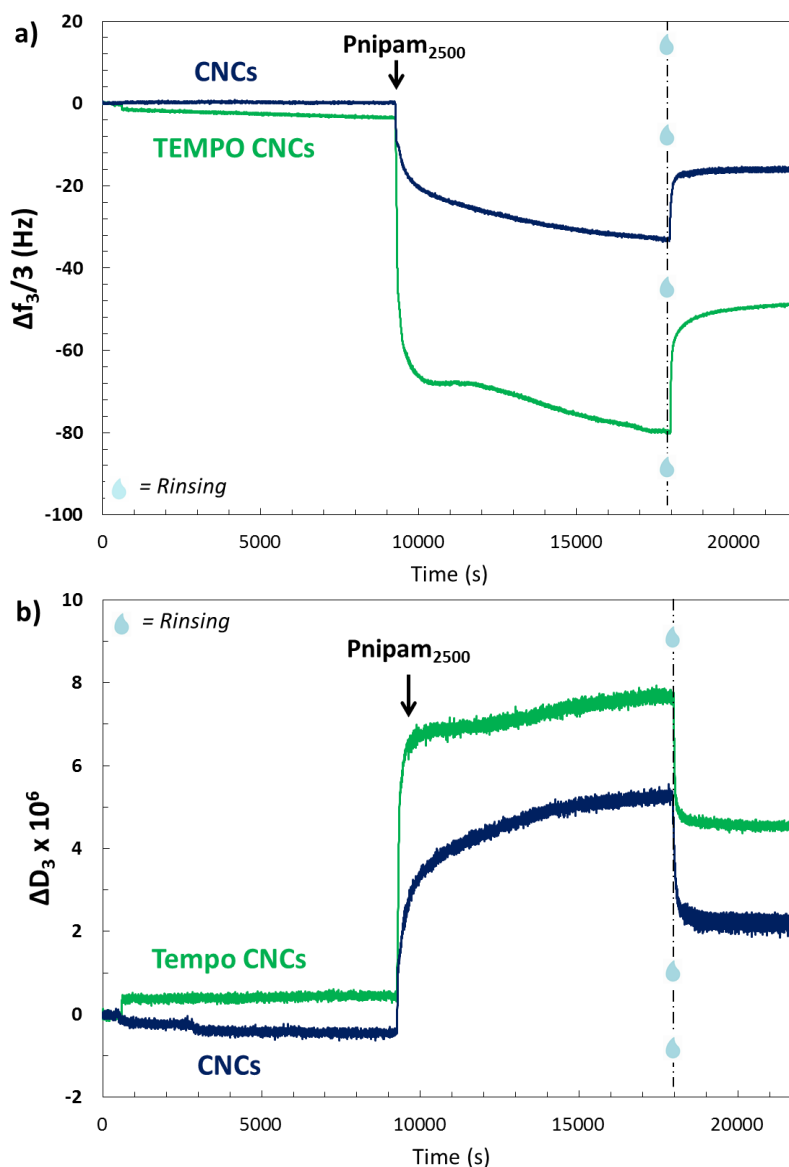


**Figure 2:** Real time QCM-d measurements present adsorption of Pnipam<sub>2500</sub> in shift frequency  $\Delta f_3$  normalized by dividing all values by  $n=3$  (a) and dissipation  $\Delta D_3$  (b) of overtone 3 on cellulosic films of CNCs and TEMPO CNCs. The vertical arrows indicate the time of Pnipam<sub>2500</sub> injection in the QCM-d module. The droplet symbols correspond to the rinsing with MilliQ water after adsorption. The adsorption was measured at 20°C, pH 6, flow rate at 100  $\mu\text{L}/\text{min}$  and at concentration of 0.1 wt%.

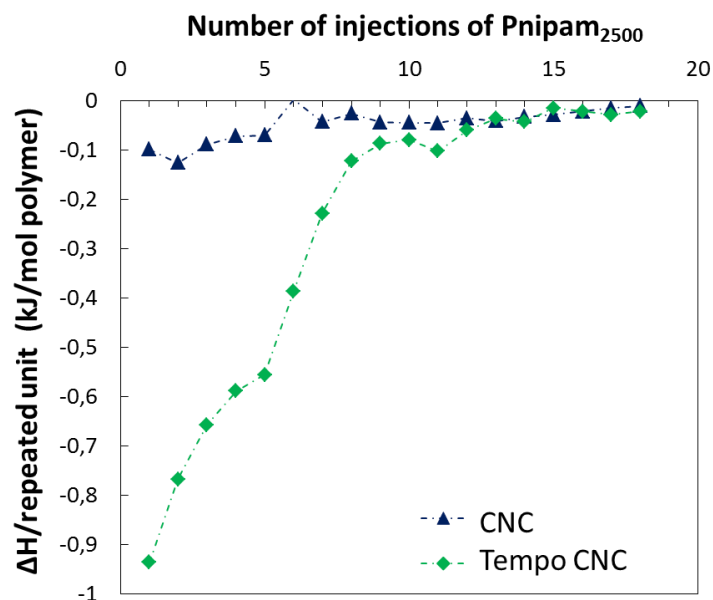
**Figure 2** presents the QCM-d measurements of the Pnipam<sub>2500</sub> adsorption to CNCs films. Two different cellulose surfaces were tested: unmodified sulfated CNCs and TEMPO CNCs. In both cases, measurements were performed at pH 6. Both CNCs are negatively charged at this pH,  $-\text{OSO}_3^-$  and  $-\text{COO}^-$  respectively. The existence of negative charges on the surface of CNCs, which is normally neutral, is due to the presence of sulfate ester ion ( $\text{SO}_3^-$ ) from the sulfuric acid hydrolysis. The Pnipam<sub>2500</sub> has an amine end group. The pKa of amine is close to 9. In the pH used in this study, the Pnipam<sub>2500</sub> is positively charged at the amine site (-

$\text{NH}_3^+$ ). Conditions are satisfied for a electrostatic interaction. **Figure 2a** and **2b** show the long plateau region at the beginning of the experiment which corresponds to the water swelling of cellulosic films. After polymer injection, sharp decrease in the frequency corresponding to adsorption of Pnipam<sub>2500</sub> on surfaces (**Figure 2a**). After rinsing, both cases present a decreasing in the frequency which corresponds to the release of loosely entangled (but unbound) polymer on the cellulosic surface. The final shift in frequency is 16.8 Hz and 45.6 Hz for CNCs and TEMPO CNCs respectively. Both associated dissipations (**Figure 2b**) show the same behavior, with a value higher with TEMPO CNCs. Dissipation values are small compared to examples from the literature (Reid et al., 2017; Vuoriluoto et al., 2015) due to the small polymer length and tighter adsorption (Pnipam<sub>2500</sub> is more an oligomer than a polymer with a repeated unit of about 22). **Table 1** shows the mass adsorbed calculated from these QCM-d measurements using Sauerbrey equation.

**Table 1:** QCM-d frequency and dissipation changes during Pnipam<sub>2500</sub> adsorption on CNCs and TEMPO CNCs with adsorbed amounts (**Equation 1**) and layer thickness of Pnipam<sub>2500</sub> on CNCs and TEMPO CNCs. Cellulose density is 1.6.

	$\Delta f_3/3$ (Hz)	$\Delta D_3$ ( $\times 10^6$ )	$\Delta m$ ( $\text{mg}\cdot\text{m}^{-2}$ )	$\Delta e$ (nm)
CNCs	-16.8	2.6	$3.0 \pm 0.1$	1.7
TEMPO CNCs	-45.6	4	$8.1 \pm 0.1$	5.0

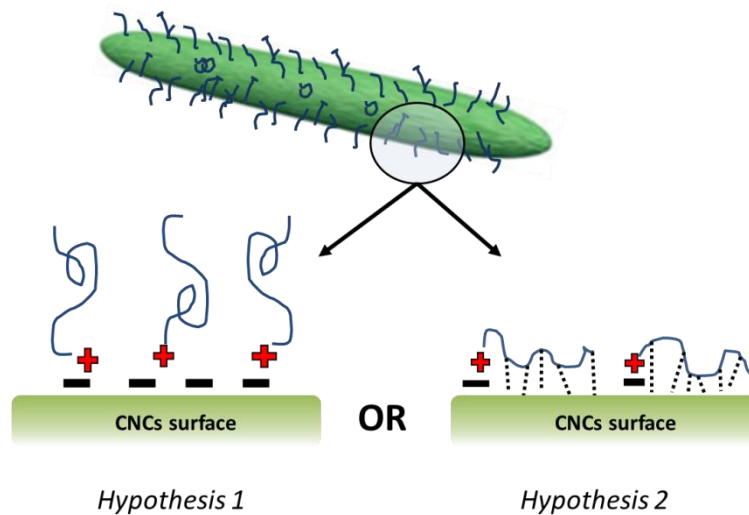
At the end of the QCM-d experiments on sulfated CNCs, the amount of polymer adsorbed after rinsing is  $3.0 \pm 0.1 \text{ mg}\cdot\text{m}^{-2}$  and the thickness of the polymer layer is  $\sim 1.7 \text{ nm}$ . These values are in accordance with a limited adsorption of Pnipam<sub>2500</sub> on CNCs surface. Besides, on TEMPO CNCs, the amount of polymer adsorbed is  $8.1 \pm 0.1 \text{ mg}\cdot\text{m}^{-2}$  and the thickness of polymer is  $\sim 5.0 \text{ nm}$ . Due to the presence of several negative charges (carboxylic acid in  $-\text{COO}^-$  form), the adsorption is 2.5 times higher than the results for CNCs. QCM-d experiments demonstrate the adsorption of Pnipam<sub>2500</sub> onto CNC films but does not necessarily correspond to polymer-CNC behavior in suspension. The adsorption behavior of Pnipam<sub>2500</sub> to CNCs and TEMPO CNCs in suspension can be explored via ITC. In this case, ITC experiments give complementary and additional information about the driving forces responsible for Pnipam<sub>2500</sub> adsorption to nanoparticles. This experiment measures the energy released or consumed during the reaction (i.e., the adsorption of PNIPAM to the surface of particles) via the molar heat of injection  $\Delta H$  ( $\text{kJ}\cdot\text{mol}^{-1}$ ). **Figure 3** shows these results for sulfated CNCs and TEMPO CNCs.



**Figure 3:** Molar heat of injection per repeated unit for the titration of 2.5 wt% of Pnipam<sub>2500</sub> polymer into suspension of 1 wt% CNCs (blue  $\Delta$ ) or 1 wt% TEMPO CNCs (green  $\diamond$ ). The heat of dilution measured for Pnipam<sub>2500</sub> in MilliQ water has been subtracted from the titration curves  $\Delta H$  of this figure.

**Figure 3** shows a clear difference between the molar heat of injection of Pnipam<sub>2500</sub> on CNCs and Tempo CNCs suspension. Normalized by the number of PNIPAM repeat units, adsorption on CNCs presents a  $\Delta H$  about -0.1 kJ/mol. This interaction is lightly exothermic and the surface saturation by polymer occurs quickly. On TEMPO CNCs, the molar heat of injection is maximized with a value of -0.95 kJ/mol. As  $\Delta H$  is negative, the interaction between Pnipam<sub>2500</sub> and TEMPO CNCs is exothermic and enthalpically driven as expected by anionic-cationic interaction. These results are in accordance with the QCM-d conclusions: Pnipam<sub>2500</sub> adsorbs to both types of CNCs but significantly more adsorption occurs with Tempo CNCs compared to sulfated CNCs, likely because the TEMPO CNCs have a higher surface charge density.

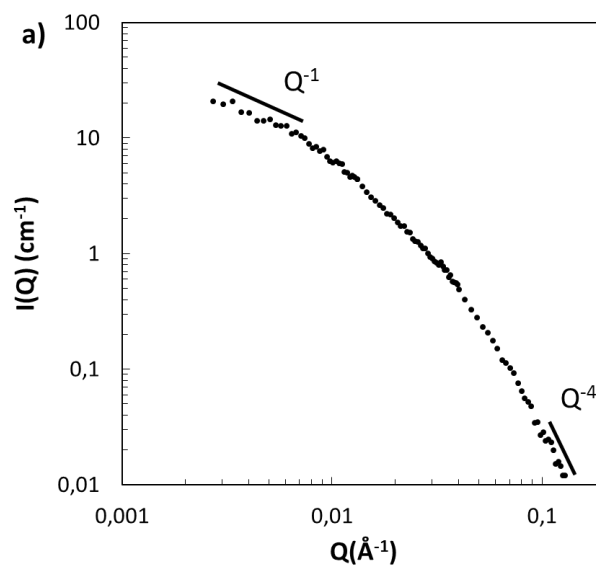
As hydrogen bonding is also possible between cellulose OH groups and amide groups in the Pnipam<sub>2500</sub> repeat unit, it was interesting to investigate polymer configuration at CNCs surface to understand whether the primary interaction is with the PNIPAM end group (amine) or the polymer repeat units/backbone. Neutron scattering is ideally suited for this investigation. Two adsorption hypotheses are depicted schematically in **Figure 4** showing either end-on brush-like adsorption or a flatter adsorbed conformation. The following SANS investigations focus on TEMPO CNCs with Pnipam<sub>2500</sub>.



**Figure 4:** Adsorption hypotheses: 1) ionic bonds and 2) ionic and hydrogen bonds.

### 2.3.3. Small angle neutron scattering (SANS) of PnIPam<sub>2500</sub> and TEMPO CNCs

SANS measurements were performed to understand the structure and organization of PnIPam<sub>2500</sub> on TEMPO CNCs after adsorption in aqueous suspension. The question was: have we created a brush system bound to the CNC surfaces only through the amine terminal groups? This technique is well adapted for such soft matter questions. Indeed the neutron wavelength probes a characteristic size between 1 and 100 nm, which is a well-adapted to describe conformation and organization between CNCs and polymers. This technique is not destructive and the final result is an average value representative of the macroscopic sample organization.



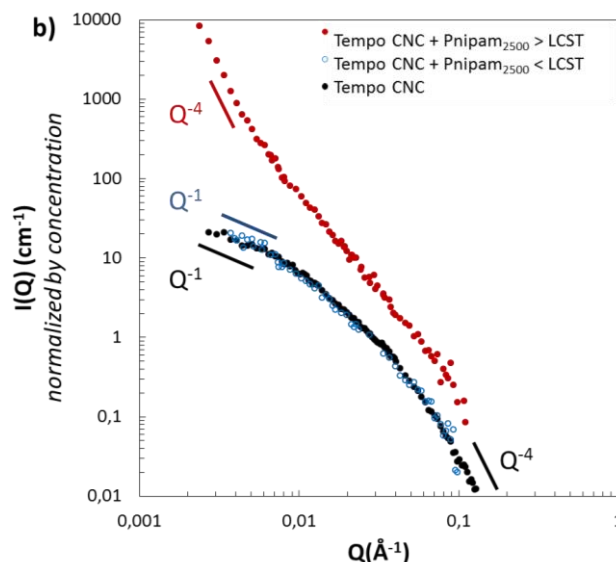


**Figure 4:** SANS curves for a) 1 wt% TEMPO CNCs at 20°C and b) 0.25 wt% TEMPO CNCs mixed with 0.75 wt% Pnipam<sub>2500</sub> system under and above the LCST (TEMPO CNC curves was added with a down shift for superposition). Slope fitting curves are indicated on each graph.

**Figure 4a** shows the SANS results for Tempo oxidized CNCs. In the small  $Q$  range, the intensity decays with a  $Q^{-1}$  slope, which is representative of rod-shaped particles. In the high  $Q$  region, a  $Q^{-4}$  slope is observed, which shows that TEMPO CNCs exhibit a sharp interface with the solvent. By fitting this curve using the form factor of a parallelepiped rod using the SasView software, dimensions of  $110 \times 17 \times 4 \text{ nm}^3$  could be extracted, which are in good agreement with our TEM measurements (**Figure 1**). It has to be noted that the length of Tempo CNC estimated by SANS is not accurate, since measurements at lower  $Q$  values would be required. In literature, PNIPAM polymer was already studied by SANS experiment by Kubota et al. in 1990 (Kubota et al., 1990). They proposed an equation which links the molecular weight of PNIPAM polymer and its radius of gyration (**Equation 2**).

$$(2) \quad R_g = \alpha \times M_w^{0.54}$$

Where  $R_g$  is the radius of gyration of polymer in Å,  $\alpha$  is a coefficient equal to 0.22 and  $M_w$  is the molecular weight of the polymer in  $\text{g} \cdot \text{mol}^{-1}$ . In the present study, the gyration radius of Pnipam<sub>2500</sub> via this equation is 1.5 nm.

The SANS spectra of a sample corresponding to Pnipam<sub>2500</sub> polymer adsorbed on TEMPO CNCs is shown in **Figure 4b** at temperatures both below and above the LCST of PNIPAM. Below the LCST, the system presents a SANS curve very similar to the one of TEMPO CNCs (**Figure 4a** and added on the graph for a better readability). The adsorbed system does not

show any sign of aggregation under the LCST, i.e. a good dispersion of individualized particles is preserved after polymer adsorption. Only a very minor increase in the scattering intensity at low  $Q$  values can be observed after polymer adsorption, which qualitatively shows that a low amount of polymer is adsorbed at the CNC surface and/or that adsorbed chains rather lay flat on the cellulose surface and do not form a thick and dense polymer shell. The radii of gyration were calculated from a Guinier plot (Glatter and Kratky, 1982) in both cases (**Figure 5**) and extracted values are summarized in **Table 2**.

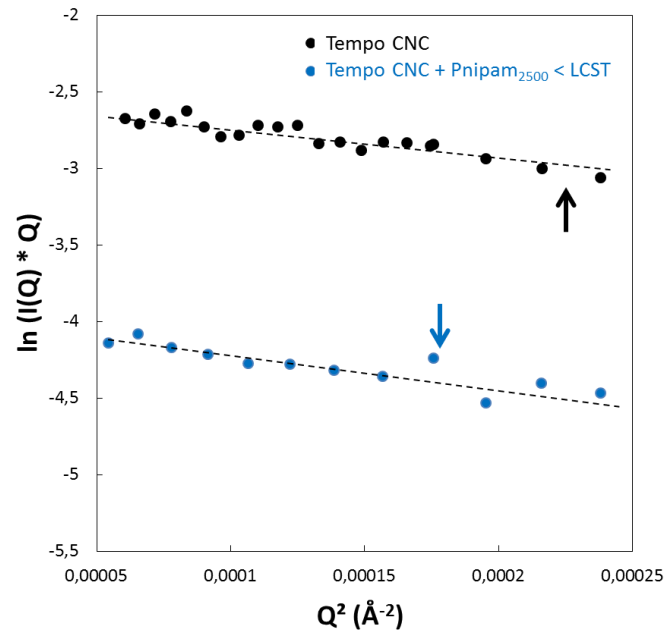


**Figure 5:** SANS measurements present as Guinier Law:  $\ln(Q \times I(Q)) = f(Q^2)$  for TEMPO CNCs and TEMPO CNCs mixed with Pnipam<sub>2500</sub> under the LCST. Arrows indicates  $Q_{max}$  values corresponding to  $1/R_g$ , above this value the Guinier law is not respected ( $Q \times R_g > 1$ ) (Glatter and Kratky, 1982).

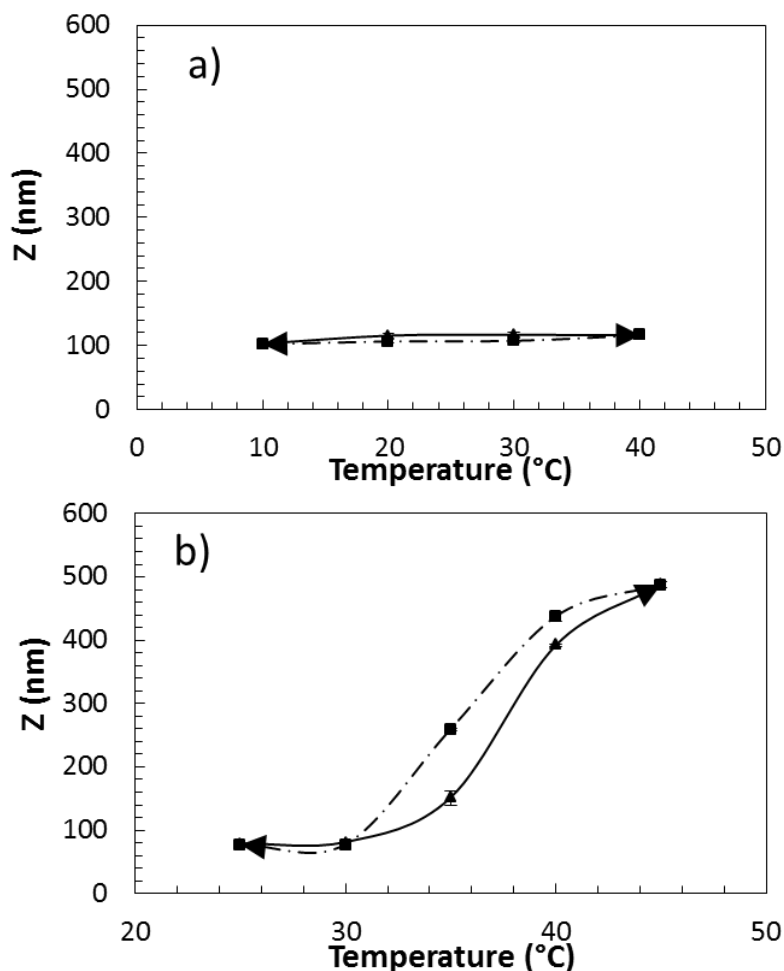
**Table 2:** Slope, gyration radius and polymer thickness isolated according to the Guinier law for each suspension of this study.<sup>a</sup> Gyration radius is calculated from **Equation 2**.

	Slope (Å <sup>-2</sup> )	R <sub>g</sub> (nm)	Polymer thickness (nm)
TEMPO CNC	-1800	6.0	-
Pnipam <sub>2500</sub>		1.5 <sup>a</sup>	-
TEMPO CNC + Pnipam <sub>2500</sub> (< LCST)	-2180	6.6	0.6

For TEMPO CNCs, the radius is 6 nm. Using the calculation of Kubota et al. (Kubota et al., 1990), Pnipam<sub>2500</sub> shows a gyration radius of 1.5 nm. After polymer adsorption on TEMPO CNCs surface the radius increases to 6.6 nm, which corresponds to a polymer shell of about

0.3 nm around a CNC core of about 6 nm. The thickness of the polymer shell is thus well-below the radius of gyration of isolated swollen polymer chains. Consequently, SANS data tend to show the Pnipam<sub>2500</sub> adsorb on TEMPO CNCs in an extended conformation on the surface. This measurement is in concordance with the *hypothesis 2* in **Figure 3**. Ionic linkage between CNCs carboxylic ends and polymer amine ends is completed with hydrogen bonds on the CNCs surface. Above the LCST, the SANS spectrum indicates the presence of large-size aggregates, as shown by the  $Q^{-4}$  behavior in the small  $Q$  region. These aggregates most probably arise from attractive interactions that develop between the polymer shells at temperatures higher than the LCST.

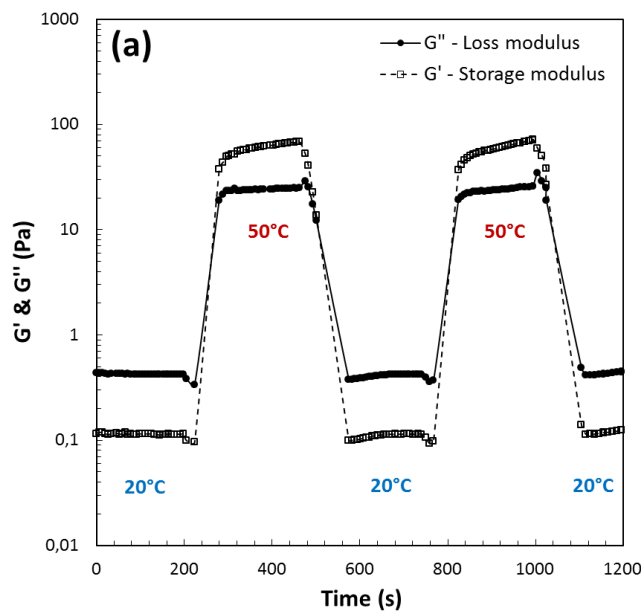
#### 2.3.4. DLS of Pnipam<sub>2500</sub> adsorbed on TEMPO CNCs system



**Figure 6:** DLS curves showing “apparent particle size” for (a) TEMPO CNCs at 0.1 wt% and (b) TEMPO CNCs+Pnipam<sub>2500</sub> at 0.1 wt% (ratio at 25% TEMPO CNCs and 75% Pnipam<sub>2500</sub>) as a function of temperature. Full line: increasing temperature and dotted line: decreasing temperature.

In order to complete the SANS results, which reveal the surface conformation at the nanometer scale, dynamic light scattering (DLS) experiments were carried out to show the microscopic behavior and stimuli responsive aggregation of PNIPAM-based CNCs. According to DLS, TEMPO CNCs (**Figure 6a**) are not modified by the temperature variation and the hydrodynamic radius is  $110 \pm 5$  nm. Referring to the literature (Fujishige et al., 1989; Wu, 1998), PNIPAM shows sensitivity to the temperature. In works of Kubota (Fujishige et al., 1989; Kubota et al., 1990; Senff and Richtering, 1999; Wu, 1998) and Wu (Wang and Wu, 1999; Wu, 1998), under the LCST ( $\sim 34^\circ\text{C}$ ), PNIPAM polymer presents a coil conformation with hydrodynamic diameter about 100 nm. Above the LCST, the polymer turns into a collapse globule conformation and presents a hydrodynamic diameter of about 20 nm. An interesting behavior is observed for the system based on the adsorption of Pnipam<sub>2500</sub> on TEMPO CNCs (**Figure 6b**). Under the LCST of the system, the hydrodynamic radius is close to the TEMPO CNCs value about  $\sim 100$  nm (Pnipam<sub>2500</sub> does not affect the values). This result supports the *hypothesis 2*. After the LCST, the radius sharply increases to a radius of  $\sim 500$  nm. After several temperature cycles, the CNCs system presents the same hysteresis and returns to its original state (colloidal stable suspension). DLS experiments show the full thermo-reversibility of the system based on TEMPO CNCs adsorbed with Pnipam<sub>2500</sub>.

### 2.3.5. Viscoelasticity properties of thermo-responsive hydrogel based on TEMPO CNCs and Pnipam<sub>2500</sub>



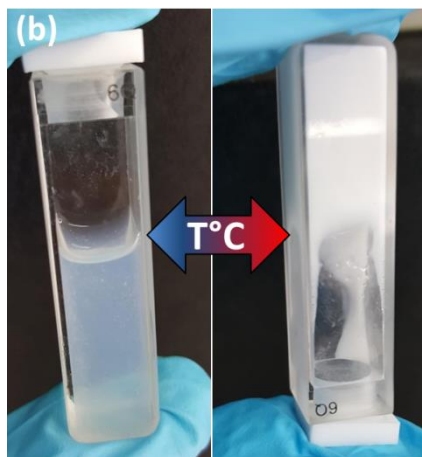


**Figure 7:** (a) Viscoelastic behavior of TEMPO CNCs (10 wt%) adsorbed with Pnipam<sub>2500</sub> (7 wt%) at 20°C and 50°C. Oscillatory measurement were performed at  $\tau_0 = 0.2$  Pa and  $f_0 = 0.5$  Hz. (b) Image of the thermo-reversible behavior of hydrogel based on TEMPO CNCs and Pnipam2500

**Figure 7a** presents the viscoelastic rheological behavior of a highly concentrated suspension composed of 7 wt% of Pnipam<sub>2500</sub> and 10 wt% TEMPO CNCs. Under the LCST, the suspension exhibits a liquid behavior with  $G''$  superior to  $G'$ . Then, when the temperature reached the LCST, the storage modulus ( $G'$ ) is higher than the loss modulus ( $G''$ ) which is characteristic of a gel behavior. **Figure 7b** shows this thermo-reversibility. A more detail study of rheology behavior of such hydrogel is presented in *Chapter III.2*.

## 2.4. Conclusions

The adsorption of Pnipam<sub>2500</sub> on cellulose nanocrystals (CNCs) is demonstrated in this work using several tools like QCM-d, ITC and SANS. The negative charges present on the CNCs surface (resulting from the sulfuric acid hydrolysis process), are sufficient to allow for polymer adsorption. Additionally, this adsorption is clearly larger after TEMPO oxidation of the CNCs which imparts a larger number of negative surface charges from carboxylic groups. In both types of CNCs, ITC measurements reveal that the interaction between Pnipam<sub>2500</sub> and CNCs or TEMPO CNCs are enthalpically driven (anionic-cationic interaction). For temperature below the LCST, a small shell of polymer chains around CNCs is observed by SANS indicating that the polymer conformation is elongated on CNCs surface. Above the LCST, hydrophobic attractive interactions between the collapsed polymer chains induce aggregation (hydrodynamic radius about 500 nm by DLS). The thermo-reversible gelation of the polymer adsorbed CNCs suspension was highlighted by viscoelastic measurement. This behavior is explained by the formation and disruption of link between aggregate formed above the LCST by the Pnipam<sub>2500</sub> adsorbed on CNCs. This thermo-reversibility provides new variety of functionalities to CNCs and paves the way to advanced smart materials based on CNCs.



## Conclusions

The challenge of this chapter was to (i) functionalize CNCs particles with thermo-responsive polymer in accordance with green chemistry principles. To realize green grafting, two main strategies were developed.

In *Chapter II.1*, the grafting strategy was investigated with a polymer commonly used for biomedical application: Poly(N-isopropylacrylamide). The PNIPAM used in this work is an oligomer ( $DP \approx 22$ ) with amine ends. Pnipam<sub>2500</sub> has been grafted onto TEMPO CNCs in combination with EDC and NHS during a peptidic coupling in aqueous media. The grafting efficiency was studied through various experiments. Nonetheless, at the end of this chapter, some questions are still pending on the presence of adsorbed polymer on the surface of CNCs in place of the grafted polymer. Rheological measurements and other indirect measurements reveal difference between adsorbed versus grafted system. Our assumption is that the grafted system is actually a mix of adsorbed and grafted Pnipam<sub>2500</sub>. This configuration influences rheological properties and surely the surface conformation of Pnipam<sub>2500</sub> as detailed in following *Chapter III.2*.

In *Chapter II.2*, the second strategy has been developed with only the polymer adsorption on the surface of negatively charged TEMPO CNCs. The question open in this *Chapter II.2* concerned the possibility and the configuration of a PNIPAM adsorption through the amine groups by hydrogen bonds or by electrostatic adsorption. Experiments reveal the adsorption of Amino-PNIPAM on CNCs was due to electrostatic attraction. In presence of polymer in excess, the final hydrogel presents promising thermo-reversible behavior for injection facilities applications.

Thermo-reversible hydrogel with a liquid-gel transition close to body temperature have been developed in this chapter. The next *Chapter III* will discuss more in details on the rheological properties of these CNCs hydrogels and tests adsorption of a longer thermosensitive block copolymers based on the encouraging results of last sub chapter.



## References

- Abitbol, T., Rivkin, A., Cao, Y., Nevo, Y., Abraham, E., Ben-Shalom, T., Lapidot, S., and Shoseyov, O. (2016). Nanocellulose, a tiny fiber with huge applications. *Curr. Opin. Biotechnol.* *39*, 76–88.
- Ahmadi, M., Madadlou, A., and Saboury, A.A. (2016). Whey protein aerogel as blended with cellulose crystalline particles or loaded with fish oil. *Food Chem.* *196*, 1016–1022.
- Alarcón, C. de las H., Pennadam, S., and Alexander, C. (2005). Stimuli responsive polymers for biomedical applications. *Chem Soc Rev* *34*, 276–285.
- Alosmanov, R., Wolski, K., and Zapotoczny, S. (2017). Grafting of thermosensitive poly(N-isopropylacrylamide) from wet bacterial cellulose sheets to improve its swelling-drying ability. *Cellulose* *24*, 285–293.
- Araki, J., Wada, M., and Kuga, S. (2001). Steric Stabilization of a Cellulose Microcrystal Suspension by Poly(ethylene glycol) Grafting. *Langmuir* *17*, 21–27.
- Atalla, R.H., and VanderHart, D.L. (1999). The role of solid state <sup>13</sup>C NMR spectroscopy in studies of the nature of native celluloses. *Solid State Nucl. Magn. Reson.* *15*, 1–19.
- Aulin, C., Varga, I., Claesson, P.M., Wågberg, L., and Lindström, T. (2008). Buildup of Polyelectrolyte Multilayers of Polyethyleneimine and Microfibrillated Cellulose Studied by in Situ Dual-Polarization Interferometry and Quartz Crystal Microbalance with Dissipation. *Langmuir* *24*, 2509–2518.
- Azzam, F., Heux, L., Putaux, J.-L., and Jean, B. (2010). Preparation By Grafting Onto, Characterization, and Properties of Thermally Responsive Polymer-Decorated Cellulose Nanocrystals. *Biomacromolecules* *11*, 3652–3659.
- Azzam, F., Siqueira, E., Fort, S., Hassaini, R., Pignon, F., Travelet, C., Putaux, J.-L., and Jean, B. (2016). Tunable Aggregation and Gelation of Thermoresponsive Suspensions of Polymer-Grafted Cellulose Nanocrystals. *Biomacromolecules* *17*, 2112–2119.
- Batmaz, R., Mohammed, N., Zaman, M., Minhas, G., Berry, R.M., and Tam, K.C. (2014). Cellulose nanocrystals as promising adsorbents for the removal of cationic dyes. *Cellulose* *21*, 1655–1665.
- Bawa, P., Pillay, V., Choonara, Y.E., and du Toit, L.C. (2009). Stimuli-responsive polymers and their applications in drug delivery. *Biomed. Mater.* *4*, 022001.
- Boluk, Y., Zhao, L., and Incani, V. (2012). Dispersions of nanocrystalline cellulose in aqueous polymer solutions: structure formation of colloidal rods. *Langmuir* *28*, 6114–6123.
- Bras, J., Viet, D., Bruzzese, C., and Dufresne, A. (2011). Correlation between stiffness of sheets prepared from cellulose whiskers and nanoparticles dimensions. *Carbohydr. Polym.* *84*, 211–215.
- Brûlet, A., Lairez, D., Lapp, A., and Cotton, J.-P. (2007). Improvement of data treatment in small-angle neutron scattering. *J. Appl. Crystallogr.* *40*, 165–177.
- Bulpitt, P., and Aeschlimann, D. (1999). New strategy for chemical modification of hyaluronic acid: Preparation of functionalized derivatives and their use in the formation of novel biocompatible hydrogels. *J. Biomed. Mater. Res.* *47*, 152–169.
- Cabane, E., Zhang, X., Langowska, K., Palivan, C.G., and Meier, W. (2012). Stimuli-Responsive Polymers and Their Applications in Nanomedicine. *Biointerphases* *7*, 9.
- Caddick, S. (1995). Microwave assisted organic reactions. *Tetrahedron* *51*, 10403–10432.
- Camarero Espinosa, S., Rothen-Rutishauser, B., Johan Foster, E., and Weder, C. (2016). Articular cartilage: from formation to tissue engineering. *Biomater. Sci.* *4*, 734–767.

- Cao, Z., Ge, H., and Lai, S. (2001). Studies on synthesis and adsorption properties of chitosan cross-linked by glutaraldehyde and Cu(II) as template under microwave irradiation. *Eur. Polym. J.* *37*, 2141–2143.
- Carlmark, A., Larsson, E., and Malmström, E. (2012). Grafting of cellulose by ring-opening polymerisation—A review. *Eur. Polym. J.* *48*, 1646–1659.
- Chauve, G., and Bras, J. (2014). Industrial point of view of nanocellulose materials and their possible applications. *Handb. Green Mater.* World Sci. 233–252.
- Chen, J., Wang, J., Zhang, X., and Jin, Y. (2008). Microwave-assisted green synthesis of silver nanoparticles by carboxymethyl cellulose sodium and silver nitrate. *Mater. Chem. Phys.* *108*, 421–424.
- Chen, X., Huang, L., Sun, H.-J., Cheng, S.Z.D., Zhu, M., and Yang, G. (2014). Stimuli-Responsive Nanocomposite: Potential Injectable Embolization Agent. *Macromol. Rapid Commun.* *35*, 579–584.
- Da Silva Perez, D., Montanari, S., and Vignon, M.R. (2003). TEMPO-Mediated Oxidation of Cellulose III. *Biomacromolecules* *4*, 1417–1425.
- Danks, T.N. (1999). Microwave assisted synthesis of pyrroles. *Tetrahedron Lett.* *40*, 3957–3960.
- De France, K.J., Chan, K.J.W., Cranston, E.D., and Hoare, T. (2016). Enhanced Mechanical Properties in Cellulose Nanocrystal–Poly(oligoethylene glycol methacrylate) Injectable Nanocomposite Hydrogels through Control of Physical and Chemical Cross-Linking. *Biomacromolecules* *17*, 649–660.
- De France, K.J., Hoare, T., and Cranston, E.D. (2017). Review of Hydrogels and Aerogels Containing Nanocellulose. *Chem. Mater.* *29*, 4609–4631.
- Deshayes, S., Liagre, M., Loupy, A., Luche, J.-L., and Petit, A. (1999). Microwave activation in phase transfer catalysis. *Tetrahedron* *55*, 10851–10870.
- Domingues, R.M.A., Gomes, M.E., and Reis, R.L. (2014). The Potential of Cellulose Nanocrystals in Tissue Engineering Strategies. *Biomacromolecules* *15*, 2327–2346.
- Dong, S., and Roman, M. (2007). Fluorescently Labeled Cellulose Nanocrystals for Bioimaging Applications. *J. Am. Chem. Soc.* *129*, 13810–13811.
- Dong, X.M., and Gray, D.G. (1997). Effect of Counterions on Ordered Phase Formation in Suspensions of Charged Rodlike Cellulose Crystallites. *Langmuir* *13*, 2404–2409.
- Dong, X.M., Kimura, T., Revol, J.-F., and Gray, D.G. (1996). Effects of Ionic Strength on the Isotropic–Chiral Nematic Phase Transition of Suspensions of Cellulose Crystallites. *Langmuir* *12*, 2076–2082.
- Dufresne, A. (2013a). Nanocellulose: a new ageless bionanomaterial. *Mater. Today* *16*, 220–227.
- Dufresne, A. (2013b). Nanocellulose: from nature to high performance tailored materials (Walter de Gruyter).
- Eichhorn, S.J., Dufresne, A., Aranguren, M., Marcovich, N.E., Capadona, J.R., Rowan, S.J., Weder, C., Thielemans, W., Roman, M., Renneckar, S., et al. (2010). Review: current international research into cellulose nanofibres and nanocomposites. *J. Mater. Sci.* *45*, 1–33.
- Endes, C., Camarero-Espinosa, S., Mueller, S., Foster, E.J., Petri-Fink, A., Rothen-Rutishauser, B., Weder, C., and Clift, M.J.D. (2016). A critical review of the current knowledge regarding the biological impact of nanocellulose. *J. Nanobiotechnology* *14*, 78.
- Eyley, S., and Thielemans, W. (2014). Surface modification of cellulose nanocrystals. *Nanoscale* *6*, 7764–7779.

- Filpponen, I., and Argyropoulos, D.S. (2010). Regular Linking of Cellulose Nanocrystals via Click Chemistry: Synthesis and Formation of Cellulose Nanoplatelet Gels. *Biomacromolecules* *11*, 1060–1066.
- Follain, N., Marais, M.-F., Montanari, S., and Vignon, M.R. (2010). Coupling onto surface carboxylated cellulose nanocrystals. *Polymer* *51*, 5332–5344.
- Fujishige, S., Kubota, K., and Ando, I. (1989). Phase transition of aqueous solutions of poly (N-isopropylacrylamide) and poly (N-isopropylmethacrylamide). *J. Phys. Chem.* *93*, 3311–3313.
- Gabriel, C., Gabriel, S., Grant, E.H., Grant, E.H., Halstead, B.S.J., and Mingos, D.M.P. (1998). Dielectric parameters relevant to microwave dielectric heating. *Chem. Soc. Rev.* *27*, 213–224.
- Gedye, R., Smith, F., Westaway, K., Ali, H., Baldisera, L., Laberge, L., and Rousell, J. (1986). The use of microwave ovens for rapid organic synthesis. *Tetrahedron Lett.* *27*, 279–282.
- Gicquel, E., Martin, C., Yanez, J.G., and Bras, J. (2017). Cellulose nanocrystals as new bio-based coating layer for improving fiber-based mechanical and barrier properties. *J. Mater. Sci.* *52*, 3048–3061.
- Giguere, R.J., Bray, T.L., Duncan, S.M., and Majetich, G. (1986). Application of commercial microwave ovens to organic synthesis. *Tetrahedron Lett.* *27*, 4945–4948.
- Glatter, O., and Kratky, O. (1982). *Small angle X-ray scattering* (Academic press).
- Grishkewich, N., Akhlaghi, S.P., Zhaoling, Y., Berry, R., and Tam, K.C. (2016). Cellulose nanocrystal-poly(oligo(ethylene glycol) methacrylate) brushes with tunable LCSTs. *Carbohydr. Polym.* *144*, 215–222.
- Habibi, Y. (2014). Key advances in the chemical modification of nanocelluloses. *Chem. Soc. Rev.* *43*, 1519–1542.
- Habibi, Y., Chanzy, H., and Vignon, M.R. (2006). TEMPO-mediated surface oxidation of cellulose whiskers. *Cellulose* *13*, 679–687.
- Habibi, Y., Lucia, L.A., and Rojas, O.J. (2010). Cellulose Nanocrystals: Chemistry, Self-Assembly, and Applications. *Chem. Rev.* *110*, 3479–3500.
- Haqani, M., Roghani-Mamaqani, H., and Salami-Kalajahi, M. (2017). Synthesis of dual-sensitive nanocrystalline cellulose-grafted block copolymers of N-isopropylacrylamide and acrylic acid by reversible addition-fragmentation chain transfer polymerization. *Cellulose* *24*, 2241–2254.
- Hebeish, A., Farag, S., Sharaf, S., and Shaheen, T.I. (2014). Thermal responsive hydrogels based on semi interpenetrating network of poly(NIPAM) and cellulose nanowhiskers. *Carbohydr. Polym.* *102*, 159–166.
- Hemraz, U.D., Lu, A., Sunasee, R., and Boluk, Y. (2014). Structure of poly(N-isopropylacrylamide) brushes and steric stability of their grafted cellulose nanocrystal dispersions. *J. Colloid Interface Sci.* *430*, 157–165.
- Hoeng, F., Denneulin, A., Neuman, C., and Bras, J. (2015). Charge density modification of carboxylated cellulose nanocrystals for stable silver nanoparticles suspension preparation. *J. Nanoparticle Res.* *17*, 244.
- Hoeng, F., Denneulin, A., and Bras, J. (2016). Use of nanocellulose in printed electronics: a review. *Nanoscale* *8*, 13131–13154.
- Hoffman, A.S. (2013). Stimuli-responsive polymers: Biomedical applications and challenges for clinical translation. *Adv. Drug Deliv. Rev.* *65*, 10–16.
- Irwin, E.F., Ho, J.E., Kane, S.R., and Healy, K.E. (2005). Analysis of Interpenetrating Polymer Networks via Quartz Crystal Microbalance with Dissipation Monitoring. *Langmuir* *21*, 5529–5536.

- Isogai, A., Saito, T., and Fukuzumi, H. (2011). TEMPO-oxidized cellulose nanofibers. *Nanoscale* 3, 71–85.
- J. Eichhorn, S. (2011). Cellulose nanowhiskers: promising materials for advanced applications. *Soft Matter* 7, 303–315.
- Jorfi, M., and Foster, E.J. (2015). Recent advances in nanocellulose for biomedical applications. *J. Appl. Polym. Sci.* 132.
- Kan, K.H.M., Li, J., Wijesekera, K., and Cranston, E.D. (2013). Polymer-Grafted Cellulose Nanocrystals as pH-Responsive Reversible Flocculants. *Biomacromolecules* 14, 3130–3139.
- Kappe, C.O. (2004). Controlled Microwave Heating in Modern Organic Synthesis. *Angew. Chem. Int. Ed.* 43, 6250–6284.
- Kappe, C.O. (2008). Microwave dielectric heating in synthetic organic chemistry. *Chem. Soc. Rev.* 37, 1127–1139.
- Karabulut, E., Pettersson, T., Ankerfors, M., and Wågberg, L. (2012). Adhesive Layer-by-Layer Films of Carboxymethylated Cellulose Nanofibril–Dopamine Covalent Bioconjugates Inspired by Marine Mussel Threads. *ACS Nano* 6, 4731–4739.
- Kaur, L., and Gupta, G.D. (2017). A review on microwave assisted grafting of polymers. *Int. J. Pharm. Sci. Res.* 8, 422.
- Klemm, D., Kramer, F., Moritz, S., Lindström, T., Ankerfors, M., Gray, D., and Dorris, A. (2011). Nanocelluloses: A New Family of Nature-Based Materials. *Angew. Chem. Int. Ed.* 50, 5438–5466.
- Kloser, E., and Gray, D.G. (2010). Surface Grafting of Cellulose Nanocrystals with Poly(ethylene oxide) in Aqueous Media. *Langmuir* 26, 13450–13456.
- Krivosheeva, O., Sababi, M., Dedinaite, A., and Claesson, P.M. (2013). Nanostructured Composite Layers of Mussel Adhesive Protein and Ceria Nanoparticles. *Langmuir* 29, 9551–9561.
- Kubota, K., Fujishige, S., and Ando, I. (1990). Solution properties of poly (N-isopropylacrylamide) in water. *Polym J* 22, 15–20.
- Lai, H., Chen, Q., and Wu, P. (2013). The core–shell structure of PNIPAM collapsed chain conformation induces a bimodal transition on cooling. *Soft Matter* 9, 3985.
- Larsson, E., Sanchez, C.C., Porsch, C., Karabulut, E., Wågberg, L., and Carlmark, A. (2013). Thermo-responsive nanofibrillated cellulose by polyelectrolyte adsorption. *Eur. Polym. J.* 49, 2689–2696.
- Lavoine, N., Bras, J., Saito, T., and Isogai, A. (2016). Improvement of the Thermal Stability of TEMPO-Oxidized Cellulose Nanofibrils by Heat-Induced Conversion of Ionic Bonds to Amide Bonds. *Macromol. Rapid Commun.* 37, 1033–1039.
- Lew, A., Krutzik, P.O., Hart, M.E., and Chamberlin, A.R. (2002). Increasing Rates of Reaction: Microwave-Assisted Organic Synthesis for Combinatorial Chemistry. *J. Comb. Chem.* 4, 95–105.
- Li, F., Biagioni, P., Bollani, M., Maccagnan, A., and Piergiovanni, L. (2013). Multi-functional coating of cellulose nanocrystals for flexible packaging applications. *Cellulose* 20, 2491–2504.
- Li, S.-M., Jia, N., Ma, M.-G., Zhang, Z., Liu, Q.-H., and Sun, R.-C. (2011). Cellulose–silver nanocomposites: Microwave-assisted synthesis, characterization, their thermal stability, and antimicrobial property. *Carbohydr. Polym.* 86, 441–447.
- Lin, N., and Dufresne, A. (2014). Nanocellulose in biomedicine: current status and future prospect. *Eur. Polym. J.* 59, 302–325.

- Lin, C.-X., Zhan, H.-Y., Liu, M.-H., Fu, S.-Y., and Huang, L.-H. (2010). Rapid homogeneous preparation of cellulose graft copolymer in BMIMCL under microwave irradiation. *J. Appl. Polym. Sci.* *118*, 399–404.
- Lin, N., Chen, G., Huang, J., Dufresne, A., and Chang, P.R. (2009). Effects of polymer-grafted natural nanocrystals on the structure and mechanical properties of poly(lactic acid): A case of cellulose whisker-graft-polycaprolactone. *J. Appl. Polym. Sci.* *113*, 3417–3425.
- Lu, Z., Fan, L., Zheng, H., Lu, Q., Liao, Y., and Huang, B. (2013). Preparation, characterization and optimization of nanocellulose whiskers by simultaneously ultrasonic wave and microwave assisted. *Bioresour. Technol.* *146*, 82–88.
- Mariano, M., El Kissi, N., and Dufresne, A. (2014). Cellulose nanocrystals and related nanocomposites: Review of some properties and challenges. *J. Polym. Sci. Part B Polym. Phys.* *52*, 791–806.
- Mingos, M.P., and Baghurst (1991). Tilden Lecture. Applications of microwave dielectric heating effects to synthetic problems in chemistry. *Chem. Soc. Rev.* *20*, 1–47.
- Missoum, K., Bras, J., and Belgacem, M.N. (2012). Organization of aliphatic chains grafted on nanofibrillated cellulose and influence on final properties. *Cellulose* *19*, 1957–1973.
- Montanari, S., Rountani, M., Heux, L., and Vignon, M.R. (2005). Topochemistry of carboxylated cellulose nanocrystals resulting from TEMPO-mediated oxidation. *Macromolecules* *38*, 1665–1671.
- Moon, R.J., Martini, A., Nairn, J., Simonsen, J., and Youngblood, J. (2011). Cellulose nanomaterials review: structure, properties and nanocomposites. *Chem. Soc. Rev.* *40*, 3941.
- Naseri, N., Deepa, B., Mathew, A.P., Oksman, K., and Girandon, L. (2016). Nanocellulose-Based Interpenetrating Polymer Network (IPN) Hydrogels for Cartilage Applications. *Biomacromolecules* *17*, 3714–3723.
- Okahata, Y., Noguchi, H., and Seki, T. (1986). Thermoselective permeation from a polymer-grafted capsule membrane. *Macromolecules* *19*, 493–494.
- Oksman, K., Mathew, A.P., Bismarck, A., Rojas, O., and Sain, M. (2014). *Handbook of Green Materials: Processing Technologies, Properties and Applications: Volume 5* (World Scientific).
- Orozco, A., Ahmad, M., Rooney, D., and Walker, G. (2007). Dilute Acid Hydrolysis of Cellulose and Cellulosic Bio-Waste Using a Microwave Reactor System. *Process Saf. Environ. Prot.* *85*, 446–449.
- Pelton, R. (2010). Poly(N-isopropylacrylamide) (PNIPAM) is never hydrophobic. *J. Colloid Interface Sci.* *348*, 673–674.
- Pentlavalli, S., Chambers, P., Sathy, B.N., O'Doherty, M., Chalanqui, M., Kelly, D.J., Haut-Donahue, T., McCarthy, H.O., and Dunne, N.J. (2017). Simple Radical Polymerization of Poly (Alginate-Graft-N-Isopropylacrylamide) Injectable Thermoresponsive Hydrogel with the Potential for Localized and Sustained Delivery of Stem Cells and Bioactive Molecules. *Macromol. Biosci.* *10.1002/mabi.201700118*.
- Plunkett, K.N., Zhu, X., Moore, J.S., and Leckband, D.E. (2006). PNIPAM Chain Collapse Depends on the Molecular Weight and Grafting Density. *Langmuir* *22*, 4259–4266.
- Polshettiwar, V., and Varma, R.S. (2008). Microwave-Assisted Organic Synthesis and Transformations using Benign Reaction Media. *Acc. Chem. Res.* *41*, 629–639.
- Rånby, B.G. (1951). Fibrous macromolecular systems. Cellulose and muscle. The colloidal properties of cellulose micelles. *Discuss. Faraday Soc.* *11*, 158–164.
- Reid, M., Villalobos, M., and Cranston, E. (2016). Cellulose Nanocrystal Interactions Probed by Thin Film Swelling to Predict Dispersibility. *Nanoscale* *8*, 12247–12257.

- Reid, M.S., Villalobos, M., and Cranston, E.D. (2017). The Role of Hydrogen Bonding in Non-Ionic Polymer Adsorption to Cellulose Nanocrystals and Silica Colloids. *Curr. Opin. Colloid Interface Sci.* *29*, 76–82.
- Reineke, T.M. (2016). Stimuli-Responsive Polymers for Biological Detection and Delivery. *ACS Macro Lett.* *5*, 14–18.
- Revol, J.-F., Bradford, H., Giasson, J., Marchessault, R.H., and Gray, D.G. (1992). Helicoidal self-ordering of cellulose microfibrils in aqueous suspension. *Int. J. Biol. Macromol.* *14*, 170–172.
- Rodahl, M., Höök, F., Krozer, A., Brzezinski, P., and Kasemo, B. (1995). Quartz crystal microbalance setup for frequency and  $Q$ -factor measurements in gaseous and liquid environments. *Rev. Sci. Instrum.* *66*, 3924–3930.
- Satgé, C., Verneuil, B., Branland, P., Granet, R., Krausz, P., Rozier, J., and Petit, C. (2002). Rapid homogeneous esterification of cellulose induced by microwave irradiation. *Carbohydr. Polym.* *49*, 373–376.
- Sauerbrey, G.Z. (1959). Use of quartz vibration for weighing thin films on a microbalance. *J Phys.* *155*, 206–212.
- Schattling, P., D. Jochum, F., and Theato, P. (2014). Multi-stimuli responsive polymers – the all-in-one talents. *Polym. Chem.* *5*, 25–36.
- Schild, H.G. (1992). Poly(N-isopropylacrylamide): experiment, theory and application. *Prog. Polym. Sci.* *17*, 163–249.
- Senff, H., and Richtering, W. (1999). Temperature sensitive microgel suspensions: Colloidal phase behavior and rheology of soft spheres. *J. Chem. Phys.* *111*, 1705–1711.
- Siqueira, G., Bras, J., and Dufresne, A. (2010a). Cellulosic Bionanocomposites: A Review of Preparation, Properties and Applications. *Polymers* *2*, 728–765.
- Siqueira, G., Bras, J., and Dufresne, A. (2010b). New Process of Chemical Grafting of Cellulose Nanoparticles with a Long Chain Isocyanate. *Langmuir* *26*, 402–411.
- Siqueira, G., Bras, J., and Dufresne, A. (2010c). Cellulosic Bionanocomposites: A Review of Preparation, Properties and Applications. *Polymers* *2*, 728–765.
- Tang, J., Sisler, J., Grishkewich, N., and Tam, K.C. (2017). Functionalization of cellulose nanocrystals for advanced applications. *J. Colloid Interface Sci.* *494*, 397–409.
- Urruzola, I., Robles, E., Serrano, L., and Labidi, J. (2014). Nanopaper from almond (*Prunus dulcis*) shell. *Cellulose* *21*, 1619–1629.
- Velazquez-Campoy, A., and Freire, E. (2006). Isothermal titration calorimetry to determine association constants for high-affinity ligands. *Nat. Protoc.* *1*, 186–191.
- Voinova, M.V., Rodahl, M., Jonson, M., and Kasemo, B. (1999). Viscoelastic acoustic response of layered polymer films at fluid-solid interfaces: continuum mechanics approach. *Phys. Scr.* *59*, 391–396.
- Vuoriluoto, M., Orelma, H., Johansson, L.-S., Zhu, B., Poutanen, M., Walther, A., Laine, J., and Rojas, O.J. (2015). Effect of Molecular Architecture of PDMAEMA–POEGMA Random and Block Copolymers on Their Adsorption on Regenerated and Anionic Nanocelluloses and Evidence of Interfacial Water Expulsion. *J. Phys. Chem. B* *119*, 15275–15286.
- Wang, X., and Wu, C. (1999). Light-Scattering Study of Coil-to-Globule Transition of a Poly(N-isopropylacrylamide) Chain in Deuterated Water. *Macromolecules* *32*, 4299–4301.
- Wei, M., Gao, Y., Li, X., and Serpe, M.J. (2017). Stimuli-responsive polymers and their applications. *Polym Chem* *8*, 127–143.

Wu, C. (1998). Globule-to-Coil Transition of a Single Homopolymer Chain in Solution. *Phys. Rev. Lett.* *80*, 4092–4094.

Wu, W., Huang, F., Pan, S., Mu, W., Meng, X., Yang, H., Xu, Z., Ragauskas, A.J., and Deng, Y. (2015). Thermo-responsive and fluorescent cellulose nanocrystals grafted with polymer brushes. *J. Mater. Chem. A* *3*, 1995–2005.

Yang, X., and Cranston, E.D. (2014). Chemically cross-linked cellulose nanocrystal aerogels with shape recovery and superabsorbent properties. *Chem. Mater.* *26*, 6016–6025.

Zhang, Z., and Zhao, Z.K. (2009). Solid acid and microwave-assisted hydrolysis of cellulose in ionic liquid. *Carbohydr. Res.* *344*, 2069–2072.

Zhang, J., Wu, Q., Li, M.-C., Song, K., Sun, X., Lee, S.-Y., and Lei, T. (2017). Thermoresponsive Copolymer Poly(N-Vinylcaprolactam) Grafted Cellulose Nanocrystals: Synthesis, Structure, and Properties. *ACS Sustain. Chem. Eng.* *5*, 7439–7447.

Zoppe, J.O., Habibi, Y., Rojas, O.J., Venditti, R.A., Johansson, L.-S., Efimenko, K., Österberg, M., and Laine, J. (2010). Poly(N-isopropylacrylamide) Brushes Grafted from Cellulose Nanocrystals via Surface-Initiated Single-Electron Transfer Living Radical Polymerization. *Biomacromolecules* *11*, 2683–2691.

Zoppe, J.O., Österberg, M., Venditti, R.A., Laine, J., and Rojas, O.J. (2011). Surface Interaction Forces of Cellulose Nanocrystals Grafted with Thermoresponsive Polymer Brushes. *Biomacromolecules* *12*, 2788–2796.

Zubik, K., Singhsa, P., Wang, Y., Manuspiya, H., and Narain, R. (2017). Thermo-Responsive Poly(N-Isopropylacrylamide)-Cellulose Nanocrystals Hybrid Hydrogels for Wound Dressing. *Polymers* *9*, 119.



# Chapter III

## Rheological study of CNCs hydrogels

---



## Table of content

<b>Introduction</b> .....	163
<b>1. Impact of sonication on the rheological and colloidal properties of high concentrated cellulose nanocrystals suspensions</b> .....	165
1.1. Introduction.....	166
1.2. Materials and Methods .....	169
1.2.1. Materials.....	169
1.2.2. CNCs suspension characterization .....	169
1.2.3. Small-angle X-ray scattering (SAXS) .....	170
1.2.4. CNCs dispersion and dilution.....	170
1.2.5. CNCs suspension concentration .....	171
1.2.6. CNCs phase diagram .....	171
1.2.7. Rheological experiments on CNCs suspensions .....	171
1.3. Results .....	172
1.3.1. CNCs morphology .....	172
1.3.2. Phase behavior and microstructure after sonication at high concentration.....	173
1.3.3. Interparticle distance in static conditions.....	175
1.3.4. Influence of sonication on the rheological behavior.....	176
1.3.5. Concentration effect on the CNC rheological behavior .....	180
1.4. Discussion.....	183
1.5. Conclusions.....	186
<b>2. Cellulose nanocrystals grafted with Poly(N-isopropyl acrylamide) suspensions as thermo-sensitive hydrogel</b> .....	187
2.1. Introduction.....	188
2.2. Materials and Methods .....	190
2.2.1. Materials.....	190
2.2.2. Carboxylation of cellulose nanocrystals by TEMPO oxidation .....	190
2.2.3. Polymer grafting by peptidic coupling in aqueous media .....	191
2.2.4. Increasing of the CNC-g-Pnipam <sub>2500</sub> suspension concentration .....	191
2.2.5. Transmission electron microscopy (TEM) .....	191
2.2.6. Small angle neutron scattering: Polymer conformation .....	192
2.2.7. Rheological experiments on thermo-reversible hydrogel.....	192
2.3. Results and discussion.....	193
2.3.1. Grafted CNCs characterization.....	193
2.3.2. SANS measurements on CNC-g-Pnipam <sub>2500</sub> .....	194
2.3.3. Rheological behavior of oxidized CNC and Pnipam <sub>2500</sub> .....	197
2.3.4. Rheological behavior and viscoelastic properties of CNC-g-Pnipam <sub>2500</sub> .....	199
2.4. Conclusions.....	203

<b>3. PDMAEMA-g-PDEGMA Polymer adsorption on carboxylated cellulose nanocrystals and corresponding thermo-sensitive hydrogel.</b>	<b>205</b>
3.1. Introduction.....	206
3.2. Materials and Methods .....	209
3.2.1. Materials.....	209
3.2.2. Carboxylation of cellulose nanocrystals by TEMPO oxidation .....	209
3.2.3. Synthesis of PDMAEMA-b-PDEGMA block copolymer with ATRP.....	210
3.2.4. Analysis of PDMAEMA-b-PDEGMA block copolymer .....	211
3.2.5. PDMAEMA-b-PDEGMA adsorption on TEMPO CNCs .....	211
3.2.6. Adsorption experiments using QCM-d.....	212
3.2.7. Adsorption experiments using the multi-parametric surface plasmon resonance spectroscopy (MP-SPR) .....	213
3.2.8. Small angle neutron scattering: Polymer conformation after adsorption .....	215
3.2.9. Rheological experiments on thermo-reversible hydrogel.....	215
3.3. Results and Discussions .....	216
3.3.1. Raw materials characterization .....	216
3.3.2. Adsorption characterization .....	217
3.3.3. SANS Analysis .....	219
3.3.4. System rheological behavior.....	223
3.4. Conclusions.....	229
<b>Conclusions.....</b>	<b>231</b>
<b>References .....</b>	<b>233</b>

# III. Rheological study of CNCs hydrogels

## Introduction

As described in *Chapter I*, CNCs present interesting rheological properties with highly viscous suspension at low shear rate and shear thinning behaviors. Combined with their biocompatibility, these systems make good candidates for the realization of injectable hydrogels. The previous part (*Chapter II*) has detailed the modification of CNCs surface through green chemistry in order to incorporate thermo-sensitive properties. In this *Chapter III*, rheological behaviors of these systems have been studied in detail in response to our second and third objectives: (ii) understanding of rheological behavior of CNCs and CNCs-polymer suspensions and (iii) realization of stimuli-responsive system based on cellulose nanocrystals and thermo-responsive polymers.

The first part of this chapter (*Chapter III.1*) will investigate the impact of sonication on the rheological and colloidal properties of classic CNCs suspensions. The knowledge of the rheological behavior of our CNCs is important to understand the thermo-responsive effect in hydrogel systems.

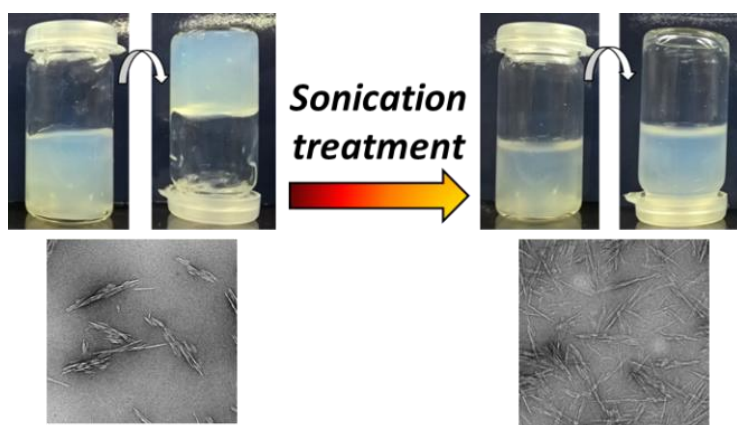
Based on the work realized in *Chapter II.1*, the *Chapter III.2* will describe the rheological thermo-reversibility of TEMPO CNCs grafted and adsorbed with Pnipam<sub>2500</sub>. Small angle neutron scattering will introduce the polymer configuration on CNCs surface of “grafted” version.

In *Chapter III.3*, a new thermo-responsive system is introduced based on previous conclusions, i.e. the electrostatic irreversible adsorption is possible but configuration on CNCs surface plays a role on final rheological properties. A block copolymer with one part dedicated to adsorption and another part dedicated to the thermo-responsive behavior and configuration has been designed in collaboration with KTH. This PDMAEMA-PDEGMA has a lower LCST and a higher molecular weight than Pnipam<sub>2500</sub>, this diblock polymer presents an important entanglement possibility with CNCs. This *Chapter III.3* will then discuss on the adsorption of diblock on TEMPO CNCs, the polymer configuration via SANS measurements and the rheological behavior of the final hydrogel system.



# 1. Impact of sonication on the rheological and colloidal properties of high concentrated cellulose nanocrystals suspensions

*This section is adapted from "Erwan GICQUEL, Candice REY, Bruno JEAN, Jean-Luc PUTAUX, Frédéric PIGNON, Julien BRAS, Céline MARTIN - Impact of sonication on the rheological and colloidal properties of high concentrated cellulose nanocrystals suspensions" Submitted in Cellulose, 2017"*



## ABSTRACT

The effect of sonication on a highly concentrated commercial suspension of cellulose nanocrystals (CNCs) and the induced resulting rheological properties have been investigated. Rheology and structural analysis techniques (atomic force microscopy, small-angle X-ray scattering, transmission electron microscopy and dynamic light scattering) were used to characterize the CNC suspension before and after sonication as a function of concentration. After sonication, the highly concentrated CNC suspension turn from a “gel” form to a “liquid” form, but no aggregates compose the never freeze-dried suspension (proved by AFM and TEM analysis). The phase diagram of the liquid crystalline part for both systems was determined, and flow rheology performed to understand the behavior as a function of concentration. Sonication induced a decrease of the inter-particle distance, a strong decrease of the viscosity and a high change in the liquid crystal behavior. Nevertheless, sonicated and non-sonicated suspensions were stable over time. The CNCs suspension presents CNCs packed together by 2-4 CNCs and after sonication, CNCs are individualized.

**Keywords:** Cellulose nanocrystals (CNCs), rheology, sonication, chiral nematic liquid crystal, microstructure, small-angle X-ray scattering (SAXS).

## 1.1. Introduction

As biodegradable, renewable, non-toxic and highly performant nanomaterials, cellulose nanocrystals (CNCs) have evolved from a laboratory curiosity to a technical material, which has attracted industrial attention. These rod-like nanoparticles, CNCs are now commonly obtained by acid hydrolysis of cellulosic material since 1950's at about 2-5% solid content (Rånby, 1951; Revol et al., 1992). CNCs are now produced in several countries at pilot or commercial scale by various companies, since 2010's (Reid et al., 2017a). Their size, shape and surface properties both depend on the origin of the cellulose source and on the hydrolysis conditions (Bras et al., 2011; Dong and Gray, 1997; García et al., 2016). Owing to their specific physical properties and high aspect ratio, CNCs are used in the development of several applications in various fields (Tang et al., 2017) such as the biomedical domain (Jorfi and Foster, 2015; Lin and Dufresne, 2014; Sunasee et al., 2016), environmentally friendly nanocomposites (Mariano et al., 2014; Oksman et al., 2014; Siqueira et al., 2010a) or paper coating industry (Gicquel et al., 2017; Hoeng et al., 2017). In each cases, the rheological properties or the CNCs concentrations will play an important role. Recently, new processes have been proposed to favor industrialization and new grade delivery. It is now possible to obtain a highly concentrated suspension (up to 11 wt%) but with some amorphous cellulose due to the washing process. This study focus on this grade.

As other colloidal rods like DNA fragments, viruses, metallic oxides or chitin nanocrystals, CNCs suspensions exhibit very interesting self-organization properties: above a critical concentration, the suspension phase separates into an upper isotropic phase and a lower anisotropic chiral nematic phase (Revol et al., 1992, 1994). The formation of this phase can be explained by Onsager's theory (Onsager, 1949), which predicts the critical transition density for very high aspect ratio hard rods. This theory was further refined to take into account smaller aspect ratios, polydispersity and most importantly electrostatic interactions (Araki and Kuga, 2001; Dong and Gray, 1997; Lee, 1987). The dimensions, aspect ratio, surface charge density and surface chemistry greatly influence the phase separation behavior and the characteristics of the cholesteric liquid-crystalline phase (Azzam et al., 2016a; Lagerwall et al., 2014; Revol et al., 1994; Shafiei-Sabet et al., 2014).

The rheological behavior of aqueous CNCs suspensions stands as a major concern of high application-relevance and different studies over the past 10 years were dedicated to its comprehensive understanding (Bercea and Navard, 2000; Liu et al., 2011a, 2011b; Lu et al., 2014; Shafiei-Sabet et al., 2012, 2014; Ureña-Benavides et al., 2011; Xu et al., 2017a, 2017b). One of the important results reported is the effect of concentration and the related position in the phase diagram. The viscosity behavior, as a function of shear rate observed for CNCs suspensions corresponds to a three-region slope, typical of liquid crystalline samples, while the isotropic suspensions behave like a classic polymer solution (Bercea and Navard, 2000; Shafiei-Sabet et al., 2012). Namely, at low shear rate, a first shear-thinning region due to the alignment of chiral nematic domains is observed. At intermediate shear rates, chiral nematic domains are aligned in the flow direction and a viscosity plateau is observed. Finally, at high shear rate, chiral domains are disrupted and all CNCs align in the flow, leading to a second shear-thinning region.

Nonetheless, most of studies focus on low concentration suspension or at least use such suspension as starting material. Furthermore, limited information exists on the relationship between macroscopic rheological properties and the microscopic structure of CNCs suspensions. A couple of works involve rheology small-angle neutron, small-angle X-ray and light scattering (SANS, SAXS, and SALS, respectively) to obtain the size and morphology of CNCs rods under flow (Ebeling et al., 1999; Elazzouzi-Hafraoui et al., 2008; Mao et al., 2017; Orts et al., 1998; Schütz et al., 2015; Xu et al., 2017a). Orts et al. (Orts et al., 1998) showed that CNCs rods are oriented parallel to shear flows with increasing shear rate.

Ultrasound treatment (also called sonication) is ordinarily used at the end of the process of creation of CNCs and also to disperse CNCs aggregates in dilute suspension (Dong et al., 1996), which generally causes a decrease in viscosity in dilute concentration (Dong et al., 1998; Marchessault et al., 1961; Shafiei-Sabet et al., 2012). This viscosity variation is important and, to our knowledge, the effect of sonication on the rheological behavior and microstructure (like inter-particle distance) of highly concentrated CNCs suspension has not been studied in details.

Beck et al. (Beck et al., 2011) evaluated the impact of ultrasound energy on CNCs in dilute suspension (~3 wt%) to prepare colored solid films and control their optical properties. The

authors found that the chiral nematic pitch in the CNCs films increased with increasing sonication energy input resulting in a change in the film color. Shafiei-Sabet et al. (Shafiei-Sabet et al., 2012) investigated the effects of concentration, temperature and sonication on the microstructure and rheological behavior of aqueous CNCs suspension. They prepared suspensions from freeze-dried CNCs and reached a maximum concentration of ~7 wt%. They found that the minimum amount of sonication necessary to disperse aggregates was  $1000 \text{ J}\cdot\text{g}^{-1}$  whatever the concentration. Nonetheless, they do not observe cholesteric phase before sonication.

In the present study, never freeze-dried highly concentrated CNCs suspensions are submitted to a sonication treatment which induces in a clear change in rheological behavior (**Figure 1**). The non-sonicated suspension forms a stable gel and after sonication, the suspension is liquid and able to flow when the vial was turned upside down. Besides, cholesteric domain appears before sonication treatment. In order to highlight the origin of this phenomenon, we have studied in details, the impact of sonication on CNCs morphology and self-organization in aqueous suspension, at rest and under flow, over a wide range of concentrations (from 1 to 12 wt%).

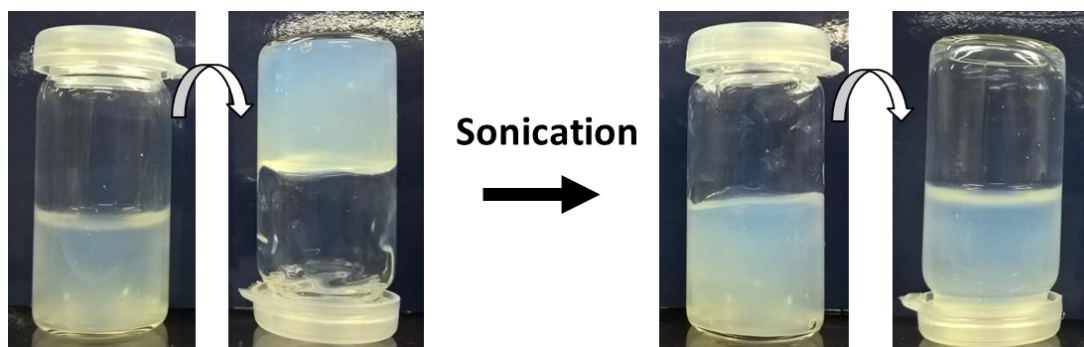


**Figure 1:** Effect of sonication ( $5000 \text{ J/g}_{\text{CNC}}$ ) of the flow properties of a 12 wt% CNC suspensions.

## 1.2. Materials and Methods

### 1.2.1. Materials

The commercial cellulose nanocrystals (CNCs) used in this study were purchased from UMaine Development Center (University of Maine, USA). These CNCs have been produced from wood pulp using sulfuric acid hydrolysis. The colloidal suspension was never freeze-dried and the dry matter content determined with a moisture analyzer (Ohaus® MB-35, Sigma-Aldrich, USA) was ~12 wt%.

### 1.2.2. CNCs suspension characterization

**Atomic force microscopy (AFM):** Individual nanoparticles of the colloidal suspension were imaged using AFM (Dimension icon®, Bruker, USA). All samples were previously diluted to  $10^{-4}$  %wt and a drop of 0.2 mL was deposited onto freshly cleaved mica plate. Samples are dried overnight under room conditions. Those samples were characterized in tapping mode using a silica coated cantilever (OTESPA® 300 kHz - 42 N/m, Bruker, USA). Scans of  $10 \times 10 \mu\text{m}^2$  and  $3.3 \times 3.3 \mu\text{m}^2$  were performed to analyze dimensions of CNCs. At least 4 images per samples were obtained. In order to measure length and height dimensions of CNCs, about 200 measurements were performed by using the software ImageJ® to obtain a representative average.

**Transmission electron microscopy (TEM):** Drops of about 0.001 %wt CNCs suspensions were deposited onto glow-discharged carbon-coated TEM grids. After 2 min, the liquid in excess was absorbed with filter paper, and prior to drying, a drop of Uranylless negative stain (Delta Microscopies, France) was deposited. After 2 min, the solution in excess was blotted and the grid was air-dried. The specimens were observed using a Philips CM200 microscope (FEI, USA) operating at 200 kV. The images were recorded with a TVIPS TemCam F216 digital camera. In order to measure length and height dimensions of CNC, about 150 measurements were performed by using the software ImageJ® to obtain a representative average.

**Dynamic light scattering (DLS):** The dynamic scattering of CNCs sample were studied using a Vasco® I DLS (Corduan Technologies). Samples were diluted in deionized water to  $10^{-2}$  wt% and the conductivity was adjusted to  $500 \mu\text{S}\cdot\text{cm}^{-1}$  by addition of NaCl solution. A non-negative least squares analysis (NNLS) was performed to calculate the hydrodynamic

diameter ( $z^*$ ) and polydispersity index (PDI). For each sample, the final values represent an average of at least 3 acquisitions with 10 measurements.

### 1.2.3. Small-angle X-ray scattering (SAXS)

SAXS measurements were carried out at the ID02 TRUSAXS beamline of the European Synchrotron Radiation Facility (ESRF, Grenoble, France). A monochromatic X-ray beam at a wavelength of 0.995 Å was used. Scattered intensities were recorded on a two-dimensional CCD detector at sample-detector distances of 2 and 10 m in order to cover a  $q$  domain ranging from  $10^{-3}$  to  $10^{-1}$  Å<sup>-1</sup>. Samples were placed in flow-through cells (diameter 1.7 mm), and were left at rest for 5 min before acquisition. The background scattering of pure water and the capillary were subtracted prior to radial integration.

**Particle size:** The scattering intensity distribution  $I(q)$  as a function of the scattering vector  $Q$  was obtained by radial integration of the two-dimensional (2D) scattering pattern. The particle length, height and thickness ( $a$ ,  $b$  and  $c$ , respectively) were extracted from the fitting of the scattering profile with the form factor of a parallelepiped using the SasView® 4.0.1 modeling software.

**Interparticle distance:** A Kratky plot (corresponding to  $q^2 \cdot I(q)$  vs  $q$ ) analysis was performed to measure the average interparticular distance,  $d$ . In this representation:  $d = 2\pi/q_{peak}$ , where  $q_{peak}$  is the position of the scattered intensity maximum.

### 1.2.4. CNCs dispersion and dilution

**Non-sonicated suspensions:** To obtain a homogeneous and well-dispersed suspension, the desired weight concentration of CNCs suspension was diluted with deionized water (pH = 6, conductivity = 1300 μs·cm<sup>-1</sup>). Then, this suspension was magnetically stirred for at least 2 hours.

**Sonicated suspensions:** The dilution was identical to that of non-sonicated dispersions. These suspensions were exposed to a dispersive energy of 5 kJ per g of dry CNCs using a 250 Watt sonication probe (Sonifier S-250A, Branson, USA) at 50% of maximum energy. To prevent thermal degradation of the CNCs during the sonication, the suspension was placed in a container with ice.

**Mechanically-homogenized dispersions:** The dilution was identical to that of non-sonicated dispersions. The suspensions were then mechanically mixed with an Ultra-turrax (IKA T25 digital) at a speed of about  $5000 \text{ tr.min}^{-1}$ .

### 1.2.5. CNCs suspension concentration

**Sonicated suspensions:** The starting solution at 12 wt% was sonicated at 5 kJ per g of CNCs using 250 Watt sonication probe (Sonifier S-250A, Branson, USA). Then, the suspension was concentrated with an EMD Millipore Amicon® bioseparations stirred cells (Merck KGaA, Darmstadt, Germany). The highest concentration was 17.6 wt%.

### 1.2.6. CNCs phase diagram

**Non-sonicated suspensions:** Samples from 1 to 12 wt% (with 1 wt% steps) were poured into 5 mL sealed glass vials and allowed to rest for at least 10 days at room temperature. These vials were observed between cross-polars and pictures were taken using a digital camera. The isotropic/anisotropic phase ratio was measured from these images.

**Sonicated suspensions:** The protocol was identical to that used for non-sonicated suspensions to prepare samples from 1 to 17.6 wt% (with 1 wt% steps).

### 1.2.7. Rheological experiments on CNCs suspensions

The rheology behavior of the aqueous CNC suspensions under shear was studied using different rotational rheometers: Physica MCR 301 (Anton-Paar, Austria) and DHR3 (TA Instruments, New Castle, DE). The tests were carried out at a temperature of  $20^\circ\text{C}$ . Shearing tests were performed with a cone-plate configuration (diameter of 50 mm and angle of  $1^\circ$  for MCR 301 and diameter of 65 mm and angle of  $2^\circ$  for DHR3). The atmosphere around the sample was saturated with water to avoid evaporation during the measurement. To control the initial state of each sample, a constant shear rate was applied. The transient response under shear was recorded until steady conditions were obtained. Steady shear viscosity vs shear rate curves was generated for each sample from a shear rate of  $0.01$  to  $1000 \text{ s}^{-1}$ . The time required to reach steady conditions was decreased with increasing shear rate. Oscillatory measurements were also performed to collect the relaxation time and the elastic behavior of each sample. The percent strain used was inside the linear viscoelastic region (LVE) as determined by performing strain sweep experiments at a frequency of 1 Hz. Then

the optimal frequency was determined by performing oscillation sweep experiments at the previously obtained strain in the LVE. These two values were fixed to achieve the storage modulus ( $G'$ , Pa) and the loss modulus ( $G''$ , Pa) before and after a strong shear deformation (up to  $100 \text{ s}^{-1}$ ).

## 1.3. Results

### 1.3.1. CNCs morphology

AFM and TEM images of CNC particles before and after sonication are shown in **Figure 2**. These data reveal changes in morphology, size and size distribution upon the sonication treatment. Before sonication, the particles clearly exhibit a composite aspect and are formed of the lateral association of elementary rod-like crystallites (**Figure 2b** and **c**). In a particle, the constituting crystallites are all parallel but their number (estimated to range between 2 and 4), size distribution and association pattern make it difficult to define a generic morphology. This composite nature of CNCs from different botanical sources have been described by other authors (Chauve et al., 2014; Elazzouzi-Hafraoui et al., 2008).

It is considered to originate from the strong lateral association of cellulose microfibrils after drying of the raw material. The strong acid hydrolysis and subsequent sonication treatments were not sufficient to break this association. It was thus possible to measure the length of the particles but more difficult to define their width. The average length was  $217 \pm 42 \text{ nm}$ , measured on AFM images. The average thickness, determined from the AFM images, was  $10 \pm 5 \text{ nm}$  (**Figure 2a**), a value which is rather close to the lateral size of the constituting crystallites and suggests that the particles have a lamellar shape.

After sonication, the particles appear to be smaller both in length and width, and the number of constituting crystallites has decreased to a few units (about 1 to 2) (**Figures 2e** and **2f**). The average length was  $150 \pm 30 \text{ nm}$  and the thickness was still  $10 \pm 5 \text{ nm}$  (**Figure 2d**). The CNC after sonication values are in line with the literature data on CNCs from wood pulp (Habibi et al., 2010; Lagerwall et al., 2014; Shafiei-Sabet et al., 2012). The decrease in dimensions was confirmed by DLS analysis, as the hydrodynamic diameter decreased from  $119 \pm 3$  to  $80 \pm 1 \text{ nm}$  after sonication (**Table 1**).

**Table 1:** Hydrodynamic size (DLS) and size distribution (AFM) of sonicated and non-sonicated CNC suspensions. The standard deviations are indicated between parentheses.

	Hydrodynamic properties		Size distribution	
	Z* (nm)	PDI	Average length (nm)	Height (nm)
Non-sonicated CNC	119 (3)	0.20	217 (42)	10 (5)
Sonicated CNC	80 (1)	0.17	150 (30)	10 (5)

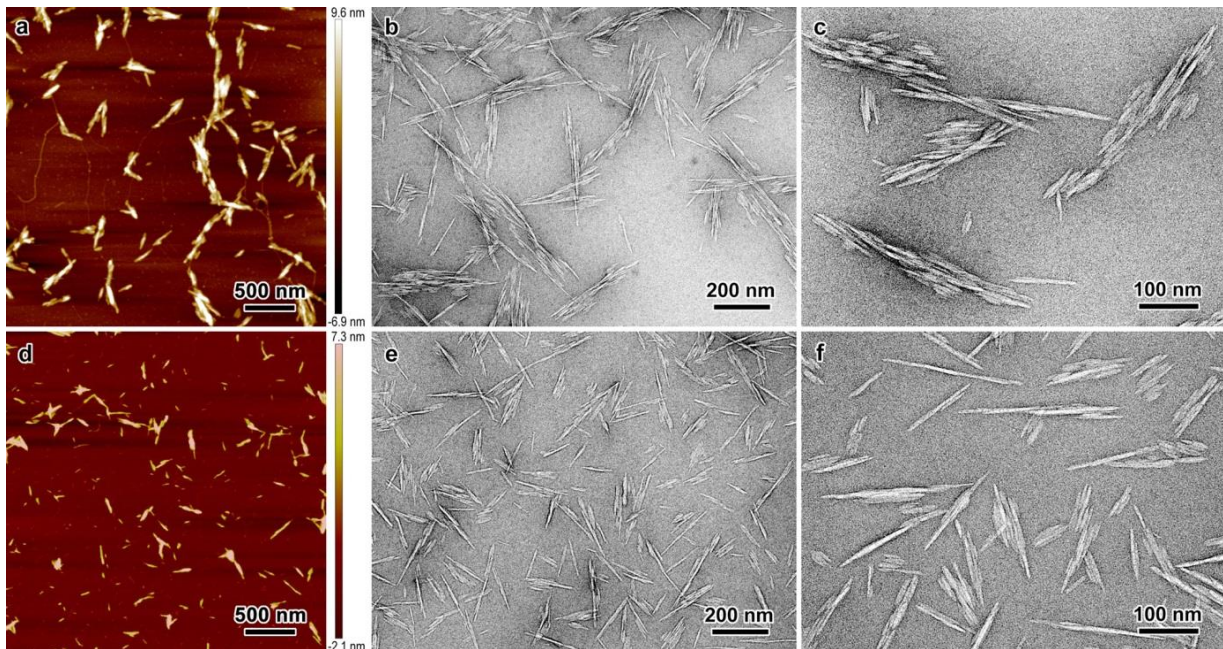


**Figure 2:** CNC morphology: a, b, c before sonication; d, e, f after sonication. a and d are AFM images while b, c, e and f are TEM images of negatively stained preparations.

### 1.3.2. Phase behavior and microstructure after sonication at high concentration

**Figure 3** presents the phase diagram for sonicated and non-sonicated CNC suspensions. In one case, the suspension at concentration about 12 wt% has been sonicated and in other case the delivered non-sonicated has been use. For non-sonicated suspensions, the full isotropic phase is constant until 5 wt%, CNC are randomly organized. Above a critical concentration about 6 wt%, a biphasic domain appears. CNCs particles start to organize themselves and a fraction of anisotropic domain emerges.

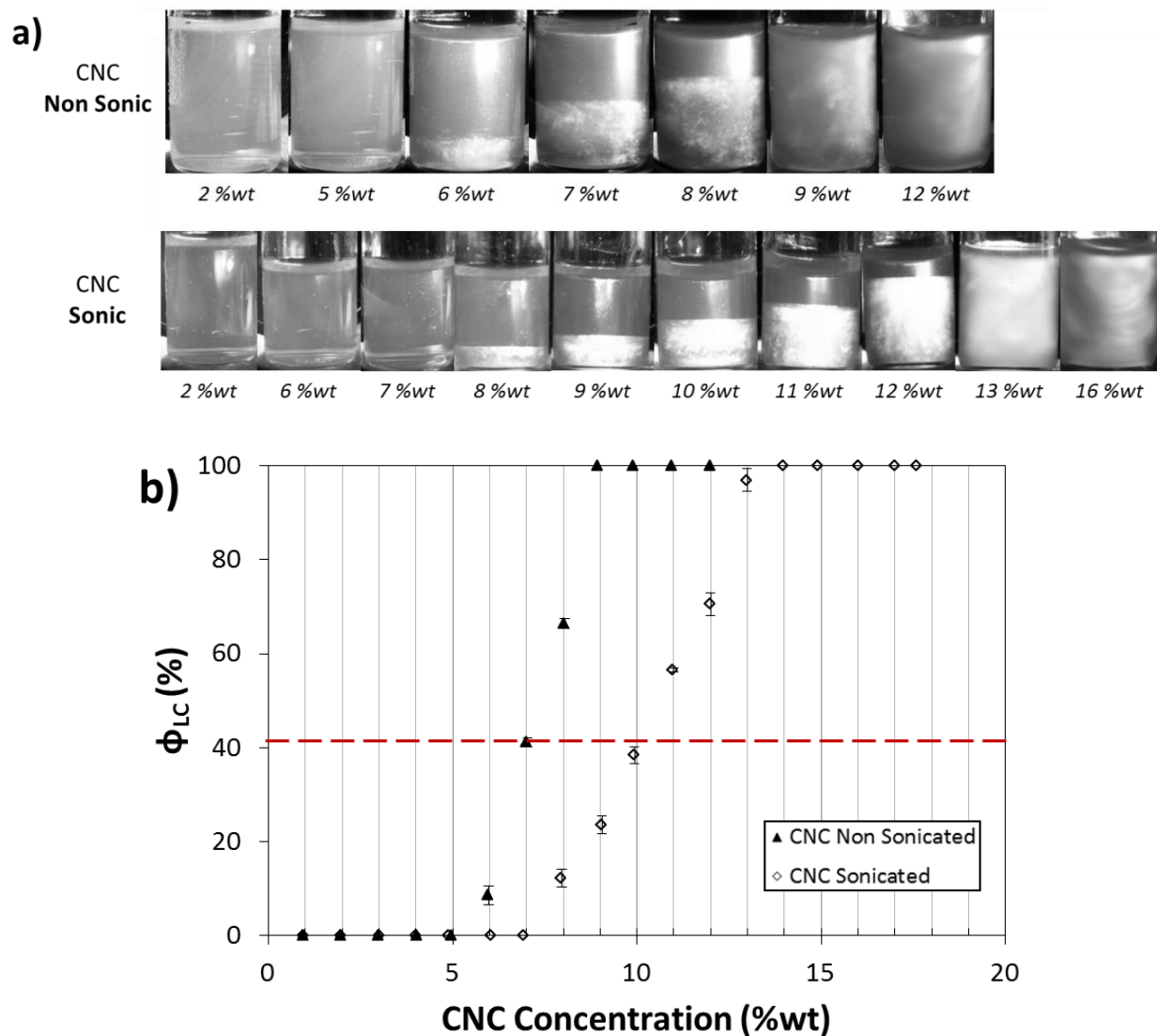


**Figure 3:** Phase behavior of aqueous CNCs suspensions after equilibration. a) photographs of vials between crossed polars showing the phase separation of CNC suspensions from 1 to 12 wt% (non-sonicated CNCs) and from 1 to 16 wt% (sonicated CNCs). The lower liquid crystalline phase (anisotropic) is white while the upper isotropic phase appears dark. b) Volume fraction of liquid crystalline phase ( $\phi_{LC}$  in vol%) as a function of the solid weight in the CNC suspensions. ▲ and ◇ correspond to non-sonicated and sonicated CNC suspensions, respectively. The error bars represent the standard deviation of the fitted Gaussian peaks. The dash line indicates  $\phi_{LC}$  equal to 40 vol%, which are further discussed.

The liquid crystal volume fraction  $\phi_{LC}$  increases with increasing suspension concentration. The maximum  $\phi_{LC}$  is obtained above 9 wt% and a total anisotropic gel is obtained. These results are in agreement with those recently reported by Xu et al. (Xu et al., 2017b). The phase separation is time-dependent and it takes several days (5-7 days in this case) for the suspension to equilibrate.

After sonication, the phase diagram of the suspension is significantly different. The critical CNCs concentration, at which the liquid-crystalline phase appears, shifts to 7 wt%. The maximum critical concentration increases to 13 wt% with the formation of an anisotropic birefringent gel and the phase equilibrium is reached much faster (20 h).

### 1.3.3. Interparticle distance in static conditions

In order to understand the effect of sonication on the interparticle distance, structural analyses at different length scales were performed by SAXS. **Figure 4** shows the evolution of the average distance between CNCs with the concentration of the suspension. Before or after the sonication, the behavior is the same and respects a power law. With the concentration increasing, the interparticle distance quickly decreases and reaches a minimum close to 30 nm in the concentration range probed. Both power law fits exhibit a power index close to  $-1/2$ . A power law index of  $-1/2$  is characteristic of the signal of long cylinder in hexagonal arrangement, also described as rod-shaped particles (Baravian et al., 2010). The CNCs' shape is conserved through the sonication treatment. During sonication, at CNCs volume fraction constant, the repartition of particles is modified. In particular, the splitting induced by sonication drastically modified the form factor from 2 to 4.

Does the modification of the volume fraction  $\phi$  is sufficient to explain the variation of the rheological behavior after sonication (presented and discussed in following section)? The  $a$ ,  $b$  and  $c$  characteristic dimensions of CNCs were obtained by plotting the intensity distribution  $I(q)$  as a function of scattering vector  $q$  and fitting the graph with mathematic model for the 1%wt CNC suspension. Different models were used and the parallelepiped one presents the best fitting. After sonication, CNCs are individualized and the characteristic dimension  $a$ ,  $b$ ,  $c$  are  $121 \times 20 \times 5 \text{ nm}^3$ . Nonetheless, before sonication, CNCs dimensions are  $114 \times 60 \times 4 \text{ nm}^3$ . The length obtained for both systems needs more investigation due to problem of fitting with the  $Q$  range used in this study. Besides, a high polydispersity appears in the calculation of the dimension  $b$  for non-sonicated CNCs. To clearly conclude on the CNCs size before sonication, more investigations in the high  $Q$  range are necessary.

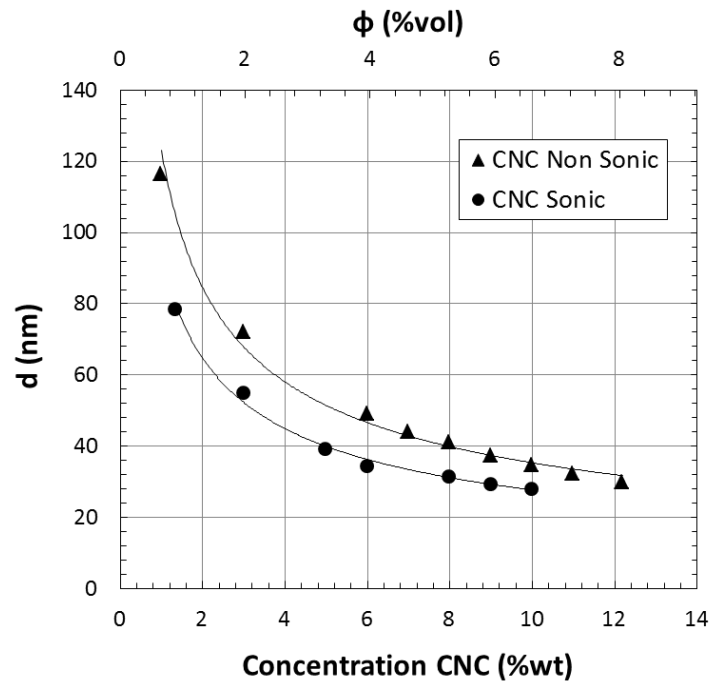


**Figure 4:** Average CNC center-to-center interparticle distance  $d$  as a function of concentration (in wt%, bottom scale) or volume fraction ( $\phi$  in vol%, top scale) in suspensions at different concentrations, deduced from the Kratky SAXS plot ( $q^2 \cdot I(q) = f[q]$ ). CNC were exposed (●) or not exposed (▲) to sonication. Interpolation curves correspond to a power law model. The power law equation is  $y = 93x^{-0.53}$  and  $y = 123x^{-0.54}$  for sonicated and non-sonicated CNC suspensions, respectively.

#### 1.3.4. Influence of sonication on the rheological behavior

To complete the static and the microstructure studies, this paper investigates the rheological behavior of the commercial suspension at 12 wt%.

##### *Effect of mechanical treatment on CNCs rheology*

**Figure 5** compares the effect of sonication and mechanical homogenization on the rheological behavior of the suspension at 12 wt%. The non-sonicated initial CNCs suspension exhibits a shear-thinning behavior. When the shear rate increases from  $0.1$  to  $1000 \text{ s}^{-1}$ , the viscosity drastically decreases from  $500$  to  $0.08 \text{ Pa}\cdot\text{s}$ , respectively, and respects a power law ( $y = 49.65x^{0.06}$ ). As shown in **Figure 1**, the suspension is in a gel-like form and do not flow when the vial was turned upside down.

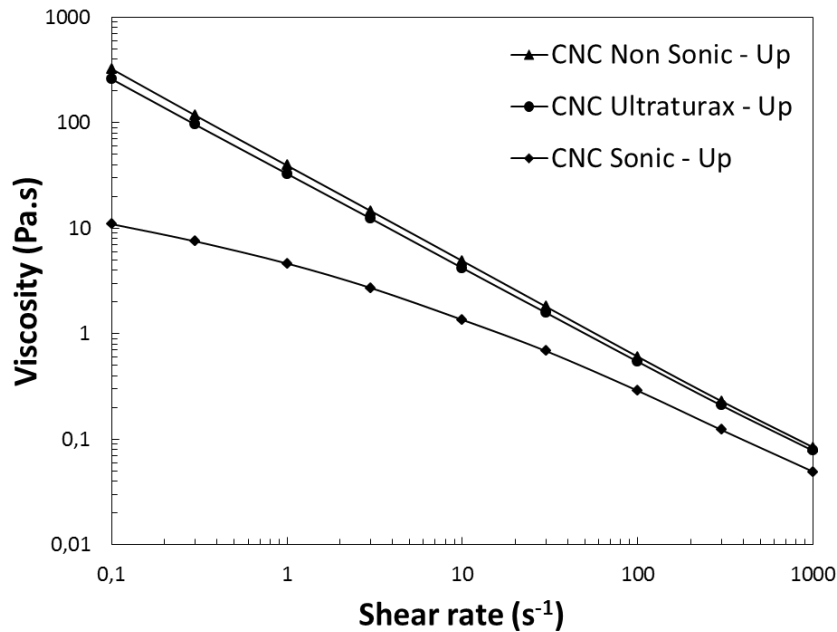


**Figure 5:** Flow curves of CNCs suspensions treated by sonication and mechanical homogenization. Full lines correspond to the increasing shear.

After a strong mechanical homogenization, the CNCs suspension do not exhibit any change in behavior compared to the non-sonicated suspension. Only sonication changes the organization of CNCs in volume and, consequently, the rheological behavior. **Figure 1** shows that the suspension was liquid and flowed when the vial was turned upside down.

### ***Influence of aging time after sonication***

**Figure 6** presents the evolution in time of the rheological behavior for 12 wt% CNCs commercial suspension after ultra-sonication treatment. Before sonication, the rheological behavior for the same suspension does not present time evolution. On this figure, two behaviors are identified and separated by a critical shear rate  $\dot{\gamma}_c$ . Below this value, the suspension is on a plateau region. Then above this value, a shear-thinning region appears.  $\dot{\gamma}_c$  decreases when relaxation time after sonication increased. In details, just after sonication, the maximum viscosity at low shear rate is close to 0.04 Pa·s and decreases to 0.016 Pa·s at 1000 s<sup>-1</sup>. During the following hour, the critical shear rate  $\dot{\gamma}_c$  does not move (20 s<sup>-1</sup>) but the viscosity slightly increases. The characteristic value  $\dot{\gamma}_c$ , and the general viscosity, change after one day of relaxation. As previously presented, the biphasic domain reaches equilibrium within one day. The viscosity increases because of reorganization of CNCs in suspension from randomly to liquid crystal phase. The sonication does not significantly change important properties of cellulose nanocrystals, but change the ions double layer

(originating from the hydrolysis process that has not been removed during the purification steps). After more than a year of relaxation the viscosity at low shear rate increases to 9 Pa·s and  $\dot{\gamma}_c$  decreases to  $2.5 \text{ s}^{-1}$ . The growth of chiral domains and their possible alignment under shear in the same axes could explain this increasing.

This suspension never comes back to the rheological behavior of the non-sonicated suspension but recovers its original behavior after very long relaxation times.

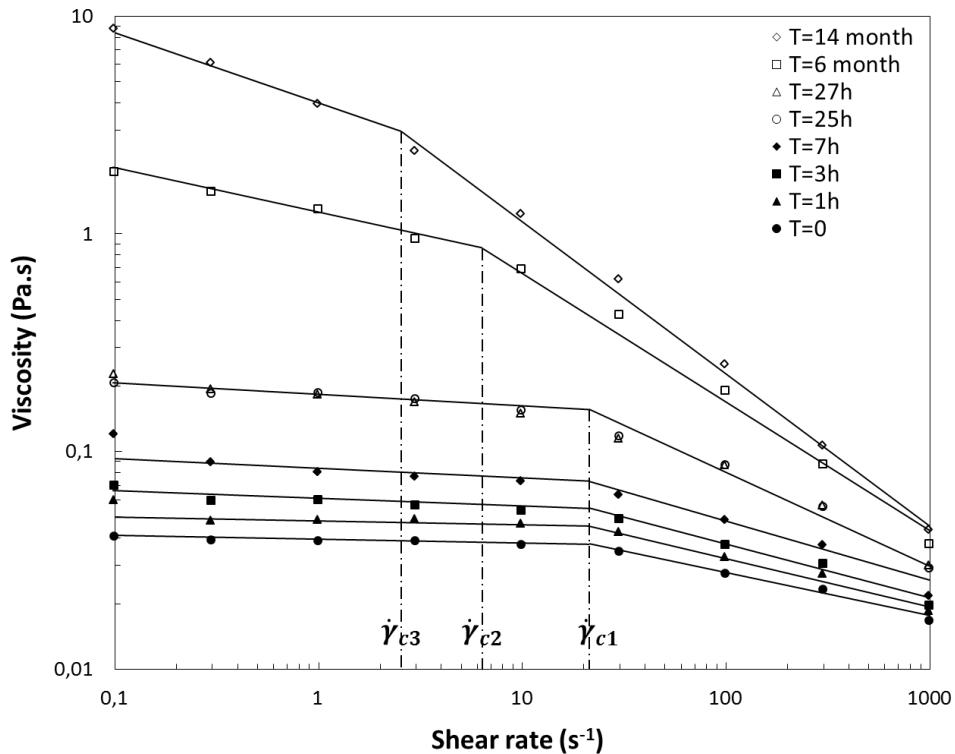


**Figure 6:** Flow curve represents the rheological behavior depending on the time evolution of 12 wt% CNCs suspensions after sonication. Plateau regions and critical shear rate ( $\dot{\gamma}_c$ ) are indicated in full and dotted lines, respectively.  $\dot{\gamma}_{c1}$ ,  $\dot{\gamma}_{c2}$  and  $\dot{\gamma}_{c3}$  are equal to 20, 6 and  $2.5 \text{ s}^{-1}$ , respectively.

In order to understand the viscoelastic properties and the restructuration after shear rate of both 12 wt% suspensions, oscillation experiments were performed. A constant strain within the linear viscoelastic (LVE) region was applied in order to keep the structural organization unchanged and probe the non-flowing samples. A strong deformation ( $\dot{\gamma} = 1000 \text{ s}^{-1}$ ) largely out of the LVE was then applied to break the system and organize CNC. Then again, a constant strain within the LVE was applied.  $G'$  (elastic modulus in Pa) and  $G''$  (viscous modulus in Pa) values quantify respectively the solid and liquid behavior of the CNC suspension.

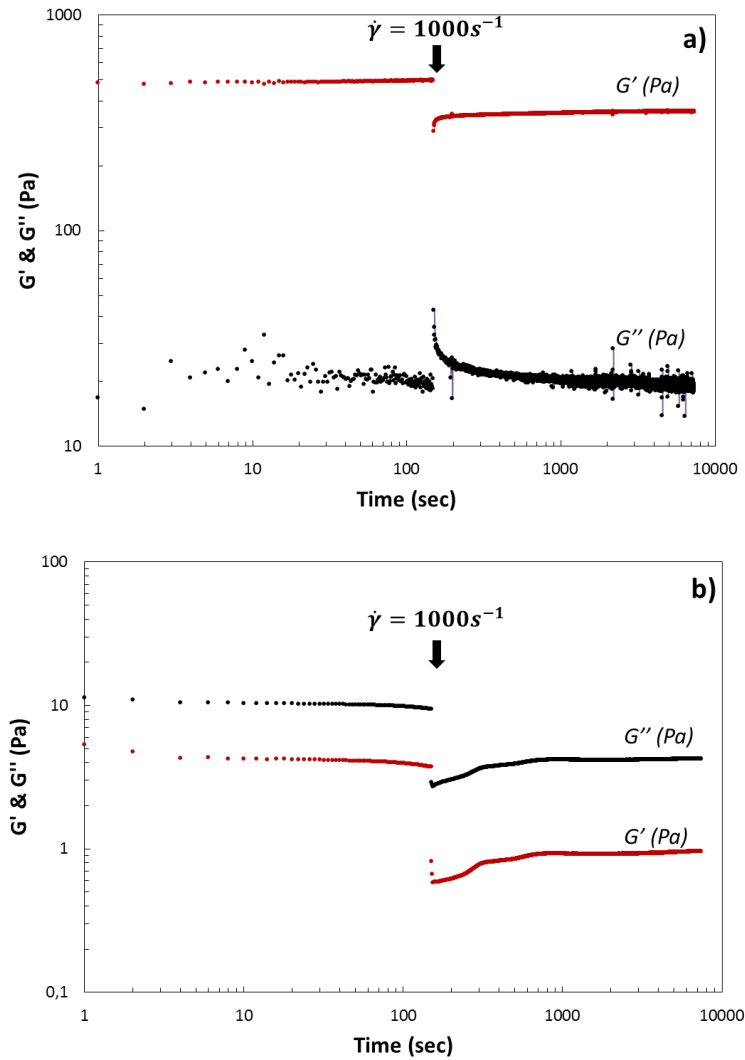


**Figure 7:** Evolution of  $G'$  (Pa) and  $G''$  (Pa) for non-sonicated (a) and sonicated (b) CNC suspensions.

With these values, the loss factor  $\tan \delta$  can be calculated according **Equation 1**:

$$(1) \quad \tan \delta = G''/G'$$

In this equation, if  $\tan \delta$  is lower than 1, the elastic modulus ( $G'$ ) dominates the system and the suspension behaves like a solid. In the opposite case, if  $\tan \delta$  is higher than 1, the viscous modulus ( $G''$ ) controls the system and the material is dominated by a liquid behavior.

The evolution of  $\tan \delta$  is presented in **Figure 7** and summarized in **Table 2**. In the original state of 12%wt commercial non sonic suspension, the loss factor is inferior to 1 indicating a dominant elastic behavior. Referring to **Figure 5**, by applying a strong shear rate the general viscosity decreases from 500 to 0.08 Pa·s (respectively 0.1 to 1000  $\text{s}^{-1}$ ). Upon strong deformation, the suspension recover quickly (200 s) its gel-like behavior with a loss of factor of 0.06.

**Table 2:** Synthesis of  $\tan \delta$  measurements obtained with  $G'$  (elastic modulus in Pa) and  $G''$  (viscous modulus in Pa) before and just after applying a shear rate of  $1000\text{s}^{-1}$  on 12 wt% CNCs suspension.

	Before deformation			After $\dot{\gamma} = 1000\text{ s}^{-1}$		
	$G'$ (Pa)	$G''$ (Pa)	$\tan \delta$	$G'$ (Pa)	$G''$ (Pa)	$\tan \delta$
Non-sonicated	490	20	<b>0.04</b>	355	20	<b>0.06</b>
Sonicated	4	10	<b>2.5</b>	1	4	<b>4</b>

After sonication, the system is driven by the viscous modulus and presents a loss factor about 2.5. The material is dominated by a liquid behavior. After high shear rate, the loss factor keeps superior to 1.

Regarding these results, only an ultrasonic treatment clearly modifies the nature of highly concentrated CNCs suspension from university of Maine. The viscosity decreases from 500 to 10 Pa·s after this treatment (at  $0.1\text{ s}^{-1}$ ). The rheological forces, which drive both suspensions, change from gel-like form to liquid form.

### 1.3.5. Concentration effect on the CNC rheological behavior

**Figure 8** shows the steady-state flow curves for CNCs suspension in deionized water at different concentrations ranging from 1 to 12 wt%. In complement, **Table 3** presents the power law parameters obtained from fitting regions of the flows curves.

In **Figure 8a**, CNCs without sonication treatment are investigated. A recent study shows results on the CNC from Maine suspension behavior without sonication effect (Xu et al., 2017b). These results are close to our results, however all concentration were not evaluated in the publication. CNCs suspensions are near-Newtonian liquid for concentration below 3%wt, referred to a flow index  $n$  close to 1 (**Table 3**). By increasing the amount of CNCs in the suspension (4-5 wt%), at low shear rate ( $<1\text{ s}^{-1}$ ) the CNCs suspensions exhibit a plateau close to a zero-shear viscosity plateau and at high shear rate a shear-thinning behavior ( $0.9 > n > 0.5$ ). In **Figure 3** these concentrations are in the fully isotropic region. Then for 6-8%wt CNC suspensions, corresponding to the apparition of the liquid crystal phase on the **Figure 3**, the rheological behavior change to a multi-phase curve as explained in the publication of Xu (Xu et al., 2017b). The consistency  $K$  starts to increase for a 7 wt% CNCs suspension, which corresponds to  $\sim 40$  vol% of volume fraction of liquid crystalline phase. For high shear rate, a significant shear thinning appear with a power law exponent from 0.5 to 0.3. The slight shear-thinning at low shear rates may indicate some association between the

CNC rods. At higher concentrations, which correspond to the fully anisotropic domain of the liquid crystals form, samples present strong shear-thinning behavior on all the range of shear rates. The flow index  $n$  decreased close to zero for 12 wt% CNCs, this CNCs suspension presents a response characteristic to a yield stress fluid. The presence of closely packed structure locks the rods motion due to an excessive concentration.

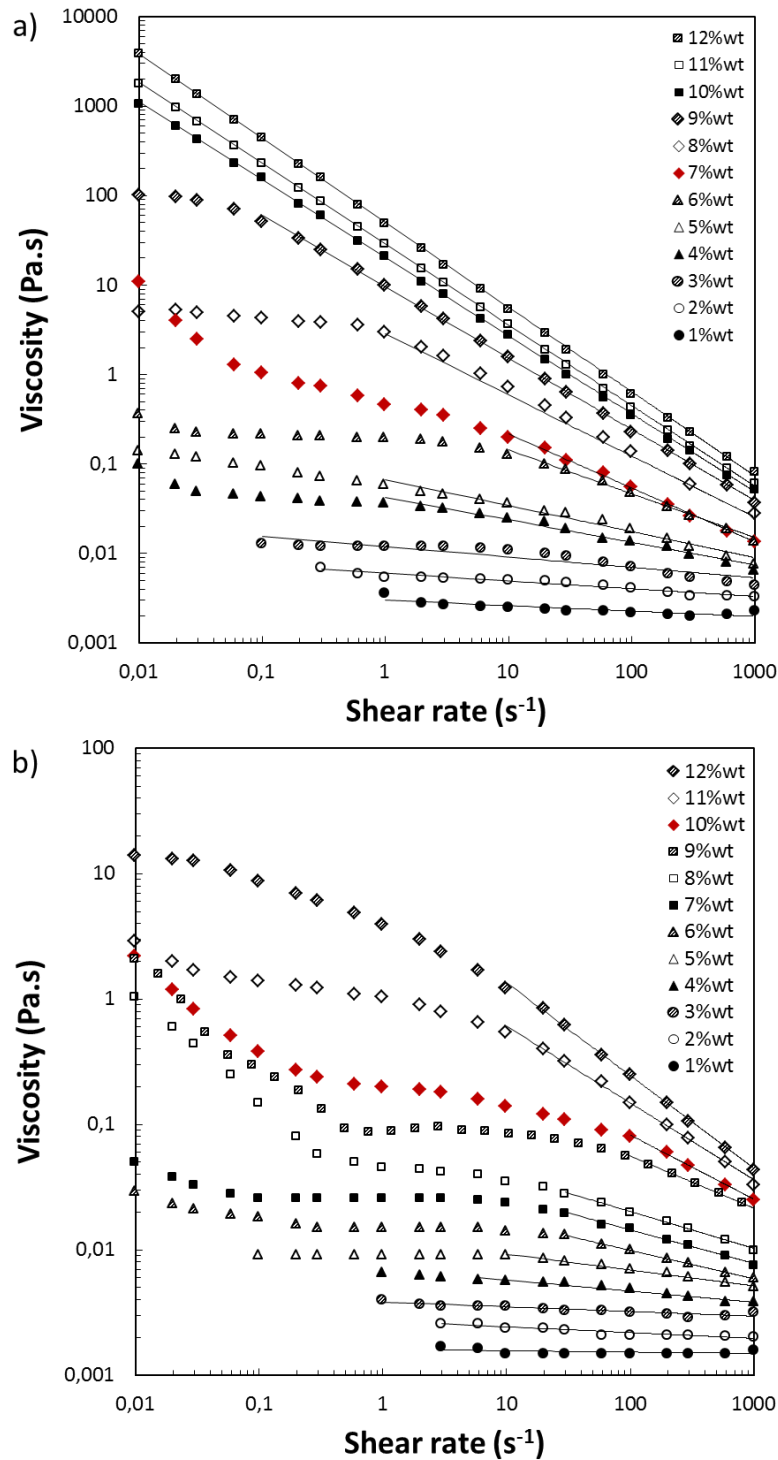


**Figure 8:** Investigation on shear rheology of 1-12 wt% CNCs suspension in water: apparent viscosity as function of shear rate for CNC before (a) and after sonication (b). Red diamond corresponds to  $\phi_{LC}$  close to 40 vol%.

		wt%	1	2	3	4	5	6	7	8	9	10	11	12
CNC Non-sonicated	$K (Pa \cdot s^{-n})$		0.003	0.006	0.023	0.048	0.09	0.053	0.71	2.77	9.35	20.39	28.671	49.65
	$n$		0.97	0.92	0.89	0.73	0.65	0.48	0.43	0.32	0.21	0.13	0.1	0.06
Sonicated CNC	$K (Pa \cdot s^{-n})$		0.002	0.003	0.004	0.007	0.012	0.024	0.045	0.077	0.386	0.515	2.423	4.93
	$n$		0.97	0.96	0.96	0.92	0.87	0.81	0.75	0.71	0.58	0.57	0.39	0.34

**Table 3:** A list of the power law ( $\eta = K \cdot \dot{\gamma}^{n-1}$ ) parameters obtained from fitting regions of the flow curves in **Figure 8**.

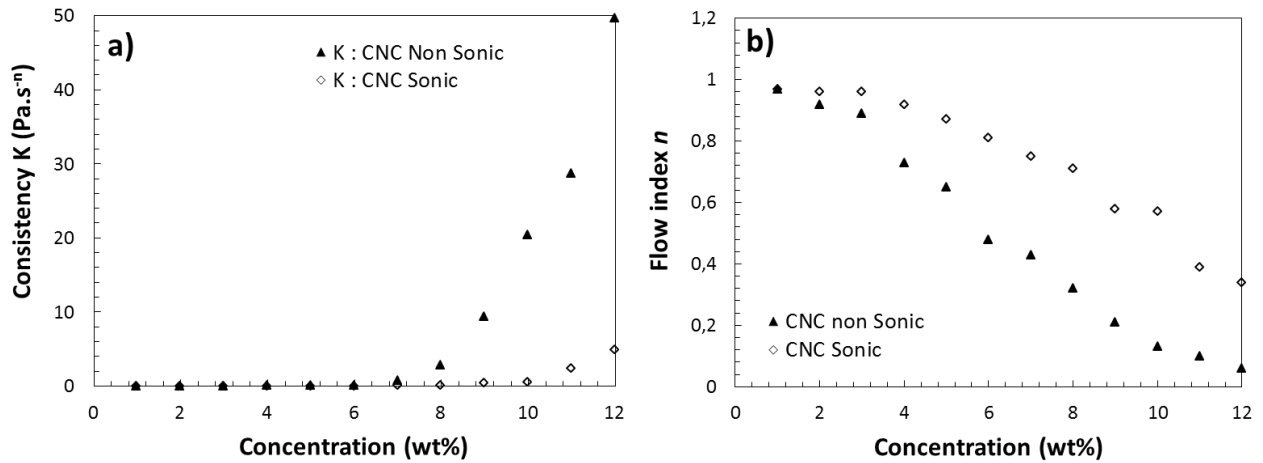


**Figure 9:** Plot of the power law parameters for CNCs before and after sonication, referring to **Table 3**: a) consistency  $K$  and b) flow index  $n$  versus CNCs concentration.

In **Figure 8b**, the rheological behavior of CNC suspension after sonication is exposed. Refers to **Figure 3** the presence of anisotropic region start at 7 wt% and is full at 13 wt%. CNCs suspension at 1-4%wt exhibits a near-Newtonian behavior with  $n$  between 1 and 0.9 (**Table 3**). For 5-7 wt%, at mid shear rate ( $< 10 \text{ s}^{-1}$ ) the CNCs suspensions exhibit a plateau region and at high shear rate a shear-thinning behavior ( $0.75 < n < 0.87$ ). A slight shear thinning at lower shear rate could be associated to the disruption of the largest chiral nematic domain in smaller chiral nematic domains. Then for concentration 8, 9 and 10%wt a three-region behavior was observed, typical of liquid crystalline samples (Bercea and Navard, 2000; Shafiei-Sabet et al., 2012). At low shear rate ( $< 0.1 \text{ s}^{-1}$ ), the viscosity decreases because of the dissociation of the largest chiral nematic domains in smaller chiral nematic domains. Then, for middle range shear rate (1 to  $30 \text{ s}^{-1}$ ), the plateau in viscosity could be associated to the increasing alignment of these chiral domains in the flow direction. Similarly to the non-sonicated suspension, the consistency  $K$  starts to increase for a volume fraction of liquid crystalline phase close to  $\sim 40 \text{ vol\%}$ , which corresponds to 10 wt% of sonicated CNC suspension. At high shear rate, a significant shear thinning appears and the viscosity

decreases: chiral domains are broken and CNC will be dissociated and aligned in the flow direction. For higher concentration, the behavior in three-region disappears and a two slope fitting appears. At  $0.1 < \dot{\gamma} < 10 \text{ s}^{-1}$ , the nematic domains have been organized in the shear flow direction. For high shear rate ( $>10 \text{ s}^{-1}$ ), the power law parameter  $n$  decreases under 0.4 and a shear-thinning behavior is observed. Nematic domains are dissociated and mostly alone CNCs are aligned with the flow.

## 1.4. Discussion

By comparing both systems (sonicated and non-sonicated suspensions) on **Figure 8**, ultrasonic treatment changes irreversibly the viscosity and the organization of the CNC suspension. At high concentration and low shear rate, the viscosity drastically decreases (example: from 4000 to 14 Pa·s at 12 wt% and  $0.01 \text{ s}^{-1}$ ). At low concentration, the same observation appears, but the gap is smaller (example: from 0.1 to 0.007 Pa·s at 4 wt% and  $0.01 \text{ s}^{-1}$ ). When the shear rate increases, both systems present a shear-thinning behavior and the final viscosity is similar. At a 3 wt% CNC concentration, both systems exhibit a near Newtonian behavior.

Concerning the shear-thinning part, when the index flow  $n$  is close to 1, the system is near a Newtonian one. When  $n$  decreased, the system becomes gel-like form and finishes as solid form. As shown in **Figure 9** and **Table 3**, the consistency  $K$  for sonicated suspension is always lower than the consistency of non-sonicated suspension, and the power law parameter  $n$  is always superior for system after sonication. Non sonicated CNCs suspensions have a power law parameter which decreases when the concentration increases, and at 12 wt%  $n$  is equal to 0.06. This system is in a strong gel form (visually demonstrated in **Figure 1**). After sonication, the suspension loses this properties and becomes a liquid system ( $n = 0.34$  at 12 wt%).

By comparing **Figure 8** and the phase diagram in **Figure 3** for both systems, rheological results present three behavior regions which correspond to the three domains in the phase diagram. In the full isotropic domain, both systems present a near Newtonian nature. A plateau region appears for low shear rate: CNCs start to organize themselves with their neighbor but the liquid crystal phase does not appear. It is the beginning of the shear-thinning properties. In the biphasic domain, both systems present three rheological behavior

regions as described in literature (Ureña-Benavides et al., 2011). In the full anisotropic region, the non-sonicated suspension is totally shear-thinning. In the case of 12 wt% sonicated suspension (**Figure 3b**), the system is not totally anisotropic ( $\phi_{LC} = 70 \text{ vol\%}$ ). On **Figure 6**, the sonicated CNC suspension presents, at a shear rate inferior to  $10 \text{ s}^{-1}$ , a first region corresponding to the organization of the nematic domain along the shear direction. At high shear rate ( $> 10 \text{ s}^{-1}$ ), a shear-thinning behavior is observed and the viscosity decreases from  $10 \text{ Pa}\cdot\text{s}$  at  $0.1 \text{ s}^{-1}$  to  $0.05 \text{ Pa}\cdot\text{s}$  at  $1000 \text{ s}^{-1}$ .

This behavior could be attributed to the presence of aggregate in the CNCs suspension before sonication. Some recent works explore these hypothesis (Ureña-Benavides et al., 2011; Xu et al., 2017a) but the authors used freeze-dried CNCs in their studies. This process involved the formation of aggregates. In our study, CNCs suspensions have never been freeze-dried and do not normally present aggregates. As shown in **Figure 2**, AFM and TEM images show well organized CNC in the non-sonicated suspension. Aggregates are normally composed of CNCs randomly packed. Nevertheless, before sonication, CNCs studied in this work present small aligned packet (on AFM measurement, the section is similar but the length is higher).

In **Figure 3**, the commercial suspension presents biphasic region in phase diagram easily obtained in 5-7 days (for CNCs prepared from wood it take couple of weeks). A fully dispersed suspension presents a liquid-crystalline phase. In the presence of aggregates, the suspension never obtains a liquid crystal phase. This phase corresponds to a chiral nematic phase which exhibits chirality. It corresponds to a twisting of CNCs perpendicular to the director, with the CNCs axis parallel to the director and presents a helicoidally structure (Beck et al., 2011; Dong et al., 1996; Habibi et al., 2010; Lagerwall et al., 2014; Schütz et al., 2015). The chiral pitch  $p$  refers to the distance over which CNCs undergo a full  $360^\circ$  twist, is linked with the inter-particle distance  $d$ . **Figure 4** presents this particular mean distance between each CNC (SAXS measurement). In both case (sonicated or non-sonicated suspension), the evolution of this distance with the concentration decreases and respects a power law with a power index equal to  $-1/2$ . This index is typical of rods like particles shape (Baravian et al., 2010). In the presence of aggregates, this set value cannot exist because of randomly packed particles.

A particular case is identified on **Figure 9**, the consistency  $K$  drastically increases at 7 wt% for non-sonicated CNCs suspension and at 10 wt% for the sonicated CNCs suspension. To obtain the same volume fraction of liquid crystals in the suspension, a 7 wt% non-sonicated suspension corresponds to a 10 wt% sonicated one. In both case, the volume fraction of liquid crystalline is close to 40 vol% (star symbol in **Figure 3**). In **Figure 8**, red diamonds highlight these two cases. Rheological behaviors of no-sonicated and sonicated CNCs suspension are similar. The sonication do not modify the rheological behavior of CNCs suspension, but changes the relative concentration when the three rheological behavior regions appeared. This observation highlights the fact that the suspension before sonication is not aggregated (in the case of aggregation, the general behavior is totally different (Xu et al., 2017a)).

In conclusion, before sonication, CNCs suspension presents cholesteric domain (**Figure 4**), a typical crystal liquid behavior of nanocellulose (**Figure 3**) and the standard rheological behavior of CNCs (Shafiei-Sabet et al., 2012; Ureña-Benavides et al., 2011) (**Figure 8**). These suspensions did not show an aggregate suspension behavior. After sonication, suspension presents rods particles (**Figure 4**) with interparticle distance smaller than in a non-sonicated CNCs suspension at the same concentration. Cholesteric domain appears for higher concentration than the non-sonicated CNCs. The rheological behavior is similar to the non-sonicated suspension. But, as the sonication induces a lateral fragmentation of the particles and a decreasing of the form factor of domains, the typical behavior of liquid crystals appears for higher concentration (10 wt% compared to 7 wt%). Sonication effect is irreversible on CNCs (**Figure 6**).

*Some publications discuss on the surface modification of the physico-chemistry of CNCs particles by the sonication effect. This modification was presented as a diminution of ions present in the electrical double layer around CNCs (Beck et al., 2011, 2012). As perspectives on this project, it will be attractive to focus on the electrical/ions liberation during the sonication to explain the rheological change.*

## 1.5. Conclusions

The microstructure and the rheological behavior of a highly concentrated suspension of cellulose nanocrystals from University of Maine have been studied, and the behavior of never freeze-dried non-sonicated and sonicated suspensions were compared. The sonication treatment does not change the rod size particle but induces a decrease of the suspension viscosity. Both suspensions present three-region phase diagrams which correspond to three different microstructural transitions: isotropic region, biphasic region (coexistence of isotropic and chiral nematic form) and a birefringent gel. The sonication effect changes the slope of the biphasic region and the general viscosity of each concentration. At 12 wt%, the suspension is a “gel” before sonication and turns totally to “liquid” form after sonication treatment. The microstructure, and in particular the inter-particle distance  $d$ , is changed by this treatment. The power law, which drives the decrease of  $d$  with the increase of the concentration, is conserved and shifts down after sonication. This indicates a diminution of the pitch between CNC, and a diminution of the particles form factor. The associated index is  $\frac{1}{2}$ , and it is characteristic of rod-shaped particles. We proved that the rheological modification is not due to the presence of aggregates in suspension, but due to the modification of the particle form factor.

The viscosity profile of the non-sonic CNC suspensions shows a single shear-thinning behavior over the whole range of shear rates for concentration higher than 9 wt%. By decreasing the concentration, a three region behavior appears then followed by a Newtonian plateau for concentration under 3 %wt. After sonication, the system is stable again but presents a high diminution of viscosity and shear-thinning slope. By decreasing the viscosity, a notable three region plateau typical of liquid-crystal appears. Then a Newtonian plateau drives the system for concentration lower than 4 wt%.

In this paper we describe the behavior of a commercial CNCs suspension before and after sonication at high concentration. This suspension is used in a lot of applied work to industry, and we are thinking that this study will open new opportunities for industrial application with nanocrystalline cellulose like shear-thinning polymer, injectable or pump-ability liquid and matrices reinforcement.



## 2.1. Introduction

During the last ten years, researchers and industrials were attracted by the realization of functional and 'smart' materials. As renewable and bio-compatible building blocks, cellulose nanocrystals (CNCs) are now commonly recognized for the design of hydrogel architecture (Abitbol et al., 2016; De France et al., 2017; Salas et al., 2014; Tang et al., 2017). The industrial availability and the price decreasing facilitate the translation from laboratory to industrial project (Chauve and Bras, 2014; Tang et al., 2017). CNCs are crystalline rods-like nanoparticles isolated via acid hydrolysis of abundant cellulosic fibers. CNCs display several unique properties such as: high and tunable aspect ratio (Bras et al., 2011), low density ( $1.606 \text{ g}\cdot\text{cm}^{-3}$ ) (Klemm et al., 2011), high specific surface area ( $300\text{-}800 \text{ m}^2\cdot\text{g}^{-1}$ ) (Habibi, 2014), excellent mechanical properties (Dufresne, 2013; J. Eichhorn, 2011; Oksman et al., 2014; Siqueira et al., 2010b) and the capacity to self-organize into liquid crystalline phases in aqueous media (Bardet et al., 2015; Dong and Gray, 1997; Revol et al., 1992).

In 'smart' material field, one of the most promising applications of CNCs is biomedical applications and in particular the possibility to use these hydrogels for injectable system, tissues engineering or Wound dressing (De France et al., 2016; Domingues et al., 2014, 2015; Jorfi and Foster, 2015; Lin and Dufresne, 2014; Naseri et al., 2016; Yang et al., 2013b). The question of toxicology and safety issues of CNCs are often ask and recent study confirms the absence of cells toxicity when injected as suspension in body (Dong et al., 2012; Kovacs et al., 2010; Roman, 2015).

In some medical applications, the hydrogel should be liquid at room temperature in order to be injectable for example by the syringe nozzle; but with high viscosity at body temperature. This is the case for drug vector delivery or ageless cosmetic injection. Thermo-sensitive hydrogels are used in promising cases (Cha et al., 2012; Hebeish et al., 2014; Hemraz et al., 2014). A large range of thermo-responsive polymers existed (Jeong et al., 2002), the most popular is Poly(N-isopropylacrylamide) also named PNIPAM. This polymer is biocompatible but also presents the particularity of a lower critical system temperature (LCST) about  $\sim 34^\circ\text{C}$ , which is ideal for physiological injectable system. In this study, we have choose to graft CNCs with PNIPAM.

Already several polymer grafting strategies have been reported on CNCs (Carlmark et al., 2012; Eyley and Thielemans, 2014; Habibi, 2014; Tang et al., 2017). Among them, the “grafting from” strategy has been reported in different case and also for stimuli-responsive polymers grafting. For example, Zoppe et al. (Zoppe et al., 2010) synthesized Poly(N-isopropylacrylamide) chains on CNCs via Single Electron Transfer-Living Radical Polymerization (SET-LRP). Hemraz et al. (Hemraz et al., 2014) investigated then recently the rheological impact of the grafting density of the system developed by Zoppe and in particular the thermo-reversibility during temperature ramps. Meanwhile, Zeinali et al. (Zeinali et al., 2014) and Haqani et al. (Haqani et al., 2017) grafted dual pH and thermo-sensitive copolymers of N-isopropylacrylamide and acrylic acid (AA) on CNCs via reversible addition fragmentation chain transfer (RAFT) polymerization. In an interesting work, Grishkewich et al. (Grishkewich et al., 2016) grafted poly(oligo(ethylene glycol)methacrylate) (POEGMA) through free-radical polymerization (FRP). Most of this grafting is successful but presents the drawback of using homopolymers and toxic solvent or reagent. New solutions are then expected. Recently, the “grafting onto” strategy has been reported in literature for attaching stimuli responsive polymers on CNCs surface. In a recent interesting work, Azzam et al. (Azzam et al., 2010, 2016b) grafted Jeffamine polyetheramine on TEMPO CNCs via peptidic coupling and the second study was in aqueous conditions. In these studies, sterically stabilization of CNCs suspension was produced in a large range of organic solvent and a thermo-reversibility was revealed.

Recently we proposed to graft thermo-responsive PNIPAM using the “grafting onto” strategy via peptidic coupling in aqueous condition onto oxidized CNCs (*Chapter II.1*). Promising grafting result were obtained and even optimized through microwave assisted reaction. In the present work, we investigate the rheological behavior of these PNIPAM grafted CNCs obtained via peptidic coupling. In particular, the thermal reversibility and the maximum of the elastic modulus will be tested, in order to develop injectable hydrogel for biomedical applications.

## 2.2. Materials and Methods

### 2.2.1. Materials

Cellulose nanocrystals (CNCs) from wood were purchased from UMaine process Development Center (University of Maine, USA). The colloidal suspension of ~12 wt% was produced using sulfuric acid hydrolysis process and has been never freeze-dried. Poly(N-isopropylacrylamide) with amine terminated were purchased from Sigma-Aldrich (USA) with molecular weight of 2500 g·mol<sup>-1</sup>. The LCST is close to 34°C. For the TEMPO oxidation of CNCs surface, following chemicals were purchased from Sigma-Aldrich: 2,2,6,6-Tetramethyl-1-piperidinyloxy (TEMPO, 2564-83-2), Sodium hypochlorite (NaClO, 12%wt, 7681-52-9) and Sodium bromide (NaBr, 7647-15-6). For the peptidic grafting, chemicals are purchased from Sigma-Aldrich: N-(3-Dimethylaminopropyl)-N'-ethylcarbodiimide hydrochloride (EDC, 25952-53-8) and N-Hydroxysuccinimide (NHS, 6066-82-6). Other chemicals were purchased from Sigma-Aldrich. Distilled water was used for all experiments.

### 2.2.2. Carboxylation of cellulose nanocrystals by TEMPO oxidation

CNCs from commercial suspension were oxidized via TEMPO-mediation using previously reported procedure (Habibi et al., 2006). In brief, 11g of CNCs were dispersed with ultrasonic energy (5 kJ·g<sub>CNC</sub> with 250 Watt sonic probe at 50% of maximum energy during 15 minutes) in 730mL of distilled water. TEMPO (323 mg, 2.07 mmol) and NaBr (3.564 mg, 34.61 mmol) were dissolved in 250mL of deionized water by magnetic stirring and slowly added to the CNCs suspension. Then, the oxidation process starts with the addition dropwise of 66 g (0.12M) of NaClO. The reaction run during 3 h at room temperature, and the pH was maintained between 10 and 10.5 by addition of sodium hydroxide solution (NaOH) at 0.5M. Finally, 40mL of ethanol was added in order to quench the oxidation reaction. Three washing steps by centrifugation (10 000 rpm, 30 min) with hydrochloric acid (HCl) at 0.5M were done in order to remove the highest part of oxidant compounds. This suspension was dialyzed against distilled water at least one week until a neutral pH was obtained (membrane 6-8 kDa). TEMPO CNCs were stored in the fridge at constant neutral pH to allow the CNC to be in their carboxylate form.

### 2.2.3. Polymer grafting by peptidic coupling in aqueous media

The grafted of amide-terminated polymer was achieved through peptidic coupling according to our recent work (*Chapter II.1*). In brief, in a TEMPO CNCs suspension of ~1 wt% at pH 4.5, 2mL of aqueous solution containing N-(3-(dimethylamino)propyl)-N'-ethylcarbodiimide hydrochloride (EDC) was added to the suspension and stirred during 30 min following by the same amount of N-hydroxysuccimide (NHS) stirred during 30 min. The pH was then adjusted to 7.5-8.0 before the addition of 10mL of an aqueous suspension containing Pnipam<sub>2500</sub>-NH<sub>2</sub>. The reaction lasted 48 h at room temperature under stirring and the resulting suspension was dialyzed against distilled water to remove excess reagents including non-grafted PNIPAM<sub>2500</sub> at least one week until neutral pH is obtained. Pnipam<sub>2500</sub> grafted CNCs will be referred to as CNC-g-Pnipam<sub>2500</sub> respectively.

### 2.2.4. Increasing of the CNC-g-Pnipam<sub>2500</sub> suspension concentration

The suspension resulting from the grafting process via peptidic coupling has a concentration of about 1.35 wt%. This concentration was used directly without any modification for small angle neutron scattering and for rheological investigation. Besides, in order to increase the hydrogel properties, this suspension was concentrated at 6.1 wt%. Concentration by evaporation at 40°C of the suspension was achieved on a hot plate under magnetic stirring.

### 2.2.5. Transmission electron microscopy (TEM)

Drops of about 0.001 %wt of CNCs suspension were deposited onto glow-discharged carbon-coated TEM grids. After 2 minutes, the liquid in excess was absorbed with filter paper, and prior to drying, a drop of Urany-Less (Delta Microscopies, France) was deposited on the specimen. Then, after 2 minutes, the solution in excess was adsorbed and the grid was dried under room temperature. The sampling was observed using a Philips CM200 (FEI, USA) operating at 200 kV. This protocol was adapted to account for the LCST of the grafted thermosensitive polymer (~34°C). In a first case, TEM specimens were prepared at room temperature. In a second case, TEM specimens were prepared with CNC-g-Pnipam<sub>2500</sub> suspension and Urany-Less solution both preheated at 50°C.

### 2.2.6. Small angle neutron scattering: Polymer conformation

In order to investigate the polymer conformation on the surface of CNCs after Pnipam<sub>2500</sub> adsorption, small angle neutron scattering (SANS) experiments were performed. The concentrations of the different suspensions measured are 1 wt% for TEMPO CNCs, 0.75 wt% for Pnipam<sub>2500</sub> and 1.35 wt% or 6.1 wt% of CNC-g-Pnipam<sub>2500</sub>. As SANS is sensitive to the isotopic composition, all samples were dialyzed against deuterium oxide (D<sub>2</sub>O) in order to obtain the best contrast possible and to minimize the incoherent scattering due to hydrogen. SANS experiments were carried out using the PA20 spectrometer at Laboratoire Léon Brillouin (CEA, Saclay, France). A large range of scattering vector,  $Q$ , between 0.0024 and 0.44 Å<sup>-1</sup> was probed using three different neutron wavelength/sample-detector distances (5 Å/18 m, 5 Å/8 m, and 5 Å/1.5 m). Samples were studied at 20°C and 40°C, i.e. respectively below and above the polymer LCST. Samples were loaded in quartz cells (Hellma) with a path length equal to 2 mm. The averaged spectra were corrected for solvent (D<sub>2</sub>O), cell, and incoherent scattering (cell with 1 mm of H<sub>2</sub>O) as well as for background noise (Brûlet et al., 2007) and spectra  $I(Q) = f(Q)$  on an absolute scale were obtained. The data were fitted using the SasView® 4.0.1 modeling software.

### 2.2.7. Rheological experiments on thermo-reversible hydrogel

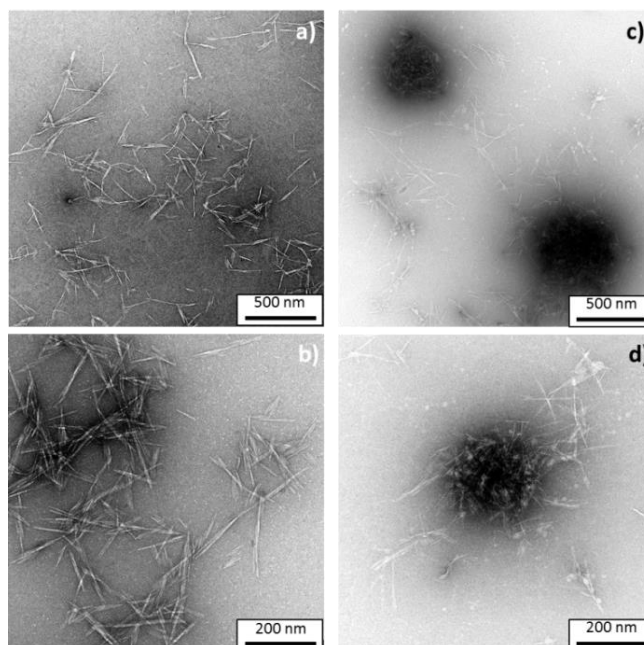
The rheology behaviors of the aqueous suspensions of CNC-g-Pnipam<sub>2500</sub> and CNC-g-Pnipam<sub>5500</sub> under shear were studied using rotational rheometer Physica MCR 301 (Anton-Paar, Austria). To investigate the temperature effect and the reversibility of these systems, tests were carried out under the LCST (20°C) and above the LCST (40°C). Start-up shearing tests were performed with a cone-plate configuration (diameter of 50mm and angle of 1°). The atmosphere around the sample was saturated with water to avoid evaporation during the measurement. To control the initial state of each sample, a constant shear rate was applied at 0.1 s<sup>-1</sup> during 30 seconds, following by 30 seconds without shear rate for stabilization. The transient response under shear was recorded until steady conditions were obtained. Steady shear viscosity versus shear rate curves was generated for each sample from a shear rate of 0.01 to 1000 s<sup>-1</sup>. The time required to attain steady conditions was decreased with increasing shear rate.

Viscoelastic properties of polymer-grafted CNCs suspensions were carried out in the oscillatory mode with a rheometer Physica MCR 301 (Anton-Paar, Austria) with a cone-plate configuration (diameter of 50mm and angle of 1°). Oscillatory measurements were performed to collect transition from liquid to gel of each sample. The strain used was inside the linear viscoelastic region (LVE) as determined by performing strain sweep experiments at a frequency of 1 Hz. Then the optimal frequency was determined by performing oscillation sweep experiments at the previously obtained strain in the LVE. These two values were fixed to achieve the storage modulus ( $G'$ , Pa) and the loss modulus ( $G''$ , Pa) during a slow linear temperature increasing from 25°C to 45°C (temperature ramp 1°C per min). At least duplicate were performed.

## 2.3. Results and discussion

### 2.3.1. Grafted CNCs characterization

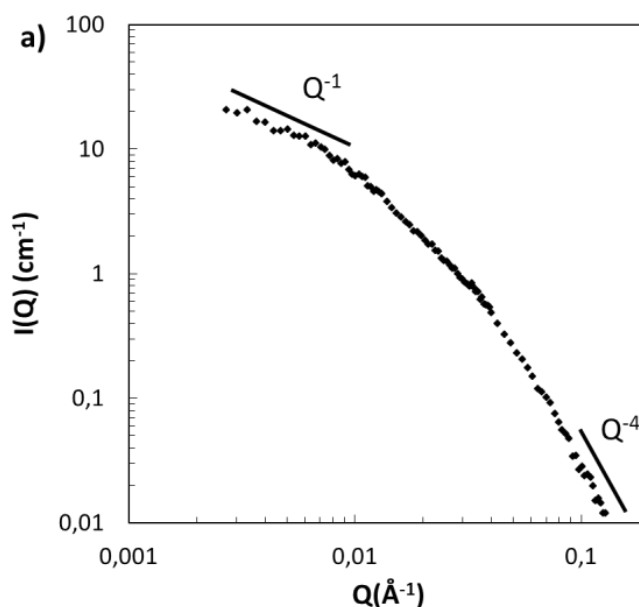
As shown in our previous study (*Chapter II.1*), thermo-responsive Pnipam<sub>2500</sub> can be successfully covalently grafted onto CNCs using the 'grafting onto' strategy, in particular peptidic coupling after TEMPO oxidation. A degree of oxidation of about 0.2 (carboxylic acid present at 20%) and a final degree of polymer substitution of about 0.07 (grafting yield about 30%) are obtained. In spite of low grafting amount, **Figure 1** from our previous work (*Chapter II.1*) presents the TEM images of the system under and above the LCST. It reveals that the system exhibits a thermal sensitivity thanks to the presence of polymer on the surface. Furthermore, the low amount of grafting density suggests that grafted polymer chains are in a mushroom regime without polymer neighbor interaction. Small angle neutron scattering (SANS) were performed in this study in order to investigate and prove this conformation.



**Figure 1:** TEM images of b)-c) CNC-g-Pnipam<sub>2500</sub> deposited on TEM grid at 20°C and c)-d) CNC-g-Pnipam<sub>2500</sub> deposited at 50°C. Pictures are representatives of each sample.

### 2.3.2. SANS measurements on CNC-g-Pnipam<sub>2500</sub>

SANS measurements were performed in this work in order to investigate the structure and organization of PNIPAM<sub>2500</sub> grafted on the surface of CNCs. This technique is well adapted for soft matter. In particular, the neutron wavelength opens access to characteristic size between 1 and 100 nm, which is a well-adapted scale to describe conformation and organization of CNC and CNC-g-Pnipam<sub>2500</sub>. This technique is not destructive and the final result is an average information representative of the macroscopic sample.



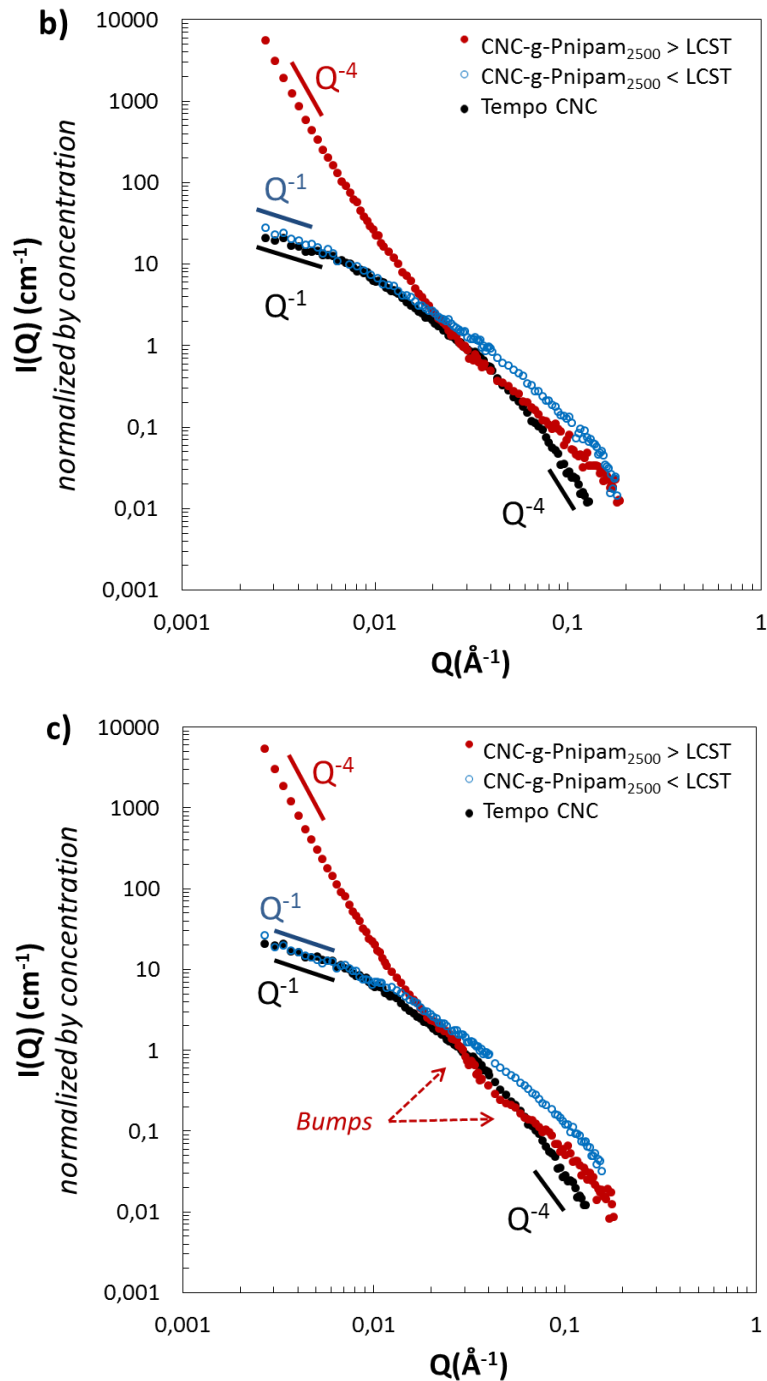


**Figure 2:** a) SANS analysis of TEMPO CNCs at 1 wt%. SANS analysis of CNC-g-Pnipam<sub>2500</sub> presenting on the same graph: TEMPO CNCs, CNC-g-Pnipam<sub>2500</sub> under and above the LCST. CNC-g-Pnipam<sub>2500</sub> is presented at a concentration of b) 1.35 wt% and c) 6.1 wt%.  $I(Q)$  was normalized by the suspension concentration. Slope fitting curves are indicated on each graph.

**Figure 2a** shows the SANS measurements for TEMPO CNCs. In the small values of  $Q$ , the relative intensity decreases with a slope of  $Q^{-1}$ , this is representative of rod-shape particles. At high values of  $Q$ , the slope is  $Q^{-4}$  which qualified a smooth and distinct interface with the solvent. By fitting this curves with SasView, TEMPO CNCs size are  $110 \times 17 \times 4 \text{ nm}^3$ . These

values are close to TEM measurements. Nonetheless, the length of TEMPO CNCs estimated by SANS is not completely exact but only a good approximation. Data in highest  $Q$  vector are required for more precise value. Concerning the Pnipam<sub>2500</sub> under its LCST, the gyration radius is calculated with the equation of Kubota et al. (Kubota et al., 1990), and described as following:  $R_g = \alpha \times M_w^{0.54}$ . Where  $R_g$  is the gyration radius of polymer in nm,  $\alpha$  is a coefficient equal to 0.022 and  $M_w$  is the molecular weight of the polymer in  $\text{g}\cdot\text{mol}^{-1}$ . In the case of PNIPAM<sub>2500</sub>, the gyration radius is 1.5 nm.

**Figure 2b** presents SANS measurements of CNC-g-Pnipam<sub>2500</sub> at 1.35 wt%. In this total amount, the concentration TEMPO CNCs in the suspension is evaluated at 0.35 wt% with 1 wt% of Pnipam<sub>2500</sub>. At this low concentration, diffused intensity can only be attributed to the object form factor in suspension. Under the LCST and compared to the SANS curve of Tempo CNCs, CNC-g-Pnipam<sub>2500</sub> indicate a similar shape and fitting for the lower  $Q$  values ( $< 0.01 \text{ \AA}^{-1}$ ). It suggests that no aggregates are present in the suspension under the LCST (slope in  $Q^{-1}$ ). For the highest  $Q$  values ( $> 0.07 \text{ \AA}^{-1}$ ), the intensity  $I(Q)$  of CNC-g-Pnipam<sub>2500</sub> is superior to the TEMPO CNCs intensity. This increasing value might be due to the presence of polymer on the surface of CNCs which increase the roughness of the surface. The SANS curves were cut at  $0.15 \text{ \AA}^{-1}$  because a too high noise from the presence of H<sub>2</sub>O in suspension, so the polymer configuration on the surface cannot be evaluated. We suspected a slope of  $Q^{-2}$  which is characteristic of random coil (de Gennes, 1980). Above the LCST, in the small values of  $Q$ , the slope of the curve drastically increase to  $Q^{-3}$ . It indicates the presence of aggregates in the suspension, due to the connection of CNC-g-Pnipam<sub>2500</sub> in the suspension. In middle range of  $Q$ , the system intensity fits with the shape of CNCs. In high  $Q$  values ( $> 0.1 \text{ \AA}^{-1}$ ), the slope is close to  $Q^{-3}$  which is representative of polymer collapse globule on the surface of CNCs.

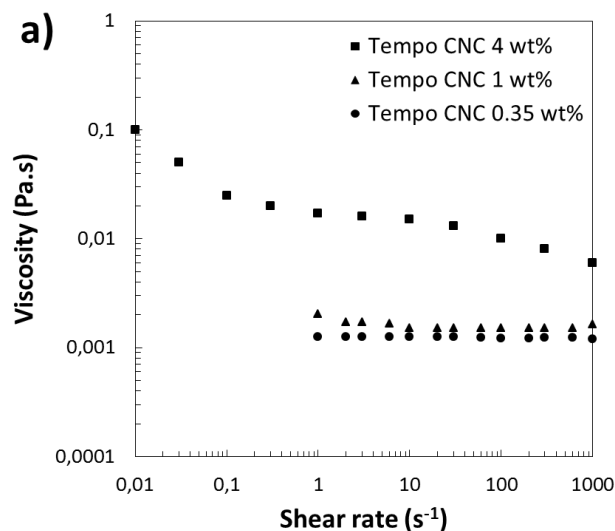
**Figure 2c** presents SANS measurements of CNC-g-Pnipam<sub>2500</sub> at 6.1 wt%. The diffused intensity is always attributed to the form factor of CNCs. Under and above the LCST, similar results than **Figure 2b** are shown. At low  $Q$  values, the Flory index is  $1/3$  (slope  $Q^{-3}$ ) which is characteristic of the polymer in collapse globules conformation (De Gennes, 1979; Flory, 1953). At this concentration, in middle range of  $Q$  values, “bumps” are identified on the graph. They could be attributed to the form factor or structure factor (repeated distance between object due to the concentration). In this case, the CNCs amount in the final

suspension is close to 1.6 wt% (for 4.5 wt% of Pnipam<sub>2500</sub>). So, these “bump” correspond to the form factor of spherical aggregates (a spherical fitting present minima and maxima for  $2\pi$  rotation), which is in concordance with the **Figure 1c-d**.

Up to our knowledge, even if some studies focus on rheology of PNIPAM grafted from the surface of CNCs (Hemraz et al., 2014; Zoppe et al., 2010; Zubik et al., 2017), none of them tried to understand surface conformation by using this neutron scattering characterization. SANS measurements were used to describe and characterize CNCs (Bonini et al., 2002; Cherhal et al., 2015; Mao et al., 2017; Terech et al., 1999). Only study from co-author with Jeffamine provides data on the polymer conformation on the CNCs surface. In their case, aggregates were smaller above the LCST and collapse polymer were easily identified in the high Q values. The polymer thickness was estimated as equal to the gyration radius of Jeffamine (i.e. 1.5 nm).

### 2.3.3. Rheological behavior of oxidized CNC and Pnipam<sub>2500</sub>

In the literature on PNIPAM polymer, the volume transition has been studied for macroscopic gels and also for micro-gels and linear PNIPAM chains where the coil to globule transition is of particular interest (Kubota et al., 1990; Schild, 1992; Senff and Richtering, 1999; Stieger et al., 2004). Nonetheless, up to our knowledge, only few studies discuss on rheological properties of PNIPAM micro-gels (Aubry et al., 2003; Kiminta et al., 1995; Stieger et al., 2004) and none on the rheology of PNIPAM polymer.



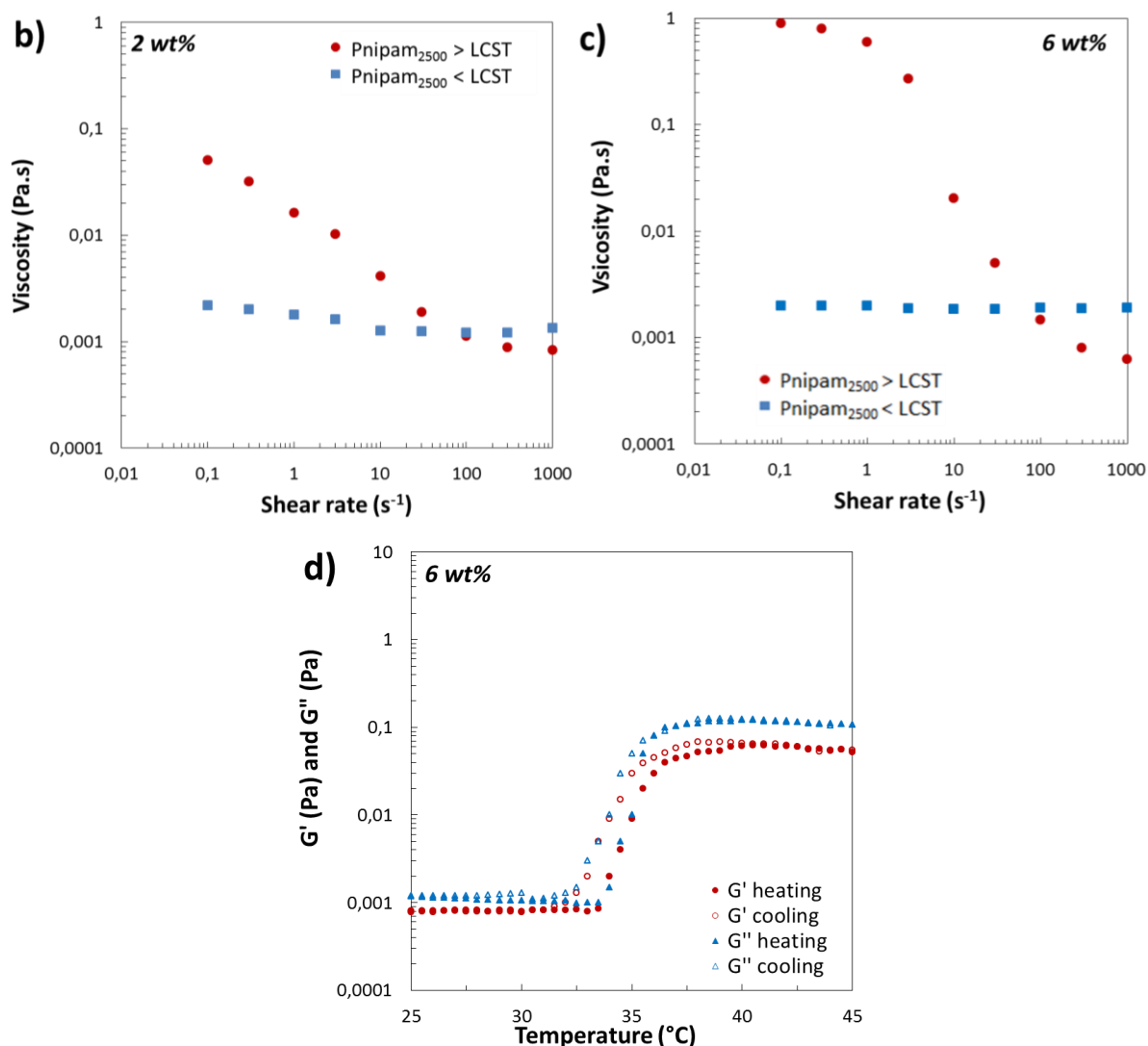


**Figure 3:** Flow curves of a) TEMPO CNCs at 0.35 wt% (circle), 1 wt% (triangle) and 4 wt% (square), Pnipam<sub>2500</sub> at 2 wt% (b) and 6 wt% (c) under (square) and above (circle) the polymer LCST. Viscoelastic properties of Pnipam<sub>2500</sub> at 6 wt% (d), full symbols and empty symbol represent respectively the heating and cooling behavior of  $G'$  and  $G''$  between 25 and 45°C (ramp of 1°C per minutes). Oscillatory measurements were performed at  $\tau_0 = 0.1$  Pa and  $f_0 = 0.1$  Hz.

**Figure 3** presents flow curves and viscoelastic properties of different raw materials used in this study. TEMPO CNCs rheological behavior (**Figure 3a**) is shown at different concentration. The maximum viscosity of CNC at a shear rate of  $0.1 \text{ s}^{-1}$  is never crossing  $0.1 \text{ Pa}\cdot\text{s}$ , and the rheology behavior is near Newtonian at low concentration. At 4 wt%, the flow curves presents the typical rheological behavior of liquid crystalline suspension, namely a three slope behavior characteristic of chiral nematic phase (Shafiei-Sabet et al., 2012; Ureña-Benavides et al., 2011; Wu et al., 2014). This particular behavior is behavior is detailed in *Chapter III.1*. TEMPO CNCs does not present a variation in viscoelastic properties and present a liquid form whatever the temperature is (the loss modulus  $G''$  is always higher than the storage modulus  $G'$ ).

**Figure 3b** presents the rheological behavior of Pnipam<sub>2500</sub> at 2 wt% and at different temperatures (under and above the LCST  $\sim 34^\circ\text{C}$ ). Under the LCST, Pnipam<sub>2500</sub> is close to a Newtonian fluid. Nonetheless, when the temperature increases, the polymer presents a viscosity increasing from 2 to 80 mPa·s at a shear rate of  $0.1 \text{ s}^{-1}$ . This viscosity quickly decreases when the shear rate increases due to a probably destruction of the very weak network. At a concentration of about 6 wt%, Pnipam<sub>2500</sub> presents the same behavior with a maximum in viscosity of 1 Pa·s at a shear rate of  $0.1 \text{ s}^{-1}$  (**Figure 3c**). The weak network resists to the shear rate since  $1 \text{ s}^{-1}$ , then identical destruction than 2 wt% appears. **Figure 3d** shows the viscoelastic properties of Pnipam<sub>2500</sub> at 6 wt%. The concentration of 6 wt% chosen for this figure is representative of the maximum amount of polymer used in this study. Whatever the temperature is, the system is in liquid form ( $G''$  is slightly higher than  $G'$ ). When the LCST is reached, the general values of  $G'$  and  $G''$  increase but the liquid form is conserved. It is probably due to a too low concentration and low DP of Pnipam<sub>2500</sub> which formed a weak network (observed in Figure 3b). The Pnipam<sub>2500</sub> presents a reversible behavior, but with a hysteresis during the cooling temperature probably due to a polymer weak entanglement. Up to our knowledge, the rheological behavior of oligomer of Pnipam<sub>2500</sub> was never reported in literature.

#### 2.3.4. Rheological behavior and viscoelastic properties of CNC-g-Pnipam<sub>2500</sub>

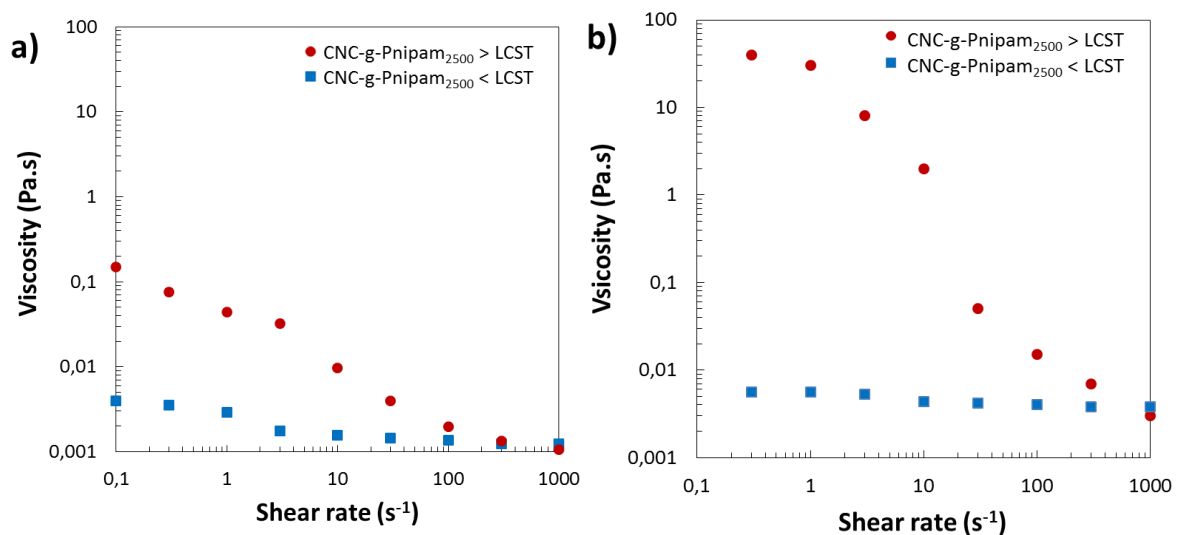


**Figure 4:** Flow curves presenting the rheological behavior under (square) and above (circle) the LCST of the Pnipam<sub>2500</sub> for a) CNC-g-Pnipam<sub>2500</sub> at 1.35 wt% and b) CNC-g-Pnipam<sub>2500</sub> at 6.1 wt%.

At the end of the grafting process, CNC-g-Pnipam<sub>2500</sub> suspension has a total concentration of about  $1.35 \pm 0.02$  wt%. It corresponds to approximately 0.35 wt% of CNCs for 1 wt% of Pnipam<sub>2500</sub>. **Figure 4a** presents the rheological behavior of this suspension. Under the LCST, the grafted system behaves as a shear thinning fluid: viscosity slightly decreases when the shear rate increases. By crossing with the results of **Figure 3a b**, the grafting system exhibits a viscosity a little bit higher than each system alone. A small synergic effect is then revealed. By applying a temperature superior to the LCST ( $\sim 34^\circ\text{C}$ ), the suspension still behaves as a shear thinning fluid with a level of viscosity higher than the level reaches under the LCST. The CNC-g-Pnipam<sub>2500</sub> exhibits a shear thinning behavior similar to the normal behavior of a CNCs suspension (Shafiei-Sabet et al., 2012; Ureña-Benavides et al., 2011). Besides, comparing with **Figure 3a-b**, a small synergic effect is then revealed.

Nevertheless, with 0.35 wt% of CNCs in the suspension after grafting, the network and entanglement is too low to reveal a thermo-sensitive hydrogel. Thereby, the concentration of the suspension was increased to 6.1 wt% by evaporation. **Figure 4b** presents the rheological behavior of the 6.1 wt% CNC-g-Pnipam<sub>2500</sub> suspension. It corresponds to approximately 1.6 wt% of TEMPO CNCs with 4.5 wt% of Pnipam<sub>2500</sub>. Under the LCST of the system, the viscosity is constant at 0.005 Pa·s along all the range of shear rate. On **Figure 3a** and **3 c**, both systems present a viscosity at 0.0022 Pa·s. A slight synergetic effect exists after grafting of TEMPO CNCs and Pnipam<sub>2500</sub>. This result is intensifying above the LCST. At a shear rate of  $0.1 \text{ s}^{-1}$ , TEMPO CNCs and Pnipam<sub>2500</sub> exhibit a viscosity of 0.001 and 1 Pa·s, respectively. On the grafted system, the viscosity increases up to 40 Pa·s which reveals a clear synergic effect due to the peptidic grafting of Pnipam<sub>2500</sub> on the CNCs surface. The maximum viscosity Pnipam<sub>2500</sub> at 6 wt% (**Figure 3c**) never increased up to 1 Pa·s. On the flow curve of CNC-g-Pnipam<sub>2500</sub> after the LCST (**Figure 4b**), a first behavior is observed until a shear rate of  $10 \text{ s}^{-1}$  is reached. It corresponds to the polymer and CNCs entanglement network. When the shear rate reaches  $10 \text{ s}^{-1}$ , the system viscosity decreases drastically under 0.1 Pa·s. The deformation is too strong to allow the grafted system to maintain its network structure. To complete this proof of the realization of a thermo-sensitive hydrogel, viscoelastic behavior was investigated in order to prove the thermal reversibility (**Figure 5**). PNIPAM is known to have a reversible phase transition (Kubota et al., 1990; Schild, 1992), we are expecting a similar thermo-reversibility of the grafted suspension.

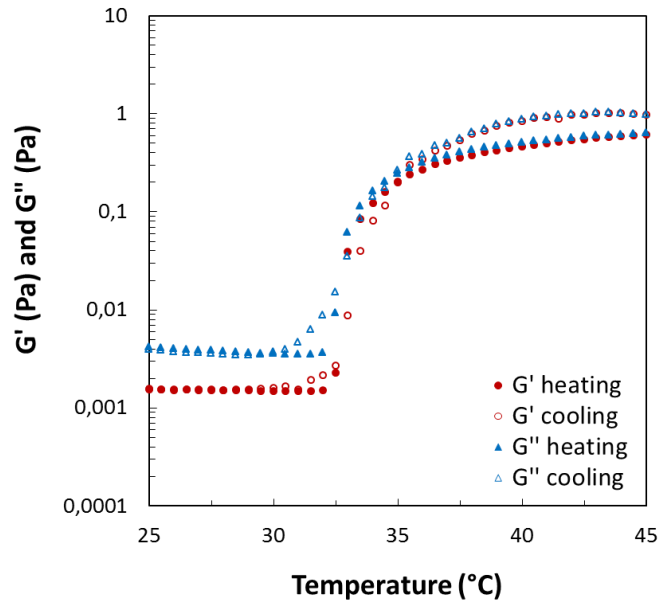


**Figure 5:** Viscoelastic behavior of CNC-g-Pnipam2500 at 6.1 wt%. Oscillatory measurement were performed at  $\tau_0 = 0.1$  Pa and  $f_0 = 0.2$  Hz.

The thermo-responsivity of stable CNC-g-Pnipam<sub>2500</sub> suspension was investigated by measuring the viscoelastic properties: dynamic storage modulus  $G'$  and dynamic loss modulus  $G''$  in heating and cooling cycle in the range of 25 to 45°C (**Figure 5**). At a temperature under 34°C, the polymer Pnipam<sub>2500</sub> chains are extended in the solvent due to their hydrophilic nature. The system is stable in suspension due to the colloidal stability of CNCs and the steric repulsion of the polymer brushes.  $G'$  is inferior to  $G''$  which is characteristic to a system in liquid form. When the temperature reached 34°C, both  $G'$  and  $G''$  values drastically increase. The transition temperature of the system is close to 34°C which is a little bit higher than the LCST of the free polymer Pnipam<sub>2500</sub> (34°C) (Suzuki et al., 2010). The polymer chains collapse on the CNCs surface and form a thin hydrophobic layer. The grafted system changes from a liquid to a gel form ( $G' > G''$ ). Contrary to grafting from strategy investigated in some works with final  $G'$  superior to 10 Pa (Hemraz et al., 2014; Zoppe et al., 2010), the low molecular weight of Pnipam<sub>2500</sub> allows the system to keep a colloidal stability above the LCST. As presented in our recent work (*Chapter II.1*) and in **Figure 1**, the system presents collapse aggregates of CNC-g-Pnipam<sub>2500</sub> which creates a network in the suspension. Upon cooling, CNC-g-Pnipam<sub>2500</sub> network exhibits a return to initial state without a clear presence of hysteresis. This is an interesting property of grafted polymer on CNCs surface via a green grafting process. These thermal cycles have been reproduced several times on the same sample and they are fully reversible.

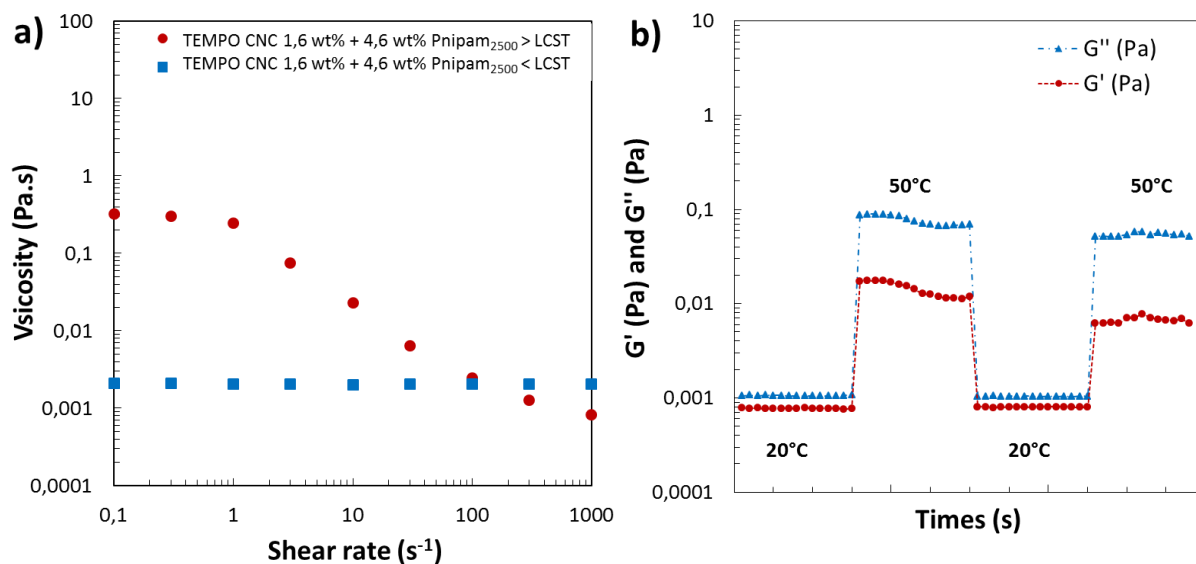


**Figure 6:** Pnipam<sub>2500</sub> at 4.6 wt% mixed with 1.6 wt% of TEMPO CNCs: a) Flow curves presenting the rheological behavior under (blue square) and above (red circle) the LCST and (b) Viscoelastic behavior with oscillatory measurement were performed at  $\tau_0 = 0.1$  Pa and  $f_0 = 0.1$  Hz.

As described in *Chapter II.1*, elemental analysis or FTIR are not enough to prove the grafting efficiency due to the large presence of amine in the PNIPAM polymer. **Figure 6** shows an indirect proof of the grafting efficiency via flow curve and viscoelastic measurements. In this figure, TEMPO CNCs at 1.6 wt% and Pnipam<sub>2500</sub> at 4.5 wt% have been mixed together without coupling agent (EDC and NHS) in respect with the ratio CNCs/PNIPAM obtained during the grafting process. By comparing the **Figure 4b** and **Figure 6a**, under LCST both systems are liquid and reveal a similar flow curve. Nonetheless, at a shear rate of  $0.1 \text{ s}^{-1}$  and above the LCST, the viscosity of the grafted system is two decades higher than the adsorbed system, respectively 40 and  $0.3 \text{ Pa}\cdot\text{s}$ . On **Figure 6b**, under and above the LCST, the system shows a liquid behavior ( $G'' > G'$ ) with loss and elastic modulus 50 times smaller than the grafted system (**Figure 5**).

Whatever the system is grafted or mixed, the hydrogel presents a thermo-sensitivity with a clear increase of the viscosity when the LCST is reached. However, a real differentiation is highlighted between grafted and adsorbed Pnipam<sub>2500</sub> on TEMPO CNCs at same concentration. Both systems are different which argue on the grafting efficiency in *Chapter II.1*.

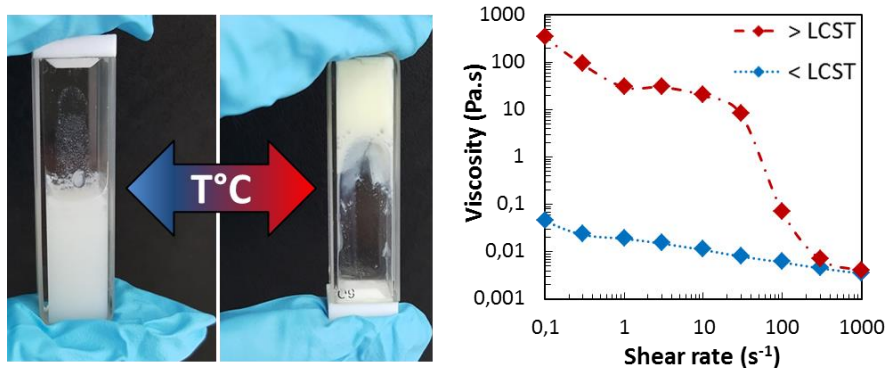
## 2.4. Conclusions

Thermo-reversible Pnipam2500 were successfully grafted on TEMPO CNCs via a green peptidic grafting as verified in our recent work (*Chapter II.1*). Small angle neutron scattering measurements were performed in order to detail the core shell configuration of polymer around the CNCs at different temperature. Pnipam<sub>2500</sub> polymer seems to be in random coil conformation on the CNCs surface under the LCST. Above this critical temperature, the system collapse and aggregates are created. By investigating the rheological behavior of the grafted system, we clearly identified a synergetic effect and a stable colloidal behavior whatever the concentration is. In particular, CNC-g-Pnipam<sub>2500</sub> presents a liquid to hydrogel reversible behavior when concentration is close to 6%, tunable by external temperature stimuli. At high concentration, the thermo-reversible gelation of the CNCs grafted suspension was attributed to the formation and rupture of connections between aggregates forming above the polymer LCST. The realization of a green, sustainable and thermo-sensitive hydrogel based on CNCs paves the way to several applications such as smart biomedical injectable system.



### 3. PDMAEMA-g-PDEGMA Polymer adsorption on carboxylated cellulose nanocrystals and corresponding thermo-sensitive hydrogel.

*This section is adapted from "Erwan GICQUEL, Céline MARTIN, Quentin GAUTHIER, Joakim ENGSTRÖM, Clara ABBATTISTA, Anna CARLMARK, Emily D. CRANSTON, Bruno JEAN, Julien BRAS - PDMAEMA-g-PDEGMA Polymer adsorption on carboxylated cellulose nanocrystals and corresponding thermo-sensitive hydrogel. Submitted in Biomacromolecules, 2017"*



#### ABSTRACT

This study investigates the adsorption on oxidized cellulose nanocrystals (TEMPO CNCs) of a block copolymers composed with a thermo-responsive block based on poly(di(ethylene glycol) methyl ether methacrylate) (PDEGMA) and a quaternized poly(2-(dimethylamino)ethylmethacrylate) (PDMAEMA) polyelectrolyte block. PDMAEMA-*b*-PDEGMA presents a lower critical solution temperature (LCST) between 26 and 28°C and was synthesized by Atom transfer radical polymerization (ATRP). The extent and dynamics of quaternized PDMAEMA-*b*-POEGMA adsorption on nanocrystals has been determined by using electromechanical and optical techniques, named respectively, quartz crystal microbalance (QCM-d) and surface Plasmon resonance (SPR). A clear ionic adsorption is identified on TEMPO CNCs (COO<sup>-</sup>) with the quaternized PDMAEMA. Small angle neutron scattering (SANS) experiments have been also performed to investigate the polymer conformation onto TEMPO CNCs surface and the core-shell behavior around nanocrystals. Besides, gyration radiuses of different systems have been characterized up to the Guinier plateau extended to very small scattering vector  $Q$ . The reversible liquid to gel transition with temperature change is clearly observed with rheological measurements. Outstanding

properties are obtained for best ratio as shown by an increase of 4 decades in viscosity at low shear. These stimuli functionalities on bio-based hydrogel pave the way to the design of smart CNCs-based materials for application in injectable biomedical system

**Keywords:** Cellulose nanocrystals, PDMAEMA-b-PDEGMA, small angle neutron scattering, rheology, hydrogel, thermo-responsive, stimuli-responsive, QCM-d, MP-SPR

### 3.1. Introduction

From the last 20 years, laboratory and industrial research focuses its interest into the design of new bio-based advanced materials. To follow these specifications a new range of materials is used: the nanocellulose. Cellulose is one of the most abundant polymers in nature. This nanoscale material presents very interesting properties like biodegradability, combined with good mechanical properties or gel like suspension. Owing to their specific physical properties and high aspect ratio, Cellulose Nanocrystals (CNCs) obtained by cellulose hydrolysis are used in several applications like environmentally friendly nanocomposites (Dufresne, 2013; Eichhorn et al., 2010; Oksman et al., 2014; Siqueira et al., 2010c), biomedical applications (Camarero Espinosa et al., 2016; Domingues et al., 2014; Endes et al., 2016; Jorfi and Foster, 2015; Klemm et al., 2011; Lin and Dufresne, 2014; Naseri et al., 2016), coatings & printing electronics (Gicquel et al., 2017; Hoeng et al., 2016; Li et al., 2013) or hydrogels & aerogel (De France et al., 2016, 2017; Eichhorn et al., 2010). Complementary, responsive polymers raise awareness on their ability to present changes triggered by external stimuli (pH, temperature, light, redox-activity,...) (Azzam et al., 2016b; Schattling et al., 2014; Way et al., 2012; Wu et al., 2015). Addition on the surface of a stimuli-responsive functionality can be used to control the release of chemicals from the surface or the interactions with other compounds (Tripathy et al., 2002). This ability is interesting for biomedical applications, responsive surfaces or sensors.

CNCs surface modification with thermo-sensitive polymer can enhance significantly the potential application of CNC systems (Abitbol et al., 2016; Eyley and Thielemans, 2014; J. Eichhorn, 2011; Tang et al., 2017). Several chemical modification approaches have previously been presented: covalent and non-covalent (Habibi, 2014). For the covalent modification, new properties can be implemented to CNCs by modifying the numerous hydroxyl group at their surface. "Grafting onto" and "grafting from" strategies are both

investigated in literature to modified cellulose with sensitive polymer chains (Azzam et al., 2010; Espino-Pérez et al., 2014; Hakalahti et al., 2016; Krouit et al., 2008; Vuoriluoto et al., 2015; Wu et al., 2015; Yang et al., 2013a; Zoppe et al., 2010). Most of them use complex strategy or toxic compounds which strongly limit upscaling and obviously their use in biomedical. The non-covalent approach is based on the adsorption by ionic, non-ionic or electrostatic interaction of ions, molecules or polymers on the cellulose surface. Rare studies investigate the adsorption of sensitive polymer or monomer on CNC/CNF (Chang and Zhang, 2011; Utsel et al., 2010). In some cases, block copolymers have been synthesized with one block realized with polyelectrolyte polymer and the other with a thermo-sensitive polymer. The polyelectrolyte block will be adsorbed to opposite charge surfaces and the responsive properties of the thermo-responsive block will bound to the surface (Ingverud et al., 2016; Larsson et al., 2013; Masci et al., 2012; Vuoriluoto et al., 2015). In the recent study of Larsson et al. (Larsson et al., 2013), three block copolymers, containing a thermo-responsive block based on poly(di(ethylene glycol) methyl ether methacrylate) (PDEGMA with a lower critical solution temperature (LCST) tuned between 26 and 28°C) and a quaternized poly(2-(dimethylamino)ethylmethacrylate) (PDMAEMA) polyelectrolyte block, were synthesized by ATRP and then adsorbed on cellulose nano-fibrils in water suspension. Adsorption at room temperature was investigated by dynamic light scattering (DLS) and quartz crystal microbalance with dissipation monitoring (QCM-d) but no study on rheology of such suspensions have been investigated.

The rheological behavior of aqueous CNCs suspension has been studied in details during the past 10 years (Bercea and Navard, 2000; Liu et al., 2011a, 2011b; Lu et al., 2014; Shafiei-Sabet et al., 2012, 2014; Ureña-Benavides et al., 2011; Xu et al., 2017a, 2017b). The shear flow, applied to the suspension of nanocrystals, modifies the microstructure and the orientation of the rods like particles. Above a critical mass concentration, the CNC suspensions are shear-thinning: when the shear rate increases, the viscosity decreases. Some studies give an explanation on what is happening on the microstructure of CNCs (Bercea and Navard, 2000; Shafiei-Sabet et al., 2012).

The expected rheological behavior for system with CNCs and thermo-reversible polymer is a reversible liquid form below the LCST (with a Newtonian behavior) to a hard hydrogel above the LCST (with a viscosity higher than 100 Pa·s at  $1\text{ s}^{-1}$ ). This reversible behavior is

investigated in recent scientific publications for release of drugs (Sanna et al., 2013), stabilization of emulsion (Zoppe et al., 2012), gel entanglement structure (Zhou et al., 2011) or bio-reversible hydrogel (Azzam et al., 2016b; Hemraz et al., 2014).

In this study, a block copolymer composed with a PDEGMA based thermo-responsive block and PDMAEMA polyelectrolyte block was synthesized. Then this diblock was adsorbed by anionic/cationic interaction on TEMPO CNCs in water suspension (schematic on **Figure 1**). The final system is a thermo-responsive bio-based materials without any chemical grafting performed on the CNC surface and prepared in aqueous condition. Small angle neutron scattering (SANS) experiments were performed to understand the diblock polymer behavior in suspension and on the surface of CNCs (mushroom conformation, collapsed chain,...). This technique is a non-destructive one and gives access to the nanoparticles shape, the gyration radius and the specific surface area. Finally, the rheological behavior of the bio-based system was carried out to reveal the gel reversibility tuned by the external temperature.

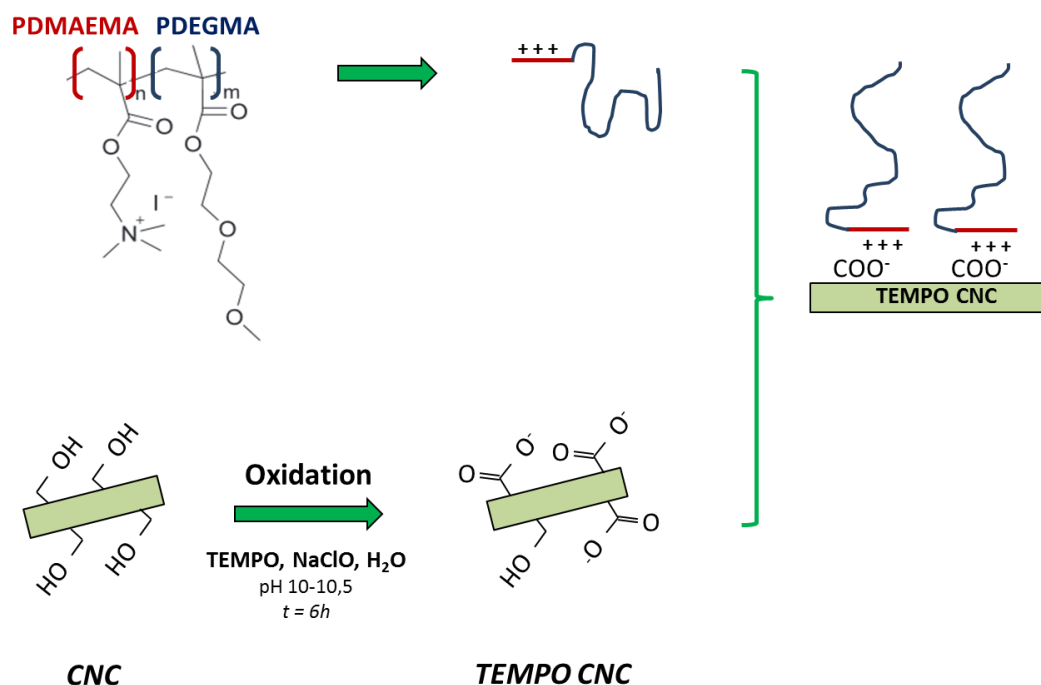


**Figure 1:** General schematic of diblock adsorption on oxidized cellulose nanocrystals

## 3.2. Materials and Methods

### 3.2.1. Materials

Colloidal suspension of ~12%wt commercial cellulose nanocrystal (CNCs) was purchased from UMaine Development Center (University of Maine, USA). They have been produced from wood pulp using sulfuric acid hydrolysis process and have been never freeze-dried. The dry matter was measured using a moisture analyzer (Ohaus® MB-35, Sigma-Aldrich, USA). For the TEMPO oxidation, following chemicals are purchased from Sigma-Aldrich: 2,2,6,6-Tetramethyl-1-piperidinyloxy (TEMPO, 2564-83-2), sodium hypochlorite (NaClO, 12%wt, 7681-52-9) and sodium bromide (NaBr, 7647-15-6). Other chemicals were purchased from Sigma-Aldrich. Ethyl  $\alpha$ -bromoisobutyrate (EBiB) (98%), 1,1,4,7,10, 10-hexamethyltriethylenetetramine (HMTETA) (97%), copper(I)chloride (99%), copper(II)chloride (97%) were purchased from Sigma–Aldrich. Iodomethane (P99%) was purchased from Riedel-de Haën. 2-(Dimethylamino)ethyl methacrylate (DMAEMA) (98%, Aldrich) and Di(ethylene glycol)methyl ether methacrylate (DEGMA) (95%, Aldrich) was activated by passing through a column with basic and neutral aluminum oxide, respectively. Diethyl ether (P99.8%), acetone (100%), dichloromethane (DCM) (P99.8%), Tetrahydrofuran (THF) (99.7%) and n-heptane (99.8%) were purchased from VWR. Distilled water was used for all experiments.

### 3.2.2. Carboxylation of cellulose nanocrystals by TEMPO oxidation

CNCs were subjected to TEMPO oxidation using a previously reported procedure (Habibi et al., 2006). 11 g of CNCs were dispersed in 730mL of distilled water. Then, this suspension was exposed to an ultrasonic dispersive energy of 5 kJ per gram of dry CNCs using a 250 Watt sonication probe (Sonifier S-250A, Branson, USA) at 50% of maximum energy. TEMPO (323 mg, 2.07 mmol) and NaBr (3.564 mg, 34.61 mmol) were dissolved in 250mL of deionized water by magnetic stirring and slowly added to the CNCs suspension. Then, 66 g (0.12M) of NaClO suspension was added dropwise to the suspension to start the oxidation. The mixture was stirring for 3 h at room temperature. The pH condition of the suspension was maintained between 10 and 10.5 by addition of sodium hydroxide solution (NaOH) at 0.5M during the reaction. Reaction was then quenched by the addition of ethanol (40 ml) and the suspension color turned from yellow to white. The resulting CNCs were washed with

hydrochloric acid (HCl) at 0.5M, to decrease the pH to 1-2, at least three times by centrifugation (10 000 rpm, 30 min). After the last centrifugation, oxidized CNCs were dispersed again in distilled water using the minimum volume to recover all CNCs. This suspension was dialyzed against distilled water at least one week until a neutral pH was obtained (membrane 6-8 kDa). TEMPO CNCs were stored in the fridge at constant neutral pH to allow CNCs to be in their carboxylate form.

### 3.2.3. Synthesis of PDMAEMA-b-PDEGMA block copolymer with ATRP

Following previously reported method (Larsson et al., 2013) for synthesizing PDMAEMA macro initiator and chain extension with PDEGMA using EBiB as ATRP initiator together with HMTETA and Cu(I)Cl (Initiator:Ligand:Halide in a 1:2:1 ratio). Synthesis of macro initiator PDMAEMA was performed in a 100 mL round bottom flask, by first introducing of acetone (45 g, target 50wt% to monomer), HMTETA (2.08 mL, 7.63 mmol) and EBiB (560.1  $\mu$ L, 3.82 mmol) under magnetic stirring. The flask was put in an ice bath and DMAEMA (45 g, 286.24 mmol) was added, followed by sealing with rubber septum, vacuum for 5 min and argon filling for 5 min. Before activation of the reaction, Cu(I)Cl (37.8 mg, 3.81 mmol) was added under argon flow to the flask followed by two more vacuum/argon cycles and then immersed in pre-heated oil bath at 50 °C. The reaction was left for around 1 hour if none or low inhibition, targeting 30% conversion, as measured by  $^1\text{H-NMR}$ . The reaction was quenched by addition of 150 mg Cu(II)Cl followed by a cycle of vacuum and argon to ensure living end-groups. The reaction mixture was passed through a column of neutral aluminum oxide to remove all the copper compounds, followed by two precipitations in cold heptane. The final polymer was left to dry under vacuum over a night and analyzed by  $^1\text{H-NMR}$  and DMF-SEC. Chain extension was done according to previous method(Larsson et al., 2013), targeting a monomer conversion of DEGMA around 25% and achieve DP 400 of PDEGMA block. Typical experiment was done by adding PDMAEMA macroinitiator (840 mg, 0.134 mmol) in a 50 mL round bottom flask followed by addition of acetone (40.35 g, target 50wt% to monomer DEGMA). Flask was then immersed in ice bath. Addition of HMTETA (72.87  $\mu$ L, 0.268 mmol) and DEGMA (40.35 g, 214.4 mmol for reaction DP 1600) was done under argon flow and followed by sealing with rubber septum and a vacuum/argon cycle. Exactly like the synthesis of macroinitiator the chain extension was activated by addition of Cu(I)Cl (13.26 mg, 0.134 mmol) and ran at 50°C in oil bath after two vacuum/argon cycles. The resulting

polymer was terminated by letting in air, and purified by two precipitations in cold heptane. The final block copolymer was analyzed with  $^1\text{H-NMR}$  and DMF-SEC. Typical experiment for quarternisation of the block copolymer PDMAEMA-*b*-PDEGMA was performed in a beaker following previous method (Larsson et al., 2013). The use of iodomethane gives a three times excess stoichiometric amount to DMAEMA units (ca DP25). Iodomethane were pre-dissolved in 15 mL THF and added dropwise to a beaker with PDMAEMA-*b*-PDEGMA (2 g) in THF (25 mL) and left over night to react under vigorous stirring and precipitated in cold heptane, then redissolved in water and precipitated in cold acetone, followed by final isolation via freeze-drying.

#### 3.2.4. Analysis of PDMAEMA-*b*-PDEGMA block copolymer

$^1\text{H-NMR}$  spectra were recorded at room temperature with the aid of a Bruker Avance 400 MHz spectrometer, using  $\text{CDCl}_3$  and  $\text{D}_2\text{O}$  as solvents.  $^1\text{H-NMR}$  was used to analyze both polymerization kinetics and conversion of monomer to polymer and to estimate degree of quarternisation of DMAEMA units in the block copolymer. Size exclusion chromatography (SEC) was performed, using dimethylformamide (DMF) ( $0.2 \text{ ml min}^{-1}$ ) as the mobile phase at  $50^\circ\text{C}$ , using a TOSOH EcoSEC HLC-8320GPC system equipped with an EcoSEC RI detector and three columns (PSS PFG 5  $\mu\text{m}$ ; Microguard,  $100 \text{ \AA}$ , and  $300 \text{ \AA}$ ) (MW resolving range: 300–100,000 Da) from PSS GmbH. Molecular weight ( $M_n$  and  $M_w$ ) and  $\bar{D}_N$  were calculated using a conventional calibration method with linear poly(methyl methacrylate) (PMMA) standards. Corrections for flow rate fluctuations were made using toluene as an internal standard. PSS WinGPC Unity software version 7.2 was used to process data.

Polyelectrolyte titration (PET) was used to measure the charge density of the block copolymers, using a 716 DMS Titrino from Metrohm (Switzerland). Potassium polyvinyl sulfate (KPVS) was used as the titrant, and orthotoluidine blue (OTB) was used as the indicator. The color change was recorded with a fotoelektrischer Messkopf 2000 from BASF and the amount of KPVS needed to reach the equilibrium point was calculated according to the method developed by Horn (Horn, 1978).

#### 3.2.5. PDMAEMA-*b*-PDEGMA adsorption on TEMPO CNCs

The adsorption of PDMAEMA-*b*-PDEGMA block on TEMPO CNCs was performed at  $15^\circ\text{C}$ , a temperature inferior to the lower critical solution temperature (LCST) of the diblock:  $24^\circ\text{C}$ .

Freeze-dried diblock was directly added to the suspension of nanocellulose at different weight percent, and dispersed by magnetic stirring during four hours. To obtain a polymer in mushroom state on the surface of CNCs, the distance between two polymers needs to be superior to two times the gyration radius. A square with side equal to two times the gyration radius represents the surface occupied by a polymer. Then the available surface of CNC is divided by this square, and the theoretical maximum diblock per CNC is presented in

**Equation 1:**

$$(1) \quad N_{max} = \frac{2ab + 2ac}{4R_g^2}$$

Where  $N_{max}$  is the maximum amount of diblock on CNCs,  $a, b$  and  $c$  are the length, thickness and height of CNCs in nm ( $150 \times 10 \times 10 \text{ nm}^3$  referred to AFM measurement) and  $R_g$  the gyration radius in nm.

### 3.2.6. Adsorption experiments using QCM-d

Cellulose model surfaces were prepared on quartz crystals microbalance with dissipation (QCM-d) crystals coated with Gold (QX 301), supplied by Biolin Scientific AB (Sweden). QCM-d sensors were washed using piranha cleaning (Hydrogen peroxide  $\text{H}_2\text{O}_2$  mix with sulfuric acid  $\text{H}_2\text{SO}_4$ , ratio 1:3) during 20 minutes, then rinsed with deionized water and dried with  $\text{N}_2$ . Next, sensor was spin-coated with a suspension of Polyethylenimine at 0.1 mM (PEI, Sigma-Aldrich), at 4000 rpm for 30 seconds using a spin coater (SPIN150i Tabletop, spin coating POLOS, The Netherlands) and rinsed with deionized water to remove unbounding polymer from the surface. Finally, colloidal suspension of TEMPO CNCs (1 %wt) were spin-coated and rinsed using the same protocol. The films were heat-treated at  $80^\circ\text{C}$  over night to ensure stability in aqueous media. The total covering of the spin coating was verified by atomic force measurements (AFM).

The interactions between nanocellulose and diblock, via the adsorbed amount, were measured using a quartz crystal microbalance with dissipation (QCM-d, E1 model, Biolin Scientific Holding AB, Gothenburg, Sweden). Crystals coated with CNCs were mounted in the QCM-d chamber and exposed to a flow of MilliQ water to create a stable baseline before diblock injection (two hours). All experiments were conducted at constant temperature of  $18^\circ\text{C}$ . Then the diblock was injected with a rate flow of 17 mL/h and a concentration of 1 mM. After reaching plateau region, a rinsing step with a flow of MilliQ water was applied.

The principles of the technique have been described by Rodahl et al. (Rodahl et al., 1995). The change in resonance frequency is related to the mass added to the crystal, and thus adsorption or desorption of material induces a frequency shift. QTools software (version 3.0.15, Biolin) was used for data analysis of frequency and dissipation data (overtones 1, 3, 5, 7, 9, 11 and 13). The estimated adsorbed polymer amount ( $\Delta m$ ) was calculating using the Sauerbrey equation (**Equation 2**) (Sauerbrey, 1959) with assumption that the created film is rigid. Calculation is valid if the dissipation change is inferior to 10 times the frequency change,  $\Delta f$ ) (Irwin et al., 2005; Voinova et al., 1999), uniform on the crystal and mass is small compared to the mass of the crystal (Vuoriluoto et al., 2015). Besides, studies have shown that there is only a small difference between Sauerbrey and more advanced viscoelastic models like Voigt (Aulin et al., 2008; Karabulut et al., 2012; Krivosheeva et al., 2013).

$$(2) \quad \Delta m = -C \frac{\Delta F}{n}$$

$C$  is a constant related to the density and thickness of the quartz crystals with a value of  $17.7 \text{ ng}\cdot\text{cm}^{-2}\cdot\text{Hz}^{-1}$  for 5 MHz crystal (provided by the manufacturer),  $\Delta F$  is the change in frequency and  $n$  is the overtone number. In this study the third overtone was used for the calculation of  $\Delta m$ . Q-tools frequency values are normalized, so  $n=1$  is utilized.

### 3.2.7. Adsorption experiments using the multi-parametric surface plasmon resonance spectroscopy (MP-SPR)

Cellulose model surfaces were prepared on MP-SPR gold crystals coated with  $\text{SiO}_2$  (SPR102- $\text{SiO}_2$ ), supplied by BioNavis (Finland). MP-SPR sensors were washed using piranha cleaning (**Caution:** hydrogen peroxide  $\text{H}_2\text{O}_2$  mix with sulfuric acid  $\text{H}_2\text{SO}_4$ , ratio 1:3) during 20 minutes, then rinsed with deionized water and dried with  $\text{N}_2$ . Next, sensor was spin-coated with a suspension of TEMPO CNCs at 2 wt% at 4000 rpm for 30 seconds with an increasing ramp of 7 seconds (SPIN150i Tabletop, spin coating POLOS, The Netherlands). Films were heat-treated at  $80^\circ\text{C}$  over night to ensure CNCs films linkage on the surface. Sensors are then rinsed with deionized water to remove unbounding CNCs from the surface and heat-treated at  $80^\circ\text{C}$  for 2 hours. The full cover of sensors was verified by AFM.

Diblock adsorption on TEMPO CNCs was monitored in real time with a MP-SPR (Navi 200, BioNavis, Ylöjärvi, Finland) and “full angular scan” curves ( $40\text{-}77^\circ$ ) were collected. Detailed

information about the optical and flow systems are presented in the work of Liang et al. (Liang et al., 2010). The SPR concept is highly sensitive to changes in refractive index near the sensor surface and is described as followed. A laser is reflected on the surface of the sensor at a specific angle of incidence. Through the analyzed solution and solid layer interface, surface plasmon are excited which leads to a sharp dip in the reflected laser intensity (named the SPR peak). When something is adsorbed on the sensor, changes occur in the reflected light energy and angles of maximum reflection intensity (Schasfoort and Tudos, 2008). In the system used in this work, laser wavelengths of 785 and 670 nm with a spot size of 500x500  $\mu\text{m}$  were simultaneously used. Cellulosic films were swollen under constant MilliQ water flow of 100  $\mu\text{L}\cdot\text{min}^{-1}$  at 18°C during 1 hour for equilibration (more details in the work of Reid et al. (Reid et al., 2016)). Thanks to results at these two wavelengths, data can be fitting by the Fresnel equations using the software *Winspall 3.01* (Max-Planck Institute for Polymer Research, Mainz, Germany) (Bensselfelt et al., 2016; Reid et al., 2016).

Nevertheless, in the present work, the polymer adsorption is so intense inducing a SPR peak for 670 nm out of instrument scope. Experiments were then focused on the 785 nm wavelength, with different polymer concentrations from 0.005 to 0.2 wt%. **Equation 3**, was used to determine the thickness of the adsorbed layer in nanometer (Jung et al., 1998).

$$(3) \quad d = \frac{l_d}{2} \times \frac{\Delta SPR_{angle}}{m(n_a - n_0)}$$

Where  $\Delta SPR_{angle}$  is the SPR angle change during adsorption,  $l_d$  the characteristic evanescent electromagnetic field decay length, estimated as 0.37 of the light wavelength (240 nm),  $m$  is sensor sensitivity factor (109.94°),  $n_0$  and  $n_a$  are the refractive index of the bulk solution (1.334) and adsorbed substance, respectively. The  $n_a$  refractive index was estimated as 1.46 for the block copolymers (based on POEGMA) (Lee et al., 2007). Then, the polymer adsorb amounts per unit area were calculated with **Equation 4** (Campbell and Kim, 2007).

$$(4) \quad \Delta m = d \times \rho$$

Where  $d$  is the thickness of the adsorbed layer and  $\rho$  is the packing density of the adsorbed polymer. Based on the results of Feng et al. (Feng et al., 2006), the value of  $\rho$  is about 1.12  $\text{g}\cdot\text{cm}^{-3}$ .

### 3.2.8. Small angle neutron scattering: Polymer conformation after adsorption

In order to investigate the polymer conformation on the surface of CNCs after diblock adsorption, small angle neutron scattering (SANS) experiments were performed. The concentrations of the different suspensions measured are 1 wt% for TEMPO CNCs, 1 wt% for diblock and 1wt% of diblock adsorbed on 1 wt% TEMPO CNCs. As SANS is sensitive to the isotopic composition, all samples were dialyzed against deuterium oxide ( $D_2O$ ) in order to obtain the best contrast possible and to minimize the incoherent scattering due to hydrogen. SANS experiments were carried out using the PA20 spectrometer at Laboratoire Léon Brillouin (CEA, Saclay, France). A large range of scattering vector,  $Q$ , between 0.0024 and  $0.44 \text{ \AA}^{-1}$  was probed using three different neutron wavelength/sample-detector distances ( $5 \text{ \AA}/18 \text{ m}$ ,  $5 \text{ \AA}/8 \text{ m}$ , and  $5 \text{ \AA}/1.5 \text{ m}$ ). Samples were studied at  $20^\circ\text{C}$  and  $40^\circ\text{C}$ , i.e. respectively below and above the polymer LCST. Samples were loaded in quartz cells (Hellma) with a path length equal to 2 mm. The averaged spectra were corrected for solvent ( $D_2O$ ), cell, and incoherent scattering (cell with 1 mm of  $H_2O$ ) as well as for background noise (Brûlet et al., 2007) and spectra  $I(Q) = f(Q)$  on an absolute scale were obtained. The data were fitted using the SasView<sup>®</sup> 4.0.1 modeling software.

### 3.2.9. Rheological experiments on thermo-reversible hydrogel

The rheological behavior of the hydrogel under shear was studied using rotational rheometer Physica MCR 301 and MCR 302 (Anton-Paar, Austria). To investigate the temperature effect and the reversibility of these systems, tests were carried out under the LCST ( $15^\circ\text{C}$ ) and above the LCST ( $40^\circ\text{C}$ ). Start-up shearing tests were performed with a cone-plate configuration (diameter of 50mm and angle of  $1^\circ$ ). The atmosphere around the sample was saturated with water to avoid evaporation during the measurement.

To control the initial state of each sample, a constant shear rate was applied ( $10 \text{ s}^{-1}$  for 30 seconds). The transient response under shear was recorded until steady conditions were obtained.

Steady shear viscosity versus shear rate curves was generated for each sample from a shear rate of 0.01 to  $1000 \text{ s}^{-1}$ . The time required to reach steady conditions was decreased with increasing shear rate.

### 3.3. Results and Discussions

#### 3.3.1. Raw materials characterization

##### *Tempo oxidation of Cellulose Nanocrystals (CNCs) characterization*

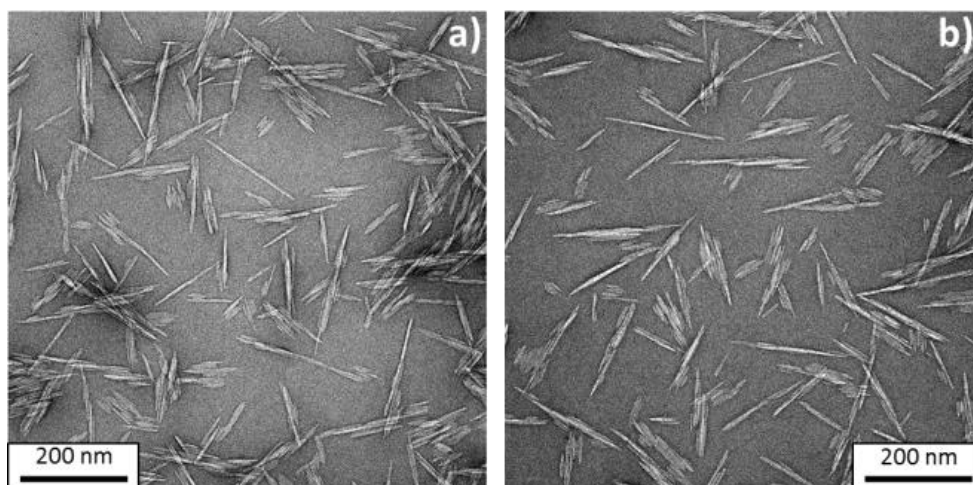


**Figure 2:** TEM images of a) CNCs and b) TEMPO CNCs.

After extraction from wood, CNCs exhibit a rod-like shape, presented in **Figure 2a**. Size measurements on TEM images show an average length of  $150 \pm 30$  nm and a section of  $10 \pm 5$  nm. These values are comparable with the literature data (Habibi et al., 2010). After TEMPO oxidation, TEMPO CNCs sizes are similar to CNCs (**Figure 2b**).

Aqueous commercial CNCs suspensions were carboxylate using TEMPO oxidation process. Via conductometric titration (as described in *Chapter II.1*), a degree of oxidation of 0.25 (mol/mol of anhydroglucose unit) and an oxidation rate of  $1450 \mu\text{mol}\cdot\text{g}^{-1}$  were obtained.

##### ***Synthesis of PDMAEMA-*b*-PDEGMA block copolymer with ATRP***

PDMAEMA-*b*-PDEGMA block copolymer synthesise was successfully done utilizing Cu(I)-mediated ATRP. It is resulting in a relatively narrow macro-initiator followed by successful chain extension, as can be judged by SEC-results in **Table 1**. In spite of the low molecular weight, the charge density of PDMAEMA is high. PDEGMA molecular weight is much longer for favoring the stimuli responsive properties.

**Table 1:** Data for the polymerization of PDMAEMA-*b*-PDEGMA block copolymer

Sample	$M_n^a$ [g/mol]	$M_n^b$ ( $\bar{D}_N$ ) [g/mol]	Charge density [meq/g] <sup>c</sup>
PDMAEMA macroinitiator	3 700	7 060 (1.20)	3.065
PDMAEMA- <i>b</i> -PDEGMA	39 000	119 700 (1.21)	0.340

<sup>a</sup> From <sup>1</sup>H-NMR conversion 30% PDMAEMA and 25% of DEGMA block <sup>b</sup> From analysis in DMF-SEC <sup>c</sup> Measured with PET

### 3.3.2. Adsorption characterization

#### Adsorption characterization

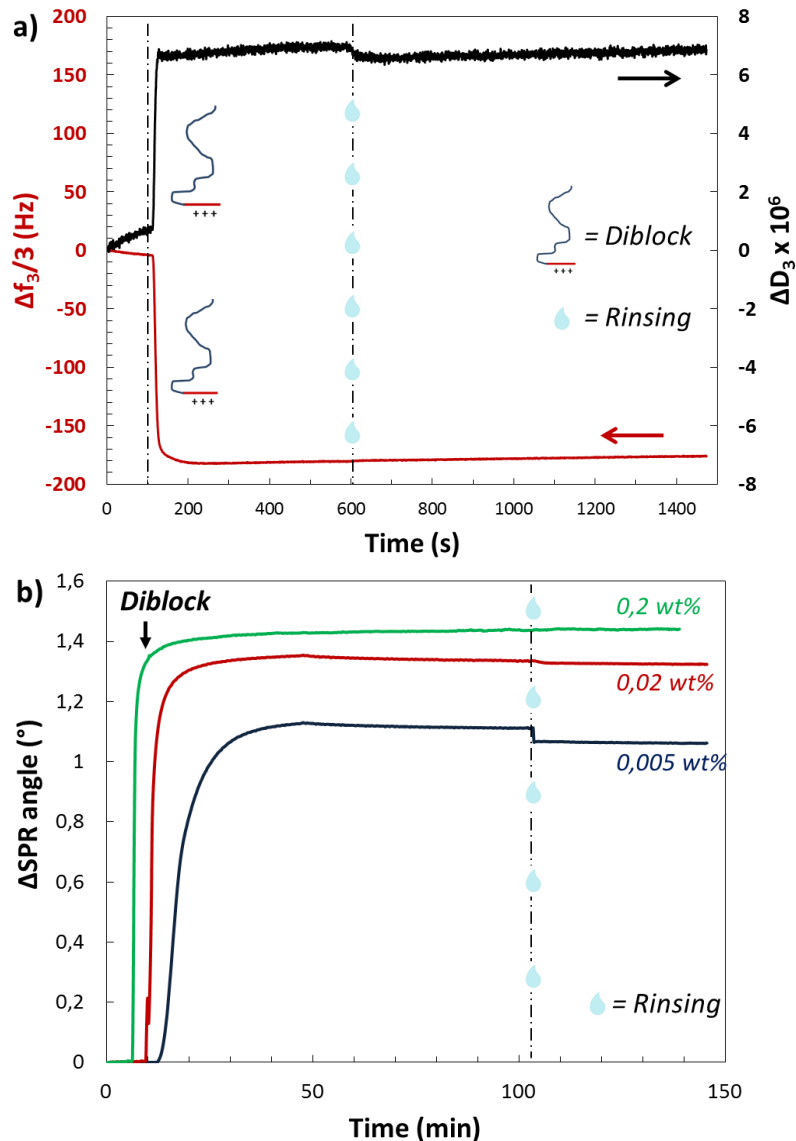


**Figure 3:** a) QCM-d measurements present adsorption of diblock on films of TEMPO CNCs. The adsorption was measured at 15°C, pH 5.5, flow rate at 300  $\mu$ L/min and concentration of 10 mM (0.05 wt%). The diblock PDMAEMA-*b*-PDEGMA is injected at 100 seconds (pH = 5.4) and the rinsing with MilliQ water starts at 600 seconds (pH = 5.5).  $\Delta F_3$  (left axis) and  $\Delta D_3$  (right axis) are respectively the shift in frequency and in dissipation of the measurement for the overtone 3. b) MP-SPR measurements present Diblock adsorption on TEMPO CNCs. Adsorption was carried out at 18°C, pH 6, flow rate of 100  $\mu$ L/min, laser wavelength 785 nm and different diblock concentration were tested.

**Figure 3** presents QCM-d adsorption experiments with PDMAEMA-*b*-PDEGMA block copolymer. They were carried out on TEMPO CNCs surfaces (**Figure 3a**). Measurements were performed at pH equal to 5.5. As previously described by Vuoriluoto et al. (Vuoriluoto et al., 2015) and Larsson et al. (Larsson et al., 2013), the PDMAEMA block contains tertiary amine groups which are quaternized (permanent cationic charges) by methylation. Besides, PEG molecules do not present a real affinity with the surface of CNCs on their own (Reid et al., 2017b) or regenerated cellulose (Vuoriluoto et al., 2015). In the work of Vuoriluoto et al. (Vuoriluoto et al., 2015), TEMPO cellulose nanofibrils show a very fast adsorption thanks to the presence of negative charges on the surface (carboxylic acid form at the experiment pH). An electrostatic interaction was proved by QCM-d and MP-SPR measurements. **Table 2** summarizes values from QCM-d and MP-SPR measurements described as following.

**Table 2:** QCM-d Frequency and dissipation changes during PDMAEMA-*b*-PDEGMA adsorption on TEMPO CNCs (**Equation 2**), layer thickness (**Equation 3**) and adsorbed amounts (**Equation 4**) of diblock on TEMPO CNCs.

Surface	QCM-d			MP-SPR	
	$\Delta F_3$ (Hz)	$\Delta D_3$ ( $10^6$ )	$\Delta m$ ( $\text{mg}\cdot\text{m}^{-2}$ )	$d$ (nm)	$\Delta m$ ( $\text{mg}\cdot\text{m}^{-2}$ )
TEMPO CNCs	-175.8	6.9	$30.0 \pm 0.1$	12.5	$14.0 \pm 0.4$

In the present study on QCM-d, the diblock amount ( $\Delta m$ ) adsorbed on TEMPO CNCs (**Figure 3a**) is estimated using the Sauerbrey equation (**Equation 2**) at  $30.0 \pm 0.1 \text{ mg}\cdot\text{m}^{-2}$ . At pH 5.5, carboxylic ends of TEMPO CNCs are negatively charged and can easily create an electrostatic link with the PDMAEMA block. Thereby, the density of diblock on the surface of TEMPO CNCs is high. It is well-known that QCM-d measurements are affected by water coupling (Vuoriluoto et al., 2015) and CNCs are highly hydrophilic material. The multi parametric surface plasmon resonance (MP-SPR) technique was used to highlight the efficiency of block copolymer adsorption on TEMPO CNCs. This technique evaluates the refractive index of the multi-layer cake after polymer adsorption and is not affected by water coupling.

PDMAEMA-*b*-PDEGMA copolymers adsorption on TEMPO CNCs (**Figure 3b**) monitored with MP-SPR were immediate, as the adsorption plateau was reached in a few minutes. Besides, the rinsing steps did not remove a significant amount of diblock, as the  $\Delta \text{SPR}_{\text{angle}}$  was not

modified. This behavior is typical for adsorption driven by electrostatic interaction (Hoogeveen et al., 1996). On the **Figure 3b**, different diblock concentration were injected (from 0.005 wt% to 0.2 wt%) on TEMPO CNCs surface and then rinsing. In each case, the rinsing did not remove diblock from the CNCs surface. This result indicates an irreversible polymer adsorption on TEMPO CNCs. The three cases presented show an increasing of the  $\Delta SPR_{angle}$  of 1.1, 1.32, 1.44 for respectively 0.005, 0.02, 0.2 wt% of diblock injected. At 0.2 wt%, the thickness is about 12.5 nm and the adsorbed mass  $\Delta m$  about  $14.0 \pm 0.4 \text{ mg}\cdot\text{m}^{-2}$ . These measurements indicate that the adsorption of block copolymers on TEMPO CNCs did not fully covered the surface until 0.2 wt%. Negative charges are still available from carboxylic groups on the surface.

By comparing QCM-d and SPR measurements, it is clear that the presence of a large amount of negative charges induce a strong adsorption on the surface. Nonetheless, a high difference exists between these two technics. In QCM-d results, the adsorbed mass is overestimated compared to MP-SPR results. Indeed, QCM-d measurements are affected by water coupling which increased the measured mass and the model calculation of Sauerbrey overestimates the mass adsorbed in the case of non-rigid polymer (it is the case for PDMAEMA-*b*-PDEGMA copolymer).

### 3.3.3. SANS Analysis

SANS measurements were performed in this work in order to investigate the structure and organization of TEMPO CNCs adsorbed with diblock. This technique is well adapted for soft matter. In particular, the neutron wavelength opens access to characteristic size between 1 and 100 nm, which is a well-adapted scale to describe configuration and organization of TEMPO CNCs and diblock system. This technique is a not destructive and the final result is an average information representative of the macroscopic sample.

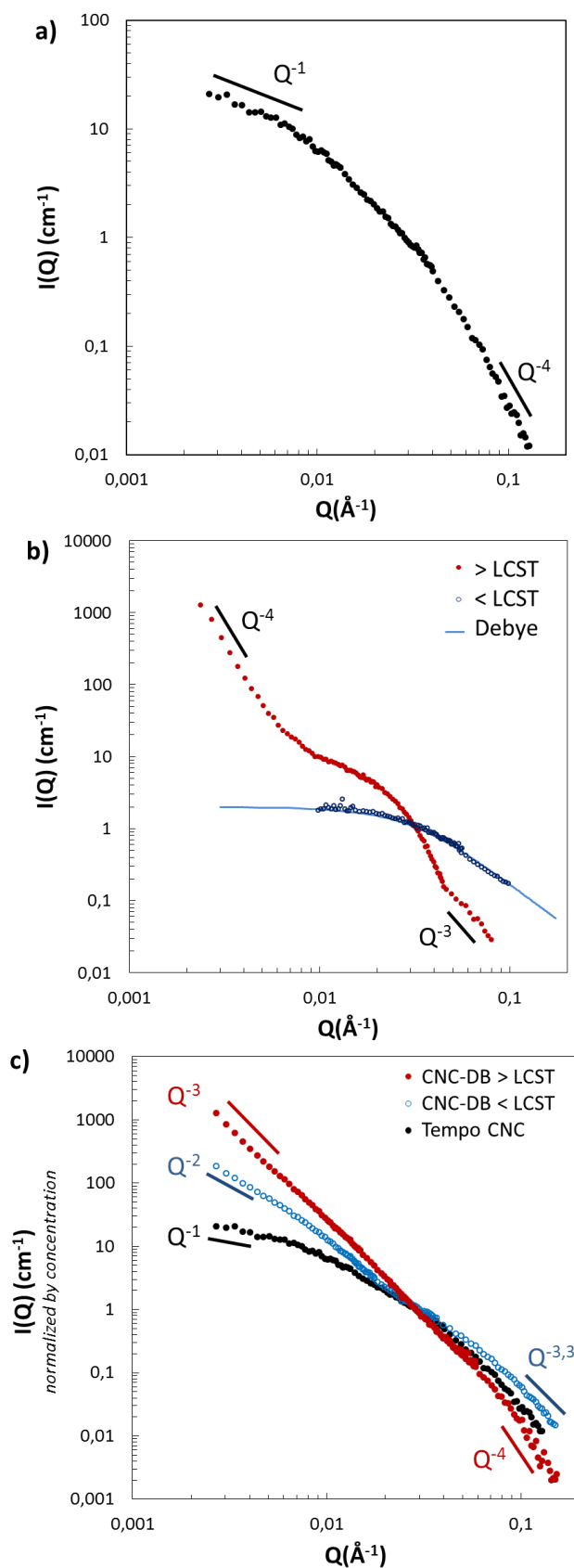


**Figure 4:** SANS curves for a) TEMPO CNCs at 20°C, b) PDMAEMA-PDEGMA block copolymer before and after the LCST and c) TEMPO CNCs (black dot), TEMPO CNCs mixed with diblock system under (blue ring) and above the LCST (red dot).  $I(Q)$  was normalized by the suspension concentration. Slope fitting curves are indicated on each graph.

**Figure 4a** shows the SANS results for TEMPO CNCs. In the small values of  $Q$ , the relative intensity decreases with a slope of  $Q^{-1}$ , this is representative of rods-shape particles. At high values of  $Q$ , the slope is  $Q^{-4}$  and it is qualified a smooth and distinct interface with the solvent. By fitting these curves with SasView, TEMPO CNCs sizes are  $110 \times 17 \times 4 \text{ nm}^3$ . These values are close to TEM measurements. Nonetheless, the length of TEMPO CNCs estimated by SANS is not exact and required data in highest  $Q$  vector. **Figure 4b** shows SANS results for diblock under an above the LCST (about  $24^\circ\text{C}$ ). The shape of the polymer under the LCST fits with the function of Debye (Ewart et al., 1946). The polymer gyration radius extracted from this function is about 4.8 nm. The exact fitting with the function of Debye of the polymer corresponds to a polymer in good solvent condition without aggregates. Nevertheless, after LCST, the intensity  $I(Q)$  presents a slope about  $Q^{-4}$  to  $Q^{-3}$  for the small  $Q$  values and high  $Q$  values, respectively. These high slopes are characteristic of polymer aggregation and collapse chain in theta solvent. Besides, the “bump” on the graph is due to a clearly identified and reproducible form, probably a spherical form of aggregates (a spherical fitting present minima and maxima for  $2\pi$  rotation). **Figure 4c** presents SANS measurements for system based on TEMPO CNCs and diblock under and above the LCST ( $24^\circ\text{C}$  for PDMAEMA-*b*-PDEGMA). Under the LCST, the intensity is not a linear combination between TEMPO CNCs and diblock and presents higher values. In small  $Q$  values, the slope is  $Q^{-2}$ . Small aggregates or bigger particles seem to be present in the suspension. At  $Q$  values superior to  $0.07 \text{ \AA}^{-1}$ , the slope is  $Q^{-3.3}$ . The polymer signature on the surface is weak. Indeed, at  $Q^{-4}$  it corresponds to a net interface between system and medium. At  $Q^{-2}$  the polymer is in good solvent (random coil) whereas at  $Q^{-3}$  the polymer is in collapse globule (normally above the LCST). The surface of decorated CNCs exhibits a smooth roughness due to the presence of block copolymer adsorbed on the crystals. However, it is difficult to determine if diblock is collapsed on the surface or presents a net core-shell around CNCs due to lake of signal in  $Q$  values superior to  $0.1 \text{ \AA}^{-1}$ . After the LCST and for small  $Q$  values, the high increasing on intensity ( $Q^{-3}$  to  $Q^{-4}$ ) corresponds to apparition of aggregates in the suspension. The general shape of CNCs disappears because of huge size of aggregates which are bigger than the maximum accessible size in the  $Q$  value range on this study. Besides, for  $Q$  values superior to  $0.05 \text{ \AA}^{-1}$ , aggregate presents a net interface with probably a characteristic size (slope  $Q^{-4}$ ).

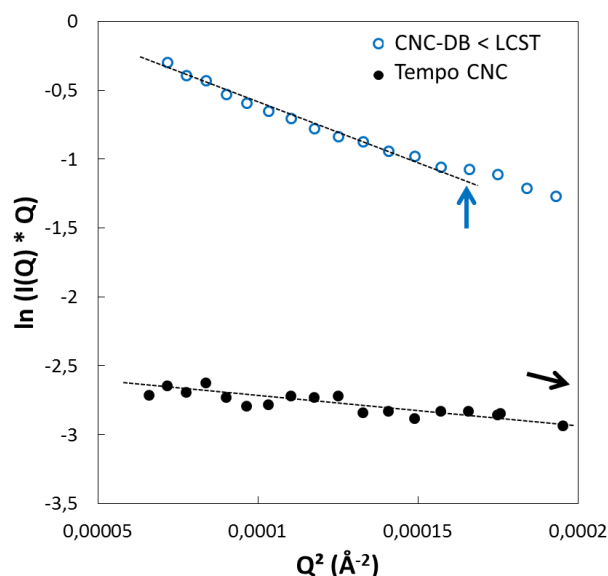


**Figure 5:** SANS measurements present as Guinier Law:  $\ln(Q \times I(Q)) = f(Q^2)$  for TEMPO CNCs and TEMPO CNCs mix with diblock under the LCST. Arrows indicates  $Q_{max}$  values corresponding to  $1/R_g$ , above this value the Guinier law is not respected ( $Q \times R_g > 1$ ) (Glatter and Kratky, 1982).

**Figure 5** and **Table 3** present Guinier law fitting and gyration radius isolated from the law. For TEMPO CNCs, the radius is 6 nm which is corresponding approximately to the section of CNCs. Thanks to the fitting with the function of Debye, the block copolymer shows a gyration radius of 4.8 nm. After polymer adsorption on TEMPO CNC surface, the radius increases to 15.8 nm. The polymer shell around TEMPO CNCs is about 9.8 nm. This value is close to two times the gyration radius of diblock. The polymer configuration is in mushroom state around CNCs for a ratio of 1 between CNCs and diblock.

**Table 3:** Slope, gyration radius and polymer thickness isolated thanks to the Guinier law for each suspension of this study. <sup>a</sup> Gyration radius is extracted from function of Debye.

	Slope ( $\text{\AA}^{-2}$ )	$R_g$ (nm)	Polymer thickness (nm)
TEMPO CNC	-2100	6	-
Diblock	-	4.8 <sup>a</sup>	-
TEMPO CNC + Diblock (< LCST)	-12500	15.8	9.8

### 3.3.4. Hydrogel rheological behavior

#### *Rheological behavior of TEMPO CNCs and Diblock*

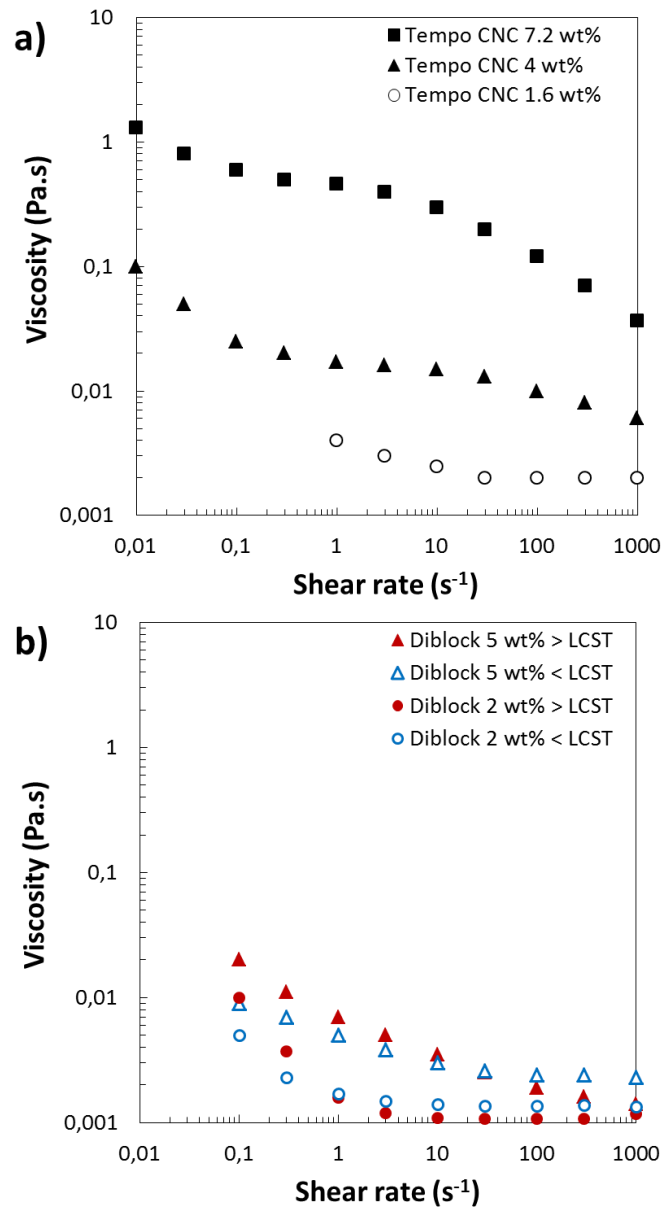


**Figure 6:** Flow curves of a) TEMPO CNCs at 1.6, 4 and 7.2 wt% at 20°C and b) diblock at 2 and 5 wt% under (15°C) and above (40°C) its LCST.

**Figure 6** presents flow curves of different raw materials used in this study. TEMPO CNCs rheological behavior (**Figure 6a**) is shown at different concentrations. Rheological behavior of dilute suspension is close to a Newtonian one. When the concentration increases, this behavior is changed to a shear thinning one and a three slope behavior at higher shear rate appears. It is characteristic of chiral nematic phase as for non-oxidized CNCs (Shafiei-Sabet et al., 2012; Ureña-Benavides et al., 2011; Wu et al., 2014). **Figure 6b** presents the rheological

behavior of diblock at different concentrations and temperatures (under and above the LCST of the thermo-sensitive polymer). The PDEGMA block is thermo-sensitive as exposed in previous work (Larsson et al., 2013). Whatever the concentration is (up to 5 wt%), the viscosity is never superior to 0.2 Pa·s at shear rate of 0.1 s<sup>-1</sup>. Besides, no clear difference appears in its viscosity when the LCST is reached. The absence of difference in behavior between these two temperatures is probably due to the absence of polymer's network entanglement at this concentration when the LCST is reached. Under the LCST, diblock are in random coil and does not resist to the shear rate. Above the LCST diblock precipitate. Nevertheless, in absence of anchorage, collapse globules of diblock flow under the action of shear rate.

### ***Influence of TEMPO CNCs on the rheological behavior of diblock solution***

In order to investigate the impact of TEMPO CNCs on diblock solution, a solution at 3 wt% of diblock was first fixed. Then, three cases were experimented: TEMPO CNCs in large excess (**Figure 7a**), an equal ratio between TEMPO CNCs and diblock (**Figure 7b**) and TEMPO CNCs in low concentration (**Figure 7c**). Previous results of QCM-d and MP-SPR certify the irreversible adsorption on TEMPO CNCs surface.

Referred to SANS measurements, an equal proportion of diblock and TEMPO CNCs involves a polymer configuration in mushroom state on the surface of CNCs. So, in the ratio in **Figure 7a** and **7b**, no polymers are in excess and they are totally adsorbed on TEMPO CNCs. At a shear rate of 0.1 s<sup>-1</sup>, the viscosity of TEMPO CNCs (**Figure 6a**) and diblock (**Figure 6b**) is under 1 Pa·s. After diblock adsorption, viscosity is highly impacted by the adsorption of diblock and reaches 100 Pa·s (**Figure 7a** and **7b**). Then, when the shear rate increases, a shear thinning behavior (due to the presence of CNCs) appears. However, when the LCST is reached, no modification of the rheological behavior is revealed. In these both cases, a significant synergic effect is revealed but no clear thermal impact was shown. This result is probably due the creation of a network of diblock and TEMPO CNCs. The high excess of CNCs cannot allow the thermal reversibility of diblock.

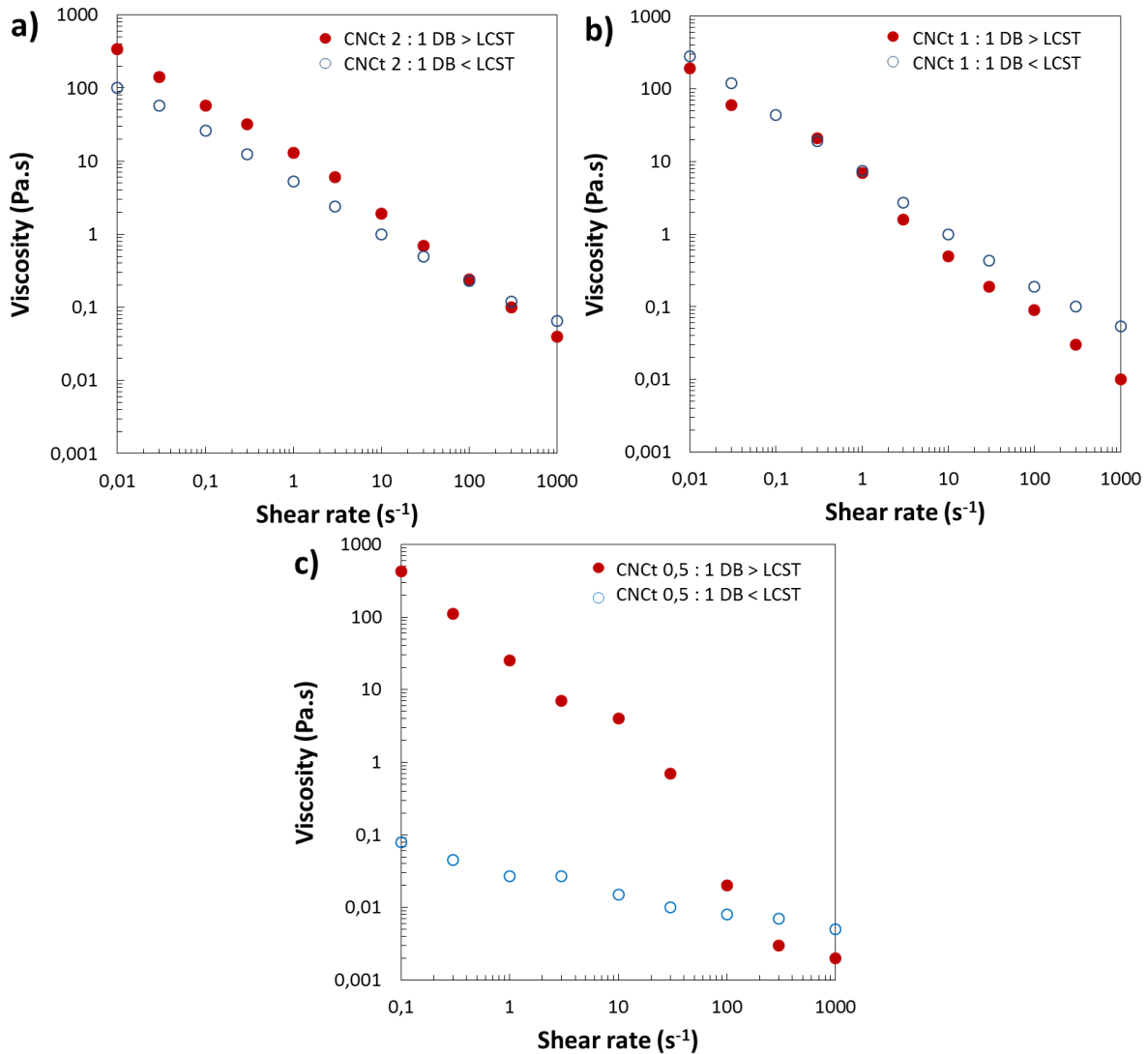


**Figure 7:** Flow curves under (ring) and above (dot) the LCST of a 3 wt% diblock solution with a) 6 wt% TEMPO CNCs (ratio 2:1), b) 3 wt% TEMPO CNCs (ratio 1:1) and c) 1.5 wt% TEMPO CNCs (ratio 0.5:1).

Furthermore, the rheological behavior of **Figure 7c** is completely different. It shows the impact of a small amount of TEMPO CNCs on the diblock behavior with 1.5 wt% of TEMPO CNCs added to 3 wt% of diblock. Indeed, under the LCST no clear synergetic effect is identified despite of diblock in large excess. Nonetheless, when the temperature reaches the LCST, a considerable thermal answer is revealed with an increasing in viscosity of almost four decades at low shear rate (0.1 to 400 Pa·s at 0.1 s<sup>-1</sup>). Then at higher shear rate (> 10 s<sup>-1</sup>), the viscosity drastically decreases because of network destruction. To conclude on this case, the small amount of TEMPO CNCs probably acts as a cross-linker or interpenetrated network in a matrix of diblock. Under the LCST, the system flows without link between each diblock/TEMPO CNCs group. Above the LCST, diblock collapse in the suspension and TEMPO CNCs act as an anchor between each group. The system turns in a “gel” behavior.

### ***Influence of the ratio between TEMPO CNCs and diblock on the rheological behavior***

In this second part of the rheology study, the final concentration of the suspension was fixed at 5 wt% and the influence on the rheological behavior of the ratio between TEMPO CNCs and diblock was evaluated (**Figure 8**). As suggested by QCM-d experiments (**Figure 3a**) and MP-SPR measurements (**Figure 3b**), diblock polymer presents a high tendency to be irreversibly adsorbed on TEMPO CNCs. According to these results, four ratios were selected: TEMPO CNCs in excess, equivalent ratio between diblock and TEMPO CNCs, diblock in excess and diblock in a large excess.

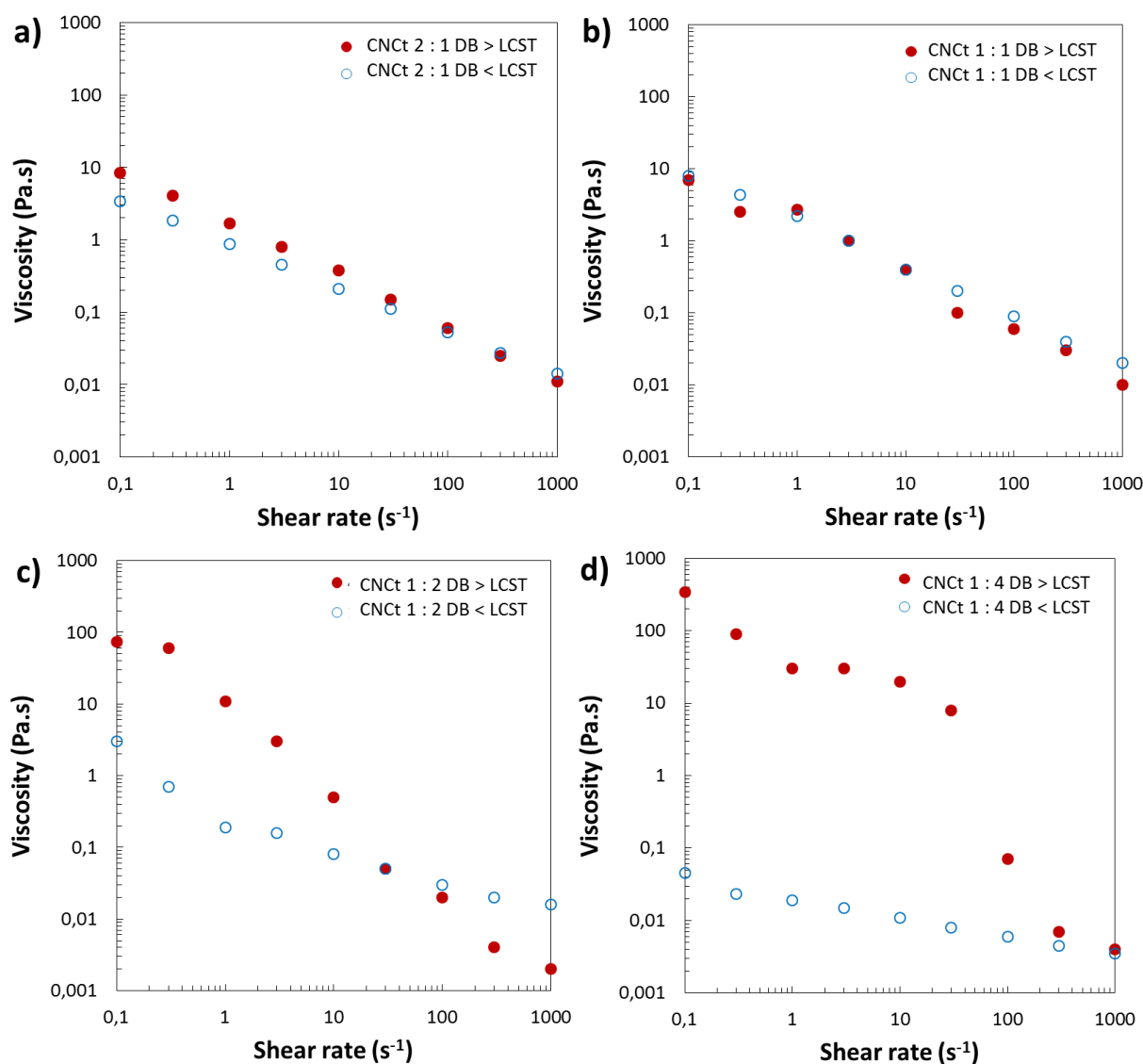


**Figure 8:** Flow curves (ring) and above (dot) the LCST for final system concentration of 5 wt% with different ratio of TEMPO CNCs for diblock of a) 2:1, b) 1:1, c) 1:2 and d) 1:4.

The **Figure 8a** and **8b** present the rheological behavior of TEMPO CNCs in excess against diblock for an identical suspension concentration of 5 wt%. Referring to SANS measurements, the equal proportion seems to be the limit for a polymer configuration in mushroom state on the surface of TEMPO CNCs. All polymers are adsorbed on the surface of TEMPO CNCs. Indeed, a significant synergic effect is revealed but no clear thermal impact was shown. The viscosity is smaller than the viscosity of **Figure 7** (10 against 200 Pa·s) due to lots of TEMPO CNCs in the suspension which influenced the rheological behavior. The high excess of CNCs cannot allow the thermal answer of diblock.

By comparison with **Figure 7**, a large amount of diblock against TEMPO CNCs seems to create a thermo-responsive system. In a consistent manner (**Figure 8c**), a significant thermo-sensitivity appears with diblock in excess. Under the LCST, the flow curve presents a similar viscosity than **Figures 8a** and **8b**. Besides, above the LCST, the viscosity increases for low shear rate ( $< 1 \text{ s}^{-1}$ ). The diblock amount is sufficient to allow its thermal answer in the suspension. At higher shear rate ( $> 3 \text{ s}^{-1}$ ), the system structure is broken due to the shear. At shear rate superior to  $100 \text{ s}^{-1}$ , the viscosity falls under  $0.01 \text{ Pa}\cdot\text{s}$  because of the expulsion of aggregates out of the suspension by the centrifuge effect (visual observation after rheological experiment).

**Figure 8d** shows a very promising thermo-responsive result with a large excess of diblock compared to TEMPO CNCs. Under the LCST, the system exhibits low viscosities ( $< 0.1 \text{ Pa}\cdot\text{s}$ ) since the amount TEMPO CNCs is minimal ( $< 1 \text{ wt}\%$ ). No clear synergic effect is shown under the LCST, probably due to the small amount of CNCs in suspension. However, above the LCST, the system displays an impressive thermo-sensitive behavior. At a shear rate of  $0.1 \text{ s}^{-1}$ , the viscosity is increasing about 760 times when the LCST is reached ( $340 \text{ Pa}\cdot\text{s}$ ). Up to  $30 \text{ s}^{-1}$ , a plateau in viscosity is observed. It traduces the resistance of adsorbed systems to flow; probably due to the network of thermo-responsive polymer cross-linked by TEMPO CNCs. Then, after a critical shear rate of  $30 \text{ s}^{-1}$ , the network is broken and a sharp decrease of viscosity is observed. This last ratio presents a thermo-reversible system with a 'liquid' to 'gel' behavior tuned by the external temperature. The same conclusion is obtained than the previous test: an important excess of diblock allows the suspension to form a thermo-reversible hydrogel by synergistic effect. **Figure 9** tries to draw these systems behaviors.

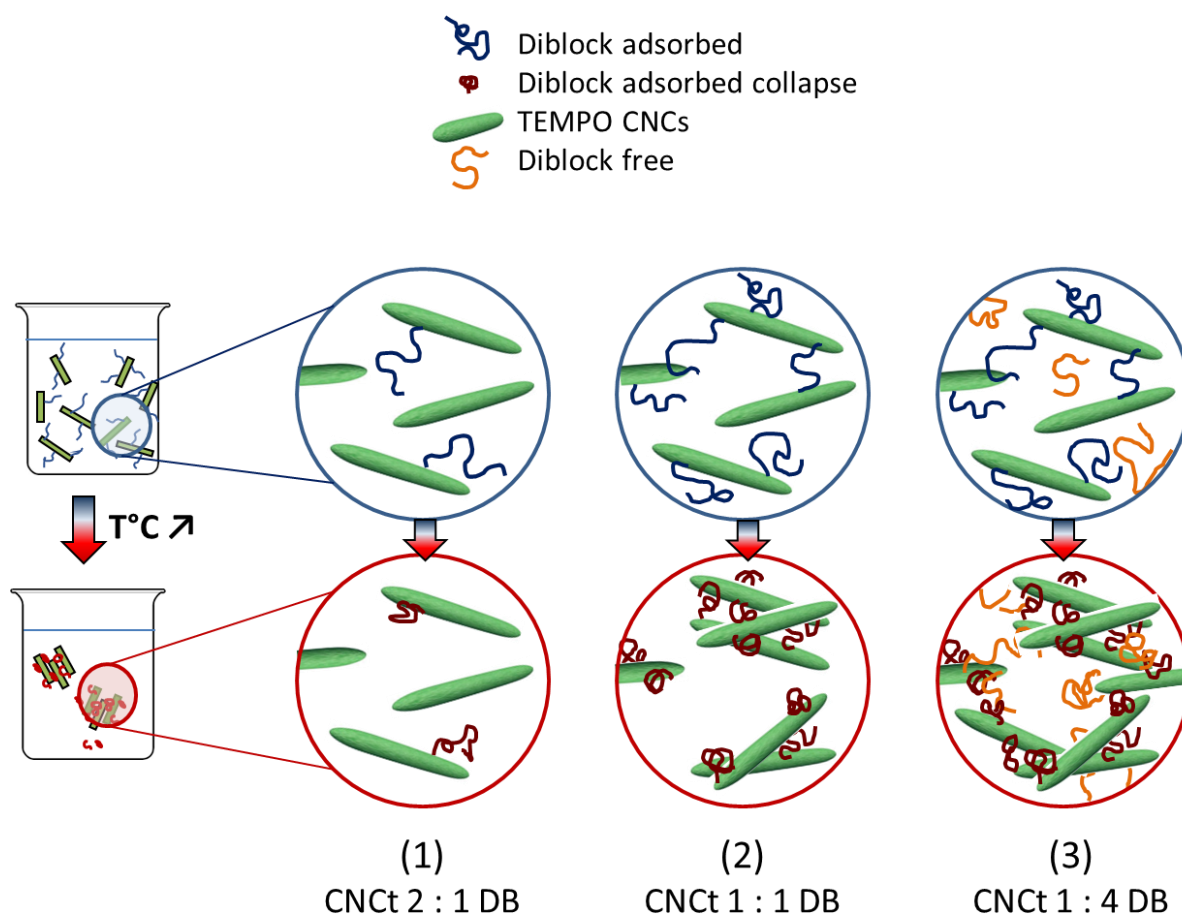


**Figure 9:** Scheme of the three characteristic behavior identified in this work with concentration (wt%): (1) TEMPO CNCs  $\gg$  Diblock, (2) TEMPO CNCs = Diblock and (3) TEMPO CNCs  $\ll$  Diblock (free diblock in excess in the suspension)

Due to the strong adsorption between TEMPO CNCs and diblock, it is possible to create thermo-responsive hydrogel with dilute suspension of nanocrystals. Under the LCST, the system is 'liquid' and above the LCST it becomes a 'gel'. Besides, while the ratio is very important, the maximum viscosity can also be tuned by increasing the final concentration. Viscosities superior to 3000 Pa.s (at  $0.1 \text{ s}^{-1}$ ) were obtained in particular ratio but a phase separation was observed.

### 3.4. Conclusions

In this work, we examined the thermo-reversible behavior of a hydrogel based on cellulose nanocrystals and thermo-responsive polymer. A quaternized diblock of PDMAEMA-*b*-PDEGMA was adsorbed on TEMPO CNCs. QCM-d and MP-SPR measurements proved the ionic adsorption on the TEMPO CNCs surface due to the large amount of negative charges from carboxylic groups on the CNCs surface. Via SANS experiments, we displayed the mushroom configuration of the polymer on the CNCs surface. The thermo-responsive ends are in swollen coil conformation with highly hydrated chains. They can interact with the suspension and neighbor polymer when the critical temperature LCST is reached. PDMAEMA-*b*-PDEGMA diblock become more hydrophobic and turn in a collapsed globule on the CNCs surface which interact with other adsorbed CNCs and create aggregates (Flory index in SANS measurements is inferior to  $\frac{1}{2}$ ). Synergetic effect between TEMPO CNCs and diblock was shown by rheological flow curves experiments. Nevertheless, only a high excess of diblock in the suspension exhibits a relevant thermo-reversible behavior above the polymer LCST. A transition 'liquid' under the LCST to 'gel' above the LCST is shown. When the LCST is reached, polymers turn in collapse hydrophobic configuration on the CNCs surface and attract its neighbor nanoparticles. Then, non-adsorbed polymers connect these particles aggregates and form a hydrogel. This promising thermo-responsive functionality on bio-based particles paves the way to the design of injectable hydrogel for surgery or anesthetic medicine.



## Conclusions

In the present **Chapter III**, two challenges of this Ph.D. were discussed: (ii) understanding of rheological behavior of CNCs and CNCs-polymer suspensions and (iii) realization of stimuli-responsive suspensions based on cellulose nanocrystals and thermo-responsive polymers.

In *Chapter III.1*, the effect of sonication on a highly concentrated suspension of CNCs and the resulting modification on rheological properties have been investigated. The commercial CNCs suspension presents a gel behavior at high concentration without aggregates. After sonication at high concentration, the suspension turns into a liquid behavior. Sonication modified the form factor of particles and onto assembly of CNCs.

In *Chapter III.2*, the specific rheology of thermo-responsive hydrogels based on CNC-g-Pnipam<sub>2500</sub>, developed in *Chapter II.1*, has been studied. Results are promising. The viscosity of the system reaches 40 Pa·s when the temperature is superior to the LCST. This hydrogel is reversible via external temperature stimuli. The Pnipam<sub>2500</sub> adsorption strategy was detailed, and the thermo-responsivity has been weaker than the grafted one (argument in favor of the grafting efficiency in *Chapter II.1*).

With *Chapter III.3*, a new thermo-sensitive polymer has been introduced in this Ph.D. project: PDMAEMA-PDEGMA. This diblock exhibits highly positive charges (on PDMAEMA) which are easily adsorbed on the negative surface of TEMPO CNCs. After adsorption, the thermo-sensitive polymer (e.g. PDEGMA) was in swollen coil conformation with highly hydrated chains. At specific ratio (excess of diblock) the suspension built a network via polymer entanglement with CNCs as cross-linker or interpenetrated network in the hydrogel. The strong thermo-reversibility property of hydrogel has been allowed by excess of diblock in the suspension and its synergy with CNCs

To conclude this chapter, the presence - via polymer adsorption or grafting - of thermo-responsive polymers on the TEMPO CNCs surface allows the creation of reversible hydrogel tuned by external temperature. These hydrogels open the way of biomedical applications such as injectable surgery. The following **Chapter IV** details couple of possible application of those different hydrogels.



## References

- Abitbol, T., Rivkin, A., Cao, Y., Nevo, Y., Abraham, E., Ben-Shalom, T., Lapidot, S., and Shoseyov, O. (2016). Nanocellulose, a tiny fiber with huge applications. *Curr. Opin. Biotechnol.* *39*, 76–88.
- Araki, J., and Kuga, S. (2001). Effect of Trace Electrolyte on Liquid Crystal Type of Cellulose Microcrystals. *Langmuir* *17*, 4493–4496.
- Aubry, T., Bossard, F., Staikos, G., and Bokias, G. (2003). Rheological study of semidilute aqueous solutions of a thermoassociative copolymer. *J. Rheol.* *47*, 577–587.
- Aulin, C., Varga, I., Claesson, P.M., Wågberg, L., and Lindström, T. (2008). Buildup of Polyelectrolyte Multilayers of Polyethyleneimine and Microfibrillated Cellulose Studied by in Situ Dual-Polarization Interferometry and Quartz Crystal Microbalance with Dissipation. *Langmuir* *24*, 2509–2518.
- Azzam, F., Heux, L., Putaux, J.-L., and Jean, B. (2010). Preparation By Grafting Onto, Characterization, and Properties of Thermally Responsive Polymer-Decorated Cellulose Nanocrystals. *Biomacromolecules* *11*, 3652–3659.
- Azzam, F., Heux, L., and Jean, B. (2016a). Adjustment of the chiral nematic phase properties of cellulose nanocrystals by polymer grafting. *Langmuir* *32*, 4305–4312.
- Azzam, F., Siqueira, E., Fort, S., Hassaini, R., Pignon, F., Travelet, C., Putaux, J.-L., and Jean, B. (2016b). Tunable Aggregation and Gelation of Thermoresponsive Suspensions of Polymer-Grafted Cellulose Nanocrystals. *Biomacromolecules* *17*, 2112–2119.
- Baravian, C., Michot, L.J., Paineau, E., Bihannic, I., Davidson, P., Impéror-Clerc, M., Belamie, E., and Levitz, P. (2010). An effective geometrical approach to the structure of colloidal suspensions of very anisometric particles. *EPL Europhys. Lett.* *90*, 36005.
- Bardet, R., Belgacem, N., and Bras, J. (2015). Flexibility and Color Monitoring of Cellulose Nanocrystal Iridescent Solid Films Using Anionic or Neutral Polymers. *ACS Appl. Mater. Interfaces* *7*, 4010–4018.
- Beck, S., Bouchard, J., and Berry, R. (2011). Controlling the Reflection Wavelength of Iridescent Solid Films of Nanocrystalline Cellulose. *Biomacromolecules* *12*, 167–172.
- Beck, S., Bouchard, J., and Berry, R. (2012). Dispersibility in Water of Dried Nanocrystalline Cellulose. *Biomacromolecules* *13*, 1486–1494.
- Bensselfelt, T., Cranston, E.D., Ondaral, S., Johansson, E., Brumer, H., Rutland, M.W., and Wågberg, L. (2016). Adsorption of Xyloglucan onto Cellulose Surfaces of Different Morphologies: An Entropy-Driven Process. *Biomacromolecules* *17*, 2801–2811.
- Bercea, M., and Navard, P. (2000). Shear Dynamics of Aqueous Suspensions of Cellulose Whiskers. *Macromolecules* *33*, 6011–6016.
- Bonini, C., Heux, L., Cavallé, J.-Y., Lindner, P., Dewhurst, C., and Terech, P. (2002). Rodlike Cellulose Whiskers Coated with Surfactant: A Small-Angle Neutron Scattering Characterization. *Langmuir* *18*, 3311–3314.
- Bras, J., Viet, D., Bruzzese, C., and Dufresne, A. (2011). Correlation between stiffness of sheets prepared from cellulose whiskers and nanoparticles dimensions. *Carbohydr. Polym.* *84*, 211–215.
- Brûlet, A., Lairez, D., Lapp, A., and Cotton, J.-P. (2007). Improvement of data treatment in small-angle neutron scattering. *J. Appl. Crystallogr.* *40*, 165–177.
- Camarero Espinosa, S., Rothen-Rutishauser, B., Johan Foster, E., and Weder, C. (2016). Articular cartilage: from formation to tissue engineering. *Biomater. Sci.* *4*, 734–767.

- Campbell, C.T., and Kim, G. (2007). SPR microscopy and its applications to high-throughput analyses of biomolecular binding events and their kinetics. *Biomaterials* 28, 2380–2392.
- Carlmark, A., Larsson, E., and Malmström, E. (2012). Grafting of cellulose by ring-opening polymerisation—A review. *Eur. Polym. J.* 48, 1646–1659.
- Cha, R., He, Z., and Ni, Y. (2012). Preparation and characterization of thermal/pH-sensitive hydrogel from carboxylated nanocrystalline cellulose. *Carbohydr. Polym.* 88, 713–718.
- Chang, C., and Zhang, L. (2011). Cellulose-based hydrogels: Present status and application prospects. *Carbohydr. Polym.* 84, 40–53.
- Chauve, G., and Bras, J. (2014). Industrial point of view of nanocellulose materials and their possible applications. *Handb. Green Mater.* World Sci. 233–252.
- Chauve, G., Frascini, C., and Jean, B. (2014). Separation of cellulose nanocrystals. *Handb. Green Mater. Process. Technol. Prop. Appl.* World Sci Pub Co Lond. 73–87.
- Cherhal, F., Cousin, F., and Capron, I. (2015). Influence of Charge Density and Ionic Strength on the Aggregation Process of Cellulose Nanocrystals in Aqueous Suspension, as Revealed by Small-Angle Neutron Scattering. *Langmuir* 31, 5596–5602.
- De France, K.J., Chan, K.J.W., Cranston, E.D., and Hoare, T. (2016). Enhanced Mechanical Properties in Cellulose Nanocrystal–Poly(oligoethylene glycol methacrylate) Injectable Nanocomposite Hydrogels through Control of Physical and Chemical Cross-Linking. *Biomacromolecules* 17, 649–660.
- De France, K.J., Hoare, T., and Cranston, E.D. (2017). Review of Hydrogels and Aerogels Containing Nanocellulose. *Chem. Mater.* 29, 4609–4631.
- De Gennes, P.-G. (1979). *Scaling concepts in polymer physics* (Cornell university press).
- Domingues, R.M.A., Gomes, M.E., and Reis, R.L. (2014). The Potential of Cellulose Nanocrystals in Tissue Engineering Strategies. *Biomacromolecules* 15, 2327–2346.
- Domingues, R.M.A., Silva, M., Gershovich, P., Betta, S., Babo, P., Caridade, S.G., Mano, J.F., Motta, A., Reis, R.L., and Gomes, M.E. (2015). Development of Injectable Hyaluronic Acid/Cellulose Nanocrystals Bionanocomposite Hydrogels for Tissue Engineering Applications. *Bioconjug. Chem.* 26, 1571–1581.
- Dong, X.M., and Gray, D.G. (1997). Effect of Counterions on Ordered Phase Formation in Suspensions of Charged Rodlike Cellulose Crystallites. *Langmuir* 13, 2404–2409.
- Dong, S., Hirani, A.A., Colacino, K.R., Lee, Y.W., and Roman, M. (2012). Cytotoxicity and cellular uptake of cellulose nanocrystals. *Nano LIFE* 02, 1241006.
- Dong, X.M., Kimura, T., Revol, J.-F., and Gray, D.G. (1996). Effects of Ionic Strength on the Isotropic–Chiral Nematic Phase Transition of Suspensions of Cellulose Crystallites. *Langmuir* 12, 2076–2082.
- Dong, X.M., Revol, J.-F., and Gray, D.G. (1998). Effect of microcrystallite preparation conditions on the formation of colloid crystals of cellulose. *Cellulose* 5, 19–32.
- Dufresne, A. (2013). Nanocellulose: a new ageless bionanomaterial. *Mater. Today* 16, 220–227.
- Ebeling, T., Paillet, M., Borsali, R., Diat, O., Dufresne, A., Cavaille, J.Y., Chanzy, H., and others (1999). Shear-induced orientation phenomena in suspensions of cellulose microcrystals, revealed by small angle X-ray scattering. *Langmuir* 15, 6123–6126.
- Eichhorn, S.J., Dufresne, A., Aranguren, M., Marcovich, N.E., Capadona, J.R., Rowan, S.J., Weder, C., Thielemans, W., Roman, M., Renneckar, S., et al. (2010). Review: current international research into cellulose nanofibres and nanocomposites. *J. Mater. Sci.* 45, 1–33.

- Elazzouzi-Hafraoui, S., Nishiyama, Y., Putaux, J.-L., Heux, L., Dubreuil, F., and Rochas, C. (2008). The Shape and Size Distribution of Crystalline Nanoparticles Prepared by Acid Hydrolysis of Native Cellulose. *Biomacromolecules* *9*, 57–65.
- Endes, C., Camarero-Espinosa, S., Mueller, S., Foster, E.J., Petri-Fink, A., Rothen-Rutishauser, B., Weder, C., and Clift, M.J.D. (2016). A critical review of the current knowledge regarding the biological impact of nanocellulose. *J. Nanobiotechnology* *14*, 78.
- Espino-Pérez, E., Domenek, S., Belgacem, N., Sillard, C., and Bras, J. (2014). Green Process for Chemical Functionalization of Nanocellulose with Carboxylic Acids. *Biomacromolecules* *15*, 4551–4560.
- Ewart, R.H., Roe, C.P., Debye, P., and McCartney, J.R. (1946). The Determination of Polymeric Molecular Weights by Light Scattering in Solvent-Precipitant Systems. *J. Chem. Phys.* *14*, 687–695.
- Eyley, S., and Thielemans, W. (2014). Surface modification of cellulose nanocrystals. *Nanoscale* *6*, 7764–7779.
- Feng, W., Zhu, S., Ishihara, K., and Brash, J.L. (2006). Protein resistant surfaces: Comparison of acrylate graft polymers bearing oligo-ethylene oxide and phosphorylcholine side chains. *Biointerphases* *1*, 50–60.
- Flory, P.J. (1953). *Principles of polymer chemistry* (Cornell University Press).
- García, A., Gandini, A., Labidi, J., Belgacem, N., and Bras, J. (2016). Industrial and crop wastes: A new source for nanocellulose biorefinery. *Ind. Crops Prod.* *93*, 26–38.
- de Gennes, P.G. (1980). Conformations of Polymers Attached to an Interface. *Macromolecules* *13*, 1069–1075.
- Gicquel, E., Martin, C., Yanez, J.G., and Bras, J. (2017). Cellulose nanocrystals as new bio-based coating layer for improving fiber-based mechanical and barrier properties. *J. Mater. Sci.* *52*, 3048–3061.
- Glatter, O., and Kratky, O. (1982). *Small angle X-ray scattering* (Academic press).
- Grishkewich, N., Akhlaghi, S.P., Zhaoling, Y., Berry, R., and Tam, K.C. (2016). Cellulose nanocrystal-poly(oligo(ethylene glycol) methacrylate) brushes with tunable LCSTs. *Carbohydr. Polym.* *144*, 215–222.
- Habibi, Y. (2014). Key advances in the chemical modification of nanocelluloses. *Chem. Soc. Rev.* *43*, 1519–1542.
- Habibi, Y., Chanzy, H., and Vignon, M.R. (2006). TEMPO-mediated surface oxidation of cellulose whiskers. *Cellulose* *13*, 679–687.
- Habibi, Y., Lucia, L.A., and Rojas, O.J. (2010). Cellulose Nanocrystals: Chemistry, Self-Assembly, and Applications. *Chem. Rev.* *110*, 3479–3500.
- Hakalahti, M., Mautner, A., Johansson, L.-S., Hänninen, T., Setälä, H., Kontturi, E., Bismarck, A., and Tammelin, T. (2016). Direct Interfacial Modification of Nanocellulose Films for Thermoresponsive Membrane Templates. *ACS Appl. Mater. Interfaces* *8*, 2923–2927.
- Haqani, M., Roghani-Mamaqani, H., and Salami-Kalajahi, M. (2017). Synthesis of dual-sensitive nanocrystalline cellulose-grafted block copolymers of N-isopropylacrylamide and acrylic acid by reversible addition-fragmentation chain transfer polymerization. *Cellulose* *24*, 2241–2254.
- Hebeish, A., Farag, S., Sharaf, S., and Shaheen, T.I. (2014). Thermal responsive hydrogels based on semi interpenetrating network of poly(NIPAm) and cellulose nanowhiskers. *Carbohydr. Polym.* *102*, 159–166.

- Hemraz, U.D., Lu, A., Sunasee, R., and Boluk, Y. (2014). Structure of poly(N-isopropylacrylamide) brushes and steric stability of their grafted cellulose nanocrystal dispersions. *J. Colloid Interface Sci.* *430*, 157–165.
- Hoeng, F., Denneulin, A., and Bras, J. (2016). Use of nanocellulose in printed electronics: a review. *Nanoscale* *8*, 13131–13154.
- Hoeng, F., Bras, J., Gicquel, E., Krosnicki, G., and Denneulin, A. (2017). Inkjet printing of nanocellulose–silver ink onto nanocellulose coated cardboard. *RSC Adv.* *7*, 15372–15381.
- Hoogeveen, N.G., Stuart, M.A.C., and Fler, G.J. (1996). Polyelectrolyte adsorption on oxides: II. Reversibility and exchange. *J. Colloid Interface Sci.* *182*, 146–157.
- Horn, D. (1978). Optisches Zweistrahlverfahren zur Bestimmung von Polyelektrolyten in Wasser und zur Messung der Polymeradsorption an Grenzflächen. *SpringerLink* 251–264.
- Ingverud, T., Larsson, E., Hemmer, G., Rojas, R., Malkoch, M., and Carlmark, A. (2016). High water-content thermoresponsive hydrogels via electrostatic macrocrosslinking of cellulose nanofibrils. *J. Polym. Sci. Part Polym. Chem.* *54*, 3415–3424.
- Irwin, E.F., Ho, J.E., Kane, S.R., and Healy, K.E. (2005). Analysis of Interpenetrating Polymer Networks via Quartz Crystal Microbalance with Dissipation Monitoring. *Langmuir* *21*, 5529–5536.
- J. Eichhorn, S. (2011). Cellulose nanowhiskers: promising materials for advanced applications. *Soft Matter* *7*, 303–315.
- Jeong, B., Kim, S.W., and Bae, Y.H. (2002). Thermosensitive sol-gel reversible hydrogels. *Adv. Drug Deliv. Rev.* *54*, 37–51.
- Jorfi, M., and Foster, E.J. (2015). Recent advances in nanocellulose for biomedical applications. *J. Appl. Polym. Sci.* *132*.
- Jung, L.S., Campbell, C.T., Chinowsky, T.M., Mar, M.N., and Yee, S.S. (1998). Quantitative interpretation of the response of surface plasmon resonance sensors to adsorbed films. *Langmuir* *14*, 5636–5648.
- Karabulut, E., Pettersson, T., Ankerfors, M., and Wågberg, L. (2012). Adhesive Layer-by-Layer Films of Carboxymethylated Cellulose Nanofibril–Dopamine Covalent Bioconjugates Inspired by Marine Mussel Threads. *ACS Nano* *6*, 4731–4739.
- Kiminta, D.Ö., Luckham, P.F., and Lenon, S. (1995). The rheology of deformable and thermoresponsive microgel particles. *Polymer* *36*, 4827–4831.
- Klemm, D., Kramer, F., Moritz, S., Lindström, T., Ankerfors, M., Gray, D., and Dorris, A. (2011). Nanocelluloses: A New Family of Nature-Based Materials. *Angew. Chem. Int. Ed.* *50*, 5438–5466.
- Kovacs, T., Naish, V., O'Connor, B., Blaise, C., Gagné, F., Hall, L., Trudeau, V., and Martel, P. (2010). An ecotoxicological characterization of nanocrystalline cellulose (NCC). *Nanotoxicology* *4*, 255–270.
- Krivosheeva, O., Sababi, M., Dedinaite, A., and Claesson, P.M. (2013). Nanostructured Composite Layers of Mussel Adhesive Protein and Ceria Nanoparticles. *Langmuir* *29*, 9551–9561.
- Krouit, M., Bras, J., and Belgacem, M.N. (2008). Cellulose surface grafting with polycaprolactone by heterogeneous click-chemistry. *Eur. Polym. J.* *44*, 4074–4081.
- Kubota, K., Fujishige, S., and Ando, I. (1990). Solution properties of poly (N-isopropylacrylamide) in water. *Polym J* *22*, 15–20.
- Lagerwall, J.P., Schütz, C., Salajkova, M., Noh, J., Park, J.H., Scalia, G., and Bergström, L. (2014). Cellulose nanocrystal-based materials: from liquid crystal self-assembly and glass formation to multifunctional thin films. *NPG Asia Mater.* *6*, e80.

- Larsson, E., Sanchez, C.C., Porsch, C., Karabulut, E., Wågberg, L., and Carlmark, A. (2013). Thermo-responsive nanofibrillated cellulose by polyelectrolyte adsorption. *Eur. Polym. J.* *49*, 2689–2696.
- Lee, S.-D. (1987). A numerical investigation of nematic ordering based on a simple hard-rod model. *J. Chem. Phys.* *87*, 4972–4974.
- Lee, B.S., Chi, Y.S., Lee, K.-B., Kim, Y.-G., and Choi, I.S. (2007). Functionalization of poly (oligo (ethylene glycol) methacrylate) films on gold and Si/SiO<sub>2</sub> for immobilization of proteins and cells: SPR and QCM studies. *Biomacromolecules* *8*, 3922–3929.
- Li, F., Biagioni, P., Bollani, M., Maccagnan, A., and Piergiovanni, L. (2013). Multi-functional coating of cellulose nanocrystals for flexible packaging applications. *Cellulose* *20*, 2491–2504.
- Liang, H., Miranto, H., Granqvist, N., Sadowski, J.W., Viitala, T., Wang, B., and Yliperttula, M. (2010). Surface plasmon resonance instrument as a refractometer for liquids and ultrathin films. *Sens. Actuators B Chem.* *149*, 212–220.
- Lin, N., and Dufresne, A. (2014). Nanocellulose in biomedicine: current status and future prospect. *Eur. Polym. J.* *59*, 302–325.
- Liu, D., Chen, X., Yue, Y., Chen, M., and Wu, Q. (2011a). Structure and rheology of nanocrystalline cellulose. *Carbohydr. Polym.* *84*, 316–322.
- Liu, H., Wang, D., Song, Z., and Shang, S. (2011b). Preparation of silver nanoparticles on cellulose nanocrystals and the application in electrochemical detection of DNA hybridization. *Cellulose* *18*, 67–74.
- Lu, A., Hemraz, U., Khalili, Z., and Boluk, Y. (2014). Unique viscoelastic behaviors of colloidal nanocrystalline cellulose aqueous suspensions. *Cellulose* *21*, 1239–1250.
- Mao, Y., Liu, K., Zhan, C., Geng, L., Chu, B., and Hsiao, B.S. (2017). Characterization of Nanocellulose Using Small-Angle Neutron, X-ray, and Dynamic Light Scattering Techniques. *J. Phys. Chem. B* *121*, 1340–1351.
- Marchessault, R.H., Morehead, F.F., and Koch, M.J. (1961). Some hydrodynamic properties of neutral suspensions of cellulose crystallites as related to size and shape. *J. Colloid Sci.* *16*, 327–344.
- Mariano, M., El Kissi, N., and Dufresne, A. (2014). Cellulose nanocrystals and related nanocomposites: Review of some properties and challenges. *J. Polym. Sci. Part B Polym. Phys.* *52*, 791–806.
- Masci, G., Ladogana, R.D., and Cametti, C. (2012). Assemblies of Thermoresponsive Diblock Copolymers: Micelle and Vesicle Formation Investigated by Means of Dielectric Relaxation Spectroscopy. *J. Phys. Chem. B* *116*, 2121–2130.
- Naseri, N., Deepa, B., Mathew, A.P., Oksman, K., and Girandon, L. (2016). Nanocellulose-Based Interpenetrating Polymer Network (IPN) Hydrogels for Cartilage Applications. *Biomacromolecules* *17*, 3714–3723.
- Oksman, K., Mathew, A.P., Bismarck, A., Rojas, O., and Sain, M. (2014). *Handbook of Green Materials: Processing Technologies, Properties and Applications: Volume 5* (World Scientific).
- Onsager, L. (1949). The Effects of Shape on the Interaction of Colloidal Particles. *Ann. N. Y. Acad. Sci.* *51*, 627–659.
- Orts, W.J., Godbout, L., Marchessault, R.H., and Revol, J.-F. (1998). Enhanced Ordering of Liquid Crystalline Suspensions of Cellulose Microfibrils: A Small Angle Neutron Scattering Study. *Macromolecules* *31*, 5717–5725.
- Rånby, B.G. (1951). Fibrous macromolecular systems. Cellulose and muscle. The colloidal properties of cellulose micelles. *Discuss. Faraday Soc.* *11*, 158–164.

- Reid, M., Villalobos, M., and Cranston, E. (2016). Cellulose Nanocrystal Interactions Probed by Thin Film Swelling to Predict Dispersibility. *Nanoscale* 8, 12247–12257.
- Reid, M.S., Villalobos, M., and Cranston, E.D. (2017a). Benchmarking Cellulose Nanocrystals: From the Laboratory to Industrial Production. *Langmuir* 33, 1583–1598.
- Reid, M.S., Villalobos, M., and Cranston, E.D. (2017b). The Role of Hydrogen Bonding in Non-Ionic Polymer Adsorption to Cellulose Nanocrystals and Silica Colloids. *Curr. Opin. Colloid Interface Sci.* 29, 76–82.
- Revol, J.-F., Bradford, H., Giasson, J., Marchessault, R.H., and Gray, D.G. (1992). Helicoidal self-ordering of cellulose microfibrils in aqueous suspension. *Int. J. Biol. Macromol.* 14, 170–172.
- Revol, J.-F., Godbout, L., Dong, X.-M., Gray, D.G., Chanzy, H., and Maret, G. (1994). Chiral nematic suspensions of cellulose crystallites; phase separation and magnetic field orientation. *Liq. Cryst.* 16, 127–134.
- Rodahl, M., Höök, F., Krozer, A., Brzezinski, P., and Kasemo, B. (1995). Quartz crystal microbalance setup for frequency and  $Q$ -factor measurements in gaseous and liquid environments. *Rev. Sci. Instrum.* 66, 3924–3930.
- Roman, M. (2015). Toxicity of Cellulose Nanocrystals: A Review. *Ind. Biotechnol.* 11, 25–33.
- Salas, C., Nypelö, T., Rodriguez-Abreu, C., Carrillo, C., and Rojas, O.J. (2014). Nanocellulose properties and applications in colloids and interfaces. *Curr. Opin. Colloid Interface Sci.* 19, 383–396.
- Sanna, R., Fortunati, E., Alzari, V., Nuvoli, D., Terenzi, A., Casula, M.F., Kenny, J.M., and Mariani, A. (2013). Poly(N-vinylcaprolactam) nanocomposites containing nanocrystalline cellulose: a green approach to thermoresponsive hydrogels. *Cellulose* 20, 2393–2402.
- Sauerbrey, G.Z. (1959). Use of quartz vibration for weighing thin films on a microbalance. *J Phys.* 155, 206–212.
- Schasfoort, R.B.M., and Tudos, A.J. (2008). *Handbook of Surface Plasmon Resonance* Royal Society of Chemistry (London).
- Schattling, P., D. Jochum, F., and Theato, P. (2014). Multi-stimuli responsive polymers – the all-in-one talents. *Polym. Chem.* 5, 25–36.
- Schild, H.G. (1992). Poly(N-isopropylacrylamide): experiment, theory and application. *Prog. Polym. Sci.* 17, 163–249.
- Schütz, C., Agthe, M., Fall, A.B., Gordeyeva, K., Guccini, V., Salajková, M., Plivelic, T.S., Lagerwall, J.P.F., Salazar-Alvarez, G., and Bergström, L. (2015). Rod Packing in Chiral Nematic Cellulose Nanocrystal Dispersions Studied by Small-Angle X-ray Scattering and Laser Diffraction. *Langmuir* 31, 6507–6513.
- Senff, H., and Richtering, W. (1999). Temperature sensitive microgel suspensions: Colloidal phase behavior and rheology of soft spheres. *J. Chem. Phys.* 111, 1705–1711.
- Shafiei-Sabet, S., Hamad, W.Y., and Hatzikiriakos, S.G. (2012). Rheology of nanocrystalline cellulose aqueous suspensions. *Langmuir ACS J. Surf. Colloids* 28, 17124–17133.
- Shafiei-Sabet, S., Hamad, W.Y., and Hatzikiriakos, S.G. (2014). Ionic strength effects on the microstructure and shear rheology of cellulose nanocrystal suspensions. *Cellulose* 21, 3347–3359.
- Siqueira, G., Bras, J., and Dufresne, A. (2010a). Cellulosic Bionanocomposites: A Review of Preparation, Properties and Applications. *Polymers* 2, 728–765.
- Siqueira, G., Tapin-Lingua, S., Bras, J., Perez, D. da S., and Dufresne, A. (2010b). Morphological investigation of nanoparticles obtained from combined mechanical shearing, and enzymatic and acid hydrolysis of sisal fibers. *Cellulose* 17, 1147–1158.

- Siqueira, G., Bras, J., and Dufresne, A. (2010c). Cellulosic Bionanocomposites: A Review of Preparation, Properties and Applications. *Polymers* 2, 728–765.
- Stieger, M., Pedersen, J.S., Lindner, P., and Richtering, W. (2004). Are Thermoresponsive Microgels Model Systems for Concentrated Colloidal Suspensions? A Rheology and Small-Angle Neutron Scattering Study. *Langmuir* 20, 7283–7292.
- Sunasee, R., Hemraz, U.D., and Ckless, K. (2016). Cellulose nanocrystals: a versatile nanoplatform for emerging biomedical applications. *Expert Opin. Drug Deliv.* 13, 1243–1256.
- Suzuki, H., Nurul, H.M., Seki, T., Kawamoto, T., Haga, H., Kawabata, K., and Takeoka, Y. (2010). Precise Synthesis and Physicochemical Properties of High-Density Polymer Brushes designed with Poly( *N* - isopropylacrylamide). *Macromolecules* 43, 9945–9956.
- Tang, J., Sisler, J., Grishkewich, N., and Tam, K.C. (2017). Functionalization of cellulose nanocrystals for advanced applications. *J. Colloid Interface Sci.* 494, 397–409.
- Terech, P., Chazeau, L., and Cavaille, J.Y. (1999). A Small-Angle Scattering Study of Cellulose Whiskers in Aqueous Suspensions. *Macromolecules* 32, 1872–1875.
- Tripathy, S.K., Kumar, J., and Nalwa, H.S. (2002). *Handbook of Polyelectrolytes and Their Applications: Applications of polyelectrolytes and theoretical models* (American Scientific Publishers).
- Ureña-Benavides, E.E., Ao, G., Davis, V.A., and Kitchens, C.L. (2011). Rheology and Phase Behavior of Lyotropic Cellulose Nanocrystal Suspensions. *Macromolecules* 44, 8990–8998.
- Utsel, S., Malmström, E.E., Carlmark, A., and Wågberg, L. (2010). Thermoresponsive nanocomposites from multilayers of nanofibrillated cellulose and specially designed *N*-isopropylacrylamide based polymers. *Soft Matter* 6, 342–352.
- Voinova, M.V., Rodahl, M., Jonson, M., and Kasemo, B. (1999). Viscoelastic acoustic response of layered polymer films at fluid-solid interfaces: continuum mechanics approach. *Phys. Scr.* 59, 391–396.
- Vuoriluoto, M., Orelma, H., Johansson, L.-S., Zhu, B., Poutanen, M., Walther, A., Laine, J., and Rojas, O.J. (2015). Effect of Molecular Architecture of PDMAEMA–POEGMA Random and Block Copolymers on Their Adsorption on Regenerated and Anionic Nanocelluloses and Evidence of Interfacial Water Expulsion. *J. Phys. Chem. B* 119, 15275–15286.
- Way, A.E., Hsu, L., Shanmuganathan, K., Weder, C., and Rowan, S.J. (2012). pH-Responsive Cellulose Nanocrystal Gels and Nanocomposites. *ACS Macro Lett.* 1, 1001–1006.
- Wu, Q., Meng, Y., Wang, S., Li, Y., Fu, S., Ma, L., and Harper, D. (2014). Rheological Behavior of Cellulose Nanocrystal Suspension: Influence of Concentration and Aspect Ratio. *J. Appl. Polym. Sci.* 131, 40525.
- Wu, W., Huang, F., Pan, S., Mu, W., Meng, X., Yang, H., Xu, Z., Ragauskas, A.J., and Deng, Y. (2015). Thermo-responsive and fluorescent cellulose nanocrystals grafted with polymer brushes. *J. Mater. Chem. A* 3, 1995–2005.
- Xu, H.-N., Tang, Y.-Y., and Ouyang, X.-K. (2017a). Shear-Induced Breakup of Cellulose Nanocrystal Aggregates. *Langmuir* 33, 235–242.
- Xu, Y., Atrens, A.D., and Stokes, J.R. (2017b). Rheology and microstructure of aqueous suspensions of nanocrystalline cellulose rods. *J. Colloid Interface Sci.* 496, 130–140.
- Yang, H., Zhu, H., Hendrix, M.M.R.M., Lousberg, N.J.H.G.M., de With, G., Esteves, A.C.C., and Xin, J.H. (2013a). Temperature-Triggered Collection and Release of Water from Fogs by a Sponge-Like Cotton Fabric. *Adv. Mater.* 25, 1150–1154.

- Yang, X., Bakaic, E., Hoare, T., and Cranston, E.D. (2013b). Injectable Polysaccharide Hydrogels Reinforced with Cellulose Nanocrystals: Morphology, Rheology, Degradation, and Cytotoxicity. *Biomacromolecules* *14*, 4447–4455.
- Zeinali, E., Haddadi-Asl, V., and Roghani-Mamaqani, H. (2014). Nanocrystalline cellulose grafted random copolymers of N-isopropylacrylamide and acrylic acid synthesized by RAFT polymerization: effect of different acrylic acid contents on LCST behavior. *RSC Adv.* *4*, 31428–31442.
- Zhou, C., Wu, Q., and Zhang, Q. (2011). Dynamic rheology studies of in situ polymerization process of polyacrylamide–cellulose nanocrystal composite hydrogels. *Colloid Polym. Sci.* *289*, 247–255.
- Zoppe, J.O., Habibi, Y., Rojas, O.J., Venditti, R.A., Johansson, L.-S., Efimenko, K., Österberg, M., and Laine, J. (2010). Poly(N-isopropylacrylamide) Brushes Grafted from Cellulose Nanocrystals via Surface-Initiated Single-Electron Transfer Living Radical Polymerization. *Biomacromolecules* *11*, 2683–2691.
- Zoppe, J.O., Venditti, R.A., and Rojas, O.J. (2012). Pickering emulsions stabilized by cellulose nanocrystals grafted with thermo-responsive polymer brushes. *J. Colloid Interface Sci.* *369*, 202–209.
- Zubik, K., Singhsa, P., Wang, Y., Manuspiya, H., and Narain, R. (2017). Thermo-Responsive Poly(N-Isopropylacrylamide)-Cellulose Nanocrystals Hybrid Hydrogels for Wound Dressing. *Polymers* *9*, 119.

# Chapter IV

## Smart materials and CNCs

---



## Table of content

<b>Introduction</b> .....	245
<b>1. Cellulose nanocrystals as new bio-based coating layer for improving fiber-based mechanical &amp; barrier properties</b> .....	247
1.1. Introduction.....	248
1.2. Materials and Methods .....	249
1.2.1. Materials.....	249
1.2.2. CNCs suspension characterization .....	250
1.2.3. Coating process .....	251
1.2.4. Paper characterization.....	251
1.3. Results and Discussion.....	253
1.3.1. CNC characterization .....	253
1.3.2. The impact of the coating process on structural properties of samples .....	254
1.3.3. Influence of CNC coating on mechanical, texture and surface properties of paper....	259
1.3.4. Barrier properties of CNC-coated paper samples .....	262
1.3.5. The effect of PEG addition on barrier properties of paper .....	265
1.4. Conclusion .....	267
<b>2. Thermo-reversible cellulose nanocrystals system coated on cellulosic substrate: a water reversible surface</b> .....	269
2.1. Introduction.....	269
2.2. Materials and Methods .....	271
2.2.1. Materials.....	271
2.2.2. Carboxylation of cellulose nanocrystals by TEMPO oxidation .....	272
2.2.3. Synthesis of PDMAEMA-co-PDEGMA block copolymer with ATRP .....	272
2.2.4. Thermo-reversible system based on polymer adsorption on TEMPO CNCs .....	272
2.2.5. Adsorption experiments using the Quartz Crystal Microbalance with dissipation (QCM-d)	272
2.2.6. Coating process .....	273
2.2.7. Contact angle.....	273
2.3. Results and discussion .....	273
2.3.1. Polymers adsorption.....	273
2.3.2. Thermo-reversible surface with Pnipam <sub>2500</sub> .....	274
2.3.3. Surface comparison .....	277
2.4. Conclusion .....	278

<b>3. Thermo-responsive hydrogel based on Cellulose nanocrystals for injectable applications ...</b>	<b>279</b>
3.1. Introduction.....	279
3.2. Materials and Methods .....	281
3.2.1. Materials.....	281
3.2.2. Carboxylation of cellulose nanocrystals by TEMPO oxidation .....	281
3.2.3. Hydrogel system preparation .....	281
3.2.4. Hydrogel rheological measurements .....	282
3.2.5. Hydrogels test of injection in PBS .....	282
3.3. Results and discussions on hyaluronic acid hydrogels .....	283
3.3.1. Impact of TEMPO CNCs on HA hydrogels .....	283
3.3.2. Thermo-responsive Pnipam <sub>5500</sub> effect on HA hydrogels .....	285
3.3.3. Discussion on thermo-responsive hydrogels based on diblock and TEMPO CNCs for injectable applications.....	289
3.4. Conclusions.....	292
<b>Conclusions .....</b>	<b>293</b>
<b>References .....</b>	<b>295</b>

# IV. Smart materials and CNCs

## Introduction

In the *Chapter I*, a review of applications for hydrogel based on CNCs were presented in details. Thermo-responsive hydrogels based on CNCs were only slightly investigated in literature. In this context our fourth objective takes place: (iv) the development of “smart” and high added values applications with thermo-responsive CNCs hydrogels.

To complete the chemical grafting of thermo-responsive polymer on CNCs (*Chapter II*) and the rheological behavior of such system (*Chapter III*), this *Chapter IV* investigates the potential applications of our thermo-responsive hydrogels.

In the first part (*Chapter IV.1*), the influence of classic CNCs coating on paper is studied. This cellulosic layer modifies the surface and should improve mechanical and barrier properties of substrate.

Then, after incorporation of thermo-responsive polymer (PNIPAM or diblock) in the CNCs hydrogel, the coated surface properties will be investigated in *Chapter IV.2*. In particular, the hydrophobic-hydrophilic properties of the surface are tested.

A final part (*Chapter IV.3*) will developed the potential applications in biomedical field for injectable system. The idea is to take advantages of the thermo-reversibility of our hydrogels to facilitate the injection through a syringe needle but produce a strong and well organize gel inside the body. Tests are carried out with hyaluronic acid and/or with our best CNCs polymer system. The chapter is mainly some proofs of concept that this CNCs and their thermo-sensitive systems could be of interest for some smart applications.



# 1. Cellulose nanocrystals as new bio-based coating layer for improving fiber-based mechanical & barrier properties

*This section is adapted from “Erwan GICQUEL, Céline MARTIN, José GARRIDO YANEZ, Julien BRAS - Cellulose nanocrystals as new bio-based coating layer for improving fiber-based mechanical & barrier properties. Journal of Materials Science 52, 6 2017”*

## ABSTRACT

Cellulose nanocrystal (CNC) materials have several environmental advantages (e.g., these materials are bio-based, biodegradable, and biocompatible) but can also provide strong reinforcement, a strong barrier, or a specific physical color by self-organization. Meanwhile, industries are undergoing constant innovation and require a new packaging solution. New bio-based and high-performance water-based coatings are expected for example in the fiber-based industry. In response to these demands, in this study, we explored the elaboration of new smart paper by coating fiber-based materials with CNC for possible use in packaging. Particularly, we investigated application of a 100% CNC layer onto a substrate. Mainly due to the cost and limited availability of CNC on a large scale, few studies have examined these opportunities. Other challenges are the possible orientation of CNC under shear stress and stiffness of the final coating layer.

In this study, several layers of CNC were deposited onto a paper material using the bar-coating process to improve relevant properties of the paper surface. Surface analyses (atomic force microscopy, scanning electron microscopy, and transmission electron microscopy) were performed to elucidate the CNC network at the paper surface. Structural and mechanical properties of the final materials were evaluated. New results were obtained about the organization of CNC on paper during the coating. In addition, results of general interest were obtained about barrier properties. The air barrier and grease resistance of this new smart paper impart new properties only to the paper coated with CNC. To complete this research, a small amount of polyethylene glycol was added to reinforce the brittle CNC coating and to improve barrier properties of the paper.

**Keywords:** Cellulose nanocrystals, Nanocrystals, paper coating, barrier properties

## 1.1. Introduction

Cellulose nanocrystals (CNC) have attracted the interest of researchers for several decades since they were discovered by Rånby et al. (Rånby and Ribic, 1950) and Marchessault et al. (Marchessault et al., 1959) in the 60s. The attention given to CNC increased recently in particular in the broad field of materials science and new technologies, owing to industrialization of CNC starting in 2010. It is possible to buy such CNC in a large quantity and implement new high-value applications. Indeed, a lot of reviews on CNC (Eichhorn et al., 2010; Habibi et al., 2010; Moon et al., 2011), on hydrogels & aerogels (Yang et al., 2015), nanocomposites (Dufresne, 2013a; Klemm et al., 2011; Siqueira et al., 2010), and on biomedical materials (Domingues et al., 2014; Lin and Dufresne, 2014; Lin et al., 2016) clearly reveal interest in various CNC applications. It is worth noting the exponential increase in the number of patents concerning a large range of practical applications of CNC (Charreau et al., 2013; García et al., 2016).

Bio-based nanoparticles are obtained by acid hydrolysis of a cellulosic material (e.g., wood, cotton, ramie, sisal, and tunicate). The amorphous part of cellulose is removed by this process, and pure nanocrystals are obtained after sonication of the batch.

CNC are favorable in terms of biodegradability, renewability, and abundance but also well-defined dimensions and excellent mechanical properties (Siqueira et al., 2010). CNC are characterized by their high elastic modulus ( $\sim 150 \pm 50$  GPa) and high tensile strength ( $\sim 7.5$  GPa). Moreover, CNC have a high aspect ratio: a diameter of  $\sim 5$  nm to several tens of nanometers and length of  $\sim 100$  nm to a few micrometers (Habibi et al., 2010). Both dimensions depend mainly on the cellulose sources (Bras et al., 2011). These specifics interest researchers historically mainly in relation to addition of nanocellulose to a polymer matrix to reinforce mechanical properties of the polymer (Herrera et al., 2014; Lee et al., 2014; Mariano et al., 2014).

As for cellulose nanofibrils (CNF) and their use in paper, two reviews were recently published (Bardet and Bras, 2014; Brodin et al., 2014), whereas nothing is available on CNC in this field. This is due to the smaller dimensions (mainly in the length) that prevent the use of CNC in the wet-end part of the process without very low retention in the bulk of paper. Indeed, the only possibility is to use CNC as a coating or impregnation suspension. Addition of a small

amount of CNC to a polymer matrix is being studied visually to improve a film's mechanical or barrier properties (Paralikar et al., 2008; Roohani et al., 2008; Siqueira et al., 2009). Nonetheless, CNC are rarely used alone or in a slurry with subsequent coating of a cellulosic substrate (Aspler et al., 2015). To the best of our knowledge, no scientific papers deal with this concept, and there are only a few conference papers on this topic (Gicquel et al., 2016a, 2016b).

Some coatings of plastic films have proven to have beneficial effects on the gas barrier. For example, one research group (Mascheroni et al., 2016) confirmed a positive impact of polyethylene terephthalate PET: a decrease in oxygen permeability by several percentage points (down to 90%). Nonetheless, contrary to CNF already applied to films (Fujisawa et al., 2011) or to paper (Aulin and Ström, 2013; Lavoine et al., 2014a; Rodionova et al., 2010) for improvement of barrier properties, only a few research papers describe coating of a substrate with a 100% CNC layer. Some studies deal with roughness and printing applications (Penttilä et al., 2013) or antifog effects on a film (Li et al., 2013). This state of affairs is also due to the cost, the limited availability of CNC on a large scale, or the very low solid content of suspensions. This situation is changing at present.

This study addresses coating of a cellulosic substrate with CNC. In particular, the coating of paper with CNC alone is studied by means of a coating process to investigate surface and barrier properties. A neutral polymer was also used to improve the layer flexibility and prevent surface fractures.

## **1.2. Materials and Methods**

### **1.2.1. Materials**

Commercial CNC were delivered as a colloidal suspension. It was purchased from the UMaine Process Development Center (University of Maine, USA) and had been produced from wood pulp using the sulfuric acid hydrolysis process. The dry matter of the commercial CNC suspension was 10%wt, as measured by means of a moisture analyzer (Ohaus® MB-35, Sigma-Aldrich, USA).

The base paper material was uncoated and non-calendered paper with a basis weight of  $56 \text{ g}\cdot\text{m}^{-2}$ , kindly provided by an industrial partner. It is classically used as a substrate to be coated for packaging applications.

Polyethylene glycol (PEG) with the molecular weight of 200 g/mol was purchased from Sigma-Aldrich (USA). Deionized water was used in all experiments ( $5 \text{ }\mu\text{S}/\text{cm}$ ).

### 1.2.2. CNCs suspension characterization

**Atomic force microscopy (AFM):** Individual nanoparticles of the colloidal suspension were imaged using an atomic force microscope (Dimension icon<sup>®</sup>, Bruker, USA). All samples were diluted to  $10^{-4}$  wt% beforehand, and a drop of 0.2 mL was deposited onto a freshly cleaved mica plate. Samples were dried overnight under ambient conditions. Those samples were characterized in tapping mode using a silica-coated cantilever (OTESPA<sup>®</sup> 300 kHz - 42 N/m, Bruker, USA). Scans of  $10 \times 10 \text{ }\mu\text{m}^2$  and  $3.3 \times 3.3 \text{ }\mu\text{m}^2$  were performed to analyze dimensions of CNC. At least 4 images per sample were obtained, and the most representative one was selected for the figures. To measure dimensions of a CNC,  $\sim 200$  measurements were performed in the software ImageJ<sup>®</sup> to obtain a representative average.

**Transmission electron microscopy (TEM):** Drops of  $\sim 0.001$  wt% of a CNC suspension were deposited onto glow-discharged carbon-coated TEM grids. After 2 minutes, the excess liquid was absorbed with filter paper, and prior to drying, a drop of Urany-Less (Delta Microscopies, France) was deposited on the specimen. After 2 minutes, the excess solution was aspirated, and the grid was dried at room temperature. The samples were examined using a Philips CM200 (FEI, USA) operating at 200 kV. At least 3 images per sample were captured, and the most representative ones were selected for the figures.

**Suspension viscosity:** The rheology behavior of the CNC suspensions under shear was studied using a rotational rheometer from Anton-Paar (Physica MCR 301, Austria). The tests were carried out at a temperature of  $20^\circ\text{C}$ . Start-up shearing tests were performed with a cone-plate configuration (diameter of 50mm and angle of  $1^\circ$ ). The atmosphere around the sample was saturated with water to avoid evaporation during the measurement. In these start-up tests, a constant shear stress was suddenly applied to the sample whose initial state is controlled. The transient response under shear was recorded until steady conditions were

achieved. The shear rate values in the steady regime were then used to establish flow curves for the dispersions under shear.

### 1.2.3. Coating process

The CNC suspension at 10%wt was applied directly to paper samples (A4 format in the machine direction) with a bar-coating process (Endupap, France). A smooth Mayer bar was used with a coating speed of  $5 \text{ cm}\cdot\text{s}^{-1}$ . Then, coated paper samples were dried under tension by means of a contact drying system at  $105^\circ\text{C}$  for 3 min. These steps were repeated one to eight times in order to improve application of CNC layers to paper. As reference samples, paper samples were coated with deionized water by following the same experimental conditions. Reference samples were treated the same number of times as the CNC-coated samples.

In the last part of this study, PEG was added to the CNC slurry before coating. PEG at  $200 \text{ g}\cdot\text{mol}^{-1}$  was in liquid form. The CNC suspension and the PEG solution were mixed with a homogenizer (Ultraturrax T8®, IKA, France) for 3 minutes at room temperature. Then, the slurry was degassed in an ultrasound bath for 5 minutes.

### 1.2.4. Paper characterization

Each sample was maintained at a temperature of  $23^\circ\text{C}$  and relative humidity of 50% for at least 24 h before characterization.

**Weight:** According to the ISO standard 534:2011, the basic weight and the CNC coating weight for each sample were determined by measuring the weight of at least 10 samples of  $10 \times 10 \text{ cm}^2$  on a digital scale (Mettler Toledo,  $\pm 0.0001 \text{ g}$  of precision). The final data in this paper represent an average of at least 10 measurements.

**Thickness:** According to the ISO standard 536:2011, the sample thickness was determined with a micrometer (Adamel Lhomargy,  $\pm 0.001 \text{ mm}$  precision) and is presented as an average of at least 10 measurements for each  $10 \times 10 \text{ cm}^2$  sample.

**Scanning electron microscopy (SEM):** For each sample, CNC-coated paper or base paper, a cross-section and surface were examined in SEM images (Quanta200®, FEI, the Netherlands). Cross-sections of the samples were obtained by placing the samples between two pieces of

paper on each side to prevent rounding of the edges caused by the pressure exerted by the razor's edge. The samples were mounted onto a metallic substrate recovered with carbon tape. To analyze a specimen by SEM, the specimen was slightly coated with an Au/Pb charge in order to obtain a conductive surface. The Everhart Thornley – Secondary electron detector (ETD) was also used for coated paper surfaces. The working distance was 10.0 mm with voltage of 10.0 kV at the magnification of  $\times 100$  or  $\times 400$  for surfaces and  $\times 600$  or  $\times 2500$  for cross-sections. At least 10 images were captured per sample, and the most representative ones were selected for the figures.

**Field emission gun-scanning transmission electron microscopy (FEG-STEM):** This method was used to complete SEM pictures for strong focus on the paper surface. Samples were prepared by fixing a paper sample on a metallic substrate. Images were obtained on a Zeiss Ultra 55<sup>®</sup> microscope in secondary electron mode, at accelerating voltage (EHT) of 5 kV and a working distance of 6.3 mm. Magnification of 50 000 was attained, and at least 5 images per sample were recorded.

**AFM:** Smaller pieces ( $5 \times 5 \text{ mm}^2$ ) of CNC-coated paper varieties were glued onto an aluminum plate. The samples were characterized in tapping mode. Pictures were recorded under ambient conditions (temperature and relative humidity). At least 4 images per sample were obtained.

**Tensile stiffness test:** Using a method adapted from the ISO standard 1924-2/3, samples were studied by means of a Lorentzen & Wettre<sup>®</sup> Tensile Tester (Sweden). The speed was fixed at  $10 \text{ mm}\cdot\text{min}^{-1}$ , and the sample initial length was 100 mm. Under the standard conditions of humidity and temperature, Young's modulus, breaking length, and elongation at break of each sample were measured. At least 6 measurements were carried out to obtain an average value.

**Bending stiffness:** It was measured with a Kodak stiffness tester (Lhomargy<sup>®</sup>, France) using ISO standard 5629 with an average based on at least 6 specimens.

**Burst Index:** The burst index (Adamel Lhomargy EC 0.5, France) was evaluated according to the ISO standard 2758/2759. Six measurements were done for each sample to obtain an average value.

**Surface gloss:** It was quantified using REFO Gloss meters (Lange). Three angles were evaluated: 20°, 60°, and 85°, according to the ISO standard 2813:2014. At least 4 measurements were carried out to obtain an average.

**Grease test TAPPI:** According to the standard T-454, the grease penetration into the sample was measured with red turpentine oil. The examination of the oil penetration was conducted every 15 seconds for the first minutes, then once a minute during 5 minutes.

**Air permeability:** According to the ISO standard 5636, paper samples were tested by means of the system of “Mariotte” vases. The tests were conducted using a sample area of 2 cm<sup>2</sup> and a vacuum of 2.5 kPa. At least five measurements were done to calculate an average value.

**Oxygen permeability (PO<sub>2</sub>):** According to the standard ASM F1927-07, PO<sub>2</sub> was monitored at 23°C and relative humidity of 0% by the equal pressure method and on an oxygen permeation analyzer (Systech ILLINOIS, M8001 oxygen permeation analyser®). The samples were conditioned for 24 h at room temperature. The specific exchange surface was 3.14 cm<sup>2</sup>. The assessments were run until stable values were obtained. The experiments were carried out in duplicate.

## 1.3. Results and Discussion

### 1.3.1. CNC characterization

It is well known that CNC have a rodlike shape, as confirmed by characterization in **Figure 1**. Measurements showed the average length of  $150 \pm 30$  nm and a section thickness of  $10 \pm 5$  nm. These values are in line with the literature data on CNC from wood pulp (Habibi et al., 2010). At high concentrations of CNCs in the suspension, a gel-like substance was obtained judging by visual inspection.

Because CNC are obtained by sulfuric acid hydrolysis, it is possible that a part of the cellulose was transformed into cellulose II. To test this hypothesis, <sup>13</sup>C nuclear magnetic resonance (NMR) analysis was performed (not shown), and the presence of 15% of cellulose II and 85% of cellulose I was confirmed. It is important to know the viscosity of this suspension to confirm its suitability for coating. In the paper industry, the classic coating slurry has

consisted of pigments, a binder (non-biodegradable), and water. In contrast, the CNC suspension is only composed of water and nanocrystals (100% biodegradable). In this study, the concentration of the CNC suspension was 10 %wt, and the values obtained without sonication are 320 Pa·s and 0.08 Pa·s for shear rates of 0.1 and 1000 s<sup>-1</sup>, respectively, showing obvious shear thinning behavior, in agreement with the literature data (Bercea and Navard, 2000).

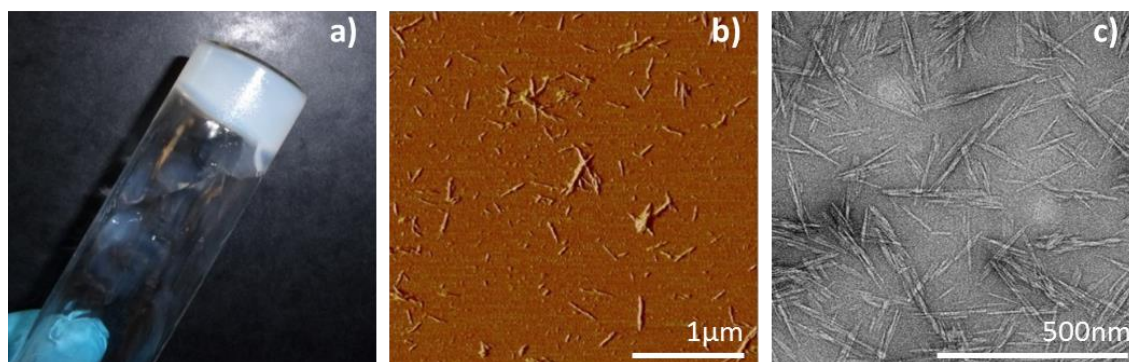


**Figure 1** Characterization of CNC: (a) picture of the CNC suspension (10%wt), (b) AFM image and (c) TEM image from wood pulp.

The viscosity was in agreement with our expectations for coating of paper substrates. A more detailed study on CNC suspension rheology and organization under shear stress was recently presented by our team using SAXS (Small-Angle X-ray Scattering) and a rheometer (Pignon, 2016).

### 1.3.2. The impact of the coating process on structural properties of samples

The CNC suspension is composed of 90%wt of water. During the one-sided coating process, a major part of water will be introduced into paper (throughout full thickness) and will thus influence the fiber network. Multiple drying steps will also strongly affect paper structure as detailed recently in a study on coating with a CNF suspension (Lavoine et al., 2014b). Regarding the results presented in this section, a paper substrate after 4 coating procedures with CNC is compared with the paper after 4 coatings with water to evaluate the water deformation effects in the material. Characterization by SEM, FEG-STEM, and AFM was carried out to obtain qualitative and quantitative data about the coating surface.

With only one layer of coating, the CNC coat weight is extremely low ( $\sim 0.10 \text{ g}\cdot\text{m}^{-2}$ ). It cannot even be observed on SEM pictures (**Figure 2**). To increase the coat weight without increasing

the concentration of CNC in the suspension, several CNC layers were applied one by one (after drying of each layer). For four and eight CNC coatings, a coat weight of almost  $2.6 \pm 0.3$  and  $4.6 \pm 0.9 \text{ g}\cdot\text{m}^{-2}$ , respectively, was reached. The surface of paper samples was clearly recovered by CNC as depicted in **Figure 2**. **Table 1** details the coat weights for increasing numbers of CNC layers and water layers.

Some researchers (Lavoine et al., 2014b) showed similar results in the case of CNF, using bar coating and a size press process. After 5 layers of CNF, almost  $5 \text{ g}\cdot\text{m}^{-2}$  was deposited onto the paper. Investigators need to keep in mind that the substrate (similar in the two studies) is considered an intermediate substrate without any previous sizing or a coating layer. Thus, no clear differences between the two types of nanocellulose were observed, even though the results are suggestive of greater penetration of CNC.

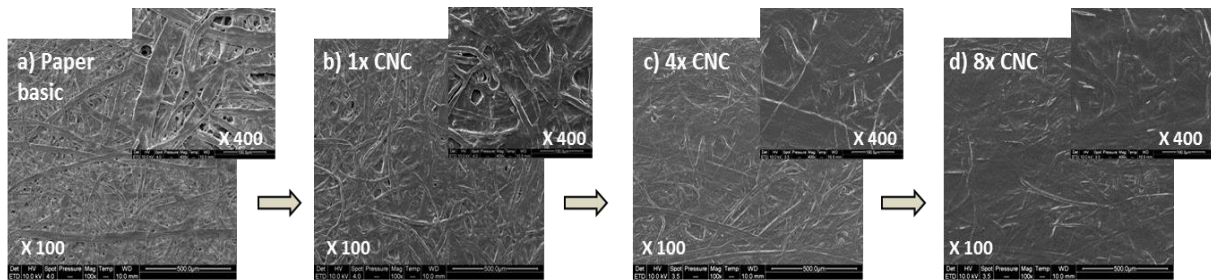


**Figure 2:** Surface SEM images ( $\times 100$  and  $\times 400$ ) of the base paper and the CNC coated samples using secondary electron detector: (a) base paper, (b) (c) and (d) paper samples with  $\times 1$ ,  $\times 4$ ,  $\times 8$  CNC coating respectively.

**Figure 3** illustrates multiscale analysis of the base paper surface versus paper coated with CNC. Each characterization method (SEM, FEG-STEM, and AFM) offers a different focus on the surface of the substrate from magnification  $100\times$  ( $\sim 1 \times 1 \text{ mm}^2$ ) to  $800\times$  ( $\sim 3 \times 3 \mu\text{m}^2$ ). Fig. 3b and 3f reveals that CNC have covered the surface of the substrates. This finding is confirmed by FEG-STEM and AFM figures showing in detail the surface of the substrate after coating. Picture 3d represents the paper base surface for dimensions  $3 \times 3 \mu\text{m}^2$ . The nanoroughness of the samples was  $\sim 195 \pm 20 \text{ nm}$ . In the case of a CNC-coated surface (Fig. 3h), these values decreased drastically to  $20 \pm 5 \text{ nm}$ . Coating a substrate with the CNC suspension remarkably changes nanoroughness of the surface by turning it into a smooth surface.

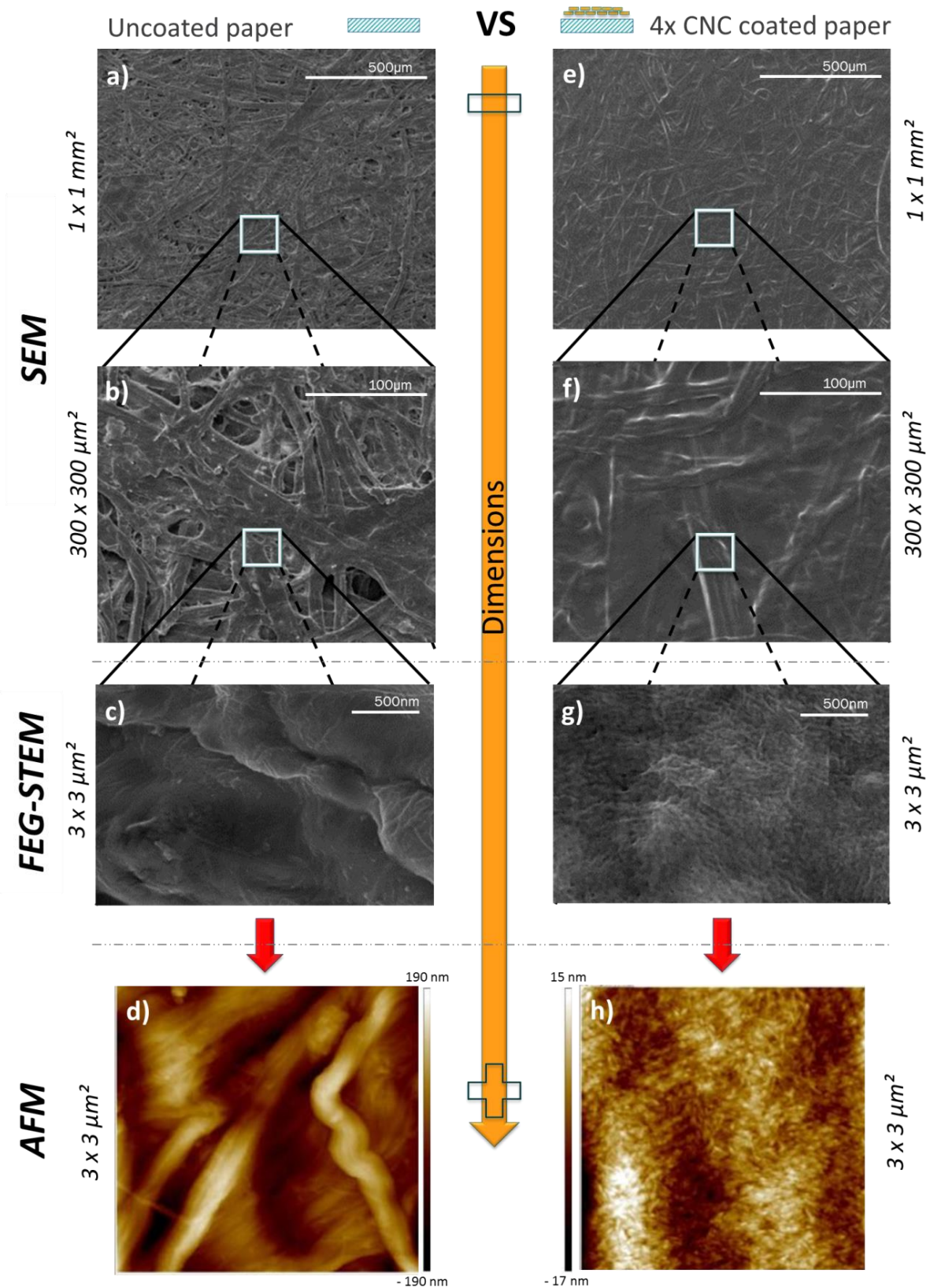


**Figure 3:** Multiscale microscopy analysis of the paper surface before and after the coating process with different tools: Surface analysis by SEM a) 1x1 mm<sup>2</sup> and b) 300x300 μm<sup>2</sup>, FEG-STEM c) 3x3 μm<sup>2</sup> and AFM d) 3x3 μm<sup>2</sup> for base paper after four water coatings and similar characterization after four coatings of a CNC suspension, respectively e), f), g) and h).

Surface analysis of a cross-section of paper was also conducted before and after coating. **Figure 4** shows that the CNC layers restore the surface by increasing smoothness and decreasing roughness. **Figure 4b** and more precisely **Figure 4e** shows the impact of water on the paper. In **Table 1**, data on paper coated with water or CNC are quite similar. By comparison with the base paper, thickness of each sample notably increased (from 15% to 22%). This increase is essentially due to the effect of successive wetting and drying cycles.

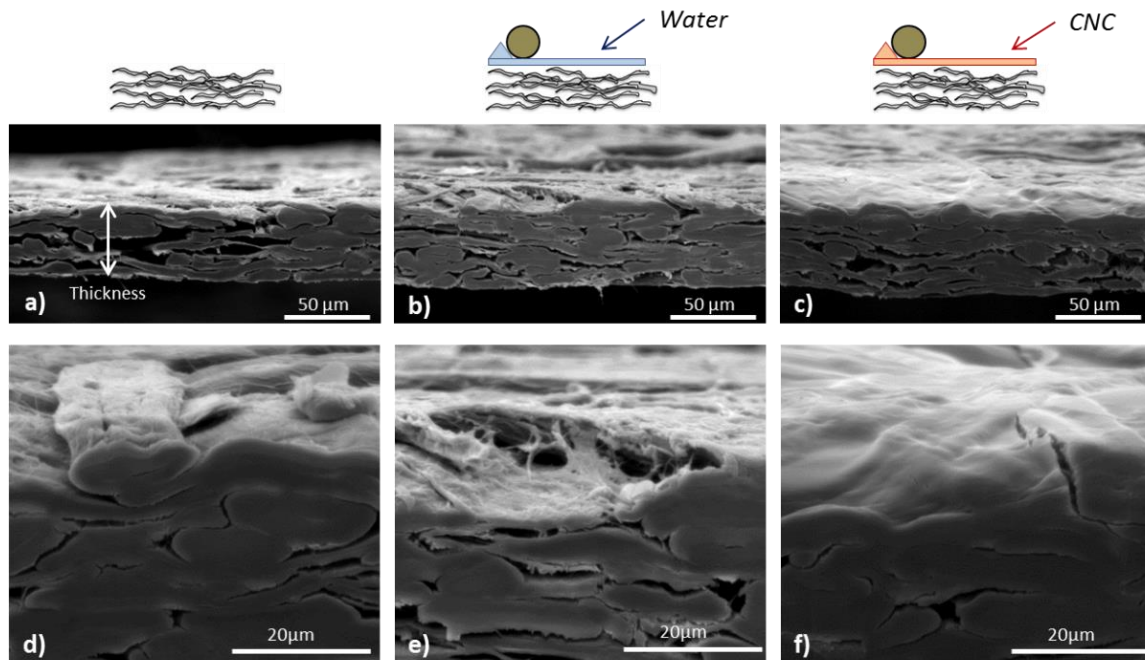


**Figure 4:** Two scales (magnitude  $\times 100$  and  $\times 400$ ) SEM images of the cross-section of base paper a)-d),  $\times 4$  water coated paper b)-e) and  $\times 4$  CNC-coated paper c)-f).

The presence of fractures and cracks obviously strongly influences the barrier properties of substrates. In the case of CNC coating, the surface is brittle because of the intrinsic CNC properties and structure. Contrary to CNF entanglement, CNC particles are stiff and unbending. Therefore, the network and the organization created during the coating are very rigid and brittle like CNC films, as shown in Fig. 4f. In the case of CNC, the mechanism is a stacking of rigid cellulose “bricks”, but it is entanglement of flexible cellulose “laces” for CNF. On the right side of this picture, the coat is split along the substrate fiber. These fractures will obviously have a strong impact on the barrier properties of samples.

Usually, a paper substrate is considered well-coated for barrier applications starting at the coat weight of  $\sim 8 \text{ g}\cdot\text{m}^{-2}$ . According to the standard deviations, in this study, only the samples coated 4 or 8 times will be studied, using as a reference the 4- and 8-time water-coated paper samples.

**Table 1** Comparison of the mechanical and surface properties of the water coated and CNC coated samples.

	Thickness ( $\mu\text{m}$ )		CNC coat weight ( $\text{g}\cdot\text{m}^{-2}$ )	Intrinsic permeability K ( $\text{nm}^2$ )	Gloss (% reflection of light) at $85^\circ$	Burst Index ( $\text{kPa}\cdot\text{m}^2\cdot\text{g}^{-1}$ )	Bending stiffness ( $\text{mN}\cdot\text{m}^{-1}$ )	
	Micrometer						MD	CD
Base paper	$56 \pm 2$		0	$10100 \pm 900$	$7,3 \pm 0,2$	$2,8 \pm 0,1$	0,07	0,03
1x H <sub>2</sub> O	$61 \pm 1$		0	$11520 \pm 654$	$7,2 \pm 0,3$	$3,2 \pm 0,1$	0,12	0,03
CNC	$60 \pm 1$		$0,10 \pm 0,05$	$4860 \pm 466$	$8,4 \pm 0,3$	$3,3 \pm 0,1$	0,06	0,03
4x H <sub>2</sub> O	$61 \pm 1$		0	$11860 \pm 460$	$5,9 \pm 0,3$	$3,2 \pm 0,1$	0,11	0,03
CNC	$62 \pm 1$		$2,56 \pm 0,25$	$880 \pm 300$	$9,6 \pm 0,7$	$3,4 \pm 0,1$	0,12	0,03
8x H <sub>2</sub> O	$62 \pm 1$		0	$17200 \pm 500$	$5,3 \pm 0,5$	$4,5 \pm 0,1$	0,15	0,05
CNC	$66 \pm 1$		$4,58 \pm 0,91$	$1160 \pm 333$	$13,8 \pm 3,3$	$4,3 \pm 0,1$	0,63	0,47

	Young's modulus (GPa)		Elongation at break (%)		Breaking length (km)		Tensile strength index ( $\text{Nm}\cdot\text{g}^{-1}$ )	
	MD	CD	MD	CD	MD	CD	MD	CD
Base paper	$7,8 \pm 0,4$	$3,7 \pm 0,1$	$1,5 \pm 0,1$	$4,2 \pm 0,3$	$6,2 \pm 0,3$	$3,3 \pm 0,1$	$60,3 \pm 2,5$	$32,5 \pm 1,0$
1x H <sub>2</sub> O	$5,9 \pm 0,2$	$2,8 \pm 0,2$	$1,6 \pm 0,1$	$4,5 \pm 0,3$	$6,1 \pm 0,2$	$3,5 \pm 0,1$	$59,5 \pm 2,4$	$34,2 \pm 0,8$
CNC	$6,4 \pm 0,1$	$2,7 \pm 0,2$	$1,7 \pm 0,1$	$4,7 \pm 0,3$	$6,6 \pm 0,1$	$3,4 \pm 0,1$	$64,8 \pm 1,0$	$33,4 \pm 1,2$
4x H <sub>2</sub> O	$5,4 \pm 0,3$	$2,6 \pm 0,1$	$1,8 \pm 0,2$	$4,0 \pm 0,7$	$6,0 \pm 0,1$	$3,3 \pm 0,1$	$58,9 \pm 0,2$	$31,9 \pm 1,1$
CNC	$5,3 \pm 0,3$	$2,5 \pm 0,3$	$2,0 \pm 0,2$	$5,3 \pm 0,2$	$6,3 \pm 0,1$	$3,4 \pm 0,1$	$61,9 \pm 0,3$	$32,9 \pm 1,3$
8x H <sub>2</sub> O	$5,5 \pm 0,6$	$2,8 \pm 0,3$	$1,7 \pm 0,1$	$4 \pm 0,2$	$5,8 \pm 0,4$	$3,4 \pm 0,1$	$57,3 \pm 4,0$	$33,2 \pm 1,4$
CNC	$6,2 \pm 0,4$	$2,3 \pm 0,3$	$1,9 \pm 0,3$	$4,9 \pm 0,4$	$6,0 \pm 0,4$	$3,2 \pm 0,1$	$58,8 \pm 3,5$	$31,6 \pm 0,4$

MD : Machine direction

CD : Cross direction

Paper basis weight :  $43.1 \pm 0.3 \text{ g}\cdot\text{m}^{-2}$

### 1.3.3. Influence of CNC coating on mechanical, texture and surface properties of paper

All the mechanical properties are summarized in **Table 1**.

Young's modulus of the paper samples is affected by the successive wetting/drying cycles. All values for water-treated paper samples (CNC or only water) are lower than Young's modulus value of the base paper. This phenomenon can be explained by penetration of water into the structure during the coating treatment. The network between fibers is irreversibly modified and the mechanical properties are slightly worsened.

Whatever the amount of CNC on the paper, Young's modulus slightly decreases because of the large amount of water (CNC solid content is only 10% w/w) in the process. The loss is almost 30% for machine and cross directions of the paper. The CNC coat weights deposited are not sufficient to counterbalance the effects of water treatment on the samples.

As expected, slight worsening of other mechanical properties (elongation at break, breaking length, and tensile strength) is also induced by these successive wetting/drying cycles in water. Some investigators have shown that the addition of CNF to the surface of paper (Lavoine et al., 2014a) or cardboard (Lavoine et al., 2014b) improves these properties. No clear effect of the presence or absence of CNCs in the coating can be deduced from the standard deviations in mechanical properties (**Table 1**). We can conclude that the stacking of CNC does not reinforce the structure as compared to the entanglement of CNF.

CNC are mainly deposited on the *surface* of samples. These coating layers should affect bending stiffness of the coated sample because the external layers usually influence bending more strongly than internal structure.

Wetting/drying cycles affect the bending stiffness whenever CNC are not used in the suspension for coating. Immediately after the first cycle, bending stiffness increased up to 71% for the water-treatment sample. Probably because of the volume mass of the paper, which increased by approximately 10% (**Table 1**), the bending needs more energy to find the vibration harmonic of the sample's structure. Bending stiffness is directly affected by this factor (thickness, volume mass). At the same time, drying of the sample has been implemented by contact and under tension in the machine direction of the substrate;

therefore, cellulose fibers are elongated in the sample and dry asymmetrically (yielding a larger number of OH-bonds on one side). These combined effects could explain the increase of the bending stiffness value.

In the case of the CNC-coated sample, **Table 1** shows improvement of the bending property of samples (maximum +900% for the 8× CNC coating). Values for machine direction vary from 0.07 mN·m<sup>-1</sup> for base paper to 0.15 for reference (water coated) and to 0.63 mN·m<sup>-1</sup> for CNC-coated paper. This strong increase is beneficial and is due to the creation of a CNC-organized film on the paper, which stiffens it. This stiffening of one paper side was confirmed by the burst index. This measure reflects resistance of the sample when pressure tries to break and blow up the surface. The tested sample with the higher bending stiffness and tensile strength is more resistant and has the highest burst index. This phenomenon is a combination of bulk and surface properties.

**Table 1** shows burst index values for both treated samples. In water-treated and CNC-coated samples, this value strongly increased from  $2.8 \pm 0.1$  kPa·m<sup>2</sup>·g<sup>-1</sup> for base paper to  $4.3 \pm 0.1$  kPa·m<sup>2</sup>·g<sup>-1</sup> for CNC-coated paper at  $\sim 5$  g·m<sup>-2</sup>. It is mainly caused by the successive wetting/drying cycles, which open the paper bulk and allow for greater deformation of the substrate under pressure. No obvious effect is noticeable in the presence of CNC on the paper.

As a conclusion the presence of CNC on the substrate does not significantly improve the bulk mechanical properties of the material, regardless of the number of CNC layers deposited, but strongly modifies the surface properties as shown for bending stiffness. That is why the next characterization experiments are focused on surface properties.

In the printing paper industry, gloss is an important property mainly for the magazine market. In this case, values of approximately 50-60 are expected. To increase the reflection percent value, it is necessary to add a metallic charge or a polymer to the surface (not always biosourced and renewable). In our case, the presence of CNC on the substrate clearly results in the ability to reflect light as shown in images in **Figure 5**.

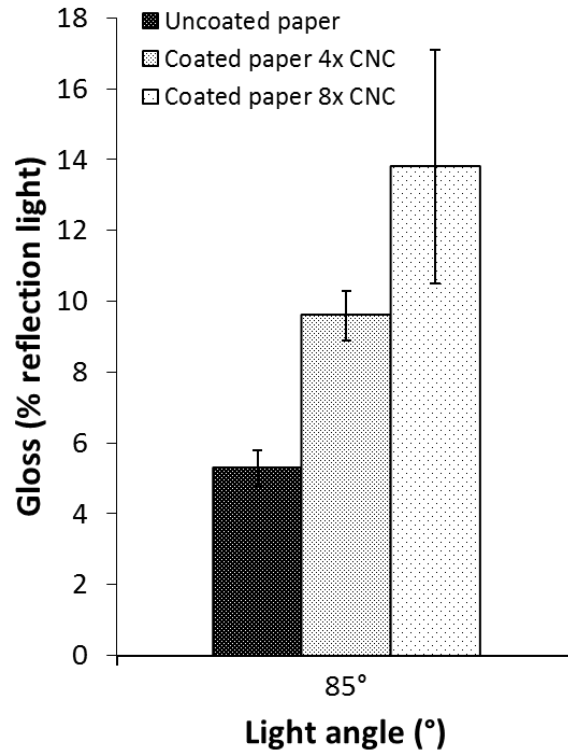


*Figure 5: Substrate gloss after successive CNC coating.*

The results on surface gloss are presented in **Table 1** and **Figure 5**. The testing involved evaluation of three angles. This study shows only the 85° gloss test, even if our reference paper sample is not adapted (very low starting gloss). The first observation is that the water-treated sample presents a smooth decrease in the brightness by ~20%. **Figure 2** shows the opening of the fiber network during wetting/drying cycles, which can explain this loss. As roughness increases, brightness decreases when the incident ray's power increases.

In the case of a CNC-coated surface, gloss increased with the number of CNC layers. These values are twofold higher for 4× CNC coating and threefold higher for 8× CNC layers.

By analyzing AFM pictures in **Figure 3**, readers can notice that the surface is smooth and the nanoroughness decreased drastically (195 to 20 nm). These gloss results favor the following conclusion: the CNC coating smooths out the surface and creates a fine network on the substrate. This seems to be the first report of such promising results. Even if gloss is still too low with this paper, other types of paper designed for printing have been tested; and a similar gloss increase was observed (proof of concept). CNC coating may be a bio-based solution for increased gloss but also to enable precise printing as shown recently in printed electronics (Hoeng et al., 2016). More detailed studies on this topic are in progress.

### 1.3.4. Barrier properties of CNC-coated paper samples

Another surface-related property can be the barrier to a liquid or gas, and it has been shown in various studies that nanocellulose (mainly CNFs) can strongly improve the gas or liquid barrier (Aulin et al., 2010; Brodin et al., 2014; Lavoine et al., 2012, 2014a; Li et al., 2013). In this study, different barrier properties (air, oxygen, and grease) have been evaluated in the water-treated and CNC-coated paper samples. The thickness values were measured with a micrometer, according to paper and paperboard standards on mechanical and barrier properties.

The analysis of the air permeability yields further information on the coating structure. It is one of the most affected barrier properties in the case of CNC-coating of paper. The results are presented in **Figure 6** and **Table 1**. The water-treated paper sample showed a strong increase in the air permeability as compared with the base paper, whereas in the CNC-coated sample, air permeability of the substrate was drastically decreased. To understand what happened, it is necessary to remember that water treatment damages the paper structure in particular by opening the fiber network; this change increases air permeability (after 8 rounds of water treatment, the permeability increases by ~70%). On the other hand, with the addition of 10%wt CNC during the bar-coating process, these values decreased by 91% (**Table 1**). The air resistance of the paper sample (intrinsic permeability of 10 000 nm<sup>2</sup>) was drastically improved (at the CNC coat weight of 2.5 g·m<sup>-2</sup>) to a value of ~880 ± 300 nm<sup>2</sup>. This value (corresponds to 4.6 g·m<sup>-2</sup>) is then modified: intrinsic permeability of ~1160 ± 330 nm<sup>2</sup>.

For a comparison with the work of another research group (Lavoine et al., 2014b) on CNF, it is necessary to have a coat weight of 8 g·m<sup>-2</sup> to improve the air resistance in an equal proportion. The thicknesses of the water-treated and CNC-coated paper samples are quite similar (**Table 1**); thus, the CNC coating clearly improves the air resistance of the paper substrate. As shown above (**Figure 3**), the network created by CNC on the substrate is highly dense and organized. It creates a smooth and strong surface that increases the air resistance of the sample coated with CNC. This observation indicates an increase in the tortuous path of the air and enhancement of the barrier properties. Because air permeability of the coating decreases with the increasing thickness of layers, and most pores are located at the surface

of the CNC layer, it follows that pores are not connected and contribute to the impermeable nature of the coating.

In the literature, numerous examples show the relation between crystallinity and permeability. Higher crystallinity is associated with lower permeability (McGonigle et al., 2004). Because CNC have a high crystallinity index ( $\sim 85 \pm 2\%$ ), this crystalline region is non-permeable and increases the path length of air diffusion.

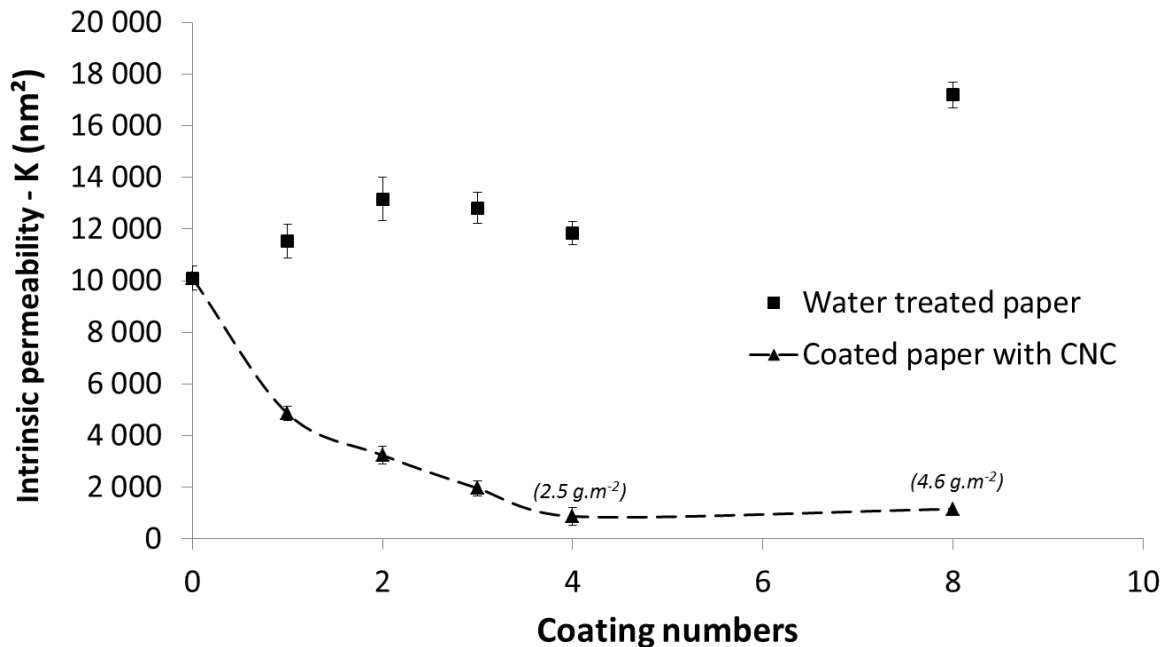


**Figure 6:** Air permeability of water-treated and CNC-coated paper samples as function of the number of coatings. The dark line with square (■) represents the water coated paper and the dash line with triangle (Δ) shows the CNC coated paper. The 0 coating number corresponds to the base paper.

Nevertheless, this obvious result on the air permeability of the CNC network on a substrate does not yield sufficient oxygen barrier properties (an experiment with an oxygen transmission rate test – OTR). The values are not measurable, i.e. higher than  $400 \text{ cm}^3 \cdot \text{m}^{-2} \cdot \text{day}^{-1} \cdot \text{kPa}^{-1}$  for paper but also for each CNC-coated sample. This situation is affected by the breakable network created by the CNC (**Figure 5f**). In the SEM pictures, some fractures are visible and have a size less than  $1 \mu\text{m}$ . Because the size of the oxygen molecule is about  $0.29 \text{ nm}$ , the network cannot block this particle alone, in contrast to the entangled network of CNF.

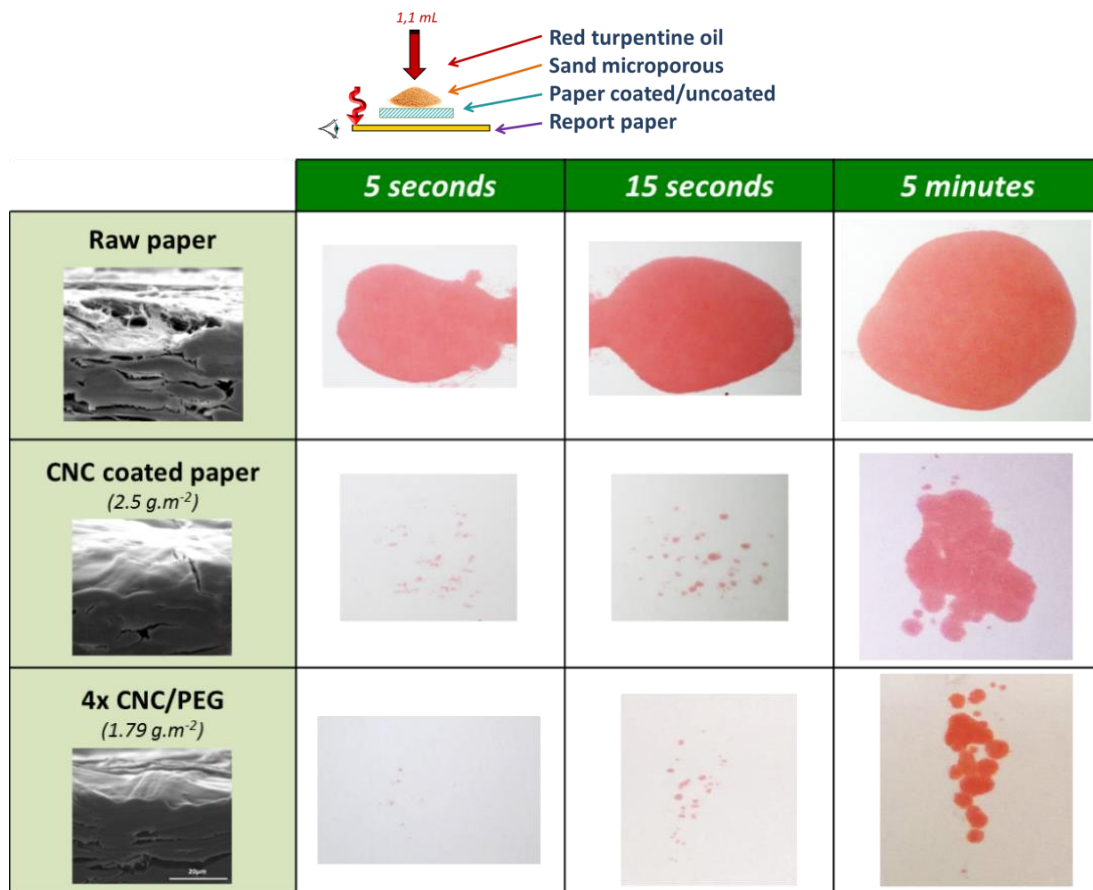


**Figure 7:** Pictures of 'report paper' after grease resistance test using Tappi T-454 on different paper: Raw paper, CNC coated, CNC + PEG coated.

As for the grease resistance, it is possible to draw a similar conclusion. To our knowledge, no one has explored the grease resistance of a CNC coating. Aulin et al. (Aulin et al., 2010), Lavoine et al. (Lavoine et al., 2012, 2014a), and Bardet et al. (Bardet and Bras, 2014) have focused their research on the oil resistance of CNF-coated paper following a different TAPPI standard (T-454, T507). They all concluded that the CNF coating can provide oil barrier properties to a cellulosic substrate because of the entanglement of fibrils on the substrate.

In the present study, the Tappi T-454 test is used to elucidate the grease penetration through paper. **Figure 7** presents these results. There is a link between air permeability and grease permeability. In most cases, the coated paper with the lowest air permeability shows high resistance to oil penetration.

The red oil penetrates the basic paper immediately ( $< 1$  s) and is instantaneously visible on the paper being studied. The CNC-coated paper is more resistant to oil because it this paper shows lower air permeability. Concerning the results from Tappi-454, the paper coated with CNC yields the first grease pin-hole at only 5 seconds. Dense, smooth, and organized CNC

coating increases the tortuosity of the network for molecules of red oil. Nonetheless, it does not stop the grease for a longer period as compared to MFC (Aulin et al., 2010). It only slowed down the penetration/migration of the oil through the paper surface. Fig. 5f shows fractures on the surface, and red oil has a way to cross the substrate. It is important to remember that the Turpentine test is one of sever liquid grease tests and has a high migration speed as compared to other oils or solid grease. Regarding applications to packaging paper, the butter test is sometimes more representative of exposure to solid grease. The coating realized in this publication resists 1 h of this exposure (data not shown) whereas paper resists only for a few minutes.

This study shows for the first time that 100% cellulose-coated paper can have lower air permeability and better grease resistance with only  $2.5 \text{ g}\cdot\text{m}^{-2}$  of CNC. This approach is promising but not sufficient if bio-based packaging applications are the ultimate goal.

### 1.3.5. The effect of PEG addition on barrier properties of paper

To prevent fracture of the layer on the surface of a substrate, PEG was added to the suspension of CNC. The objective was to counterbalance the breakable network of the CNC layer by addition of a binder. In the literature, when it is added to a CNC matrix, PEG is a “plasticizer” that can improve the CNC film’s flexibility (Bardet et al., 2015).

In the present study, a maximum of 20%wt of PEG ( $200 \text{ g}\cdot\text{mol}^{-1}$ ) was added to the fourfold CNC suspension.

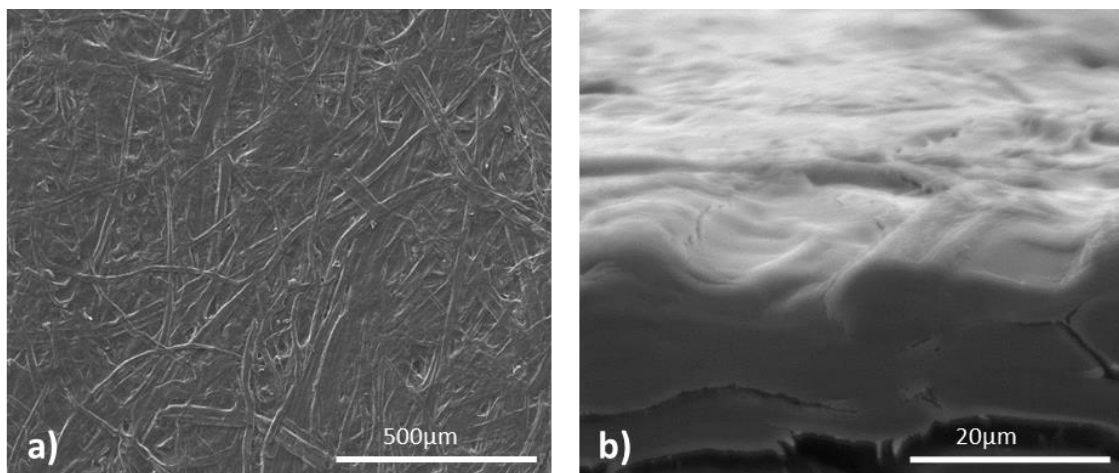


**Figure 8:** SEM images of paper coated with CNC and 20%wt of PEG as plasticizer: (a) surface (scale bar at  $500\mu\text{m}$ ) and (b) cross-section of the substrate (scale bar  $20\mu\text{m}$ ).

**Figure 8** shows an SEM image of the coated paper. It is notable that the number and size of fractures on the substrate strongly decreased. Because of the presence of PEG in the suspension, the CNC coat weight decreases to  $1.79 \pm 0.19 \text{ g}\cdot\text{m}^{-2}$  because of higher viscosity. Under these conditions, no change in the mechanical and surface properties in comparison to paper with CNC ( $2.5 \text{ g}\cdot\text{m}^{-2}$  in Table 1) is detectable. Nevertheless, as for the barrier properties, the addition of PEG to the CNC slurry improved final properties of the coated paper.

First, in terms of air permeability, after the addition of PEG to the slurry of CNC, the value is halved. The basic paper has a value of  $\sim 10100 \pm 900 \text{ nm}^2$ . Then, for CNC coating, the air permeability is reduced to  $880 \pm 300 \text{ nm}^2$ , whereas for the CNC + PEG coating, the permeability is  $474 \pm 48 \text{ nm}^2$ . The presence of PEG around nanocrystals creates a link in the network which prevents formation of holes and fractures and homogenizes the coating on the substrate.

Second, this promising result for the air permeability has a positive effect on the oxygen barrier property (experiment with the oxygen transmission rate test – OTR). The values measured start at  $390 \text{ cm}^3\cdot\text{m}^{-2}\cdot\text{day}^{-1}\cdot\text{kPa}^{-1}$  during the first minute of the test. Nonetheless, oxygen eventually diffuses through the CNC+PEG-coated sample after several minutes.

Third, the grease test has been performed according Tappi standard T-454. With addition of PEG, the first pin hole of red turpentine oil appears at 15 seconds, as shown in **Figure 8**.

To conclude this part, with the presence of PEG in the matrix of CNC, the number of fractures and holes on the coated surface drastically decreases. Barrier properties improve due to the homogeneous and strongly organized CNC layer and because of the diminution of layer stiffness. This result is promising for the packaging industry, because such low-basis weight recyclable and bio-based material (> 99% cellulose) may be used for flexible packaging with low barrier expectations, e.g., fast food paper.

## 1.4. Conclusion

This study is focused on the implementation of a 100% cellulosic material with new surface properties. In particular, the effects of pure CNC coating on mechanical and barrier properties of a paper substrate were investigated.

To our knowledge, this is the first study in which paper is coated with a suspension of pure CNC. The effect of the layer of CNC on the mechanical properties is not significant because of the creation of a film on the surface and not inside the substrate. Only the bending stiffness is improved by 900% for paper coated with  $4.5 \text{ g}\cdot\text{m}^{-2}$ . In contrast, the impact of the CNC coating is more relevant for barrier and surface properties. As for air permeability, for a CNC coat weight of  $\sim 2.5 \text{ g}\cdot\text{m}^{-2}$ , resistance of the coated material is increased by 91%. The grease resistance slightly increases and the gloss of the surface increases by  $\sim 300\%$ . The limitations that are mainly due to layer stiffness have been partially overcome by adding PEG as a plasticizer.

In conclusion, the improvement of the surface properties of cellulosic substrates can be considered a promising approach to some flexible bio-based packaging applications. Another use of the CNC coating may be, for example, printing of electronics.



## 2. Thermo-reversible cellulose nanocrystals system coated on cellulosic substrate: a water reversible surface

*Erwan GICQUEL, Quentin GAUTHIER, Céline MARTIN, Julien BRAS*

### 2.1. Introduction

With approximately 250 megatons produced annually by biomass, cellulose is considered as the most abundant organic polymer in nature (Urruzola et al., 2014). Cellulose exhibits promising properties like renewability, biocompatibility, biodegradability and mechanical resistance. Such material is classically used in textile and paper industry since centuries. Over the last years, smart applications using cellulose based materials with stimuli-responsive properties attract significant attention of the scientific and industrial communities in the field of biomedical, packaging or tissue engineering (Cabane et al., 2012; Hoffman, 2013; Wei et al., 2017). As stimuli-responsive polymer, pH and temperature sensitive are the most investigated ones. A large range of polymer exists (Wei et al., 2017), but poly(N-isopropyl acrylamide) (PNIPAM) is the most commonly used for its thermo-responsive properties in bio-medical applications. PNIPAM undergoes a temperature induced transition from hydrophilic to a more hydrophobic state at around 32°C in water (Kubota et al., 1990; Schild, 1992). In particular, stimuli-reversible surface are developed for cell adhesion/desorption (Akiyama et al., 2004; Cunliffe et al., 2003; Okano et al., 1995; Xue et al., 2017), filter membrane (Hakalahti et al., 2016; Pan et al., 2010) or cell culture (Kwon et al., 2000). First works on thermo-responsive surface have grafted specific sensitive polymer on glass (Cunliffe et al., 2003; Yakushiji et al., 1998), polystyrene (Akiyama et al., 2004; Okano et al., 1995; Wang et al., 2008) or polyethylene terephthalate (Kwon et al., 2000). Since the last decades, some researches focused on cellulosic substrate for green and renewable facilities like filter paper (Lindqvist et al., 2008; Wu et al., 2016a, 2016b), cotton fiber (Jiang et al., 2012), regenerate cellulose membrane (Pan et al., 2010) or nanocellulose film (Hakalahti et al., 2016). Although long chains polymer and high grafting densities were obtained, major drawbacks of these works are the grafting process using radical polymerization with toxic

raw materials or solvents, sensibility to oxygen and difficulty to eliminate copper catalyst or coupling agent. An opportunity in green chemistry is the polymer chemical adsorption on surface. Nonetheless, the electrolyte adsorption depends on the surface charge of the substrate which could be a limiting factor. The coating of nanocellulose, especially cellulose nanocrystals (CNCs), on cellulosic substrate has been recently shown in literature (Gicquel et al., 2016a; Lavoine et al., 2014c; Li et al., 2013). These nanocelluloses could be a solution as bio-based template to deposit sensitive polymer onto substrate.

Nanocellulose, and in particular cellulose nanocrystals (CNCs), presents unique properties including excellent mechanical strength, bio-compatibility, high surface area and low density (Abitbol et al., 2016; Habibi, 2014; Klemm et al., 2011; Moon et al., 2011; Revol et al., 1992). CNCs are rigid rod-like particles with dimension of 5 to 15 nm of diameter and 150 to 500 nm of length depending on the source (Dufresne, 2013b; Habibi et al., 2010). CNCs are the crystalline part of cellulose obtained by acid hydrolysis. To take advantage of the CNCs surface reactivity, surface oxidation by 2,2,6,6-tetramethyl-1-piperidinyloxy (TEMPO) has been widely used to introduce carboxylate groups on surface since last decade (Habibi et al., 2006). In pH condition superior to 3.4, carboxylic groups present negative charges which favor adsorption of positively charged materials. This strategy was recently proposed in literature to “connect” CNCs and cationic polymer (Larsson et al., 2013; Vuoriluoto et al., 2015).

In this study, we propose the development of a thermo-reversible paper surface properties with the presence of PNIPAM or a block copolymer of poly(di(ethylene glycol) methyl ether methacrylate) (PDEGMA) grafted with poly(2-(dimethylamino)ethylmethacrylate) (PDMAEMA). Both polymers were first adsorbed on CNCs which plays the role of template. These CNCs-polymer systems present a thermo-reversible hydrogel behavior as previously described in *Chapter III.3*. Then, they were coated on cellulosic substrate. The water contact angle was studied under and above the polymer LCST (lower critical solution temperature) in order to achieve thermo-reversible surface. **Figure 1** presents the goal of this work.

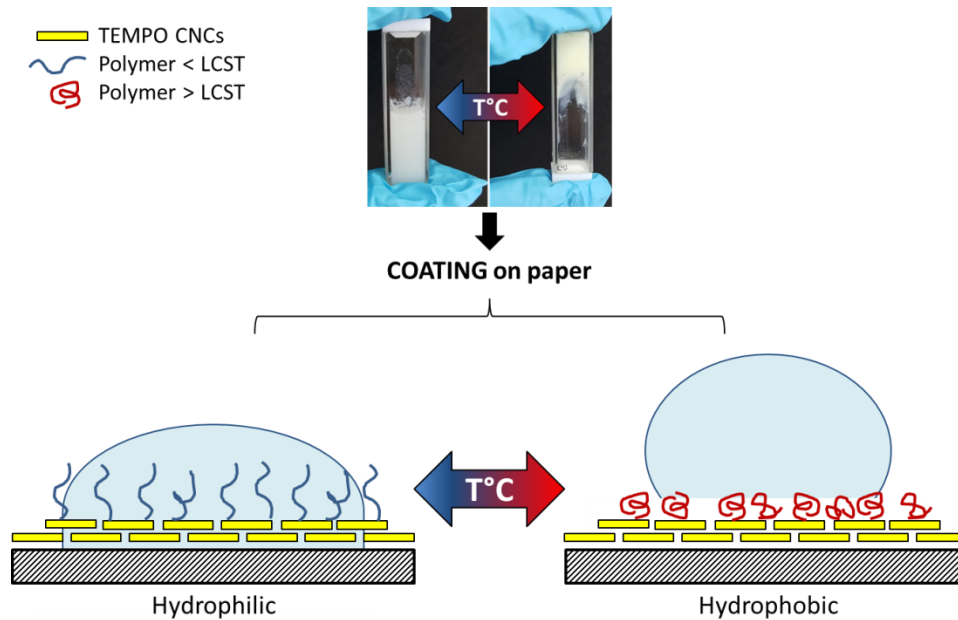


**Figure 1:** Schematic concept of thermo-responsive surface

## 2.2. Materials and Methods

### 2.2.1. Materials

Colloidal suspension of ~12%wt Commercial Cellulose Nanocrystal (CNCs) was purchased from UMaine process Development Center (University of Maine, USA). They have been produced from wood pulp using sulfuric acid hydrolysis process and have been never freeze-dried. The dry matter was measured using a moisture analyzer (Ohaus® MB-35, Sigma-Aldrich, USA). Poly(N-isopropylacrylamide) with amine terminated were purchased from Sigma-Aldrich (USA) with molecular weight of  $2500 \text{ g}\cdot\text{mol}^{-1}$ . The LCST is closed to  $32^\circ\text{C}$ . A complete list of products used for TEMPO oxidation is previously described in *Chapter II.1* of this PhD manuscript. Regarding the realization of block copolymer of PDEGMA-co-PMAEMA, details on chemical products are described in *Chapter III.3*. Distillated water was used for all experiments. The base paper material was uncoated and non-calendered paper with a basis weight of  $56 \text{ g}\cdot\text{m}^{-2}$ , kindly provided by an industrial partner. It is classically used as a substrate to be coated for packaging applications (Gicquel et al., 2016a).

### 2.2.2. Carboxylation of cellulose nanocrystals by TEMPO oxidation

In order to incorporate negative charges on the surface of CNCs, CNCs were subjected to TEMPO-mediation oxidation using a previously reported procedure (Habibi et al., 2006) and already described in previous *Chapter II* of this PhD project.

### 2.2.3. Synthesis of PDMAEMA-co-PDEGMA block copolymer with ATRP

Built on collaboration with KTH laboratory in Sweden, the realization of the block copolymer composed with laboratory synthesized PDMAEMA macro initiator and chain extension with PDEGMA via ATRP grafting process was described in details in *Chapter III.3*. It will be named Diblock in this work.

### 2.2.4. Thermo-reversible system based on polymer adsorption on TEMPO CNCs

The adsorption of Diblock on TEMPO CNCs was performed at 15°C, a temperature inferior to the LCST of the diblock: 24°C. Freeze dried diblock was directly added to the suspension of TEMPO CNCs. Referred to ratio determined in *Chapter III.3*, 2 wt% of Diblock and 8 wt% of TEMPO CNCs were adsorbed together by magnetic stirring during four hours.

The adsorption of Pnipam<sub>2500</sub> on TEMPO CNCs was performed at room temperature (< 32°C). Suspension concentrations were 8 wt% for TEMPO CNCs and 3 wt% for Pnipam<sub>2500</sub>.

### 2.2.5. Adsorption experiments using the Quartz Crystal Microbalance with dissipation (QCM-d)

Polymer adsorptions on TEMPO CNCs substrate were recorded using a quartz crystal microbalance with dissipation (QCM-d, E1 model, Biolin Scientific Holding AB, Gothenburg, Sweden). Details on the preparation of QCM-d sensor and adsorption calculation are detailed in *Chapter II.2 and III.3* of this PhD project. The estimated adsorbed polymer amount ( $\Delta m$ ) was calculating using the Sauerbrey equation (**Equation 1**) (Sauerbrey, 1959)

$$(1) \quad \Delta m = -C \frac{\Delta f}{n}$$

$C$  is a constant related to the density and thickness of the quartz crystals with a value of 17.7 ng·cm<sup>-2</sup>·Hz<sup>-1</sup> for 5 MHz crystal (provided by the manufacturer),  $\Delta f$  is the change in

frequency and  $n$  is the overtone number. In this study the third overtone was used for the calculation of  $\Delta m$ . Q-tools frequency values are normalized, so  $n=1$  is utilized.

### 2.2.6. Coating process

Polymer adsorbed CNCs suspensions were applied on paper samples with a bar-coating process (Endupap, France). A smooth Meyer bar was used with a coating speed of  $5 \text{ cm}\cdot\text{s}^{-1}$ . Then, coated paper samples were dried under tension by a contact drying system at  $105^\circ\text{C}$  for 3 min. This process was repeated four times in order to remove the paper roughness and fully covered the cellulosic fiber. The thickness obtained is about  $3 \mu\text{m}$  with a coating mass of about  $2.5 \text{ g}\cdot\text{m}^{-2}$  (Gicquel et al., 2016a).

### 2.2.7. Contact angle

Static contact angles were performed on DataPhysics Instrument (DataPhysics OCA 20) at room temperature. A  $5 \mu\text{l}$  distilled water drop with a B-BRAUN Injekt-F syringe at  $15^\circ\text{C}$  or  $50^\circ\text{C}$  was deposited on the surface and images were recorded for two minutes to record contact angle and drop volume evolution. Averages of at least 5 measurements were done for each surface to give representative results.

## 2.3. Results and discussion

### 2.3.1. Polymers adsorption

Aqueous commercial CNCs suspensions were carboxylate using TEMPO oxidation process. By conductometric titration, a degree of oxidation of 0.246 (mol/mol of anhydroglucose unit) and an oxidation rate of  $1450 (\mu\text{mol}\cdot\text{g}^{-1})$  were obtained. The adsorption of Pnipam<sub>2500</sub> and PDMAEMA-PDEGMA on TEMPO CNCs were presented in details in *Chapters II.2 and III.3*. **Figure 2** and **Table 1** summarize the QCM-d adsorption experiments.

**Table 1:** QCM-D Frequency and Dissipation changes during Pnipam<sub>2500</sub> and PDMAEMA-PDEGMA adsorption on TEMPO CNCs (*Equation 1*).

Polymer	$\Delta F_3$ (Hz)	$\Delta D_3 (10^6)$	$\Delta m (\text{mg}\cdot\text{m}^{-2})$
Pnipam <sub>2500</sub>	-45.6	4	$8.1 \pm 0.1$
PDMAEMA-PDEGMA	-175.8	6.9	$30.0 \pm 0.1$

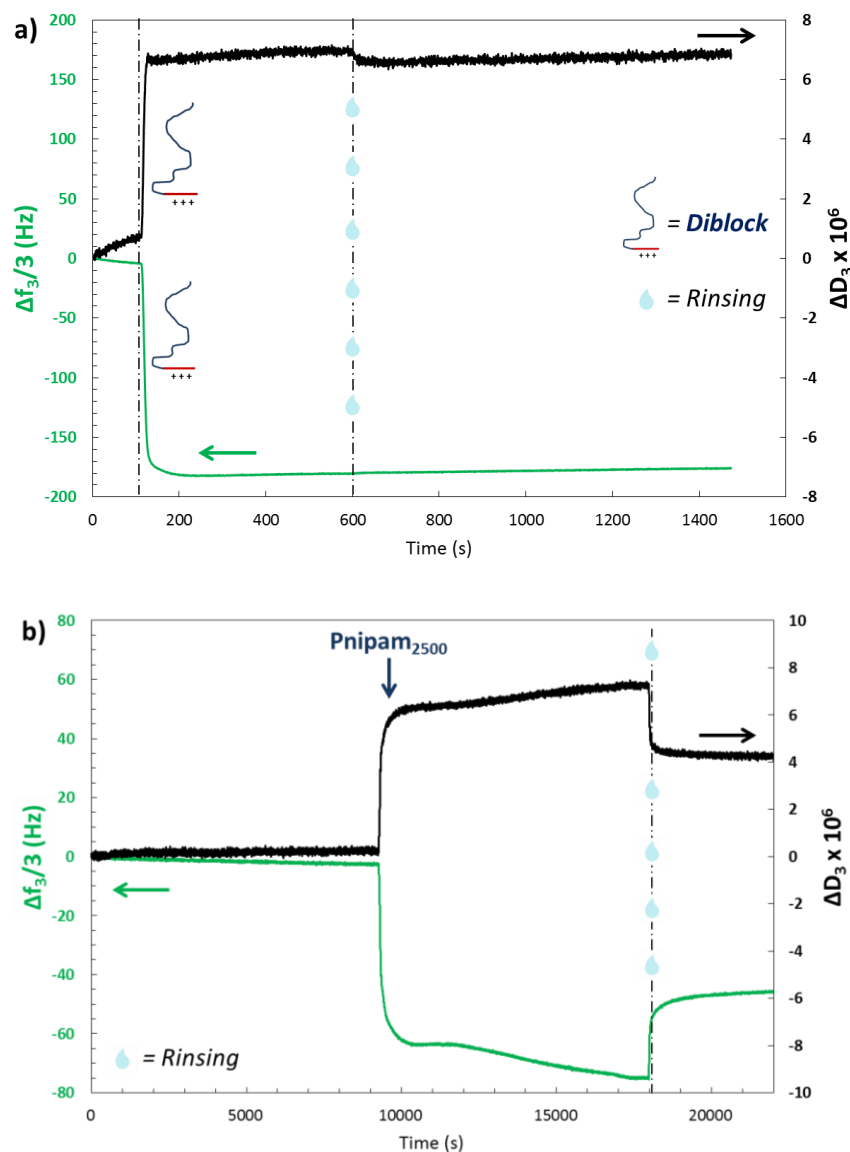


**Figure 2:** QCM-d measurements present adsorption of a) Diblock and b) Pnipam<sub>2500</sub> on TEMPO CNCs films. The adsorption was measured at 15°C, pH 6, flow rate at 17 mL/h and a concentration of 10 mM.  $\Delta F_3$  (left axis) and  $\Delta D_3$  (right axis) are respectively the shift in frequency and in dissipation of the measurement for the overtone 3.

In both cases, polymers are strongly adsorbed on TEMPO CNCs. The diblock presents a higher adsorption than Pnipam<sub>2500</sub> due to the amount of positive charges on PDMAEMA. After rinsing step, each polymer is strongly adsorbed on the surface on TEMPO CNCs and is not released.

### 2.3.2. Thermo-reversible surface with Pnipam<sub>2500</sub>

Hydrogel of TEMPO CNCs and Pnipam<sub>2500</sub> present a thermo-reversibility rheological behavior as described in Chapter II.2. **Figure 3** presents the surface behavior after four coating on paper substrate. Paper substrate is hydrophilic and shows a contact angle (CA) around 40°.

Paper adsorbs a drop of water in few seconds. **Figure 3a** presents the evolution of the contact angle (CA) depending on the external temperature after few seconds and **Figure 3b** presents the evolution of the CA with the time.

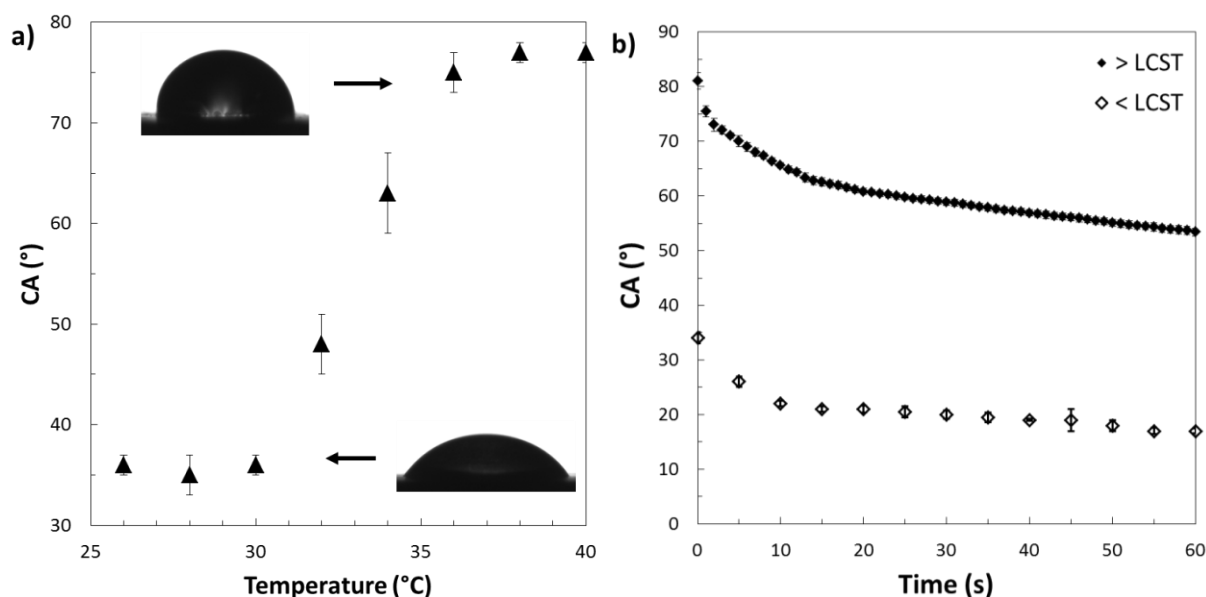


**Figure 3:** Water contact angle of paper substrate coating with hydrogel of Pnipam<sub>2500</sub> adsorbed on TEMPO CNCs depending on a) the temperature and a) the time under and above the LCST. Insert images on a) correspond to the visual contact angle under and above the LCST.

Under the LCST (e.g. 34°C), the CA of the coated paper is about  $35 \pm 2^\circ$  (**Figure 3a**). This value is closed to the CA of the raw paper used in this study ( $\sim 40 \pm 8^\circ$ ). Compared to the diblock adsorption which exhibits a high molecular length ( $\sim 40\,000\text{ g}\cdot\text{mol}^{-1}$ ), Pnipam<sub>2500</sub> have a very small molecular weight ( $2500\text{ g}\cdot\text{mol}^{-1}$ ) which does not impact surface properties under LCST. On **Figure 3b**, the CA decreases quickly after the drop deposition from  $35^\circ$  to  $20^\circ$ . Then in one minute, the CA decreases with the adsorption of the drop in the paper. In contrast, above the LCST, the Pnipam<sub>2500</sub> turns to a collapse globule in water and reveals a hydrophobic behavior. The CA on **Figure 3a** of the coated paper is about  $77 \pm 2^\circ$ . A clear thermo-sensitivity appears on the surface from  $\sim 35^\circ$  to  $\sim 75^\circ$ . It is worth to notice that deposition of a hot water (at 50°C) on classic paper surface does not induce such CA increases. Similar angle of about  $40^\circ$  is obtained for raw paper whatever the temperature is. Nonetheless, this value is not superior to  $90^\circ$  which normally indicates a hydrophobic surface. The small polymer length and a weak polymer presence are probably the limiting factors. In literature, with a high grafting density of PNIPAM and a high molecular weight (superior to  $25\,000\text{ g}\cdot\text{mol}^{-1}$ ), CA of cellulosic fiber are superior to  $120^\circ$  above the PNIPAM

LCST (Jiang et al., 2012; Wu et al., 2016a). Their processes involve harsh solvent and do not correspond to our green chemistry principle. In **Figure 3b**, the CA slowly decreases in 10 seconds from 77° to 70° due to the drop spreading on the paper surface (constant volume). Then until one minute, the CA decreases to 60° with a small adsorption in the paper. The presence of the thermo-sensitive hydrogel on the paper surface allows creating a thermo-sensitive paper. Under the LCST, the paper is hydrophilic and above the LCST, the paper gains a waterproof resistance.

### 1.1.1. Thermo-sensitivity surface with PDMAEMA-PDEGMA

Hydrogel of TEMPO CNCs and diblock present a thermo-sensitivity behavior as described in *Chapter III.3*. **Figure 4** presents the CA of the paper after coating of this hydrogel.

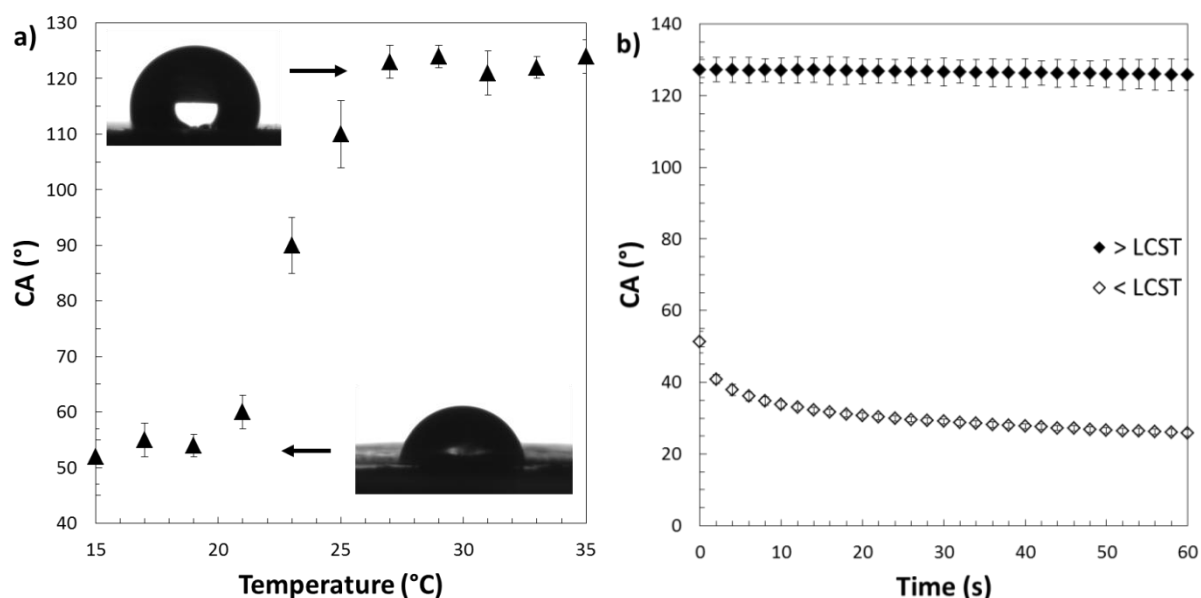


**Figure 4:** Water contact angle of paper substrate coated with hydrogel of diblock adsorbed on TEMPO CNCs depending on a) the temperature and b) the time under and above the LCST.

**Figure 4a** shows the evolution of the CA with the temperature after few seconds. Under the LCST of the polymer (around 24 °C), the CA of the coated paper is about  $50 \pm 5^\circ$ . This value is superior to the uncoated paper due the presence of several CNCs and diblock layers on the surface which increase at the drop impact the resistance to water adsorption. Besides, the presence of a long chain of polymer on the surface (even if it is in hydrophilic configuration) delays the surface hydration and increases the CA. Nonetheless, on **Figure 4b**, the CA of a water drop decreases quickly due to the paper adsorption. After 5 seconds, the drop volume

decreases which corresponds to the drop adsorption by cellulosic paper. The paper presents a small bulge at the water impact due to the cellulosic fiber swelling.

Above the LCST, the coated surface turns to hydrophobic with a CA about  $127 \pm 2^\circ$  (**Figure 4a**). On **Figure 4b**, in one minute, the CA is fixed to  $\sim 125^\circ$ . Besides, the cellulosic paper does not exhibit bulge on the water drop place. After a sufficient range of time, the drop volume decreases but it is difficult to separate the effect due to the water evaporation and the paper adsorption. In brief, the hydrogel based on diblock and TEMPO CNCs exhibits thermo-sensitivity behavior described in *Chapter III.3* (more or less hydrophilic to hydrophobic behavior). After coating, the thermo-responsive properties are present on the paper surface. Above the polymer LCST, the coated surface exhibits a hydrophobic behavior with a high resistance to the water adsorption.

### 2.3.3. Surface comparison

The apparition of hydrophobicity on a surface is due to different factors: the presence of hydrophobic particles and/or a nano roughness (Wenzel, 1936). In this study both polymers present a thermo-reversibility in presence of water and hydrophobicity due to the collapse coil conformation of polymer in water above a particular temperature (LCST). Concerning the nano roughness, the polymer length will impact it. Pnipam<sub>2500</sub> presents a molecular weight about  $2500 \text{ g}\cdot\text{mol}^{-1}$  and diblock has  $40\,000 \text{ g}\cdot\text{mol}^{-1}$ . In the Pnipam<sub>2500</sub> case, the surface roughness due to polymer is probably weak and did not cover the entire CNCs surface. A hot drop of water will find a way to pass through the polymer layer. With several coating of hydrogel on paper, when the first layer was crossing, a second one with hydrophobic properties slows down the water adsorption in paper. **Figure 5A** describes schematically this conclusion. In the case of diblock, the polymer probably presents a big dot on the paper surface above its LCST. The nano-roughness seems to be high and the drop cannot find a way to cross the layer of CNCs and diblock as resumed in **Figure 5B**. This assumption is difficult to prove but could explain the difference between the two systems.

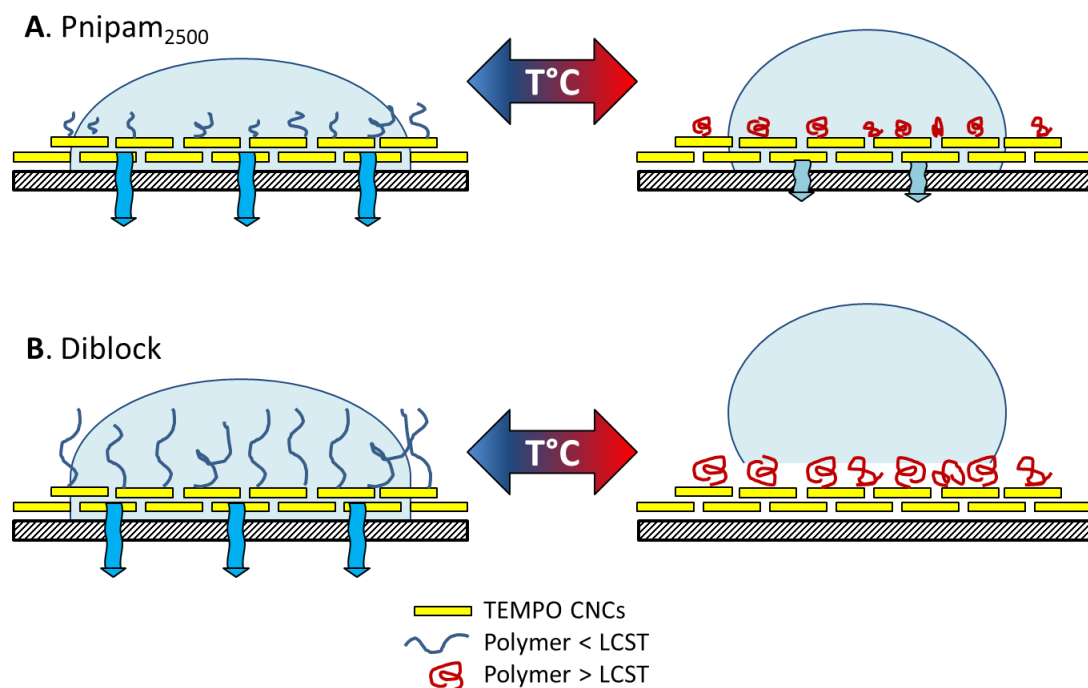


**Figure 5:** schematic representation of the contact angle of a water drop on paper coated with TEMPO CNCs and Pnipam<sub>2500</sub> (A) or TEMPO CNCs and diblock (B).

## 2.4. Conclusion

Polymer adsorption was used to incorporate thermo-sensitive properties on CNCs system. Two kind of polymer were used in this study: Pnipam<sub>2500</sub> and PDMAEMA-PDEGMA. The irreversible adsorption on naocellulose was demonstrated with QCM-d tools. These hydrogels present thermo-sensitive behavior in suspension. After coating, the thermal properties are applied on the surface of paper sheet thanks to CNCs which play the role of template. Under each polymer LCST, the contact angle of a water drop is closed to the paper contact angle ( $\sim 40^\circ$ ). Depending on the polymer length and above the LCST, the contact angle can be tuned from  $77^\circ$  to  $125^\circ$  and reveals a hydrophobic surface. In each case, the surface presents a waterproof resistance during one minute and more. These thermo-responsive surfaces, obtained via green chemistry, can be used in several applications like membrane, microfluidic, bio-compatible sensor or printing facilities (selective and hide printing in offset). Smart packaging is also an excellent opportunity with anti-counterfeit surface or salad package (adaptive water release).

## 3. Thermo-responsive hydrogel based on Cellulose nanocrystals for injectable applications

*Erwan GICQUEL, Quentin GAUTHIER, Céline MARTIN, Julien BRAS*

### 3.1. Introduction

As already detailed in **Chapter 1**, cellulose nanocrystals (CNCs) reveal interesting and promising properties for highly added values applications (Oksman et al., 2014) like good mechanical properties, biodegradability, biocompatibility and high surface area. This greatly contributes to their potential use in regenerative medicine (Domingues et al., 2014). Indeed we can highlight in recent literature the possibility to use CNCs as a classic reinforcement for environmentally friendly nanocomposite (Dufresne, 2013a; Eichhorn et al., 2010; Mariano et al., 2014) or as hydrogels in biomedical applications (Camarero Espinosa et al., 2016; Domingues et al., 2014; Endes et al., 2016; Jorfi and Foster, 2015; Klemm et al., 2011; Lin and Dufresne, 2014; Naseri et al., 2016). In both cases, the CNC surface is usually functionalized for a better compatibility, implementation of new functions (i.e. antimicrobial) or the monitoring of drug delivery. Among this strategy, only very few researchers tried the preparation of CNCs stimuli-responsive hydrogel. This smart hydrogels opens possibility to use reversible hydrogel for cosmetic or therapeutic biomedical injection facilities. The idea is to form a solid gel in situ into the body after injection of a liquid behavior hydrogel. The main advantage of this hydrogel is the possibility to adapt to the defect shape inside the body, to reinforce wrinkled skin and to be easily laden with cells and/or drugs. Besides, this principle is minimally invasive surgery for patients.

In order to develop these biomedical applications, we were interested by the behavior of CNCs hydrogel in presence of hyaluronic acid (HA). HA is nowadays the main component used in aesthetic medicine in particular in injectable systems for skin rejuvenation or lubricating articulations. HA is a high-molecular-mass linear polysaccharide of alternating D-glucuronic acid and N-acetyl-D-glucosamine. HA is present in tissues and body fluids of vertebrates and some bacteria. Its presence in natural extracellular matrix plays a major role in cellular survival, tissue hydration and lubricate functions (Fraser et al., 1997). HA presents

unique properties like good biocompatibility, gel-forming properties (Bothner and Wik, 1987), non-immunogenic and ability to be easily modified, which paves the way to use it as hydrogel in tissue engineering and regenerative medicine (Burdick and Prestwich, 2011; Kogan et al., 2006; Sze et al., 2016). Recent studies have focused on the development of HA-based injectable hydrogels (Bae et al., 2013; Domingues et al., 2014, 2015; Li et al., 2012; Peroglio et al., 2012). Nonetheless, their clinical applications are restraining by limited mechanical properties and degradation rates associated (Collins and Birkinshaw, 2008; Jeon et al., 2007). Recent works introduce natural based cellulose nanocrystals (CNCs), resulting in an improvement of HA-based hydrogel mechanical properties (Domingues et al., 2015; Yang et al., 2013).

The present work will discuss on the possibilities to use previously designed hydrogel systems for biomedical injection. All systems prepared during this PhD work are exposed to injection test in hot (i.e. close to body temperature) phosphate buffer saline (PBS) in order to investigate their stability. The first system studied is the rheological effect of integration of TEMPO CNCs in HA hydrogel. CNCs will act as cross-linkers and increases the HA stability. The first challenge is to decrease the general cost of HA hydrogel without modification of rheological properties and to increase the injection facility. The second system incorporates Poly(N-isopropyl acrylamide) (PNIPAM) in order to add a thermo-reversibility functionality to HA/CNCs based hydrogels. Injection facility and highly elastic hydrogel are targeted with this polymer adsorption. A third system (without HA hydrogel) details the hydrogel behavior during injection tests of a thermo-responsive polymer PDMAEMA-PDEGMA adsorbed onto oxidized CNCs (details in *Chapter III.3*). Such system is the best thermo-responsive suspension as shown in our previous rheology studies and should be adapted to body injections.

## 3.2. Materials and Methods

### 3.2.1. Materials

Cellulose nanocrystals (CNCs) were purchased from UMaine Development Center (University of Maine, USA). They were produced from wood pulp via sulfuric acid hydrolysis process. The commercial colloidal suspension presents a concentration of about ~12%wt Poly(N-isopropylacrylamide) with amine terminated was purchased from Sigma-Aldrich (USA). The molecular weight is about  $5500 \text{ g}\cdot\text{mol}^{-1}$ , and the LCST is about  $32^\circ\text{C}$ . Hyaluronic acid (HA) was also provided by an industrial partner (Vivacy) and presents a high molecular weight fibers ( $3 \times 10^6 \text{ Da}$ ) with a level of purity of 85,7%. For the TEMPO oxidation, following chemicals are purchased from Sigma-Aldrich: 2,2,6,6-Tetramethyl-1-piperidinyloxy (TEMPO, 2564-83-2), Sodium hypochlorite ( $\text{NaClO}$ , 10-15%wt, 7681-52-9) and Sodium bromide ( $\text{NaBr}$ , 7647-15-6). Phosphate buffer saline (PBS) from Sigma-Aldrich was used for hydrogel injection test. DiBlock polymer is a block co-polymer PDMAEMA-PDEGMA synthesized by a KTH partner as previously described in *Chapter III.3*.

### 3.2.2. Carboxylation of cellulose nanocrystals by TEMPO oxidation

In order to incorporate carboxylic acid ends and negative charges on the surface of CNCs, CNCs were subjected to TEMPO-mediation oxidation using a previously reported procedure (Habibi et al., 2006) and already described in previous *Chapter II and III* of this PhD project. Conductometric titration was performed to extract the carboxylic content on the CNCs surface as previously described in *Chapter II*.

### 3.2.3. Hydrogel system preparation

As first system, 1.2 wt% of hyaluronic acid fibers were hydrated and dispersed in a suspension of 7.2 wt% TEMPO CNCs during 24h, with regular agitation at  $20^\circ\text{C}$ . A second suspension of 9 wt% of TEMPO CNCs was mixed with 7 wt% of Pnipam<sub>5500</sub> powder by magnetic stirring at  $20^\circ\text{C}$  following procedure detailed in the *Chapter II.2*. This second suspension was then mixed with 1.2 wt% of HA fibers during 24h at  $20^\circ\text{C}$  for hydration and dispersion.

The adsorption of a diblock polymer on TEMPO CNCs was performed at 15°C, a temperature inferior to the Lower Critical System Temperature (LCST) of the diblock: 24°C. Freeze dried diblock was directly added to the suspension of TEMPO CNCs. Referred to ratio determined in *Chapter III.3*, 4 wt% of Diblock and 1 wt% of TEMPO CNCs were adsorbed together by magnetic stirring during four hours.

#### **3.2.4. Hydrogel rheological measurements**

The rheological behaviors of hydrogel under shear were studied using rotational rheometer Physica MCR 301 (Anton-Paar, Austria). To investigate the temperature effect and the reversibility of systems based on thermo-responsive polymer, tests were carried out under the LCST (15°C) and above the LCST (40°C) close to body temperature. Start-up shearing tests were performed with a cone-plate configuration (diameter of 50mm and angle of 1°). The atmosphere around the sample was saturated with water to avoid evaporation during the measurement. To control the initial state of each sample, a constant shear rate was applied ( $10 \text{ s}^{-1}$  for 30 seconds) followed by a standing time of 30 seconds. The transient response under shear was recorded until steady conditions were obtained. Steady shear viscosity versus shear rate curves was generated as duplicates for each sample from a shear rate of 0.01 to  $1000 \text{ s}^{-1}$ . The time required to reach steady conditions was decreased with increasing shear rate. At least duplicate were performed.

Viscoelastic properties of hydrogels were carried out in the oscillatory mode with a rheometer Physica MCR 301 (Anton-Paar, Austria) with a cone-plate configuration (diameter of 50mm and angle of 1°). The optimal frequency used was inside the linear viscoelastic region (LVE) as determined by performing strain sweep experiments at 3 Pa. In all case, a frequency about 1 Hz was obtained and fixed to achieve the storage modulus ( $G'$ , Pa) and the loss modulus ( $G''$ , Pa) during a strain ramp. At least duplicate were performed.

#### **3.2.5. Hydrogels test of injection in PBS**

Different hydrogel systems tests of injection facility were performed in PBS under and above the polymer LCST. A syringe (B-BRAUN Injekt-F syringe) with a volume of 5 mL was used with a needle (Terumo dental needle 0.30x13 mm). The appearances of the hydrogels before and after injection were observed and photographed by a digital camera.

### 3.3. Results and discussions on hyaluronic acid hydrogels

A large range of hyaluronic acid (HA) is available in commercial production. In order to understand the impact of hydrogel based on CNCs on HA hydrogel properties, we focus this work on hydrogel realized via hydration of HA fibers. This limits the presence of other product from industry (like Mannitol) which could corrupt the phenomenon's understanding.

#### 3.3.1. Impact of TEMPO CNCs on HA hydrogels

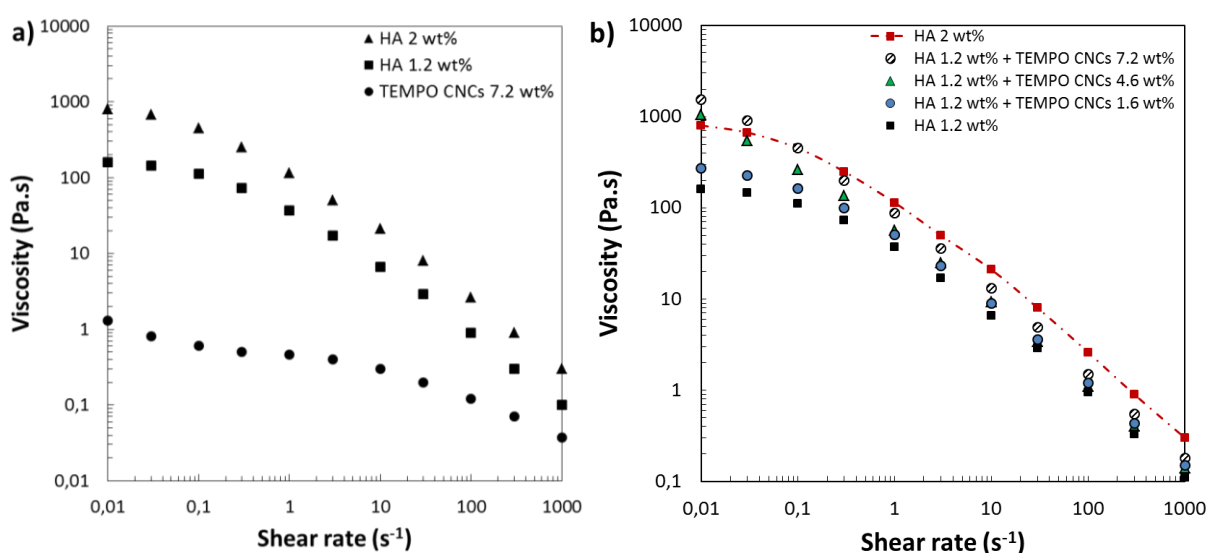


**Figure 1:** Flow curves of a) TEMPO CNCs at 7.2 wt%, Hyaluronic acid (HA) fibers at 1.2 and 2 wt% and b) addition of TEMPO CNCs from 1.6 to 7.2 wt% in HA solution at 1.2 wt%. On b) the square with guide lines corresponds to the commercial suspension behavior.

As already said, HA are industrially used in biomedical hydrogel applications but only few studies incorporated CNC and even less researchers have tested oxidized CNCs. **Figure 1a** presents the evolution of viscosity depending on the shear rate of oxidized CNCs, HA and mix of both. TEMPO CNCs at high concentration (7.2 wt% in this work) presents a three regions behavior typical of liquid crystalline particles organization (Shafiei-Sabet et al., 2012; Ureña-Benavides et al., 2011) as previously described in *Chapter III.1*. The maximum of viscosity is close to 1 Pa.s and the suspension behaves as a shear-thinning fluid. In the case of HA hydrogels, the commercial hydrogel has a concentration about 2 wt%. The flow curve on the top in the **Figure 1a** presents the evolution of this viscosity. HA hydrogels present a shear-thinning behavior with a maximum viscosity of about 1000 Pa.s at 0.01 s<sup>-1</sup>, and a minimum close to 1 Pa.s at 1000 s<sup>-1</sup>. Under 0.1 s<sup>-1</sup>, a small plateau region corresponds to the entanglement of HA fibers in the solution. After this shear rate, the network is broken and

HA fibers are organized in the direction of the flow. At 1.2 wt%, HA hydrogels present similar behavior than the 2 wt% hydrogel with a maximum viscosity divided by 10.

One of the expectations of those hydrogel based on HA and TEMPO CNCs is to present a similar rheological behavior than the commercial HA hydrogel and a storage modulus ( $G'$ ) superior to 100 Pa. One advantage of adding CNCs is a price benefits: 1g of commercial HA hydrogel is between 500 and 2000€ depending on the molecular weight (sigma-Aldrich) and 1g of dried CNCs is about 0.05€. After TEMPO oxidation, the price of 1g TEMPO CNCs is about 2€. The HA hydration properties should also be maintained. CNC might also be a drug carrier once functionalized or adsorbed with drug like chlorhexidine or anti-cancer drugs for example.

**Figure 1b** introduces the impact of presence of TEMPO CNCs on HA hydrogel. The flow curve with square symbols guide line is the commercial objective. By increasing the amount of TEMPO CNCs from 1 wt% to 7.2 wt% in water, the rheological behavior of 1.2 wt% HA hydrogel will be equal to the behavior of 2 wt% commercial HA hydrogel. TEMPO CNCs act as a cross linkers in HA hydrogel and increase the viscosity of the final product. The addition of TEMPO CNCs to hyaluronic leads to increase the viscosity at low shear rate ( $< 0.3 \text{ s}^{-1}$ ). Besides, at highest shear rate ( $> 10 \text{ s}^{-1}$ ), the viscosity is smaller than the commercial HA hydrogel and presents a high shear-thinning behavior. This point is of interest for injection. Through the syringe, a high shear rate is applied and the hydrogel can be easily injected. At low shear rate (e.g. in the body), the hydrogel returns to a “solid” gel with an elastic modulus of about 300 Pa (loss modulus  $G''$  is close to 115 Pa).

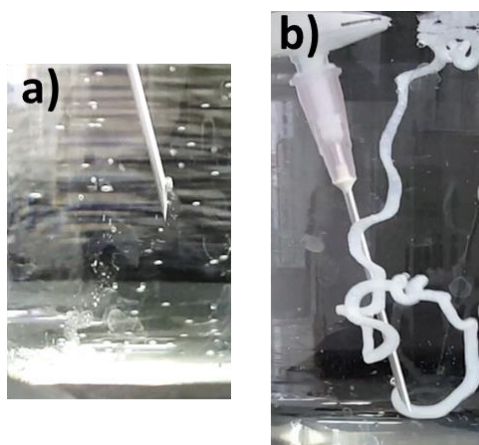


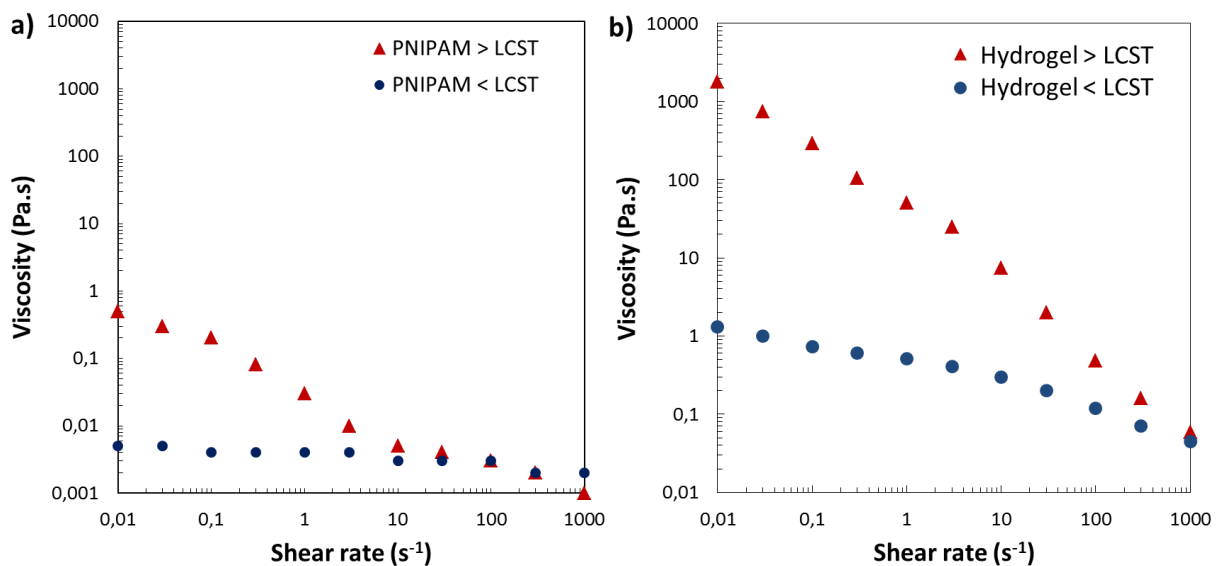
**Figure 2:** Images of a) HA hydrogels at 2 wt% (Gel 1) and b) 1.2 wt% HA + 7.2 wt% TEMPO CNCs (Gel 2) in hot PBS.

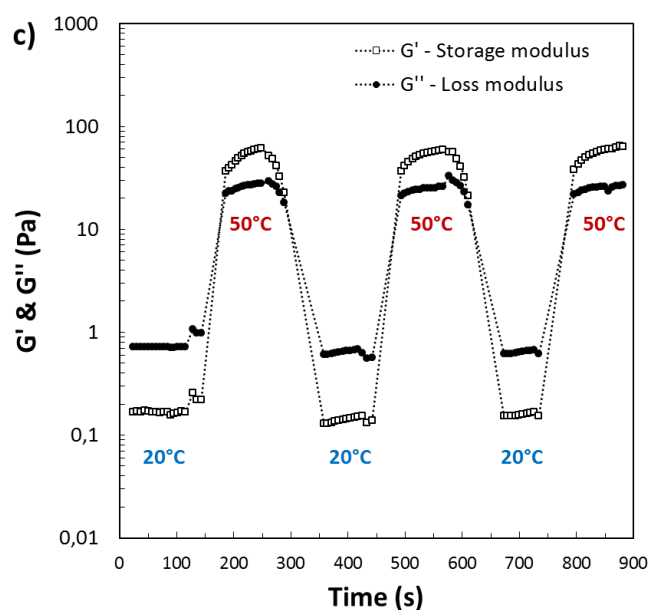
**Figure 2** presents images of both injectable hydrogels in hot PBS ( $\sim 37^\circ\text{C}$ ): Gel 1 (2 wt% of HA fibers hydrogel) and Gel 2 (1.2 wt% of HA fibers mixed with 7.2 wt% of TEMPO CNCs). Gel 2 (**Figure 2b**) is more white than Gel 1 (**Figure 2a**) due to the presence of particles inside the suspension which modified the light diffraction of the hydrogel. Gel 2 presents also a smaller density than Gel 1 (hydrogel floats on water). Both gels are in filament form in PBS after injection. This form is maintained during several hours before a collapse configuration. On the time investigated in this study (maximum 6 hours), none of each hydrogels were dissolved in the hot PBS. This CNC –HA mixture seems promising and the idea is now to add a thermo-responsive behavior to favor their injection.

### 3.3.2. Thermo-responsive Pnipam<sub>5500</sub> effect on HA hydrogels

*In the following section, we will discuss on the injection of hydrogel based on PNIPAM and TEMPO CNCs defined in Chapter II.2. The molecular weight of PNIPAM is  $5500\text{ g}\cdot\text{mol}^{-1}$ . It is two times the length of the Pnipam<sub>2500</sub> used in Chapter II.2 in order to favor the entanglement inside the hydrogel and increase the mechanical strength. Previous experiments with Pnipam<sub>2500</sub> were also tested without relevant results in hot PBS (immediate dispersion).*

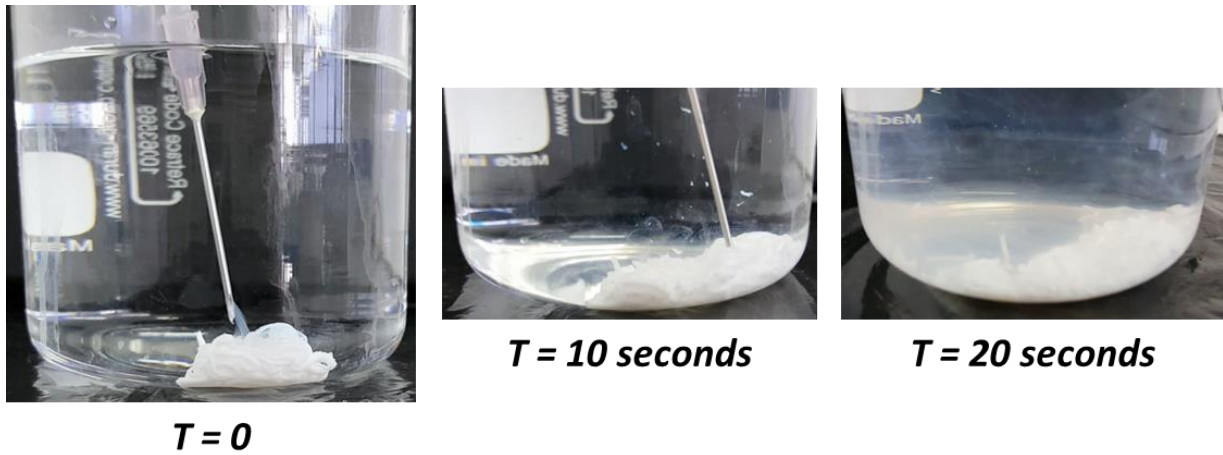
The following **Figure 3** presents the rheological behavior of the Pnipam<sub>5500</sub> alone (**Figure 3a**), in hydrogel with TEMPO CNCs (**Figure 3b**) and the viscoelastic properties of the final hydrogel (**Figure 3c**) under and above the polymer LCST.





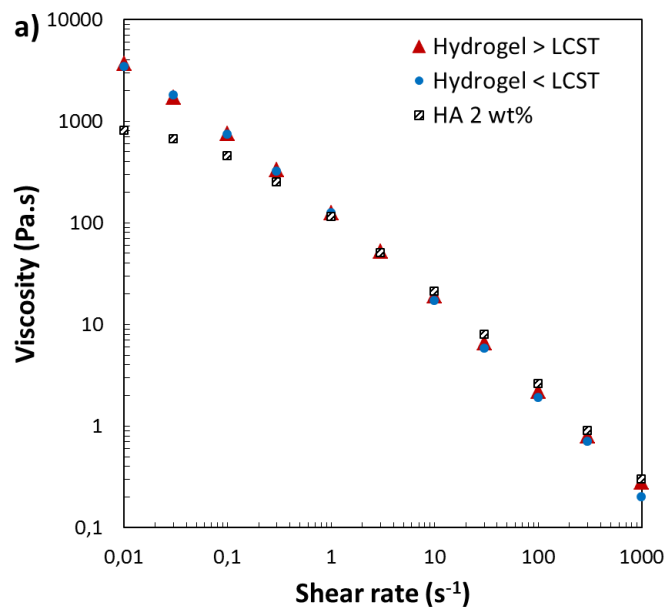
**Figure 3:** flow curves of a) 9 wt% Pnipam<sub>5500</sub>, b) 9 wt% Pnipam<sub>5500</sub> + 7 wt% TEMPO CNCs under and above the polymer LCST. Viscoelastic behavior c) of hydrogel based on 9 wt% Pnipam<sub>5500</sub> + 7 wt% TEMPO CNCs depending on the external temperature.

Pnipam<sub>5500</sub> presents a small thermo-responsive behavior (**Figure 3a**) under and above its LCST. The small entanglement of collapsed polymer is destroyed when the shear rate increases ( $> 1 \text{ s}^{-1}$ ). After adsorption with TEMPO CNCs (demonstrated in *Chapter II.2*), the new system (**Figure 3b**) presents a similar behavior under the LCST than TEMPO CNCs in suspension (**Figure 1a**). Nonetheless, above the LCST, the viscosity drastically increases to 2000 Pa·s at low shear rate. When the shear rate increases, the system exhibits a shear-thinning behavior due to the presence of CNCs in the hydrogel. TEMPO CNCs participate in the construction of the entanglement of polymer. **Figure 3c** reveals the thermo-reversibility of the hydrogel depending on the temperature. Under the LCST, viscoelastic measurements present a liquid behavior ( $G' < G''$ ) while above the LCST the system is in gel form ( $G' > G''$ ). After several cycles of heating and cooling, the hydrogel presents exactly the same reversibility. Compared to our previous results (*Chapter II.2*), the polymer's length has a clear impact on the hydrogel's mechanical strength. However, as shown in **Figure 4**, the hydrogel is dissolved in less than one minute in hot PBS.



**Figure 4:** Images of hydrogel based on 9 wt% Pnipam<sub>5500</sub> + 7 wt% TEMPO CNCs in hot PBS depending on the time.

In order to improve the hydrogel stability, HA fibers were mixed with this previous PNIPAM-CNCs based hydrogels. **Figure 5a** shows the rheological behavior of hydrogel based on HA fibers, Pnipam<sub>5500</sub> and TEMPO CNCs. Whatever the temperature is, the hydrogel does not present a thermo-responsive behavior. It is probably due to the strong entanglement with HA fibers which do not allow PNIPAM to modify the viscosity. Besides, by comparing with a 2 wt% HA fibers suspension at a shear rate superior to  $0.3 \text{ s}^{-1}$ , the hydrogel composed with 1.2 wt% of HA fibers, 9 wt% Pnipam<sub>5500</sub> and 7 wt% TEMPO CNCs presents identical rheological behavior. Under a shear rate about  $0.3 \text{ s}^{-1}$ , the viscosity is higher than the commercial material (up to 3500 Pa·s).



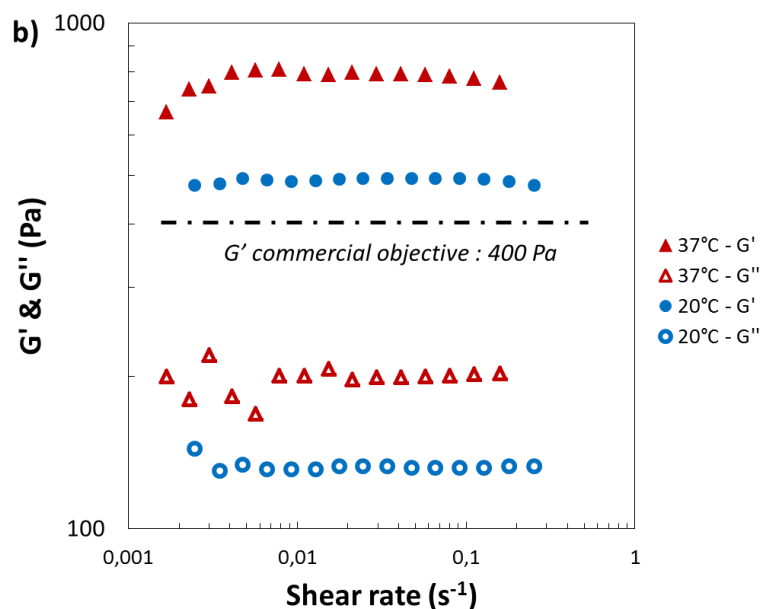


**Figure 5:** a) Flow curves of hydrogel composed with 9 wt% Pnipam<sub>5500</sub>, 7 wt% TEMPO CNCs and 1.2 wt% HA fibers under and above the polymer LCST. The flow curve of HA commercial concentration is shown on the graph for comparison. b) Viscoelastic behavior of this hydrogel around the LCST. Dashed line underline the storage modulus of HA commercial product.

On **Figure 5b**, under the PNIPAM LCST ( $\sim 32^{\circ}\text{C}$ ) the hydrogel present a highly gel form with a storage modulus  $G'$  about 500 Pa and a loss modulus  $G''$  about 130 Pa. Above the LCST, these values increase to 800 Pa and 200 Pa for  $G'$  and  $G''$ , respectively. In both case, these values are superior to industrial objectives. Although flow properties seem to be not modifying by the temperature, the hydrogel's elastic properties are impacted. With the presence of Pnipam<sub>5500</sub> and TEMPO CNCs in the HA hydrogel, it is possible to divide by 2 the amount of HA fibers and positively increase the properties of commercial HA hydrogel. **Figure 6** shows the visual injection of this hydrogel in hot PBS. The hydrogel forms a filament after injection. After 2 hours, the Pnipam<sub>5500</sub> in excess in the hydrogel seems to be released in the hot PBS (white solution).

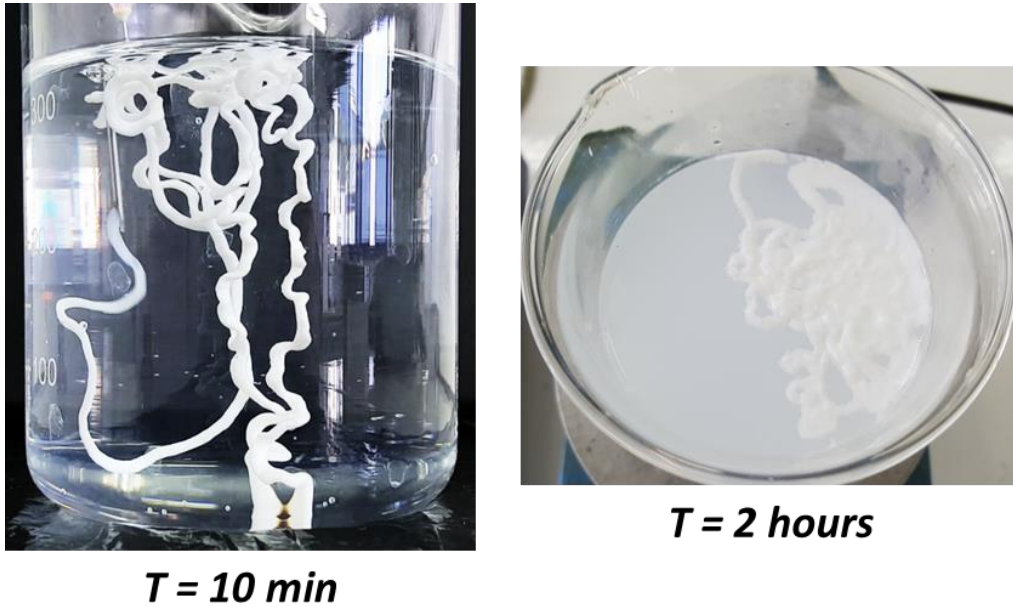


**Figure 6:** Images of hydrogel based on 1.2 wt% HA fibers + 9 wt% Pnipam<sub>5500</sub> + 7 wt% TEMPO CNCs in hot PBS depending on the time.

These hydrogels based on hyaluronic acid need to be optimized but it seems that presence of CNC can help in preparation of stiffer gel structure. This part was just preliminary results and it is clear that influence of concentration of PNIPAM, its adsorption, its chain length or its functionalization should be analyzed for a better understanding. The strong interest for designing new injectable systems lead us to carry on this qualitative study with the best thermo-responsive hydrogel prepared in previous chapters The following section will develop the injectable facilities of hydrogels based on TEMPO CNCs and diblock (details in Chapter III.3).

### 3.3.3. Discussion on thermo-responsive hydrogels based on diblock and TEMPO CNCs for injectable applications

The adsorption of diblock composed with PDMAEMA-PDEGMA on TEMPO CNCs was already described in details in *Chapter III.3*. A clear and strong adsorption due to electrostatic charges was highlighted. The ratio explored in the present section is diblock in high excess (four times the TEMPO CNCs content). This hydrogel presents the best thermo-responsive properties in rheological measurements as shown in **Figure 7**.

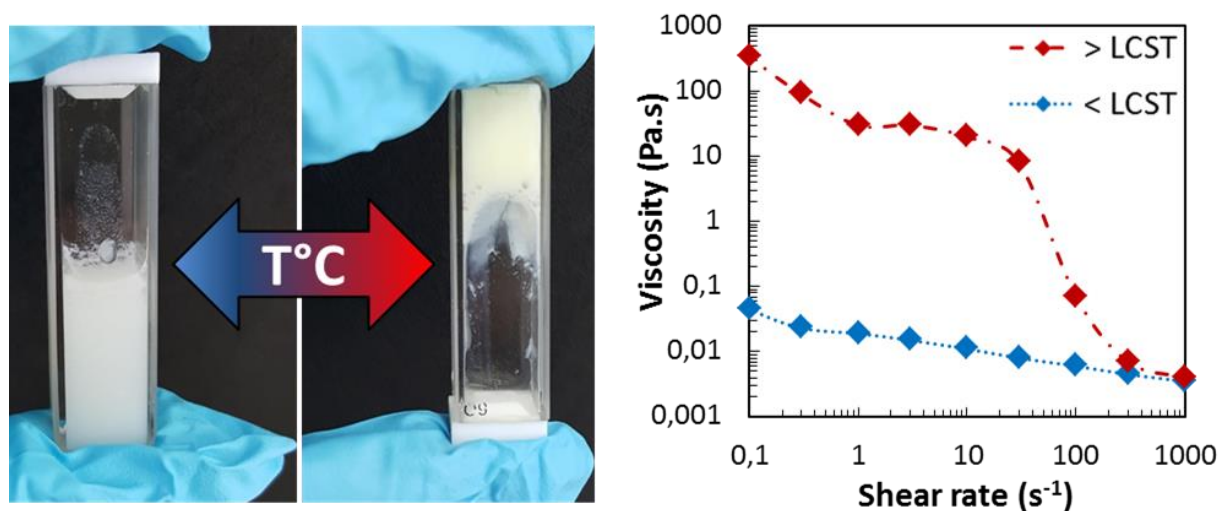


**Figure 7:** Images of reversible diblock hydrogels (left) and flow curves under and above the LCST for 4.5 wt% system (right) from Chapter III.3.

On the **Figure 7**, images clearly show the thermo-sensitivity of the diblock-CNCs hydrogel when the temperature reach the polymer LCST. In the flow curves, under the LCST, the diblock-CNCs hydrogel shows a viscosity under 0.1 Pa·s for the all range of shear rate. The hydrogel is in liquid form. Above the LCST, the hydrogel exhibits a very high viscosity (about 400 Pa·s at 0.1 s<sup>-1</sup>) and a gel behavior since a shear rate about 30 s<sup>-1</sup>. The *Chapter III.3* gives more details on the hydrogel's rheological behavior.

On **figure 8**, hydrogel injections in cold and hot PBS were tested. Under the diblock LCST (~22°C), the thermo-responsive hydrogel is in liquid form and easy to handle with syringe. During injection in cold PBS (**figure 8a**) and after injection (**figure 8b**), the thermo-sensitive liquid is immediately dispersed in the PBS solution. This observation shows the absence of interaction between PBS and diblock and their quick dilution in liquid. In contrast, in solution of PBS at temperature close to body (i.e. above the diblock LCST), the hydrogel presents a gel-form. During injection (**figure 8c**) and 4 hours later (**figure 8d**) the thermo-responsive system forms a durable hydrogel without polymer release in PBS solution. Even after several days in hot water the gel is still homogeneous and stiff. Such materials could have strong interest in wrinkled skin reparation. These results are very promising. Of course, several other properties should be studied in details and collaboration with a company expert in this field is under discussion to carry on this study.

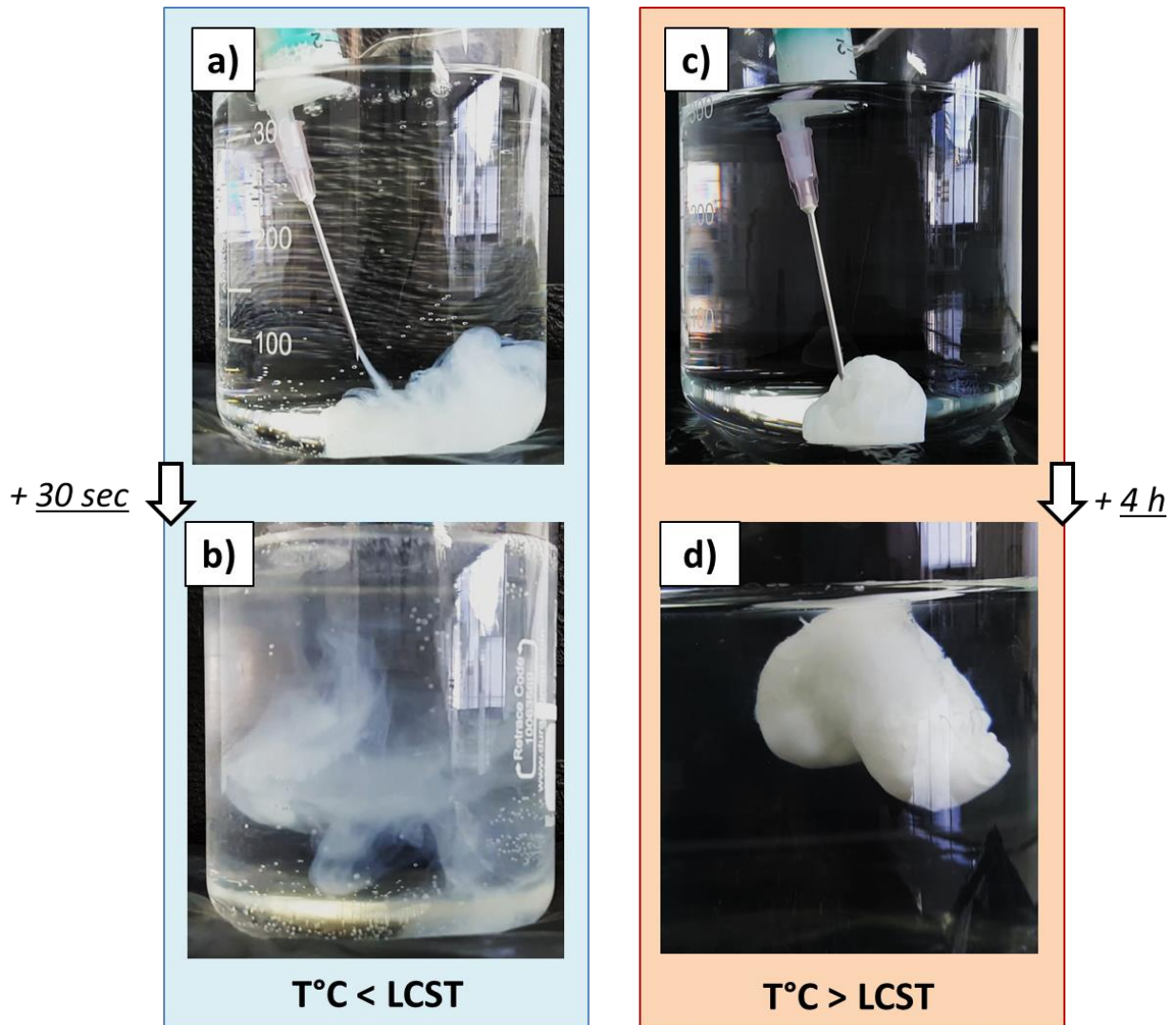


**Figure 8:** Images of 4 wt% diblock adsorbed in 1 wt% TEMPO CNCs hydrogel under the LCST (a-b) and above the LCST (c-d). a) and c) corresponds to injection in PBS. b) and d) show the time evolution of the hydrogel in PBS depending on the temperature, b) 30 seconds later and d) 4 hours later.

### 3.4. Conclusions

Promising hydrogels developed in this Ph.D. were tested for injection applications. A part of them were also mixed with hyaluronic acid for biomedical injection system. HA hydrogel are used in biomedical for injection applications with an expensive price. By addition of CNCs in the HA hydrogel, we have proved that it is possible to divide by 2 the HA amount (the final price too) and maintain the same rheological properties.

PNIPAM based hydrogels present interesting viscoelastic properties and shear-thinning behavior, which are important for injection facilities. PNIPAM and TEMPO CNCs hydrogel exhibits excellent rheological properties but after injection in PBS, the cohesion between polymer and CNCs is partially destructed. After addition of HA fibers in this hydrogel, a more cohesive gel is formed with very encouraging elasticity behavior. However, after a couple of hours, the hydrogel releases a part of PNIPAM in the external solution.

The final promising hydrogel is based on PDMAEMA-PDEGMA block copolymer adsorbed on TEMPO CNCs. Excellent rheological properties were reported in previous chapter. In injection tests, this hydrogel turns in a dense and strong gel in hot PBS. No polymer release was reported in our experiments time.

Each of these hydrogels present interesting possibilities for future applications in surgery injection or anesthetic medicine. They need more investigation on the mechanical strength and the release test, but this is a first step for CNCs hydrogel applications.

## Conclusions

In the present **Chapter IV** thermo-responsive hydrogel based on CNCs were exploited in the development of “smart” and high added values applications (fourth challenge).

In the *Chapter IV.1*, pure CNCs suspensions were coated on paper substrate. Surface properties have been impacted by this cellulosic layer. While mechanicals properties were not significantly impacted, the surface and barrier properties were positively modified. The surface resistance against air and grease were increased due to the presence of CNCs layers but the crack possibility limits their impact and new properties should be targeted as in *Chapter IV.2*.

Indeed, in *Chapter IV.2*, the thermo-responsive hydrogels (*Chapter II.2* and *III.3*) were coated on paper substrate to evaluate its hydrophilic-hydrophobic reversibility. This study revealed the thermo-response of the substrate. Under polymer LCST, the surface was hydrophilic and above this temperature the paper was hydrophobic. These properties open the way for bio-compatible sensor or specific smart packaging.

To complete the work on thermo-responsive hydrogels of this Ph.D., biomedical injectable application has been tested in *Chapter IV.3*. Each different hydrogels were submitted to injection in PBS in order to evaluate their strength in aqueous conditions. Experiments were also done with hyaluronic acid classically used for biomedical application in wound healing or anesthetic surgery. Results were very promising. Our best system based on the block copolymer adsorption shows qualitatively the transition from liquid behavior (easily injectable) to strong and permanent gel at body temperature.

These last results should be analyzed more in details and contacts with a company are in progress. Nevertheless, such preliminary results provide a proof of concept on these CNCs thermo-sensitive systems which could have promising applications in smart materials.



## References

- Abitbol, T., Rivkin, A., Cao, Y., Nevo, Y., Abraham, E., Ben-Shalom, T., Lapidot, S., and Shoseyov, O. (2016). Nanocellulose, a tiny fiber with huge applications. *Curr. Opin. Biotechnol.* *39*, 76–88.
- Akiyama, Y., Kikuchi, A., Yamato, M., and Okano, T. (2004). Ultrathin Poly(N-isopropylacrylamide) Grafted Layer on Polystyrene Surfaces for Cell Adhesion/Detachment Control. *Langmuir* *20*, 5506–5511.
- Aspler, J.S., Zou, X., Laleg, M., Manfred, T., and Grennon, J. (2015). Print quality on thin coatings of cellulose nanocrystals.
- Aulin, C., and Ström, G. (2013). Multilayered Alkyd Resin/Nanocellulose Coatings for Use in Renewable Packaging Solutions with a High Level of Moisture Resistance. *Ind. Eng. Chem. Res.* *52*, 2582–2589.
- Aulin, C., Gällstedt, M., and Lindström, T. (2010). Oxygen and oil barrier properties of microfibrillated cellulose films and coatings. *Cellulose* *17*, 559–574.
- Bae, K.H., Wang, L.-S., and Kurisawa, M. (2013). Injectable biodegradable hydrogels: progress and challenges. *J. Mater. Chem. B* *1*, 5371–5388.
- Bardet, R., and Bras, J. (2014). Cellulose Nanofibers and Their Use in Paper Industry. In *Handbook of Green Materials : Processing Technologies, Properties and Applications*, pp. 207–232.
- Bardet, R., Belgacem, N., and Bras, J. (2015). Flexibility and Color Monitoring of Cellulose Nanocrystal Iridescent Solid Films Using Anionic or Neutral Polymers. *ACS Appl. Mater. Interfaces* *7*, 4010–4018.
- Bercea, M., and Navard, P. (2000). Shear Dynamics of Aqueous Suspensions of Cellulose Whiskers. *Macromolecules* *33*, 6011–6016.
- Bothner, H., and Wik, O. (1987). Rheology of hyaluronate. *Acta Otolaryngol. (Stockh.)* *104*, 25–30.
- Bras, J., Viet, D., Bruzzese, C., and Dufresne, A. (2011). Correlation between stiffness of sheets prepared from cellulose whiskers and nanoparticles dimensions. *Carbohydr. Polym.* *84*, 211–215.
- Brodin, F.W., Gregersen, O.W., and Syverud, K. (2014). Cellulose nanofibrils: Challenges and possibilities as a paper additive or coating material—A review. *Nord. Pulp Pap. Res. J.* *29*, 156–166.
- Burdick, J.A., and Prestwich, G.D. (2011). Hyaluronic acid hydrogels for biomedical applications. *Adv. Mater.* *23*, H41–H56.
- Cabane, E., Zhang, X., Langowska, K., Palivan, C.G., and Meier, W. (2012). Stimuli-Responsive Polymers and Their Applications in Nanomedicine. *Biointerphases* *7*, 9.
- Camarero Espinosa, S., Rothen-Rutishauser, B., Johan Foster, E., and Weder, C. (2016). Articular cartilage: from formation to tissue engineering. *Biomater. Sci.* *4*, 734–767.
- Charreau, H., L. Foresti, M., and Vazquez, A. (2013). Nanocellulose Patents Trends: A Comprehensive Review on Patents on Cellulose Nanocrystals, Microfibrillated and Bacterial Cellulose. *Recent Pat. Nanotechnol.* *7*, 56–80.
- Collins, M.N., and Birkinshaw, C. (2008). Physical properties of crosslinked hyaluronic acid hydrogels. *J. Mater. Sci. Mater. Med.* *19*, 3335–3343.
- Cunliffe, D., de las Heras Alarcón, C., Peters, V., Smith, J.R., and Alexander, C. (2003). Thermoresponsive Surface-Grafted Poly( N – isopropylacrylamide) Copolymers: Effect of Phase Transitions on Protein and Bacterial Attachment. *Langmuir* *19*, 2888–2899.

- Domingues, R.M.A., Gomes, M.E., and Reis, R.L. (2014). The Potential of Cellulose Nanocrystals in Tissue Engineering Strategies. *Biomacromolecules* 15, 2327–2346.
- Domingues, R.M.A., Silva, M., Gershovich, P., Betta, S., Babo, P., Caridade, S.G., Mano, J.F., Motta, A., Reis, R.L., and Gomes, M.E. (2015). Development of Injectable Hyaluronic Acid/Cellulose Nanocrystals Bionanocomposite Hydrogels for Tissue Engineering Applications. *Bioconjug. Chem.* 26, 1571–1581.
- Dufresne, A. (2013a). Nanocellulose: a new ageless bionanomaterial. *Mater. Today* 16, 220–227.
- Dufresne, A. (2013b). Nanocellulose: from nature to high performance tailored materials (Walter de Gruyter).
- Eichhorn, S.J., Dufresne, A., Aranguren, M., Marcovich, N.E., Capadona, J.R., Rowan, S.J., Weder, C., Thielemans, W., Roman, M., Renneckar, S., et al. (2010). Review: current international research into cellulose nanofibres and nanocomposites. *J. Mater. Sci.* 45, 1–33.
- Endes, C., Camarero-Espinosa, S., Mueller, S., Foster, E.J., Petri-Fink, A., Rothen-Rutishauser, B., Weder, C., and Clift, M.J.D. (2016). A critical review of the current knowledge regarding the biological impact of nanocellulose. *J. Nanobiotechnology* 14, 78.
- Fraser, J.R.E., Laurent, T.C., and Laurent, U.B.G. (1997). Hyaluronan: its nature, distribution, functions and turnover. *J. Intern. Med.* 242, 27–33.
- Fujisawa, S., Okita, Y., Fukuzumi, H., Saito, T., and Isogai, A. (2011). Preparation and characterization of TEMPO-oxidized cellulose nanofibril films with free carboxyl groups. *Carbohydr. Polym.* 84, 579–583.
- García, A., Gandini, A., Labidi, J., Belgacem, N., and Bras, J. (2016). Industrial and crop wastes: A new source for nanocellulose biorefinery. *Ind. Crops Prod.* 93, 26–38.
- Gicquel, E., Martin, C., and Bras, J. (2016a). Cellulose Nanocrystals as new bio based coating layer for improving fiber-based barrier properties (2016 International conference on Nanotechnology for renewable Materials (Tappi Nano 2016) Grenoble, FRANCE).
- Gicquel, E., Bras, J., Martin, C., Jean, B., and Pignon, F. (2016b). Stimuli responsive cellulose nanocrystals hydrogel for smart applications (American Chemical Society (ACS 2016), San Diego, USA).
- Habibi, Y. (2014). Key advances in the chemical modification of nanocelluloses. *Chem. Soc. Rev.* 43, 1519–1542.
- Habibi, Y., Chanzy, H., and Vignon, M.R. (2006). TEMPO-mediated surface oxidation of cellulose whiskers. *Cellulose* 13, 679–687.
- Habibi, Y., Lucia, L.A., and Rojas, O.J. (2010). Cellulose Nanocrystals: Chemistry, Self-Assembly, and Applications. *Chem. Rev.* 110, 3479–3500.
- Hakalahti, M., Mautner, A., Johansson, L.-S., Hänninen, T., Setälä, H., Kontturi, E., Bismarck, A., and Tammelin, T. (2016). Direct Interfacial Modification of Nanocellulose Films for Thermoresponsive Membrane Templates. *ACS Appl. Mater. Interfaces* 8, 2923–2927.
- Herrera, M.A., Mathew, A.P., and Oksman, K. (2014). Gas permeability and selectivity of cellulose nanocrystals films (layers) deposited by spin coating. *Carbohydr. Polym.* 112, 494–501.
- Hoffman, A.S. (2013). Stimuli-responsive polymers: Biomedical applications and challenges for clinical translation. *Adv. Drug Deliv. Rev.* 65, 10–16.
- Jeon, O., Song, S.J., Lee, K.-J., Park, M.H., Lee, S.-H., Hahn, S.K., Kim, S., and Kim, B.-S. (2007). Mechanical properties and degradation behaviors of hyaluronic acid hydrogels cross-linked at various cross-linking densities. *Carbohydr. Polym.* 70, 251–257.

- Jiang, C., Wang, Q., and Wang, T. (2012). Thermoresponsive PNIPAAm-modified cotton fabric surfaces that switch between superhydrophilicity and superhydrophobicity. *Appl. Surf. Sci.* *258*, 4888–4892.
- Jorfi, M., and Foster, E.J. (2015). Recent advances in nanocellulose for biomedical applications. *J. Appl. Polym. Sci.* *132*.
- Klemm, D., Kramer, F., Moritz, S., Lindström, T., Ankerfors, M., Gray, D., and Dorris, A. (2011). Nanocelluloses: A New Family of Nature-Based Materials. *Angew. Chem. Int. Ed.* *50*, 5438–5466.
- Kogan, G., Šoltés, L., Stern, R., and Gemeiner, P. (2006). Hyaluronic acid: a natural biopolymer with a broad range of biomedical and industrial applications. *Biotechnol. Lett.* *29*, 17–25.
- Kubota, K., Fujishige, S., and Ando, I. (1990). Solution properties of poly (N-isopropylacrylamide) in water. *Polym J* *22*, 15–20.
- Kwon, O.H., Kikuchi, A., Yamato, M., Sakurai, Y., and Okano, T. (2000). Rapid cell sheet detachment from Poly(N-isopropylacrylamide)-grafted porous cell culture membranes. *J. Biomed. Mater. Res.* *50*, 82–89.
- Larsson, E., Sanchez, C.C., Porsch, C., Karabulut, E., Wågberg, L., and Carlmark, A. (2013). Thermo-responsive nanofibrillated cellulose by polyelectrolyte adsorption. *Eur. Polym. J.* *49*, 2689–2696.
- Lavoine, N., Desloges, I., Dufresne, A., and Bras, J. (2012). Microfibrillated cellulose – Its barrier properties and applications in cellulosic materials: A review. *Carbohydr. Polym.* *90*, 735–764.
- Lavoine, N., Bras, J., and Desloges, I. (2014a). Mechanical and barrier properties of cardboard and 3D packaging coated with microfibrillated cellulose. *J. Appl. Polym. Sci.* *131*, 40106.
- Lavoine, N., Desloges, I., Khelifi, B., and Bras, J. (2014b). Impact of different coating processes of microfibrillated cellulose on the mechanical and barrier properties of paper. *J. Mater. Sci.* *49*, 2879–2893.
- Lavoine, N., Desloges, I., and Bras, J. (2014c). Microfibrillated cellulose coatings as new release systems for active packaging. *Carbohydr. Polym.* *103*, 528–537.
- Lee, K.-Y., Aitomäki, Y., Berglund, L.A., Oksman, K., and Bismarck, A. (2014). On the use of nanocellulose as reinforcement in polymer matrix composites. *Compos. Sci. Technol.* *105*, 15–27.
- Li, F., Biagioni, P., Bollani, M., Maccagnan, A., and Piergiovanni, L. (2013). Multi-functional coating of cellulose nanocrystals for flexible packaging applications. *Cellulose* *20*, 2491–2504.
- Li, Y., Rodrigues, J., and Tomás, H. (2012). Injectable and biodegradable hydrogels: gelation, biodegradation and biomedical applications. *Chem. Soc. Rev.* *41*, 2193–2221.
- Lin, N., and Dufresne, A. (2014). Nanocellulose in biomedicine: current status and future prospect. *Eur. Polym. J.* *59*, 302–325.
- Lin, N., Gèze, A., Wouessidjewe, D., Huang, J., and Dufresne, A. (2016). Biocompatible Double-Membrane Hydrogels from Cationic Cellulose Nanocrystals and Anionic Alginate as Complexing Drugs Codelivery. *ACS Appl. Mater. Interfaces* *8*, 6880–6889.
- Lindqvist, J., Nyström, D., Östmark, E., Antoni, P., Carlmark, A., Johansson, M., Hult, A., and Malmström, E. (2008). Intelligent Dual-Responsive Cellulose Surfaces via Surface-Initiated ATRP. *Biomacromolecules* *9*, 2139–2145.
- Marchessault, R.H., Morehead, F.F., and Walter, N.M. (1959). Liquid Crystal Systems from Fibrillar Polysaccharides. *Nature* *184*, 632–633.
- Mariano, M., El Kissi, N., and Dufresne, A. (2014). Cellulose nanocrystals and related nanocomposites: Review of some properties and challenges. *J. Polym. Sci. Part B Polym. Phys.* *52*, 791–806.

- Mascheroni, E., Rampazzo, R., Ortenzi, M.A., Piva, G., Bonetti, S., and Piergiovanni, L. (2016). Comparison of cellulose nanocrystals obtained by sulfuric acid hydrolysis and ammonium persulfate, to be used as coating on flexible food-packaging materials. *Cellulose* 23, 779–793.
- McGonigle, E.-A., Liggat, J.J., Pethrick, R.A., Jenkins, S.D., Daly, J.H., and Hayward, D. (2004). Permeability of N<sub>2</sub>, Ar, He, O<sub>2</sub>, and CO<sub>2</sub> through as-extruded amorphous and biaxially oriented polyester films: Dependence on chain mobility. *J. Polym. Sci. Part B Polym. Phys.* 42, 2916–2929.
- Moon, R.J., Martini, A., Nairn, J., Simonsen, J., and Youngblood, J. (2011). Cellulose nanomaterials review: structure, properties and nanocomposites. *Chem. Soc. Rev.* 40, 3941.
- Mulvihill, M.J., Beach, E.S., Zimmerman, J.B., and Anastas, P.T. (2011). Green Chemistry and Green Engineering: A Framework for Sustainable Technology Development. *Annu. Rev. Environ. Resour.* 36, 271–293.
- Naseri, N., Deepa, B., Mathew, A.P., Oksman, K., and Girandon, L. (2016). Nanocellulose-Based Interpenetrating Polymer Network (IPN) Hydrogels for Cartilage Applications. *Biomacromolecules* 17, 3714–3723.
- Okano, T., Kikuchi, A., Sakurai, Y., Takei, Y., and Ogata, N. (1995). Temperature-responsive poly (N-isopropylacrylamide) as a modulator for alteration of hydrophilic/hydrophobic surface properties to control activation/inactivation of platelets. *J. Controlled Release* 36, 125–133.
- Oksman, K., Mathew, A.P., Bismarck, A., Rojas, O., and Sain, M. (2014). *Handbook of Green Materials: Processing Technologies, Properties and Applications: Volume 5* (World Scientific).
- Pan, K., Zhang, X., Ren, R., and Cao, B. (2010). Double stimuli-responsive membranes grafted with block copolymer by ATRP method. *J. Membr. Sci.* 356, 133–137.
- Paralakar, S.A., Simonsen, J., and Lombardi, J. (2008). Poly(vinyl alcohol)/cellulose nanocrystal barrier membranes. *J. Membr. Sci.* 320, 248–258.
- Penttilä, A., Sievänen, J., Torvinen, K., Ojanperä, K., and Ketoja, J.A. (2013). Filler-nanocellulose substrate for printed electronics: experiments and model approach to structure and conductivity. *Cellulose* 20, 1413–1424.
- Peroglio, M., Grad, S., Mortisen, D., Sprecher, C.M., Illien-Jünger, S., Alini, M., and Eglin, D. (2012). Injectable thermoreversible hyaluronan-based hydrogels for nucleus pulposus cell encapsulation. *Eur. Spine J.* 21, 839–849.
- Pignon, F. (2016). Structure and rheological behavior of CNC dispersions probed by local birefringence and in-situ Rheo-SAXS (2016 International conference on nanotechnology for renewable materials (Tappi NANO 2016) Grenoble, FRANCE)).
- Rånby, B.G., and Ribí, E. (1950). Über den feinbau der zellulose. *Experientia* 6, 12–14.
- Revol, J.-F., Bradford, H., Giasson, J., Marchessault, R.H., and Gray, D.G. (1992). Helicoidal self-ordering of cellulose microfibrils in aqueous suspension. *Int. J. Biol. Macromol.* 14, 170–172.
- Rodionova, G., Lenes, M., Eriksen, Ø., and Gregersen, Ø. (2010). Surface chemical modification of microfibrillated cellulose: improvement of barrier properties for packaging applications. *Cellulose* 18, 127–134.
- Roohani, M., Habibi, Y., Belgacem, N.M., Ebrahim, G., Karimi, A.N., and Dufresne, A. (2008). Cellulose whiskers reinforced polyvinyl alcohol copolymers nanocomposites. *Eur. Polym. J.* 44, 2489–2498.
- Sauerbrey, G.Z. (1959). Use of quartz vibration for weighing thin films on a microbalance. *J Phys.* 155, 206–212.
- Schild, H.G. (1992). Poly(N-isopropylacrylamide): experiment, theory and application. *Prog. Polym. Sci.* 17, 163–249.

- Shafiei-Sabet, S., Hamad, W.Y., and Hatzikiriakos, S.G. (2012). Rheology of nanocrystalline cellulose aqueous suspensions. *Langmuir ACS J. Surf. Colloids* 28, 17124–17133.
- Siqueira, G., Bras, J., and Dufresne, A. (2009). Cellulose Whiskers versus Microfibrils: Influence of the Nature of the Nanoparticle and its Surface Functionalization on the Thermal and Mechanical Properties of Nanocomposites. *Biomacromolecules* 10, 425–432.
- Siqueira, G., Bras, J., and Dufresne, A. (2010). Cellulosic Bionanocomposites: A Review of Preparation, Properties and Applications. *Polymers* 2, 728–765.
- Sze, J.H., Brownlie, J.C., and Love, C.A. (2016). Biotechnological production of hyaluronic acid: a mini review. *3 Biotech* 6, 67.
- Ureña-Benavides, E.E., Ao, G., Davis, V.A., and Kitchens, C.L. (2011). Rheology and Phase Behavior of Lyotropic Cellulose Nanocrystal Suspensions. *Macromolecules* 44, 8990–8998.
- Urruzola, I., Robles, E., Serrano, L., and Labidi, J. (2014). Nanopaper from almond (*Prunus dulcis*) shell. *Cellulose* 21, 1619–1629.
- Vuoriluoto, M., Orelma, H., Johansson, L.-S., Zhu, B., Poutanen, M., Walther, A., Laine, J., and Rojas, O.J. (2015). Effect of Molecular Architecture of PDMAEMA–POEGMA Random and Block Copolymers on Their Adsorption on Regenerated and Anionic Nanocelluloses and Evidence of Interfacial Water Expulsion. *J. Phys. Chem. B* 119, 15275–15286.
- Wang, N., Zhao, Y., and Jiang, L. (2008). Low-Cost, Thermoresponsive Wettability of Surfaces: Poly(N-isopropylacrylamide)/Polystyrene Composite Films Prepared by Electrospinning. *Macromol. Rapid Commun.* 29, 485–489.
- Wei, M., Gao, Y., Li, X., and Serpe, M.J. (2017). Stimuli-responsive polymers and their applications. *Polym Chem* 8, 127–143.
- Wenzel, R.N. (1936). Resistance of solid surfaces to wetting by water. *Ind. Eng. Chem.* 28, 988–994.
- Wu, W., Li, J., Zhu, W., Jing, Y., and Dai, H. (2016a). Thermo-responsive cellulose paper via ARGET ATRP. *Fibers Polym.* 17, 495–501.
- Wu, W., Song, R., Li, J., and Zhuang, Z. (2016b). Thermo-responsive cellulose papers grafted with poly (di (ethylene glycol) methyl ether methacrylate). *J. Bioresour. Bioprod.* 1, 127–131.
- Xue, X., Thiagarajan, L., Braim, S., Saunders, B.R., Shakesheff, K.M., and Alexander, C. (2017). Upper critical solution temperature thermo-responsive polymer brushes and a mechanism for controlled cell attachment. *J Mater Chem B* 5, 4926–4933.
- Yakushiji, T., Sakai, K., Kikuchi, A., Aoyagi, T., Sakurai, Y., and Okano, T. (1998). Graft architectural effects on thermoresponsive wettability changes of poly (N-isopropylacrylamide)-modified surfaces. *Langmuir* 14, 4657–4662.
- Yang, X., Bakaic, E., Hoare, T., and Cranston, E.D. (2013). Injectable Polysaccharide Hydrogels Reinforced with Cellulose Nanocrystals: Morphology, Rheology, Degradation, and Cytotoxicity. *Biomacromolecules* 14, 4447–4455.
- Yang, X., Shi, K., Zhitomirsky, I., and Cranston, E.D. (2015). Cellulose Nanocrystal Aerogels as Universal 3D Lightweight Substrates for Supercapacitor Materials. *Adv. Mater.* 27, 6104–6109.



# General conclusion and perspectives

---



## General conclusions and perspectives

The main objective of this Ph.D. project was the realization of thermo-responsive hydrogels using cellulose nanocrystals as building blocks for high added values applications. The contribution of nanocellulose in the rheological behavior of such reversible hydrogels tuned by the temperature has been investigated. Indeed, the **Chapter I** highlights the recent interest to use CNCs in biocompatible system, especially for their chemistry and rheological properties. The axes of our research have been defined in accordance with the state of the art as:

- (i) Establish a green process for grafting stimuli-responsive polymers onto CNCs
- (ii) Understand rheological behaviors of thermo-responsive hydrogels based on CNCs
- (iii) Develop “smart” and high added values biomaterials for applications in packaging and biomedical gel suspensions.

The **Chapter I** proposes a synthetic literature review about the chemical modification of CNCs and the shear thinning rheological behavior of these nanoparticles. Very rare works have been focused on using the shear thinning properties of CNCs for injection in biomedical. Even if a few previous studies deal with either CNCs grafting of stimuli responsive polymer or CNCs interaction with stimuli responsive polymers, up to our knowledge, none of them has tried the CNCs coupling with thermo-responsive polymer in accordance with green chemistry principle for rheological understanding in biomedical application. It is worth noting that the novelty of the topic is high as 70% of publications on stimuli-responsive systems based on CNCs were published since the beginning of this Ph.D. project in 2014.

At the beginning of this Ph.D. project, only rare studies have precisely evaluated the use of CNCs as building blocks in the network of thermo-responsive polymers. At the writing point of this manuscript (2017), 16 papers discuss on the presence of stimuli-responsive polymers on the surface of CNCs. Besides, almost no study deals with the green grafting process of thermo-responsive polymer on CNCs and focuses on the rheological behavior.

This Ph.D. manuscript was built as a multiscale analysis of these systems: from the nanoscale modification to the macroscopic applications, as illustrated by the **Figure 1**.

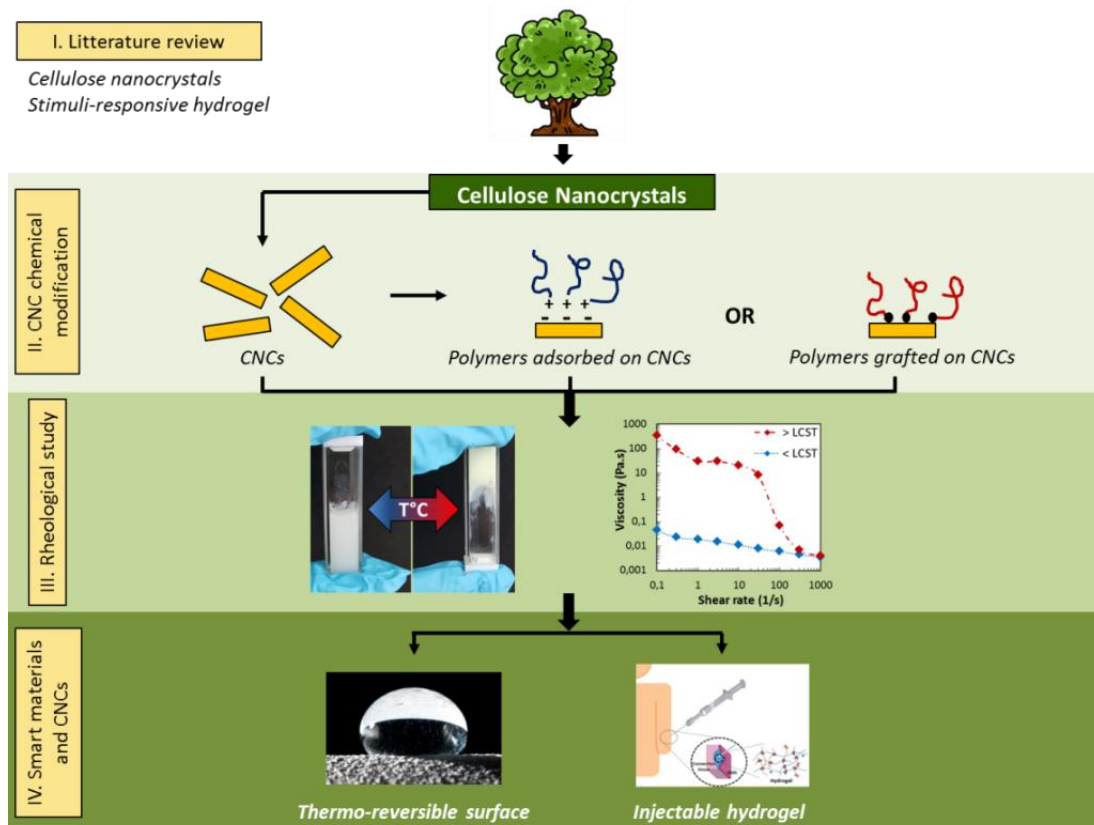


**Figure 1:** Schematic illustration of the Ph.D. project

This Ph.D. work contribution (6 papers) provides innovative and promising way to design thermo-responsive hydrogels. Two major strategies have been developed in this project: the polymer **adsorption** and the polymer **grafting** on the surface of CNCs.

Before the discussion on the design of thermo-responsive hydrogels, **preliminary investigations** were carried out on the **CNCs** materials. The rheological behavior study of commercial CNCs was developed, and particularly the sonication effect on the CNCs structure at high concentration (*Chapter III.1*). SAXS experiments were performed to understand the inter-particle distance depending on the suspension concentration. It was shown that this distance decreases after sonication due to a diminution in the form factor. Nonetheless, the suspension before and after sonication does not present aggregates and exhibits a cholesteric behavior. Then, the coating of CNCs suspension on 100% cellulosic substrate improves the barrier properties against air and grease of the surface (*Chapter IV.1*). Among those results, CNCs coating has been proved to be efficient for the printing facilities on porous and cellulosic substrates by limiting the ink diffusion through the substrate.

**Table 1** summarizes the key results and also the associated perspectives of these preliminary sections.

**Table 1:** Key results and perspectives of CNCs materials

<i>Scientific issue</i>	<i>Key results</i>	<i>Perspectives</i>
<b>CNCs rheological behavior</b> <i>(III.1)</i>	Sonication on high concentrated CNCs suspension decreases the viscosity by the modification of the particles form factor	SAXS experiments to identify the nano-structuration under flow
	CNCs are not broken due to sonication up to 5 kJ/g of dry CNCs	
	Sonication impacts the evolution of the inter-particular distance	Comparison of CNCs types
	Detailed rheology behavior of a well-known commercial CNCs suspension	CNCs orientation under flow and impact of ultra-sounds
	Details on the structuration under flow	
<b>CNCs coating on cellulosic substrate</b> <i>(IV.1)</i>	CNCs suspension can be processed by coating	Coating on other kind of substrate to remove the substrate roughness (PET, baking paper)
	CNCs layers increase barrier properties against grease and air	
	100% cellulosic barrier film obtained	Solution to delete all fracture in CNCs layers (plasticizer, microcapsule, soluble polymer like PVOH).
	CNCs layers does not impact substrate mechanical properties	
	PEG addition deletes a part of microfractures in layer and improves the barrier properties	

In the **first strategy**, the **grafting** of poly(N-isopropyl acrylamide) - **PNIPAM** - were developed on **TEMPO CNCs**. The covalent bound between TEMPO CNCs and PNIPAM with amine ends were investigated in *Chapter II.1*. Through peptidic grafting, the presence of mix of grafted PNIPAM and adsorbed PNIPAM on the surface of CNCs was presented. Microwaves assisted reaction reveals promising results on the possibility to reduce the reaction time from 72h to 6 min. Promising results on the rheological behavior of the grafted system (versus the only adsorbed CNCs) show an important thermo-reversibility behavior (*Chapter III.2*). **Table 2** summarizes the key results and perspectives of this grafting strategy. The second challenge of this Ph.D. project is a success through the design of a thermo-responsive hydrogel based on CNCs.

**Table 2: Key results and perspectives of PNIPAM grafted on TEMPO CNCs**

<i>Scientific issue</i>	<i>Key results</i>	<i>Perspectives</i>
<b>PNIPAM peptidic grafting on CNCs (II.1)</b>	Peptidic coupling is realized with 100% green chemistry	
	Heterogenic “grafting onto” is efficient in green condition and aqueous media	Improve most of washing steps efficiency / purification
	Presence of PNIPAM is revealed after washing steps on CNCs - grafted and adsorbed	Optimization of microwaves assisted reaction and influence of microwave onto adsorption
	Microwave increases the presence and facility to graft and/or adsorb PNIPAM on TEMPO CNCs	Trials with longer polymer molecular weight to increase the network possibility
	Microwave decreases the reaction time from 72h to 6 min	
<b>Rheological behavior of CNC-g-Pnipam (III.2)</b>		Increase of the polymer chain length → higher thermo-reversibility network
	The design of thermo-responsive hydrogel is successful	
	High rheological behavior depending on the temperature are obtained	Development of injection facilities and biomedical applications
	‘Liquid’ at room temperature ‘Gel’ at body temperature	Check the release in body of hydrogels based on CNCs and polymer
	Shear thinning properties is conserved on the final system	Biocompatibility and biodegradability in vivo analysis
	PNIPAM adsorbed on TEMPO CNCs provides excellent thermo-reversible rheological behavior	Mechanical strength and swelling ratio of hydrogel in biomedical applications

The **second strategy** has been developed on the polymer **adsorption** on **TEMPO CNCs**. Two polymers were tested: **PNIPAM** and **Diblock copolymers** - PDMAEMA-PDEGMA.

The **PNIPAM adsorption** was evaluated following previously results in *Chapter II.1* which introduces the potential presence of adsorbed polymer after peptidic grafting. We dedicated a section on the investigation of this polymer adsorption. **Table 3** summarizes the key results and perspectives of the PNIPAM adsorption.

Thanks to the presence of amine ends on PNIPAM, the adsorption seems to be very efficient and irreversible between carboxylic ends (negatively charged) and amine ends (positively charged) (*Chapter II.2*). Interesting rheological properties are shown (*Chapter II.2*) with a thermo-reversibility when the PNIPAM is in excess in the suspension. At the same ratio than

the grafted one, no real synergic effect is revealed (argument in favor of the grafting efficiency). The entanglement above the polymer LCST is probably due to a crosslinking effect with TEMPO CNCs. Different applications were tested (*Chapter IV.2 and IV.3*) for this system. After coating on a cellulosic substrate, preliminary results reveals the reversibility of the surface from hydrophilic (under the LCST) to resistant against water penetration (above the LCST). Besides, injectable tests for biomedical applications show that in presence of hyaluronic acid, a consistent hydrogel is created after injection in PBS. However, polymer release appears after a couple of minutes. Those proofs of concept confirm it seems possible to answer to the third challenge of this Ph.D. dedicated to smart applications. However results were not sufficient and it has been decided to improve adsorption with a cationic polymer and increase molecular weight (and so the chain length) of the thermosensitive polymer to check if an optimization was possible with the use of the Diblock copolymer.

**Table 3:** Key results and perspectives of PNIPAM-NH<sub>2</sub> adsorption on TEMPO CNCs

<i>Scientific issue</i>	<i>Key results</i>	<i>Perspectives</i>
<b>PNIPAM-NH<sub>2</sub> adsorption on TEMPO CNCs</b> <i>(II.2)</i>	Adsorption was proved via QCM-d, MP-SPR and ITC	pH and salt impact on the adsorption
	Electrostatic connection drive the adsorption	Trials with a longer amino PNIPAM
	SANS shows random coil configuration around CNCs (core-shell)	SANS: investigation on the polymer configuration depending on the ratio
<b>Rheological behavior</b> <i>(II.2)</i>	A synergic effect between PNIPAM and TEMPO CNCs was shown	Investigation of the structuration under flow in SAXS
	In excess of PNIPAM, hydrogels reveals a thermo-reversibility behavior where CNCs probably act as cross-linkers	Trials with a longer amino PNIPAM
	This hydrogel present weaker reversibility than CNC-g-PNIPAM	
<b>Thermo-responsive surface</b> <i>(IV.2)</i>	Contact Angle (CA) is tuned by temperature: 20 to 70° on 100% cellulosic substrate	Release test of polymer for packaging applications
	> LCST, resistance to water adsorption < LCST, absence of resistance: swelling	Tests with other support like PET (hydrophobic)
<b>Injectable application</b> <i>(IV.3)</i>	Hydrogel without HA is dispersed in PBS even if the LCST is reached	Optimization to prevent the polymer release after injection
	With HA: strong entanglement when LCST is reached	Hydrogel test: swelling ratio, ageing...
	BUT release of PNIPAM in PBS solution	TEMPO CNCs biocompatibility

The **diblock adsorption** on TEMPO CNCs was proved unequivocally with a fast and irreversible adsorption (*Chapter III.3*). This point strongly impacts the fluid rheological properties. Outstanding thermo-reversible behavior is revealed, with an increase in viscosity of about 4 decades after reaching the LCST for the best ratio of CNC and diblock (1:4). The adsorbed system presents a ‘liquid’ to ‘gel’ behavior and confirms the synergistic effect between diblock polymers and CNCs.

This very interesting hydrogels made of diblock adsorbed on TEMPO CNCs have been tested in high added values applications: thermo-responsive surface (*Chapter IV.2*) and injectable hydrogel (*Chapter IV.3*). The coating on cellulosic substrates provides them a thermo-sensitive answer. Under the LCST, the substrate is highly hydrophilic and above the LCST, the surface is hydrophobic. The contact angle passes from 40° to 120° by changing only temperature! Besides, the final hydrogel can be injected (as it is a liquid at room temperature) in hot PBS and then forms a strong viscous material without degradation in time and polymer release. These final proofs of concept are of interest for future collaborations with biomedical industry. **Table 4** summarizes the key results and open questions of the diblock adsorption on TEMPO CNCs.

**Table 4:** Key results and perspectives of diblock adsorbed on TEMPO CNCs

<i>Scientific issue</i>	<i>Key results</i>	<i>Perspectives</i>
<b>Diblock adsorption on TEMPO CNCs</b> <i>(III.3)</i>	High amount of diblock is adsorbed on TEMPO CNC by electrolytic connection	SANS: investigate the polymer configuration depending on the ratio
	SANS reveals a core-shell diblock decoration	Modify the amount of charge on TEMPO CNCs to increase the rheological properties  Change chain length of each polymer block
<b>Rheological behavior</b> <i>(III.3)</i>	Synergic effect between diblock and TEMPO CNCs is shown	
	Without diblock in excess, hydrogel present a gel structure whatever the temperature is	SAXS: CNCs organization and structuration under flow
	With diblock in excess, hydrogel present a high thermo-reversibility rheological behavior	Effect on drying energy
	‘Liquid’ at room temperature ‘Gel’ at body temperature  Viscosity > 100 Pa·s above the LCST	

<b>Thermo-responsive surface (IV.2)</b>	CA is tuned by temperature: 40 to 120° on 100% cellulosic substrate due to nano roughness and thermo-reversible polymer > LCST, hydrophobic at least 10 min < LCST, water swelling	Interest on the surface releasing in packaging applications Anti-counterfeiting and microfluidic applications
<b>Injectable application (IV.3)</b>	> LCST: hydrogel is dispersed in PBS < LCST: hydrogel of diblock is not degrade for several hours without polymer release in PBS	Hydrogel test: swelling ratio, ageing... TEMPO CNCs and diblock biocompatibility Test the matching with other biocompatible polymer like HA

As a conclusion, this work provides interesting results for the development of thermo-responsive hydrogels and associated applications. At the beginning of this project, very few studies have reported the use of nanocellulose as building blocks in thermo-responsive systems through green chemistry or even only adsorptions. In respect with the initial idea of the combination of CNCs and thermo-responsive polymers in aqueous media, positive results have been obtained. The rheological understanding of these thermo-responsive systems opens doors for promising potential in biomedical applications.

We hope that this study can be considered as an important step in modification of CNCs suspensions in order to incorporated smart properties on their surface like thermo-sensitive properties and also on the investigation of the rheology of these particular systems. The development of industrial solutions with each system proposed in this work and the valorization of each one could be the next step of this project.



# French abstract

---



## Résumé Français

### Extended French abstract

Avec la fin des énergies fossiles et en réponse à la forte demande des matériaux de 'haute performance', une nouvelle génération de matériaux 'bio' (biosourcés, biocompatibles, biodégradables) et 'intelligents' (fonctionnalités, performances, stimulables) a vu le jour.

Parallèlement, l'évolution des outils de recherche et des procédés d'ingénierie a permis de découvrir la cellulose dans ses plus petites dimensions. Les **nanocelluloses** sont certes renouvelables, biodégradables et biocompatibles mais surtout attractives pour leurs propriétés spécifiques et remarquables (aspect de forme élevé, excellentes propriétés mécaniques, grande réactivité chimique, capacité à former des gels avec un très faible taux de matière). Deux catégories existent en relation avec le mode d'extraction des nanocelluloses tel qu'illustré dans la **figure 1** : les nanocristaux de cellulose (CNCs) et les nanofibrilles de cellulose (CNFs).

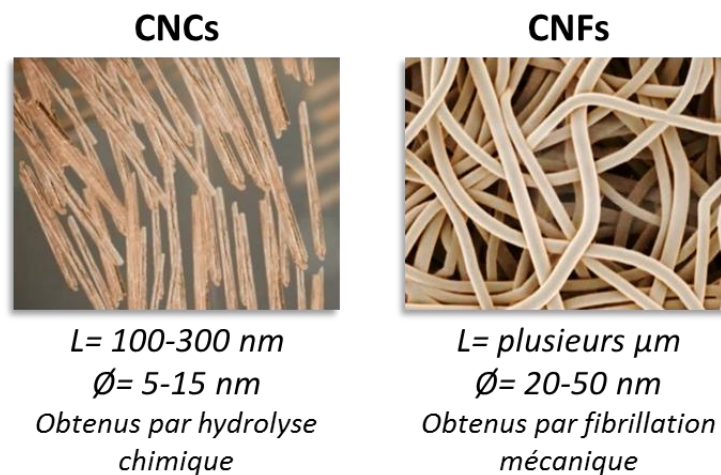


**Figure 1** : Vue schématique des CNCs et des CNFs

Les CNFs se présentent sous la forme de longs filaments flexibles, alors que les CNCs sont considérés comme des bâtonnets rigides de taille nanométrique. Ces derniers sont étudiés depuis les années soixante mais commercialisés uniquement depuis 2010. Ces CNCs ont permis le développement de matériaux nouveaux et performants pour une large gamme d'applications présentées dans la **figure 2**.

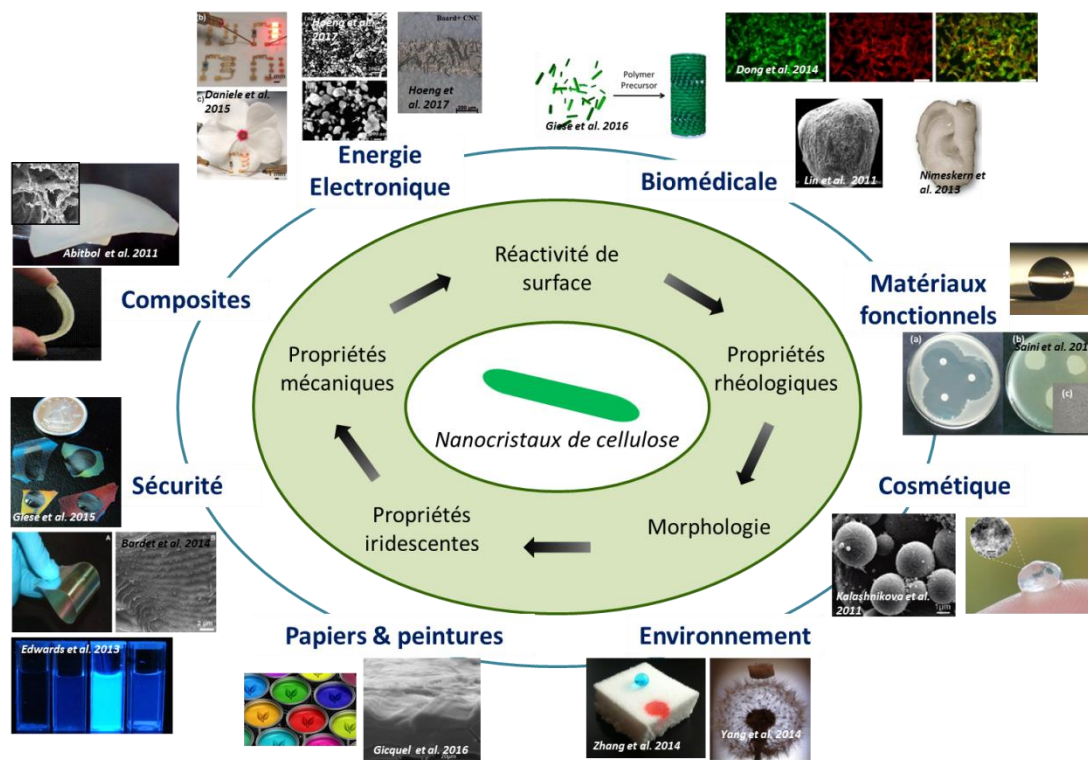


**Figure 2 :** Divers champs d'applications pour les nanocristaux de cellulose

Parmi ces nombreuses applications potentielles, les hydrogels à base de CNCs sont en plein essor avec notamment un fort potentiel pour le biomédical. Afin d'apporter une forte valeur ajoutée, l'intégration de polymères stimulables - notamment thermosensibles - aux CNCs a débuté il y a quelques années. Néanmoins, les principes de la chimie verte sont rarement utilisés dans ces systèmes.

C'est dans ce contexte que le LGP2 (UMR CNRS 5518), laboratoire français expert en Nanocellulose, a décidé de lancer un projet de thèse Ministérielle nommé RHEONANO. Ce projet a profité d'un support partiel de la part de l'institut Carnot PolyNat (Investissement d'avenir - accord de subvention n°ANR-11-CARN-007-01). Le titre de ce projet est '*Développement d'hydrogels de Nanocristaux de cellulose stimulables pour des applications fonctionnelles*'.

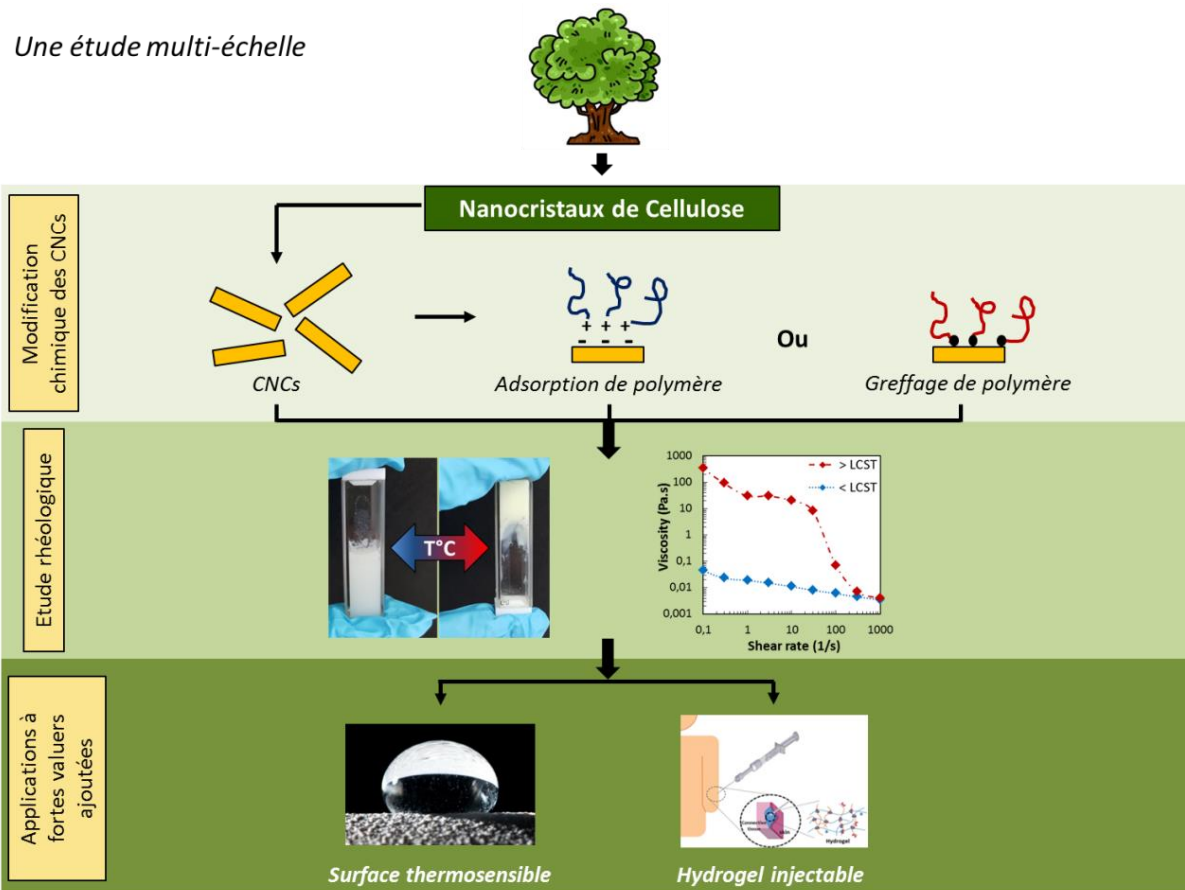
Ainsi, le but de ce projet est de réaliser des hydrogels (environ 90% d'eau) composés de particules biosourcées - les nanocristaux de cellulose - couplées à des polymères aux propriétés thermosensibles. L'intérêt de ces hydrogels se trouve entre autres dans les applications du domaine biomédical. L'idée est de créer des systèmes qui seraient liquides à température ambiante puis qui se transformeraient en gel visqueux à la température du

corps humain. Il est facile d’imaginer les nombreuses possibilités offertes tels que le soin des plaies, les injections réparatrices ou encore la chirurgie esthétique. De plus, la science des matériaux y trouve aussi un intérêt dans le développement de surfaces tantôt hydrophobes tantôt hydrophiles par modification de la température dans le domaine de l’emballage ou de l’anti-contrefaçon.

En réponse à l’état de l’art actuel, plusieurs verrous ont été identifiés et définissent les objectifs du projet:

- (i) Réaliser des hydrogels thermosensibles basés sur les CNCs via un procédé répondant aux principes de chimie verte.
- (ii) Comprendre le comportement rhéologique de ces gels thermosensibles.
- (iii) Trouver et développer des applications à forte valeur ajoutée pour ces biomatériaux uniques.

La **figure 3** suivante illustre le déroulement du projet ainsi que celui du présent manuscrit.



Deux stratégies ont été choisies pour la préparation des systèmes thermosensibles : l'adsorption et le greffage peptidique de polymères. Tous deux ont été réalisés en milieu aqueux et dans des conditions facilement up-scalable.

Dans la **première stratégie** du projet, les **nanocristaux de cellulose** sont utilisés comme support du greffage de **polymères thermosensibles**. Afin de respecter les principes de la chimie verte, un **greffage peptidique** (ou amidation) a été réalisé. Le principe est de faire réagir une amine (présent sur le polymère) avec une fonction carboxylique (issue d'une oxydation des hydroxyles des CNCs) en présence d'agents couplant (EDC et NHS) en milieu aqueux. Ce greffage s'effectue à température ambiante sans l'ajout de solvant ou produit nocif. Le polymère est ajouté déjà polymérisé pour une stratégie de greffage « onto ». Pour ses propriétés de biocompatibilité et pour sa LCST proche de la température du corps humain ( $\sim 34^\circ\text{C}$ ), le Poly(N-isopropylacrylamide) - ou **PNIPAM** - a été choisi en vue d'applications dans le biomédical. Une première étude sur la réalisation du greffage a été menée et tend à prouver l'apparition d'une liaison chimique. Une question reste ouverte sur la possibilité d'un mélange de PNIPAM adsorbé et de PNIPAM greffé sur la surface des CNCs à l'issue du greffage. Le comportement rhéologique de la suspension ainsi obtenue a été par la suite détaillé. Des résultats clés ont été obtenus concernant la conformation des polymères greffés en surface des CNCs ainsi que l'évolution de la viscosité et sa **réversibilité** activée par la température. A température ambiante, l'hydrogel est liquide et à température biologique celui-ci se transforme en gel. La **figure 4** illustre cette première stratégie.

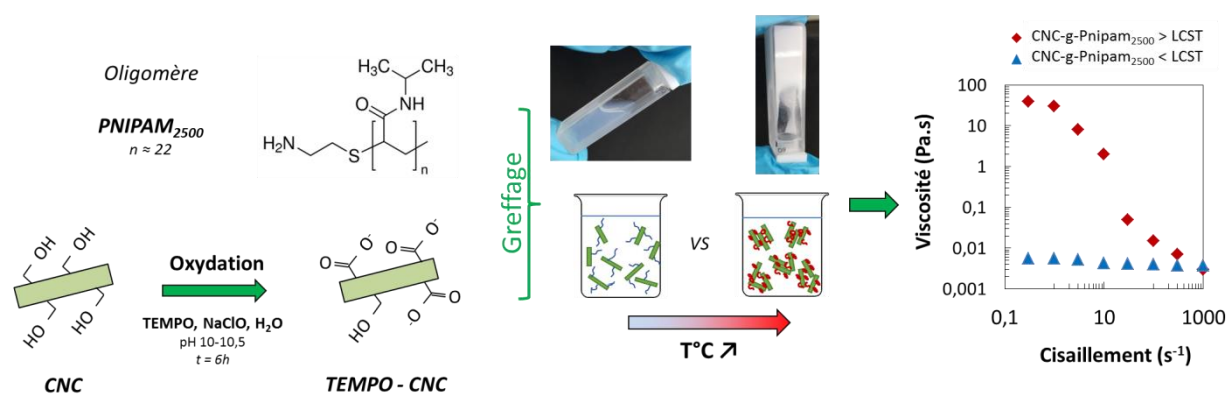


**Figure 4** : Illustration schématique des principaux résultats obtenus au cours de l'étude sur le greffage peptidique du PNIPAM.

Une comparaison avec du PNIPAM « seulement » adsorbé sur les CNCs a été réalisée. A partir d'une concentration critique de 6% massique, la présence de polymère thermosensible dans le mélange fait apparaître les propriétés de réversibilité visée dans cette étude. Cependant à concentration équivalente, la viscosité au repos et la tenue du gel est plus faible que le PNIPAM greffé sur les CNCs de la 1<sup>ère</sup> stratégie. Suivant l'application visée, cette stratégie à l'avantage d'être facilement mise en œuvre et très rapide (10 minutes contre 72 heures).

Dans cette première stratégie, il est clairement montré que le greffage est plus intéressant que l'adsorption au niveau rhéologique, sûrement dû à sa conformation. Toutefois il est aussi démontré que l'adsorption irréversible du PNIPAM est déjà très efficace pour modifier les comportements des suspensions de CNCs.

C'est pour cette raison que dans la **seconde stratégie** du projet, nous nous sommes concentrés sur les **nanocristaux de cellulose** comme support de l'**adsorption** d'un **bloc copolymère** constitué de PDMAEMA (polymère chargé pour favoriser l'adsorption) et de PDEGMA (polymère thermosensible). Le block copolymère a été facilement et fortement adsorbé sur les CNCs précédemment oxydés. Il a été montré que le ratio de polymère avait une très forte influence sur l'enchevêtrement et sur la tenue mécanique du gel ainsi formé. Ce système présente des propriétés de thermo-réversibilité remarquable telles qu'illustrées dans la **Figure 5** et le changement de température permet de multiplier par quasi 10000 la valeur de viscosité à faible cisaillement dans le cas du meilleur ratio (ratio 1:4, diblock en excès) à la plus forte concentration (5% massique au total).

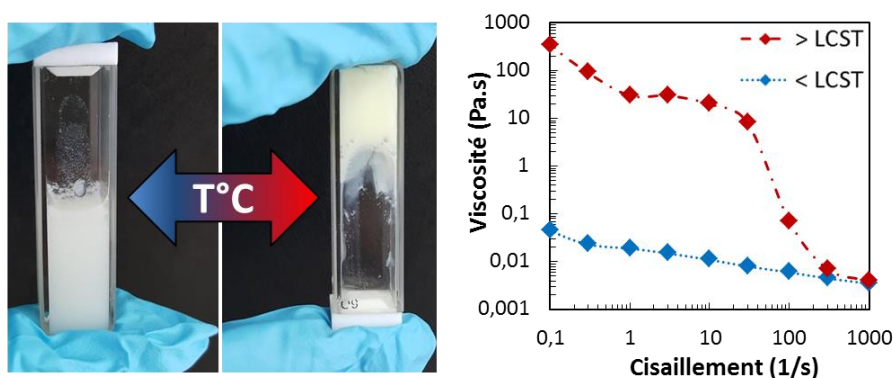


**Figure 5** : illustration schématique de l'étude des hydrogels thermoréversibles constitués de blocs copolymères.

Pour confirmer l'intérêt de ces nouveaux gels, l'étude s'est concentrée sur les applications potentielles des systèmes les plus prometteurs.

Dans un premier lieu, le **couchage des hydrogels thermosensibles** sur des supports celluloseux a été réalisé. Les propriétés thermoréversibles des hydrogels sont transférées sur la surface des substrats. A basse température, le support est hydrophile et adsorbe toute goutte d'eau. A l'inverse, à température supérieure à la LCST des polymères, le support devient hydrophobe pendant plusieurs minutes. C'est un résultat clé dans le développement de papiers fonctionnels pour l'emballage, la contrefaçon voir la micro-fluidique. La **figure 6a** illustre cette sensibilité thermique.

Dans un second lieu, l'**injection des gels thermosensibles** pour des applications dans le biomédical ont été évaluées. L'hydrogel constitué du block copolymère fournit des résultats très prometteurs et engageants. Comme illustrés par la **figure 6b**, l'injection dans un liquide à température du corps humain se traduit par le passage d'un état liquide (donc injectable) à température ambiante à un gel visqueux structuré. Ce n'est qu'une preuve de concept mais elle semble démontrer à elle-seule le fort intérêt pour ces nouveaux hydrogels thermosensibles.

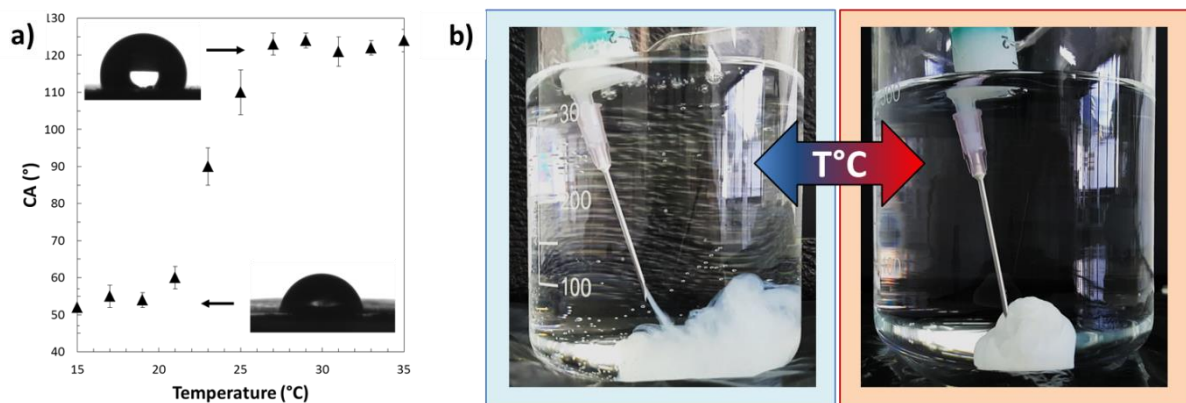


**Figure 6 :** a) illustration des surfaces thermosensibles obtenues après couchage des hydrogels et b) illustration de l'injectabilité des hydrogels thermosensibles dans le PBS.

Pour conclure, au cours de ce projet des suspensions hybrides combinant nanocristaux de cellulose et polymères thermosensibles ont été formulées. Les comportements rhéologiques et les potentielles applications ont été étudiés en détail aboutissant à l'écriture de 6 articles scientifiques.

Ce travail propose une étude physico-chimique complète de la réalisation et du comportement d'hydrogels thermosensibles à base de nanocristaux de cellulose dans des conditions aqueuses.

Les résultats de ce projet étant prometteurs, les perspectives futures sont tournées vers la compréhension de la structuration sous écoulement des systèmes de polymères thermosensibles ainsi que sur l'étude de la tenue mécanique des hydrogels dans le temps et sous la contrainte d'une articulation après injection. Quoiqu'il en soit, cette thèse permet de confirmer tout l'intérêt de ces suspensions hybrides thermosensibles et permet d'envisager de nombreuses applications industrielles.



# Appendix - Posters

---



# Grafting process optimization of stimuli responsive polymer onto cellulose nanocrystals via peptidic coupling.

Vivek HITASHI<sup>1</sup>, Erwan GICQUEL<sup>2</sup>, Céline MARTIN<sup>2</sup>, Julien BRAS<sup>2</sup>, Bruno JEAN<sup>1</sup>

<sup>1</sup> Centre de Recherches sur les Macromolécules Végétales – CERMAV-CNRS – Grenoble UJF, France

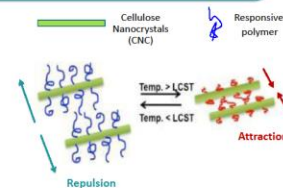
<sup>2</sup> Laboratory of Pulp and Paper Science and Graphic Arts – LGP2 UMR 5518 / CNRS – Grenoble INP – Agefpi, France



## Abstract

Despite their numerous properties such as **renewability, high specific surface area, excellent mechanical properties, light weight, or non-toxicity**, cellulose nanocrystals (CNCs) still require a fine tuning of their surface properties to be used as building blocks for materials with advanced functionalities. There is therefore a need for the development of efficient, fast and water-based chemical grafting processes onto these nanoparticles. The **successful grafting of thermosensitive polyetheramines onto CNCs** has already been reported <sup>1</sup>, but **long reaction times** (a few days) and purification procedure (1 week dialysis) are required, limiting the production of large amounts of surface decorated CNCs.

In this study, we have investigated the optimization of the grafting of amine-terminated thermo-responsive polymers onto carboxylated CNCs by **peptidic coupling**. Conductimetric titration measurements and solid-state NMR data show that the **use of micro-wave assisted peptidic coupling reaction in water** is able to achieve in only **6 minutes a covalent polymer grafting** with a degree of substitution comparable to the one obtained in 72 h without the use of a micro-wave reactor. The obtained thermosensitive polymer decorated CNCs display a **thermoreversible aggregation/redispersion behavior**, as shown by dynamic light scattering and transmission electron microscopy data. Additionally, it was shown that the use of ultrafiltration instead of static dialysis leads to a decrease of the purification time from 1 week to 12 h. This **successful optimized green grafting** of thermosensitive polymers onto CNCs constitutes a new development towards the preparation of **smart functional CNC-based materials**.



## Materials & Methods

### Cellulose nanocrystals (CNC)

CNC suspension has been produced by University of Maine (US) from softwood. Concentration suspension is almost 11%wt.

Several characterizations have been performed and are presented below:

AFM	Length	nm	150 ± 30
	Thickness	nm	10 ± 5
	Aspect ratio	-	10
XRD	Crystallinity index	%	85 ± 2
DLS	Hydrodynamic diameter z*	nm	75 ± 2
	Polydispersity index (PDI)	-	0.14
TGA	Ash content	%	1.5
	T°C Cellulose degradation	°C	220
CT	Sulfure content	µeq/g	206 ± 16

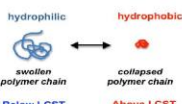


AFM: Atomic Force Microscopy, DLS: Dynamic Light Scattering, TGA: Thermogravimetric analysis, CT: Conductimetric Titration, XRD: X-Ray Diffraction

### Thermoresponsive polymers

- Jeffamine : M2070, M2005 were donated by Huntsman Corporation.
- PNIPAM : Poly(N-isopropylacrylamide) with -NH<sub>2</sub> terminated was purchased from Sigma-Aldrich.

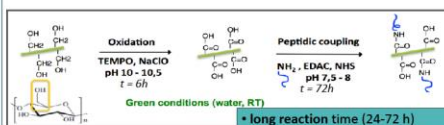
	M <sub>w</sub>	LCST
M2070	2000	65°C
M2005	2000	16°C
PNIPAM	2500	32°C



LCST : Lower critical solution temperature

### Peptidic grafting in aqueous media

CNC with Tempo oxidation are suspended in deionized water. **10 molar equivalents of PNIPAM-NH<sub>2</sub> or Jeffamine, 4 equivalents of EDAC (N-(3-dimethylaminopropyl)-N'-ethylcarbodiimide hydrochloride) and NHS (N-hydroxysuccinimide)** was added for the coupling reaction.



- long reaction time (24-72 h)
- purification itself takes few days.

### Tools for grafting process optimization

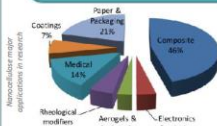
**Microwave Reactor (CERMAV)** : Initiator Classic microwave reactor (BIOTAGE) is using to perform micro-wave-assisted peptide coupling in water. **↑ temperature → thousand times faster** than traditional reflux conditions.

Reaction : pH : 7.5-8 & reaction : **6 min at 100°C**

**Ultrafiltration Cell (CERMAV)** : Purification after chemical modification was performed with Ultrafiltration cell (Amicon). **High pressure deionized water is injected → 10 times faster** than normal conditions.

Dialysis : **overnight purification** in Amicon ultrafiltration cell.

## Introduction



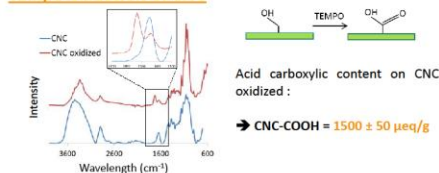
Since last decades, cellulose nanocrystals (CNC) and their properties know a strong interest and they have been the subject of many studies by industrials and/or academic consortia <sup>2,3</sup>.

The target of this study is to decorate CNC with thermosensitive polymer. Two thermosensitive polymer have been investigated : **Jeffamine & Poly(N-isopropylacrylamide) (Pnipam)**. This study is a part of one Polynat Carnot Institute project between 3 laboratories (CERMAV, LGP2 and LRP).



## Results & discussion

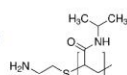
### Tempo oxidation of CNC



Acid carboxylic content on CNC oxidized :  
**→ CNC-COOH = 1500 ± 50 µeq/g**

### PNIPAM – NH<sub>2</sub>

Pnipam LCST is close to body temperature, easy to tune, desired polymer for potential applications.

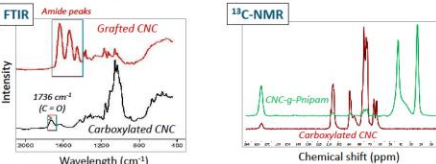


Conductimetric titration shows strange results



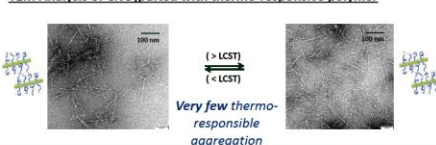
→ Conductometry suggests almost **100% of grafting**.

### Elemental analysis



→ Characteristic cellulose peaks are very low.  
 → Grafted suspension carries **large excess of free polymer** which is not grafted.

### TEM Analysis of CNC grafted with thermo-responsive polymer



### JEFFAMINE

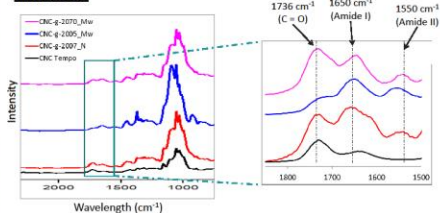


Conductimetric titration shows indicative results for grafting

	DO	DS	Yield (%)	Duration
Jeffamine 2005 – Normal (N)	0.21	0.032	15.4	72 h
Jeffamine 2005 – Microwave (Mw)	0.22	0.033	15.4	6 min

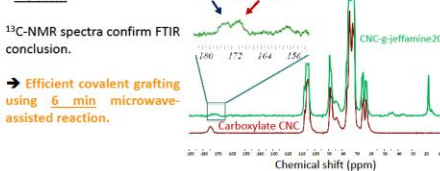
→ Same grafting yield is obtained with both reaction system.  
 → Microwave reaction **strongly decreases time reaction**.

### FTIR Spectra



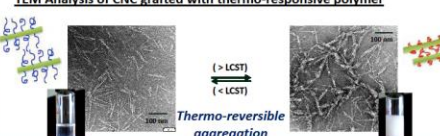
→ **Clear proof of grafting on CNC** : Carbonyl groups peaks (1740 cm<sup>-1</sup>) disappear in favor of Amide peaks (1650 cm<sup>-1</sup>).

### 13C-NMR



→ **Efficient covalent grafting using 6 min microwave-assisted reaction.**

### TEM Analysis of CNC grafted with thermo-responsive polymer



## Characterizations

- TEM images were obtained with a Philips CM200 transmission electron microscope using an acceleration voltage of 80 kV.
- <sup>13</sup>C-NMR : experiments were performed with a Bruker Avance DSX 400MHz spectrometer operating at 100.6 MHz for <sup>13</sup>C.
- **Infra-red spectra** were obtained using FTIR Perkin-Elmer spectrum 65, 16 scans on KBr pellet.
- Grafting efficiency were checked by classical conductimetric titration .

### References:

- Azzam F. & al., Biomacromolecules 2010
- Sun & al., Surface Chemistry 2004
- Dufresne, Materials today 2013

### Acknowledgment :

This work has been partially supported by the PolyNat Carnot Institute (Investissements d'Avenir - grant agreement n°ANR-11-CARN-007-01). This research was made possible thanks to the facilities of the TekLCell platform funded by the Région Rhône-Alpes (ERDF: European regional development fund).

LGP2, 461 rue de la papeterie, CS10065, 38402 Saint-Martin-d'Hères, France

## Conclusions & Perspectives

- **Covalent grafting** of a thermo-responsive polymer on CNC surface using **Microwave Reactor**.
- **Ultrafiltration is a good solution** but need some improvements.
- **Reversible thermo-aggregation** behavior of grafted CNCs with Jeffamine. Still some questions for Pnipam.

- Washing steps optimization.
- CNC direct grafting with esterification.
- CNC + PNIPAM-NH<sub>2</sub> adsorption understanding.



Bruno.Jean@cermav-cnrs.fr  
 Julien.Bras@lgp2.grenoble-inp.fr  
 Erwan.Gicquel@lgp2.grenoble-inp.fr



# Cellulose Nanocrystals as new bio based coating for improving fiber-based mechanical & barrier properties

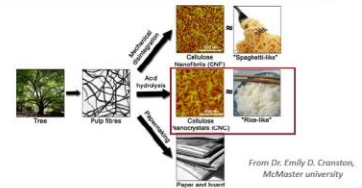
Erwan GICQUEL, Céline MARTIN, Cécile SILLARD, Julien BRAS

Laboratory of Pulp and Paper Science and Graphic Arts – LGP2 UMR 5518 / CNRS – Grenoble INP – Agefpi, France

## Abstract

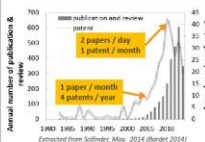
Cellulose Nanocrystals (CNC) are well known since 1960's but their recent industrialization (since 2011) opens new opportunities in high volume applications. Indeed, such materials present several **environmental advantages** (bio-based, biodegradable, biocompatible) but also can confer strong reinforcement, **high barrier properties** or specific physical color by auto organization. Meanwhile, industries are in constant innovation and require **new packaging solution**. New bio-based and high performance water-based coatings are expected for example in fiber-based industry. In response of these demands, this study investigates the elaboration of a **new smart paper by coated cellulose nanocrystals (CNC)** on fiber-based material for packaging.

To improve the properties of the paper surface, several layers of CNC have been deposited onto paper material using **bar coating process**. AFM, SEM, TEM analysis have been performed to highlight the **CNC network at the paper surface**. Results of high interest are discovered about the barrier properties. **Air barrier and grease resistance** of this new smart paper give new properties to the **paper only coated with CNC**.



From Dr. Emily D. Cranston, McMaster university

## Introduction



Since last decades, cellulose nanocrystals (CNC) and their properties know a strong interest and they have been the subject of many studies by industrials and/or academic consortia<sup>1,2</sup>.

Some publications deal with the use of Microfibrillated Cellulose on Paper for their properties<sup>3,4</sup>. However, **researches on paper only coated with CNC are not investigated**.

This study is a part of one Polynat Carnot Institute project between 3 laboratories (CERMAV, LGP2 and LRP).



## Materials & Methods

### Cellulose nanocrystals (CNC)

CNC suspension has been produced by University of Maine (US) from softwood. Concentration suspension is almost 11%wt. Several characterizations have been performed and are presented below:

AFM	Length	nm	150 ± 30
	Thickness	nm	10 ± 5
	Aspect ratio	-	10
XRD	Crystallinity index	%	85 ± 2
DLS	Hydrodynamic diameter z*	nm	75 ± 2
	Polydispersity index (PDI)	-	0.14
TGA	Ash content	%	1.5
	T°C Cellulose degradation	°C	220
CT	Sulfure content	µm/g	206 ± 16



AFM: Atomic Force Microscopy, DLS: Dynamic Light Scattering, TGA: Thermogravimetric analysis, CT: Conductometric Titration, XRD: X-Ray Diffraction

### Bar coating & paper

- Paper : calendered paper with basis weight of 43 g.m<sup>-2</sup>, made with non-bleached pulp, commercial used for packaging.
- Bar coating process : CNC suspension was coated onto paper samples with a bar coating process (Endupap, France) at speed of 5 cm.s<sup>-1</sup>. The coated papers were then dried with a contact drying system under tension at 105°C for 3 min. Steps are repeated at least 4 times.



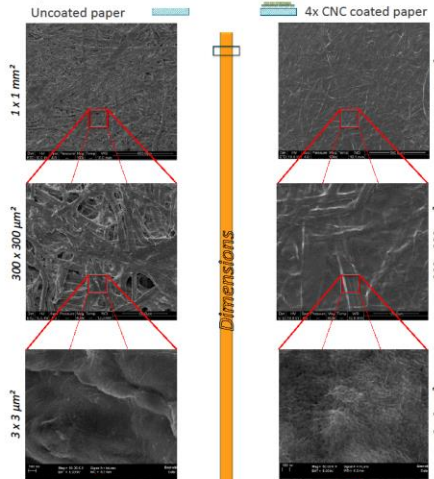
### Characterization

- SEM images were obtained with Quanta 200 environmental scanning electron microscope under vacuum at an operating voltage of 10 kV.
- AFM pictures were imaged at 3x3µm<sup>2</sup> using Atomic Force Microscope from Nanoscope III<sup>®</sup>, Veeco, Canada.
- Air permeability : is measured with "Mariotte vase" in respect of standard ISO 5636.
- Grease test : coated surface is exposed during 1 min to red color vegetal oil in standard respect ISO 16532-1:2008. Oil penetration through paper is looked and the report paper is analyzed.
- Contact angle : surface tension measurement was performed with DataPhysics equipment.
- Brightness : light reflection at 20, 60, 85° (REFO Glossmeters, Lange).

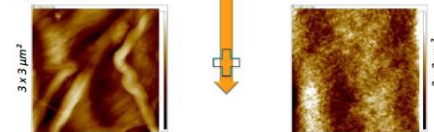
## Results & discussion

### Surface morphology analysis

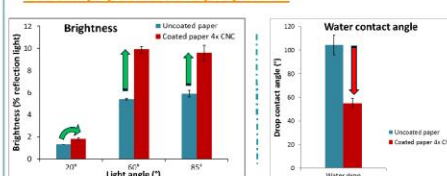
SEM pictures :



AFM pictures :

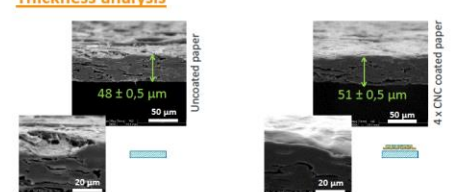


### Coated paper surface properties



- **Brightness** : Benefic effects of CNC coating on the brightness : + 5% of brightness (normally obtained by addition of polymer, latex, ...)
- **Water contact angle** : Negative effects on the paper. After coating, the surface is closed to cellulose water contact angle (60°).

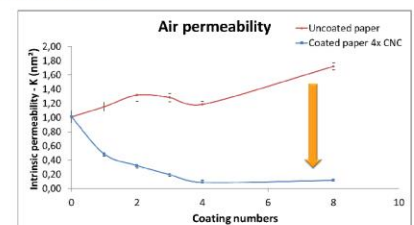
### Thickness analysis



- Roughness : 150 ± 20 nm (uncoated) to 20 ± 3 nm (CNC coated).
- After CNC coating, paper surface turns to **smooth aspect**.

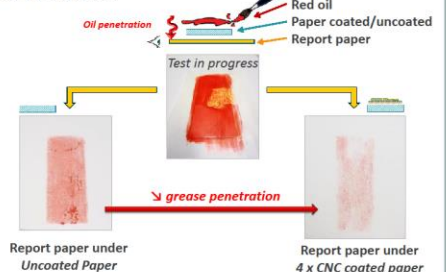
### Barrier properties

Air permeability :



- **High decrease** of air permeability thanks to CNC layers (1,70 to 0,10 ± 0,03 nm<sup>2</sup>)
- Thanks to fine network of CNC on paper, air debit through the surface strongly decreases : 420 ml air/min to 40 ml air /min

Grease resistance :



- After 4x CNC coating, 50% of red color oil is **stopped** compare to basic paper.
- WTR and PO<sub>2</sub> was investigated BUT because of the **high heterogeneity and stiffness** of the coating, results are not representative.

## Conclusions

- It is possible to coat paper with **only Cellulose Nanocrystals**.
- **Roughness strongly decrease** after CNC coating.
- **Barrier properties** : air permeability strongly decreases & Grease resistance increases.

## Perspectives

- Improve **homogeneity and flexibility** of CNC coating.
- Knowledge on **CNC organization on paper**, under the bar coater.
- Control if surface is adapted for specific applications (**printed electronics**).
- Investigation on different coating process.
- Coating with **thermo-responsive CNC** to create smart coatings.

### References:

1. Sun & al., Surface Chemistry 2004
2. Dufresne, Materials today 2013
3. Li & al., Cellulose 2013
4. Lavoinne & al., Applied Polymer Science 2013
5. Lavoinne & al., Journal of materials sciences 2014



### Acknowledgment :

This work has been partially supported by the PolyNat Carnot Institute (Investissements d'Avenir - grant agreement n°ANR-11-CARN-007-01). This research was made possible thanks to the facilities of the TokiCell platform funded by the Région Rhône-Alpes (ERDF: European regional development fund).

Julien.Bras@lgp2.grenoble-inp.fr  
Erwan.Gicquel@lgp2.grenoble-inp.fr

LGP2, 461 rue de la papeterie, CS10065, 38402 Saint-Martin-d'Hères, France





# Cellulose Nanocrystals as new bio-based support in thermo-responsive hydrogels for bio-compatible smart applications

Erwan GICQUEL, Clara ABBATTISTA, Bruno JEAN, Frédéric PIGNON, Céline MARTIN, Julien BRAS

Laboratory of Pulp and Paper Science and Graphic Arts – LGP2 UMR 5518 / CNRS – Grenoble INP – Agefpi, France

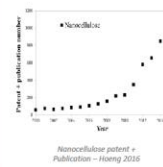
## Abstract

The proposed innovative approach has been to investigate the realization and characterization of **thermo-sensitive bio-based hydrogels**. In order to create these hydrogels, thermo-responsive polymers are grafted by **green chemistry** (onto and from chemistry) or **adsorbed** on CNC<sup>1,2,3</sup>. Well-known for their Low Critical Solution Transition (LCST) at the interface between room and human body temperature, Poly(N-isopropylacrylamide) (Pnipam) has been used. The **idea** is to produce a **bio-compatible, bio-based and renewable hydrogel for smart applications**.

In this study, different parameters are carried out. The external stimuli temperature was changed to control and estimate the **repeatability** of the **liquid form to gel** form hydrogel. Rheological and structure under shear flow of these thermo-responsive hydrogel were examined. Finally, the concentration of grafted CNC inside the hydrogel was customized to improve the network of the system.



## Introduction



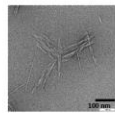
Society requires nowadays innovating technological solutions to develop **high added value bio-products**. In response to these requirements, Cellulose Nanocrystals (CNC) is of high interest for several smart applications like biomedical hydrogels, cosmetic and fiber based industries<sup>4</sup>. Concerning **hydrogels**, their rheological properties and structure under shear flow are more and more studied by the scientific community<sup>5,6</sup>.

## Materials & Methods

### Cellulose nanocrystals (CNC)

CNC suspension has been produced by University of Maine (US) from softwood. Concentration suspension is almost 11%wt and used after sonication. Several characterizations have been performed and are presented below:

AFM	Length	nm	150 ± 30
	Thickness <td>nm</td> <td>10 ± 5</td>	nm	10 ± 5
	Aspect ratio <td>-</td> <td>10</td>	-	10
XRD	Crystallinity index	%	85 ± 2
DLS	Hydrodynamic diameter z*	nm	75 ± 2
	Polydispersity index (PDI)	-	0.14
CT	Sulfure content	µeq/g	206 ± 16



CNC by TEM

AFM: Atomic Force Microscopy, DLS: Dynamic Light Scattering, CT: Conductimetric Titration, XRD: X-Ray Diffraction

### Thermo-sensitive polymer

**P-Nipam** : Poly(N-isopropylacrylamide) with -NH<sub>2</sub> terminated purchased from Sigma-Aldrich. It was used for peptidic grafting and adsorption on CNC. Because of Mw = 2 500 g/mol and DP = 25, this polymer is more an Oligomer : Oligo(N-isopropylacrylamide) / O-Nipam.

### Peptidic grafting in aqueous media

CNC with Tempo oxidation are suspended in deionized water. **10 molar equivalents** of PNIPAM-NH<sub>2</sub> or Jeffamine, **4 equivalents** of EDAC (N-(3-dimethylaminopropyl)-N'-ethylcarbodiimide hydrochloride) and NHS (N-hydroxysuccinimide) was added for the coupling reaction.

### Rheology behavior

The rheological behavior of suspensions was studying using a speed rotating rheometer (Anton paar MCR 301) at different temperatures. Shear test were carried out with a cone-plate configuration.

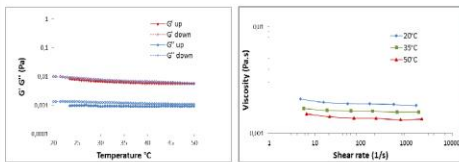
- 1- Constant shear rate was applied to the sample whose initial state is controlled, from 1s<sup>-1</sup> to 1000 s<sup>-1</sup>, to obtain flow curve.
- 2- Oscillatory deformation was performed to understand the elastic part of the suspension. G' & G'' (Pa) was studied depending of the temperature of the system.



## Results & Discussions

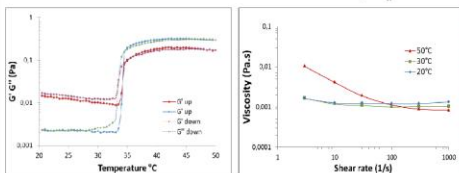
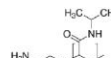
### Rheological behavior of the raw material

#### CNC at 2%wt :



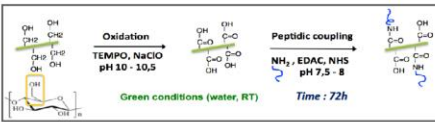
- CNC at low concentration are in **liquid** configuration (G' > G'')
- Temperature have **no impact** on the suspension.

#### O-Nipam at 5%wt:



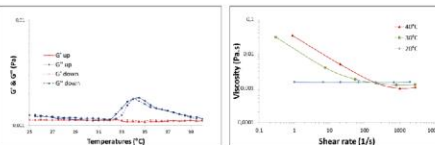
- **Liquid <-> gel** structure before and after the LCST.
- No clear impact of the temperature on the viscosity.
- Oligomer of Onipam after LCST aggregate** together and are ejected because of the rotation of the rheometer.

### Peptidic grafting : CNC graft with Onipam



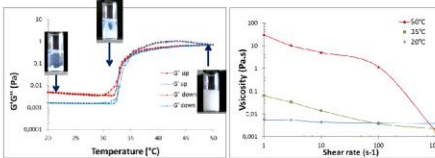
- Grafting rate : **85%**
- Conductimetric titration and FTIR was performed to confirm the grafting

#### CNC-g-Onipam : 1,35%wt (0,35%wt CNC + 1%wt Onipam)



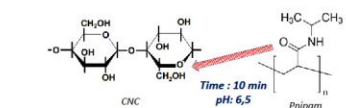
- CNC concentration is too low. No clear impact on the rheological elastic properties.

#### CNC-g-Onipam : 6,1%wt (1,1%wt CNC + 5%wt Onipam)



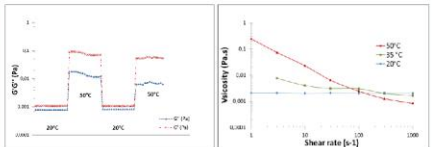
- Viscosity increase from **0,01 Pa.s to 50 Pa.s**
- **Liquid <-> gel** structure before and after the LCST & **reversibility**
- At 1 s<sup>-1</sup>, the **viscosity is x10 000** when the temperature cross the LCST

### Adsorption : CNC decorate with Onipam



- **Hydrogen bonds** between C=O on Pnipam and OH on CNC
- QCM-D was performed to confirm the adsorption on CNC

#### 1,1%wt CNC + 5%wt Onipam



- Low effect of the temperature on the elastic behavior. Gel form isn't formed when the temperature increased but a **reversible system**
- At 1 s<sup>-1</sup>, the **viscosity is x100** when the temperature cross the LCST

#### CNC concentration impact :

✓ When concentration increase, the viscosity increased

	1,35%wt	6,1%wt
$\dot{\gamma} = 1 \text{ s}^{-1}, 20^\circ\text{C}$	0,001 Pa.s	0,007 Pa.s
$\dot{\gamma} = 1 \text{ s}^{-1}, 50^\circ\text{C}$	0,05 Pa.s	50 Pa.s

X 10 000

#### Adsorbed VS grafted :

- ✓ Polymer grafted on CNC have a strong rheological reversible answer contrary to adsorption.

	Grafted	Adsorbed
$\dot{\gamma} = 1 \text{ s}^{-1}, 20^\circ\text{C}$	0,007 Pa.s	0,003 Pa.s
$\dot{\gamma} = 1 \text{ s}^{-1}, 50^\circ\text{C}$	50 Pa.s	0,3 Pa.s

## Conclusions

- It is possible to realize **strong & thermo-sensitive hydrogel by green grafting**
- Adsorption can create a network and a small hydrogel without a clear reversible properties BUT grafting performed the strongest hydrogel
- Realization of a **bio-compatible, bio-based and renewable hydrogel for smart applications** (cosmetic, coating, ...)

## Perspectives

- Test other thermosensitive polymer : **Diblock, long Pnipam, Jeffamine, ...**
- Study more in details the **concentration effect**
- **Optimize** the hydrogel to increase the Viscosity to 1 000 Pa.s
- Create CNC-g-Pnipam by **living radical polymerization** to increase the length of the Pnipam brushes

### References:

1. Azzam et al., Biomacromolecules 2010
2. Hemraz et al., Journal of Colloid and Interface Science 2014
3. Larsson et al., European Polymer Journal 2013
4. Yang et al., Advance materials 2015
5. Salas et al., Current Opinion in Colloid & Interface Science 2014
6. Wu et al., Journal of Applied Polymer Science 2014



### Acknowledgment :

This work has been partially supported by the PolyNat Carnot Institute (Investissements d'Avenir - grant agreement n°ANR-11-CARN-007-01). This research was made possible thanks to the facilities of the TekliCell platform funded by the Région Rhône-Alpes (ERDF: European regional development fund).

Julien.Bras@lgp2.grenoble-inp.fr  
Erwan.Gicquel@lgp2.grenoble-inp.fr





### **Résumé Anglais - English Abstract**

This project consists to develop and study new hybrid structures based on nanocelluloses and stimuli-responsive polymers, in particular, thermo-responsive polymers. Nanocelluloses - nanoparticles extracted from cellulose - exist in two forms: cellulose nanocrystals (CNCs) and cellulose nanofibrils (CNFs). This study focused on the design of CNCs hydrogels with stimuli-responsive polymers. Several thermo-responsive polymers have been used for their biocompatibility and lower critical solution temperature (LCST) close to body temperature. This work consisted of (i) preparation of systems using the principles of green chemistry, (ii) the rheological study of these thermo-sensitive hydrogels, and (iii) the development of smart applications for these unique biomaterials. Through the use of state of the art technologies (SANS, SAXS), physicochemical interactions between the polymers and CNCs have been studied. The use of block copolymers made it possible to create CNCs-based hydrogels with specific rheological properties: liquid at ambient temperature to gel at body temperature. These hydrogels can be used in the creation of injectable systems for biomedical applications, as well as thermosensitive surfaces.

**Key-words:** *Cellulose nanocrystals, hydrogel, thermo-responsive, stimuli-responsive*

### **Résumé Français - French Abstract**

L'originalité de ce projet consiste au développement et à l'étude de nouvelles structures hybrides à base de nanocelluloses et de polymères stimulables. En particulier, c'est le design d'hydrogels aux propriétés thermosensibles qui est visé. Les nanocelluloses - nanoparticules issues de la cellulose - sont de deux types : les nanocristaux de cellulose (CNCs) et les nanofibrilles de cellulose (CNFs) et possèdent des propriétés bien particulières. Cette étude s'est concentrée sur l'élaboration d'hydrogels de CNCs. Plusieurs polymères thermosensibles ont été utilisés pour leur biocompatibilité et leur température de solution critique (LCST) aux abords de la température du corps humain. Ce travail a consisté en (i) la préparation des systèmes sur les principes de la chimie verte, (ii) l'étude rhéologique de ces gels thermosensibles et (iii) l'élaboration d'applications à forte valeur ajoutée pour ces biomatériaux uniques. A travers l'utilisation de grands équipements (SANS, SAXS), les interactions physico-chimiques CNCs/polymères ont été étudiées. L'utilisation de block copolymères a permis l'obtention de suspensions de CNCs aux propriétés rhéologiques spécifiques : de liquide à température ambiante à gel à température du corps humain. D'un point de vue applicatif, les hydrogels ainsi réalisés ont permis le déploiement de systèmes injectables pour le biomédical ainsi que des surfaces thermosensibles.

**Mots clés :** *Nanocristaux de cellulose, hydrogel, thermosensible, stimuable*